# ENGINEERED TISSUES USING BIOACTIVE HYDROGELS

EDITED BY: Di Huang, Zongliang Wang, Sushila Maharjan and Yi Deng
PUBLISHED IN: Frontiers in Bioengineering and Biotechnology

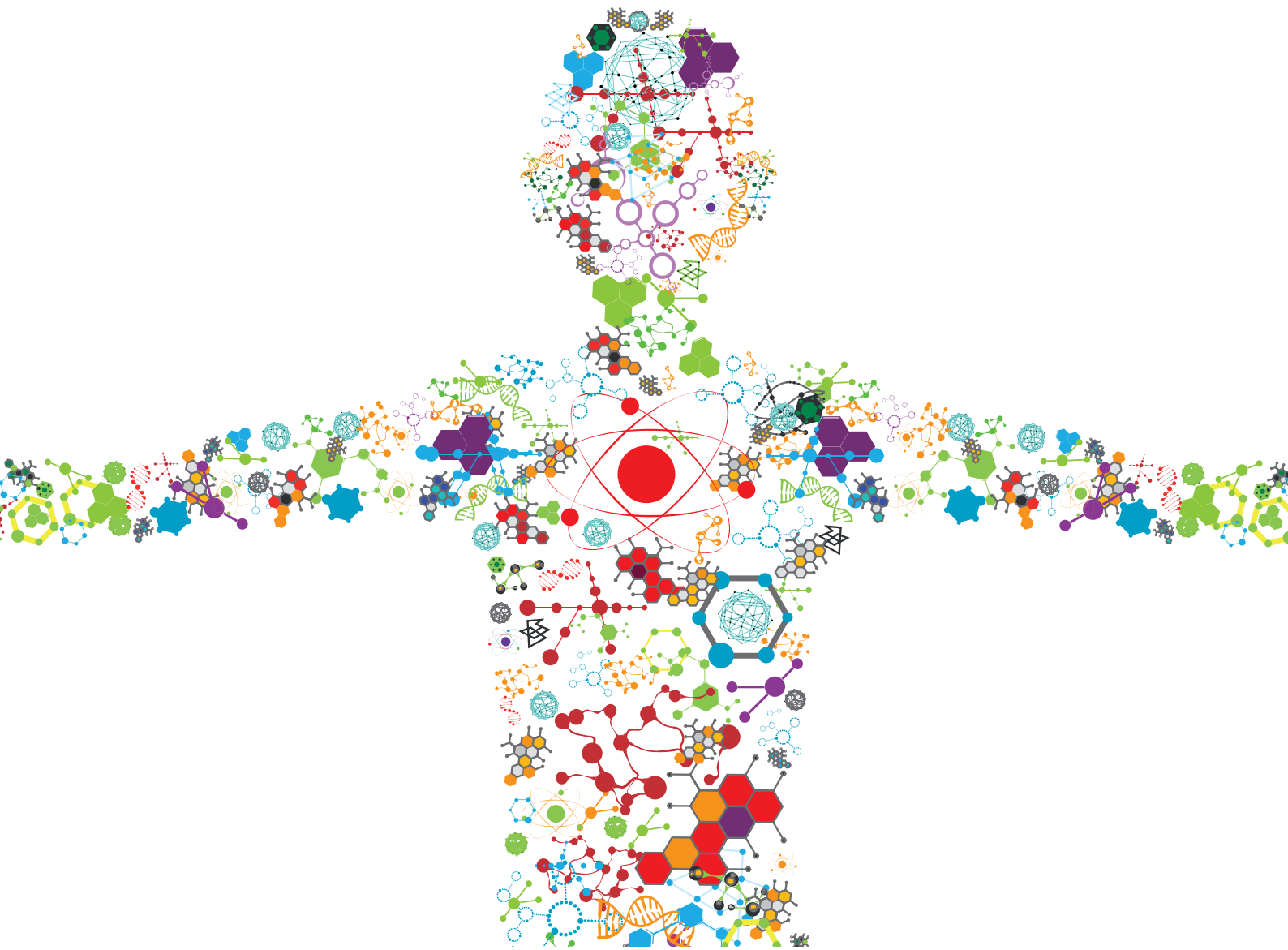

frontiers Research Topics

ISSN 1664-8714
ISBN 978-2-88976-836-3
DOI 10.3389/978-2-88976-836-3

## About Frontiers

Frontiers is more than just an open-access publisher of scholarly articles: it is a pioneering approach to the world of academia, radically improving the way scholarly research is managed. The grand vision of Frontiers is a world where all people have an equal opportunity to seek, share and generate knowledge. Frontiers provides immediate and permanent online open access to all its publications, but this alone is not enough to realize our grand goals.

## Frontiers Journal Series

The Frontiers Journal Series is a multi-tier and interdisciplinary set of open-access, online journals, promising a paradigm shift from the current review, selection and dissemination processes in academic publishing. All Frontiers journals are driven by researchers for researchers; therefore, they constitute a service to the scholarly community. At the same time, the Frontiers Journal Series operates on a revolutionary invention, the tiered publishing system, initially addressing specific communities of scholars, and gradually climbing up to broader public understanding, thus serving the interests of the lay society, too.

## Dedication to Quality

Each Frontiers article is a landmark of the highest quality, thanks to genuinely collaborative interactions between authors and review editors, who include some of the world's best academicians. Research must be certified by peers before entering a stream of knowledge that may eventually reach the public - and shape society; therefore, Frontiers only applies the most rigorous and unbiased reviews.
Frontiers revolutionizes research publishing by freely delivering the most outstanding research, evaluated with no bias from both the academic and social point of view. By applying the most advanced information technologies, Frontiers is catapulting scholarly publishing into a new generation.

## What are Frontiers Research Topics?

Frontiers Research Topics are very popular trademarks of the Frontiers Journals Series: they are collections of at least ten articles, all centered on a particular subject. With their unique mix of varied contributions from Original Research to Review Articles, Frontiers Research Topics unify the most influential researchers, the latest key findings and historical advances in a hot research area! Find out more on how to host your own Frontiers Research Topic or contribute to one as an author by contacting the Frontiers Editorial Office: frontiersin.org/about/contact

# ENGINEERED TISSUES USING BIOACTIVE HYDROGELS

Topic Editors:
**Di Huang,** Taiyuan University of Technology, China
**Zongliang Wang,** Changchun Institute of Applied Chemistry, Chinese Academy of Sciences (CAS), China
**Sushila Maharjan,** Brigham and Women's Hospital, Harvard Medical School, United States
**Yi Deng,** Sichuan University, China

**Citation:** Huang, D., Wang, Z., Maharjan, S., Deng, Y., eds. (2022). Engineered Tissues Using Bioactive Hydrogels. Lausanne: Frontiers Media SA.
doi: 10.3389/978-2-88976-836-3

# Table of Contents

frontiers | Frontiers in Bioengineering and Biotechnology

TYPE Editorial
PUBLISHED 22 July 2022
DOI 10.3389/fbioe.2022.975907



OPEN ACCESS

EDITED AND REVIEWED BY
Hasan Uludag,
University of Alberta, Canada

*CORRESPONDENCE
Yi Deng,
dengyibandeng@scu.edu.cn
Sushila Maharjan,
smaharjan@bwh.harvard.edu
Zongliang Wang,
wangzl@ciac.ac.cn
Di Huang,
huangjw2067@163.com

SPECIALTY SECTION
This article was submitted to Biomaterials, a section of the journal Frontiers in Bioengineering and Biotechnology

RECEIVED 22 June 2022
ACCEPTED 27 June 2022
PUBLISHED 22 July 2022

CITATION
Qin M, Deng Y, Maharjan S, Wang Z and Huang D (2022), Editorial: Engineered tissues using bioactive hydrogels. *Front. Bioeng. Biotechnol.* 10:975907. doi: 10.3389/fbioe.2022.975907



# Editorial: Engineered tissues using bioactive hydrogels

Miao Qin[1], Yi Deng[2]*, Sushila Maharjan[3]*, Zongliang Wang[4]* and Di Huang[1]*

[1]Research Center for Nano-Biomaterials and Regenerative Medicine, College of Biomedical Engineering, Taiyuan University of Technology, Taiyuan, China, [2]State Key Laboratory of Polymer Materials Engineering, School of Chemical Engineering, Sichuan University, Chengdu, China, [3]Division of Engineering in Medicine, Department of Medicine, Brigham and Women's Hospital and Harvard Medical School, Boston, MA, United States, [4]Key Laboratory of Polymer Ecomaterials, Changchun Institute of Applied Chemistry, Chinese Academy of Sciences, Changchun, China

KEYWORDS

**tissue engineering, extracellular matrix, 3D structure, bioactive, hydrogels**

Editorial on the Research Topic
Engineered tissues using bioactive hydrogels

Tissue damage, dysfunction and organ failure remain great challenges to cure, which have been the major causes of human morbidity and mortality. According to studies, the global cost associated with organ dysfunction and failure has been projected to hundreds of billions of dollars every year. Therefore, the regeneration of human tissues and organs have been widely explored to repair or replace defective tissues and organs while restoring their functions, thereby improving health and life quality. Several technologies including surgical reconstruction, organ transplant, *in situ* induced regeneration and tissue engineering have been employed to achieve regeneration of tissues and organs. Among these approaches, tissue engineering holds the promising approach to engineer various tissues and organs with the potential to meet the future needs of patients requiring the repair, replace and regeneration of tissues and organs.

Hydrogels have been proven to be promising candidates in tissue engineering field due to the distinct three-dimensional network structure and excellent biocompatibility, which could provide extracellular matrix like microenvironments and stimulus response properties in human tissues and organs. Consequently, endeavor has been pursued on the investigation of hydrogels for mimicking human tissues such as bone, skin, muscle, and so on. However, the clinical applications of hydrogels are still hampered owing to the intrinsic characteristics including poor mechanical performances, low bioactivity, uncontrollable degradation process, which leaves a huge gap compared to real human tissues. Among these drawbacks, insufficient bioactivity is the primary obstacle to be overcome for researchers, which exert a significant influence on tissue regeneration. To address this thorny issue, plenty of strategies such as introducing cells and bioactive molecules into hydrogels have been conducted. Even though bioactivity of the hydrogels has been improved, there still remain a large number of challenges that restrict their

application in clinics. A variety of factors, such as the loading efficiency of cells and bioactive molecules, the interaction between hydrogels and bioactive molecules, the biostability of hydrogel-based engineered tissues system, etc., should be considered in hydrogel-based engineered tissues before their clinical application.

In this Research Topic, we present a number of interesting studies related to the development of bioactive hydrogels for mimicking tissues to facilitate the repair and regeneration of defective tissues. Broadly, there are two approaches towards recreating engineered tissues *in vitro*. One is development and fabrication of bioactive hydrogels. For example, Sun et al. have designed a composite hydrogel with antibacterial property for skin repair. They have fabricated decellularized ECM-based bio-scaffolds to promote remodeling of skin tissues. Similarly, Wu et al. have constructed injectable small extracellular vesicles laden hydrogel for accelerating bone regeneration. While Xu et al. have developed hybrid aerogel scaffold for osteonecrosis repair, Yu et al. have synthesized bio-hydrogel cell delivery system for retarding intervertebral disc degeneration. Furthermore, Wang et al. have summarized the application of bioactive hydrogels in intrauterine adhesion treatment and Lv et al. have summarized new treatment ideas in spinal cord injuries using hydrogels.

The other approach is utilization of different technologies. For instance, Sun et al. have shown the promising prospects of exosome-laden hydrogels in bone repair and Xin et al. have introduced versatile design strategies of bioactive hydrogels against osteomyelitis. Furthermore, Liu et al. have demonstrated the merits of 3D printing technology-based hydrogel in bone repair and reconstruction. With the encouraging strategies and approaches, we believe that the new paradigm will be introduced into tissue engineering field using bioactive hydrogels, which will advance the engineering of tissues and organs *in vitro* for their use in clinics.

## Author contributions

All authors listed have made a substantial, direct, and intellectual contribution to the work and approved it for publication.

## Conflict of interest

The authors declare that the research was conducted in the absence of any commercial or financial relationships that could be construed as a potential conflict of interest.

## Publisher's note

frontiers in Bioengineering and Biotechnology

REVIEW
published: 21 September 2021
doi: 10.3389/fbioe.2021.760943

# Application of Bioactive Hydrogels for Functional Treatment of Intrauterine Adhesion

*Jingying Wang, Chao Yang, Yuxin Xie, Xiaoxu Chen, Ting Jiang, Jing Tian, Sihui Hu and Yingli Lu**

*Department of Obstetrics and Gynecology, The Second Hospital, Jilin University, Changchun, China*

Intrauterine adhesion (IUA) is a common endometrial disease and one of the main causes of infertility in women of childbearing age. Current treatment strategies, such as hysteroscopic adhesion resection, hysteroscopic transcervical resection of adhesion (TCRA), the use of local hormone drugs, and anti-adhesion scaffold implantation, do not provide a satisfactory pregnancy outcome for moderate-severe IUA, which presents a great challenge in reproductive medicine. With the development of material engineering, various bioactive and functional hydrogels have been developed using natural and synthetic biomaterials. These hydrogels are not only used as barely physical barriers but are also designed as vectors of hormone drugs, growth factors, and stem cells. These characteristics give bioactive hydrogels potentially important roles in the prevention and treatment of IUA. However, there is still no systematic review or consensus on the current advances and future research direction in this field. Herein, we review recent advances in bioactive hydrogels as physical anti-adhesion barriers, *in situ* drug delivery systems, and 3D cell delivery and culture systems for seeded cells in IUA treatment. In addition, current limitations and future perspectives are presented for further research guidance, which may provide a comprehensive understanding of the application of bioactive hydrogels in intrauterine adhesion treatment.

**Keywords: bioactive hydrogel, reproductive medicine, drug delivery system, stem cell therapy, intrauterine adhesion**

OPEN ACCESS

***Edited by:***
*Zongliang Wang,*
*Changchun Institute of Applied Chemistry, Chinese Academy of Sciences, China*

***Reviewed by:***
*Yilong Cheng,*
*Xi'an Jiaotong University, China*
*Jin Zhang,*
*Fuzhou University, China*
*Shuangjiang Yu,*
*Hangzhou Normal University, China*

****Correspondence:***
*Yingli Lu*
*luyl@jlu.edu.cn*

***Specialty section:***
*This article was submitted to Biomaterials, a section of the journal Frontiers in Bioengineering and Biotechnology*

***Received:*** *19 August 2021*
***Accepted:*** *09 September 2021*
***Published:*** *21 September 2021*

***Citation:***
*Wang J, Yang C, Xie Y, Chen X, Jiang T, Tian J, Hu S and Lu Y (2021) Application of Bioactive Hydrogels for Functional Treatment of Intrauterine Adhesion. Front. Bioeng. Biotechnol. 9:760943. doi: 10.3389/fbioe.2021.760943*

## INTRODUCTION

The uterus is composed of three tissue layers, namely, the endometrium, myometrium, and perimetrium (Mancini and Pensabene, 2019). The endometrium is the innermost layer composed of epithelial and stromal components; it is a unique tissue that undergoes a repetitive cycle of cell proliferation, differentiation, and shedding during the reproductive years of a woman's life, providing the "fertile ground" for embryo implantation (Lv et al., 2021). Intrauterine adhesion (IUA) is a result of endometrial injury and infection caused by unsafe abortion and poor maternal care, which can lead to partial or complete occlusion of the uterine cavity, resulting in periodic abdominal pain, oligomenorrhea, amenorrhea, even infertility (Liao et al., 2021). A normal endometrium is a determinant of fertility, and IUA is recorded to be the second most common cause of female infertility after fallopian tube obstruction (Wei et al., 2020). As for IUA treatment, current therapies include hysteroscopic adhesiolysis, TCRA, hormonal therapy, and anti-adhesion material implantation, including the intrauterine device (IUD) (Huang et al., 2020a; Han et al., 2020). Although current treatment strategies have achieved positive effects in some cases, the prognosis of

patients with severe IUA is unsatisfactory, and the incidence of re-adhesion after the operation is still high (Young and Evans-Hoeker, 2014). Thus, patients always accept adjuvant therapy after operation to avoid the recurrence of re-adhesion after surgery (Li et al., 2021). To date, clinicians have already applied biomaterials such as hyaluronic acid (HA) and INTERCEED®—an absorbable adhesion barrier made of oxidized regenerated cellulose—after surgery in IUA patients to prevent postoperative re-adhesion (Zhang et al., 2020a). In addition, numerous adjuvant therapies and biomaterials, including bioactive hydrogels, can be selected for those patients who suffer from severe IUA. With the rapid development of regenerative medicine and tissue engineering, in addition to applying traditional adjuvant therapy to IUA patients, clinicians are also seeking the potential of endometrial regeneration through tissue engineering.

Hydrogels are formed by water-soluble or hydrophilic polymers through certain chemical or physical cross-linking, and are composed of a hydrophilic three-dimensional (3D) network structure. The hydrogels swell rapidly in water and can retain a large volume of water without dissolving in this swollen state, which is very similar to soft tissue (Milcovich et al., 2017; Manna et al., 2019). Hydrogels are widely applied in the field of tissue engineering owing to their excellent properties in drug release, 3D cell culture, and simulation of an extracellular matrix (Chang et al., 2018). In the treatment of IUA, the bioactive hydrogels show potential in anti-adhesion and endometrial reconstruction. In order to improve the biocompatibility, reduce the potential cytotoxicity, and adapt to the special pathological microenvironment of the IUA, researchers have further constructed and optimized hydrogels (Tang et al., 2018). Although hydrogels have performed outstandingly in tissue regeneration, cell culture, and drug delivery, their application in the field of reproductive medicine is still in the exploratory stage. Only a limited number of hydrogel products and technologies have been successfully used in humans (Huang and Ding, 2019).

In this review, we summarize the latest advances in hydrogels as a therapeutic option for IUA. This article focuses on the latest research regarding hydrogels as physical anti-adhesion barriers, *in situ* drug delivery systems, and 3D cell delivery and culture systems, in order to improve their application in IUA (**Scheme 1**).

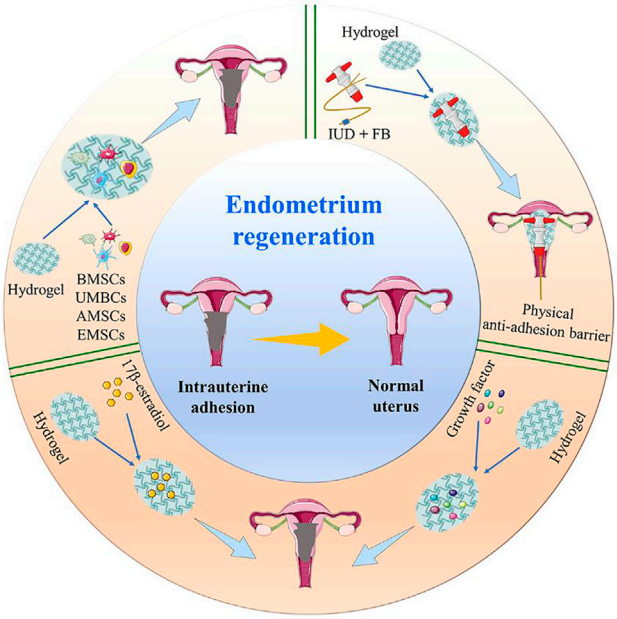


**SCHEME 1 |** Advances in bioactive hydrogels as a therapeutic option for IUA.

## THE DESIGN OF HYDROGELS FOR IUA

The design of hydrogels for biomedical applications needs to consider the purpose of the application and the disease-specific microenvironment. IUA can be characterized as endometrial fibrosis, where the intrauterine walls partially or completely adhere to each other, thus resulting in narrowing or disappearance of the uterine cavity (Carbonnel et al., 2021). The characteristic pathological change of IUA is endometrial injury, which has become a primary factor resulting in oligomenorrhea and related complications (Xu et al., 2020). During natural repair of an endometrial lesion, the luminal epithelial cells are largely lost and are replaced by inactive columnar endometrial epithelium, the stroma is replaced by fibrous tissue, the endometrium becomes significantly thinner and loses response to estrogen and progesterone (Zhao et al., 2016). As mentioned previously, the major aim of the application of bioactive hydrogels is to prevent the recurrence of adhesion and to promote endometrial regeneration. To be an ideal biomaterial for patients with IUA, biocompatibility, immunogenicity, mechanics, degradability, the possibility of infection and transmission of disease, the ability to promote stem cell recruitment, intimal repair and reproductive function recovery, drug-controlled release, availability and even ethical issues should be taken into consideration (López-Martínez et al., 2021). Therefore, the design strategy for bioactive hydrogels should consider the purpose of the application and the disease-specific microenvironment of IUA.

Firstly, one of the main characteristics of the hydrogels used for anti-IUA barrier materials is its ability to form a mechanical intrauterine cavity to decrease the formation of fibrous tissue. The uterine cavity is surrounded by a muscular layer of interlacing smooth muscle fibers, which usually causes the uterine cavity to collapse during the postoperative healing process unless it is mechanically distended. Since the uterine cavity is varied in size and shape, the bioactive hydrogels which can adjust themselves to different uterine cavities may fully promote endometrium regeneration. Moreover, the speed of degradation of the hydrogels needs to be manageable to avoid rapid degradation because they must remain in the uterine cavity for a certain time to resist adhesion recurrence (Wang et al., 2020a). After the healing process is completed, the bioactive hydrogels as barriers must be degraded or absorbed naturally, rather than remaining as a foreign body. Among the hydrogel systems sensitive to stimuli,

thermosensitive hydrogels are the most extensively studied. Depending on the properties, thermosensitive matrices are divided into systems showing lower critical solution temperature (LCST) or upper critical solution temperature (UCST) (Kasiński et al., 2020). In this field, temperature-responsive hydrogels have attracted the attention of researchers; especially the hydrogels that are liquid at room temperature and can be rapidly gelled at physiological temperature around specific tissues (Kapoor and Kundu, 2016). The most important hydrogels for biomedical applications are systems with LCST close to the physiological temperature. This type of hydrogel is widely used in anti-adhesion materials because of the ease of its control and its rapid response to physical and chemical changes (Keskin et al., 2019). Compared to other hydrogels, temperature-responsive hydrogels can mechanically help shape the normal uterine cavity and prevent postoperative IUA (Han et al., 2016).

Secondly, hydrogels applied in IUA treatment should have controllable release profiles. As a simple and efficient platform for controlled release and delivery, the ideal bioactive hydrogels embed growth factors, drugs, and stem cells with therapeutic functions within their 3D structure. These drugs are released through the pores, hydrolysis of bonds, or self-degradation of the hydrogels, allowing the drugs to be applied to the uterine cavity wound after surgery with a sustained profile to promote regeneration of the endometrium (Sheth et al., 2019). Chemically crosslinked hydrogels usually provide a stable polymer network with slow degradation kinetics. For patients with severe IUA, where there is almost no normal functional endometrial tissue in the uterine cavity, stem cell transplantation is a potential option for the promotion of endometrial regeneration. Under such circumstances, the ideal bioactive hydrogels need to create a 3D cell delivery and culture system that is conducive to transplanted stem cell survival, proliferation, and directed differentiation (Cervelló et al., 2015).

Depending on the source, hydrogels can be divided into natural hydrogels and synthetic hydrogels. Natural hydrogels (e.g., HA, alginate, chitosan, collagen, and polyethylene glycol) have already been widely used in the field of regenerative medicine (Liu et al., 2020a). They are generally highly biocompatible, as reflected in their successful use in the peritoneum and other sites *in vivo* (T et al., 2016). Their biocompatibility is promoted by a high-water content and a physiochemical similarity to the native extracellular matrix, both compositionally (particularly in the case of carbohydrate-based hydrogels) and mechanically (Larrañeta et al., 2018). The naturally derived materials often have desirable biological properties and can influence cell function, but some natural hydrogels are limited by poor mechanical strength and fast degradation profiles (Rastogi and Kandasubramanian, 2019). In contrast, synthetic polymers provide appropriate 3D environments and have the desired mechanical strengths. However, they lack the bioactive properties of natural materials. Therefore, it is necessary to produce hybrid materials by combining synthetic and natural polymers, and to retain the desirable characteristics of both materials (Liu et al., 2018).

To date, hydrogels used in clinical settings can only achieve physical anti-adhesion. Bioactive hydrogels with controlled release and suitable culture microenvironment have not been widely used in the treatment of IUA. Hydrogels have been widely exploited with the aim of achieving drug delivery directly into the vaginal mucosa for hormone therapy, owing to their attractive features such as the increased drug residence time at the targeted sites and control of drug release rates after hysteroscopic transcervical resection of adhesion (TCRA) (Shamloo et al., 2018).

## THE APPLICATION OF BIOACTIVE HYDROGELS IN IUA

The excellent biocompatibility, controllable mechanical properties, the ability of incorporating therapeutic agents for sustained release, and encapsulating seed cells at physiological conditions make bioactive hydrogel an ideal option for IUA treatment and endometrial regeneration. Several factors should be considered carefully, such as vascularization, native cell recruitment, and scar inhibition (Owusu-Akyaw et al., 2019). In the field of IUA treatment, hydrogels are broadly applied as space-filling agents, delivery vehicles for bioactive substances, and 3D structures that organize cells and present stimuli to ensure the repair of the damaged endometrium (Grover et al., 2012). Herein, we summarize the progress in hydrogel research for endometrial regeneration and IUA treatment from the following three aspects; namely, bioactive hydrogels as physical anti-adhesion barriers, *in situ* drug delivery systems, and 3D cell delivery and culture systems.

### Bioactive Hydrogels as Absorbable Physical Anti-Adhesion Barriers in IUA

Generally speaking, the main methods for the treatment of IUA are transabdominal or hysteroscopic resection of the adhesion; but while the former creates appreciable tissue injury, the latter has a high risk of recurrence, and postoperative uterine cavity wounds often quickly form new adhesions (Bhandari et al., 2015). Therefore, positive preventive measures should be taken for IUA after operation. Currently, strategies to reduce the rate of recurrence and improve reproductive outcomes in cases of severe IUA include the use of an IUD, Foley balloon (FB), amnion graft applied over a FB, and an oxidized and regenerated cellulose adhesion barrier (INTERCEED®), with the aim of maintaining the uterine lumen (Ugboaja et al., 2017). However, there are several shortcomings of IUD and FB in preventing the recurrence of IUA. IUD has a potential risk factor of infection (Sun et al., 2018a), and is only effective in preventing re-adhesion (Chi et al., 2018). To solve the problem, some studies investigated the potential benefits of hydrogels as physical anti-adhesion barriers to prevent recurrence in IUA after hysteroscopic adhesiolysis (**Table 1**).

Compared with patients using an IUD alone, the combination of an oxidized, regenerated cellulose adhesion barrier (INTERCEED®) and an IUD could regain an adhesion-free

**TABLE 1 |** Summary of bioactive hydrogels as physical barriers used in IUA.

| Physical barrier | Biomaterial | Model | Strength | References |
|---|---|---|---|---|
| IUD + Hydrogel | New crosslinked hyaluronan gel | Human | The application of new crosslinked hyaluronan gel significantly reduces IUA formation | Li et al. (2019) |
| Hydrogel | New crosslinked hyaluronan gel | Human | New crosslinked hyaluronan gel appears to be able to reduce the formation of IUA | Can et al. (2018) |
| IUD + Hydrogel | New crosslinked hyaluronan gel | Human | Better endometrial thickness values were observed in those who received new crosslinked hyaluronan gel either alone or in combination with an IUD | Pabuçcu et al. (2019) |
| Hydrogel | ABT13107 | Human | ABT13107 is non-inferior to the highly viscous hyaluronic acid anti-adhesive barrier in IUA formation after hysteroscopic surgery | Lee et al. (2020) |
| FB + Hydrogel | Auto-crosslinked hyaluronic acid gel | Human | Auto-crosslinked HA gel could be able to reduce IUA, decrease adhesion severity, and improve menopause postoperatively | Xiao et al. (2015) |
| Hydrogel | Hyaluronic acid gel | Human | Reduce the risk of postoperative IUA | Tafti et al. (2021) |

uterine cavity and significantly shorten the conception interval (Cai et al., 2017). A comprehensive treatment strategy of intrauterine injection of HA hydrogel combined with a balloon urinary catheter and IUD insertion, and oral estrogen following hysteroscopic adhesiolysis, was investigated in moderate-severe IUA patients (Xiong et al., 2020). The results indicated that this combined strategy prevented the recurrence of IUA to a certain extent. Moreover, evidence indicated that the combination of IUD and anti-adhesion hydrogel had a more satisfactory effect than applying an IUD alone (Can et al., 2018; Li et al., 2019). Lin *et al.* (Lin et al., 2013) found that the insertion of an intrauterine balloon or IUD was more effective than the use of HA gel alone in the prevention of IUA reformation. Furthermore, Pabuçcu *et al.* (Pabuçcu et al., 2019) found that endometrial thickness was significantly enhanced when applying a new crosslinked hyaluronan gel with an IUD after hysteroscopic adhesiolysis. Although many studies have shown that an IUD combined with hydrogels can reduce IUA recurrence, in some cases the clinical pregnancy rate of these patients is not improved. Therefore, in-depth research is needed to explore whether the application of hydrogels can improve pregnancy outcomes for infertile patients. It may be that the pure hydrogels only play an anti-adhesion role, and are unable to promote the regeneration and functional recovery of the endometrium. Therefore, it is necessary to optimize the design to prepare functional bioactive hydrogels that are conducive to endometrial repair and functional regeneration of the endometrium.

Huang *et al.* (Huang et al., 2020b) tested patented intrauterine scaffolds made of amino acids as a barrier in the treatment of recurrent IUA with poor prognosis. The results showed that the menstrual volume returned to normal, and the recovery rate of amenorrhea increased significantly after scaffold implantation. However, the recurrence rate of IUA was still up to 25%, which indicated that although intrauterine scaffolds may be an effective therapy, they still need to be further optimized.

In addition, although ordinary HA gel can mechanically support the uterine cavity, because of its rapid degradation it cannot stay inside the uterine cavity for a prolonged duration, therefore the anti-adhesion effect is not satisfactory (Azumaguchi et al., 2019). A meta-analysis addressing the use of HA gel to prevent IUA after intrauterine surgery showed that HA gel can reduce the incidence of re-adhesion in mild cases following intrauterine surgery (Fei et al., 2020; Zheng et al., 2020). While there was also research showed that the application of auto-cross-linked HA gel was unable to reduce the recurrence rate of IUA following hysteroscopic adhesiolysis (Zhou et al., 2021). ABT13107, a newly developed thermo-responsive sol-gel made from non-animal derived HA and synthetic poloxamers, had been studied regarding preventing the recurrence of IUA (Lee et al., 2020). Moreover, a randomized double-blind controlled clinical trial (RCT) was conducted to evaluate the efficacy and safety of auto-crosslinked HA gel for preventing IUA after hysteroscopic adhesiolysis; the results indicated that auto-crosslinked HA gel may be able to reduce IUA, decrease adhesion severity, and improve menopause postoperatively (Xiao et al., 2015). A meta-analysis exploring whether the application of HA gel can reduce the recurrence rate of IUA after hysteroscopic adhesiolysis showed that HA gel could reduce the recurrence rate of IUA, but had no significant effect on postoperative pregnancy rate (Fei et al., 2019). In addition, another study compared the effect of adjuvant therapy on the prevention and treatment of IUA and found that an alginate hyaluronate-carboxymethylcellulose membrane (ACH) was most effective in preventing IUA progression (Yan and Xu, 2018). Chenite *et al.* indicated that sodium hyaluronate or a hydrogel prepared using hydroxybutyl chitosan (HBC) and polyphosphate can reduce the occurrence of postoperative IUA. However, owing to the lack of viscosity of sodium hyaluronate or HBC hydrogel, they are not easily retained in the uterine cavity. Thus, it cannot completely isolate uterine wounds, which affects its ability to prevent IUA. Therefore, after developing and optimizing hydrogels with potential anti-adhesion ability combined with a physical anti-adhesion barrier for IUA, bioactive hydrogels overcome some drawbacks of original natural hydrogels, the prevention and treatment have great clinical significance (Kowalski et al., 2019).

## Bioactive Hydrogels as *in situ* Drug Delivery Systems for Endometrial Regeneration

With the development of tissue engineering, it is possible to use biomaterials to repair and replace damaged tissues and organs

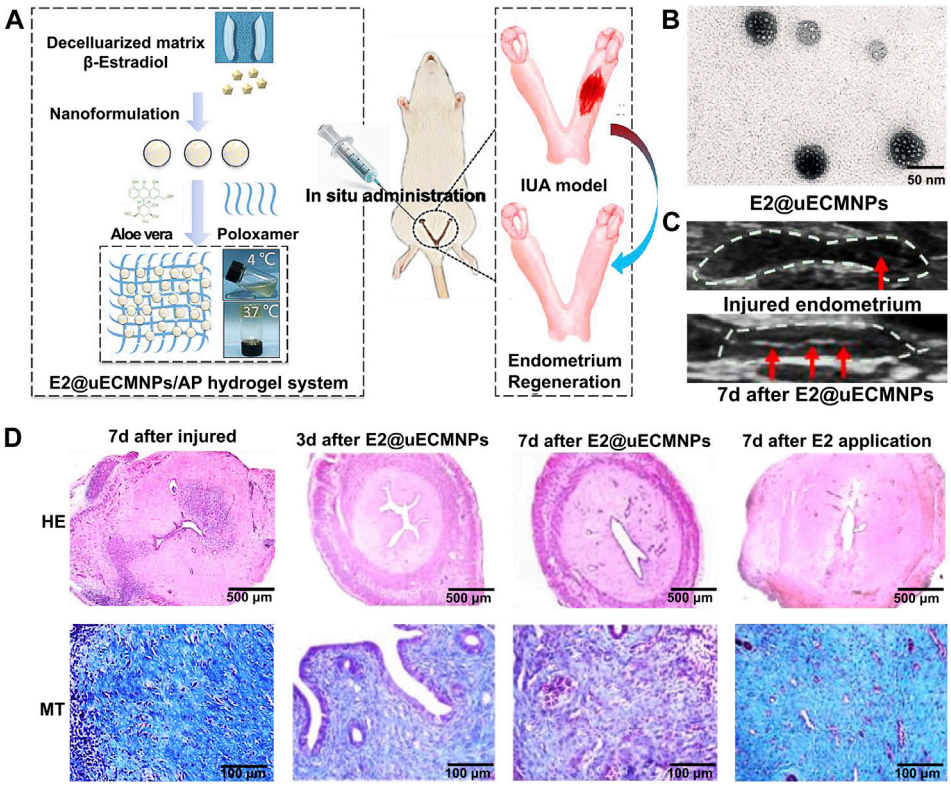


**FIGURE 1 |** An overview of E2@uECMNPs/AP hydrogel system with multi-therapeutic effects to promote endometrial regeneration for the prevention of IUA. **(A)** Schematic graphs of E2@uECMNPs/AP hydrogel system. **(B)** TEM images of E2@uECMNPs. **(C)** Comparison of ultrasound images of the injured endometrium with or without E2@uECMNPs treatment. **(D)** H&E staining (HE) and Masson staining (MT) of the uterus from IUA rat's uteri and IUA rats uteri receiving different treatments on day 3 and 7 after injury. Reproduced with permission (Yao et al., 2020). Copyright 2020, Elsevier Ltd.

(Kwon et al., 2018). The application of bioactive hydrogels in IUA endometrial tissue regeneration is still in the exploratory stage. However, the use of bioactive hydrogels as a local drug delivery system to release specific drugs for regulating the specific pathological environment of IUA has great potential for application in endometrial regeneration. Hydrogels have attracted noticeable interest for their use in drug delivery owing to their unique physical properties. The high porosity that characterizes hydrogels can easily be adjusted by controlling the density of cross-links in their matrix and their affinity to water (Ávila-Salas et al., 2019). Their porous structure also allows drugs to be loaded and then released. The topical application of hydrogels can effectively be used in drug delivery that can help to alleviate the symptoms of many pathological conditions. *In situ* drug delivery systems have become a popular treatment owing to their combination of a physical barrier and controlled drug release. Hydrogels made of hydrophilic polymers with large amounts of water are suitable for drug delivery when applied to IUA patients. Drugs such as β-estradiol can be delivered by hydrogel scaffolds for various purposes including endometrial regeneration (Lam et al., 2014). Furthermore, the use of stimuli-responsive hydrogels brings many possibilities in drug delivery systems.

## Bioactive Hydrogels as *in situ* Drug Delivery Systems Through Vaginal Administration

The large surface area and abundant blood flow in the vagina are excellent for promoting drug absorption (Ci et al., 2017). Vaginal administration has no first-pass effect and has low enzyme activity; therefore, drugs can perform local treatment, and can also enter the systemic circulation. Thermosensitive hydrogels are easily administered vaginally, and are administered in a low viscous form at room temperature (Domiński et al., 2019). After entering the vagina, the hydrogel spreads rapidly into the folded area of the vaginal mucosa and forms a gel at body temperature (Liu et al., 2017). Stromal cell-derived factor-1α (SDF-1α) is a chemokine protein with the ability of recruiting endogenous cells, that can accelerate the regeneration of multiple tissues. In order to obtain a superior effect, Qi *et al.* (Wenbo et al., 2020) prepared an SDF-1α-loaded-chitosan-heparin hydrogel with controlled drug release ability. Seven days after treatment, uteri treated with SDF-1α incorporating a hydrogel gave both mechanical support to the uterine cavity and also initiated regeneration of the endometrium by recruiting c-kit positive stem cells to the injury site. Cai *et al.* (Cai et al., 2019) studied the incorporation of SDF-1α within a silk fibroin-bacterial cellulose (SF-BC) membrane that promoted the regeneration

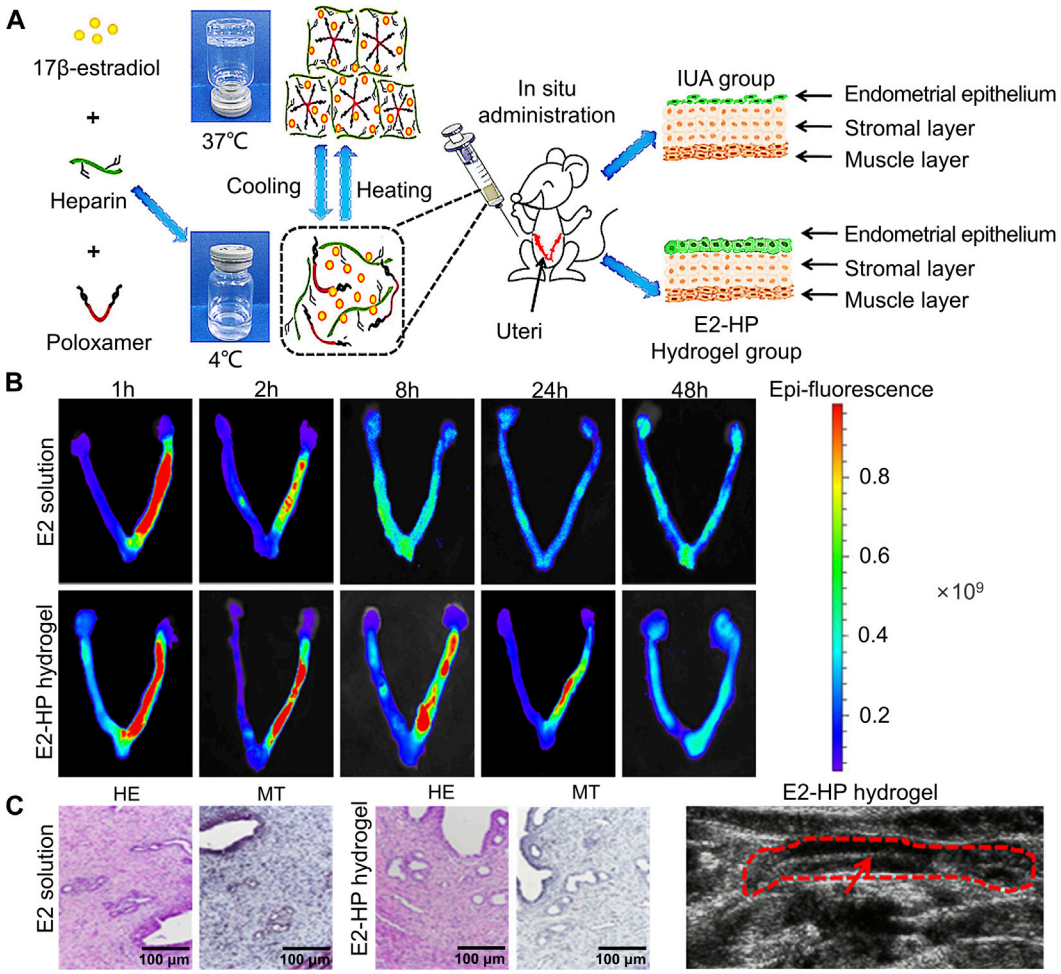


**FIGURE 2 |** Construction of E2-HP hydrogel and *in-situ* administration effect. **(A)** Schematic diagram of E2-HP hydrogel as an *in-situ* administration drug for the treatment of IUA. **(B)** The penetration and retention of different FITC-E2 formulations in the uterus after *in-situ* administration. **(C)** Comparison of H&E staining (HE) and Masson's staining (MT) of endometrium at 14 days after different treatments. **(D)** Ultrasound images of the endometrium after E2-HP hydrogel treatment. Reproduced with permission (Zhang et al., 2017). Copyright 2021 Dove Press Ltd.

of a full-depth uterine injury and also improved the pregnancy outcome of the damaged uterus.

Aloe has been reported as an ideal organic component to mix with poloxamer to form a more biologically friendly thermosensitive hydrogel system (Baghersad et al., 2018). Aloe-poloxamer (AP) hybrid hydrogel has been fabricated for treating IUA, which can achieve a better therapeutic effect with prolonged retention time within the uterine cavity compared to poloxamer gel. This study showed that AP hydrogel can serve as a biologically active delivery carrier for β-estradiol and that it can synergistically promote morphological, structural, and functional repair of the injured uterus (Yao et al., 2020) (**Figures 1A–D**). The E2@uECMNPs/AP hydrogel itself acts as a physical barrier during the early stage of the injury. Its multiple components, including β-estradiol, synergistically exert pro-healing effects and promote endometrial regeneration. From the perspective of anti-adhesion therapy and sustained drug release, hydrogels have potential implications for vaginal administration in the treatment of IUA.

## Drug Delivery Through Injectable Bioactive Hydrogels

The use of injectable hydrogels, where the solution–gel transition occurs at the site of administration, may shorten the duration of treatment, reduce the risk of infection of the implanted site, and prevent scarring (Asai et al., 2012). To date, various studies have investigated the possibility of this therapy in animal models (Sun et al., 2018b; Jian et al., 2018; Jiang et al., 2019). The injectable SDF-1α release hydrogel exhibited long-term recruiting of hematopoietic stem cells (HSCs) and achieved better effects than a one-off injection of SDF-1α solution. This hydrogel could be a candidate for uterine injury healing and other wound dressing drug delivery systems. Because of their biocompatibility, biodegradability, and tissue adhesion, chitosan and HA are also suitable as a matrix for injectable *in*

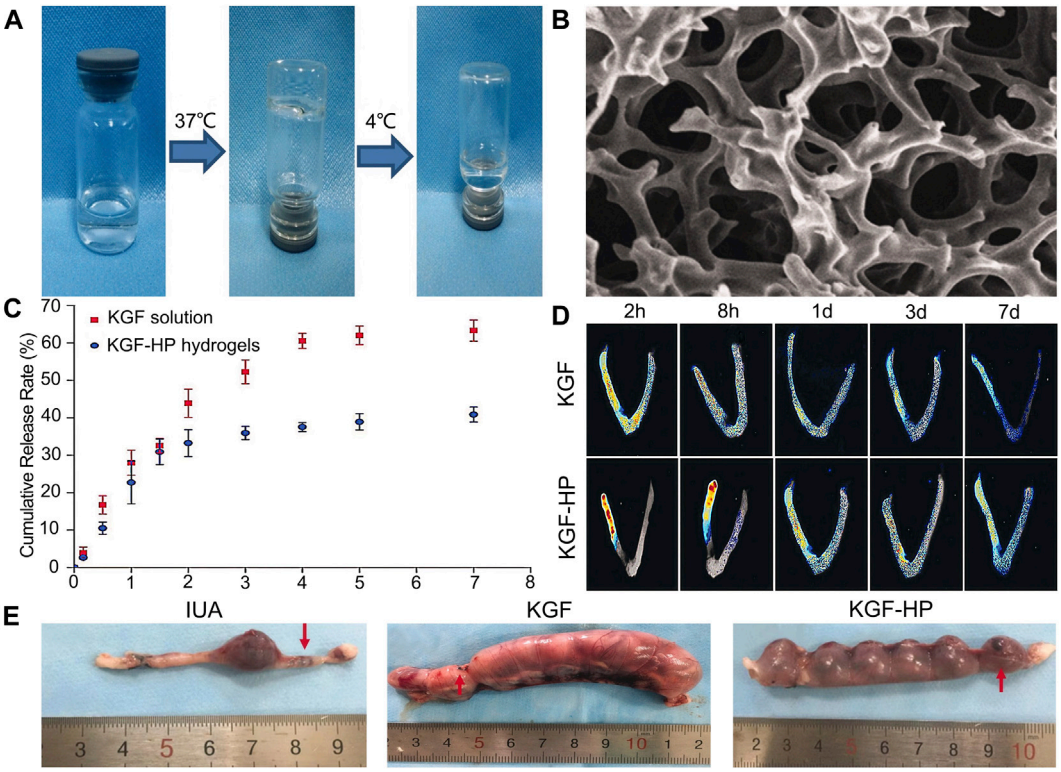


**FIGURE 3 |** Construction of KGF-loaded HP hydrogel and its curative effect. **(A)** The temperature-dependent appearance of KGF-loaded HP hydrogel. **(B)** SEM images of the lyophilized KGF-loaded HP hydrogel. **(C)** The cumulative release profile of free KGF solution and KGF-HP hydrogel. **(D)** Representative fluorescence images of an intact rat uteri after treatment with FITC-labeled KGF or KGF-loaded HP hydrogel. **(E)** Representative images of embryo implantation for rats treated by different formulations. Reproduced with permission (Xu et al., 2017). Copyright 2017 Taylor & Francis Group.

*situ* hydrogels for drug, gene delivery, and tissue repair through invasive surgery (Lu et al., 2019).

The role of new bioactive hydrogel scaffolds, such as heparin-poloxamer (HP), and gelatin meth acryloyl (GelMA), in uterine cavity repair has attracted growing attention, and they can be used as sustained-release drug delivery systems to effectively promote endometrial repair in IUA animal models (Wu et al., 2019). Zhang *et al.* (Zhang et al., 2017) injected the combination of different drugs (hormone or growth factor) with thermosensitive, sustained drug delivery systems based on HP hydrogels to rat's uteri (**Figures 2A–D**). The study demonstrated that the encapsulation of 17 β-estradiol into HP hydrogels can increase the drug concentration at the injured area while reducing the blood concentration, because it can be administered by *in situ* injection. Keratinocyte growth factor (KGF), a potent repair factor for epithelial tissues, had been encapsulated into HP hydrogels, and the KGF-loaded HP hydrogel delivered a sustained release of long duration and prolonged retention of the encapsulated KGF in the injured endometrium, thus improving endometrial recovery in a rat model compared to the administration of KGF alone (**Figures 3A–E**) (Xu et al., 2017). However, at present, the above synthetic biological scaffolds are generally expensive and have not been widely used in clinical settings. In animal experiments, most injectable bioactive hydrogels are administrated through the myometrium rather than the cervical canal. However, gynecologists usually apply anti-adhesion hydrogel through the cervical canal for IUA patients after hysteroscopic adhesiolysis. Though these hydrogels are all injectable, different administrations make it is not clear whether these patients can benefit from injectable bioactive hydrogels.

## Bioactive Hydrogels as 3D Cell Delivery and Culture Systems in IUA

Stem cell therapies have been demonstrated to be promising and multifunctional alternatives to traditional drug therapy. To date, numerous maladies have been modeled in animals to test the efficacy and safety of a range of cellular therapies. However, the difficulty lies in the normal expansion of stem cells in cell therapy. There are two crucial factors that influence stem cell expansion, which are biochemical composition and the physical properties of the matrix (Madl et al., 2018). One crucial physical regulator of stem cell fate is matrix stiffness. Interestingly, bioactive hydrogels can be fabricated as culture systems with a tunable stiffness that encompasses a physiological range. Owing to their high-water content, porosity, and soft consistency, bioactive hydrogels can closely simulate natural living tissue. In addition, by adjusting the biochemical composition of the hydrogel or encapsulated drugs, they can

**TABLE 2 |** Summary of bioactive hydrogels in cell therapy in IUA.

| Cell | Biomaterial | Model | Molecule/pathway | Strength | References |
|---|---|---|---|---|---|
| - | Chitosan-heparin hydrogels | Sprague-Dawley rats | Downregulated expression of TGF-β<br>Upregulated expression of VEGF | SDF-1α/CXCR4 axle secreted cytokine to regulate the tissue regeneration | Wenbo et al. (2020) |
| - | E2@uECMNPs/AP hydrogel | Sprague-Dawley rats | Upregulated Ki67, cytokeratin, and ER-β<br>Decreased TGF-β1 and TNF-α | Increased morphological recovery and decreased uterine fibrosis rate | Yao et al. (2020) |
| - | E2-Heparin-Poloxamer Hydrogel | Sprague-Dawley rats | Kisspeptin; ERK1/2 and MAPKs p38 pathways | Facilitate the regeneration<br>Inhibiting the cell apoptosis in IUA model | Zhang et al. (2020b) |
| dEMSCs | Hyaluronic acid fibrinogen/thrombin hydrogel (HA + F + T50 gel) | Sprague-Dawley rats | Increased expression of PECAM and IGF-1<br>VEGF and LIF expression are also increased | Expression and secretion of molecules essential for embryonic implantation<br>Shortens time window between cell transplantation and embryo transfer | Kim et al. (2019) |
| MSC-Sec | Crosslinked hyaluronic acid gel | Sprague-Dawley rats | - | Creates a sustained release system<br>Thicker endometrium and more glands were observed after treatment | Liu et al. (2019) |
| BMSCs | Pluronic F-127-vitminC hydrogel | Sprague-Dawley rats | Restored cytokeratin, von Willebrand Factor (vWF)<br>Decreased interleukin-1β (IL-1β) | Vc promoted the survival and health of PF-127-encapsulated BMSCs *in vitro*<br>Thicker endometrium membrane<br>More glands and fewer areas of fibrosis | Yang et al. (2017) |
| Oral mucosal epithelial cells OMECs | Lyophilized amniotic membrane | Sprague-Dawley rats | VEGF expression is increased | Effective in preventing fibrosis with improved regeneration of endometrium and endometrial glands in the rat model of IUA | Chen et al. (2019) |
| hUCMSC | Collagen | Sprague-Dawley rats | Increased the expression of HuNu and vimentin in a IUA-induced rat model<br>Protein levels of the p-transcriptional co-activator with PDZ-binding motif, stromal cell-derived factor-1, and C-X-C chemokine receptor type 4 were upregulated | Increased number of endometrial glands and reduced area of fibrosis | Liu et al. (2020b) |
| UC-MSCs | Collagen | Human | - | 38.4% participants had a successful pregnancy | Cao et al. (2018) |
| UC-MSC-derived exosomes | Collagen | Sprague-Dawley rats | Increased the expression of the estrogen receptor α/progesterone receptor | Endometrium regeneration<br>Collagen remodeling<br>Increased the expression of the estrogen receptor α/progesterone receptor<br>Restored fertility<br>Reduced inflammation, and increased anti-inflammatory responses | Xin et al. (2020) |
| hiMSCs | Alginate and gelatin | Sprague-Dawley rats | Integrin αv β3 and LIF were significantly higher in the cell-loaded scaffold group | Promoted the recovery of the endometrial histomorphology (endometrial tissue and gland regeneration) and the regeneration of endometrial cells (stromal cells and epithelial cells) and endothelial cells<br>Improved endometrial receptivity functional indicators | Ji et al. (2020) |
| ADSCs-derived exosomes | PEG | Sprague-Dawley rats | Significant increases in VEGF, LIF, avβ3, and IGF-1 expression | Promote HUVEC proliferation, migration, and tube formation *in vitro*<br>Exhibited a robust ability to induce neovascularization and tissue regeneration while suppressing localized fibrosis *in vivo*<br>Regenerated endometrial tissue was more receptive to embryos, leading to higher rates of pregnancy | Pan et al. (2020) |

*hAECs: human amnion epithelial cells; bFGF: basic fibroblast growth factor; VEGF: vascular endothelial growth factor; IGF-1: insulin-like growth factor-1; COL1A1: collagen type I alpha 1; TIMP-1: tissue inhibitor of metalloproteinase-1; TGF-β: transforming growth factor-β; PDGF-C: platelet-derived growth factor-C; THBS1: thrombospondin-1; CTGF: connective tissue growth factor; ER-β: estrogen receptor β; E2@uECMNPs/AP hydrogel: nanoparticulate decellularized uterus (uECMNPs) encapsulated β-estradiol thermosensitive aloe-poloxamer hydrogel; MenSCs: menstrual blood stem cells; BMSCs: bone marrow-derived stem cells; dEMSCs: decidualized endometrial stromal cells; MSC-Sec: mesenchymal stem cell-secretome; UC-MSCs: umbilical cord-derived mesenchymal stromal cells; ADSCs: adipose stem cells.*

also regulate the fate of stem cells. Therefore, functional bioactive hydrogels make it easier to transport stem cells to injured the endometrium with good vitality and differentiation potential. At present, there are ongoing studies on the advantages and disadvantages of different bioactive hydrogels applied in stem cell therapies in IUA. A summary of bioactive hydrogels in stem cell therapy in IUA is listed. The advantages of the mentioned hydrogels are also listed (**Table 2**). According to **Table 2**, the endometrium regeneration associated molecules are well improved. Another highlight of bioactive hydrogel used in stem cell therapy is that it can decrease uterine fibrosis rate and promote endometrial glands growth.

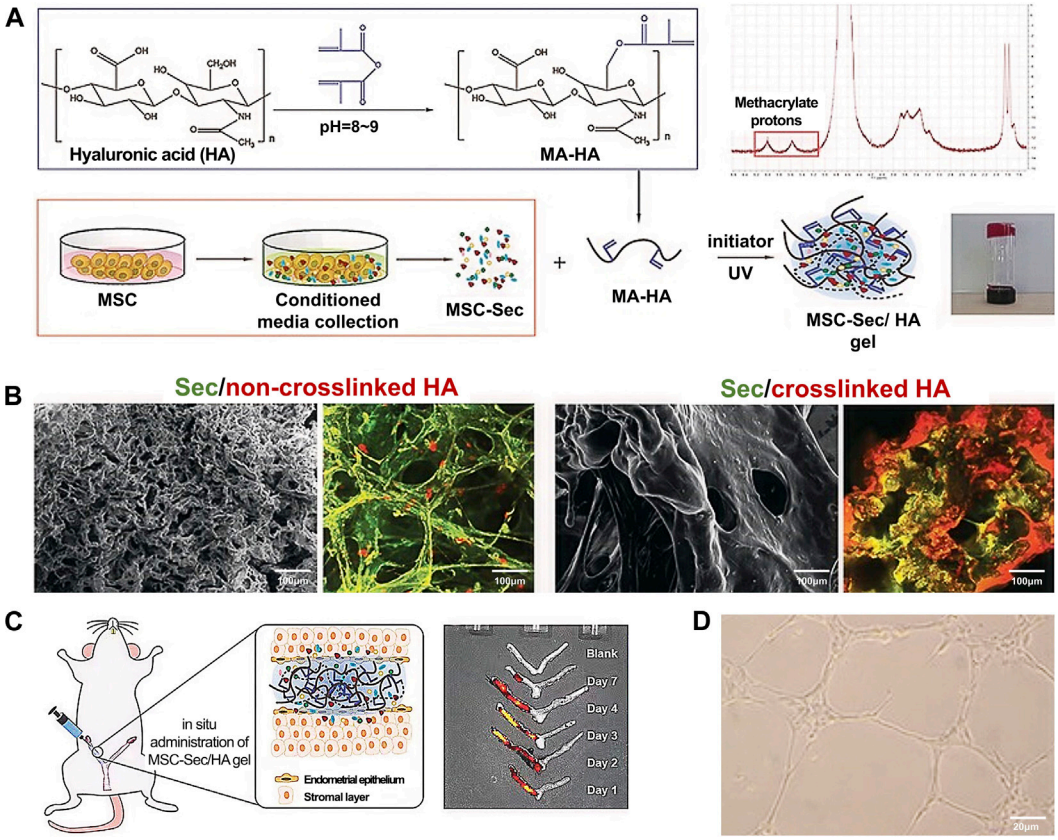


**FIGURE 4 |** Fabrication and characterization of MSC-Sec-loaded crosslinked HA gel. **(A)** Schematic showing the synthesis of MSC-Sec-loaded, crosslinked HA gel and the state of HA gel at room temperature when the bottle is upside down. **(B)** Representative SEM and color-depth projection confocal images of MSC-Sec/non-crosslinked HA and MSC-Sec/crosslinked HA; green represents MSC-Sec, red represents HA. **(C)** MSC-Sec/HA gel injection and a rodent model of endometrial injury. **(D)** The tube-formation ability of human umbilical vein endothelial cells is enhanced in the MSC-Sec-treated group. Reproduced with permission (Liu et al., 2019). Copyright 2019 WILEY-VCH Verlag GmbH & Co. KGaA, Weinheim.

## Hyaluronic Acid

HA may be an appropriate hydrogel for endometrial regeneration therapeutics. Nevertheless, HA gels have a natural half-life of just 1–2 days (Carruthers and Carruthers, 2007). Moreover, the half-life may be even shorter in the uterus owing to aqueous dilution. In order to optimize the short half-life of natural HA, Kim *et al.* (Kim et al., 2019) constructed endometrium-tailored HA/fibrin composite hydrogel and demonstrated the significant regenerative effects of the *in vitro* processed isotopic cells encapsulated in composite scaffold materials. The expression of *PECAM* and *IGF-1*, which are neovascularization- and decidua-specific genes, were significantly increased. Vascular endothelial growth factor (VEGF) and leukemia inhibitory factor (LIF) expression were also increased in the HA-fibrin-thrombin 50 mg (HA-F-T50) composite hydrogel. Moreover, an attempt at pregnancy was possible as early as 2 weeks after treatment, and successful *in vivo* embryonic implantation and development in the regenerated recipient model was confirmed at 7 days after embryo transformation in a murine uterine synechiae model. Despite limited evidence of its efficiency in the human body, further studies should be carried out to optimize this promising technology.

Liu *et al.* (Liu et al., 2019) fabricated a control-released, intrauterine-administered mesenchymal stem cell-secretome (MSC-Sec)-loaded, crosslinked HA gel, that was developed as a therapy to restore injured endometrial morphology and fertility in a rat model of AS (**Figures 4A–D**). This crosslinked HA gel can be used in stem cell therapy because it can bypass the tumorigenic risks associated with stem cell therapies and help maintain the promising effect of MSC-Sec on endometrial and endothelial cells.

## Other Hydrogels

Apart from HA hydrogel, Pluronic F-127 is a synthetic Food and Drug Administration (FDA)-approved compound which has several advantages, including low toxicity, biocompatibility, and thermo-reversibility. It is widely used in drug delivery and *in vivo* tissue engineering because it can form into a hydrogel at physiological temperatures. BMSCs and Vitamin C encapsulated Pluronic F-127 hydrogel was prepared to promote restoration of damaged IUA endometrium *in vivo*; the vitamin C promoted BMSCs survival and growth in the hydrogel (Yang et al., 2017).

In another study, Liu *et al.* (Liu et al., 2020b) used collagen scaffold loading with human umbilical cord mesenchymal stem

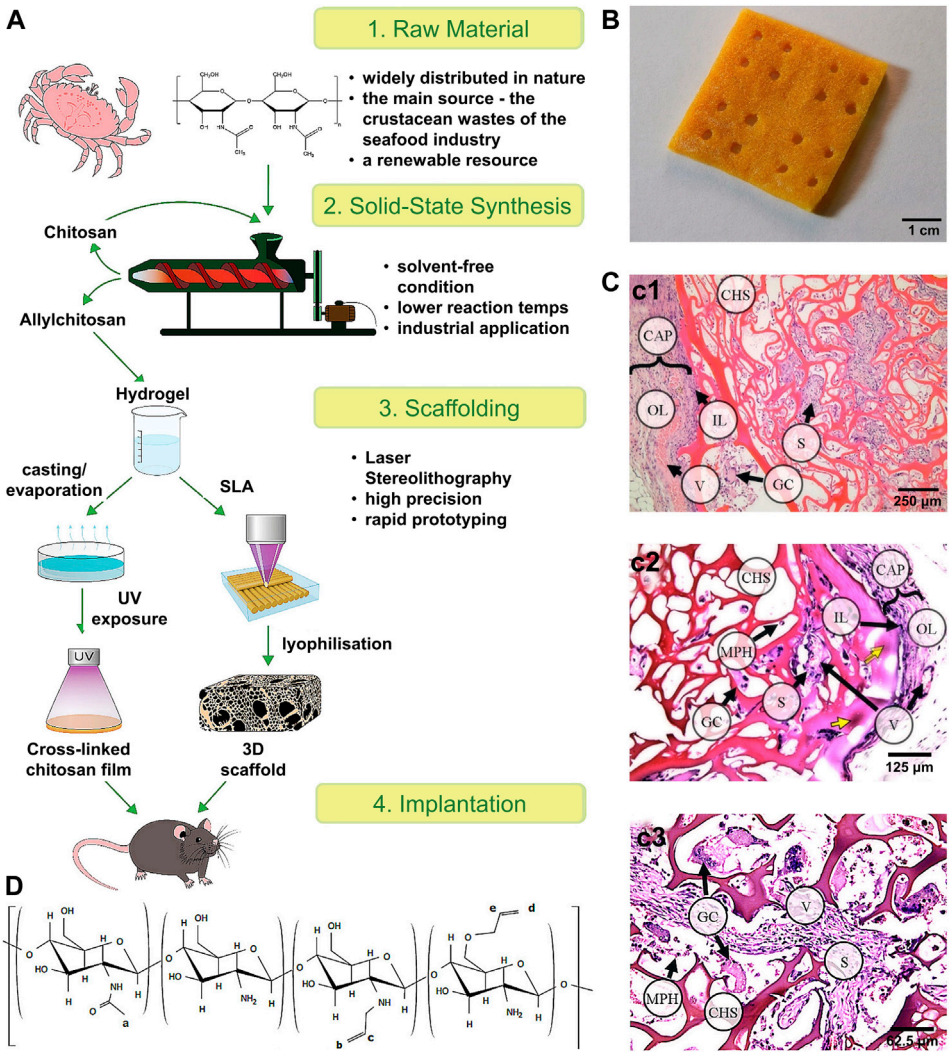


**FIGURE 5 |** Scheme of the experimental work and the tissue reaction to the 3D scaffold. **(A)** Scheme of the experimental work. **(B)** 3D porous allylchitosans scaffold (the chitosan sponges) after freeze drying. **(C)** Tissue reaction to the porous 3D scaffolds based on allylchitosans. c1) 30 days: the chitosan sponge (CHS) material was oxyphilic; c2) 60 days: a basophilic focus (yellow arrows) in the surface septa of the CHS material; and c3) 90 days: deep CHS sections: most of the scaffold septa were moderately basophilic. **(D)** The structure of the synthesized allylchitosans. Reproduced with permission (Bardakova et al., 2019). Copyright 2021, Elsevier Ltd.

cells (hUCMSCs) to increase the number of endometrial glands and reduced the area of fibrosis, suggesting that the combination of the collagen scaffold and hUCMSCs may be an alternative approach for treating IUA. Moreover, the hUCMSCs-collagen scaffold had passed through a phase I clinical trial and obtained a satisfactory outcome, where around 38.4% of participants underwent a successful pregnancy without complications associated with stem cell therapy (Cao et al., 2018).

In terms of 3D bioactive hydrogel scaffolds, chitosan is a biopolymer with a unique set of biological and physicochemical properties (Pan et al., 2020). Thus, Ksenia *et al.* (Carruthers and Carruthers, 2007) successfully formed different scale structures of chitosan and further tested their biomechanical quality and biocompatibility to demonstrate the prospects of their broad biological application (**Figures 5A–D**). Furthermore, Ji *et al.* (Ji et al., 2020) studied the application of 3D bioprinting of a human iPSC-derived MSC-loaded scaffold for repair of the uterine endometrium. The results showed that the endothelial cells and endometrial cells regenerated, and the dysfunctional endometrium was partially restored (**Figures 6A–E**).

Recently, bioactive hydrogels laden with stem cell exosomes have been developed for endometrial regeneration. The advantages of hydrogel treatment include the potential for sustained exosome release, resulting in the maintenance of higher local concentrations of pharmacologically important compounds for extended periods, and reducing the need for repeated dosing in a clinical setting, thus making them a promising candidate for use in exosome-based endometrial repair applications (Pan et al., 2020). Lin *et al.* (Lin et al.,

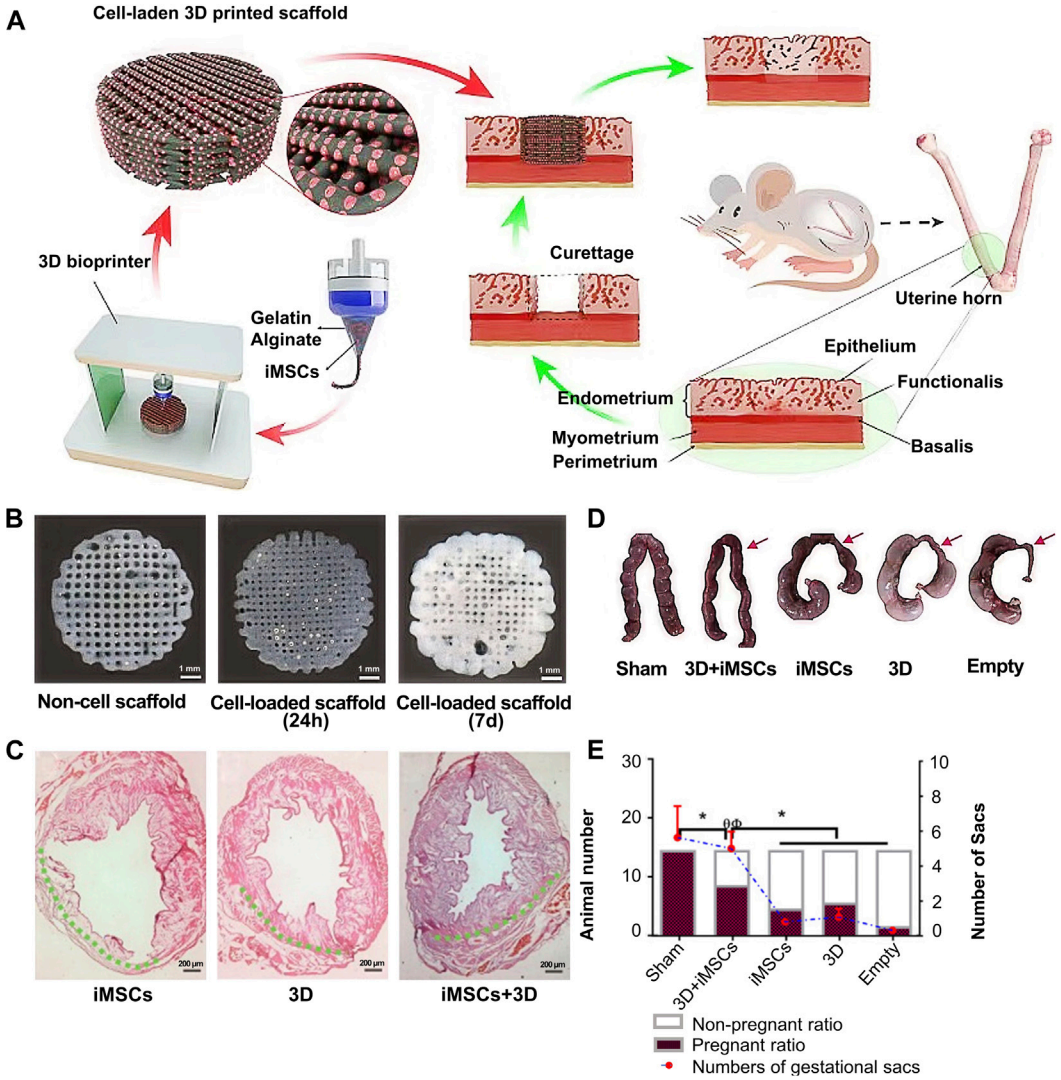


**FIGURE 6 |** Whole overview of 3D bioprinting a human iPSC-derived MSC-loaded scaffold. **(A)** The whole preparation procedure of an alginate–gelatin hydrogel scaffold and scaffold implantation. **(B)** Picture of the original alginate-gelatin hydrogel and cell-loaded scaffold at 24 h and 7 d **(C)** H&E stain of the endometrium after cell implantation, scaffold implantation, and cell-loaded scaffold implantation. **(D–E)** Outcome of endometrial receptivity after cell-loaded scaffold implantation. Reproduced with permission (Ji et al., 2020). Copyright 2021, Elsevier Ltd.

2021) developed a microenvironment-protected exosome-hydrogel for endometrial regeneration (**Figures 7A–C**). This PEG hydrogel was injectable, antibacterial, and facilitated controlled ADSC-exo release in order to promote endometrial regeneration.

## CURRENT LIMITATIONS AND FUTURE PERSPECTIVES

Despite their many advantageous properties, hydrogels also have several limitations. With the continuous progress of related research, the disadvantages of natural hydrogels are being gradually revealed. Although some natural hydrogels such as HA and alginate have already shown superiority over other hydrogels, the opportunity to improve current hydrogel implementations is still very promising. Researchers are gradually improving the structure of hydrogels by changing the polymer type and optimizing fabrication methods. The low tensile strength of many hydrogels limits their use in load-bearing applications, resulting in displacement of the hydrogel from a targeted local site. Because the hydrophobic compounds have limited loading quantity and homogeneity in hydrogel matrices, hydrogels are limited to carrying hydrophilic drugs (Zagórska-Dziok and Sobczak, 2020).

### Physical Anti-Adhesion Barriers

According to the published research (Du et al., 2020), anti-adhesion hydrogels are usually placed in the uterine cavity to prevent recurrence after operation. However, the effect of anti-

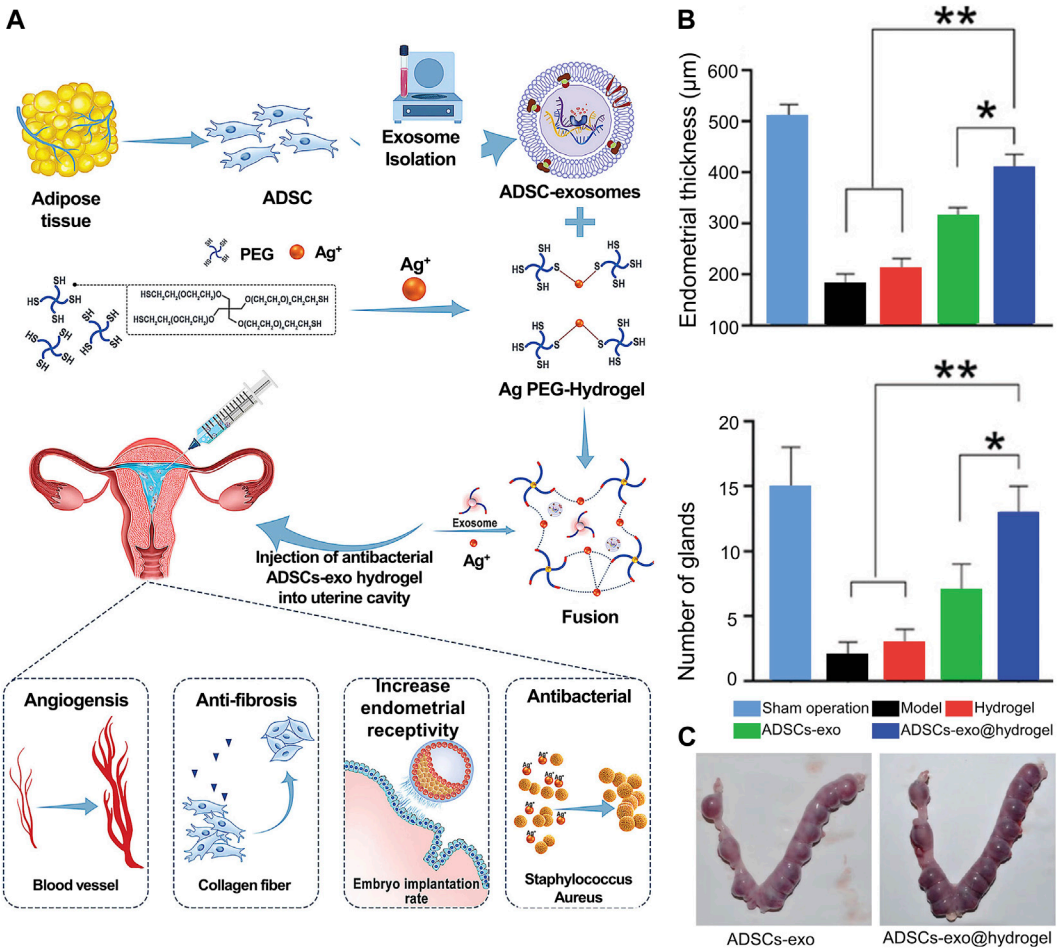


**FIGURE 7 |** Whole overview of ADSC-exosome-hydrogel. **(A)** Preparation procedures of ADSCs-exosome hydrogel. **(B)** Performance of ADSC-exosome-hydrogel in endometrial regeneration. **(C)** Performance of ADSC-exosome-hydrogel in endometrial receptivity. Reproduced with permission (Lin et al., 2021). Copyright 2021 WILEY-VCH Verlag GmbH & Co. KGaA, Weinheim.

adhesion hydrogels alone is less satisfactory than that of a combination of hydrogels and IUD. The reason why hydrogels cannot become the first-line therapy in endometrial regeneration is that most hydrogel applications in the prevention of IUA are still less satisfactory than a traditional IUD. Moreover, hydrogels do not have sufficient mechanical strength to shape a normal uterine cavity throughout a complete treatment. Unlike traditional IUD, some hydrogels in liquid are able to transform to sodium gel after entering uteri, which may help more efficient formation of the uterine cavity in various sizes. It is known that most IUA patients in childbearing age hope to improve fertility through IUA treatment. However, some bioactive hydrogels as physical barriers cannot assist in the formation of a normal functional endometrium for embryo implantation because they cannot meet the requirement of excellent cell culture system and sufficient mechanical strength. Therefore, future research needs to address the optimization of bioactive hydrogels as physical barriers to increase their strength in shaping a normal uterine cavity while still maintaining the capacity of controllable degradation.

## Drug Delivery Systems

As mentioned previously, hydrogels can be applied as *in situ* drug delivery systems for sustained release drugs to promote endometrial regeneration in patients with IUA. Compared with traditional hormone replacement therapy, this method may reduce the incidence of related risks like breast hyperplasia caused by oral estrogen in treating IUA. Several experiments that demonstrate that the effectiveness of a hydrogel-based drug delivery model in treating IUA have used animal models, and there has been limited evidence of clinical practice in human (Wang et al., 2020b). Whether hydrogels as *in situ* drug delivery systems are more beneficial than traditional drug delivery is still not clear in humans. Moreover, the hydrated nature of hydrogels can make terminal sterilization difficult and time-consuming (Lima et al., 2020). In the future, hydrogels with multiple concurrent functions may be a satisfactory way of treating IUA, which can provide both mechanical structure in forming the uterine cavity, and also be a stable *in situ* drug delivery system.

### Stem Cell Therapy

Because of their structural features, bioactive hydrogels are widely used as 3D cell culture systems. With the recent broader understanding that stem cells and stem cell derivatives can promote endometrial repair, the value of 3D hydrogel scaffolds that can simulate the living environment of cells and promote the transmission of stem cells and their secretions has become particularly prominent. Therefore, some studies have explored the application of hydrogels in IUA cell therapy. Many animal experiments have shown that, compared with traditional cell therapy, the application of hydrogels as a 3D culture environment produces superior outcomes in endometrial regeneration, and the improvement of endometrial receptivity is evident. However, despite exhibiting promising results in animal experiments, the application of hydrogels in stem cell therapy is still largely restricted to the experimental stage owing to its critical pitfalls and drawbacks such as safety issues, poor cell survival, and high cost.

Currently, one of the biggest concerns regarding stem cell therapy is the tumorigenic complications caused by uncontrollable stem cell implantation. Thus, the future study of hydrogels used in stem cell therapy could focus on controllable cell growth offering a better therapeutic approach while avoiding related complications. Moreover, the existing cell loaded hydrogels face the problem that the supply of oxygen and nutrients is limited by diffusion kinetics. For example, 3D printed hydrogels still require surface modification, such as chemical methods to carry integrin (for endometrial cells) and increase the survival rate of the seeded cells, by inducing cell-oriented differentiation, or by maturing the scaffold in a bioreactor before implantation (Wen et al., 2019). Therefore, selecting and optimizing bioactive hydrogels is important in obtaining better results and for their application in treating IUA.

## CONCLUSION

IUA is a common endometrial disease and one of the main causes of infertility in women of childbearing age. Owing to their excellent properties—such as good biocompatibility, degradability, and controlled drug release—bioactive hydrogels play an important role in the prevention and treatment of IUA and have great potential for application in the clinical setting. Bioactive hydrogels can be used as physical anti-adhesion barriers, and can also act as drug delivery systems for hormone drugs, multiple factors, and 3D cell delivery and culture systems in IUA treatment. These characteristics show that a combination of hydrogels and traditional intrauterine adhesion treatment can have a significant therapeutic effect on IUA and improve pregnancy success rates. While most researches ongoing are based on animal experiments, the mechanism behind the therapeutic effect of bioactive hydrogel in IUA treatment is not clear. The optimization on the safety and effectiveness of bioactive hydrogels is valuable to researchers in the future.

## AUTHOR CONTRIBUTIONS

JW and YL conceptualized, designed, and wrote the manuscript. CY and YX drafted the manuscript, reviewed the literature. TJ and XC designed the figure and table. YL, JT, and SH revised the manuscript. All authors approved the final version of the manuscript.

## FUNDING

This study was supported by the grants from Special Fund for Health of Jilin Province Finance Department (Grant No. ZXWSTZXEY034).

## ACKNOWLEDGMENTS

We thank He Liu (The Second Hospital of Jilin University) for his very enlightening comments and improving the quality of English language in this article.

## REFERENCES

Asai, D., Xu, D., Liu, W., Garcia Quiroz, F., Callahan, D. J., Zalutsky, M. R., et al. (2012). Protein Polymer Hydrogels by *In Situ*, Rapid and Reversible Self-Gelation. *Biomaterials* 33 (21), 5451–5458. doi:10.1016/j.biomaterials.2012.03.083

Ávila-Salas, F., Marican, A., Pinochet, S., Carreño, G., Valdés, O., Venegas, B., et al. (2019). Film Dressings Based on Hydrogels: Simultaneous and Sustained-Release of Bioactive Compounds with Wound Healing Properties. *Pharmaceutics* 11 (9), 447. doi:10.3390/pharmaceutics11090447

Azumaguchi, A., Henmi, H., and Saito, T. (2019). Efficacy of Silicone Sheet as a Personalized Barrier for Preventing Adhesion Reformation after Hysteroscopic Adhesiolysis of Intrauterine Adhesions. *Reprod. Med. Biol.* 18 (4), 378–383. doi:10.1002/rmb2.12294

Baghersad, S., Hajir Bahrami, S., Mohammadi, M. R., Mojtahedi, M. R. M., and Milan, P. B. (2018). Development of Biodegradable Electrospun Gelatin/aloe-Vera/poly(ε-caprolactone) Hybrid Nanofibrous Scaffold for Application as Skin Substitutes. *Mater. Sci. Eng. C* 93, 367–379. doi:10.1016/j.msec.2018.08.020

Bardakova, K. N., Akopova, T. A., Kurkov, A. V., Goncharuk, G. P., Butnaru, D. V., Burdukovskii, V. F., et al. (2019). From Aggregates to Porous Three-Dimensional Scaffolds through a Mechanochemical Approach to Design Photosensitive Chitosan Derivatives. *Mar. Drugs* 17 (1), 48. doi:10.3390/md17010048

Bhandari, S., Bhave, P., Ganguly, I., Baxi, A., and Agarwal, P. (2015). Reproductive Outcome of Patients with Asherman's Syndrome: A SAIMS Experience. *J. Reprod. Infertil* 16 (4), 229–235.

Cai, H., Qiao, L., Song, K., and He, Y. (2017). Oxidized, Regenerated Cellulose Adhesion Barrier Plus Intrauterine Device Prevents Recurrence after Adhesiolysis for Moderate to Severe Intrauterine Adhesions. *J. minimally invasive Gynecol.* 24 (1), 80–88. doi:10.1016/j.jmig.2016.09.021

Cai, H., Wu, B., Li, Y., Liu, Y., Shi, L., Gong, L., et al. (2019). Local Delivery of Silk-Cellulose Incorporated with Stromal Cell-Derived Factor-1α Functionally Improves the Uterus Repair. *Tissue Eng. A* 25 (21-22), 1514–1526. doi:10.1089/ten.TEA.2018.0283

Can, S., Kirpinar, G., Dural, O., Karamustafaoglu, B. B., Tas, I. S., Yasa, C., et al. (2018). Efficacy of a New Crosslinked Hyaluronan Gel in the Prevention of Intrauterine Adhesions. *JSLS* 22 (4), e2018.00036. doi:10.4293/jsls.2018.00036

Cao, Y., Sun, H., Zhu, H., Zhu, X., Tang, X., Yan, G., et al. (2018). Allogeneic Cell Therapy Using Umbilical Cord MSCs on Collagen Scaffolds for Patients with Recurrent Uterine Adhesion: a Phase I Clinical Trial. *Stem Cel Res Ther* 9 (1), 192. doi:10.1186/s13287-018-0904-3

Carbonnel, M., Pirtea, P., de Ziegler, D., and Ayoubi, J. M. (2021). Uterine Factors in Recurrent Pregnancy Losses. *Fertil. Sterility* 115 (3), 538–545. doi:10.1016/j.fertnstert.2020.12.003

Carruthers, A., and Carruthers, J. (2007). Non???Animal-Based Hyaluronic Acid Fillers: Scientific and Technical Considerations. *Plast. Reconstr. Surg.* 120 (6 Suppl. l), 33s–40s. doi:10.1097/01.prs.0000248808.75700.5f

Cervelló, I., Santamaría, X., Miyazaki, K., Maruyama, T., and Simón, C. (2015). Cell Therapy and Tissue Engineering from and toward the Uterus. *Semin. Reprod. Med.* 33 (5), 366–372. doi:10.1055/s-0035-1559581

Chang, J., He, J., Mao, M., Zhou, W., Lei, Q., Li, X., et al. (2018). Advanced Material Strategies for Next-Generation Additive Manufacturing. *Materials* 11 (1), 166. doi:10.3390/ma11010166

Chen, X., Sun, J., Li, X., Mao, L., Cui, L., and Bai, W. (2019). Transplantation of Oral Mucosal Epithelial Cells Seeded on Decellularized and Lyophilized Amniotic Membrane for the Regeneration of Injured Endometrium. *Stem Cel Res Ther* 10 (1), 107. doi:10.1186/s13287-019-1179-z

Chi, Y., He, P., Lei, L., Lan, Y., Hu, J., Meng, Y., et al. (2018). Transdermal Estrogen Gel and Oral Aspirin Combination Therapy Improves Fertility Prognosis via the Promotion of Endometrial Receptivity in Moderate to Severe Intrauterine Adhesion. *Mol. Med. Rep.* 17 (5), 6337–6344. doi:10.3892/mmr.2018.8685

Ci, L., Huang, Z., Liu, Y., Liu, Z., Wei, G., and Lu, W. (2017). Amino-functionalized Poloxamer 407 with Both Mucoadhesive and Thermosensitive Properties: Preparation, Characterization and Application in a Vaginal Drug Delivery System. *Acta pharmaceutica Sinica B* 7 (5), 593–602. doi:10.1016/j.apsb.2017.03.002

Domiński, A., Konieczny, T., and Kurcok, P. (2019). α-Cyclodextrin-Based Polypseudorotaxane Hydrogels. *Materials* 13 (1), 133. doi:10.3390/ma13010133

Du, X., Hou, Y., Wu, L., Li, S., Yu, A., Kong, D., et al. (2020). An Anti-infective Hydrogel Adhesive with Non-swelling and Robust Mechanical Properties for Sutureless Wound Closure. *J. Mater. Chem. B* 8 (26), 5682–5693. doi:10.1039/d0tb00640h

Fei, Z., Bin, Z., Xin, X., Fei, H., and Yuechong, C. (2019). Meta-analysis on the Use of Hyaluronic Acid Gel to Prevent Recurrence of Intrauterine Adhesion after Hysteroscopic Adhesiolysis. *Taiwanese J. Obstet. Gynecol.* 58 (6), 731–736. doi:10.1016/j.tjog.2019.09.002

Fei, Z., Xin, X., Fei, H., and Yuechong, C. (2020). Meta-analysis of the Use of Hyaluronic Acid Gel to Prevent Intrauterine Adhesions after Miscarriage. *Eur. J. Obstet. Gynecol. Reprod. Biol.* 244, 1–4. doi:10.1016/j.ejogrb.2019.10.018

Grover, G. N., Lam, J., Nguyen, T. H., Segura, T., and Maynard, H. D. (2012). Biocompatible Hydrogels by Oxime Click Chemistry. *Biomacromolecules* 13 (10), 3013–3017. doi:10.1021/bm301346e

Han, X., Ma, Y., Lu, X., Li, W., Xia, E., Li, T.-C., et al. (2020). Transplantation of Human Adipose Stem Cells Using Acellular Human Amniotic Membrane Improves Angiogenesis in Injured Endometrial Tissue in a Rat Intrauterine Adhesion Model. *Cel Transpl.* 29, 096368972095205. doi:10.1177/0963689720952055

Han, Y., Liu, S., Mao, H., Tian, L., and Ning, W. (2016). Synthesis of Novel Temperature- and pH-Sensitive ABA Triblock Copolymers P(DEAEMA-co-MEO2MA-co-OEGMA)-b-PEG-b-P(DEAEMA-co-MEO2MA-co-OEGMA): Micellization, Sol-Gel Transitions, and Sustained BSA Release. *Polymers* 8 (11), 367. doi:10.3390/polym8110367

Huang, C., and Ding, D.-C. (2019). Outcomes of Adhesion Barriers in Gynecologic Surgeries. *Medicine (Baltimore)* 98 (50), e18391. doi:10.1097/md.0000000000018391

Huang, H., Zou, L., Zhang, A., Zhao, X., Xu, D., and Xue, M. (2020). A Preliminary Study on a Patented Intrauterine Stent in the Treatment of Recurrent Intrauterine Adhesions with Poor Prognosis. *Ann. Transl Med.* 8 (4), 57. doi:10.21037/atm.2020.01.77

Huang, X.-W., Lin, M.-M., Zhao, H.-Q., Powell, M., Wang, Y.-Q., Zheng, R.-R., et al. (2020). A Prospective Randomized Controlled Trial Comparing Two Different Treatments of Intrauterine Adhesions. *Reprod. BioMedicine Online* 40 (6), 835–841. doi:10.1016/j.rbmo.2020.02.013

Ji, W., Hou, B., Lin, W., Wang, L., Zheng, W., Li, W., et al. (2020). 3D Bioprinting a Human iPSC-Derived MSC-Loaded Scaffold for Repair of the Uterine Endometrium. *Acta Biomater.* 116, 268–284. doi:10.1016/j.actbio.2020.09.012

Jian, W.-H., Wang, H.-C., Kuan, C.-H., Chen, M.-H., Wu, H.-C., Sun, J.-S., et al. (2018). Glycosaminoglycan-based Hybrid Hydrogel Encapsulated with Polyelectrolyte Complex Nanoparticles for Endogenous Stem Cell Regulation in central Nervous System Regeneration. *Biomaterials* 174, 17–30. doi:10.1016/j.biomaterials.2018.05.009

Jiang, C., Guo, J., Cheng, H., and Feng, Y.-H. (2019). Induced Expression of Endogenous CXCR4 in iPSCs by Targeted CpG Demethylation Enhances Cell Migration toward the Ligand CXCL12. *Inflammation* 42 (1), 20–34. doi:10.1007/s10753-018-0869-5

Kapoor, S., and Kundu, S. C. (2016). Silk Protein-Based Hydrogels: Promising Advanced Materials for Biomedical Applications. *Acta Biomater.* 31, 17–32. doi:10.1016/j.actbio.2015.11.034

Kasiński, A., Zielińska-Pisklak, M., Oledzka, E., and Sobczak, M. (2020). Smart Hydrogels - Synthetic Stimuli-Responsive Antitumor Drug Release Systems. *Int. J. Nanomedicine* 15, 4541–4572. doi:10.2147/ijn.S248987

Keskin, D., Mergel, O., van der Mei, H. C., Busscher, H. J., and van Rijn, P. (2019). Inhibiting Bacterial Adhesion by Mechanically Modulated Microgel Coatings. *Biomacromolecules* 20 (1), 243–253. doi:10.1021/acs.biomac.8b01378

Kim, Y. Y., Park, K.-H., Kim, Y. J., Kim, M. S., Liu, H. C., Rosenwaks, Z., et al. (2019). Synergistic Regenerative Effects of Functionalized Endometrial Stromal Cells with Hyaluronic Acid Hydrogel in a Murine Model of Uterine Damage. *Acta Biomater.* 89, 139–151. doi:10.1016/j.actbio.2019.03.032

Kowalski, G., Kijowska, K., Witczak, M., Kuterasiński, Ł., and Łukasiewicz, M. (2019). Synthesis and Effect of Structure on Swelling Properties of Hydrogels Based on High Methylated Pectin and Acrylic Polymers. *Polymers* 11 (1), 114. doi:10.3390/polym11010114

Kwon, S. G., Kwon, Y. W., Lee, T. W., Park, G. T., and Kim, J. H. (2018). Recent Advances in Stem Cell Therapeutics and Tissue Engineering Strategies. *Biomater. Res.* 22, 36. doi:10.1186/s40824-018-0148-4

Lam, J., Kim, K., Lu, S., Tabata, Y., Scott, D. W., Mikos, A. G., et al. (2014). A Factorial Analysis of the Combined Effects of Hydrogel Fabrication Parameters on the *In Vitro* Swelling and Degradation of Oligo(poly(ethylene Glycol) Fumarate) Hydrogels. *J. Biomed. Mater. Res.* 102 (10), 3477–3487. doi:10.1002/jbm.a.35015

Larrañeta, E., Stewart, S., Ervine, M., Al-Kasasbeh, R., and Donnelly, R. (2018). Hydrogels for Hydrophobic Drug Delivery. Classification, Synthesis and Applications. *J. Funct. Biomater.* 9 (1), 13. doi:10.3390/jfb9010013

Lee, D.-Y., Lee, S. R., Kim, S. K., Joo, J. K., Lee, W. S., Shin, J.-H., et al. (2020). A New Thermo-Responsive Hyaluronic Acid Sol-Gel to Prevent Intrauterine Adhesions after Hysteroscopic Surgery: A Randomized, Non-inferiority Trial. *Yonsei Med. J.* 61 (10), 868–874. doi:10.3349/ymj.2020.61.10.868

Li, J., Huang, B., Dong, L., Zhong, Y., and Huang, Z. (2021). WJ-MSCs Intervention May Relieve Intrauterine Adhesions in Female Rats via TGF-β1-mediated Rho/ROCK Signaling Inhibition. *Mol. Med. Rep.* 23 (1), 1. doi:10.3892/mmr.2020.11646

Li, X., Wu, L., Zhou, Y., Fan, X., Huang, J., Wu, J., et al. (2019). New Crosslinked Hyaluronan Gel for the Prevention of Intrauterine Adhesions after Dilation and Curettage in Patients with Delayed Miscarriage: A Prospective, Multicenter, Randomized, Controlled Trial. *J. Minimally Invasive Gynecol.* 26 (1), 94–99. doi:10.1016/j.jmig.2018.03.032

Liao, Z., Liu, C., Wang, L., Sui, C., and Zhang, H. (2021). Therapeutic Role of Mesenchymal Stem Cell-Derived Extracellular Vesicles in Female Reproductive Diseases. *Front. Endocrinol.* 12, 665645. doi:10.3389/fendo.2021.665645

Lima, C. S. A. D., Balogh, T. S., Varca, J. P. R. O., Varca, G. H. C., Lugão, A. B., Camacho-Cruz, L. A., et al. (2020). An Updated Review of Macro, Micro, and Nanostructured Hydrogels for Biomedical and Pharmaceutical Applications. *Pharmaceutics* 12 (10), 970. doi:10.3390/pharmaceutics12100970

Lin, J., Wang, Z., Huang, J., Tang, S., Saiding, Q., Zhu, Q., et al. (2021). Microenvironment-Protected Exosome-Hydrogel for Facilitating Endometrial Regeneration, Fertility Restoration, and Live Birth of Offspring. *Small* 17 (11), 2007235. doi:10.1002/smll.202007235

Lin, X., Wei, M., Li, T. C., Huang, Q., Huang, D., Zhou, F., et al. (2013). A Comparison of Intrauterine Balloon, Intrauterine Contraceptive Device and Hyaluronic Acid Gel in the Prevention of Adhesion Reformation Following

Hysteroscopic Surgery for Asherman Syndrome: a Cohort Study. *Eur. J. Obstet. Gynecol. Reprod. Biol.* 170 (2), 512–516. doi:10.1016/j.ejogrb.2013.07.018

Liu, F., Hu, S., Yang, H., Li, Z., Huang, K., Su, T., et al. (2019). Hyaluronic Acid Hydrogel Integrated with Mesenchymal Stem Cell-Secretome to Treat Endometrial Injury in a Rat Model of Asherman's Syndrome. *Adv. Healthc. Mater.* 8 (14), 1900411. doi:10.1002/adhm.201900411

Liu, H., Wang, C., Li, C., Qin, Y., Wang, Z., Yang, F., et al. (2018). A Functional Chitosan-Based Hydrogel as a Wound Dressing and Drug Delivery System in the Treatment of Wound Healing. *RSC Adv.* 8 (14), 7533–7549. doi:10.1039/c7ra13510f

Liu, T., Weng, W., Zhang, Y., Sun, X., and Yang, H. (2020). Applications of Gelatin Methacryloyl (GelMA) Hydrogels in Microfluidic Technique-Assisted Tissue Engineering. *Molecules* 25 (22), 5305. doi:10.3390/molecules25225305

Liu, Y., Cai, J., Luo, X., Wen, H., and Luo, Y. (2020). Collagen Scaffold with Human Umbilical Cord Mesenchymal Stem Cells Remarkably Improves Intrauterine Adhesions in a Rat Model. *Gynecol. Obstet. Invest.* 85 (3), 267–276. doi:10.1159/000505691

Liu, Y., Yang, F., Feng, L., Yang, L., Chen, L., Wei, G., et al. (2017). *In Vivo* retention of Poloxamer-Based *In Situ* Hydrogels for Vaginal Application in Mouse and Rat Models. *Acta pharmaceutica Sinica B* 7 (4), 502–509. doi:10.1016/j.apsb.2017.03.003

López-Martínez, S., Rodríguez-Eguren, A., de Miguel-Gómez, L., Francés-Herrero, E., Faus, A., Díaz, A., et al. (2021). Bioengineered Endometrial Hydrogels with Growth Factors Promote Tissue Regeneration and Restore Fertility in Murine Models. *Acta Biomater.* doi:10.1016/j.actbio.2021.08.025

Lu, K.-Y., Lin, Y.-C., Lu, H.-T., Ho, Y.-C., Weng, S.-C., Tsai, M.-L., et al. (2019). A Novel Injectable *In Situ* Forming Gel Based on Carboxymethyl Hexanoyl Chitosan/hyaluronic Acid Polymer Blending for Sustained Release of Berberine. *Carbohydr. Polym.* 206, 664–673. doi:10.1016/j.carbpol.2018.11.050

Lv, H., Wu, B., Song, J., Wu, W., Cai, W., and Xu, J. (2021). Hydrogel, a Novel Therapeutic and Delivery Strategy, in the Treatment of Intrauterine Adhesions. *J. Mater. Chem. B* 9, 6536–6552. doi:10.1039/d1tb01005k

Madl, C. M., Heilshorn, S. C., and Blau, H. M. (2018). Bioengineering Strategies to Accelerate Stem Cell Therapeutics. *Nature* 557 (7705), 335–342. doi:10.1038/s41586-018-0089-z

Mancini, V., and Pensabene, V. (2019). Organs-On-Chip Models of the Female Reproductive System. *Bioengineering* 6 (4), 103. doi:10.3390/bioengineering6040103

Manna, S., Ghosh, A. K., and Mandal, S. M. (2019). Curd-Peptide Based Novel Hydrogel Inhibits Biofilm Formation, Quorum Sensing, Swimming Mortility of Multi-Antibiotic Resistant Clinical Isolates and Accelerates Wound Healing Activity. *Front. Microbiol.* 10, 951. doi:10.3389/fmicb.2019.00951

Milcovich, G., Lettieri, S., Antunes, F. E., Medronho, B., Fonseca, A. C., Coelho, J. F. J., et al. (2017). Recent Advances in Smart Biotechnology: Hydrogels and Nanocarriers for Tailored Bioactive Molecules Depot. *Adv. Colloid Interf. Sci.* 249, 163–180. doi:10.1016/j.cis.2017.05.009

Owusu-Akyaw, A., Krishnamoorthy, K., Goldsmith, L. T., and Morelli, S. S. (2019). The Role of Mesenchymal-Epithelial Transition in Endometrial Function. *Hum. Reprod. Update* 25 (1), 114–133. doi:10.1093/humupd/dmy035

Pabuçcu, E. G., Kovanci, E., Şahin, Ö., Arslanoğlu, E., Yıldız, Y., and Pabuçcu, R. (2019). New Crosslinked Hyaluronan Gel, Intrauterine Device, or Both for the Prevention of Intrauterine Adhesions. *JSLS* 23 (1), e2018.00108. doi:10.4293/jsls.2018.00108

Pan, Y., Zhao, Y., Kuang, R., Liu, H., Sun, D., Mao, T., et al. (2020). Injectable Hydrogel-Loaded Nano-Hydroxyapatite that Improves Bone Regeneration and Alveolar ridge Promotion. *Mater. Sci. Eng. C* 116, 111158. doi:10.1016/j.msec.2020.111158

Rastogi, P., and Kandasubramanian, B. (2019). Review of Alginate-Based Hydrogel Bioprinting for Application in Tissue Engineering. *Biofabrication* 11 (4), 042001. doi:10.1088/1758-5090/ab331e

Shamloo, A., Sarmadi, M., Aghababaie, Z., and Vossoughi, M. (2018). Accelerated Full-Thickness Wound Healing via Sustained bFGF Delivery Based on a PVA/chitosan/gelatin Hydrogel Incorporating PCL Microspheres. *Int. J. pharmaceutics* 537 (1-2), 278–289. doi:10.1016/j.ijpharm.2017.12.045

Sheth, S., Barnard, E., Hyatt, B., Rathinam, M., and Zustiak, S. P. (2019). Predicting Drug Release from Degradable Hydrogels Using Fluorescence Correlation Spectroscopy and Mathematical Modeling. *Front. Bioeng. Biotechnol.* 7, 410. doi:10.3389/fbioe.2019.00410

Sun, J., Mou, C., Shi, Q., Chen, B., Hou, X., Zhang, W., et al. (2018). Controlled Release of Collagen-Binding SDF-1α from the Collagen Scaffold Promoted Tendon Regeneration in a Rat Achilles Tendon Defect Model. *Biomaterials* 162, 22–33. doi:10.1016/j.biomaterials.2018.02.008

Sun, X., Xue, M., Deng, X., Lin, Y., Tan, Y., and Wei, X. (2018). Clinical Characteristic and Intraoperative Findings of Uterine Perforation Patients in Using of Intrauterine Devices (IUDs). *Gynecol. Surg.* 15 (1), 3. doi:10.1186/s10397-017-1032-2

T, M., M, D. a., Berrios I, M., Zhu, C., Gaughan, C., Weinberg, J., et al. (2016). Control Release Anesthetics to Enable an Integrated Anesthetic-Mesenchymal Stromal Cell Therapeutic. *Int. J. Anesth. Pain Med.* 2 (1), 3. doi:10.21767/2471-982x.100012

Tafti, S. Z. G., Javaheri, A., Firoozabadi, R. D., Ashkezar, S. K., and Abarghouei, H. F. (2021). Role of Hyaluronic Acid Intrauterine Injection in the Prevention of Asherman's Syndrome in Women Undergoing Uterine Septum Resection: An RCT. *Int. J. Reprod. Biomed.* 19 (4), 339–346. doi:10.18502/ijrm.v19i4.9060

Tang, J., Chen, J., Guo, J., Wei, Q., and Fan, H. (2018). Construction and Evaluation of Fibrillar Composite Hydrogel of Collagen/konjac Glucomannan for Potential Biomedical Applications. *Regen. Biomater.* 5 (4), 239–250. doi:10.1093/rb/rby018

Ugboaja, J. O., Oguejiofor, C. B., and Igwegbe, A. O. (2017). Clinico-hysteroscopic Analysis of Severe Intrauterine Adhesions Among Nigerian Infertile Women. *Pan Afr. Med. J.* 28, 226. doi:10.11604/pamj.2017.28.226.13838

Wang, L., Yu, C., Chang, T., Zhang, M., Song, S., Xiong, C., et al. (2020). *In Situ* repair Abilities of Human Umbilical Cord-Derived Mesenchymal Stem Cells and Autocrosslinked Hyaluronic Acid Gel Complex in Rhesus Monkeys with Intrauterine Adhesion. *Sci. Adv.* 6 (21), eaba6357. doi:10.1126/sciadv.aba6357

Wang, Z., Wu, J., Shi, X., Song, F., Gao, W., and Liu, S. (2020). Stereocomplexation of Poly(Lactic Acid) and Chemical Crosslinking of Ethylene Glycol Dimethacrylate (EGDMA) Double-Crosslinked Temperature/pH Dual Responsive Hydrogels. *Polymers* 12 (10), 2204. doi:10.3390/polym12102204

Wei, C., Pan, Y., Zhang, Y., Dai, Y., Jiang, L., Shi, L., et al. (2020). Overactivated Sonic Hedgehog Signaling Aggravates Intrauterine Adhesion via Inhibiting Autophagy in Endometrial Stromal Cells. *Cell Death Dis* 11 (9), 755. doi:10.1038/s41419-020-02956-2

Wen, H., Xiao, W., Biswas, S., Cong, Z.-Q., Liu, X.-M., Lam, K. S., et al. (2019). Alginate Hydrogel Modified with a Ligand Interacting with α3β1 Integrin Receptor Promotes the Differentiation of 3D Neural Spheroids toward Oligodendrocytes *In Vitro*. *ACS Appl. Mater. Inter.* 11 (6), 5821–5833. doi:10.1021/acsami.8b19438

Wenbo, Q., Lijian, X., Shuangdan, Z., Jiahua, Z., Yanpeng, T., Xuejun, Q., et al. (2020). Controlled Releasing of SDF-1α in Chitosan-Heparin Hydrogel for Endometrium Injury Healing in Rat Model. *Int. J. Biol. Macromolecules* 143, 163–172. doi:10.1016/j.ijbiomac.2019.11.184

Wu, Y., Xiang, Y., Fang, J., Li, X., Lin, Z., Dai, G., et al. (2019). The Influence of the Stiffness of GelMA Substrate on the Outgrowth of PC12 Cells. *Biosci. Rep.* 39 (1). BSR20181748. doi:10.1042/bsr20181748

Xiao, S., Wan, Y., Zou, F., Ye, M., Deng, H., Ma, J., et al. (2015). Prevention of Intrauterine Adhesion with Auto-Crosslinked Hyaluronic Acid Gel: a Prospective, Randomized, Controlled Clinical Study. *Zhonghua Fu Chan Ke Za Zhi* 50 (1), 32–36. doi:10.3760/cma.j.issn.0529-567x.2015.01.008

Xin, L., Lin, X., Zhou, F., Li, C., Wang, X., Yu, H., et al. (2020). A Scaffold Laden with Mesenchymal Stem Cell-Derived Exosomes for Promoting Endometrium Regeneration and Fertility Restoration through Macrophage Immunomodulation. *Acta Biomater.* 113, 252–266. doi:10.1016/j.actbio.2020.06.029

Xiong, Q., Zhang, T., and Su, S. (2020). A Network Meta-Analysis of Efficacy of Different Interventions in the Prevention of Postoperative Intrauterine Adhesions. *Clin. Transl Sci.* 13 (2), 372–380. doi:10.1111/cts.12721

Xu, F., Shen, X., Sun, C., Xu, X., Wang, W., and Zheng, J. (2020). The Effect of Mitomycin C on Reducing Endometrial Fibrosis for Intrauterine Adhesion. *Med. Sci. Monit.* 26, e920670. doi:10.12659/msm.920670

Xu, H.-L., Xu, J., Zhang, S.-S., Zhu, Q.-Y., Jin, B.-H., ZhuGe, D.-L., et al. (2017). Temperature-sensitive Heparin-Modified Poloxamer Hydrogel with Affinity to KGF Facilitate the Morphologic and Functional Recovery of the Injured Rat Uterus. *Drug Deliv.* 24 (1), 867–881. doi:10.1080/10717544.2017.1333173

Yan, Y., and Xu, D. (2018). The Effect of Adjuvant Treatment to Prevent and Treat Intrauterine Adhesions: A Network Meta-Analysis of Randomized Controlled

Trials. *J. minimally invasive Gynecol.* 25 (4), 589–599. doi:10.1016/j.jmig.2017.09.006

Yang, H., Wu, S., Feng, R., Huang, J., Liu, L., Liu, F., et al. (2017). Vitamin C Plus Hydrogel Facilitates Bone Marrow Stromal Cell-Mediated Endometrium Regeneration in Rats. *Stem Cel Res Ther* 8 (1), 267. doi:10.1186/s13287-017-0718-8

Yao, Q., Zheng, Y.-W., Lan, Q.-H., Wang, L.-F., Huang, Z.-W., Chen, R., et al. (2020). Aloe/poloxamer Hydrogel as an Injectable β-estradiol Delivery Scaffold with Multi-Therapeutic Effects to Promote Endometrial Regeneration for Intrauterine Adhesion Treatment. *Eur. J. Pharm. Sci.* 148, 105316. doi:10.1016/j.ejps.2020.105316

Young, S., and Evans-Hoeker, E. (2014). Endometrial Receptivity and Intrauterine Adhesive Disease. *Semin. Reprod. Med.* 32 (5), 392–401. doi:10.1055/s-0034-1376358

Zagórska-Dziok, M., and Sobczak, M. (2020). Hydrogel-Based Active Substance Release Systems for Cosmetology and Dermatology Application: A Review. *Pharmaceutics* 12 (5), 396. doi:10.3390/pharmaceutics12050396

Zhang, E., Song, B., Shi, Y., Zhu, H., Han, X., Du, H., et al. (2020). Fouling-resistant Zwitterionic Polymers for Complete Prevention of Postoperative Adhesion. *Proc. Natl. Acad. Sci. USA* 117 (50), 32046–32055. doi:10.1073/pnas.2012491117

Zhang, S.-S., Xia, W.-T., Xu, J., Xu, H.-L., Lu, C.-T., Zhao, Y.-Z., et al. (2017). Three-dimensional Structure Micelles of Heparin-Poloxamer Improve the Therapeutic Effect of 17β-Estradiol on Endometrial Regeneration for Intrauterine Adhesions in a Rat Model. *Int. J. Nanomedicine* 12, 5643–5657. doi:10.2147/ijn.S137237

Zhang, S. S., Xu, X. X., Xiang, W. W., Zhang, H. H., Lin, H. L., Shen, L. E., et al. (2020). Using 17β-estradiol Heparin-poloxamer Thermosensitive Hydrogel to Enhance the Endometrial Regeneration and Functional Recovery of Intrauterine Adhesions in a Rat Model. *FASEB j.* 34 (1), 446–457. doi:10.1096/fj.201901603RR

Zhao, G., Cao, Y., Zhu, X., Tang, X., Ding, L., Sun, H., et al. (2016). Transplantation of Collagen Scaffold with Autologous Bone Marrow Mononuclear Cells Promotes Functional Endometrium Reconstruction via Downregulating ΔNp63 Expression in Asherman's Syndrome. *Sci. China Life Sci.* 60 (4), 404–416. doi:10.1007/s11427-016-0328-y

Zheng, F., Xin, X., He, F., Liu, J., and Cui, Y. (2020). Meta-analysis on the Use of Hyaluronic Acid Gel to Prevent Intrauterine Adhesion after Intrauterine Operations. *Exp. Ther. Med.* 19 (4), 2672–2678. doi:10.3892/etm.2020.8483

Zhou, Q., Shi, X., Saravelos, S., Huang, X., Zhao, Y., Huang, R., et al. (2021). Auto-Cross-Linked Hyaluronic Acid Gel for Prevention of Intrauterine Adhesions after Hysteroscopic Adhesiolysis: A Randomized Controlled Trial. *J. minimally invasive Gynecol.* 28, 307–313. doi:10.1016/j.jmig.2020.06.030

**Conflict of Interest:** The authors declare that the research was conducted in the absence of any commercial or financial relationships that could be construed as a potential conflict of interest.

**Publisher's Note:** All claims expressed in this article are solely those of the authors and do not necessarily represent those of their affiliated organizations, or those of the publisher, the editors and the reviewers. Any product that may be evaluated in this article, or claim that may be made by its manufacturer, is not guaranteed or endorsed by the publisher.

frontiers in Bioengineering and Biotechnology

ORIGINAL RESEARCH
published: 23 December 2021
doi: 10.3389/fbioe.2021.807883

# Genipin Cross-Linked Decellularized Nucleus Pulposus Hydrogel-Like Cell Delivery System Induces Differentiation of ADSCs and Retards Intervertebral Disc Degeneration

*Lei Yu[1†], Yi Liu[1†], Jianxin Wu[2†], Shuang Wang[1], Jiangming Yu[3], Weiheng Wang[1]* and Xiaojian Ye[3]**

[1]Department of Orthopedics, Second Affiliated Hospital of Naval Medical University, Shanghai, China, [2]Department of Orthopedics, First Affiliated Hospital of Naval Medical University, Shanghai, China, [3]Department of Orthopaedics, Tongren Hospital, Shanghai Jiaotong University, Shanghai, China

OPEN ACCESS

**Edited by:**
*Di Huang,*
*Taiyuan University of Technology, China*

**Reviewed by:**
*Fengxuan Han,*
*Soochow University, China*
*Qingquan Kong,*
*Sichuan University, China*

***Correspondence:**
*Weiheng Wang*
*wangweiheng01@163.com*
*Xiaojian Ye*
*yexj2002@163.com*

*†These authors have contributed equally to this work*

**Specialty section:**
*This article was submitted to Biomaterials, a section of the journal Frontiers in Bioengineering and Biotechnology*

**Received:** 02 November 2021
**Accepted:** 03 December 2021
**Published:** 23 December 2021

**Citation:**
*Yu L, Liu Y, Wu J, Wang S, Yu J, Wang W and Ye X (2021) Genipin Cross-Linked Decellularized Nucleus Pulposus Hydrogel-Like Cell Delivery System Induces Differentiation of ADSCs and Retards Intervertebral Disc Degeneration. Front. Bioeng. Biotechnol. 9:807883. doi: 10.3389/fbioe.2021.807883*

Intervertebral disc degeneration (IDD) is the pathological basis of disc degenerative diseases (DDD). Reduction in the number of cells and degeneration of the extracellular matrix (ECM) in the nucleus pulposus (NP) are characteristics of IDD. Bio-hydrogel combined with stem cell transplantation is a promising treatment. Injectable ECM hydrogels have good biological activity and *in-situ* gelatinization. However, its biomechanics and stability are insufficient to provide adequate mechanical support for intervertebral discs and to maintain the long-term differential stimulus for seeded stem cells. In our study, we developed genipin cross-linked decellularized nucleus pulposus hydrogel (GDH) as delivery system. We evaluated the mechanical properties, stability, biocompatibility, and differentiation induction of GDH cross-linked with different concentrations of genipin *in vitro*. The GDH-loaded adipose-derived mesenchymal stem cells (ADSCs) (GDHA) were injected into the rat degenerated coccygeal intervertebral disc. The effect of intervertebral disc regeneration *in vivo* was evaluated. The results showed that GDH with 0.02% of genipin had similar elastic modulus to human nucleus pulposus, good biocompatibility, and inducibility of expressing NP-related genes. *In vivo* studies showed that GDHA improved the survival of ADSCs and improved the intervertebral height, MRI index, and histological grading score. In conclusion, GDH, as an outstanding bio-hydrogel cell delivery system, has the therapeutic potential for retarding IDD.

**Keywords: intervertebral disc degeneration, genipin, nucleus pulposus, ADSC, tissue engineering**

## INTRODUCTION

It is reported that low-back pain is currently the second leading cause of hospitalization and disability for elders, placing a serious financial burden on individuals and society (Cieza et al., 2021). Intervertebral disc degeneration (IDD) is the primary pathological basis of low-back pain. The etiology of IDD is complicated and multifaceted involving genetic, environmental, mechanical, age, and other risk factors (Henry et al., 2018). Intervertebral discs (IVDs) are composed of a central

nucleus pulposus (NP), surrounded by the annulus fibrosus and cartilaginous endplates (Eyring, 1969). The NP, usually considered the origin of IDD, is the inner part and the most hydrated region (rich in proteoglycans and collagen II) of IVD transferring axial loads radially (Fontana et al., 2015). Besides the extracellular matrix (ECM) which is enzymatically degenerated during IDD, nucleus pulposus cells (NPCs) are remarkably replaced by cells of fibroblast-like phenotype (Lipson and Muir, 19801981; Lama et al., 2021). Current clinical treatments for IDD-caused low-back pain include medication intervention, surgical depression, and fusion. However, both of them cannot reverse the pathological process of IDD. Furthermore, surgical treatment accelerates the degeneration of adjacent vertebral body segments, finally leading to adjacent vertebral disease. Therefore, there is an urgent need for a satisfactory solution to reengineer the natural properties of IVD (Benneker et al., 2014).

Bioengineering of hydrogels has become a focused researching area of rebuilding the anatomy and histological structure of IVD, being deemed as a promising therapeutic method for IDD (O'Halloran and Pandit, 2007). According to the origin of composites, hydrogels are commonly classified into natural hydrogels and synthetic hydrogels. Naturally derived hydrogels are generally composed of chitosan, alginate, hyaluronan, collagen, and agarose, which can be easily acquired from various renewable bio-tissues (Mano et al., 2007; Leyva-Gómez et al., 2018). Compared with synthetic hydrogels, natural hydrogels possess inherent biocompatibility and biodegradability, while they do not have satisfactory tunability for functional facile fabrication as fine as that of synthetic hydrogels (Tang et al., 2020). Among the natural hydrogels, injectable ECM hydrogels are particularly appealing because their 3D structure and biochemical composition are highly compatible for each distinctive tissue type. ECM has been mimicking aspects of the ECM structure and composition to host tissues which have been demonstrated to dynamically and reciprocally regulate cell behavior, such as migration, proliferation, and differentiation (Geiger et al., 2001) (Cheng et al., 2014) (Young et al., 2011). In addition, ECM hydrogels can reduce immune rejecting reactions and intrinsic enzymes that allow materials to effectively integrate with surrounding tissues (Chua et al., 2016). In our previous study, we have previously developed and reported the decellularized nucleus pulposus hydrogel (DNPH), which shows good potential in NP regeneration (Yu et al., 2020). Although DNPHs have excellent biological activity, the poor mechanical properties limited their wide use in organizations with high mechanical strength requirements, such as NP (Chan et al., 2013). Moreover, current ECM hydrogels seem to not possess sufficient mechanical properties which could match the requirement of an NP biomechanical environment (Moya and Halder, 2019). Without proper mechanical properties, there would be an absence of mechanical signals from ECM bio-scaffolds such as stiffness and elasticity to stimulate host cells and transplanted cells for proliferation and differentiation (Loebel et al., 2019; Moya and Halder, 2019). Due to the mechanical properties of the IVD, stable ECM hydrogels with good mechanical properties for supporting the survival and maturation of NP are needed urgently.

A variety of mesenchymal stem cells (MSCs) have been widely used in stem cell-based IVD engineering, including cartilage or bone marrow-derived MSCs and adipose-derived MSCs (ADSCs) (Li et al., 2021). Compared with other kinds of MSC, ADSCs are especially suitable as seed cells for tissue engineering of IVD, because they are easily accessible from renewable adipose tissue and have potential to differentiate into different cells, such as NP-like cells in specific conditions (Zuk et al., 2001; Tapp et al., 2008). In addition, the prominent paracrine secretion of ADSCs is also beneficial to modulate the microenvironment of a degenerative NP environment. However, without specific exogenous stimuli, the differentiation of ADSCs is inhibited in varying degrees, especially in various hydrogels or scaffolds (Virdi and Pethe, 2021). Among those different factors affecting MSC differentiation into NP-like cells, mechanical stimuli are essential which induce MSC transformation and secretion of NP-specific ECM (Liu et al., 2021). Therefore, in the application of ADSCs in ECM-hydrogel based IVD tissue engineering, adjusting the mechanical properties of hydrogel to an appropriate degree is important for inducing ADSC differentiation and finally rebuilding the normal structure of IVD.

Genipin, a new type of natural cross-linking agent, has the advantage of having low toxicity, having a mild cross-linking process, and the cross-linking products having a good stability and biological compatibility (Ma et al., 2014; Dupont, 2016). Particularly, some studies have shown that genipin can improve the stability and mechanical strength of scaffold. Therefore, it is rational to assume that the modification of DNPH with genipin could improve its stability and biomechanical properties for better inducing the differentiation of seed cells. In this research, we developed genipin cross-linked DNPH (GDH) as a delivery system. We evaluated the mechanical properties, stability, biocompatibility, and differentiation induction of GDH with different concentrations of genipin *in vitro* to determine the proper GDH similar to the properties of NP. Then, we verified the inducing NP-like differentiation of ADSCs exerted by GDH. Finally, we injected GDH loaded with ADSCs (GDHA) into the rats' degenerated coccygeal IVD and evaluated the rebuilding effect of GDHA on degenerated IVD *in vivo*. Our research will provide new insights and methods for exploring ECM-based injectable cell delivery systems to treat IDD.

# MATERIALS AND METHODS

## Extraction, Cultivation, and Identification of ADSCs

All the animals were obtained from the Animal Center of Naval Medical University (Shanghai, China), and all procedures were approved by the Institutional Animal Care and Use Committee of the Second Military Medical University. Male SD rats of 60-g weight were anesthetized and executed to extract primary ADSCs.

The sheared adipose tissue from the groin of rats was transferred into a working solution containing 0.1% collagen type I (Sigma, St. Louis, MO, USA) and 1% BSA (MP, Santa Ana, CA, USA) for digestion (37°C, 1 h). The residue and supernatant were removed by filtering and centrifuging, respectively. Then, the cells were collected and cultured. The culture medium was completely replaced once every 2 days. The third-generation ADSCs were used for subsequent experiments. The surface antigen (CD29, CD105, CD45, and CD90) positive rates of third-generation ADSCs were evaluated by flow cytometry (BD, San Jose, CA, USA) to identify the cell purity.

An induced differentiation medium (Cyagen Biosciences Inc., Santa Clara, CA, USA) was used to culture ADSCs for 3 weeks. Cell adipogenesis differentiation was verified by Oil Red O staining. Osteogenic differentiation was verified by alizarin red staining. Chondrogenic differentiation was verified by Alcian blue staining.

## Preparation of GDH and GDHA

A DNPH precursor was prepared, as reported in our previous study (Yu et al., 2020). Briefly, fresh bovine NP was subjected to a freeze-thaw cycle and 1% SDS for decellularization, followed by freeze-drying and grinding to powder. Firstly, the powder was digested with pepsin for 72 h at room temperature, then the pH and electrolyte were balanced at 4°C. Secondly, the DNPH precursor was cross-linked by genipin (with or without ADSCs) to form GDH at 37°C for 48 h. Notably, ADSCs and genipin were mixed at the same time (final cell concentration is $4 \times 10^6$/ml) to form ADSC 3D culture in GDHA. Both GDH and GDHA were divided to four groups according to the concentration of genipin: 0% group (without genipin), 0.01% group, 0.02% group, and 0.04% group. The properties of the hydrogels, such as mechanical properties, stability, biocompatibility *in vitro*, and differentiation of ADSCs into NPCs, were tested.

## Detection of GDH Cross-Linking Degree

The cross-linking process was reflected by gelation kinetics (within 1 h) and ninhydrin experiments, respectively. The gelation kinetics experiment was as follows: 50-μl precooled gel precursors were placed in 96-well plates, and the absorbance was measured every 2 min for a total of 60 min at 405 nm at 37°C using a Synergy HT pacemeter (BioTek, Winooski, VT, USA). The data were normalized according to **Eq. 1**. The ninhydrin experiment was follows: growth hormone deficiency (GHD) with different cross-linking times was added to a ninhydrin solution (solution of ethylene glycol monomethyl ether with 8.5/ml mg of ninhydrin and 1.5 ml/mg of hydrindantin) and incubated in boiling water for 15 min, followed by cooling to room temperature and diluting with 60% ethanol. The absorbance of the solution at 570 nm was recorded with the Synergy HT pacemeter (BioTek, Winooski, VT, USA). The amount of free amino is proportional to the absorbance of the solution. The cross-linking degree is calculated as shown in **Eq. 2**.

$$normalized\ absorbance = A - A0/Amax\ A0 \quad (1)$$

A is the absorbance, A0 is the initial absorbance, and Amax is the maximum absorbance.

$$\text{cross} - \text{linking degree} = 1 - \text{OD}(\text{cross} - \text{linking})/\text{OD}(\text{uncross} - \text{linking}) \times 100\% \quad (2)$$

## Mechanical Determination of GDH

The GDH in each group was trimmed into cylinders with a diameter of 0.7 cm and height of 0.5 cm. An Instron 4455 universal material testing machine (Biomedical Center, Donghua University, Shanghai, China) was used to perform mechanical testing. The maximum stress $\sigma$ (kPa) and maximum strain (%) of each sample were measured according to the instrument specification, and the elastic modulus E (kPa) of the samples was calculated. The calculation formula is $E = \sigma/\varepsilon$.

## Biodegradation of GDH *in vitro*

The type I collagenase solution (50 U/ml) with double antibodies (Thermo Fisher Scientific, Waltham, MA, USA) was used as the degradation solution, and the ratio of hydrogel volume (ml): degradation solution (ml) is 1:20 (Butterfield et al., 2011). The mixture was subjected to vibration and at constant temperature of 37°C. The total time of complete degradation was recorded.

## Microstructure

GDH in each group was frozen quickly with liquid nitrogen and cross-cut by a blade. The hydrogel was observed *via* cryogenic scanning electron microscopy (SEM, FEI, USA). The average mesh area was measured and calculated by software of ImageJ.

## Biocompatible Assay

GDHAs, also divided into 0%, 0.01%, 0.02%, and 0.04% groups, were prepared for three-dimensional culture. GDHAs (200 μl) were seeded in 12-well plates, and the complete medium was changed every 2 days. The monolayer culture was used as a control group. Cell proliferation and cytotoxicity were detected respectively by CCK-8 staining (Dojindo, Kumamoto, Japan) at 1, 3, and 7 days and live/dead staining at 5 days (R37601 Life Technologies, Carlsbad, CA, USA) according to the manufacturer's protocol. The number of living cells was measured by software of ImageJ, and the living cell ratio was calculated to reflect the cell viability.

## NP Phenotype Expression of ADSCs Encapsulated in GDHA

We chose 0% and 0.02% groups of GDH for ADSC 3D culture, and the monolayer culture was used as a control group. The expression levels of NP phenotype genes (collagen I, collagen II, aggrecan, sox-9) were detected at 7 and 14 days. The primers used for RT-PCR are shown in **Table 1**. The procedures were carried out as described in our previous report. Briefly, total RNA was extracted using TRIzol reagent (Thermo Fisher Scientific). cDNA was synthesized by reverse transcription, followed by real-time PCR utilizing the SYBR Premix qPCR Kit (Takara, Shiga, Japan). GAPDH was used for normalization. Relative gene expression

**TABLE 1 |** Primers used for RT-PCR analysis.

| Gene | Forward primer (5′–3′) | Reverse primer (5′–3′) |
|---|---|---|
| Collagen I | GCTCCTCTTAGGGGCCACT | ATTGGGGACCCTTAGGCCAT |
| Collagen II | GGGTCACAGAGGTTACCCAG | ACCAGGGGAACCACTCTCAC |
| Aggrecan | AGGTGTCGCTCCCCAACTAT | CTTCACAGCGGTAGATCCCAG |
| sox-9 | AGTACCCGCATCTGCACAAC | ACGAAGGGTCTCTTCTCGCT |
| GADPH | AGGTCGGTGTGAACGGATTTG | GGGGTCGTTGATGGCAACA |

data were conducted by the 2-ΔΔCT method. Each sample was tested in triplicate.

After being 2D cultured on the surface of 0% or 0.2% GDH, ADSCs were scraped off and lysed by RIPA buffer. After being quantified with a BCA protein assay kit (Thermo Fisher Scientific Inc., Waltham, MA), the proteins were separated by SDS-PAGE and transferred onto polyvinylidene fluoride (PVDF) membranes. After being blocked with 5% bovine serum albumin (BSA), the PVDF membranes were incubated with primary antibodies: collagen I (ab260043, Abcam, Cambridge, MA, USA) (ab205718); collagen II (GB11021, Servicebio, Wuhan, China); aggrecan (sc166951, Santa Cruz, Dallas, TX, USA); sox9 (ab185966, Abcam, USA); and GAPDH (ab8245). Then, the membranes were washed and incubated with species-matched peroxidase-conjugated secondary antibodies (Beyotime, Shanghai, China) at room temperature for 2 h, and an ECL kit (Millipore, Bedford, MA, USA) was used to visualize the immunoreactive bands. Finally, ImageJ software was used to calculate the band density.

## Animal and Surgical Procedures

Eighty male SD rats 3 months old were used in this experiment. When the rats hit 3 months, skeletal maturity was reached and the IVD remodeling proved irrelevant to animal growth (Hughes and Tanner, 1970). The disc degenerative disease (DDD) model was established as described by Rousseau et al. (2007). After rat anesthesia, the vertebral bodies of Co7-9 were found by palpation and confirmed by X-ray. Needles (20 G) were inserted (parallel to the end plates) into the center of the NP, rotated to 360°, and held for 30 s. After 2 weeks, 2 μl of injection in each group was injected using a microsyringe attached to a 31-G needle into the disc, and the rats were kept still (for gel *in situ*) for more than 30 min. We defined the injection time as the starting time (0 weeks). These rats were divided into 5 groups randomly: sham group (without needle puncture and treatment), control group (needle puncture and DMEM injection, ADSC group (needle puncture and ADSC injection), GDH group (needle puncture and 0.02% GDH injection), and GDHA (needle puncture and 0.02% GDHA injection). Then, the degeneration of the rat tail IVD was evaluated at 0, 4, 8, and 12 weeks after injection.

## X-Ray and MRI

At the time of 0, 4, 8, and 12 weeks after injection, the rats were anesthesia by pentobarbital sodium (50 mg/kg, intraperitoneal injection) and placed on the platform in prone position. The radiographic beam (GE Medical Systems, Buckinghamshire, UK) was adjusted to focus at the 2 target discs. Radiographs and disc height index (DHI) were obtained using the image unit with a collimator-to-film distance of 66 cm, exposure of 63 mA, and penetration power of 35 kV. At 0 and 12 weeks after injection, T2 weighting with a 7.0-T MRI scanner (GE Medical Systems, UK) was used to reveal the water content and the structure of the IVD. The parameter settings were as follows: spin echo repetition time, 2,275 ms; echo time, 80 ms; number of excitations, 8; field of view, 5 cm; slice thickness, 1.5 mm; and no phase wrap. The MRI index (NP area × T2 signal intensity) was measured by Sante DICOM free software.

## H and E and Safranin O Fast Green Stain

At the time of 0, 4, 8, and 12 weeks after injection, the rats were executed. The harvested samples were fixed by 4% paraformaldehyde, followed by de-calcification and paraffin-embedded sectioning (5 μm). The standard sagittal position is maintained during section. H and E stain and Safranin O-fast green stain were performed respectively. The histologic scores were evaluated according to the cellularity and morphology of the IVD (**Table 2**) (Han et al., 2008).

## Evaluation of the Survival and Migration of the Transplanted ADSCs

To track the ADSCs in degenerative discs, GFP-ADSCs were used in the ADSC group and the GDHA group. GFP-ADSCs were obtained from 10 green fluorescent protein (GFP)-transgenic female SD rats [50–60 g, SD-Tg (CAG-enhanced GFP) CZ-004Osb, Sina-British SIPPR/BK Lab, Animal Ltd., Shanghai, China]. The animal model established was as mentioned above. The samples were collected and cross-sectioned (5 μm) with a freezing microtome (Leica, Wetzlar, Germany) at 0, 4, 8, and 12 weeks, respectively. Then, the specimens were stained with DAPI (Servicebio, Wuhan, China) for 3 min. The survival of GFP-ADSCs excited green fluorescence under a fluorescence microscope (Leica, Wetzlar, Germany).

## Statistical Analysis

Continuous variables are presented as the mean ± SD, while categorical variables are presented as quartiles. Student's t test was used for two-group comparison, while one-way ANOVA test was used for multiple groups and intergroup comparison was assessed by the LSD t-test. $p < 0.05$ was considered statistically significant. All data were analyzed using SPSS 20.0 (IBM, Armonk, NY, USA) software. GraphPad Prism 6.0 was used for data conversion and generating the statistical graph.

# RESULTS

## Characterization of ADSCs

The results of the flow cytometry detection of cell surface antigen of ADSCs showed that the expressions of CD29 and CD90 were positive (positive rate >90%), while the expressions of CD44 and CD45 were negative (positive rate <5%, **Supplementary Figures S1A–C**). The ADSCs were cultured under different induced differentiation conditions and stained accordingly. After 2 weeks of adipogenic induction, a large number of red-stained

**TABLE 2 |** Histological grading scale.

| Cellularity and morphology | Grade |
|---|---|
| Cellularity of the AF | 1. Fibroblasts comprise more than 75% of the cells |
| | 2. Neither fibroblasts nor chondrocytes comprise more than 75% of the cells |
| | 3. Chondrocytes comprise more than 75% of the cells |
| Morphology of the AF | 1. Well-organized collagen lamellae without ruptured or serpentine fibers |
| | 2. Inward bulging, ruptured, or serpentine fibers in less than one-third of the annulus |
| | 3. Inward bulging, ruptured, or serpentine fibers in more than one-third of the annulus |
| Border between the AF and NP | 1. Normal, without any interruption |
| | 2. Minimal interruption |
| | 3. Moderate or severe interruption |
| Cellularity of the NP | 1. Normal cellularity with stellar-shaped nuclear cells evenly distributed throughout the nucleus |
| | 2. Slight decrease in the number of cells with some clustering |
| | 3. Moderate or severe decrease (>50%) in the number of cells with all the remaining cells clustered and separated by dense areas of proteoglycans |
| Morphology of the NP | 1. Round, comprising at least half of the disc area in mid-sagittal sections |
| | 2. Rounded or irregularly shaped, comprising one quarter to half of the disc area in mid-sagittal sections |
| | 3. Irregularly shaped, comprising less than one quarter of the disc area in mid-sagittal section |

fat droplets were observed in the cytoplasm after oil Red O staining. After 2 weeks of osteogenic induction, alizarin red staining showed red calcium nodules. After chondrogenic induction for about 3 weeks, Alcian blue staining showed the blue matrix inside and outside the cells (**Supplementary Figures S1D–G**). Both flow cytometry and differentiation experiments proved that most of the obtained cells were stem cells with good differentiation potential, which can be used for further experiments.

## Observation and Cross-Linking Degree Detection of GDH

The precursor of DNPH was mixed with different concentrations of genipin evenly and placed at 37°C. After 30 min, all groups were presented as opalescent translucent gel (GDH). Over time, GDH became blue and deepens gradually. After 48 h, the color of GDH was basically no longer deepened. At 48 h, the 0% group is a milky white and semi-fluid gel with a low cross-linking degree (**Figure 1A**). In the 0.01% group, the appearance was light blue and the cross-linking degree increased (**Figure 1B**); the 0.02% group with blue appearance has a higher cross-linking degree (**Figure 1C**). The 0.04% group has a dark blue appearance with the highest cross-linking degree (**Figure 1D**).

The gelation kinetics curve was obtained, and the trend of curve in each group was roughly similar (**Figure 1E**). The 0% group completed the cross-linking in about 30 min, while other groups were still cross-linking slowly after 30 min. The time-variant degree of cross-linking was measured for 48 h (once an hour) by the ninhydrin experiment (**Figure 1F**). The 0% group was basically stable within 1 h, while other groups showed a slow rise until 48 h. At the same time point, the cross-linking degree of GDH increased significantly with the increase in the concentration of genipin ($p < 0.05\%$).

## Microstructure

Hydrogels in each group appeared as a grid under a freezing microscope. The microstructure of the 0% group was porous with a smooth and regular skeleton (**Figure 2A**). With the addition of genipin, the microstructure of GDH became twisted and tough, and the pores became more irregular. GDH formed a new cross-linking on the basis of the original grid structure of DNPH. As the concentration of genipin increased, the microstructural transformation of the hydrogel became more and more obvious (**Figures 2B–D**). The average grid area, measured by software ImageJ, decreased significantly with the increase in genipin concentration ($p < 0.05\%$, **Figure 2E**).

## Mechanical and Stability Test

All groups completed the mechanical test except the 0% group, which was a too loose structure to test. The maximum stress, maximum strain, and elastic modulus of GDH at the inflection point (when the hydrogel was destroyed) were obtained according to the corresponding stress–strain curve (**Figure 3A**). Results showed that the maximum strain of the 0.01%, 0.02%, and 0.04% groups was (82.36 ± 2.50)%, (76.57 ± 5.09)%, and (68.82 ± 2.73)%, respectively; the maximum stress of each group was (4.63 ± 0.29) kPa, (8.18 ± 0.33) kPa, and (9.40 ± 0.73) kPa; and the elastic moduli were (5.62 ± 0.28) kPa, (10.70 ± 0.28) kPa, and (13.64 ± 0.63) kPa. Therefore, with the increase in genipin concentration, the maximum strain of GDH decreased significantly ($p < 0.05$, **Figure 3B**), and the maximum stress and elastic modulus increased significantly ($p < 0.05$, **Figures 3C,D**). This suggested that the elastic modulus of the corresponding GDH increased with the increase in the concentration of genipin.

The biodegradation of GDH *in vitro* was also tested. The volume of each gel gradually decreased due to the action of collagenase, and the complete degradation time of each group is shown in **Figure 3E**. The stability of GDH increased significantly with the increase in cross-linking degree ($p < 0.05\%$).

## Biocompatibility *in vitro*

Live/dead staining showed that the vast majority of cells in the control group (2D monolayer culture) and the 0%, 0.01%, and

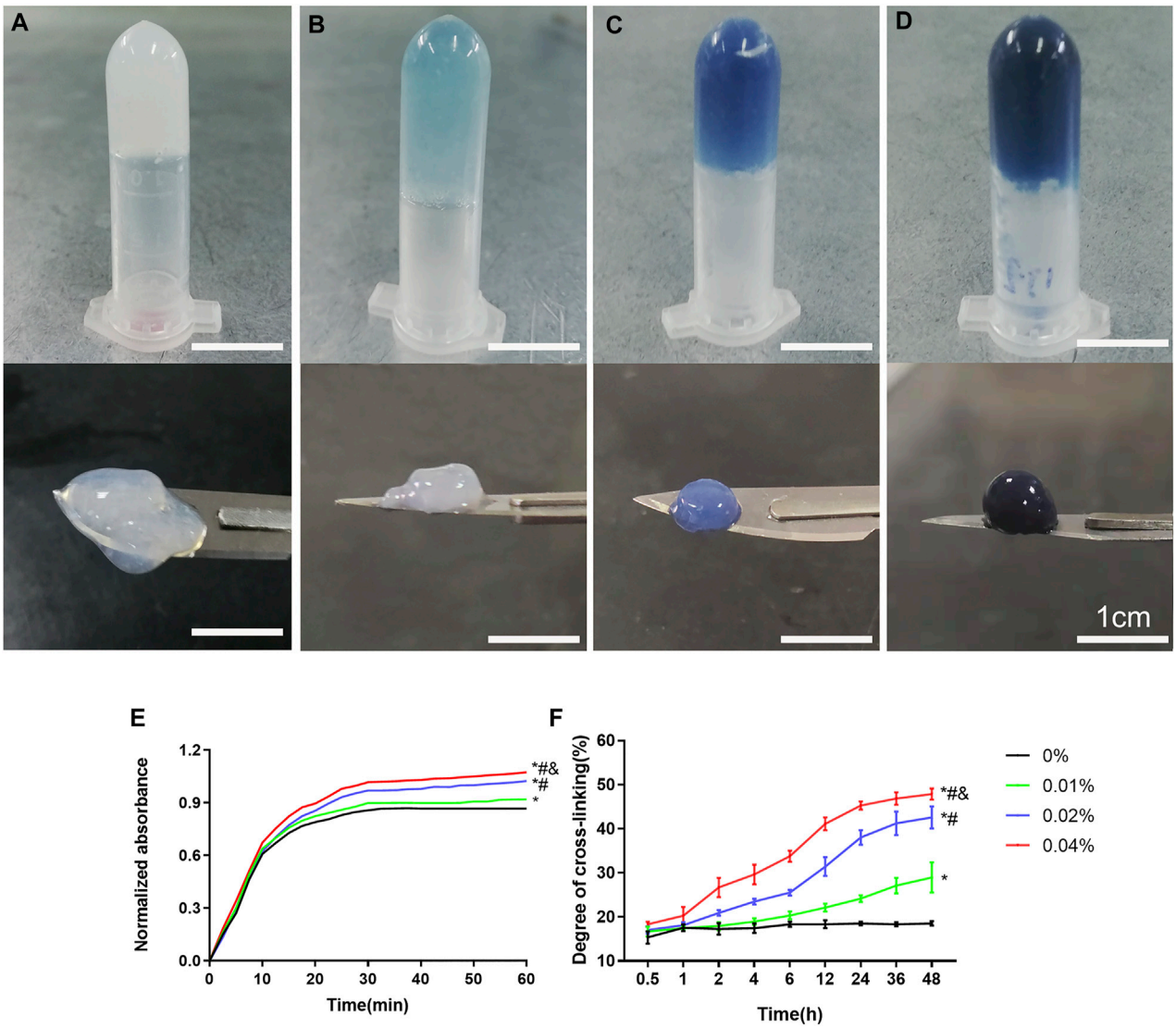


**FIGURE 1 |** The appearance and cross-linking degree of the GDH cross-linked by different concentrations of genipin for 48 h. The morphology and color of GDH shown in the 0% **(A)**, 0.01% **(B)**, 0.02% **(C),** and 0.04% **(D)** groups. **(E)**: Gelation kinetics curve; **(F)**: time-variant degree of cross-linking measured by the ninhydrin experiment. Data represented mean ± SD ($n$ = 5); $^{*}p < 0.05$, vs. 0% group; $^{\#}p < 0.05$, vs. 0.1% group; $^{\&}p < 0.05$, vs. 0.02% group. Scale bar = 1 cm.

0.02% groups were green stained (live cells); few cells were red (death cells, **Figures 4A–E**). After counting the live/dead cells, the living cell ratios were 91%, 90%, 87%, and 88%, respectively, with no significant difference between groups (control, 0%, 0.01%, 0.02% group), while a large number of red-stained cells were observed in the 0.04% group, and the living cell ratio was 52%, which was significantly lower than that in the other groups ($p <$ 0.05%, **Figures 4F**). The CCK-8 test showed that there were no significant differences of cell proliferation between the control and 0%, 0.01%, and 0.02% groups ($p > 0.05$). However, the cell proliferation in the 0.04% group was much lower than that in other groups ($p < 0.05$, **Figures 4G**). Giving a comprehensive consideration to the stability and biocompatibility of GDH, we determined that the proper concentration of genipin for cross-linking was 0.02%.

## NP-like Differentiation

As shown in **Figure 5A–D**, the expression of NP-related genes, collagen type I (Col-1), collagen type II (Col-2), aggrecan (Acan), and sox9 showed significant differences in each group ($p < 0.05$) at 7 and 14 days, while there were no significant differences in Col-1 between each group's expression at various time-points ($p > 0.05$). The comparison of aggrecan expression between the 0% and 0.02% groups showed no statistical difference ($p > 0.05$) at 7 days but increased significantly at 14 days in the 0.02% group ($p < 0.05$). The Col 2 and sox-9 expression levels in the 0.02% group were higher than those of other groups at each time. The expression of NP-related phenotype genes in ADSCs was highest in group 0.02%, followed by the 0% group, and lowest in the control group. In addition, the distinct effects of GDH with different concentrations of genipin in inducing differentiation

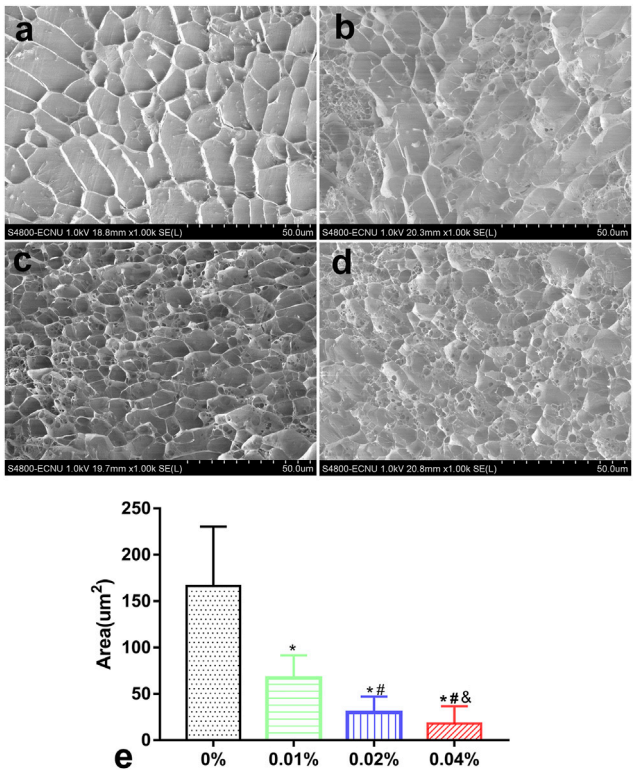


**FIGURE 2 |** The GHD microstructure observation and grid area measurement by a cryoelectron microscope. Cryoelectron microscope images of GHD in the **(A)** 0%, **(B)** 0.01%, **(C)** 0.02%, and **(D)** 0.04% groups. **(E)** The quantification of the average grid area of GHD cross-linked with genipin. Data represented mean ± SD ($n = 5$); $^{*}p < 0.05$, vs. 0% group; $^{\#}p < 0.05$, vs. 0.1% group; $^{\&}p < 0.05$, vs. 0.02% group.

of ADSCs to NP-like cells were confirmed by Western blot (**Figures 5E–I**).

## X-Ray

The changes in X-ray and DHI in each group are shown in **Figure 6**. DHIs in the control group, ADSC group, GDH group, and GDHA group were significantly lower than that in the sham group at week 0 ($p < 0.05$). Compared with the control group, ADSC group, and GDH group, the DHI in the GDHA group was significantly higher at 4, 8, and 12 weeks ($p < 0.05$). Compared with the control group, DHIs in GDH group and GDHA group were much higher at 0, 4, 8, and 12 weeks ($p < 0.05$).

## MRI

The MRI reflects the structure and water content of the IVD (**Figure 7**). In the sham group, the structure of the IVD was intact, while in other groups, the disc was damaged to varying degrees accompanied by the T2 signal change of the NP. The MRI indexes were compared and sorted. Compared with the sham group, the MRI indices of the control group, ADSC group, GDH group, and GDHA group were significantly lower at 0, 4, 8, and 12 weeks ($p < 0.05$), respectively. The structure and T2 signal of IVD in the ADSC group, GDH group, and GDHA group were improved compared with the control group ($p < 0.05$), while the MRI indices of the GDHA group at 4, 8, and 12 weeks were much higher than those in the control group, ADSC group, and GDH group ($p < 0.05$).

## Histological Staining and Grading

As shown in HE staining (**Figure 8**) and S and O staining (**Figure 9**), the histological structure of IVD (distribution of NP cells, NP content and disc height) in the sham group was regular, and the corresponding histological grading score was 5. In other groups, the disordered structure of NP and annulus fibrosus was presented. The degeneration site was occupied by fibrocartilage tissue and cells with different cell morphology or even the scar tissue. The histological grading score in each group over time is shown in **Figure 8B**. At the advanced stage (8–12 weeks), the cell distribution and tissue structure of the GDHA group were more regular and the histological grading score was significantly improved compared with other groups (except the sham group).

## Cell Tracing

For detecting the living ADSCs in GDH, we applied GFP-tagged ADSCs in building GDHA. As shown in **Figure 10A**, a small number of GFP-ADSCs with limited migration were observed, in the single ADSC group at 1 and 4 weeks. The number of cells reached the maximum at 4 weeks while it significantly decreased at 8 weeks and almost vanished at week 12 ($p < 0.05$, **Figure 10C**). In the GDHA group, GFP-ADSCs could survive in the degenerative disc and migrate to the surrounding area at weeks 1, 4, 8, and 12 (**Figure 10B**). The number of GFP-positive cells was highest at 1 and 4 weeks while it decreased gradually at 8 and 12 weeks ($p < 0.05$, **Figure 10C**).

# DISCUSSION

The NP-derived ECM hydrogels offered the possibility of regeneration to degenerate NP (Collin et al., 2011; Wang et al., 2014). However, the low elastic modulus and poor stability of the ECM hydrogels may suffer no stress and cannot sustain cells for long-term survival in degenerated IVD (Chung and Burdick, 2008). Wachs et al. (2017) and Mercuri et al. (2013) reported the study of NP ECM hydrogels *in vitro* but neglected the critical mechanical properties in IVDs (Setton and Chen, 2004). It is of great significance to improve the stability and mechanical properties of the ECM hydrogel and to clarify its effects on cell behavior and relative mechanisms. In the present study, we constructed ECM-based DNPH scaffold and made it be cross-linked with genipin to improve the mechanical mechanics and stability. Afterward, we figured out a suitable genipin cross-linking concentration (0.02%) and developed a novel genipin cross-linked decellularized NP hydrogel-like cell delivery system (DNPH) to deliver ADSCs into IVD. We demonstrated that this ADSC–genipin-DNPH complex could retard IDD significantly.

Cross-linking is a well-established technique in materials science and bioengineering, through which two or more molecules are chemically connected to enhance the mechanical

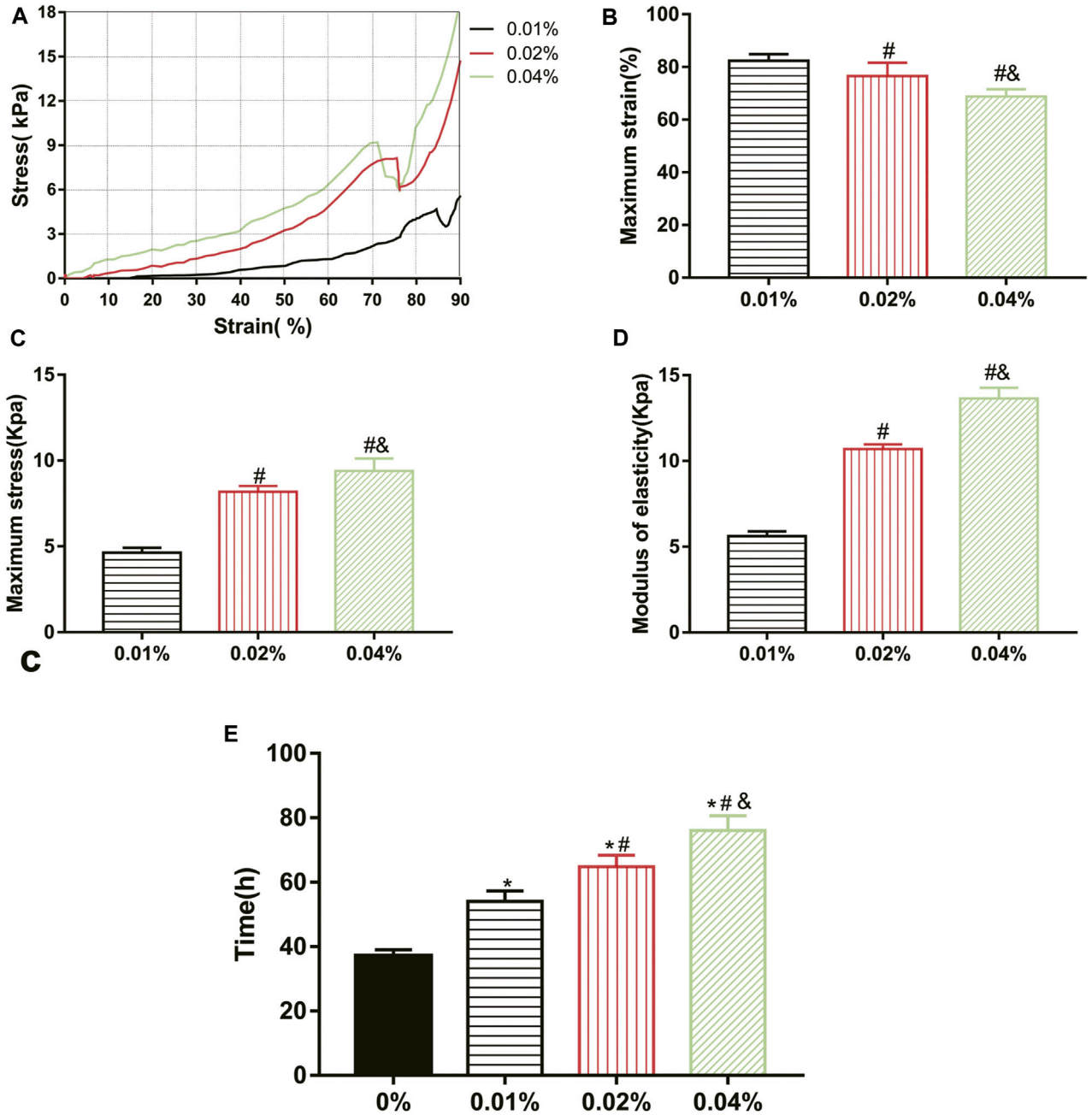


**FIGURE 3 |** Effect of genipin concentration on GDH cross-linking rule and stability. **(A)** The stress–strain curves of the GDH hydrogels with different genipin concentrations; **(B,C)** the maximum strain and maximum stress of the GDH hydrogels with different genipin concentrations; **(D)** the elastic modulus of the GDH hydrogels with different genipin concentrations; **(E)** the stability of GDH reflected by the time of complete degradation *in vitro*. Data represented mean ± SD ($n = 5$); $^{*}p <$ 0.05, vs. 0% group; $^{\#}p < 0.05$, vs. 0.1% group; $^{\&}p < 0.05$, vs. 0.02% group.

strength of tissues or biomaterials. In recent years, cross-linking has been gradually applied in the research of IDD and repair and continuously developed as a novel therapeutic strategy for the restoration of NPCs and ECM. As an essential factor for chemical cross-linking, the current available agents include glutaraldehyde, glyceraldehyde, ribose, and glucose (Wollensak and Spoerl, 2004). The biological toxicity of chemical cross-linking agents cannot be ignored during the cross-linking process, which limits their further clinical application (Sung et al., 1999). As an extract from traditional Chinese medicine, Eucommia ulmoides, genipin is a natural biological cross-linking agent with low toxicity. Due to its mechanical-enhancing properties and biocompatibility of the matrix (Muzzarelli et al., 2016), genipin has been widely used in the bioengineering research of sclera, articular cartilage, tendon,

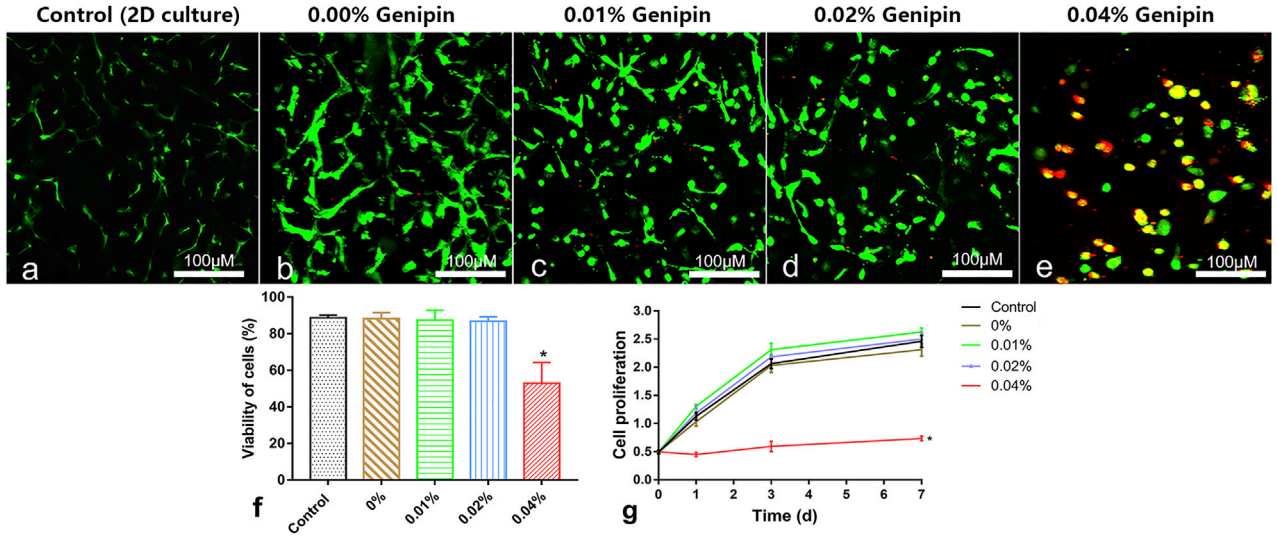


**FIGURE 4 |** Cytocompatibility measurement of the hydrogels *in vitro*. **(A–E)** Live/dead cell staining and cell morphology observed at 5 days in the 2D-cultured control group and 0%, 0.01%, 0.02%, and 0.04% groups; **(F)** the living cell ratio showing the viability of cells; **(G)** the cell proliferation tested by the CCK-8 test. Data represented mean ± SD ($n$ = 5); $^{*}p < 0.05$, vs. 0% group; $^{\#}p < 0.05$, vs. 0.1% group; $^{\&}p < 0.05$, vs. 0.02% group. Scale bar = 100 μm.

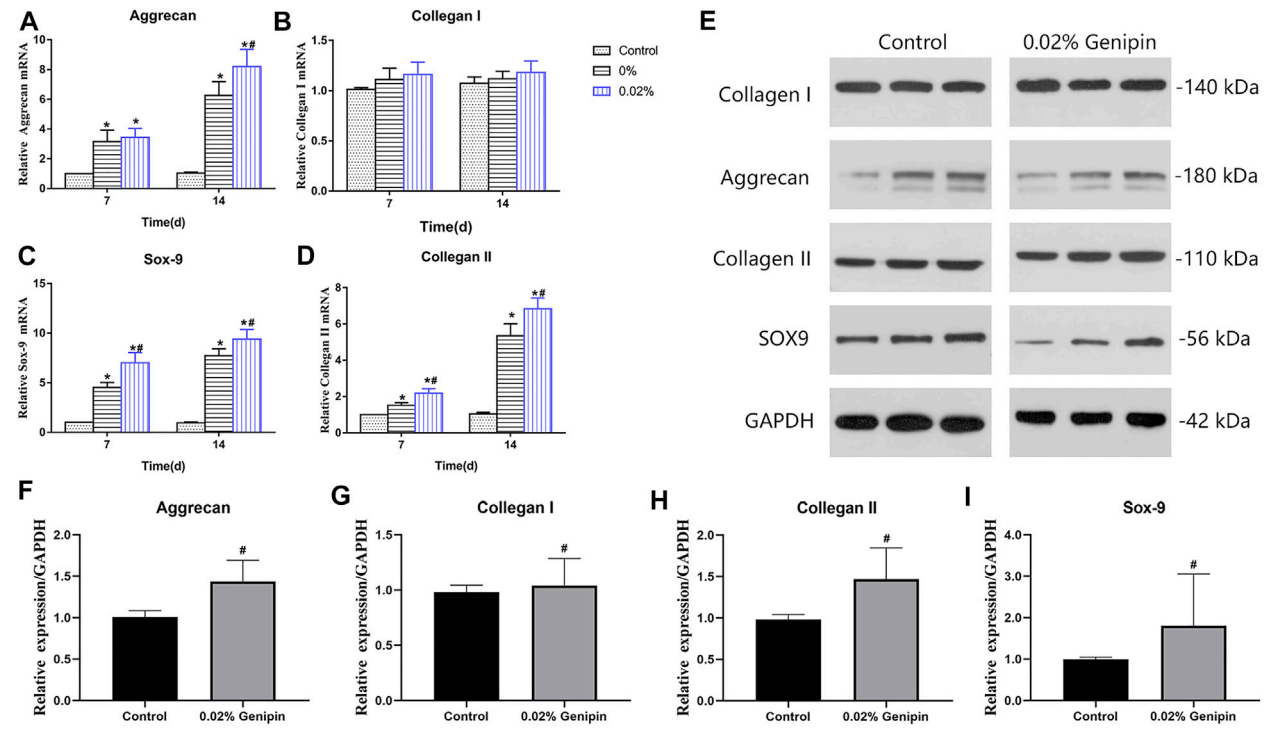


**FIGURE 5 |** Nucleus pulposus-related gene expression levels of ADSCs. Gene expression levels of Acan **(A)**, Col-I **(B)**, Sox9 **(C)**, and Col-II **(D)** were measured at 7 and 14 days. Verification of Western blot for NP-related gene expression at 7 days is shown in **(E–I)**. Data represented mean ± SD ($n$ = 5); $^{*}p < 0.05$, vs. 0% group; $^{\#}p < 0.05$, vs. 0.2% group.

and bone (Kim et al., 2010; Yan et al., 2010; Muzzarelli et al., 2015; Zhu et al., 2016). In the field of bioengineering repair for IDD, the application of genipin is still in the initial stage (Zhou et al., 2018a; Zhou et al., 2018b; Fujii et al., 2020). Zhou et al. produced the genipin cross-linked type II collagen/chondroitin sulfate composite scaffold, which had the property of *in-situ* gelation

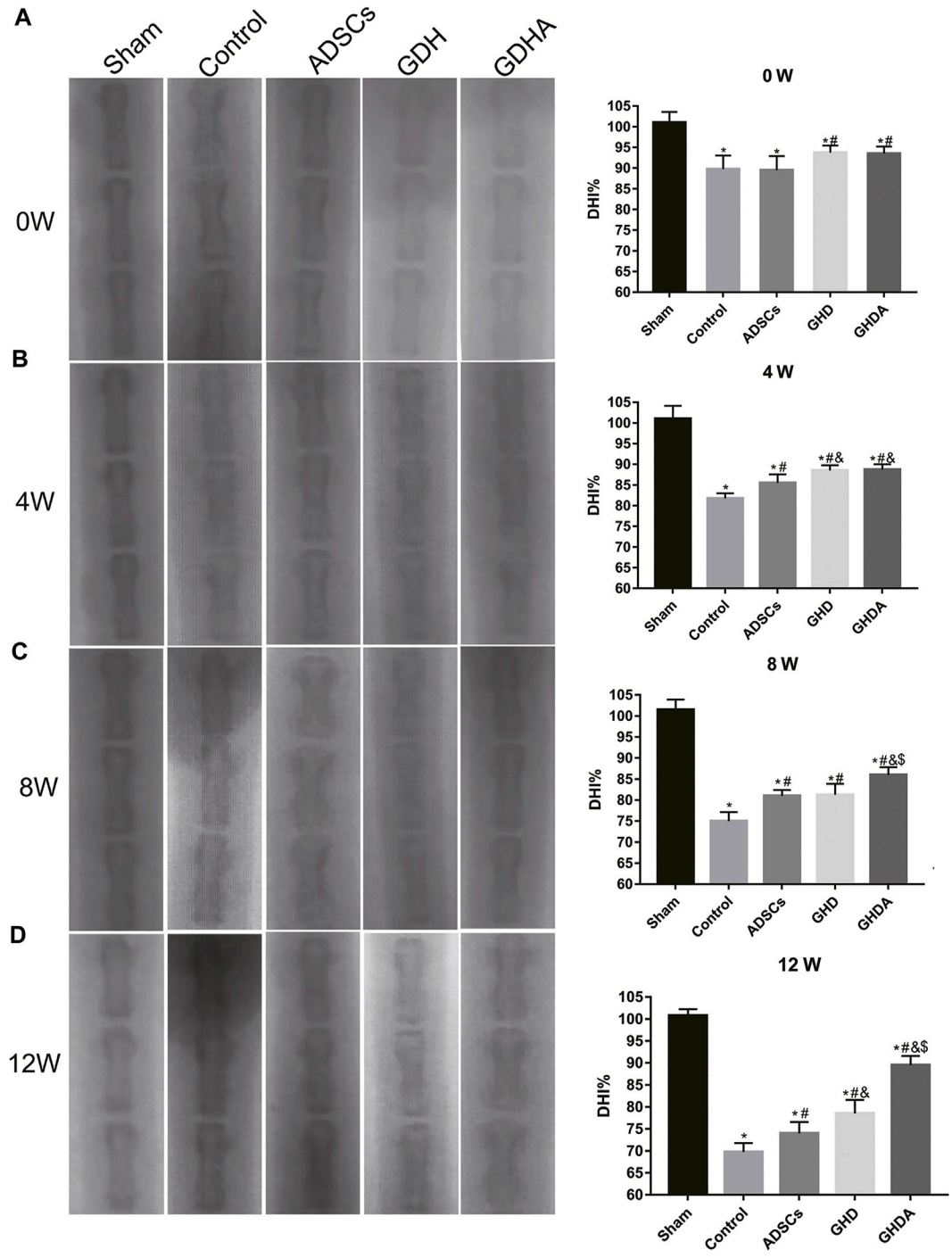


**FIGURE 6 |** Radiographs of the caudal vertebra and change of the DHI tested by X-ray at 0 **(A)**, 4 **(B)**, 8 **(C),** and 12 **(D)** weeks after injection. Data represented mean ± SD ($n$ = 5); $^{*}p < 0.05$, vs. sham group; $^{\#}p < 0.05$, vs. control group; $^{\&}p < 0.05$, vs. ADSCs group; $^{\$}p < 0.05$, vs. GHD group.

and induced adipose-derived stem cells differentiating to an NP-like phenotype *in vitro* (Zhou et al., 2018b). In addition, Zhou et al. developed a genipin-cross-linked type II collagen scaffold and found that it can promote the differentiation of adipose-derived stem cells into NP-like cells (Zhou et al., 2018a). However, whether GDH has the therapeutic effect on IDD is hitherto unclear. In the present study, the gelation kinetics and ninhydrin detection showed that the GDH was initially self-cross-linking rapidly at the first half hour, then slowed down by genipin, and finally completed in around 48 h. The cross-linking degree, elastic modulus, and resistance to enzymatic hydrolysis of the GDH were positively correlated with genipin concentration. SME

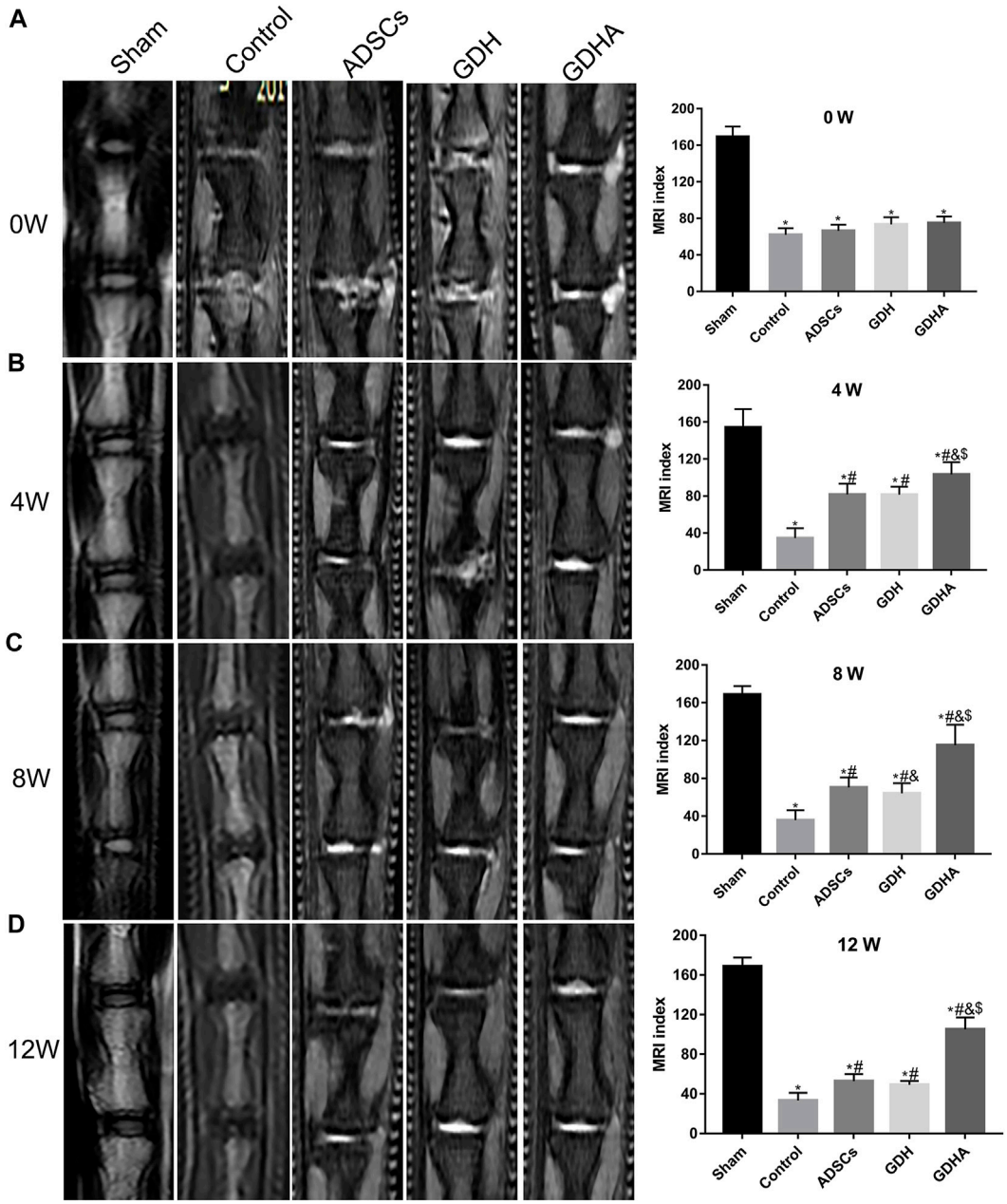


**FIGURE 7 |** Typical MRI and MRI index change in the tail discs at 0 **(A)**, 4 **(B)**, 8 **(C),** and 12 **(D)** weeks after injection. Data represented mean ± SD (n = 5); $^{*}p < 0.05$, vs. sham group; $^{\#}p < 0.05$, vs. control group; $^{\&}p < 0.05$, vs. ADSCs group; $^{\$}p < 0.05$, vs. GHD group.

showed that the mesh area in the hydrogel decreased with the increase in genipin concentration, suggesting that genipin may establish more solid cross-linking to the hydrogel. When the concentration of genipin is 0.02%–0.04%, the elastic modulus of GDH is close to human NP (about 11 kPa) (Iatridis et al., 1996).

The CCK-8 test showed that there was no significance between different groups (expect the 0.04% genipin group) at various time-points. Meanwhile, the dead/live test showed that most of the ADSCs cultured on the GDH with low concentrations of genipin (0%–0.02%) were living, which account for about 90%. However, in the 0.04% group, it showed a significant increase of dead cells, and the ratio of living cells was only 50% as well. According to these results, we deduced that the optimum concentration of genipin is 0.02%.

The gene expression of NP-related phenotypic molecules (aggrecan, Sox-9, collagen I, and collagen II) represents the matrix synthesis and reflects the NP-like differentiation of ADSCs. The RT-PCR and Western blot showed there were no significant between different groups in the expression of *Col-1* (NP-negative maker) at various time-points. Compared with the

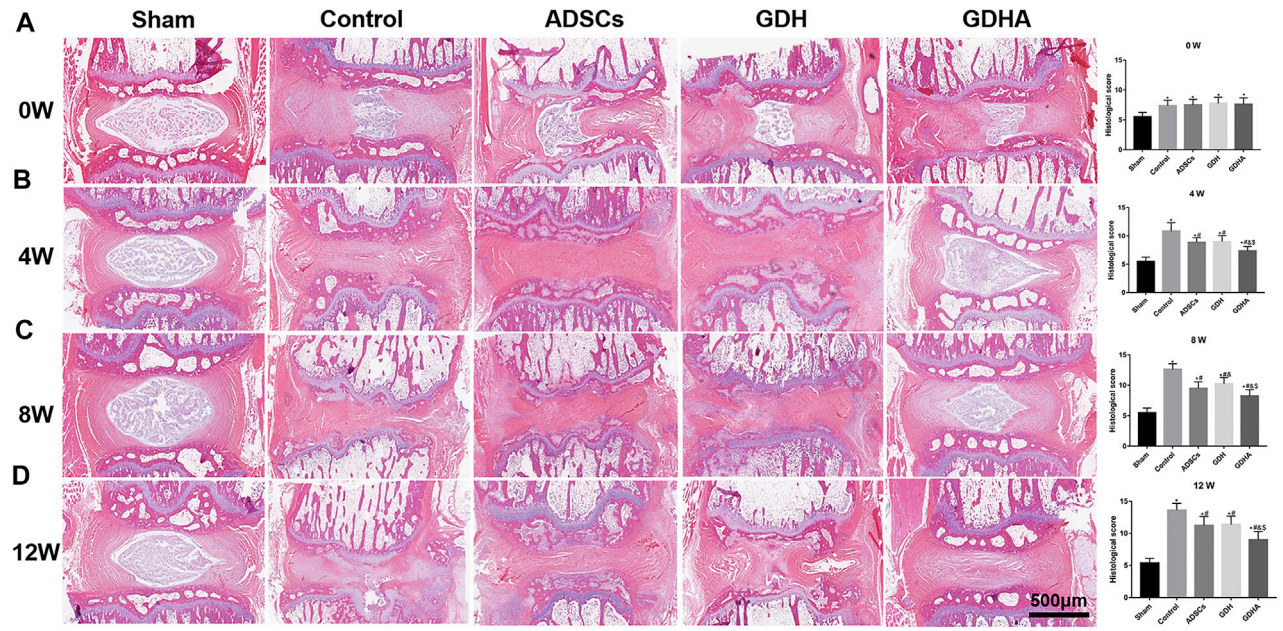


**FIGURE 8 |** Typical HE staining and histologic score change in the tail discs at 0 **(A)**, 4 **(B)**, 8 **(C),** and 12 **(D)** weeks after injection. Data represented mean ± SD ($n$ = 5); $^{*}p < 0.05$, vs. sham group; $^{\#}p < 0.05$, vs. control group; $^{\&}p < 0.05$, vs. ADSC group; $^{\$}p < 0.05$, vs. GHD group. Scale bar = 500 μm.

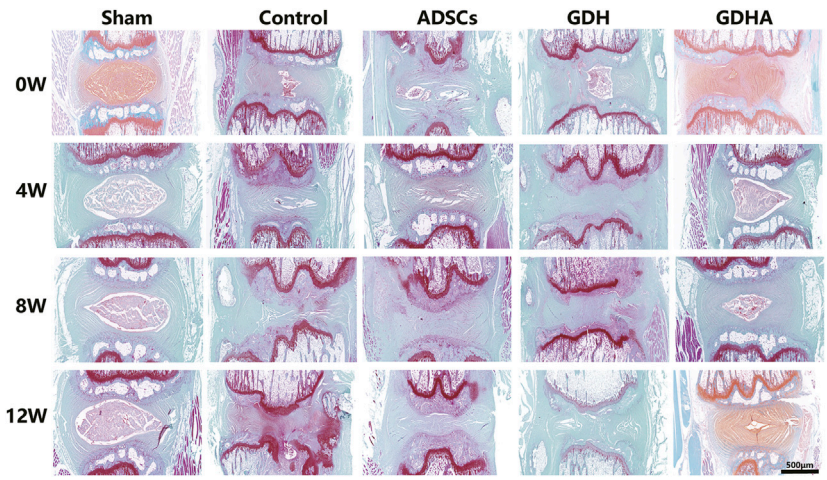


**FIGURE 9 |** Typical Safranin O–fast green (S–O) staining in the tail discs at 0 **(A)**, 4 **(B)**, 8 **(C),** and 12 **(D)** weeks after injection. Scale bar = 500 μm.

control group, gene expression levels of NP-positive markers (*Col-2*, Acan, and Sox-9) were increased in the DNPH group and reached to the highest level in the 0.02% genipin–DNPH group. This suggested that DNPH promoted the NP-like differentiating induction of DNPH which could be enhanced by genipin cross-linking. There might be several potential mechanisms contributing to this phenomenon. Firstly, ECM cross-linked by genipin leads to variations in stiffness and roughness, while its proteic composition remains unchanged (Yoo et al., 2011). Its inherent collagen II could improve the differentiation of ADSCs into NP cells (Yin et al., 2018) and promote the synthesis of ECM (Tao et al., 2016; Zhou et al., 2018b). Secondly, the stiffness of the ECM leads to the differentiation of MSCs. The mechanically related transcription coactivator (YAP/TAZ) with a PDZ-binding motif has been shown to influence the behavior of MSC by transducing signals originated from ECM mechanical cues (Dupont, 2016). Previous studies showed that MSCs have robust osteogenic capacity on a rigid matrix with a modulus of 40 kPa (Ye et al., 2015; Ye et al., 2016), while on a soft matrix (0–1 kPa) they contribute to adipogenic differentiation (Engler et al., 2006). In this study, the modulus of GDH (with 0.02% genipin) was about 11 kPa, contributing to chondroid

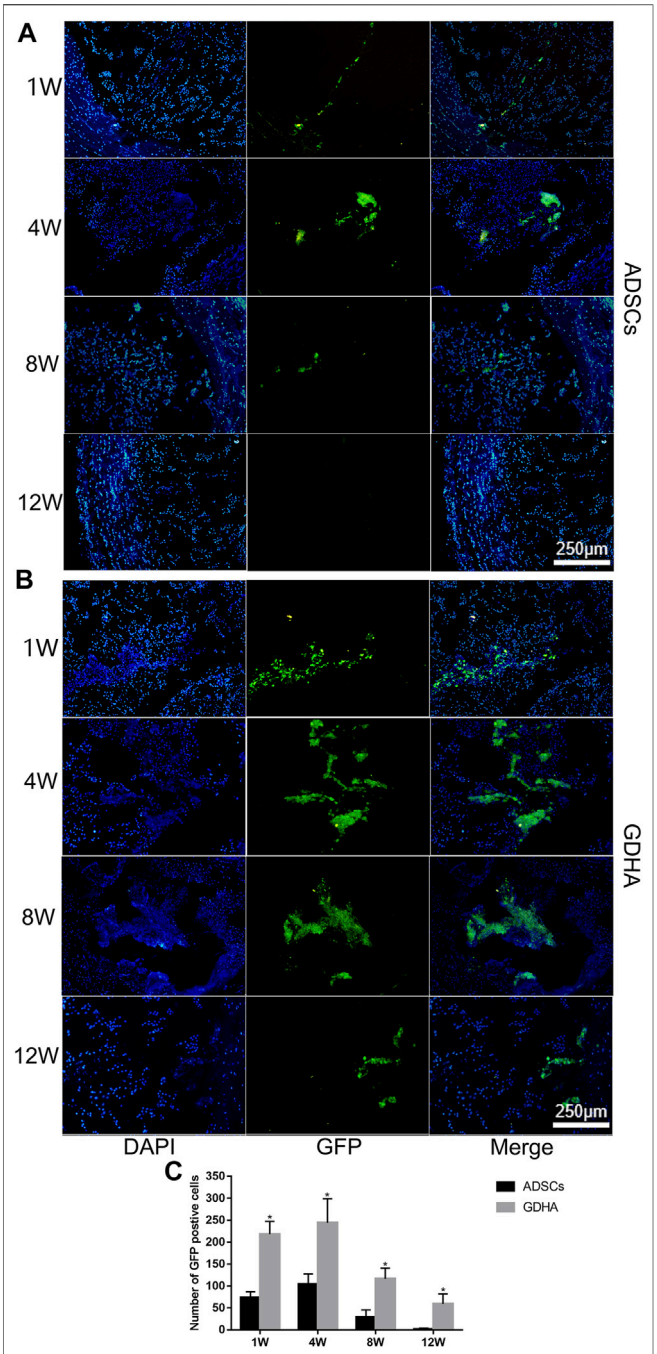


**FIGURE 10 |** The survival and migration of ADSCs in the tail discs of the ADSC group **(A)** and GDHA group **(B)** at 1, 4, 8, and 12 weeks after injection. Data represented mean ± SD ($n = 5$); $^{*}p < 0.05$, vs. sham group; $^{\#}p < 0.05$, vs. control group; $^{\&}p < 0.05$, vs. ADSC group; $^{\$}p < 0.05$, vs. GHD group. Scale bar = 250 μm.

differentiation (Akhmanova et al., 2015). Thirdly, the secondary structure and surface properties of ECM were changed in GHD (Qiu et al., 2013). SEM showed that loose mesh in DNPH changed into denser mesh in GDH. In the perspective of topological structure, surface characteristics and pore size may affect the differentiation of stem cells (Ma et al., 2018). Nevertheless, the molecular mechanism in which GDH (with 0.02% genipin) exerted specific NP differentiation–induction on ADSCs needs to be explored in further studies.

Given the differences between *in vitro* and *in vivo* environments, whether ADSCs can survive and maintain the same cytoactivity in degenerated IVD as the *in vitro* culture needs to be clarified. In the present study, the *in vivo* cell tracing showed that a few ADSCs in the ADSCs group were alive at 1 and 4 weeks, while in the GDHA group, more cells were still alive at 8 weeks and kept cytoactive, indicating that GDH could provide vital support for surviving ADSCs in IVD. Moreover, our results also showed that GDHA significantly restored the histological characteristics of degenerated IVD. Compared with the degenerative group, the intervertebral height and structure in the ADSC group were improved, while they were still worse than those in the GDHA group. Some studies have shown that the degraded NPs possess a detrimental environment (low oxygen tension, limited nutrition, acidic pH, high osmotic pressure), which has a negative impact on the function and viability of transplanted cells (Henry et al., 2018). As abovementioned, only a few ADSCs survived at 4 weeks. Considering that related ECM can be synthesized by ADSCs in the early stage, it is difficult to make ADSCs survive in the long term in harsh environments and hardly achieve continuous restoration of the IVD physiological structure. The cell tracer showed that the cells in the GDHA group could survive longer, combined with a higher elastic modulus. The DHI, MRI index, and degeneration index were improved in the GDHA group, but they were still inferior to those in the sham group. In addition, due to the improved elastic modulus and better anti-enzymatic hydrolysis performance, the intervertebral height and T2 signal values in the GDH group were higher than those in the degenerative group. Therefore, GDHA possesses superior mechanical properties and can prolong the survival time of ADSCs, which is an ideal biomaterial for IVD regeneration.

## CONCLUSION

In the present research, we developed a novel genipin cross-linked decellularized NP hydrogel-like cell delivery system to deliver ADSCs into IVD. The GDH is cross-linked with 0.02% genipin and has the ability of *in situ* gelation after injection. The GDHA cross-linking degree is moderate with an increased bio-stability and solid-like properties after gelation. Our *in vitro* results demonstrated the bio-safety of the GDHA and the stimulating effects of the GDHA on the differentiation of ADSCs to NP-like cells. We further studied the pro-regenerative effects of the GDHA delivery system on the IDD in the rat model, and we demonstrated that it could partly promote the regeneration of the degenerated NP. We hope our study can provide new clinical application of stem cell-based tissue engineering for the treatment of IDD.

## DATA AVAILABILITY STATEMENT

The raw data supporting the conclusions of this article will be made available by the authors, without undue reservation.

## ETHICS STATEMENT

The animal study was reviewed and approved by the Ethics Committee of Naval Medical University.

## AUTHOR CONTRIBUTIONS

LY, YL, and JW and performed the experimental work and contributed equally in this work. SW, YL, and JY helped in methods and analysis. All this work was under the guidance of XY and WW. All authors reviewed and approved the manuscript.

## FUNDING

This work was supported by a grant from the National Key R and D Program of China (2020YFC2008404), the National Natural Science Foundation of China (No. 82102605), and the Shanghai Sailing Program (19YF1448400).

## SUPPLEMENTARY MATERIAL

The Supplementary Material for this article can be found online at: https://www.frontiersin.org/articles/10.3389/fbioe.2021.807883/full#supplementary-material

## REFERENCES

Akhmanova, M., Osidak, E., Domogatsky, S., Rodin, S., and Domogatskaya, A. (2015). Physical, Spatial, and Molecular Aspects of Extracellular Matrix of *In Vivo* Niches and Artificial Scaffolds Relevant to Stem Cells Research. *Stem Cell Int* 2015, 167025. doi:10.1155/2015/167025

Benneker, L., Andersson, G., Iatridis, J., Sakai, D., Härtl, R., Ito, K., et al. (2014). Cell Therapy for Intervertebral Disc Repair: Advancing Cell Therapy from Bench to Clinics. *eCM* 27s, 5–11. doi:10.22203/ecm.v027sa02

Butterfield, K. C., Conovaloff, A. W., and Panitch, A. (2011). Development of Affinity-Based Delivery of NGF from a Chondroitin Sulfate Biomaterial. *Biomatter* 1 (2), 174–181. doi:10.4161/biom.18791

Chan, V., Raman, R., Cvetkovic, C., and Bashir, R. (2013). Enabling Microscale and Nanoscale Approaches for Bioengineered Cardiac Tissue. *ACS Nano* 7 (3), 1830–1837. doi:10.1021/nn401098c

Cheng, C. W., Solorio, L. D., and Alsberg, E. (2014). Decellularized Tissue and Cell-Derived Extracellular Matrices as Scaffolds for Orthopaedic Tissue Engineering. *Biotechnol. Adv.* 32 (2), 462–484. doi:10.1016/j.biotechadv.2013.12.012

Chua, I. L. S., Kim, H.-W., and Lee, J. H. (2016). Signaling of Extracellular Matrices for Tissue Regeneration and Therapeutics. *Tissue Eng. Regen. Med.* 13 (1), 1–12. doi:10.1007/s13770-016-9075-0

Chung, C., and Burdick, J. A. (2008). Engineering Cartilage Tissue. *Adv. Drug Deliv. Rev.* 60 (2), 243–262. doi:10.1016/j.addr.2007.08.027

Cieza, A., Causey, K., Kamenov, K., Hanson, S. W., Chatterji, S., and Vos, T. (2021). Global Estimates of the Need for Rehabilitation Based on the Global Burden of Disease Study 2019: a Systematic Analysis for the Global Burden of Disease Study 2019. *Lancet* 396 (10267), 2006–2017. doi:10.1016/S0140-6736(20)32340-0

Collin, E. C., Grad, S., Zeugolis, D. I., Vinatier, C. S., Clouet, J. R., Guicheux, J. J., et al. (2011). An Injectable Vehicle for Nucleus Pulposus Cell-Based Therapy. *Biomaterials* 32 (11), 2862–2870. doi:10.1016/j.biomaterials.2011.01.018

Dupont, S. (2016). Role of YAP/TAZ in Cell-Matrix Adhesion-Mediated Signalling and Mechanotransduction. *Exp. Cel Res.* 343 (1), 42–53. doi:10.1016/j.yexcr.2015.10.034

Engler, A. J., Sen, S., Sweeney, H. L., and Discher, D. E. (2006). Matrix Elasticity Directs Stem Cell Lineage Specification. *Cell* 126 (4), 677–689. doi:10.1016/j.cell.2006.06.044

Eyring, E. J. (1969). 3 the Biochemistry and Physiology of the Intervertebral Disk. *Clin. Orthopaedics Relat. Res.* 67, 16–28. doi:10.1097/00003086-196911000-00004

Fontana, G., See, E., and Pandit, A. (2015). Current Trends in Biologics Delivery to Restore Intervertebral Disc Anabolism. *Adv. Drug Deliv. Rev.* 84, 146–158. doi:10.1016/j.addr.2014.08.008

Fujii, K., Lai, A., Korda, N., Hom, W. W., Evashwick-Rogler, T. W., Nasser, P., et al. (2020). *Ex-vivo* Biomechanics of Repaired Rat Intervertebral Discs Using Genipin Crosslinked Fibrin Adhesive Hydrogel. *J. Biomech.* 113, 110100. doi:10.1016/j.jbiomech.2020.110100

Geiger, B., Bershadsky, A., Pankov, R., and Yamada, K. M. (2001). Transmembrane Crosstalk between the Extracellular Matrix and the Cytoskeleton. *Nat. Rev. Mol. Cel Biol* 2 (11), 793–805. doi:10.1038/35099066

Han, B., Zhu, K., Li, F. C., Xiao, Y. X., Feng, J., Shi, Z. L., et al. (2008). A Simple Disc Degeneration Model Induced by Percutaneous Needle Puncture in the Rat Tail. *Spine (Phila Pa 1976)* 33 (18), 1925–1934. doi:10.1097/BRS.0b013e31817c64a9

Henry, N., Clouet, J., Le Bideau, J., Le Visage, C., and Guicheux, J. (2018). Innovative Strategies for Intervertebral Disc Regenerative Medicine: From Cell Therapies to Multiscale Delivery Systems. *Biotechnol. Adv.* 36 (1), 281–294. doi:10.1016/j.biotechadv.2017.11.009

Hughes, P. C., and Tanner, J. M. (1970). The Assessment of Skeletal Maturity in the Growing Rat. *J. Anat.* 106 (Pt 2), 371–402.

Iatridis, J. C., Weidenbaum, M., Setton, L. A., and Mow, V. C. (1996). Is the Nucleus Pulposus a Solid or a Fluid? Mechanical Behaviors of the Nucleus Pulposus of the Human Intervertebral Disc. *Spine* 21 (10), 1174–1184. doi:10.1097/00007632-199605150-00009

Kim, M. S., Jun, I., Shin, Y. M., Jang, W., Kim, S. I., and Shin, H. (2010). The Development of Genipin-Crosslinked Poly(caprolactone) (PCL)/gelatin Nanofibers for Tissue Engineering Applications. *Macromol. Biosci.* 10 (1), 91–100. doi:10.1002/mabi.200900168

Lama, P., Tewari, J., Adams, M. A., and Le Maitre, C. (2021). Degenerative Physiochemical Events in the Pathological Intervertebral Disc. *Histol. Histopathol* 1, 18395. doi:10.14670/HH-18-395

Leyva-Gómez, G., Piñón-Segundo, E., Mendoza-Muñoz, N., Zambrano-Zaragoza, M. L., Mendoza-Elvira, S., Quintanar-Guerrero, D., et al. (2018). Approaches in Polymeric Nanoparticles for Vaginal Drug Delivery: A Review of the State of the Art. *Int. J. Mol. Sci.* 19 (6). 1549. doi:10.3390/ijms19061549

Li, B., Yang, Y., Wang, L., and Liu, G. (2021). Stem Cell Therapy and Exercise for Treatment of Intervertebral Disc Degeneration. *Stem Cell Int* 2021, 7982333. doi:10.1155/2021/7982333

Lipson, S. J., and Muir, H. (19801981). 1980 Volvo Award in Basic Science. Proteoglycans in Experimental Intervertebral Disc degenerationProteoglycans in Experimental Intervertebral Disc Degeneration. *Spine (Phila Pa 1976)* 6 (3), 194–210. doi:10.1097/00007632-198105000-00002

Liu, L., Liu, M., Xie, D., Liu, X., and Yan, H. (2021). Role of the Extracellular Matrix and YAP/TAZ in Cell Reprogramming. *Differentiation* 122, 1–6. doi:10.1016/j.diff.2021.11.001

Loebel, C., Mauck, R. L., and Burdick, J. A. (2019). Local Nascent Protein Deposition and Remodelling Guide Mesenchymal Stromal Cell Mechanosensing and Fate in Three-Dimensional Hydrogels. *Nat. Mater.* 18 (8), 883–891. doi:10.1038/s41563-019-0307-6

Ma, B., Wang, X., Wu, C., and Chang, J. (2014). Crosslinking Strategies for Preparation of Extracellular Matrix-Derived Cardiovascular Scaffolds. *Regenerative Biomater.* 1 (1), 81–89. doi:10.1093/rb/rbu009

Ma, J., He, Y., Liu, X., Chen, W., Wang, A., Lin, C.-Y., et al. (2018). A Novel Electrospun-Aligned Nanoyarn/three-Dimensional Porous Nanofibrous Hybrid Scaffold for Annulus Fibrosus Tissue Engineering. *Ijn* 13, 1553–1567. doi:10.2147/ijn.s143990

Mano, J. F., Silva, G. A., Azevedo, H. S., Malafaya, P. B., Sousa, R. A., Silva, S. S., et al. (2007). Natural Origin Biodegradable Systems in Tissue Engineering and Regenerative Medicine: Present Status and Some Moving Trends. *J. R. Soc. Interf.* 4 (17), 999–1030. doi:10.1098/rsif.2007.0220

Mercuri, J. J., Patnaik, S., Dion, G., Gill, S. S., Liao, J., and Simionescu, D. T. (2013). Regenerative Potential of Decellularized Porcine Nucleus Pulposus Hydrogel

Scaffolds: Stem Cell Differentiation, Matrix Remodeling, and Biocompatibility Studies. *Tissue Eng. Part. A.* 19 (7-8), 952–966. doi:10.1089/ten.TEA.2012.0088

Moya, I. M., and Halder, G. (2019). Hippo-YAP/TAZ Signalling in Organ Regeneration and Regenerative Medicine. *Nat. Rev. Mol. Cel Biol* 20 (4), 211–226. doi:10.1038/s41580-018-0086-y

Muzzarelli, R. A. A., El Mehtedi, M., Bottegoni, C., and Gigante, A. (2016). Physical Properties Imparted by Genipin to Chitosan for Tissue Regeneration with Human Stem Cells: A Review. *Int. J. Biol. Macromolecules* 93 (Pt B), 1366–1381. doi:10.1016/j.ijbiomac.2016.03.075

Muzzarelli, R., El Mehtedi, M., Bottegoni, C., Aquili, A., and Gigante, A. (2015). Genipin-Crosslinked Chitosan Gels and Scaffolds for Tissue Engineering and Regeneration of Cartilage and Bone. *Mar. Drugs* 13 (12), 7314–7338. doi:10.3390/md13127068

O'Halloran, D. M., and Pandit, A. S. (2007). Tissue-engineering Approach to Regenerating the Intervertebral Disc. *Tissue Eng.* 13 (8), 1927–1954. doi:10.1089/ten.2005.0608

Qiu, J., Li, J., Wang, G., Zheng, L., Ren, N., Liu, H., et al. (2013). *In Vitro* investigation on the Biodegradability and Biocompatibility of Genipin Cross-Linked Porcine Acellular Dermal Matrix with Intrinsic Fluorescence. *ACS Appl. Mater. Inter.* 5 (2), 344–350. doi:10.1021/am302272k

Rousseau, M. A., Ulrich, J. A., Bass, E. C., Rodriguez, A. G., Liu, J. J., and Lotz, J. C. (2007). Stab Incision for Inducing Intervertebral Disc Degeneration in the Rat. *Spine (Phila Pa 1976)* 32 (1), 17–24. doi:10.1097/01.brs.0000251013.07656.45

Setton, L. A., and Chen, J. (2004). Cell Mechanics and Mechanobiology in the Intervertebral Disc. *Spine* 29 (23), 2710–2723. doi:10.1097/01.brs.0000146050.57722.2a

Sung, H.-W., Huang, R.-N., Huang, L. L. H., and Tsai, C.-C. (1999). *In Vitro* evaluation of Cytotoxicity of a Naturally Occurring Cross-Linking Reagent for Biological Tissue Fixation. *J. Biomater. Sci. Polym. Edition* 10 (1), 63–78. doi:10.1163/156856299x00289

Tang, G., Zhou, B., Li, F., Wang, W., Liu, Y., Wang, X., et al. (2020). Advances of Naturally Derived and Synthetic Hydrogels for Intervertebral Disk Regeneration. *Front. Bioeng. Biotechnol.* 8, 745. doi:10.3389/fbioe.2020.00745

Tao, Y., Zhou, X., Liu, D., Li, H., Liang, C., Li, F., et al. (2016). Proportion of Collagen Type II in the Extracellular Matrix Promotes the Differentiation of Human Adipose-Derived Mesenchymal Stem Cells into Nucleus Pulposus Cells. *Biofactors* 42 (2), 212–223. doi:10.1002/biof.1266

Tapp, H., Deepe, R., Ingram, J. A., Kuremsky, M., Hanley, E. N., and Gruber, H. E. (2008). Adipose-derived Mesenchymal Stem Cells from the Sand Rat: Transforming Growth Factor Beta and 3D Co-culture with Human Disc Cells Stimulate Proteoglycan and Collagen Type I Rich Extracellular Matrix. *Arthritis Res. Ther.* 10 (4), R89. doi:10.1186/ar2473

Virdi, J. K., and Pethe, P. (2021). Biomaterials Regulate Mechanosensors YAP/TAZ in Stem Cell Growth and Differentiation. *Tissue Eng. Regen. Med.* 18 (2), 199–215. doi:10.1007/s13770-020-00301-4

Wachs, R. A., Hoogenboezem, E. N., Huda, H. I., Xin, S., Porvasnik, S. L., and Schmidt, C. E. (2017). Creation of an Injectable *In Situ* Gelling Native Extracellular Matrix for Nucleus Pulposus Tissue Engineering. *Spine J.* 17 (3), 435–444. doi:10.1016/j.spinee.2016.10.022

Wang, H., Zhou, Y., Huang, B., Liu, L. T., Liu, M. H., Wang, J., et al. (2014). Utilization of Stem Cells in Alginate for Nucleus Pulposus Tissue Engineering. *Tissue Eng. Part. A.* 20 (5-6), 908–920. doi:10.1089/ten.TEA.2012.0703

Wollensak, G., and Spoerl, E. (2004). Collagen Crosslinking of Human and Porcine Sclera. *J. Cataract Refract Surg.* 30 (3), 689–695. doi:10.1016/j.jcrs.2003.11.032

Yan, L.-P., Wang, Y.-J., Ren, L., Wu, G., Caridade, S. G., Fan, J.-B., et al. (2010). Genipin-cross-linked Collagen/chitosan Biomimetic Scaffolds for Articular Cartilage Tissue Engineering Applications. *J. Biomed. Mater. Res.* 95A (2), 465–475. doi:10.1002/jbm.a.32869

Ye, K., Cao, L., Li, S., Yu, L., and Ding, J. (2016). Interplay of Matrix Stiffness and Cell-Cell Contact in Regulating Differentiation of Stem Cells. *ACS Appl. Mater. Inter.* 8 (34), 21903–21913. doi:10.1021/acsami.5b09746

Ye, K., Wang, X., Cao, L., Li, S., Li, Z., Yu, L., et al. (2015). Matrix Stiffness and Nanoscale Spatial Organization of Cell-Adhesive Ligands Direct Stem Cell Fate. *Nano Lett.* 15 (7), 4720–4729. doi:10.1021/acs.nanolett.5b01619

Yin, H., Wang, Y., Sun, X., Cui, G., Sun, Z., Chen, P., et al. (2018). Functional Tissue-Engineered Microtissue Derived from Cartilage Extracellular Matrix for Articular Cartilage Regeneration. *Acta Biomater.* 77, 127–141. doi:10.1016/j.actbio.2018.07.031

Yoo, J. S., Kim, Y. J., Kim, S. H., and Choi, S. H. (2011). Study on Genipin: a New Alternative Natural Crosslinking Agent for Fixing Heterograft Tissue. *Korean J. Thorac. Cardiovasc. Surg.* 44 (3), 197–207. doi:10.5090/kjtcs.2011.44.3.197

Young, D. A., Ibrahim, D. O., Hu, D., and Christman, K. L. (2011). Injectable Hydrogel Scaffold from Decellularized Human Lipoaspirate. *Acta Biomater.* 7 (3), 1040–1049. doi:10.1016/j.actbio.2010.09.035

Yu, L., Sun, Z. J., Tan, Q. C., Wang, S., Wang, W. H., Yang, X. Q., et al. (2020). Thermosensitive Injectable Decellularized Nucleus Pulposus Hydrogel as an Ideal Biomaterial for Nucleus Pulposus Regeneration. *J. Biomater. Appl.* 35, 182–192. doi:10.1177/0885328220921328

Zhou, X., Tao, Y., Chen, E., Wang, J., Fang, W., Zhao, T., et al. (2018). Genipin-cross-linked Type II Collagen Scaffold Promotes the Differentiation of Adipose-Derived Stem Cells into Nucleus Pulposus-like Cells. *J. Biomed. Mater. Res.* 106 (5), 1258–1268. doi:10.1002/jbm.a.36325

Zhou, X., Wang, J., Fang, W., Tao, Y., Zhao, T., Xia, K., et al. (2018). Genipin Cross-Linked Type II Collagen/chondroitin Sulfate Composite Hydrogel-like Cell Delivery System Induces Differentiation of Adipose-Derived Stem Cells and Regenerates Degenerated Nucleus Pulposus. *Acta Biomater.* 71, 496–509. doi:10.1016/j.actbio.2018.03.019

Zhu, S.-Q., Zheng, L.-Y., Pan, A.-P., Yu, A.-Y., Wang, Q.-M., and Xue, A.-Q. (2016). The Efficacy and Safety of Posterior Scleral Reinforcement Using Genipin Cross-Linked Sclera for Macular Detachment and Retinoschisis in Highly Myopic Eyes. *Br. J. Ophthalmol.* 100 (11), 1470–1475. doi:10.1136/bjophthalmol-2015-308087

Zuk, P. A., Zhu, M., Mizuno, H., Huang, J., Futrell, J. W., Katz, A. J., et al. (2001). Multilineage Cells from Human Adipose Tissue: Implications for Cell-Based Therapies. *Tissue Eng.* 7 (2), 211–228. doi:10.1089/107632701300062859

**Conflict of Interest:** The authors declare that the research was conducted in the absence of any commercial or financial relationships that could be construed as a potential conflict of interest.

**Publisher's Note:** All claims expressed in this article are solely those of the authors and do not necessarily represent those of their affiliated organizations, or those of the publisher, the editors, and the reviewers. Any product that may be evaluated in this article, or claim that may be made by its manufacturer, is not guaranteed or endorsed by the publisher.

frontiers in Bioengineering and Biotechnology

ORIGINAL RESEARCH
published: 19 January 2022
doi: 10.3389/fbioe.2021.829136

# Bone Mesenchymal Stem Cell-Derived sEV-Encapsulated Thermosensitive Hydrogels Accelerate Osteogenesis and Angiogenesis by Release of Exosomal miR-21

*Di Wu[1†], Hao Qin[2†], Zixuan Wang[3†], Mingzhao Yu[1], Zhe Liu[1], Hao Peng[1], Leilei Liang[4*], Changqing Zhang[1*] and Xiaojuan Wei[5*]*

[1]Department of Orthopedic Surgery, Shanghai Jiao Tong University Affiliated Shanghai Sixth People's Hospital, Shanghai, China, [2]Center for Reproductive Medicine, Department of Obstetrics and Gynecology, Peking University Third Hospital, Beijing, China, [3]Department of Mechanical Engineering, Tsinghua University, Beijing, China, [4]National Cancer Center, Chinese Academy of Medical Sciences and Peking Union Medical College, Beijing, China, [5]Institute of Microsurgery on Extremities, Shanghai Jiao Tong University Affiliated, Shanghai Sixth People's Hospital, Shanghai, China

OPEN ACCESS

**Edited by:**
Zongliang Wang,
Changchun Institute of Applied Chemistry (CAS), China

**Reviewed by:**
Pingping Han,
The University of Queensland, Australia
Xiaoxiao Cai,
Sichuan University, China

***Correspondence:**
Xiaojuan Wei
xjweish@126.com
Changqing Zhang
zhangcq@sjtu.edu.cn
Leilei Liang
liangleilei10006@163.com

†These authors have contributed equally to this work

**Specialty section:**
This article was submitted to Biomaterials, a section of the journal Frontiers in Bioengineering and Biotechnology

**Received:** 05 December 2021
**Accepted:** 27 December 2021
**Published:** 19 January 2022

**Citation:**
Wu D, Qin H, Wang Z, Yu M, Liu Z, Peng H, Liang L, Zhang C and Wei X (2022) Bone Mesenchymal Stem Cell-Derived sEV-Encapsulated Thermosensitive Hydrogels Accelerate Osteogenesis and Angiogenesis by Release of Exosomal miR-21. Front. Bioeng. Biotechnol. 9:829136. doi: 10.3389/fbioe.2021.829136

Angiogenesis has been recognized to play an essential role in remodeling new bone (osteogenesis). Small extracellular vesicles (sEVs), the endogenously secreted nanovesicles by cells, exhibit great potential in the regeneration of bone defects and the realization of cell-free therapy. Chitosan, a natural polysaccharide, can form a thermosensitive injectable hydrogel through the addition of β-glycerophosphate. Herein, we developed injectable thermosensitive hydrogel-encapsulated sEVs derived from bone mesenchymal stem cells, which significantly prolonged delivery and release and synergistically enhanced bone regeneration. sEVs were isolated and characterized, and the physicochemical properties, release kinetics, and biocompatibility of the hydrogels were analyzed. *In vitro* experiments were performed to investigate osteogenic differentiation, cell proliferation and migration, and tube formation. Thereafter, sEVs were added to the chitosan/β-glycerophosphate hydrogel (sEV@CS/β-GP composite) to repair calvarial defects in rats. The results showed that sEV-loaded hydrogels were biocompatible, exhibiting excellent thermosensitive properties and enhancing bone regeneration. Furthermore, mechanistic studies revealed that exosomal miR-21 targeted SPRY2, thereby promoting angiogenesis. Our study provides new insights on the repair of bone defects with multifunctional controlled-sEV-release hydrogels, which shows great potential in the repair of tissues in the future.

**Keywords: thermosensitive hydrogel, small extracellular vesicle, release, bone regeneration, angiogenesis**

## INTRODUCTION

Bone defects often arise from trauma, infections, tumors, congenital malformations, or skeletal diseases, and they can heal slowly or not at all, thereby leading to life-long disabilities (Zaidi, 2007; Huey et al., 2012). Currently, the "gold standard" in the treatment of bone defects is autologous and allogeneic transplantation (Crane et al., 1995; Lopes et al., 2018). In recent years, the introduction of a variety of reconstructive materials has provided new tools for orthopedic surgeons; however, the

most important aspect of bone regeneration still lies in the identification of safe, effective, and aesthetic means for filling structural defects (Kawai et al., 2011; Bose et al., 2012; Zhang et al., 2019). Several studies on the modulatory processes of bone healing have demonstrated that angiogenesis plays an important role in bone regeneration. As such, bone tissue engineering combines the use of different cells, biological factors, scaffolds, and bone substitutes to improve osteogenic and angiogenic activities (Langer and Vacanti, 1993; Khademhosseini and Langer, 2016).

The use of bone mesenchymal stem cells (BMSCs) is an attractive approach to promote osteogenesis and angiogenesis in patients with bone defects (Fu et al., 2019). BMSCs can be easily harvested from donors, maintain osteogenic properties, and offer a low incidence of graft-versus-host disease. However, the direct transplantation of BMSCs associates with several challenges such as time- and dose-requirements, the low survival rate of locally transplanted cells, tumor formation, and immune rejection (Sissung and Figg, 2020). In addition, the role of BMSCs in tissue regeneration involves paracrine mechanisms, which stimulate immunomodulatory pathways, and small extracellular vesicles (sEVs) have been implicated in these processes (Li et al., 2018).

sEVs are membranous structures (diameter, 50–150 nm), namely, exosomes and microvesicles that are released from cells into the extracellular environment, and they participate in cell-to-cell communication (Tkach and Thery, 2016; van Niel et al., 2018; Xu et al., 2018). sEVs have important roles in the protection of their contents, such as mRNAs, miRNAs, and proteins, from degradation, as well as in the delivery of their contents to recipient cells, which are needed for cell function (He et al., 2018; Kalluri and LeBleu, 2020). sEVs possess stem cell-like pro-regenerative properties, and the application of sEVs may prevent many of the adverse effects of stem cell transplantation therapy. More importantly, sEVs do not contain MHC-I or MHC-II proteins; as such, they overcome the disadvantages of stem cell transplantation therapy and seldom induce overt immune reactions (Roccaro et al., 2013). Previous studies have demonstrated that BMSC-derived sEVs (BMSC-sEVs) exhibit similar or identical therapeutic roles to those of BMSCs used in the treatment of bone defects, and miRNAs may induce osteoblast differentiation and bone formation (Tan et al., 2020; Wang and Thomsen, 2021). For example, Liu et al. reported that BMSC-sEVs expressing miR-130a can stimulate the PTEN/AKT signaling pathway during angiogenesis and bone remodeling (Liu et al., 2019), whereas Liao et al. demonstrated that BMSC-sEVs expressing miRNA-122–5p can promote osteoblast proliferation during osteonecrosis of the femoral head (Liao et al., 2019b). Taken together, these findings suggest that exploring the underlying mechanisms of bone regeneration induced by exosomal miRNAs may improve our understanding of osteogenesis and angiogenesis, thereby promoting the development of new treatment strategies.

Recently, hydrogels have generated considerable interest in the field of bone repair, as they involve a minimally invasive injection and form into a solid-like object *in situ* (Ingavle et al., 2019; Kocak et al., 2020). Polymer-based hydrogels have been used in tissue repair due to their structural uniformity, biodegradability, high permeability, biocompatibility, improved mechanical strength, and application ease (Hoffman et al., 2013). Chitosan (CS), a type of endogenous polysaccharide, has been widely used due to its many properties, including antibacterial activity and exogenous biomineralization capability (Petit et al., 2020). Among chitosan-based hydrogels, chitosan (CS)/β-glycerophosphate (β-GP) hydrogels have received much interest because of their thermosensitive properties and injectability (Wasupalli and Verma, 2020). Thermosensitive hydrogels exist as liquids at room temperature but form gels at body temperature, that is, most thermally-responsive hydrogels are soluble below a specific temperature, which is known as the lower critical solution temperature (LCST), but they are insoluble above this temperature (Bhattarai et al., 2010).

To our knowledge, the effects of sEV-loaded CS/β-GP hydrogels on angiogenesis, which is critical for bone regeneration, have not yet been investigated (Wang et al., 2020). Here, an effort was made to fabricate a novel type of injectable hydrogel system (sEV@CS/β-GP composite) consisting of the CS/β-GP hydrogel and sEVs that was capable of forming a gel *in situ* at body temperature. The sEVs were released in a sustained and controlled manner, and the hydrogel was gradually degraded and internalized by human umbilical vein endothelial cells (HUVECs) and human BMSCs. Furthermore, the absorbed sEVs exhibited osteogenic and angiogenic properties. Previous studies have also reported that angiogenic activity was also promoted by miR-21 overexpression in BMSC-sEVs (Wu et al., 2020; Li G.-Q. et al., 2021; Zhang et al., 2021). In summary, sEV@CS/β-GP hydrogels can promote bone regeneration, which was likely mediated by miR-21 overexpression. These findings provide new insights on a promising therapeutic strategy for cell-free bone repair.

# MATERIALS AND METHODS

## Cell Culture

BMSCs, HUVECs, and HEK-293 cells were obtained from the cell bank of the Chinese Academy of Medical Sciences (Beijing, China). BMSCs were cultured in basal media (Cyagen Biosciences, Santa Clara, CA, United States), and HUVECs and HEK-293 cells were cultured in high-glucose Dulbecco's modified Eagle's medium (DMEM, Gibco BRL, Grand Island, NY, United States) supplemented with 10% fetal bovine serum (FBS) and 1% penicillin–streptomycin.

## Isolation and Characterization of sEVs

### sEV Isolation and Purification

sEVs were isolated and purified from BMSC supernatants by ultracentrifugation as previously described (Colombo et al., 2014). Before isolation, BMSCs were incubated for 48 h in medium supplemented with 10% sEV-depleted FBS (Umibio, Shanghai, China). The supernatant was collected and centrifuged at 300 × g for 10 min, 2000 × g for 20 min, and 10,000 × g for 30 min to discard the cell debris, and centrifuged at 100,000 × g for 70 min to collect the sEVs. The pelleted sEVs were washed two

times with PBS and centrifuged at 110,000 × g for 70 min to remove the contaminating proteins. All procedures were performed at 4°C, and the sEVs were resuspended in PBS.

### sEV Identification and Internalization

The size distribution of sEVs was determined by nanoparticle tracking analysis (NTA) with the NanoSight NS500 system (Malvern Instruments, Malvern, United Kingdom), and the morphology of sEVs was observed by transmission electron microscopy (TEM, Hitachi, Tokyo, Japan) as previously described (Wu et al., 2021). Western blotting was used to detect the expression of sEV-specific surface markers, including CD63, CD81, and TSG101.

The uptake of sEVs by BMSCs and HUVECs was examined by labeling sEVs with the fluorescent dye PKH26 or PKH67 (Sigma-Aldrich, Darmstadt, Germany), according to the manufacturer's instructions, which were then incubated with BMSCs or HUVECs at 37°C for 24 h. Subsequently, the cells were fixed with 4% paraformaldehyde, stained with DAPI for 10 min, and observed by confocal microscopy (Nikon, Tokyo, Japan).

## Impact of sEVs on Osteogenic Differentiation

### Alizarin Red Staining (ARS) and Alkaline Phosphatase (ALP) Activity

The osteogenic differentiation of BMSCs was carried out 24 h after the incubation of sEVs or transfection of miRNA mimic or inhibitor. Briefly, the medium was replaced with osteogenic differentiation medium (Cyagen Biosciences), which was refreshed every 72 h, supplemented with PBS (200 μL) or different concentrations of BMSC-sEVs (50 or 100 μg/ml). To assess mineralization, ARS was performed on day 14 after osteoinduction. Cells were stained with 2% ARS solution (Sigma-Aldrich) for 10 min and then washed with distilled water. To quantitatively determine matrix calcification, the cells were de-stained with 10% cetylpyridinium chloride in 10 mM sodium phosphate for 30 min, and the absorbance was measured at 562 nm.

To assess ALP activity, the ALP assay kit (Beyotime, Jiangsu, China) was used. BMSCs were cultured in osteogenic differentiation medium and lysed on days 7 and 14 with 0.1% Triton X-100 in Tris-HCl for 2 h at 4°C. *p*-Nitrophenyl phosphate was added to the cell lysates, and the samples were incubated at 37°C for 15 min. The normalized ALP activity was obtained by determining the total intracellular protein concentration with the Pierce BCA Protein Assay kit (Thermo Fisher Scientific, Waltham, MA, United States).

## Impact of sEVs on Angiogenesis

### Cell Proliferation Assay

Three groups were prepared according to the BMSC-sEVs concentration (0, 50, and 100 μg/ml), with each group consisting of quadruplicate wells. HUVECs ($5 \times 10^3$ cells/well) were inoculated into 96-well plates and treated with the different BMSC-sEVs concentrations. The medium was changed every 2 days. To assess cell viability, the Cell Counting kit-8 (CCK-8; Dojindo, Tokyo, Japan) was used. On days 1, 3, 5, and 7, the absorbance was measured at 450 nm, and the growth curve was generated. CCK8 assay was also performed to test the promoting effect of gradient concentrations (400, 200, 100, 50, 25, and 0 μg/ml) of sEVs on cell proliferation.

### Cell Migration Assay

HUVECs ($1 \times 10^4$ cells/well) were resuspended in serum-free medium and seeded into the upper chamber of Corning 8-μm pore size transwell units (Corning, NY, United States) that were housed in 24-well plates. The lower chamber was filled with DMEM supplemented with 10% sEV-depleted FBS that was pre-incubated with PBS (200 μL), BMSC-sEVs (50 μg/ml), or BMSC-sEVs (100 μg/ml). The plates were incubated at 37°C for 24 h. Thereafter, the cells attached to the upper surface of the filter membranes were removed, and those attached to the lower surface were stained with 0.1% crystal violet. Cell migration was observed by light microscopy (Leica, Solms, Germany).

### Tube Formation Assay

The *in vitro* angiogenesis assay was conducted using Matrigel basement membrane matrix (BD Biosciences, San Jose, CA, United States), according to the manufacturer's instructions. Briefly, Matrigel was thawed overnight at 4°C and added to 96-well plates (50 μL/well), which were then incubated at 37°C. Thereafter, HUVECs ($2 \times 10^4$ cells/well) were resuspended in complete medium supplemented with 10% sEV-depleted FBS pre-incubated with PBS (10 μL), BMSC-sEVs (50 μg/ml), or BMSC-sEVs (100 μg/ml). The plates were incubated at 37°C for 6 h, and tube formation was observed by inverted microscopy. Five fields from each well were randomly selected, and the total tube length was measured with ImageJ software (National Institutes of Health, Bethesda, MD, United States).

### Quantitative Real-Time PCR (RT-qPCR) Analysis

TRIzol (Invitrogen, Carlsbad, CA, United States) was used to isolate total RNA, and the Revert Aid First-Strand cDNA Synthesis kit (Vazyme, Jiangsu, China) was used to reverse transcribe RNA, according to the manufacturer's instructions. The sEV RNA Purification kit (Umibio, Shanghai, China) was used to extract miRNA, and the SYBR Green microRNA Assay kit (Applied Biosystems, Foster City, CA, United States) was used to synthesize cDNA. Real-time PCR was performed with the ABI PRISM 7900 H T system using the SYBR Green Master-Mix kit (Applied Biosystems). GAPDH and U6 were used to normalize mRNA and miRNA expression levels, respectively, and the $2^{-\Delta\Delta Ct}$ method was used to quantify the relative expression levels. All primer sequences are listed in **Table 1**.

### Western Blotting

The total protein concentrations in cells and sEVs were determined using the BCA Protein Assay kit. Proteins were separated by 10% SDS-PAGE, transferred to PVDF membranes, and probed with the appropriate primary and secondary antibodies. Immunoreactive bands were visualized using enhanced chemiluminescence reagents (Thermo Fisher Scientific) and quantified using ImageJ software. Primary

**TABLE 1 |** List of primers used.

| Gene | Primer sequence, 5′–3′ | |
|---|---|---|
| | Forward | Reverse |
| *OCN* | CACTCCTCGCCCTATTGGC | CCCTCCTGCTTGGACACAAAG |
| *OPN* | GAAGTTTCGCAGACCTGACAT | GTATGCACCATTCAACTCCTCG |
| *Runx2* | TCAACGATCTGAGATTTGTGGG | GGGGAGGATTTGTGAAGACGG |
| *VEGF* | AGCGCCGAAGTCCAGAAAAC | AGGGTCTCGATTGGATGGCA |
| *bFGF* | AGAAGAGCGACCCTCACATCA | CGGTTAGCACACACTCCTTTG |
| *ANG-1* | AGCGCCGAAGTCCAGAAAAC | TACTCTCACGACAGTTGCCAT |
| *GAPDH* | CAGGGCTGCTTTTAACTCTGG | TGGGTGGAATCATATTGGAACA |
| *U6* | TGGAACGCTTCACGAATTTGCG | GGAACGATACAGAGAAGATTAGC |

antibodies against CD63, CD81, TSG101, Calnexin, OCN, OPN, Runx2, VEGF, bFGF, ANG-1, and CD31 were obtained from Abcam (Cambridge, United Kingdom).

## Preparation and Characterization of Hydrogels

### Hydrogel Preparation

Thermosensitive CS/β-GP hydrogels were prepared as previously described (Wu et al., 2019). Briefly, 0.2 g of CS (degree of deacetylation, 95%; Sigma-Aldrich) was added to an acetic acid solution (0.1 mol/L, 10 ml) to obtain the 2% (w/v) CS solution, followed by the dropwise addition of 1 ml of 56% (w/v) β-GP solution (Merck, Darmstadt, Germany) while stirring.

### Thermosensitivity

The sol-to-gel transition behavior of the hydrogels at 37 °C was determined by the test tube inversion method (Park et al., 2012), which uses flow (sol) or no-flow (gel) criteria to assess flow when sample tubes are inverted for 30 s at a controlled temperature. The gelation time was determined by inverting the vial every 30 s. Five independent duplicate tests were performed. The gelation time was recorded, and the average value was used.

### Scanning Electron Microscopy (SEM)

Hydrogels were frozen at −80°C for 24 h and lyophilized at −40°C for 48 h in a freeze-dryer. Thereafter, the samples were cut with a sharp blade to obtain cross-sections and sputter-coated with a gold-platinum layer. Cross-sections were observed by SEM (XL30, PHILIPS, Eindhoven, Netherlands). The pore size was analyzed by ImageJ software, and the average pore size was calculated based on 50 pores in five randomly selected areas per sample.

### Viscosity

A rheometer (Kinexus Ultra, Malvern, United Kingdom) equipped with a parallel plate with a diameter of 20 mm and a gap distance of 0.5 mm was used to measure the rheological properties of the hydrogel solution. The variations in the storage (G′) and loss (G″) moduli of the samples were measured under constant strain (0.1%) and frequency (1.0 Hz). The hydrogel solution was added to the parallel plate using a temperature range of 25–45°C and a heating rate of 0.5°C/min.

### Swelling and Degradation Behaviors

Hydrogels (n = 3) were dried, weighed ($W_d$), and rehydrated in PBS for 24 h at 37°C. Samples were removed from PBS and weighed again ($W_s$) at different time points after blotting the surface with filter paper (Yuan et al., 2019). The swelling ratio was calculated as follows $(W_s - W_d)/W_d \times 100\%$

The degradation of the hydrogels was reflected in the weight loss, which was also studied in PBS at 37°C. At given time points (days 1, 4, 7, 10, 14, and 21) after blotting the surface with filter paper, the hydrogel weight was measured. The weight loss ratio was defined as follows $(W_0 - W_t)/W_0 \times 100\%$, where $W_0$ is the initial weight of the sample, and $W_t$ is the weight of the sample at a specific time point.

### Mechanical Properties Test

The mechanical properties of the hydrogels were determined with a universal mechanical analyzer (Instron, Norwood, MA, United States). Photo-crosslinked cylindrical hydrogels (n = 4) with a height of 5 mm and a diameter of 10 mm were placed on the lower plate at a speed of 1 mm/min, and the compressive force was recorded until the hydrogels were deformed by the upper plate.

### Ability of sEVs/Gel Composites to Release sEVs

sEVs ($1 \times 10^8$ particles/mL) were added to the composited hydrogels, and the release of sEVs from hydrogels was measured using the BCA Protein Assay kit. Briefly, the hydrogels were immersed in PBS in 24-well plates. At specific time points, the liquid on the surface of the hydrogels was collected, and the PBS in the wells was replaced. sEVs release was quantified and expressed as a percentage. Data were presented as mean ± SD of three replicates.

## *In Vivo* Animal Experiments

### Surgical Procedures

All procedures were approved by the Animal Research Committee of Peking Union Medical College Hospital (XHDW-2020-040), and all surgical procedures were performed in a sterile environment. Rats were anesthetized with an intraperitoneal injection of pentobarbital sodium (50 mg/kg). Thereafter, a 1.0–1.5-cm midline sagittal incision was made on the scalp, and the calvarium was exposed by blunt dissection. Two full-thickness critical-size calvarial defects with a

diameter of 5 mm each were created with a drill with a sterile bit, and 18 male rats at 8 weeks-of-age were randomly allocated into three groups as follows: PBS (control), CS/β-GP hydrogel, and CS/β-GP hydrogel with 200 μg sEVs (sEV@CS/β-GP). Thereafter, the bone defects were closed and sutured with degradable silk thread. All rats were housed individually and provided food and water in a temperature-controlled environment with regular use of prophylactic antibiotics.

### Micro-CT Analysis

Rats were euthanized at 12 weeks after surgery, and the skulls were explanted and fixed in 4% (w/v) paraformaldehyde. The morphology of the skulls was assessed using micro-computed tomography (CT) to determine the bone volume. The percentage of new bone volume to tissue volume (BV/TV), bone mineral density (BMD), trabecular number (Tb.N), and trabecular thickness (Tb.Th) were determined using Mimics software (Materialise, Leuven, Belgium).

### Histological, Immunohistochemical, and Immunofluorescence Analysis

Specimens were fixed with 4% (w/v) paraformaldehyde solution, decalcified with 5% (w/v) EDTA, dehydrated in a graded series of alcohol solutions, and embedded in paraffin. Thereafter, 5-μm-thick cross-sections from mid-defect cranial regions were stained with hematoxylin and eosin (H&E) and observed by light microscopy. Masson's trichrome staining was used to evaluate the degree of collagen maturation.

For immunohistochemical analysis, the cross-sections were treated with antigen retrieval buffer and incubated with a CD31 primary antibody (1:100) at 4°C overnight. Thereafter, the cross-sections were incubated with a secondary antibody (1:250) at room temperature, followed by staining with DAB and counterstaining with hematoxylin. CD31 immunofluorescence staining was performed to examine new capillary formation. Cross-sections were incubated a CD31 primary antibody (1: 100) at 4 °C overnight and a secondary antibody (1:250) at room temperature for 1 h in the dark.

## Exosomal miR-21-Mediated Angiogenesis by Targeting SPRY2

### Luciferase Reporter Assay

The 3′untranslated region (UTR) of wild-type (wt) and mutant (mut) SPRY2 was amplified by PCR and individually inserted into the pGL3 plasmid. HEK293 cells ($5 \times 10^4$) were seeded in 48-well plates and co-transfected with the wt or mut luciferase reporter (100 ng) and miR-21 mimics (20 nM) or negative control (NCs) as indicated. At 48 h after transfection, the relative luciferase activity was detected with the Bright-Glo luciferase Assay system (Promega, Madison, WI, United States).

### Cell Transfection

To examine the function of miR-21, HUVECs were transfected with miR-21 mimic or inhibitor and the respective NC (RiboBio, Guangzhou, China) using Lipofectamine 3000 reagent (Invitrogen). For SPRY2 overexpression, HUVECs were transfected with SPRY2 cDNA (Genechem, Shanghai, China) using Lipofectamine 3000 reagent.

### Statistical Analysis

All experiments were performed at least in triplicate. All the data are presented as the mean ± standard deviation (SD). Multiple group comparisons were performed by two-way analysis of variance with Tukey's post hoc test. Statistical analysis was carried out with GraphPad Prism 7.0 (GraphPad Software, La Jolla, CA, United States), and statistical significance was taken at (*) $p < 0.05$ and (**) $p < 0.01$.

# RESULTS

## Characterization of sEVs

sEVs were successfully isolated from BMSCs, and BMSC-sEVs were characterized by NTA analysis, TEM analysis, and western blotting. NTA analysis revealed the size distribution of the sEVs to consist of a single bell-shaped curve with a peak at approximately 120.0 nm, and the percentage of the sEVs with a diameter in the range of 30–150 nm was >99% (**Figure 1A**). TEM images showed the sEVs to be round or cup-shaped with a diameter in the range of 100–150 nm (**Figure 1B**). Western blotting analysis (**Figure 1C**) showed that sEVs, and not BMSCs, expressed CD63, CD81, and TSG101 but not calnexin (negative control). Representative fluorescence microscopy images (**Figure 1D**) showed that sEVs were observed in the cytoplasm, which was indicative of their attachment and internalization by BMSCs and HUVECs. In addition, immunoreactive PKH26 (red) and PKH67 (green) were observed around the nucleus (blue).

## Pro-Osteogenic and Pro-angiogenic Effects of BMSC-sEVs *in vitro*

The promoting proliferative effect was enhanced as the concentrations of sEVs increased, while this effect was significantly reduced or faded when sEVs were more than 200 μg/ml (**Supplementary Figure S1**). Compared with controls, the results of ARS showed that the different concentrations of sEVs could enhance mineral deposition by BMSCs on day 14, and the highest concentration of sEVs could induce matrix mineralization and calcified nodule formation (**Figure 2A**). In quantitative analysis, there was significantly more calcium accumulation in the group treated with sEVs at 100 μg/ml than that in the group treated with sEVs at 50 μg/ml or the untreated group ($p < 0.05$; **Figure 2B**). ALP activity, an indicator of early-stage osteogenic differentiation of BMSCs, was significantly higher in cells exposed to both concentrations than that in control cells on days 7 and 14 ($p < 0.05$; **Figure 2C**), and the effects were dose-dependent. The mRNA levels of *OCN*, *OPN*, and *Runx2* gradually increased in cells exposed to sEVs from days 7–14, and the protein levels of OCN, OPN, and RUNX2 significantly increased on day 14 (**Figure 2D**), indicating that BMSC-sEVs can upregulate the expression of osteogenic genes ($p < 0.05$). The most significant increases in mRNA expression

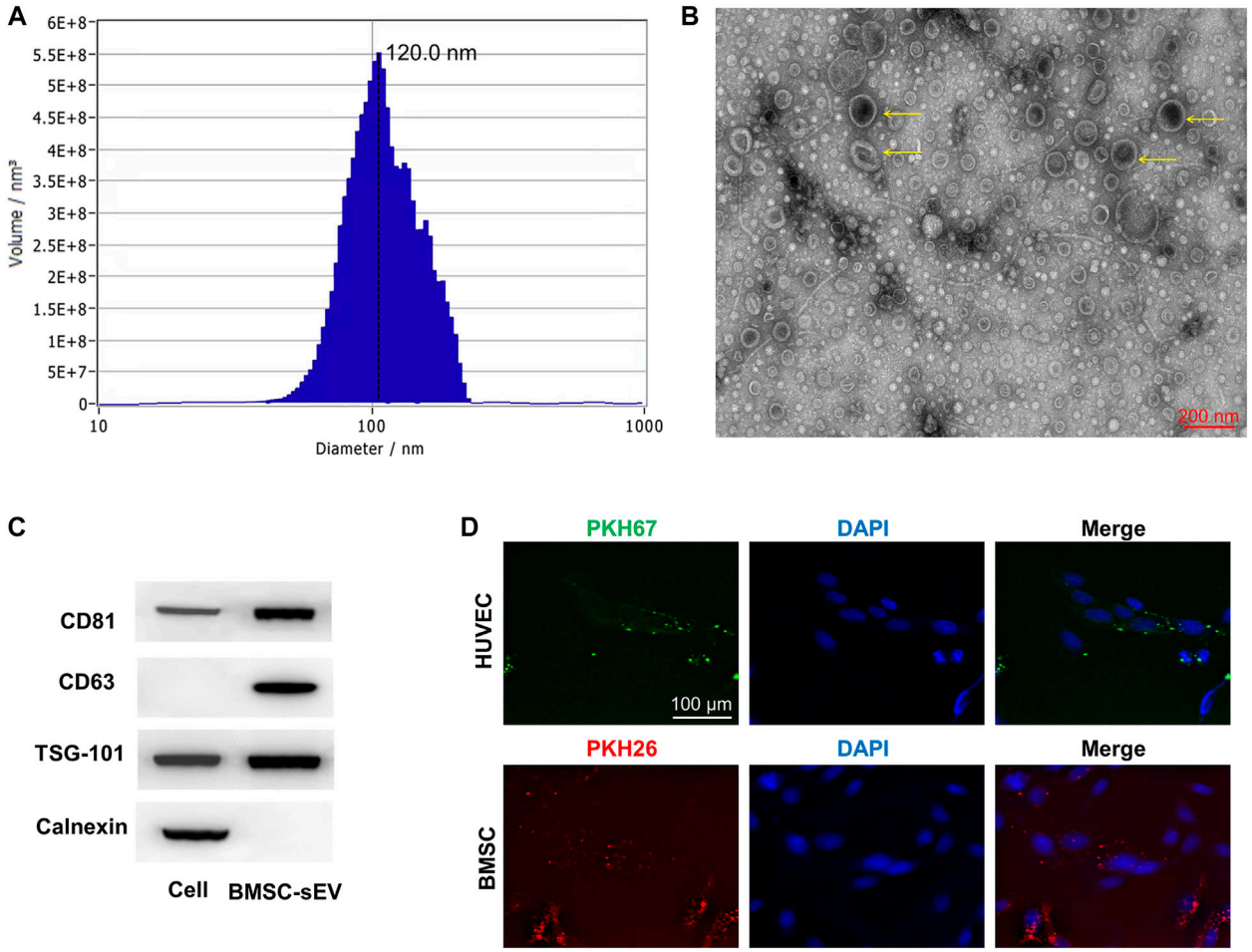


**FIGURE 1 |** Characterization and internalization of sEVs **(A)** Particle size distribution of sEVs detected by NTA and the mean diameter is 120.0 nm **(B)** Representative images of the morphology of sEVs by TEM. The yellow arrows indicate sEVs. Scale bar = 200 nm **(C)** Western blotting analysis of the exosomal proteins CD63, CD81, TSG101 and the negative marker Calnexin **(D)** Uptake of green fuorescent dye (PKH67)-labeled and red fuorescent dye (PKH26)-labeled sEVs by HUVECs and BMSCs, respectively.

were observed in cells treated with the highest concentration of sEVs (**Figure 2E**), revealing that the effects were dose-dependent.

As shown in **Figures 3A–D**, the migratory capability of HUVECs exposed to sEVs for 24 h was greater than that in control cells, and the effects were dose-dependent. Furthermore, tube formation was increased in cells treated with sEVs at a concentration of 100 μg/ml compared with those treated at a concentration of 50 μg/ml or PBS. Compared with the control group, the proliferation of HUVECs exposed to BMSC-sEVs at both concentrations was also increased on days 1, 3, 5, and 7 ($p < 0.05$), and the effects were dose-dependent (**Figure 3E**). Compared with controls, the protein levels of VEGF, bFGF, and ANG-1 increased in cells exposed to sEVs, with the highest concentration showing the most significant changes (**Figure 3F**). Likewise, compared with controls, the mRNA levels of *VEGF*, *bFGF*, and *ANG-1* increased in cells exposed to sEVs on days 4–7, and the effects were dose-dependent (**Figure 3G**). These findings indicate that BMSC-sEVs can dose-dependently promote angiogenesis.

## Characterization of sEV Release From CS/β-GP Hydrogels

As shown in **Figure 4A**, the CS/β-GP hydrogel was a colorless and transparent liquid at room temperature (25°C). It underwent a sol-to-gel transition as the temperature increased, and at physiological temperature (37°C), the CS/β-GP hydrogel transformed into a non-flowing hydrogel. SEM results revealed that the hydrogel was porous and encased in a dense, thick polymeric wall (**Figure 4B**). **Figure 4C** shows the process by which hydrogels were loaded with sEVs. To verify the sol-to-gel transition, the viscosity was examined as a function of the temperature. The hydrogels had low elastic (G′) and viscous (G″) moduli at 25°C and the intersection of G′ and G″, which was characterized as G′ < G″ (**Figure 4D**), indicating their viscous nature, while the intersection of G′ and G″ (G′ = G″) clearly revealed their gelation. Furthermore, the gap between the G′ curve and the G″ curve for sEV-loaded hydrogels was slightly smaller compared with unloaded hydrogels. These results

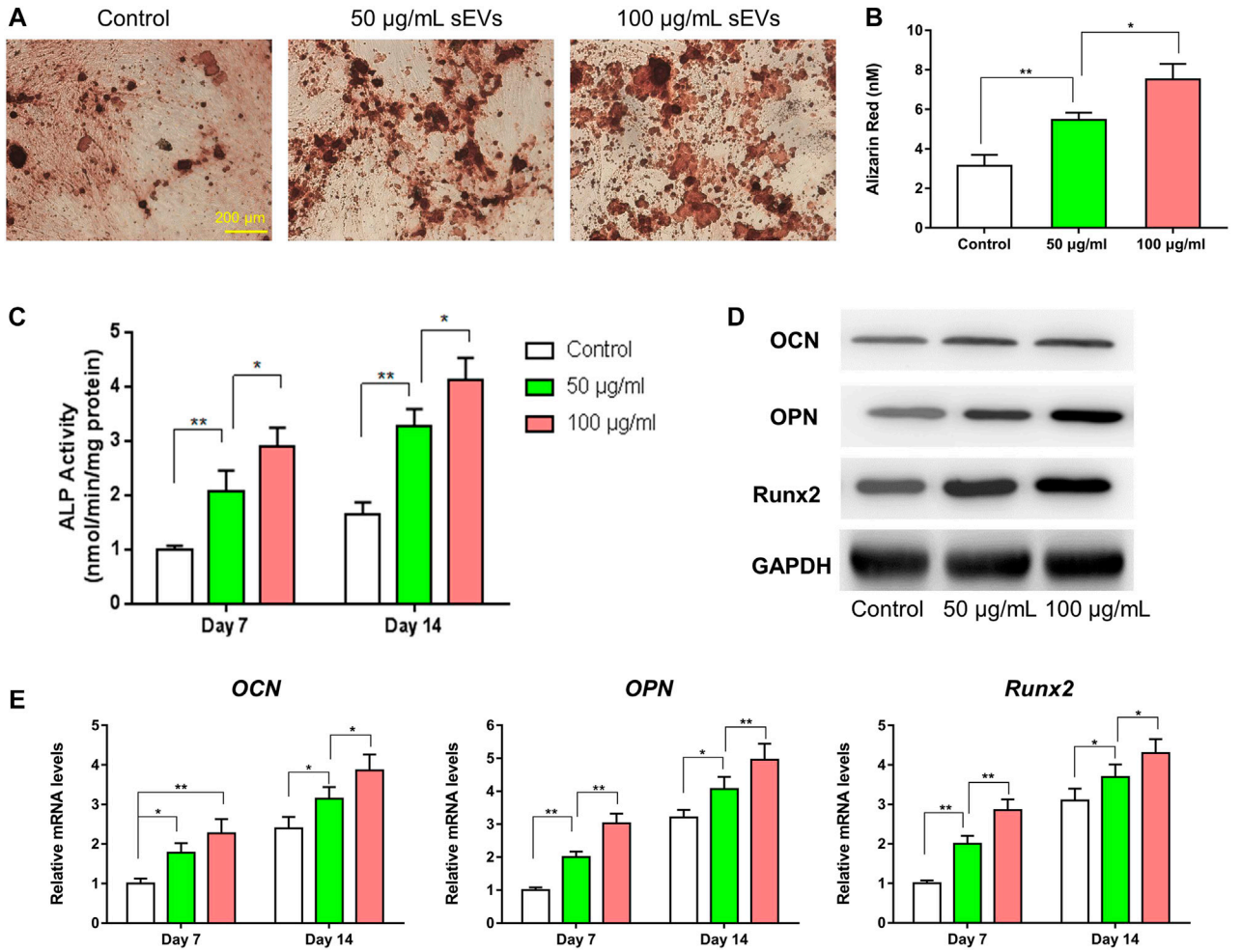


**FIGURE 2 |** Enhanced osteogenic effect of sEVs *in vitro* (*) $p < 0.05$ (**) $p < 0.01$ **(A)** ARS results from stimulation of sEVs on BMSCs after 14 days of culture. Scale bar = 200 μm **(B)** Quantitative analysis of ARS **(C)** Quantifcation of ALP staining after incubation of BMSCs with sEVs for 7 and 14 days **(D)** Western blotting assay for the protein expression of OCN, OPN, and Runx2 **(E)** mRNA level of pro-osteogenic-related genes (*OCN*, *OPN*, and *Runx2*) in BMSCs exposed to different treatments.

indicate that the hydrogel behaved as a liquid before gelation and as a gel after gelation, that is, at physiological temperature and pH.

Both CS/β-GP and sEV@CS/β-GP had good biodegradability and swelling behavior (**Figure 4E**). The swelling ratio of the hydrogel increased with time, reaching equilibrium at approximately 6 h, and there was no significant difference between the two hydrogels. Likewise, there was no difference in the weight loss of the two hydrogels, and the hydrolysis of imine bonds within the hydrogel in PBS was the likely mechanism. As shown in **Figure 4F**, there was a slight but non-significant increase in the gelation time when sEVs were added to CS/β-GP hydrogels (508 ± 21 and 569 ± 26 s). The maximal stress and strain of hydrogels were obtained from compressive curves, and the results indicated that both hydrogels had similar maximal stress and strain (**Figure 4G**). FTIR spectra revealed the addition of sEVs did not cause significant structural changes (**Figure 4H**), as the sEVs may have interacted with certain functional groups to reduce the formation of hydrogen chemical bonds. A slight increase in wavelengths (from 4,254 to 4,268 $cm^{-1}$ and 928 to 937 $cm^{-1}$) indicated that sEVs had no impact on the thermosensitive hydrogels. Moreover, the sEV@CS/β-GP hydrogel showed good slow-release performance (**Figure 4I**), with 80% of the sEVs releasing on day 8 and the release rate slowing after this time point.

## BMSC-sEVs Promote the Repair of Calvarial Defects *in vivo*

The 3D reconstruction of micro-CT images of rat calvarial defects at 12 weeks are shown in **Figure 5A**. Compared with the control group, the formation of new bone, which filled the calvarial defects, was observed in CS/β-GP and sEV@CS/β-GP groups, with the sEV@CS/β-GP group showing a greater area of newly formed bone. The repair of these bone defects was further examined using quantitative approaches, and the BMD, BV/TV ratio, and Tb.N in CS/β-GP and sEV@CS/β-GP groups

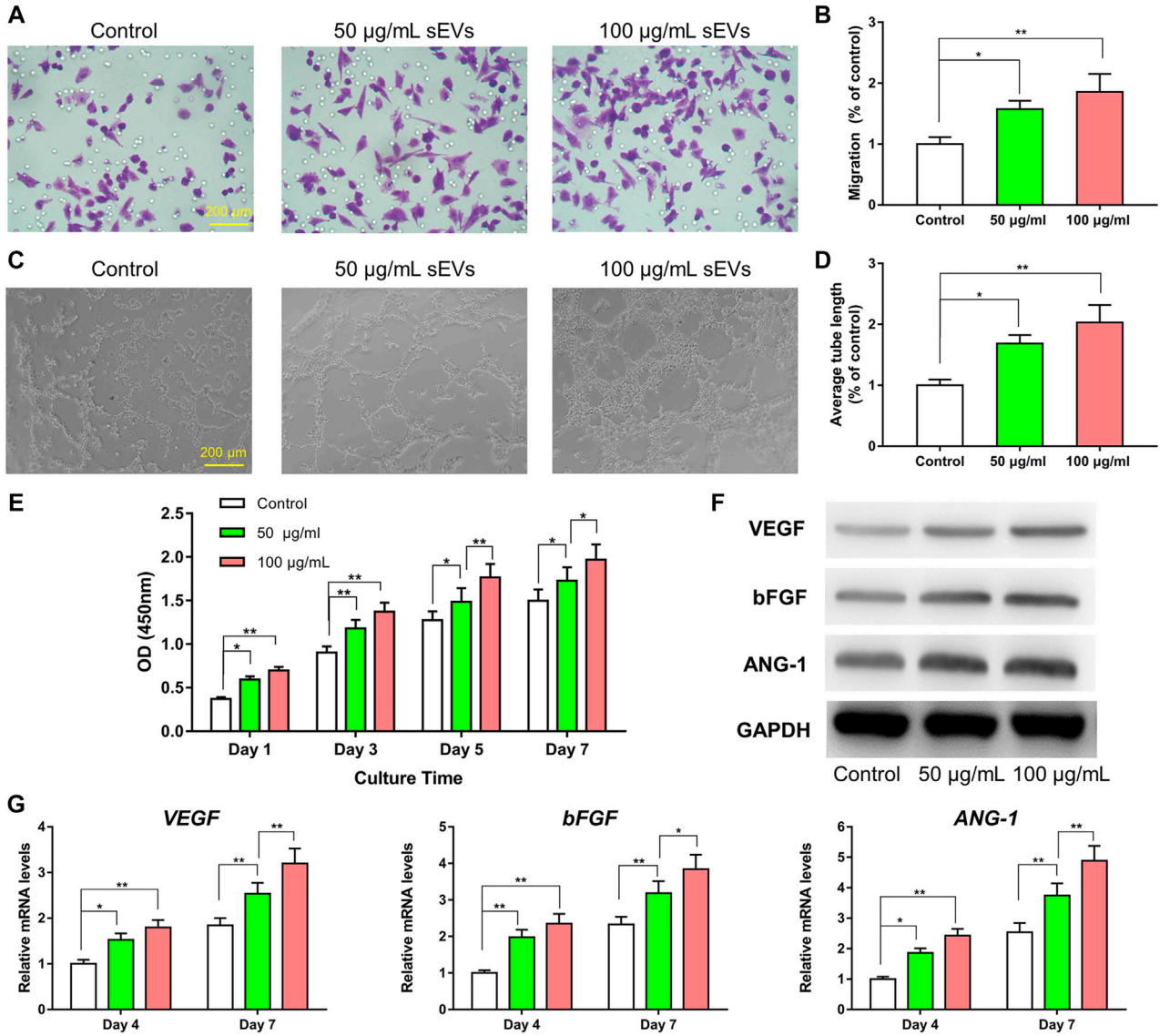


**FIGURE 3 |** Enhanced angiogenic effect of sEVs *in vitro* (*) $p < 0.05$ (**) $p < 0.01$ **(A)** Transwell assay and quantitative analysis **(B)** of the cell migration rate **(C)** Tube formation by HUVECs and quantitative analysis **(D)** of the average tube length **(E)** CCK8 assay for the proliferation of HUVECs exposed to different treatments **(F)** Western blotting assay for the protein expression of VEGF, bFGF, and ANG-1 **(G)** mRNA level of pro-angiogenic-related genes (*VEGF*, *bFGF*, and *ANG-1*).

were all significantly higher than those in the control group, indicating that the release of sEVs from hydrogels and the thermosensitive property of hydrogels improved the bone healing capacity, whereas there was no difference in the Tb.Th (**Figure 5B**). The results of histological staining indicated that the bone defects in the control group were mainly filled with fibrotic connective tissue, whereas newly formed bone was observed both along the border and in the center of the calvarial defects after application of CS/β-GP hydrogels, with sEV@CS/β-GP hydrogels showing a greater area of newly formed bone (**Figures 5C,D**, **Supplementary Figure S2,3**). These results were similar to those of micro-CT analysis. The results of CD31 immunohistochemical staining of right bone defect sections indicated that there were more CD31-positive cells in the sEV@CS/β-GP group compared with the CS/β-GP group, which was indicative of new vessel formation within the bone defect (**Figure 5E**), which was further verified by quantitative analysis (**Figures 5F,G**). These results reveal that sEVs promoted calvarial defect repair and enhanced angiogenesis and osteogenesis.

## BMSC-Derived Exosomal miR-21 Promotes Angiogenesis by Targeting SPRY2

Previous studies have reported that miR-21 is expressed at a high level in sEVs derived from BMSCs (Lv et al., 2017). As such, we analyzed miRNA expression in BMSCs using an existing GEO dataset (GSE78865) and predicted the candidate target genes of miR-21 that contributed to

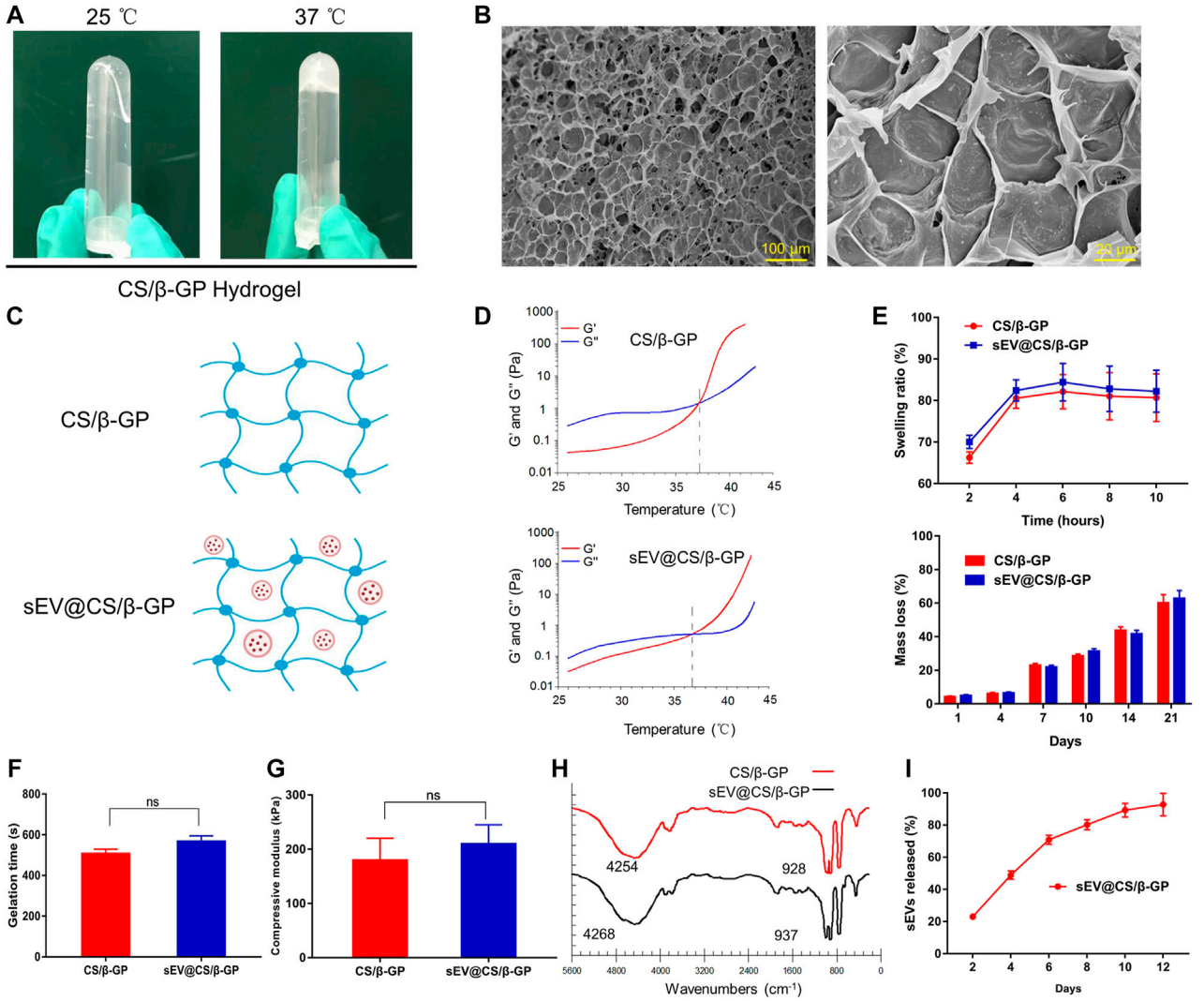


**FIGURE 4 |** Characterization and the sEV release ability of the CS/β-GP hydrogel. ns: no significant difference **(A)** Sol-to-gel transition: a photograph of CS/β-GP thermosensitive hydrogel at 25 and 37°C **(B)** SEM photomicrographs of the morphological structure of CS/β-GP hydrogel **(C)** Schematic representation of the combination of sEVs and CS/β-GP hydrogel **(D)** Typical temperature-dependent functions of G′ and G″ for CS/β-GP and sEV@CS/β-GP hydrogels **(E)** Swelling rate and mass-remaining profiles of CS/β-GP and sEV@CS/β-GP hydrogels **(F)** Gelation time of CS/β-GP and sEV@CS/β-GP hydrogels **(G)** The compressive module of CS/β-GP and sEV@CS/β-GP hydrogels **(H)** FTIR (Fourier-transform infrared) spectra of CS/β-GP and sEV@CS/β-GP hydrogels **(I)** release profiles of sEVs from the sEV@CS/β-GP hydrogel.

angiogenesis by exploring online databases, including TargetScan, miRanda and miRWalk. KEGG pathway enrichment analysis was performed for candidate target genes related to angiogenesis. To confirm the direct binding between miR-21 and the 3′-UTR of its predicted target gene SPRY2, we performed reporter assays using a luciferase reporter plasmid containing the wt or mut SPRY2 3′-UTR with the miR-21 binding site (**Figure 6A**). Transfection of HUVECs with the miR-21 mimics could reduce luciferase activity compared to transfection with the control mimic, which was indicative of direct binding between miR-21 and the SPRY2 3-′UTR (**Figure 6B**).

To further explore the relationship between exosomal miR-21 and SPRY2, rescue experiments were conducted. We transfected the miR-21 mimics or miR-NC into HUVECs, followed by co-transfection with a SPRY2-overexpressing plasmid (pcDNA-SPRY2). The results revealed that the migratory capacity of cells co-transfected with the miR-21 mimics and pcDNA-SPRY2 was enhanced compared with cells co-transfected with the miR-NC and pcDNA-SPRY2 (**Figures 6C,D**). The levels of angiogenic proteins in cells transfected with the miR-21 mimics were higher than those in control cells, and pcDNA-SPRY2 could abolish the effect of the miR-21 mimics on angiogenesis (**Figure 6E**), indicating that

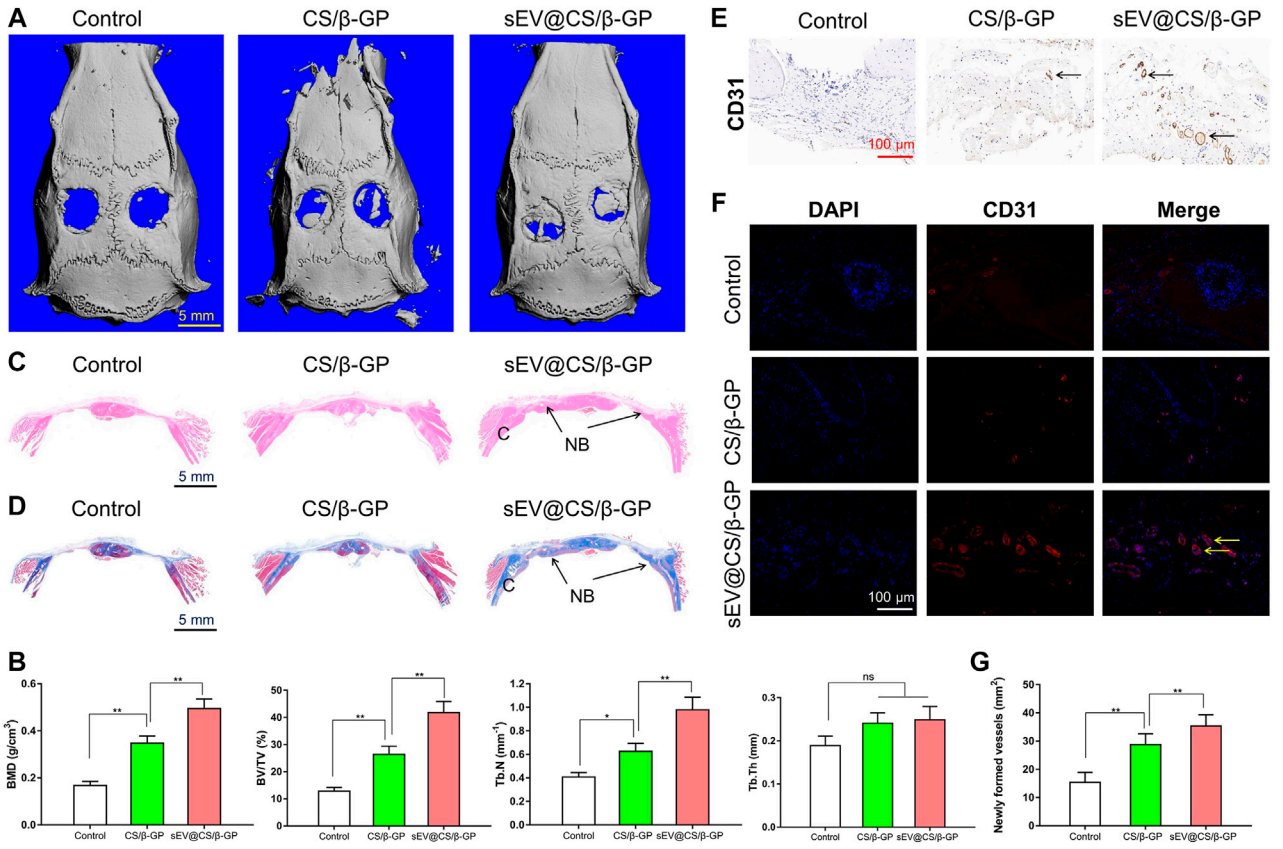


**FIGURE 5 |** sEV@CS/β-GP hydrogel promoted bone formation in critical-sized rat calvarial defects (*) $p < 0.05$ (**) $p < 0.01$, ns: no significant difference **(A)** Micro-CT images of bone defects in each group after 12 weeks. Scale bar = 5 mm **(B)** Quantitative analysis of BMD, BV/TV ratio, Tb.N and Tb.Th in the diferent groups **(C)** H&E staining and Masson's trichrome staining **(D)** in the three groups. C, cranium. NB, new bone **(E)** Immunohistochemical staining and immunofuorescence analysis **(F)** of the angiogenic marker CD31. Dark brown granules indicating positive staining are marked by black arrows, and yellow arrows mark the newly formed vessels **(G)** Quantitative analysis of newly formed vessels.

exosomal miR-21 can promote HUVEC migration and angiogenesis by targeting SPRY2.

## DISCUSSION

Angiogenesis and osteogenesis are highly coupled processes that are indispensable for bone repair (Kusumbe et al., 2014). Large bone defects caused by trauma and certain diseases may not heal naturally and require regenerative scaffold implantation to promote tissue reconstruction (Dimitriou et al., 2011). Although a variety of bioengineering techniques that promote tissue regeneration with optimized materials are currently available, vascularization after scaffold implantation is still a major challenge (Potente et al., 2011; Rouwkema and Khademhosseini, 2016; Eelen et al., 2020). The osteogenic function of cells that promote bone regeneration requires a network of microvessels, which mediate the transport of circulating of cells, oxygen, nutrients, and waste products (Laschke and Menger, 2015). Besides, Zhao et al. modified the tetrahedral framework nucleic acid (tFNA) with aptamers to form aptamer-tFNA nanostructures, tFNA-Apt02 and tFNA-AptVEGF, and they exhibited stronger angiogenesis, further provided a new and efficient proangiogenic approach (Zhao et al., 2021). Therefore, newly formed microvessels within grafts are critical for successful bone tissue engineering.

Mesenchymal stromal/stem cells (MSCs) have been widely applied because they can be obtained easily from adult tissues, as well as proliferate and differentiate into bone, adipose, or cartilage (Grayson et al., 2015). However, the direct use of MSCs for therapeutic purposes remains limited by many risk factors, such as tumor formation, thrombosis, and unwanted immune responses. Furthermore, the stimulation of localized healing by MSCs involves paracrine mechanisms (Gnecchi et al., 2005; Caplan and Correa, 2011), and the application of sEVs may overcome these limitations. Because of their ideal characteristics, sEVs are also favorable nanoscale drug carriers for the regeneration of tissues and the treatment of certain diseases (Liao et al., 2019a; Elsharkasy et al., 2020). For example, Dong et al. revealed that the use of fetal bovine serum-derived sEVs to carry Icariin could promote osteoblast proliferation and bone regeneration more effectively than Icariin alone (Dong et al., 2021). Wu et al. demonstrated that BMSC-derived sEVs and $Fe_3O_4$ nanoparticles under conditions of a static magnetic field

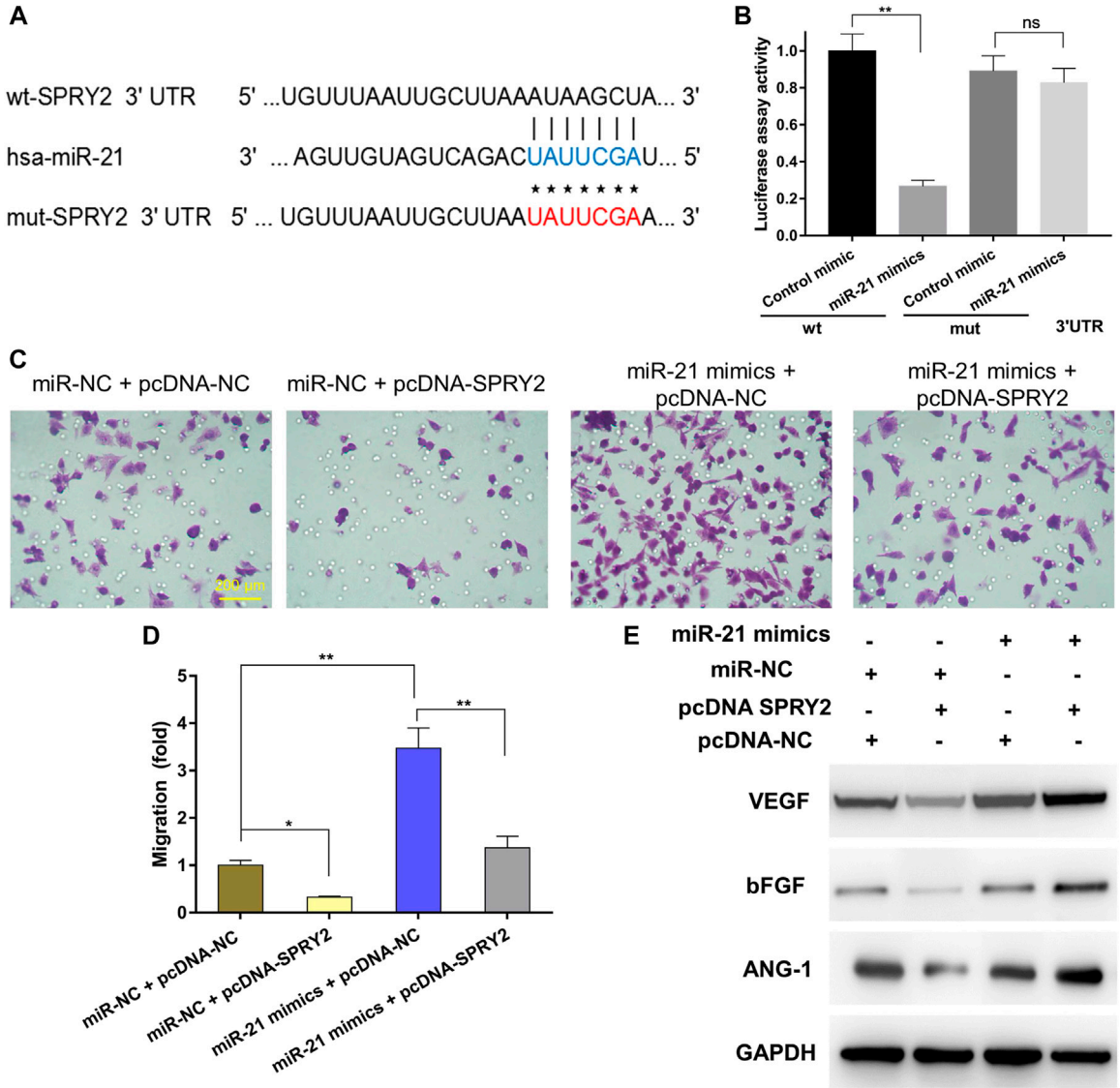


**FIGURE 6 |** Exosomal miR-21 promoted angiogenesis by targeting SPRY2 (*) $p < 0.05$ (**) $p < 0.01$, ns: no significant difference. wt, wild-type; mut, mutant; NC, negative control **(A)** The miR-21 binding sequence in the 3′-UTR of SPRY2 **(B)** The miR-21 mimics transfection reduced luciferase activity when compared to control mimics transfection, which confirms that SPRY2 are the target genes of miR-21 **(C)** The transwell assay showing the cell migration when HUVECs were co-transfected with miR-21 mimics and pcDNA-SPRY2, and the quantitative analysis **(D)** indicated overexpression of SPRY2 suppressed the upregulation of the migration rate of HUVECs by miR-21 mimics **(E)** Western blotting assays showing that overexpression of SPRY2 prevented the upregulation of VEGF, bFGF, and ANG-1 protein expression by miR-21 mimics.

could facilitate bone regeneration and enhance wound healing (Wu et al., 2020; Wu et al., 2021). In the present study, we manufactured thermosensitive hydrogels loaded with BMSC-derived sEVs that could promote bone regeneration.

Hydrogels have been widely used in tissue bioengineering, drug delivery, and cell-based therapy. A recent study reported a biphasic hydrogel for osteochondral defect regeneration, which was fabricated via a thermally reactive, rapid cross-linking method (Liao et al., 2017). CS is an excellent excipient because it is non-toxic, stable, biodegradable, and sterilizable, which makes it a versatile material with application potential in biomedical and biotechnological fields (Kumar et al., 2004). CS can form a thermosensitive injectable hydrogel through cross-linking with β-GP via ionic interactions between the ammonium groups of CS and the phosphate groups of β-GP, which can increase the gelation temperature and pH to the physiological range and restrict the immediate precipitation/deformation of the hydrogel (Bhattarai et al., 2010). The thermosetting of hydrogels has an added advantage, that is, once the homogeneous solution is injected into the tissue defect, the hydrogel forms and strengthens mechanically with time. In addition, the ability of polymer matrix hydrogels to expand and degrade makes them suitable vehicles for

the encapsulation and delivery of numerous therapeutic agents, such as cells, growth factors, drugs, and proteins, to sites of tissue damage (Xu et al., 2019; Amiryaghoubi et al., 2020). These properties are ideal for sustained drug delivery applications, and CS/β-GP hydrogels are attractive biomaterials because of their temperature sensitivity. The results of rheological experiments have revealed that the gelation time and temperature could be modulated by sEVs, as they slightly decreased the gelation time and temperature. As such, after sEV loading, the resulting sEV@CS/β-GP hydrogels are attractive biomaterials for bone repair. Petit et al. reported that thermosensitive chitosan-based stain-loaded hydrogels decreased soft tissue inflammation and induced new bone formation (Petit et al., 2020), whereas Kocak et al. demonstrated that CS and hydroxyapatite composite materials loaded with low concentrations of heparin could stimulate angiogenesis and promote bone regeneration (Kocak et al., 2020).

MiRNAs regulate gene expression and biological functions by binding to the 3′-UTR or amino acid coding sequence of target genes (Thomou et al., 2017). MiR-21, one of the most studied miRNAs, is involved in many biological processes (Kumarswamy et al., 2011). For example, Geng et al. reported that miR-21 can induce angiogenic differentiation of MSCs and promote blood vessel and bone formation (Geng et al., 2020). The role of SPRY2 in angiogenesis and the regulation of SPRY2 by the miR-23/27 cluster has been previously demonstrated (Zhou et al., 2011), as well as the regulation of SPRY2 by miR-21 (Thum et al., 2008). Li et al. fabricated the resultant bioswitchable nanocomposite by integrating the sticky-end tFNA (stFNA) and miRs (miR-21, miR-124, miR-335, and miR-2861), further promoting bone regeneration via inhibiting the expression of HDAC5 (Li S. et al., 2021). A similar research reported that exosomal miR-21 derived from umbilical MSC-sEVs promoted angiogenesis by upregulating the NOTCH1/DLL4 pathway (Zhang et al., 2021). In this study, the results of luciferase assays revealed that SPRY2 expression was increased by the miR-21 mimics. Furthermore, SPRY2 significantly inhibited HUVEC migration and proliferation and mediated the negative feedback of major growth factors such as VEGF, bFGF, and ANG-1. The results of gain-of-function and loss-of-function assays indicated that SPRY2 overexpression in HUVECs could attenuate, but not entirely abolish, the effects of the miR-21 mimics on angiogenesis.

## CONCLUSION

In summary, we developed an injectable homogeneous CS/β-GP hydrogel solution, with gelation occurring at body temperature. The hydrogel had desirable structural and physical properties that promoted bone healing, and it served as a scaffold for sEVs. The sEV-loaded hydrogel could effectively promote bone healing in a rat model by enhancing angiogenesis, which may have been mediated by the upregulation of miR-21 expression in sEVs and the regulation of SPRY2 by miR-21. This study provides a new strategy for repairing bone defects with multifunctional controlled-sEV-release hydrogels, and this sEV-based therapy shows great potential in the future.

## DATA AVAILABILITY STATEMENT

The original contributions presented in the study are included in the article/**Supplementary Material**, further inquiries can be directed to the corresponding authors.

## ETHICS STATEMENT

The animal study was reviewed and approved by Animal Research Committee of Peking Union Medical College Hospital (XHDW-2020-040), Beijing, China.

## AUTHOR CONTRIBUTIONS

DW, HQ and LL conducted most of the experimental work performance and drafted the manuscript. ZW, MY, ZL, and HP participated in data collection and related analysis. XW revised the manuscript. LL, CZ, and XW designed and supervised this project. All authors read and approved the final manuscript.

## FUNDING

This work was supported by the National Key Research and Development Project of China (Grant No. 2018YFC1106303); Innovation Project of Peking Union Medical College Graduate Student (20191002-11).

## ACKNOWLEDGMENTS

We are grateful to all the laboratory members for their technical advice and helpful discussion.

## SUPPLEMENTARY MATERIAL

The Supplementary Material for this article can be found online at: https://www.frontiersin.org/articles/10.3389/fbioe.2021.829136/full#supplementary-material

## REFERENCES

Amiryaghoubi, N., Noroozi Pesyan, N., Fathi, M., and Omidi, Y. (2020). Injectable Thermosensitive Hybrid Hydrogel Containing Graphene Oxide and Chitosan as Dental Pulp Stem Cells Scaffold for Bone Tissue Engineering. *Int. J. Biol. Macromolecules* 162, 1338–1357. doi:10.1016/j.ijbiomac.2020.06.138

Bhattarai, N., Gunn, J., and Zhang, M. (2010). Chitosan-based Hydrogels for Controlled, Localized Drug Delivery. *Adv. Drug Deliv. Rev.* 62 (1), 83–99. doi:10.1016/j.addr.2009.07.019

Bose, S., Roy, M., and Bandyopadhyay, A. (2012). Recent Advances in Bone Tissue Engineering Scaffolds. *Trends Biotechnol.* 30 (10), 546–554. doi:10.1016/j.tibtech.2012.07.005

Caplan, A. I., and Correa, D. (2011). The MSC: an Injury Drugstore. *Cell Stem Cell* 9 (1), 11–15. doi:10.1016/j.stem.2011.06.008

Colombo, M., Raposo, G., and Théry, C. (2014). Biogenesis, Secretion, and Intercellular Interactions of Exosomes and Other Extracellular Vesicles. *Annu. Rev. Cell Dev. Biol.* 30, 255–289. doi:10.1146/annurev-cellbio-101512-122326

Crane, G. M., Ishaug, S. L., and Mikos, A. G. (1995). Bone Tissue Engineering. *Nat. Med.* 1 (12), 1322–1324. doi:10.1038/nm1295-1322

Dimitriou, R., Jones, E., McGonagle, D., and Giannoudis, P. V. (2011). Bone Regeneration: Current Concepts and Future Directions. *BMC Med.* 9, 66. doi:10.1186/1741-7015-9-66

Dong, M., Wu, S., Xu, H., Yu, X., Wang, L., Bai, H., et al. (2021). FBS-derived Exosomes as a Natural Nano-Scale Carrier for Icariin Promote Osteoblast Proliferation. *Front. Bioeng. Biotechnol.* 9, 615920. doi:10.3389/fbioe.2021.615920

Eelen, G., Treps, L., Li, X., and Carmeliet, P. (2020). Basic and Therapeutic Aspects of Angiogenesis Updated. *Circ. Res.* 127 (2), 310–329. doi:10.1161/CIRCRESAHA.120.316851

Elsharkasy, O. M., Nordin, J. Z., Hagey, D. W., de Jong, O. G., Schiffelers, R. M., Andaloussi, S. E., et al. (2020). Extracellular Vesicles as Drug Delivery Systems: Why and How? *Adv. Drug Deliv. Rev.* 159, 332–343. doi:10.1016/j.addr.2020.04.004

Fu, X., Liu, G., Halim, A., Ju, Y., Luo, Q., and Song, A. G. (2019). Mesenchymal Stem Cell Migration and Tissue Repair. *Cells* 8 (8), 784. doi:10.3390/cells8080784

Geng, Z., Yu, Y., Li, Z., Ma, L., Zhu, S., Liang, Y., et al. (2020). miR-21 Promotes Osseointegration and Mineralization through Enhancing Both Osteogenic and Osteoclastic Expression. *Mater. Sci. Eng. C* 111, 110785. doi:10.1016/j.msec.2020.110785

Gnecchi, M., He, H., Liang, O. D., Melo, L. G., Morello, F., Mu, H., et al. (2005). Paracrine Action Accounts for Marked protection of Ischemic Heart by Akt-Modified Mesenchymal Stem Cells. *Nat. Med.* 11 (4), 367–368. doi:10.1038/nm0405-367

Grayson, W. L., Bunnell, B. A., Martin, E., Frazier, T., Hung, B. P., and Gimble, J. M. (2015). Stromal Cells and Stem Cells in Clinical Bone Regeneration. *Nat. Rev. Endocrinol.* 11 (3), 140–150. doi:10.1038/nrendo.2014.234

He, C., Zheng, S., Luo, Y., and Wang, B. (2018). Exosome Theranostics: Biology and Translational Medicine. *Theranostics* 8 (1), 237–255. doi:10.7150/thno.21945

Hoffman, M. D., Xie, C., Zhang, X., and Benoit, D. S. W. (2013). The Effect of Mesenchymal Stem Cells Delivered via Hydrogel-Based Tissue Engineered Periosteum on Bone Allograft Healing. *Biomaterials* 34 (35), 8887–8898. doi:10.1016/j.biomaterials.2013.08.005

Huey, D. J., Hu, J. C., and Athanasiou, K. A. (2012). Unlike Bone, Cartilage Regeneration Remains Elusive. *Science* 338 (6109), 917–921. doi:10.1126/science.1222454

Ingavle, G. C., Gionet-Gonzales, M., Vorwald, C. E., Bohannon, L. K., Clark, K., Galuppo, L. D., et al. (2019). Injectable Mineralized Microsphere-Loaded Composite Hydrogels for Bone Repair in a Sheep Bone Defect Model. *Biomaterials* 197, 119–128. doi:10.1016/j.biomaterials.2019.01.005

Kalluri, R., and LeBleu, V. S. (2020). The Biology , Function , and Biomedical Applications of Exosomes. *Science* 367 (6478). doi:10.1126/science.aau6977

Kawai, M., Mödder, U. I., Khosla, S., and Rosen, C. J. (2011). Emerging Therapeutic Opportunities for Skeletal Restoration. *Nat. Rev. Drug Discov.* 10 (2), 141–156. doi:10.1038/nrd3299

Khademhosseini, A., and Langer, R. (2016). A Decade of Progress in Tissue Engineering. *Nat. Protoc.* 11 (10), 1775–1781. doi:10.1038/nprot.2016.123

Kocak, F. Z., Talari, A. C. S., Yar, M., and Rehman, I. U. (2020). *In-Situ* Forming pH and Thermosensitive Injectable Hydrogels to Stimulate Angiogenesis: Potential Candidates for Fast Bone Regeneration Applications. *Ijms* 21 (5), 1633. doi:10.3390/ijms21051633

Kumar, M. N. V. R., Muzzarelli, R. A. A., Muzzarelli, C., Sashiwa, H., and Domb, A. J. (2004). Chitosan Chemistry and Pharmaceutical Perspectives. *Chem. Rev.* 104 (12), 6017–6084. doi:10.1021/cr030441b

Kumarswamy, R., Volkmann, I., and Thum, T. (2011). Regulation and Function of miRNA-21 in Health and Disease. *RNA Biol.* 8 (5), 706–713. doi:10.4161/rna.8.5.16154

Kusumbe, A. P., Ramasamy, S. K., and Adams, R. H. (2014). Coupling of Angiogenesis and Osteogenesis by a Specific Vessel Subtype in Bone. *Nature* 507 (7492), 323–328. doi:10.1038/nature13145

Langer, R., and Vacanti, J. P. (1993). Tissue Engineering. *Science* 260 (5110), 920–926. doi:10.1126/science.8493529

Laschke, M. W., and Menger, M. D. (2015). Adipose Tissue-Derived Microvascular Fragments: Natural Vascularization Units for Regenerative Medicine. *Trends Biotechnol.* 33 (8), 442–448. doi:10.1016/j.tibtech.2015.06.001

Li, G.-Q., Fang, Y.-X., Liu, Y., Meng, F.-R., Wu, X., Zhang, C.-W., et al. (2021a). MicroRNA-21 from Bone Marrow Mesenchymal Stem Cell-Derived Extracellular Vesicles Targets TET1 to Suppress KLF4 and Alleviate Rheumatoid Arthritis. *Ther. Adv. Chronic Dis.* 12, 204062232110073. doi:10.1177/20406223211007369

Li, S., Liu, Y., Tian, T., Zhang, T., Lin, S., Zhou, M., et al. (2021b). Bioswitchable Delivery of microRNA by Framework Nucleic Acids: Application to Bone Regeneration. *Small* 17 (47), 2104359. doi:10.1002/smll.202104359

Li, W., Liu, Y., Zhang, P., Tang, Y., Zhou, M., Jiang, W., et al. (2018). Tissue-Engineered Bone Immobilized with Human Adipose Stem Cells-Derived Exosomes Promotes Bone Regeneration. *ACS Appl. Mater. Inter.* 10 (6), 5240–5254. doi:10.1021/acsami.7b17620

Liao, J., Tian, T., Shi, S., Xie, X., Ma, Q., Li, G., et al. (2017). The Fabrication of Biomimetic Biphasic CAN-PAC Hydrogel with a Seamless Interfacial Layer Applied in Osteochondral Defect Repair. *Bone Res.* 5, 17018. doi:10.1038/boneres.2017.18

Liao, W., Du, Y., Zhang, C., Pan, F., Yao, Y., Zhang, T., et al. (2019a). Exosomes: The Next Generation of Endogenous Nanomaterials for Advanced Drug Delivery and Therapy. *Acta Biomater.* 86, 1–14. doi:10.1016/j.actbio.2018.12.045

Liao, W., Ning, Y., Xu, H.-J., Zou, W.-Z., Hu, J., Liu, X.-Z., et al. (2019b). BMSC-derived Exosomes Carrying microRNA-122-5p Promote Proliferation of Osteoblasts in Osteonecrosis of the Femoral Head. *Clin. Sci. (Lond)* 133 (18), 1955–1975. doi:10.1042/CS20181064

Liu, L., Liu, Y., Feng, C., Chang, J., Fu, R., Wu, T., et al. (2019). Lithium-containing Biomaterials Stimulate Bone Marrow Stromal Cell-Derived Exosomal miR-130a Secretion to Promote Angiogenesis. *Biomaterials* 192, 523–536. doi:10.1016/j.biomaterials.2018.11.007

Lopes, D., Martins-Cruz, C., Oliveira, M. B., and Mano, J. F. (2018). Bone Physiology as Inspiration for Tissue Regenerative Therapies. *Biomaterials* 185, 240–275. doi:10.1016/j.biomaterials.2018.09.028

Lv, C., Yang, S., Chen, X., Zhu, X., Lin, W., Wang, L., et al. (2017). MicroRNA-21 Promotes Bone Mesenchymal Stem Cells Migration *In Vitro* by Activating PI3K/Akt/MMPs Pathway. *J. Clin. Neurosci.* 46, 156–162. doi:10.1016/j.jocn.2017.07.040

Park, M. H., Joo, M. K., Choi, B. G., and Jeong, B. (2012). Biodegradable Thermogels. *Acc. Chem. Res.* 45 (3), 424–433. doi:10.1021/ar200162j

Petit, C., Batool, F., Stutz, C., Anton, N., Klymchenko, A., Vandamme, T., et al. (2020). Development of a Thermosensitive Statin Loaded Chitosan-Based Hydrogel Promoting Bone Healing. *Int. J. Pharmaceutics* 586, 119534. doi:10.1016/j.ijpharm.2020.119534

Potente, M., Gerhardt, H., and Carmeliet, P. (2011). Basic and Therapeutic Aspects of Angiogenesis. *Cell* 146 (6), 873–887. doi:10.1016/j.cell.2011.08.039

Roccaro, A. M., Sacco, A., Maiso, P., Azab, A. K., Tai, Y.-T., Reagan, M., et al. (2013). BM Mesenchymal Stromal Cell-Derived Exosomes Facilitate Multiple Myeloma Progression. *J. Clin. Invest.* 123 (4), 1542–1555. doi:10.1172/JCI66517

Rouwkema, J., and Khademhosseini, A. (2016). Vascularization and Angiogenesis in Tissue Engineering: Beyond Creating Static Networks. *Trends Biotechnol.* 34 (9), 733–745. doi:10.1016/j.tibtech.2016.03.002

Sissung, T. M., and Figg, W. D. (2020). Stem Cell Clinics: Risk of Proliferation. *Lancet Oncol.* 21 (2), 205–206. doi:10.1016/S1470-2045(19)30787-9

Tan, S. H. S., Wong, J. R. Y., Sim, S. J. Y., Tjio, C. K. E., Wong, K. L., Chew, J. R. J., et al. (2020). Mesenchymal Stem Cell Exosomes in Bone Regenerative Strategies-A Systematic Review of Preclinical Studies. *Mater. Today Bio* 7, 100067. doi:10.1016/j.mtbio.2020.100067

Thomou, T., Mori, M. A., Dreyfuss, J. M., Konishi, M., Sakaguchi, M., Wolfrum, C., et al. (2017). Adipose-derived Circulating miRNAs Regulate Gene Expression in Other Tissues. *Nature* 542 (7642), 450–455. doi:10.1038/nature21365

Thum, T., Gross, C., Fiedler, J., Fischer, T., Kissler, S., Bussen, M., et al. (2008). MicroRNA-21 Contributes to Myocardial Disease by Stimulating MAP Kinase Signalling in Fibroblasts. *Nature* 456 (7224), 980–984. doi:10.1038/nature07511

Tkach, M., and Théry, C. (2016). Communication by Extracellular Vesicles: Where We Are and where We Need to Go. *Cell* 164 (6), 1226–1232. doi:10.1016/j.cell.2016.01.043

van Niel, G., D'Angelo, G., and Raposo, G. (2018). Shedding Light on the Cell Biology of Extracellular Vesicles. *Nat. Rev. Mol. Cell Biol* 19 (4), 213–228. doi:10.1038/nrm.2017.125

Wang, L., Wang, J., Zhou, X., Sun, J., Zhu, B., Duan, C., et al. (2020). A New Self-Healing Hydrogel Containing hucMSC-Derived Exosomes Promotes Bone Regeneration. *Front. Bioeng. Biotechnol.* 8, 564731. doi:10.3389/fbioe.2020.564731

Wang, X., and Thomsen, P. (2021). Mesenchymal Stem Cell-Derived Small Extracellular Vesicles and Bone Regeneration. *Basic Clin. Pharmacol. Toxicol.* 128 (1), 18–36. doi:10.1111/bcpt.13478

Wasupalli, G. K., and Verma, D. (2020). Injectable and Thermosensitive Nanofibrous Hydrogel for Bone Tissue Engineering. *Mater. Sci. Eng. C* 107, 110343. doi:10.1016/j.msec.2019.110343

Wu, D., Chang, X., Tian, J., Kang, L., Wu, Y., Liu, J., et al. (2021). Bone Mesenchymal Stem Cells Stimulation by Magnetic Nanoparticles and a Static Magnetic Field: Release of Exosomal miR-1260a Improves Osteogenesis and Angiogenesis. *J. Nanobiotechnol* 19 (1), 209. doi:10.1186/s12951-021-00958-6

Wu, D., Kang, L., Tian, J., Wu, Y., Liu, J., Li, Z., et al. (2020). Exosomes Derived from Bone Mesenchymal Stem Cells with the Stimulation of Fe3O4 Nanoparticles and Static Magnetic Field Enhance Wound Healing through Upregulated miR-21-5p. *Ijn* 15, 7979–7993. doi:10.2147/IJN.S275650

Wu, J., Zheng, K., Huang, X., Liu, J., Liu, H., Boccaccini, A. R., et al. (2019). Thermally Triggered Injectable Chitosan/silk Fibroin/bioactive Glass Nanoparticle Hydrogels for *In-Situ* Bone Formation in Rat Calvarial Bone Defects. *Acta Biomater.* 91, 60–71. doi:10.1016/j.actbio.2019.04.023

Xu, R., Rai, A., Chen, M., Suwakulsiri, W., Greening, D. W., and Simpson, R. J. (2018). Extracellular Vesicles in Cancer - Implications for Future Improvements in Cancer Care. *Nat. Rev. Clin. Oncol.* 15 (10), 617–638. doi:10.1038/s41571-018-0036-9

Xu, X., Gu, Z., Chen, X., Shi, C., Liu, C., Liu, M., et al. (2019). An Injectable and Thermosensitive Hydrogel: Promoting Periodontal Regeneration by Controlled-Release of Aspirin and Erythropoietin. *Acta Biomater.* 86, 235–246. doi:10.1016/j.actbio.2019.01.001

Yuan, X., Amarnath Praphakar, R., Munusamy, M. A., Alarfaj, A. A., Suresh Kumar, S., and Rajan, M. (2019). Mucoadhesive Guargum Hydrogel Interconnected Chitosan-G-Polycaprolactone Micelles for Rifampicin Delivery. *Carbohydr. Polym.* 206, 1–10. doi:10.1016/j.carbpol.2018.10.098

Zaidi, M. (2007). Skeletal Remodeling in Health and Disease. *Nat. Med.* 13 (7), 791–801. doi:10.1038/nm1593

Zhang, B., Skelly, J. D., Maalouf, J. R., Ayers, D. C., and Song, J. (2019). Multifunctional Scaffolds for Facile Implantation, Spontaneous Fixation, and Accelerated Long Bone Regeneration in Rodents. *Sci. Transl. Med.* 11 (502). doi:10.1126/scitranslmed.aau7411

Zhang, Y., Xie, Y., Hao, Z., Zhou, P., Wang, P., Fang, S., et al. (2021). Umbilical Mesenchymal Stem Cell-Derived Exosome-Encapsulated Hydrogels Accelerate Bone Repair by Enhancing Angiogenesis. *ACS Appl. Mater. Inter.* 13 (16), 18472–18487. doi:10.1021/acsami.0c22671

Zhao, D., Liu, M., Li, J., Xiao, D., Peng, S., He, Q., et al. (2021). Angiogenic Aptamer-Modified Tetrahedral Framework Nucleic Acid Promotes Angiogenesis *In Vitro* and *In Vivo*. *ACS Appl. Mater. Inter.* 13 (25), 29439–29449. doi:10.1021/acsami.1c08565

Zhou, Q., Gallagher, R., Ufret-Vincenty, R., Li, X., Olson, E. N., and Wang, S. (2011). Regulation of Angiogenesis and Choroidal Neovascularization by Members of microRNA-23 27 24 Clusters. *Proc. Natl. Acad. Sci.* 108 (20), 8287–8292. doi:10.1073/pnas.1105254108

**Conflict of Interest:** The authors declare that the research was conducted in the absence of any commercial or financial relationships that could be construed as a potential conflict of interest.

**Publisher's Note:** All claims expressed in this article are solely those of the authors and do not necessarily represent those of their affiliated organizations, or those of the publisher, the editors and the reviewers. Any product that may be evaluated in this article, or claim that may be made by its manufacturer, is not guaranteed or endorsed by the publisher.

frontiers in Bioengineering and Biotechnology

ORIGINAL RESEARCH
published: 08 March 2022
doi: 10.3389/fbioe.2022.825231

# *In vitro* and *in vivo* Repair Effects of the NCF-Col-NHA Aerogel Scaffold Loaded With SOST Monoclonal Antibody and SDF-1 in Steroid-Induced Osteonecrosis

*Bing Xu*[1,2†], *Zeyu Luo*[1†], *Duan Wang*[1], *Zeyu Huang*[1], *Zongke Zhou*[1] and *Haoyang Wang*[*,1]

[1]Department of Orthopaedic, West China Hospital, Orthopedic Research Institute, Sichuan University, ChengDu, China, [2]Department of Orthopaedic Surgery, Chengdu Second People's Hospital, ChengDu, China

In the current study, we synthesized nanocellulose (NCF)-collagen (Col)-nano hydroxyapatite (NHA) organic-inorganic hybrid aerogels loaded with stromal cell derived factor-1 (SDF-1) and sclerostin monoclonal antibody (SOST McAb) and investigated their ability to repair steroid-induced osteonecrosis. Rabbit bone marrow mesenchymal stem cells (BMSCs) and human vascular endothelial cells (HUVECs) were used for the *in vitro* study. A rabbit steroid-induced osteonecrosis model was used for the *in vivo* study. The best elastic modulus reached 12.95 ± 4.77 MPa with a mean compressive property of 0.4067 ± 0.084 MPa for the scaffold containing 100% mass fraction. The average pore diameter of the aerogel was 75 ± 18 μm with a porosity of more than 90% (96.4 ± 1.6%). The aerogel-loaded SDF-1 and SOST were released at 40–50% from the material within the initial 3 h and maintained a stable release for more than 21 days. The *in vitro* study showed osteogenesis and vascularization capabilities of the scaffold. The *in vivo* study showed that rabbits received implantation of the scaffold with SOST McAb and SDF-1 showed the best osteogenesis of the osteonecrosis zone in the femoral head. Imaging examination revealed that most of the necrotic area of the femoral head was repaired. These results suggest that this hybrid aerogel scaffold could be used for future steroid-induced osteonecrosis repair.

**Keywords: aerogel, steroid-induced osteonecrosis, bone repair, sost, bone regenaration**

OPEN ACCESS

***Edited by:***
*Di Huang,*
*Taiyuan University of Technology, China*

***Reviewed by:***
*Guosheng Tang,*
*Guangzhou Medical University, China*
*Xiao Yang,*
*City University of Hong Kong, Hong Kong SAR China*

***Correspondence:**
*Haoyang Wang*
*wanghaoyang-scu@163.com*

*†These authors have contributed equally to this work*

***Specialty section:***
*This article was submitted to Biomaterials, a section of the journal Frontiers in Bioengineering and Biotechnology*

***Received:*** *30 November 2021*
***Accepted:*** *11 February 2022*
***Published:*** *08 March 2022*

***Citation:***
*Xu B, Luo Z, Wang D, Huang Z, Zhou Z and Wang H (2022) In vitro and in vivo Repair Effects of the NCF-Col-NHA Aerogel Scaffold Loaded With SOST Monoclonal Antibody and SDF-1 in Steroid-Induced Osteonecrosis. Front. Bioeng. Biotechnol. 10:825231. doi: 10.3389/fbioe.2022.825231*

## INTRODUCTION

Steroid-induced osteonecrosis of the femoral head (ONFH) is due to long-term use or a high dose of glucocorticoids in a short time (Wang et al., 2018). Great health-related burdens, including pain and work ability loss, were caused by the disease. Because of the sclerotic zone around the necrotic area of the femoral head, it is difficult for conventional drugs to reach the necrotic area through blood circulation, and which is one of the reasons why there are currently no effective therapeutic drugs for ONFH (García-Gareta et al., 2015; Wang et al., 2016). Through drilling, decompression is the most commonly used surgical method for head protection treatment for osteonecrosis, and two-thirds of patients seek total hip arthroplasty at the end stage (Peng et al., 2018).

An aerogel is a type of special gel that uses gas to replace the liquid in the gel without essentially changing the network structure or volume of the gel itself (Moon et al., 2011). It has the characteristics of a micrometer porous structure, high porosity, and ultralow density. In addition, it has the maximum internal surface area of the same volume in the material at present (Cai et al., 2014; Barrios et al., 2019). Nanocellulose has a wide range of sources, low price, nontoxicity, biodegradability, excellent mechanical properties, and biocompatibility and can serve as an ideal raw material for the synthesis of aerogels (Long et al., 2018). Inorganic-organic hybrid nanocellulose has or exceeds the performance advantages of single-component nanomaterials: 1) Inorganic-organic hybrid nanocellulose aerogel has the advantages of traditional aerogel properties (low density, superior strength). That is, the pore size, strength, and elastic modulus of the material can be adjusted by changing the content of the composition so that it has a wider control range of elastic modulus and excellent mechanical properties, and has the natural advantage of becoming a hard tissue repair material (Kontturi et al., 2018; Wu et al., 2018). 2) Inorganic-organic hybrid nanocellulose aerogels have high biocompatibility and degradability. Cai et al. used natural nanocellulose aerogel microspheres as the medium for coculture with 3T3NIH cells, and the cells were colonized and grew well in the medium in which nanofiber aerogel microspheres were used as the growth skeleton (Cai et al., 2014). 3) The high porosity and specific surface area of inorganic-organic hybrid nanocellulose aerogels can carry more drugs, and the controllable and adjustable drug release rate enables them to be used as carriers of drugs or bone-induced cytokines. The maximum drug-carrying capacity and stable drug release capacity were achieved at a constant volume. Studies have demonstrated that the drug release of aerogel scaffolds can reach a peak quickly and maintain the peak drug dose for a long time (Zhao et al., 2015; Bhandari et al., 2017; Kéri et al., 2020). These superior properties provide a theoretical basis for the application of inorganic-organic hybrid cellulose aerogels in the field of bone defect repair.

In the repair of bone defects, it is necessary to recruit stem cells to gather in the defect area and differentiate in a direction conducive to bone formation. SDF-1 (stromal cell-derived factor-1) is an important chemokine secreted by bone marrow stromal cells that play an important role in progenitor cell homing, hematopoiesis, angiogenesis, and immunity. Studies have shown that SDF-1 binds to CXC chemokine receptor-4 (CXCR4) to activate CXCR4 receptor coupled G protein, to activate the P13K/PKC/NF-kb pathway and other pathways to recruit BMSCs, to promote BMSCs to secrete II collagen and glycosaminoglycan, to induce BMSCs to differentiate into osteoblasts, and to promote new bone formation. SDF-1 can also recruit vascular endothelial progenitor cells (EPCs) to promote angiogenesis and provide support for the repair of bone defects (Takahashi et al., 2020; Tamari et al., 2020). The coding gene of sclerostin encodes a protein polypeptide secreted by osteocytes that inhibits the growth of bone tissue because the expression of SOST is highly tissue specific. Inhibiting the secretion of sclerostin and weakening its activity can increase osteogenesis. At present, it has been confirmed that a specific antibody against SOST can antagonize the effect of SOST, ensure the normal transduction of the classical WNT signaling pathway and the normal physiological function of BMP, and make bone formation activity proceed smoothly (Korn et al., 2019; Scheiber et al., 2019). Nanohydroxyapatite (NHA) and type I collagen are components of bone tissue, and a large number of basic and clinical studies have confirmed the role of nanohydroxyapatite and type I collagen in the process of bone tissue repair. Nanocellulose has a large number of carboxyl groups that can be combined with any organic or inorganic particles through covalent or noncovalent bonds (Dong et al., 2013). Some researchers have successfully prepared new nanocellulose-based hybrid materials with uniform NHA distribution and have shown excellent biocompatibility and biomechanical properties (Jiang et al., 2013; Wang et al., 2019).

In the current study, we aimed to synthesize elastic aerogel scaffolds containing nanocellulose, nanohydroxyapatite, and type I collagen. Meanwhile, we used nanocellulose to carry SDF-1 and SOST McAb to observe the effect of this new material on the proliferation and differentiation of BMSCs and HUVECs *in vitro* and the repair of steroid-induced ONFH *in vivo*.

# MATERIALS AND METHODS

## Reagents

Information on the reagents used in the current study is listed in **Supplementary Table S1**.

## Preparation of Scaffolds

Our previous studies showed that when the ratio of nanocellulose (NCF): collagen (Collagen, Col) = 2: 1, a uniform and stable three-dimensional porous scaffold was formed, the pore structure of the scaffold changed little, and the pore diameter was uniform. NCF and Col at 2:1 were arranged into a 1.0% (w/v) suspension in deionized water, the pH was adjusted to 4, and different contents of NHA (NHA: NCF/Col = 50, 100, 150, and 200%) were added to the NCF/Col mixture and then stirred at 1,000 rpm/min until there was no granular NHA in the mixture. Then, under stirring at 300 rpm/min, γ-(2.3 epoxide) propyltrimethoxysilane was added dropwise to the mixed solution of NCF-Col-NHA, and the cross-linking reaction was continuously stirred for 48 h. The mold rested at 0–44°C for 4 h and then was replaced in tert-butanol solvent for 24 h, during which tert-butanol was replaced every 8 h. Finally, the sample was freeze-dried at −20°C for 48 h to obtain the NCF-Col-NHA aerogel scaffold (**Figure 1A**).

## Mechanical Properties and Characterization of NCF-Col-NHA Aerogel

The NCF-Col-NHA aerogels were treated with a hairdryer, and a copper sulfate dryer was placed to adjust humidity. The compressive strength of aerogel scaffolds with different NHA contents was tested by a constant loading pressure tester (compression speed 10 N per second, Instron, United States), and NCF-Col-NHA aerogel scaffolds with good mechanical

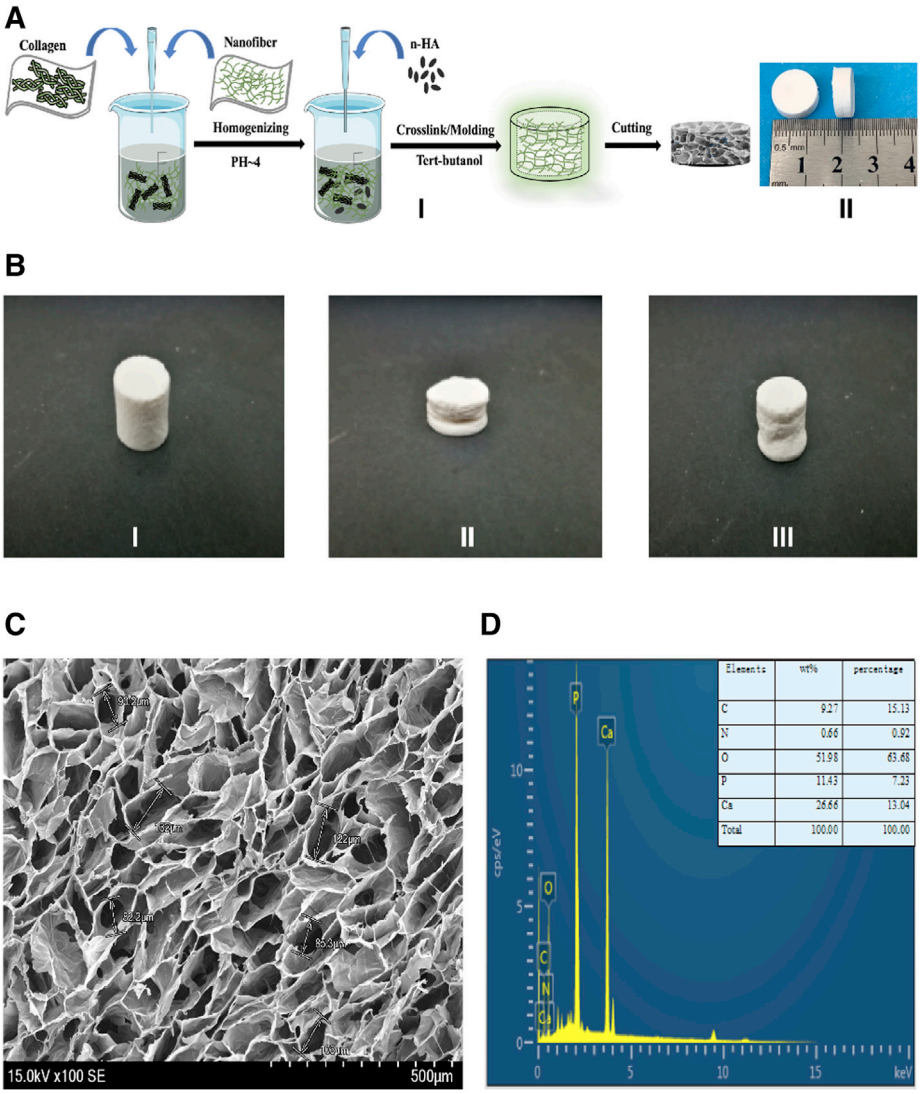


**FIGURE 1 |** The fabrication process, characterization of the NCF-Col-NHA aerogel scaffold **(A).** The fabrication process and appearance of NCF-Col-NHA aerogel scaffolds. I) show the manufacturing process of aerogel scaffolds: NCF and Col were mixed at a ratio of 2:1, stirred under PH4 conditions, and then added NHA, to get NCF-Col-NHA hydrogel. After replacing the water in the hydrogel with tert-butanol, the NCF-Col-NHA aerogel scaffold was obtained by freeze-drying at-20 °C for 48 h. II) is the finished product of the aerogel scaffold, which is the white porous scaffold **(B).** The shape of NCF-Col-NHA aerogel scaffolds could be restored after compression. **(C)** Morphological observation and elemental analysis of NCF-Col-NHA aerogel scaffolds. Observed under an electron microscope, NCF-Col-NHA aerogel is a porous structure with large and small pores connected **(D).** The elemental analysis of aerogel scaffold, phosphorus (P), calcium (Ca), oxygen (O), and carbon (C) are the main element.

strength were selected to carry SOST McAb + SDF-1. The NCF-Col-NHA aerogel with excellent mechanical strength was packed in separate bags and disinfected with ethylene oxide, and then 40 μl SOST McAb (1 μg/ml), 40 μl SDF-1 (1 μg/ml), 40 μl SOST McAb (1 μg/ml) and 40 μl SDF-1 (1 μg/ml) were dripped under aseptic conditions. After freeze-drying, aerogels loaded with SOST McAb, aerogels loaded with SDF-1, and aerogels loaded with SOST McAb + SDF-1 were obtained. The porosity of the aerogel scaffolds with different NHA contents was measured by the anhydrous ethanol replacement method. The sample was immersed in silica gel in a dryer for 48 h. The specific steps were as follows: the NCF-Col-NHA aerogel was immersed in anhydrous ethanol and weighed 24 h later, and five parallel groups were established to take the average value and calculate the standard deviation. The calculation formula is (W and $W_0$ are the initial mass and 24-h mass of the sample, respectively; V and $V_0$ are the initial volumes and 24-h volume of anhydrous ethanol, respectively).

The micromorphology and internal structure of the NCF-Col-NHA aerogel were observed by scanning electron microscopy (SEM, Nova SEM450, FEI, United States): longitudinal sections of the NCF-Col-NHA aerogel scaffold were obtained after rapid extraction with liquid nitrogen at low temperature. After drying, the sample was set on the sample table to spray gold. The

acceleration voltages of desktop SEM and field emission SEM are 5 and 20 kV, respectively. After SEM scanning, the selected area was scanned by an energy dispersive spectrometer (XSAM800, Kratos), and the surface morphology (pore diameter, porosity) and element composition of the NCF-Col-HA scaffold were analyzed. Aerogel scaffolds with excellent mechanical properties and characterization were selected for follow-up experiments.

## Detection of Degradation and Drug Release Rate of Aerogel Scaffolds in vitro

The NCF-Col-NHA aerogel scaffolds were immersed in a polyethylene plastic pipe containing SBF at a material: liquid ratio of 1:30 (g/ml). The polyethylene plastic pipe was made airtight and placed on a constant temperature shaker at 37°C at a rate of 120 rpm. The degradation experiments were performed *in vitro* for 120 days. The samples were removed and washed with deionized water ultrasound and anhydrous ethanol 3 times at 1, 7, 14, 21, 28, 42, 84, and 110 days. The samples were placed in a vacuum drying oven at 50°C for 12 h and weighed with an electronic balance. The weight of the scaffold is ($W_0$) before drying and ($W_1$) after drying. The weight loss rate (WL%) was calculated according to the mass loss of the scaffold before and after immersion:

The NCF-Col-NHA aerogel with excellent mechanical strength was packed in separate bags and disinfected with ethylene oxide, and then 40 μl SOST McAb (1 μg/ml), 40 μl SDF-1 (1 μg/ml), 40 μl SOST McAb (1 μg/ml) and 40 μl SDF-1 (1 μg/ml) were dripped under aseptic conditions. After freeze-drying, aerogels loaded with SOST McAb, aerogels loaded with SDF-1, and aerogels loaded with SOST McAb + SDF-1 were obtained. The same volume of materials with different drugs (aerogels loaded with SOST McAb only, aerogels loaded with SDF-1 only, and aerogels loaded with SOST McAb + SDF-1) and the control group (aerogel scaffold without drug-loaded) were placed in a centrifuge tube containing 1 ml PBS and placed in a constant temperature concussion box at 37°C with a vibration frequency of 60 times per minute. At the predetermined time, the leach liquor was taken to detect the concentration of SDF-1 and SOST monoclonal antibodies, and the drug release curve was drawn.

## Biological Properties of Aerogel Scaffolds in vitro

BMSCs from New Zealand rabbits were isolated according to established protocols and cultured in DMEM supplemented with 10% fetal bovine serum and 1% penicillin-streptomycin at 37°C in a 5% $CO_2$ incubator. The confluent cells were detached with a 0.25% trypsin mixture, and the isolated cells were subcultured in equal parts. Third-passage cells were employed to conduct the following experiment.

The same amount of aerogel scaffold with different drugs was placed into the DMEM culture, shaken in a constant temperature concussion box at 37°C for 72 h, and then filtered with a 22 μm filter to obtain the extracts. The cytotoxicity test was carried out according to the biological evaluation of GB/T16886.5-2003 medical devices. A BMSC suspension with a density of $1 \times 10^4$ cells/ml was added to a 96-well cell culture plate, and different aerogel scaffold extracts were added to the culture medium after cell attachment. Group I was aerogel extract without loading drugs, Group II was the extract of aerogel loaded with SOST McAb, Group III was the extract of aerogel loaded with SDF-1, Group IV extracted from aerogel loaded with SOST McAb + SDF-1, and Group V was the control group, with just the DMEM culture medium. There were ten holes in each group. The cells were cultured at 37°C, 5% $CO_2$ saturated humidity constant temperature incubator, and the culture medium was refreshed every 2 days. Quantitative analysis was performed with the CCK-8 kit on the 1st, 3rd, 5th, and 7th days, and the absorbance (OD value) of each well at 450 nm wavelength was detected by an automatic enzyme labeling instrument (Bio–Rad, United States). The relative growth rate (RGR) of BMSCs was estimated according to the OD value to evaluate cytotoxicity. RGR calculation formula: (Ren et al., 2008). According to the methods in the literature, the live/dead assay was carried out in each group after 3 days of culture (Zhang et al., 2019).

BMSCs and HUVCs were seeded on different scaffolds placed in 12-well culture plates at a density of $1 \times 10^5$ cells/well, incubated at a constant temperature of 37°C, 5% $CO_2$, and saturated humidity in an incubator for 5 h, allowing the cells to adhere to the scaffolds. Group I was the scaffold not loaded with drugs, Group II was the scaffold loaded with SOST McAb, Group III was the scaffold loaded with SDF-1, and Group IV was the scaffold loaded with SOST McAb + SDF-1. Four days later, the scaffolds were placed in 2.5% glutaraldehyde solution, moved to the refrigerator at 4°C for 24 h, and then gently rinsed with PBS solution three times. The material was gradient dehydrated with different concentrations of tert-butyl alcohol solution (50, 70, 90, 95, and 100%) and then vacuum freeze-dried for 24 h. Dried scaffolds were sprayed with gold, and the growth of cells on the surface of aerogel scaffolds was observed by electron microscopy. After being treated according to the standard process, the BMSCs and HUVCs were stained with iFluor555-labeled phalloidin and diaminphenyl indoles (DAPI). The cell morphology was observed by laser confocal microscopy, and the image was analyzed by ImageProPlus software. The cell spreading area and nuclear area of intact cells in the visual field were measured. The ratio of the cell spreading area to the nuclear area was calculated. *Transwell Test*.

The effect of scaffolds on the migration ability of BMSCs and HUVECs was examined by Transwell experiments. Group I was aerogel without drug loading, Group II was aerogel loaded with SOST McAb, Group III was aerogel loaded with SDF-1, Group IV was scaffold loaded with SOST McAb + SDF-1, and Group V was a simple culture medium group. The extract of each group was put into the Transwell chamber. The BMSC or HUVEC suspension ($1 \times 10^5$ cells/ml, 100 μl) was dripped into the chamber. After 24 h of incubation, the Transwell chamber was removed, and the number of cells migrating through the floor membrane of the small ventricle was calculated. The test was repeated three times.

## HUVEC Tubule Formation Assay

A tubule formation assay was used to determine the ability of extracts of different scaffolds to induce HUVEC tubule formation. The grouping was the same as 2.6. Matrigel was spread in a 15-well plate for tubule formation at 50 μl per well and incubated for 30 min. The HUVEC suspension was prepared with $1.5 \times 10^4$ cells per well, and 30 μl of 1% scaffold extract was added. There were 3 wells in each group, and they were incubated for 12 h. Five random visual fields were taken under a light microscope, and the tube volume was analyzed by ImageJ. The upper layer of liquid in the well was carefully absorbed, 50 μl of calcein was added to stain the cells in each well, and the cells were incubated at room temperature for 30 min away from light. Then, a fluorescein isothiocyanate (FITC) filter was used to collect the pictures.

## ALP Activity and Cell Mineralization

P3 rabbit BMSCs were cocultured with different aerogel scaffolds for 7 days (Group I was aerogel without drug loading, Group II was aerogel loaded with SOST McAb, Group III was aerogel loaded with SDF-1, and Group IV was aerogel scaffold loaded with SOST McAb + SDF-1). One milliliter of 0.1% Triton X-100 cell lysate was added to each well and frozen-thawed repeatedly at 37°C and −20°C three times. The obtained cell lysate was transferred into a centrifuge tube and centrifuged at 15,000 r/minute for 5 min. Each group absorbed 30 μl of the supernatant from the centrifuge tube. The ALP measurement was performed according to the operating instructions of the ELISA kit, the OD value was measured at 450 nm by an enzyme labeling instrument, and the OD values in each group were compared.

In the mineralization experiment, we had five groups: Group I was aerogel extract without a drug, Group II was aerogel extract loaded with SOST McAb, Group III was aerogel extract loaded with SDF-1, Group IV was aerogel extract loaded with SOST McAb + SDF-1, and Group V was FBS medium. A third-generation rabbit BMSC suspension with a concentration of $1 \times 10^5$ cells/ml was added to the wells (1 ml per well) and cultured at 37°C, 5% $CO_2$, and saturated humidity. The culture medium was changed every 2 days, and alizarin red staining was performed after 14 days. Calcium nodules were observed under the microscope.

## In vivo Study

The experimental scheme was approved by the Ethics Committee of West China Hospital of Sichuan University (Ethical approval No. 2020379A, 12.31.2020), and the experimental process strictly complied with the requirements of "Guiding opinions on being kind to Experimental Animals".

The modified lipopolysaccharide and hormone modeling method was used to establish a model of hormone-induced osteonecrosis in rabbits (Zhao et al., 2020). Firstly, the rabbits were injected with 10 μg/kg of lipopolysaccharide (LPS; Sigma) intravenously. After 24 h, they were injected once a day intramuscularly with 40 mg/kg of methylprednisolone (MPS) for the following 3 days. Penicillin 4,00,000 U was injected intramuscularly into each rabbit before treatment and then continued for 5 days. Four weeks later, the success of the model was assessed by imaging (X-ray, micro-CT) and histological examination. After successful modeling, the rabbits were randomly divided into five groups. After anesthesia, the rabbits were fixed on the operating table. Open the hip joint capsule near the greater trochanter to expose the femoral head, then use a 3.5 mm Kirschner wire to drill a 5 mm depth hole in the junction area of the femoral head and neck toward the necrotic area in the femoral head. The corresponding aerogel scaffold was implanted into the hole by a tweezer according to the experimental design. Aerogel scaffolds without drugs were implanted in Group I, aerogel scaffolds with SOST monoclonal antibody were implanted in Group II, aerogel scaffolds with SDF-1 were implanted in Group III, aerogel scaffolds with SOST monoclonal antibody + SDF-1 were implanted in Group IV, and nothing was implanted in Group V. The implant material was 0.4 cm in diameter with a 0.5 cm high cylinder (**Figure 8A**). All aerogel scaffolds were disinfected with ethylene oxide at low temperature (Disinfection Center of West China Hospital of Sichuan University). Each rabbit was injected with 4,00,000 U penicillin intramuscularly for three consecutive days. The samples were taken 12 weeks after the operation.

The specimens of the proximal femur were scanned using X-ray and micro-CT (SCANCO Medical AG vivaCT80). The area of the aerogel scaffold was selected as the region of interest (ROI) to form a three-dimensional image. The analysis parameters included bone mineral density (BMD), number of trabeculae (Tb. N), trabecular thickness (Tb. Th.3D), trabecular space (Tb. Sp.3D), and bone volume/tissue volume (BV/TV) (Bodnyk et al., 2020). The NCF-Col-NHA aerogel region in the scanned layer is reconstructed according to the scaffold, the part of bone growth in the material, and the density of the cavity with different grayscale and marked with different colors.

The removed femoral head was fixed with 10% paraformaldehyde solution and then cut and polished with a slicer to obtain thin slices with a thickness of approximately 20–30 μm, which were stained with HE and methylene blue-magenta. After vacuum critical drying, the tissue sections of each group were sprayed with gold. The bonding degree between the implanted aerogel scaffold and the host bone was observed bySEM.

## Osteogenic and Angiogenic Gene Expression

Quantitative real-time polymerase chain reaction (qRT-PCR) was conducted to determine osteogenic and angiogenic gene expression. Total RNA was extracted from the femoral head using TRIzol reagent and then reverse-transcribed according to the synthesized *VEGF*, *ALP*, and *BMP-2* gene primers by a reverse transcription kit (**Supplementary Table S2**). Then, qRT-PCR detection was carried out. Glyceraldehyde 3-phosphate dehydrogenase (*GAPDH*) was used as an internal reference for data standardization. Compared with the normal femoral head, the relative expression level of target gene mRNA was analyzed and calculated, and the expression of VEGF, ALP, and BMP-2

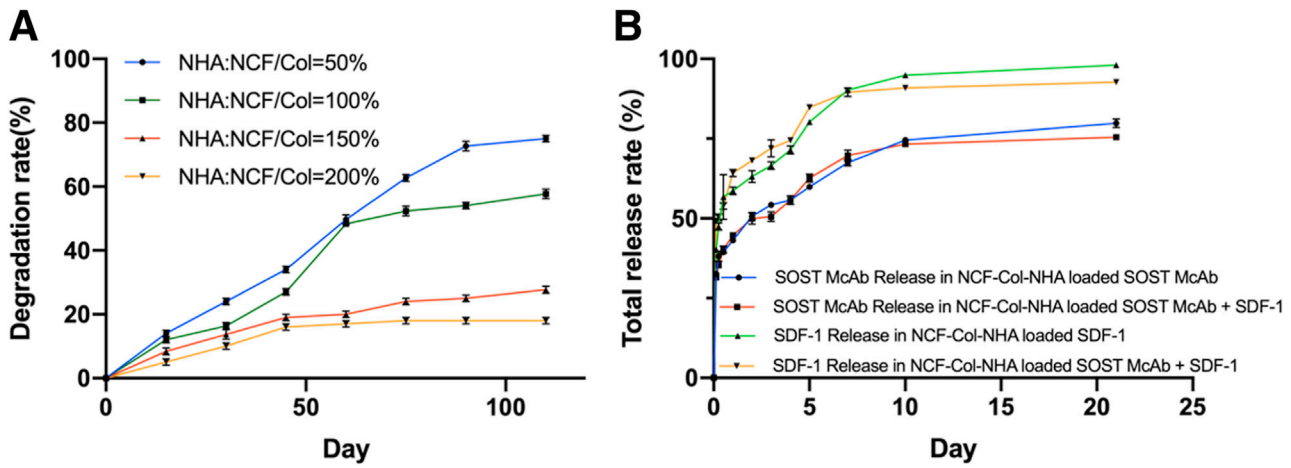


**FIGURE 2 |** The degradation curve and drug release curve of the NCF-Col-NHA aerogel scaffolds *in vitro*. **(A)** *In vitro* degradation curve of NCF-Col-NHA aerogel scaffolds with different NHA content. The less NHA content, the faster the material degrades **(B).** Drug release curve of aerogel scaffolds loaded with different drugs. There was no difference in release rate between SOST McAb and SDF-1, whether co-loaded or individually loaded on aerogel scaffolds.

protein was detected by Western blot according to the standard flow.

## Health Status of Organs

12th weeks after the operation, the liver, spleen, and kidney tissues of each group were taken and stained with HE, and the health status of each organ was observed.

## Statistical Analysis

All of the experiments were conducted in triplicate. One-way ANOVA followed by the least significant difference (LSD) test and Student–Newman–Keuls (SNK) test were performed to determine significant differences using IBM SPSS 20.0. $p < 0.05$ was considered statistically significant.

# RESULTS

## Mechanical Properties and Characterization of the NCF-Col-NHA Aerogel Scaffold

Aerogels with different mass fractions of NHAs have different compressive properties (50% HA: 0.3550 ± 0.0353 MPa; 100% HA: 0.4067 ± 0.084 MPa; 150% HA: 0.3641 ± 0.0506 MPa; 200% HA: 0.4262 ± 0.0209 MPa) and elastic modulus (50% HA: 4.25 ± 0.41 MPa; 100% HA: 12.95 ± 4.77 MPa; 150% HA: 8.16 ± 2.80 MPa; 200% HA: 9.36 ± 2.48 MPa). The composite aerogel scaffold with 100% NHA content recovered 95% of its deformation after compression (**Figure 1B**). Under the electron microscope, the NCF-Col-NHA composite scaffold materials with different HA contents are all through-pore structures with large pores and small pores coexisting. With increasing HA mass ratio, the pore size of the NCF-Col-NHA composite materials gradually decreased (50% HA: 90 ± 15 μm; 100% HA: 75 ± 18 μm; 150% HA: 60 ± 11 μm; 200% HA: 40 ± 13 μm). When the mass ratio of NHA was 50 and 100%, the material maintained a relatively good porous structure, but with the increase in the HA mass ratio, the pore structure of the material gradually deformed or even collapsed, and the porosity of the NCF-Col-NHA aerogel with 150 and 200% HA contents showed an obvious downward trend (50% HA: 97.3 ± 1.5%; 100% HA: 96.4 ± 1.6%; 150% HA: 89 ± 3.2%; 200% HA: 80 ± 2.3%). The composite scaffold with a 100% NHA ratio has the best mechanical strength and good porous structure, so we chose it for follow-up experiments. EDS elemental analysis showed that the main components of aerogel scaffolds included phosphorus (P), calcium (Ca), oxygen (O), and carbon (C) (**Figures 1C,D**).

## Degradation of Aerogel Scaffolds in vitro

The degradation rate of scaffolds decreased with increasing NHA content. The early stage of scaffold degradation is mainly swelling and cellulose disintegration. When the proportion of NHA is 50%, it is degraded to a certain extent, and cracks appear on the surface and interior of the material so that a large number of NCFs come into contact with simulated body fluids and swell rapidly, but the disintegration value is not reached within the range of degradation research. When the proportion of NHA was 100%, the degradation rate decreased slowly with increasing time, the NCF swelling and the degradation of Col and NHA were almost synchronized, and the degradation rate was relatively slow. For the NCF-Col-NHA aerogel with 150 and 200% NHA content, because of a large number of $Ca^{2+}$ ions in NHA, NHA reacted with -OH in NCF to form Ca-O bonds or O-Ca-O bonds, which made the tight combination of NCF and HA difficult to disintegrate. At the same time, NHA reduced the hydrophilicity of NCF, prevented the water molecules in SBF from entering the interior, and reduced the degradation rate and degradation amount. The aerogel scaffold with 100% NHA had the most suitable degradation rate (**Figure 2A**).

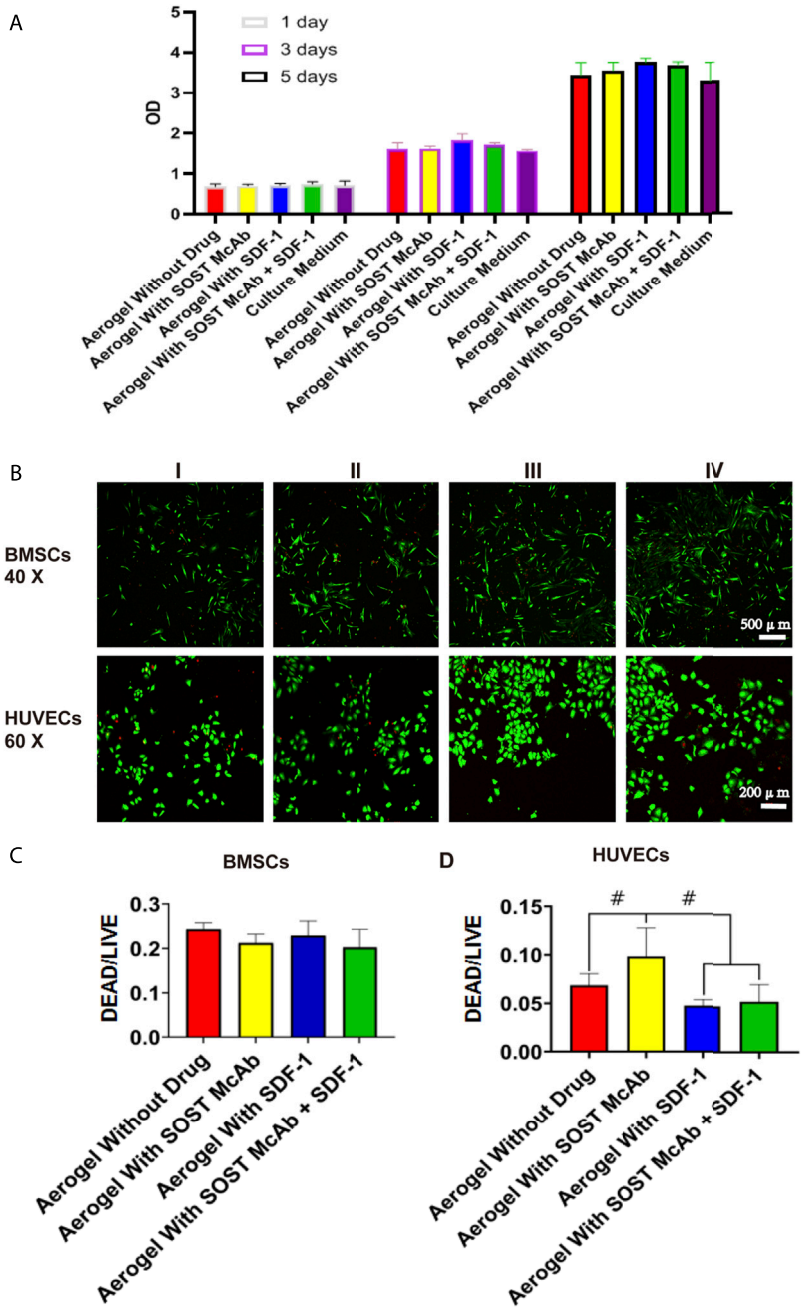


**FIGURE 3 |** The cell activity evaluation and the result of live/dead assay of the NCF-Col-NHA aerogel scaffold in vitro. Cell activity evaluation. When the extract of NCF-Col-NHA aerogel scaffolds with different drugs was co-cultured with BMSCs, the relative proliferation rate of BMSCs was between 97% and 113% **(A)**, these aerogel scaffolds had no cytotoxicity **(B–D)**. The result of live/dead assay. The BMSCs and HUVECs grow well on the aerogel scaffolds, the ratio of dead/living cells is lower than 10%. Group I, aerogel scaffold without loading drugs; Group II, aerogel scaffold loaded with SOST McAb; Group III, aerogel scaffold loaded with SDF-1; Group IV, aerogel scaffold loaded with SOST McAb + SDF-1. BMSCs, bone marrow mesenchymal stem cells; HUVECs, Human umbilical vein endothelial cells. #, $p < 0.05$.

## Drug Release Rate *in vitro*

There was no significant difference in the appearance of aerogel scaffolds loaded with different drugs, and all of them were milky white porous scaffolds. The drug release curve of the loaded NCF-Col-NHA aerogel *in vitro* shows that 40–50% of the SDF-1 and SOST McAbs were released from the material within 3 h and maintained a stable release rate in the following 21 days, and 70–80% of the drugs were involved in drug release on the 21st day. Drug release could be maintained for a longer time after Day 21. There was no difference in the release rate of SOST

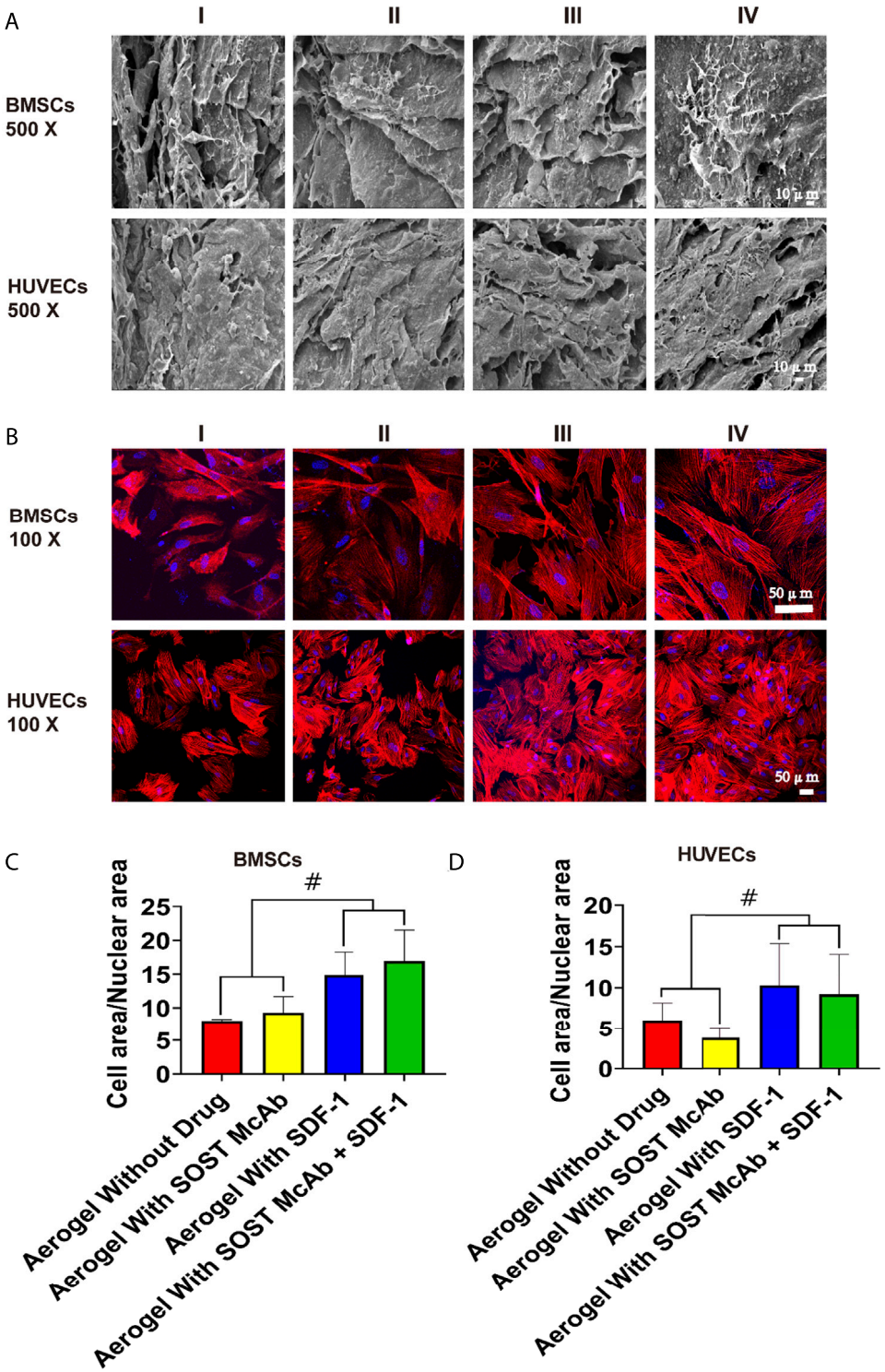


**FIGURE 4 |** The biocompatibility of the NCF-Col-NHA aerogel scaffold with BMSCs and HUVECs *in vitro*. **(A)** Under the electron microscope, BMSCs and HUVECs can adhere to the surface of aerogel scaffolds loaded with different drugs **(B–D)**. Observation on the morphology of cells on the surface of NCF-Col-NHA aerogel scaffolds. The results of iFluor555 labeled phalloidine and diaminphenyl indoles stain and cell area/nuclear area calculation showed that SDF-1 was beneficial to the adhesion and growth of BMSCs and HUVECs on the surface of the scaffolds. Group I, aerogel scaffold without loading drugs; Group II, aerogel scaffold loaded with SOST McAb; Group III, aerogel scaffold loaded with SDF-1; Group IV, aerogel scaffold loaded with SOST McAb + SDF-1. BMSCs, bone marrow mesenchymal stem cells; HUVECs, Human umbilical vein endothelial cells. #, $p < 0.05$.

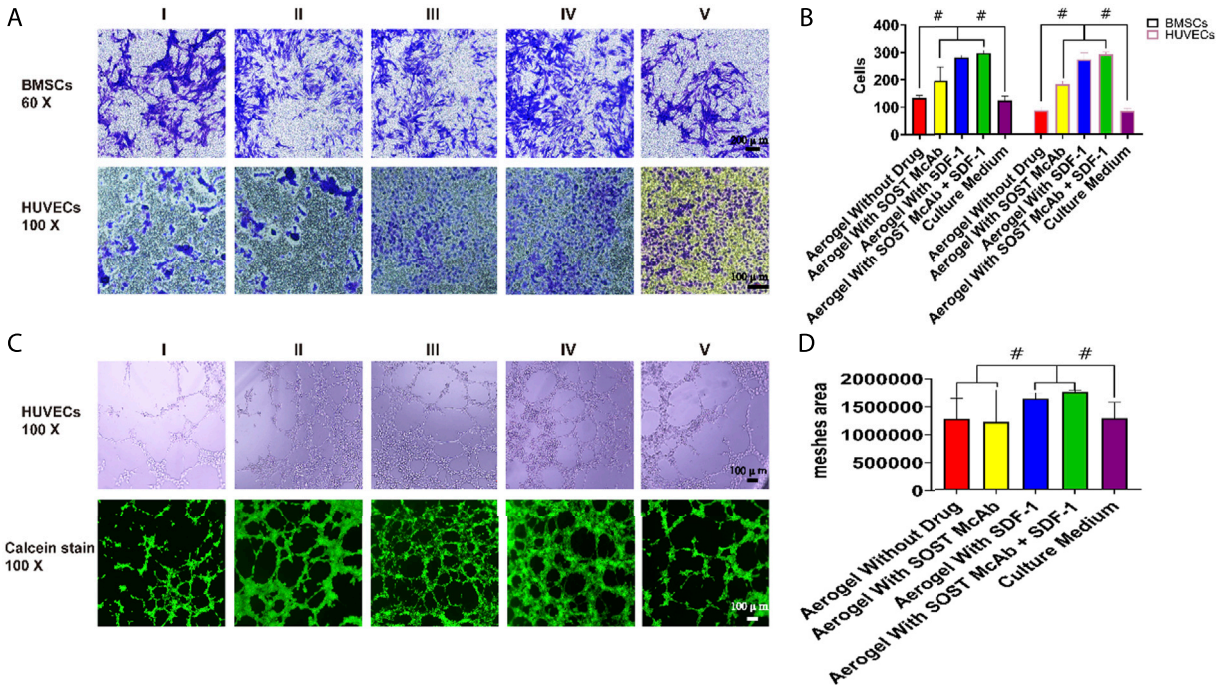


**FIGURE 5 |** The results of Transwell test and tubule formation assay. **(A,B)** Results of cell staining and cell count in Transwell test. The Transwell test shows that the extracts of aerogel scaffolds containing drugs were better than that of aerogel without drugs and common culture medium. Each bar represents a group, better Transwell test results were obtained in the extract of drug-loaded aerogel scaffolds **(C,D).** The result of HUVECs tubule formation Assay. Calcein staining results showed that the aerogel scaffold with SDF-1 had the best effect of forming tubules, and the histogram of analysis of meshes area showed the same results, the difference between groups was statistically significant. Group I, aerogel scaffold without loading drugs; Group II, aerogel scaffold loaded with SOST McAb; Group III, aerogel scaffold loaded with SDF-1; Group IV, aerogel scaffold loaded with SOST McAb + SDF-1; Group V, the control group with simple culture medium. BMSCs, bone marrow mesenchymal stem cells; HUVECs, Human umbilical vein endothelial cells. #, $p < 0.05$.

McAb and SDF-1 coloaded or separately loaded with the scaffolds (**Figure 2B**).

## *In vitro* Biological Performance

After coculture of BMSCs and the extract of different aerogel scaffolds, the RGR measured by the CCK-8 method was between 97 and 113%, and the scaffolds of each group met the toxicity requirements of biological implant materials. After BMSCs and HUVECs were grown on different groups of NCF-Col-NHA aerogels for 4 days, the living and dead cells on the materials were observed by live/dead assay. The dead cells were stained red, and the live cells were stained green. Both BMSCs and HUVECs grew well on the NCF-Col-NHA aerogel, and the ratio of dead cells was less than 10%. The ratio of HUVEC-dead cells in the aerogel group loaded with SOST monoclonal antibody was 9.94 ± 3%, which was slightly higher than that in the other groups ($p < 0.05$). There was no significant difference in the ratio of live/dead cells among the groups ($p > 0.05$) (**Figure 3**).

After BMSCs and HUVECs were cultured on different NCF-Col-NHA aerogels for 4 days, SEM revealed that both BMSCs and HUVECs could adhere to the aerogel scaffolds and grow pseudopodia. Compared with HUVECs, BMSCs had more and longer pseudopodia. The aggregation of cells on drug-loaded aerogel scaffolds was more obvious. There were more cells attached to SDF-1 aerogels and SOST McAb + SDF-1 aerogels, which may be related to the effect of SDF-1 on cell homing (**Figure 4A**). The area ratio of cytoplasm to nucleus was analyzed by Image software. The area ratio of cytoplasm to the nucleus in the aerogel group loaded with SDF-1 and SOST McAb + SDF-1 was 14.88 ± 3.39 and 16.95 ± 4.58, respectively, which was higher than that without drug loading (8.07 ± 0.20) and that loaded with SOST McAb (9.30 ± 2.42). The cytoplasmic/nuclear area ratios of HUVECs loaded with SDF-1 and SOST McAb + SDF-1 aerogels were 10.30 ± 5.07 and 9.22 ± 4.83, respectively, which were higher than those of HUVECs loaded with unloaded drugs (6.02 ± 2.11) and SOST McAb (3.76 ± 1.38) (**Figures 4B–D**).

Four hours after inoculation, the cells passing through the Transwell chamber could be seen in all groups. The average number of cells passing through the small ependyma in the group without drug aerogel was 122 ± 16 and 85 ± 9, respectively, which was lower than that in the group with drugs ($p < 0.05$). There was no significant difference between aerogel scaffolds loaded with different drugs.

Six hours after inoculation, HUVECs were arranged into a network structure. The areas of aerogels loaded with SDF-1 and SOST McAb + SDF-1 were 1650287.00 ± 99375.23 and 1768436.67 ± 29859.84, respectively, which were higher than those of the SOST McAb group (1231132.75 ± 570126.52) and unloaded drug group (1289030.50 ± 369031.77) (**Figure 5**).

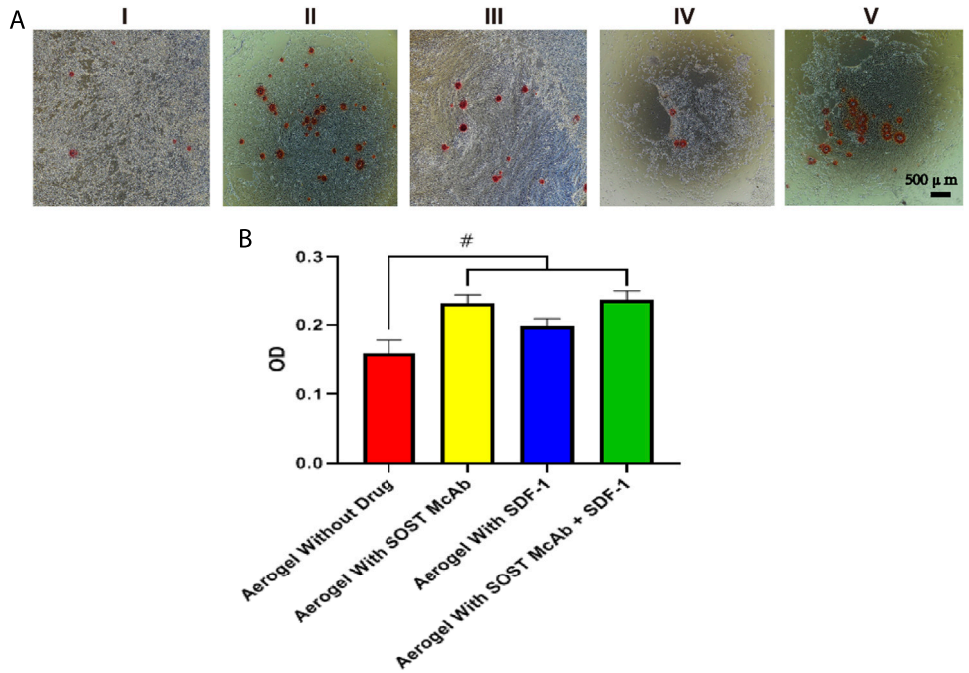


**FIGURE 6 |** The result of ALP activity and cell mineralization. **(A)** The results of alizarin red staining **(B)** alkaline phosphatase detection. The results showed that the aerogel scaffold with SOST Macb had a better osteogenic differentiation effect on BMSCs. Group I, aerogel extract without loading drugs; Group II, the extract of aerogel loaded with SOST McAb, Group III, the extract of aerogel loaded with SDF-1; Group IV, extracted from aerogel loaded with SOST McAb + SDF-1; Group V the control group with simple culture medium. #, $p < 0.05$.

## Osteogenic Differentiation

ELISA kits were used to detect the ALP content of cell lysates after coculture of aerogel scaffolds and BMSCs in each group. The OD value measured by the enzyme labeling instrument showed that the unloaded drug aerogel group was 0.16 ± 0.02, which was lower than those aerogel scaffolds with drugs ($p < 0.05$). The OD values of the McAb and McAb + SDF-1 aerogel groups were 0.23 ± 0.01 and 0.247 ± 0.02, respectively, which were higher than those of the SDF-1 aerogel scaffold ($p < 0.05$). The results of alizarin red staining showed that there were more calcium nodules in the SOST McAb and SOST McAb + SDF-1 groups (**Figure 6**).

## *In vivo* Experiments

To further study the biological performance of the aerogel scaffolds, we conducted an *in vivo* animal test for 12 weeks to confirm the bone regeneration ability of the scaffolds. In this study, 80 New Zealand rabbits were injected intramuscularly to induce steroid-induced ONFH. On the 2$^{nd}$ day after drug injection, most rabbits showed lethargy, reduced food intake, hair removal, and reduced activity, and some rabbits began to develop diarrhea. One week later, the mental state of the rabbit began to recover, and the intake of food gradually increased, but the activity of the rabbit was still less than that before the drug injection. Within 4 weeks, 20 rabbits died of upper gastrointestinal ulcers, perforation, diarrhea, and so on. When taking the model rabbit specimens, osteoporosis was found around the femoral head, the femoral cortex became thinner, and the color of the femoral head was darker than that of the normal rabbit, but there was no collapse of the femoral head. The X-ray results showed that the density of the femoral head in the model group was uneven, the trabeculae were blurred, and the trabeculae were partially interrupted. Micro-CT showed that the number of trabeculae in the model rabbits decreased, the width between the trabeculae increased, the cortex of the femoral neck became thinner, and the femoral head and trochanter were osteoporotic. The number of trabeculae (2.45 ± 0.04 /mm$^3$) and the bone volume/tissue volume (0.31 ± 0.04) were lower than those in the normal control group ($p < 0.05$). The trabecular space (0.38 ± 0.02 mm) was higher than that of the control group (0.28 ± 0.02) ($p < 0.05$), and there was no significant difference in the mineral density between the two groups. HE staining showed that the cartilage matrix and cells in the model group were normal, and the number of adipocytes and inflammatory cells in the bone trabeculae increased. In addition, the number and density of empty bone lacunae increased. The empty bone lacuna rate in the model group was 52.88 ± 1.19%, higher than that in the control group (22.73 ± 3.87%), $p < 0.05$. Steroid-induced osteonecrosis was successfully created in New Zealand rabbits to establish the animal model (**Figure 7**).

12th weeks after the operation, there was no collapse of the femoral head in any of the groups. There were still bone defects of the femoral head in the group without an aerogel scaffold implant, and the bone defects were repaired in the other four groups. X-ray and micro-CT showed that the bone defect was not completely repaired in the femoral head of the group without implanted materials. There were different degrees of high-density

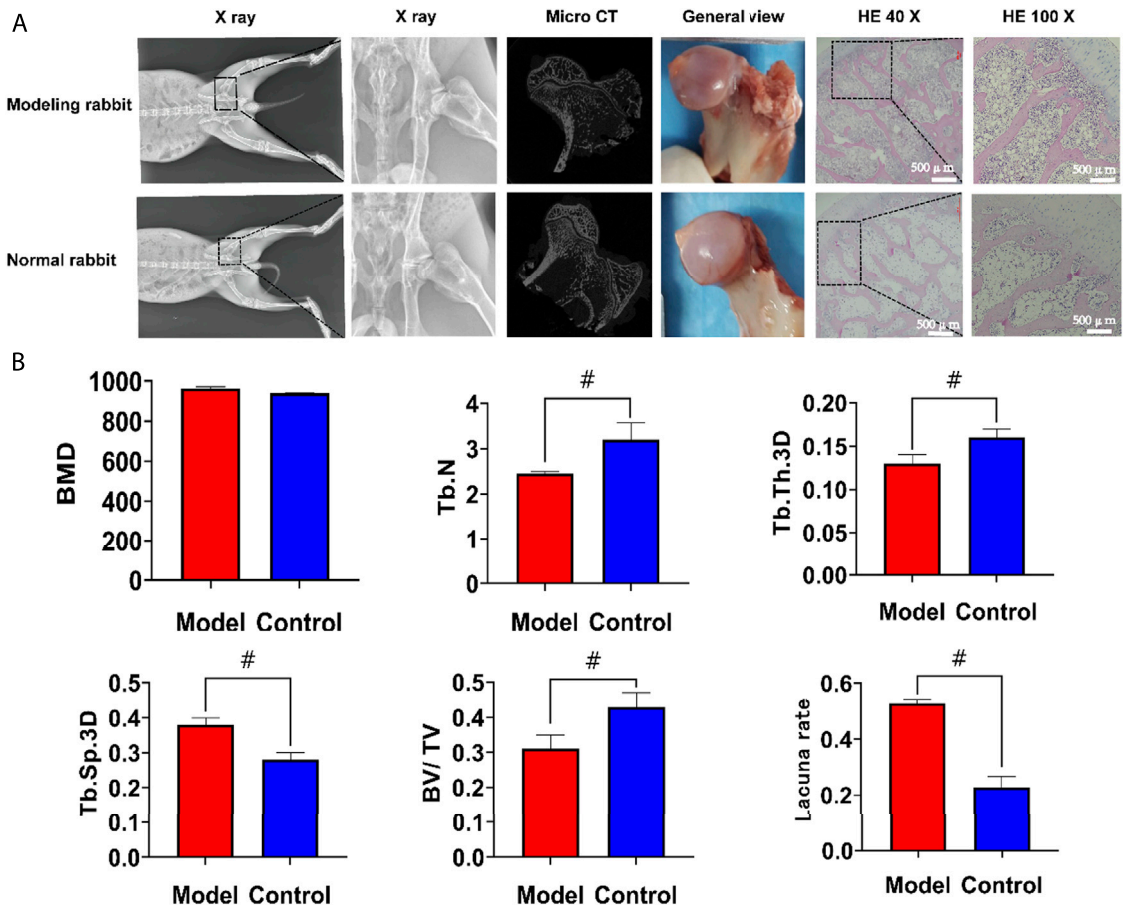


**FIGURE 7 |** The results of modeling of the steroid-induced osteonecrosis model in New Zealand rabbits. **(A)** After modeling, there was no collapse of the femoral head. Compared with the normal rabbits, the X-ray, Micro CT and HE staining showed that the trabeculae in the femoral head became thinner and the empty lacunae increased **(B).** Statistical results of regions of interest. The number of trabeculae and the bone volume/tissue volume was significantly lower than that in the normal group, the trabecular space was higher than the normal group but there was no significant difference in the mineral density between the two groups. The empty bone lacuna rate in the model group was more than 50%, which was significantly higher than that in the control group. HE, hematoxylin-eosin staining; BMD, bone mineral density; Tb. N, number of trabeculae; Tb. Th.3D, trabecular thickness; Tb. Sp.3D, trabecular space; BV/TV, bone volume/tissue volume. VEGF, vascular endothelial growth factor; BMP2, Bone Morphogenetic Protein 2; ALP, alkaline phosphatase. #, $p < 0.05$.

osteogenic images in the drilling area of the femoral heads in the other four groups. The area of aerogel implanted into the femoral head was selected as the ROI, and the analysis results showed that in the SOST McAb + SDF-1 aerogel group, the BMD was 742.14 ± 3.83 mg/ml, the trabecular thickness was 0.14 ± 0.02 mm, and the BV/TV was 0.33 ± 0.01, which was higher than those in other groups ($p < 0.05$), while the trabecular space (0.35 ± 0.01 mm) was lower than that in the other groups ($p < 0.05$). The number of bone trabeculae in the SOST McAb aerogel group and the SOST McAb + SDF-1 aerogel group was 3.04 ± 0.10/mm$^3$ and 3.51 ± 0.06/mm$^3$, respectively, which was higher than that in the other three groups ($p < 0.05$) (**Figures 8B,C**).

The results of HE staining showed that there was obvious new bone formation at the junction between the aerogel scaffold and host bone. In the group with the SOST McAb + SDF-1 aerogel scaffold, the bone grew deeper, and new bone could be observed in the center of the aerogel scaffold. However, in the group without aerogel scaffold implantation, there was only granulation tissue filling in the drilled tunnel but no discernible new bone formation. After methylene blue acid fuchsin staining, the aerogel containing hydroxyapatite was stained purplish red, the new bone tissue was light red, and the host bone tissue was red. The group implanted with the SOST McAb + SDF-1 aerogel scaffold had much more new bone formation, and the ability to encourage bone formation and repair bone defects was significantly stronger than that of the other groups (**Figure 9A**). SEM observation showed that the growth of new bone could be seen at the junction between aerogel scaffolds and host bone, and the aerogel scaffold with SDF-1 and aerogel scaffold with SOST McAb + SDF-1 was the most obvious (**Figure 8B**). The PCR results showed that the VEGF gene expression in the simple drilling decompression group and unloaded drug aerogel group was 0.002 ± 0.001 and 0.005 ± 0.001, respectively, which was lower than that in the other three groups ($p < 0.05$). The expression of the ALP gene in the simple drilling decompression group and the unloaded drug aerogel

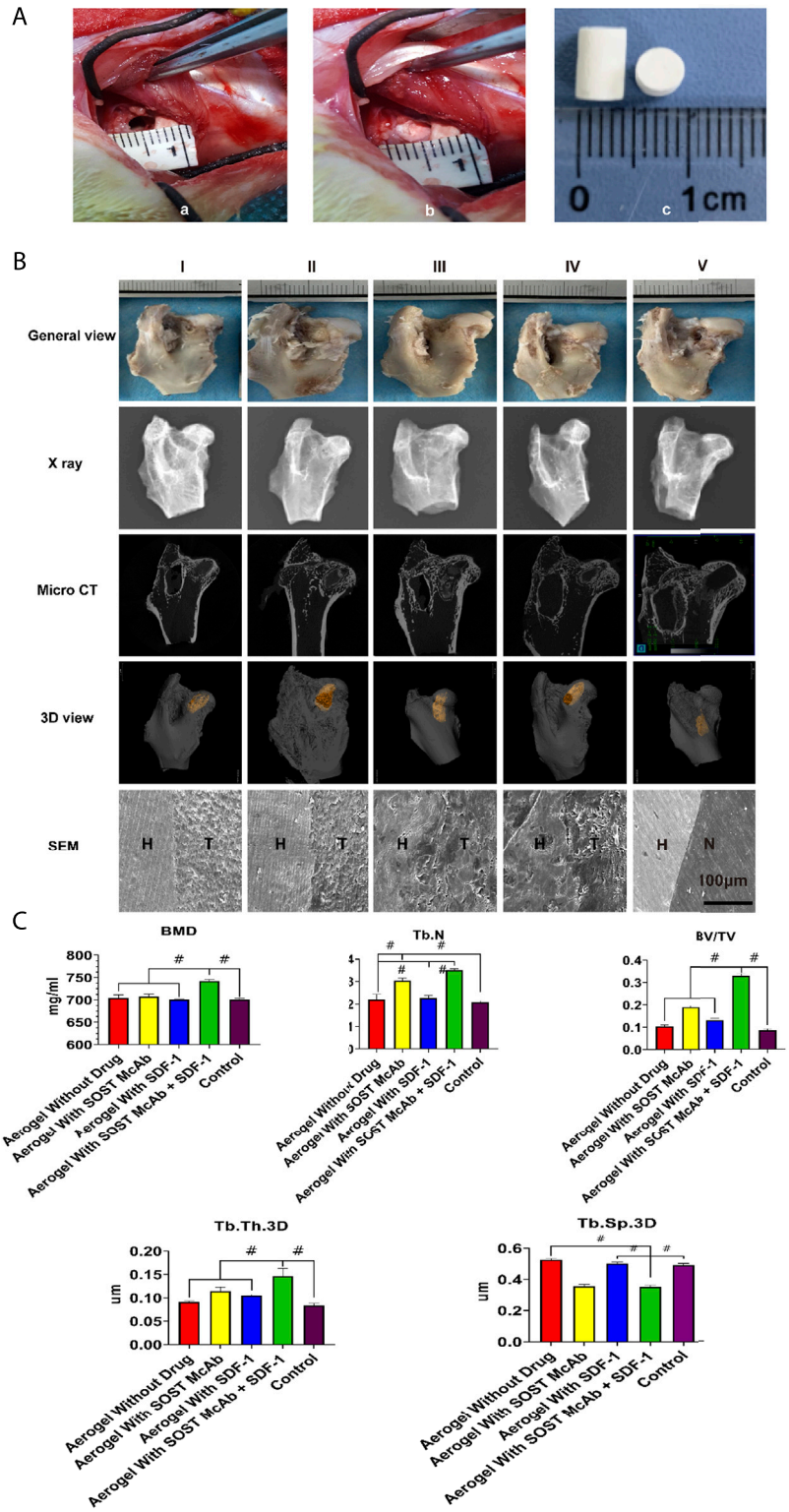


**FIGURE 8 |** The process and the results *in vivo* experiments. **(A)** the process *in vivo* experimental operation. The aerogel scaffold was implanted after drilling holes at the junction of the head and neck of the femur in rabbits. a) shows the 4 mm diameter of the hole; b) shows the implantation of the aerogel scaffold at the drill hole; c) is the diameter of the implanted aerogel stent, which is 5 mm **(B)**. Observation of New Zealand rabbits implanted with different aerogel scaffolds. There was no obvious collapse of the femoral head in all groups. X-ray and Micro CT showed that there were different degrees of new bone formation in the osteonecrosis area in the aerogel scaffold implanted group (I-IV), while in the group only drilled without aerogel implantation (V), only a small amount of new bone formed at the beginning of the

(*Continued*)

**FIGURE 8 |** hole, and the osteonecrosis area was not repaired. Under the electron microscope, there were different degrees of integration between aerogel scaffolds and host bone in the I-IV group, among which the group III and IV were the most obvious. There was no new bone formation in the osteonecrosis area of the group without aerogel scaffolds **(C)**. Results of Micro CT region of interest analysis. The bar graph shows that the group of aerogel scaffolds with SOST McAb + SDF-1 has the best bone quality. Group I aerogel scaffold without loading drugs, Group II aerogel scaffold loaded with SOST McAb, Group III aerogel scaffold loaded with SDF-1, Group IV aerogel scaffold loaded with SOST McAb + SDF-1, Group V the control group without scaffold implant, Group VI rabbit without surgery. H marked as the host bone, T marked as the aerogel scaffold, and N marked as the tunnel with granulation tissue. BMD, bone mineral density; Tb. N, number of trabeculae; Tb. Th.3D, trabecular thickness; Tb. Sp.3D, trabecular space; BV/TV, bone volume/tissue volume. #, $p < 0.05$.

group was 0.143 ± 0.001 and 0.015 ± 0.001, respectively, which was also lower than that in the other three groups ($p < 0.05$). The expression of BMP-2 in the SOST McAb-loaded group and SOST McAb + SDF-1 aerogel group was 2.63 ± 0.09 and 3.07 ± 0.02, respectively, which was higher than that in the other groups ($p < 0.05$). Analogous results were obtained by Western blot detection. The aerogel scaffold loaded with SOST McAb + SDF-1 had the best effect on promoting new bone and neovascularization (**Figure 10**).

At 12 weeks after the operation, there were no pathological abnormalities in the liver, spleen, or kidney of rabbits with aerogel scaffolds compared with rabbits without aerogel scaffolds and rabbits without surgery. It was confirmed again that the NCF-Col-NHA aerogel scaffold loaded with SOST McAb and SDF-1 had good biosafety (**Figure 9B**).

## DISCUSSION

The main purpose of this study was to design and make a porous composite scaffold with elasticity, basic recovery of deformation after compression, and the ability to induce osteogenesis and angiogenesis. This aerogel scaffold composed of nanohydroxyapatite, collagen, and nanocellulose was fabricated by improving the aerogel manufacturing process. Compared with traditional bone substitute materials, this new aerogel scaffold has the characteristics of traditional bone substitute materials; that is, it has a three-dimensional porous structure, bone conduction, and bone induction, so it is suitable for bone growth. The ideal scaffold for bone regeneration should obtain good mechanical properties. The compressive strength of the new composite scaffold developed in this study is 12.95 ± 4.77 MPa, which is within the range of compressive strength of cancellous bone (2–220 MPa) (Bose et al., 2012) and is suitable for filling cancellous bone defects of the femoral head. In our previous study, it was found that the higher the content of NHA was, the stronger the mechanical properties of the scaffold, but it affected the anti-deformation ability and porosity of the material. When the ratio of NHA to NCF-Col was 1:1, the scaffold had better mechanical strength and pore structure. The related results will be emphasized in another paper of our team. Previous studies have considered that the pore size of the most suitable material for bone growth is 100–4,400 μm, but some recent research results challenge these data. They think that micropores with pores lower than 100 μm or even nm are also suitable for bone growth, and smaller pores even show a better ability to induce bone growth (Eggli et al., 1988; Itälä et al., 2001; Bose et al., 2012). The average pore size of this new material is 75 ± 18 μm. The *in vitro* and *in vivo* results confirmed that pore sizes lower than 100 μm are suitable for bone growth. In addition, this innovative material has two outstanding characteristics: one is that it can quickly restore deformation after compression and has good plasticity, and the shape of the material can be restored to approximately 95% after compression. The scaffold can quickly restore deformation after being compressed and implanted into the bone defect area through a small orifice, and the volume of the material will be expanded to a certain extent after absorbing water or blood, fully filling the bone defect area. Second, nanocellulose acetate has a large number of carboxyl groups and a large internal surface area, which can carry more osteogenic and angiogenic drugs at the same volume (Ulker and Erkey, 2014). Our scaffolds can bind SDF-1 and SOST antibodies well and can be confirmed to have long-term and stable release, which is helpful to promote the repair of bone defects.

Excellent bone regeneration materials should have good histocompatibility. The nanocellulose acetate, nanohydroxyapatite, and collagen we selected are all materials with appropriate safety, and hydroxyapatite and type I collagen are the normal components of bone tissue (Liu et al., 2016). *In vitro*, it was found that BMSCs and HUVECs could adhere, aggregate, and exert their respective biological activities on the surface of the materials. Depending on the CCK-8 results, the proliferation of BMSCs increased on the composite aerogel scaffolds loaded with SOST monoclonal antibody and SDF-1. BMSCs and HUVECs were cocultured with scaffolds for 4 days, and the staining results of live/dead cells also showed that the scaffolds had good biocompatibility. Aerogel scaffolds loaded with SOST monoclonal antibody and SDF-1 are more conducive to cell adhesion, which provides a helpful beginning for local osteogenesis, angiogenesis, and bone defect repair centered on scaffold materials. In addition, the results of the Transwell experiment and tubule formation experiment also confirmed that the aerogel scaffold loaded with SOST monoclonal antibody + SDF-1 was more conducive to cell growth and biological activity expression than the control scaffold. This is of great importance to the repair of bone defects. *In vitro*, whether cocultured with SOST McAb + SDF-1 composite aerogel scaffold or adding composite scaffold extract to the culture medium, BMSCs showed better osteogenic activity than other groups. In this study, to more intuitively observe the effect of aerogel scaffolds with drugs on the osteogenic differentiation of BMSCs, we did not choose an osteogenic culture medium but used a common culture medium. After 14 days of culture, alizarin red staining of the five groups showed that the aerogel scaffolds carrying SOST monoclonal antibody and SOST monoclonal antibody + SDF-1 had a better effect on promoting the differentiation of BMSCs into osteoblasts than the other three groups.

One of the problems in repairing large bone defects is that it is difficult to form blood vessels in the central area of bone defects. Through the bone conduction of scaffold materials, the new bone tissue can repair and reconstruct the bone defect area while the scaffold is degraded gradually. However, due to insufficient blood

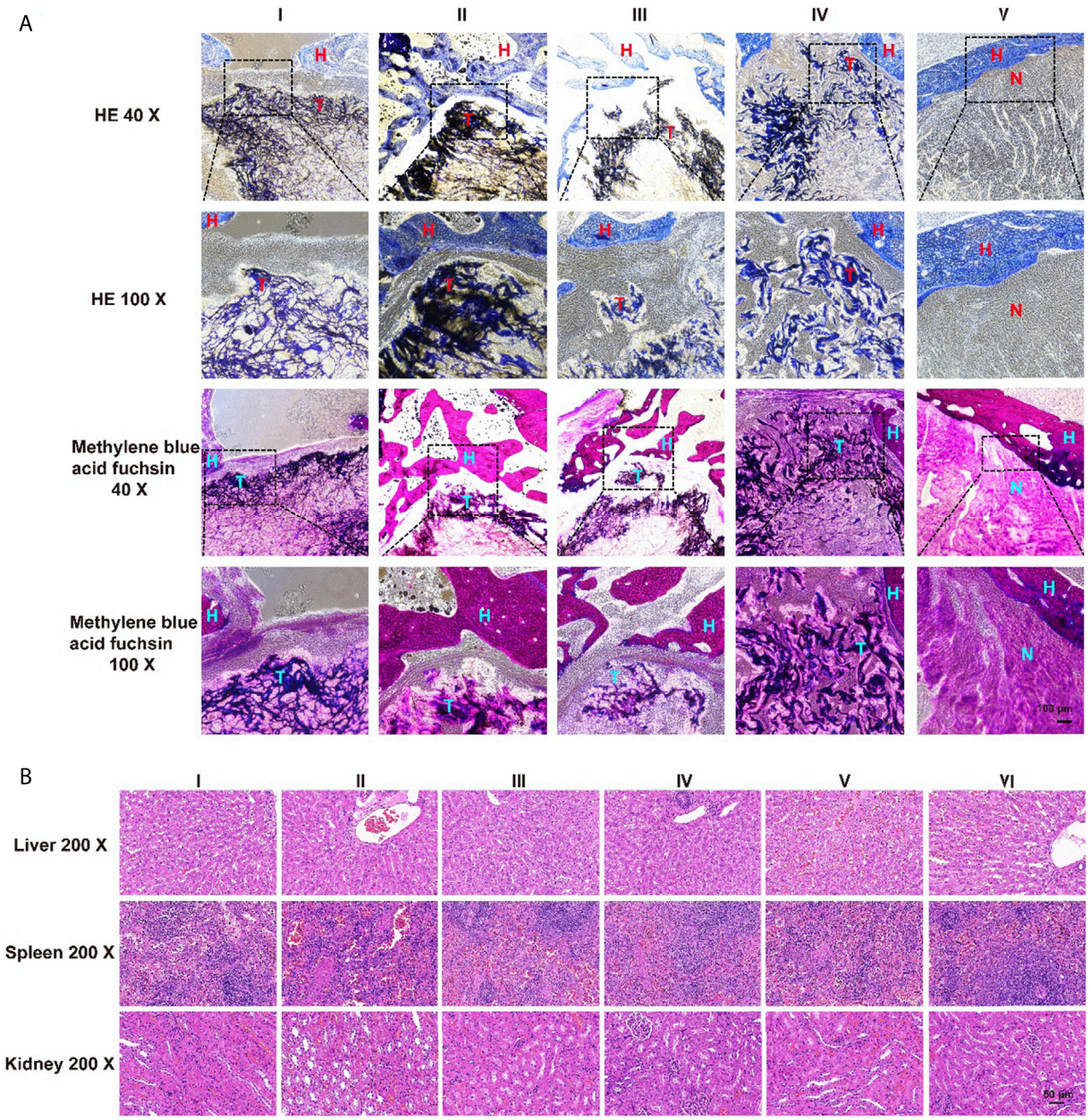


**FIGURE 9 |** The results of HE and methylene blue acid fuchsin staining and safety monitoring. **(A)** There were obvious bone formation and new bone formation at the junction between the aerogel scaffold and host bone. The ability of the aerogel scaffold carrying SOST McAb + SDF-1 to promote new bone formation was significantly higher than that of other groups **(B)**. Results of HE staining of visceral organs. 12 weeks after the operation, no pathological abnormality was found in the liver, spleen, and kidney of the rabbits in each experimental group (I-IV) compared with the group without scaffold unimplanted (V) and the of the unoperated group (VI). Group I aerogel scaffold without loading drugs, Group II aerogel scaffold loaded with SOST McAb, Group III aerogel scaffold loaded with SDF-1, Group IV aerogel scaffold loaded with SOST McAb + SDF-1, Group V the control group without scaffold implant, Group VI rabbit without surgery. H marked as the host bone, T marked as the aerogel scaffold, N marked as the tunnel with granulation tissue. HE, hematoxylin-eosin staining.

supply in the central area of the bone defect, it is unable to provide enough nutrition for the new bone and eventually leads to the failure of bone defect repair (Wendt et al., 2006; Johnson et al., 2011). SDF-1 can recruit stem cells such as bone marrow stromal cells and vascular progenitor cells through the homing effect, and SOST can increase osteogenesis through the osteogenic effect (Suen et al., 2015; Janssens et al., 2018). The results showed that the aerogels loaded with SDF-1 had an obvious effect on the migration of HUVECs and BMSCs, and the aerogels loaded with SOST had an observable osteogenic effect. The aerogel scaffold loaded with SOST monoclonal antibody and SDF-1 can cause stem cells with osteogenic and angiogenic abilities to gather at the aerogel scaffold and differentiate in a direction conducive to osteogenesis and angiogenesis. Neovascularization provides sufficient nutritional support for the central area of the

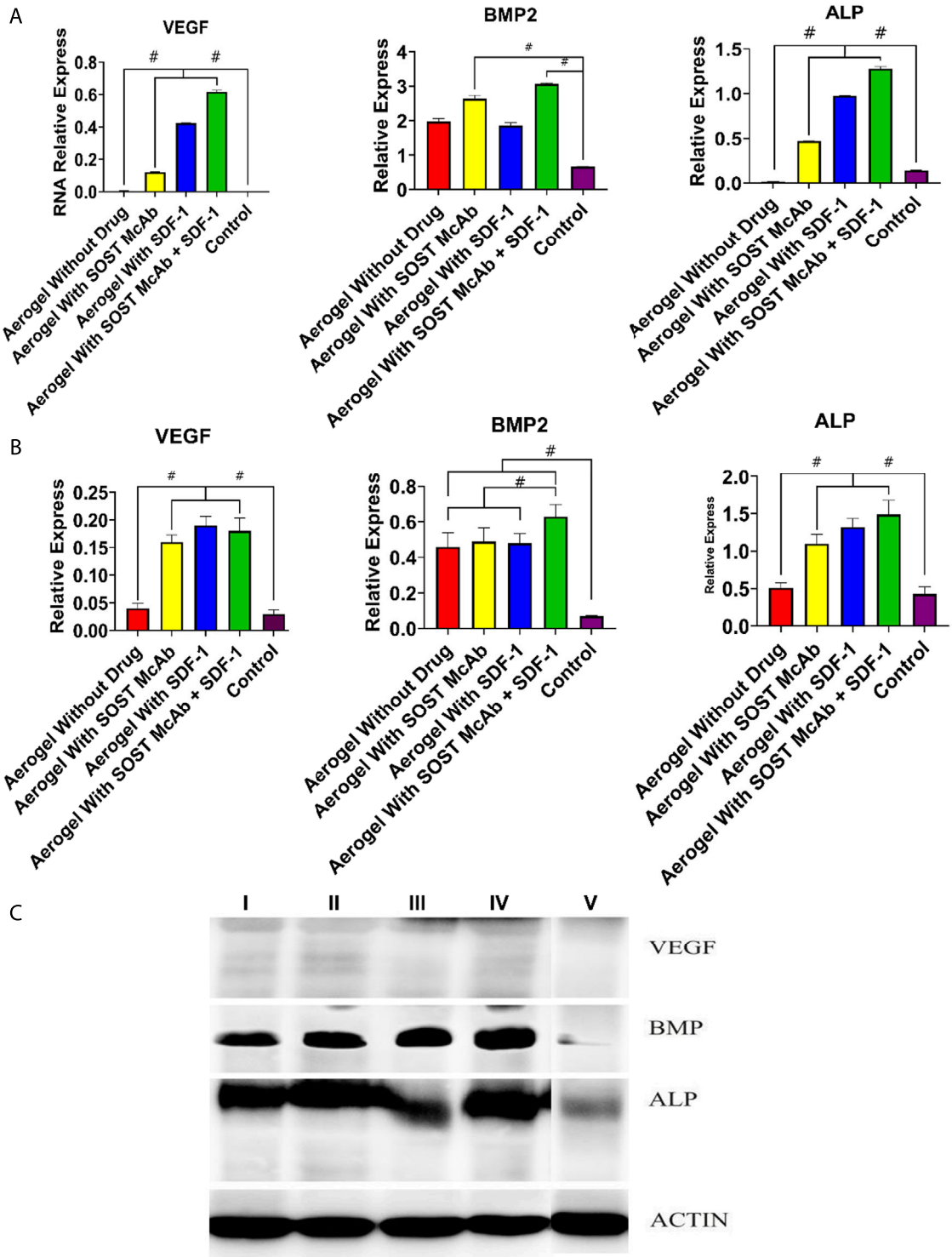


**FIGURE 10 |** Results of PCR and Western blot detection. **(A)** The results of PCR of VEGF, BMP2, and ALP **(B,C)**. The results of Western blot of VEGF, BMP2, and ALP. The bar graph showed that the aerogel loaded with SOST McAb and SDF-1 had the best effect on promoting new bone and neovascularization. Group I aerogel scaffold without loading drugs, Group II aerogel scaffold loaded with SOST McAb, Group III aerogel scaffold loaded with SDF-1, Group IV aerogel scaffold loaded with SOST McAb + SDF-1, Group V the control group without scaffold implant. VEGF, vascular endothelial growth factor; BMP2, Bone Morphogenetic Protein 2; ALP, alkaline phosphatase. #, $p < 0.05$.

bone defect and timely transport of metabolic waste, which is beneficial to the repair of bone defects, providing sufficient evidence for *in vivo* research.

There are a few difficulties in establishing a model of steroid-induced osteonecrosis in New Zealand rabbits. The combined use of lipopolysaccharide and high-dose glucocorticoids caused diarrhea, digestive tract ulcers, and death in some experimental animals (Powell et al., 2011; Xi et al., 2017). In our study, we reduced the death of experimental animals by giving proton pump inhibitors to the rabbits. After the establishment of the model, we confirmed the success of the model of ONFH by imaging and histological examination. The successful femoral head was drilled, and the scaffold material was implanted. This new composite scaffold perfectly realizes the assumption of implanting large-diameter filling materials through small diameter holes in the experiment. We utilized a 4 mm electric drill to obtain a decompressed bone tract and implanted composite scaffolds with a diameter of 5 mm to achieve good filling of bone defects. 12th weeks after the operation, no collapse of the femoral head was discovered in the rabbits by specimen observation and X-ray examination, indicating that the drilling operation controlled the disease progression of ONFH to a certain extent. The MicroCT results showed that there were more new bones in the femoral head of the experimental animals with aerogel scaffolds than in those with simple drilling. The results of RIO analysis showed that the bone repair effect of the composite aerogel scaffolds with SOST monoclonal antibody and SDF-1 was the best. Histological staining (HE staining and methylene fuchsin staining) confirmed that there was more new bone formation in the bone defect area when implanted with the SOST monoclonal antibody + SDF-1 composite aerogel scaffold. SEM showed that the fresh bone grew staggered at the interface between the aerogel scaffold and the host bone, and the bone grew deeper in the composite aerogel scaffold group with SOST monoclonal antibody + SDF-1. To further confirm that the SOST monoclonal antibody + SDF-1 composite aerogel scaffold has better osteogenic and angiogenic effects, we removed tissues from the target area to detect the osteogenic and angiogenic genes ALP, BMP2, and VEGF by fluorescence quantitative PCR and Western blot. The results showed that compared with the control and the scaffold with a single drug, the composite aerogel scaffold with SOST monoclonal antibody + SDF-1 had more advantages in osteogenesis and angiogenesis.

## CONCLUSION

In this study, an NCF-Col-NHA aerogel scaffold was successfully prepared, which has a three-dimensional porous structure, excellent anti-deformation ability, and good biomechanical properties, and successfully loaded with SOST monoclonal antibody and SDF-1, which can promote osteogenesis and angiogenesis and achieve sustained and effective drug release. The scaffold showed good osteogenic and angiogenic effects *in vitro* and *in vivo*. Tissue repair can be realized in the osteonecrosis area of steroid-induced ONFH. These results indicate that the NCF-Col-NHA aerogel scaffold with SOST McAb + SDF-1 is a promising substitute for bone repair.

## DATA AVAILABILITY STATEMENT

The original contributions presented in the study are included in the article/**Supplementary Material**, further inquiries can be directed to the corresponding author.

## ETHICS STATEMENT

The animal study was reviewed and approved by the Laboratory Animal Ethics Committee of West China Hospital of Sichuan University.

## AUTHOR CONTRIBUTIONS

BX and ZL compiled most of the manuscript, DW created the illustrations. ZH was a major contributor to guiding the experiment. HW assisted in writing and planning the manuscript, as well as making final edits. ZZ edited the manuscript. All authors contributed to the article and approved the submitted version.

## FUNDING

This research was funded by the National Natural Science Foundation of China (No. 81702128). The Foundation of Science and Technology Department of Sichuan Province (No. 2018SZ0051). The 1.3.5 project for disciplines of excellence, West China Hospital, Sichuan University (ZYJC21066).

## SUPPLEMENTARY MATERIAL

The Supplementary Material for this article can be found online at: https://www.frontiersin.org/articles/10.3389/fbioe.2022.825231/full#supplementary-material

## REFERENCES

Barrios, E., Fox, D., Li Sip, Y. Y., Catarata, R., Calderon, J. E., Azim, N., et al. (2019). Nanomaterials in Advanced, High-Performance Aerogel Composites: A Review. *Polymers (Basel)* 11 (4). 726, doi:10.3390/polym11040726

Bhandari, J., Mishra, H., Mishra, P. K., Wimmer, R., Ahmad, F. J., and Talegaonkar, S. (2017). Cellulose Nanofiber Aerogel as a Promising Biomaterial for Customized Oral Drug Delivery. *Ijn* Vol. 12, 2021–2031. doi:10.2147/ijn.s124318

Bodnyk, K. A., Kuchynsky, K. S., Balgemann, M., Stephens, B., and Hart, R. T. (2020). The Long-Term Residual Effects of Low-Magnitude Mechanical

Stimulation Therapy on Skeletal Health. *J. Biol. Eng.* 14, 9. doi:10.1186/s13036-020-0232-x

Bose, S., Roy, M., and Bandyopadhyay, A. (2012). Recent Advances in Bone Tissue Engineering Scaffolds. *Trends Biotechnology* 30 (10), 546–554. doi:10.1016/j.tibtech.2012.07.005

Cai, H., Sharma, S., Liu, W., Mu, W., Liu, W., Zhang, X., et al. (2014). Aerogel Microspheres from Natural Cellulose Nanofibrils and Their Application as Cell Culture Scaffold. *Biomacromolecules* 15 (7), 2540–2547. doi:10.1021/bm5003976

Dong, H., Snyder, J. F., Tran, D. T., and Leadore, J. L. (2013). Hydrogel, Aerogel and Film of Cellulose Nanofibrils Functionalized with Silver Nanoparticles. *Carbohydr. Polym.* 95 (2), 760–767. doi:10.1016/j.carbpol.2013.03.041

Eggli, P. S., Müller, W., and Schenk, R. K. (1988). Porous Hydroxyapatite and Tricalcium Phosphate Cylinders with Two Different Pore Size Ranges Implanted in the Cancellous Bone of Rabbits. A Comparative Histomorphometric and Histologic Study of Bony Ingrowth and Implant Substitution. *Clin. Orthop. Relat. Res.* 232, 127–138. doi:10.1097/00003086-198807000-00017

García-Gareta, E., Coathup, M. J., and Blunn, G. W. (2015). Osteoinduction of Bone Grafting Materials for Bone Repair and Regeneration. *Bone* 81, 112–121. doi:10.1016/j.bone.2015.07.007

Itälä, A. I., Ylänen, H. O., Ekholm, C., Karlsson, K. H., and Aro, H. T. (2001). Pore Diameter of More Than 100 Microm Is Not Requisite for Bone Ingrowth in Rabbits. *J. Biomed. Mater. Res.* 58 (6), 679–683.doi:10.1002/jbm.1069

Janssens, R., Struyf, S., and Proost, P. (2018). The Unique Structural and Functional Features of CXCL12. *Cell Mol Immunol* 15 (4), 299–311. doi:10.1038/cmi.2017.107

Jiang, H., Zuo, Y., Zou, Q., Wang, H., Du, J., Li, Y., et al. (2013). Biomimetic Spiral-Cylindrical Scaffold Based on Hybrid Chitosan/cellulose/nano-Hydroxyapatite Membrane for Bone Regeneration. *ACS Appl. Mater. Inter.* 5 (22), 12036–12044. doi:10.1021/am4038432

Johnson, E. O., Troupis, T., and Soucacos, P. N. (2011). Tissue-engineered Vascularized Bone Grafts: Basic Science and Clinical Relevance to Trauma and Reconstructive Microsurgery. *Microsurgery* 31 (3), 176–182. doi:10.1002/micr.20821

Kéri, M., Forgács, A., Papp, V., Bányai, I., Veres, P., Len, A., et al. (2020). Gelatin Content Governs Hydration Induced Structural Changes in Silica-Gelatin Hybrid Aerogels - Implications in Drug Delivery. *Acta Biomater.* 105, 131–145. doi:10.1016/j.actbio.2020.01.016

Kontturi, E., Laaksonen, P., Linder, M. B., NonappaGröschel, A. H., Rojas, O. J., et al. (2018). Advanced Materials through Assembly of Nanocelluloses. *Adv. Mater.* 30 (24), e1703779. doi:10.1002/adma.201703779

Korn, P., Kramer, I., Kramer, I., Schlottig, F., Tödtmann, N., Eckelt, U., et al. (2019). Systemic Sclerostin Antibody Treatment Increases Osseointegration and Biomechanical Competence of Zoledronic-Acid-Coated Dental Implants in a Rat Osteoporosis Model. *eCM* 37, 333–346. doi:10.22203/ecm.v037a20

Liu, Y., Luo, D., and Wang, T. (2016). Hierarchical Structures of Bone and Bioinspired Bone Tissue Engineering. *Small* 12 (34), 4611–4632. doi:10.1002/smll.201600626

Long, L. Y., Weng, Y. X., and Wang, Y. Z. (2018). Cellulose Aerogels: Synthesis, Applications, and Prospects. *Polymers (Basel)* 10 (6), 623. doi:10.3390/polym10060623

Moon, R. J., Martini, A., Nairn, J., Simonsen, J., and Youngblood, J. (2011). Cellulose Nanomaterials Review: Structure, Properties and Nanocomposites. *Chem. Soc. Rev.* 40 (7), 3941–3994. doi:10.1039/c0cs00108b

Peng, W., Zhang, J., Zhang, F., Zhao, Y., and Dong, W. (2018). Expression of Osteoprotegerin and Receptor Activator for the Nuclear Factor-kappaB Ligand in XACB/LV-bFGF/MSCs Transplantation for Repair of Rabbit Femoral Head Defect Necrosis. *J. Cel Biochem* 120, 1427–1434. doi:10.1002/jcb.27201

Powell, C., Chang, C., and Gershwin, M. E. (2011). Current Concepts on the Pathogenesis and Natural History of Steroid-Induced Osteonecrosis. *Clinic Rev. Allerg Immunol.* 41 (1), 102–113. doi:10.1007/s12016-010-8217-z

Ren, J., Zhao, P., Ren, T., Gu, S., and Pan, K. (2008). Poly (D,L-lactide)/nano-hydroxyapatite Composite Scaffolds for Bone Tissue Engineering and Biocompatibility Evaluation. *J. Mater. Sci. Mater. Med.* 19 (3), 1075–1082. doi:10.1007/s10856-007-3181-8

Scheiber, A. L., Barton, D. K., Khoury, B. M., Marini, J. C., Swiderski, D. L., Caird, M. S., et al. (2019). Sclerostin Antibody-Induced Changes in Bone Mass Are Site Specific in Developing Crania. *J. Bone Miner Res.* 34 (12), 2301–2310. doi:10.1002/jbmr.3858

Suen, P. K., Zhu, T. Y., Chow, D. H. K., Huang, L., Zheng, L.-Z., and Qin, L. (2015). Sclerostin Antibody Treatment Increases Bone Formation, Bone Mass and Bone Strength of Intact Bones in Adult Male Rats. *Sci. Rep.* 5, 15632. doi:10.1038/srep15632

Takahashi, R., Amano, H., Ito, Y., Eshima, K., Satoh, T., Iwamura, M., et al. (2020). Microsomal Prostaglandin E Synthase-1 Promotes Lung Metastasis via SDF-1/cxcr4-Mediated Recruitment of CD11b+Gr1+MDSCs from Bone Marrow. *Biomed. Pharmacother.* 121, 109581. doi:10.1016/j.biopha.2019.109581

Tamari, T., Kawar-Jaraisy, R., Doppelt, O., Giladi, B., Sabbah, N., and Zigdon-Giladi, H. (2020). The Paracrine Role of Endothelial Cells in Bone Formation via CXCR4/SDF-1 Pathway. *Cells* 9 (6), 1325. doi:10.3390/cells9061325

Ulker, Z., and Erkey, C. (2014). An Emerging Platform for Drug Delivery: Aerogel Based Systems. *J. Controlled Release* 177, 51–63. doi:10.1016/j.jconrel.2013.12.033

Wang, A., Ren, M., and Wang, J. (2018). The Pathogenesis of Steroid-Induced Osteonecrosis of the Femoral Head: A Systematic Review of the Literature. *Gene* 671, 103–109. doi:10.1016/j.gene.2018.05.091

Wang, D., Jang, J., Kim, K., Kim, J., and Park, C. B. (2019). "Tree to Bone": Lignin/Polycaprolactone Nanofibers for Hydroxyapatite Biomineralization. *Biomacromolecules* 20 (7), 2684–2693. doi:10.1021/acs.biomac.9b00451

Wang, X., Xu, S., Zhou, S., Xu, W., Leary, M., Choong, P., et al. (2016). Topological Design and Additive Manufacturing of Porous Metals for Bone Scaffolds and Orthopaedic Implants: A Review. *Biomaterials* 83, 127–141. doi:10.1016/j.biomaterials.2016.01.012

Wendt, D., Stroebel, S., Jakob, M., John, G. T., and Martin, I. (2006). Uniform Tissues Engineered by Seeding and Culturing Cells in 3D Scaffolds under Perfusion at Defined Oxygen Tensions. *Biorheology* 43 (34), 481–488.

Wu, Z.-Y., Liang, H.-W., Hu, B.-C., and Yu, S.-H. (2018). Emerging Carbon-Nanofiber Aerogels: Chemosynthesis versus Biosynthesis. *Angew. Chem. Int. Ed.* 57 (48), 15646–15662. doi:10.1002/anie.201802663

Xi, H., Tao, W., Jian, Z., Sun, X., Gong, X., Huang, L., et al. (2017). Levodopa Attenuates Cellular Apoptosis in Steroid-Associated Necrosis of the Femoral Head. *Exp. Ther. Med.* 13 (1), 69–74. doi:10.3892/etm.2016.3964

Zhang, Y., Wang, C., Fu, L., Ye, S., Wang, M., and Zhou, Y. (2019). Fabrication and Application of Novel Porous Scaffold In Situ-Loaded Graphene Oxide and Osteogenic Peptide by Cryogenic 3D Printing for Repairing Critical-Sized Bone Defect. *Molecules* 24 (9), 1669. doi:10.3390/molecules24091669

Zhao, J., Lu, C., He, X., Zhang, X., Zhang, W., and Zhang, X. (2015). Polyethylenimine-grafted Cellulose Nanofibril Aerogels as Versatile Vehicles for Drug Delivery. *ACS Appl. Mater. Inter.* 7 (4), 2607–2615. doi:10.1021/am507601m

Zhao, X., Alqwbani, M., Luo, Y., Chen, C., Ge, A., Wei, Y., et al. (2020). Glucocorticoids Decreased Cx43 Expression in Osteonecrosis of Femoral Head: The Effect on Proliferation and Osteogenic Differentiation of Rat BMSCs. *J. Cell. Mol. Med.* 25 (1), 484–498. doi:10.1111/jcmm.16103

**Conflict of Interest:** The authors declare that the research was conducted in the absence of any commercial or financial relationships that could be construed as a potential conflict of interest.

**Publisher's Note:** All claims expressed in this article are solely those of the authors and do not necessarily represent those of their affiliated organizations, or those of the publisher, the editors and the reviewers. Any product that may be evaluated in this article, or claim that may be made by its manufacturer, is not guaranteed or endorsed by the publisher.

frontiers | Frontiers in Bioengineering and Biotechnology

REVIEW
published: 01 April 2022
doi: 10.3389/fbioe.2022.866208

# Exosome-Laden Hydrogels: A Novel Cell-free Strategy for *In-situ* Bone Tissue Regeneration

*Jinru Sun*[1†], *Zhifeng Yin*[2†], *Xiuhui Wang*[1*] and *Jiacan Su*[1,3*]

[1]Institute of Translational Medicine, Shanghai University, Shanghai, China, [2]Department of Orthopedics, Shanghai Zhongye Hospital, Shanghai, China, [3]Department of Orthopaedics Trauma, Changhai Hospital, Second Military Medical University, Shanghai, China

*In-situ* bone tissue regeneration, which harnesses cell external microenvironment and their regenerative potential to induce cell functions and bone reconstruction through some special properties of biomaterials, has been deeply developed. In which, hydrogel was widely applied due to its 3D network structure with high water absorption and mimicking native extracellular matrix (ECM). Additionally, exosomes can participate in a variety of physiological processes such as cell differentiation, angiogenesis and tissue repair. Therefore, a novel cell-free tissue engineering (TE) using exosome-laden hydrogels has been explored and developed for bone regeneration in recent years. However, related reviews in this field are limited. Therefore, we elaborated on the shortcomings of traditional bone tissue engineering, the challenges of exosome delivery and emphasized the advantages of exosome-laden hydrogels for *in-situ* bone tissue regeneration. The encapsulation strategies of hydrogel and exosomes are listed, and the research progress and prospects of bioactive hydrogel composite system for continuous delivery of exosomes for *in-situ* bone repair are also discussed in this review.

**Keywords: hydrogels, exosomes, exosome-laden hydrogels, *in-situ bone tissue engineering*, bone regeneration**

OPEN ACCESS

***Edited by:***
*Di Huang,*
*Taiyuan University of Technology, China*

***Reviewed by:***
*Ying Yang,*
*University of Michigan, United States*
*Jingchao Li,*
*Donghua University, China*
*Chen Yang,*
*Wenzhou Institute (CAS), China*

***Correspondence:**
*Xiuhui Wang*
*blackrabbit@shu.edu.cn*
*Jiacan Su*
*drsujiacan@163.com*

[†]*These authors have contributed equally to this work*

***Specialty section:***
*This article was submitted to Biomaterials, a section of the journal Frontiers in Bioengineering and Biotechnology*

***Received:*** *31 January 2022*
***Accepted:*** *07 March 2022*
***Published:*** *01 April 2022*

***Citation:***
*Sun J, Yin Z, Wang X and Su J (2022) Exosome-Laden Hydrogels: A Novel Cell-free Strategy for In-situ Bone Tissue Regeneration. Front. Bioeng. Biotechnol. 10:866208. doi: 10.3389/fbioe.2022.866208*

## INTRODUCTION

Currently, bone replacements for skeletal defects are highly required by a majority of patients who suffered accidents or age-related diseases in clinic. It is estimated that more than two million bone grafting procedures are operated per year around the world, with more than a quarter of them operated in the United States (Campana et al., 2014). Moreover, bone grafts need over 600,000 cases in the US caused by cancer and traumatic injuries, which cost about $2.5 billion (Laurencin et al., 2006).

As we all know, autologous bone grafting is always considered as a "gold standard".

(Ho-Shui-Ling et al., 2018) for clinical treatments of bone defects while its source is limited (Zhang et al., 2019) and secondary surgery caused infection (Laurencin et al., 2006). After that, allografts was developed (Vanderstappen et al., 2015) but the immunological rejection was caused (Dimitriou et al., 2011; Zhang et al., 2019). Therefore, the limitations of autograft and allograft result in alternative bone repair strategies was highly desired and widely developed (Kempen et al., 2009; De Witte et al., 2018).

In recent years, bone tissue engineering strategy, which utilizes the cell culture and functional differentiation *in vitro* to construct bioactive bone-grafts, has been deeply developed for bone regeneration (**Figure 1A**) (Kempen et al., 2009). Among them, the

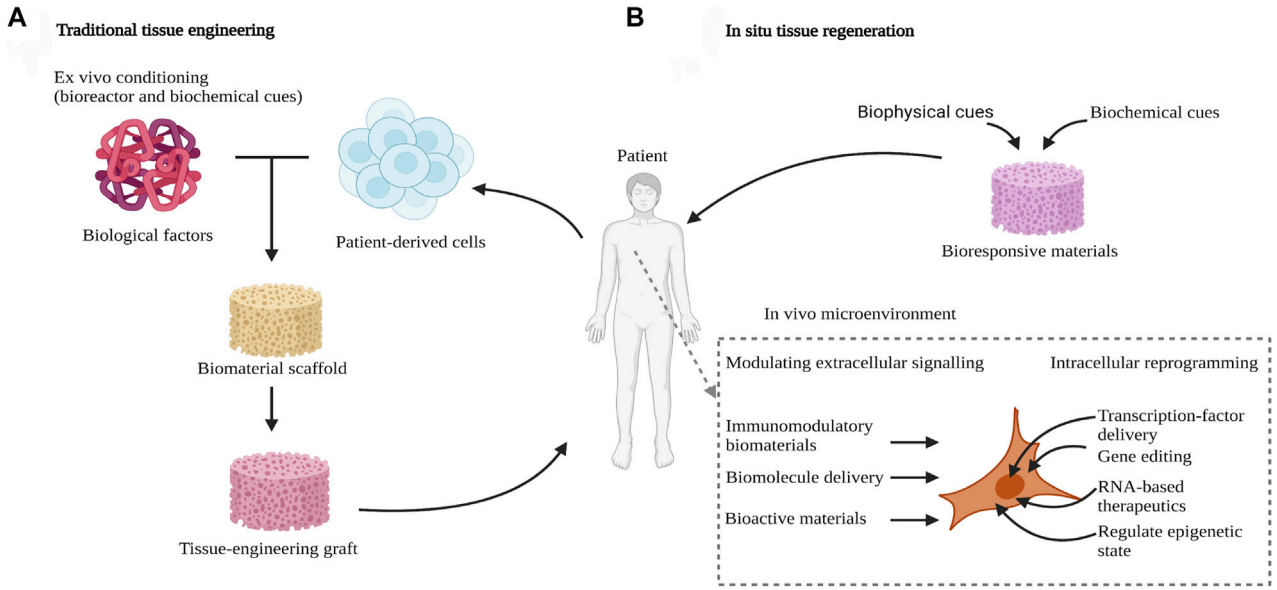


**FIGURE 1 |** *In-situ* tissue engineering. **(A)** Traditional tissue-engineering approaches require the pre-seeding of engineered scaffolds and *ex vivo* conditioning before implantation into the body. **(B)** *In situ* tissue regeneration uses bioresponsive materials that harness the innate regenerative ability of the body. These materials are loaded with biochemical and biophysical cues to recruit endogenous cells for tissue healing (Gaharwar et al., 2020). Copyright 2020, Gaharwar, A.K., Singh, I. & Khademhosseini.

major elements of bone tissue engineering are seeding cells, growth factors and biomaterial scaffolds (Petta et al., 2016; Yu et al., 2018).scaffold is a crucial factor to bone tissue engineering, which offered the space for cell growth, proliferation and differentiation (Zhang et al., 2010). To promote the three-dimensional attachment, growth and tissue regeneration of cells, the scaffold needs a large specific surface area and interconnected pores (Yu et al., 2018; Zhu et al., 2021). The biomaterials which can be used for fabricating porous scaffolds consist of inorganic ceramic, polymer and metal materials (Yan et al., 2018; Wei et al., 2022). Patients with diabetes mellitus (DM) suffer from poor bone healing ability, the 3D-printed enzyme-functionalized scaffold showed anti-inflammatory and osteogenic effects under diabetic conditions (Yang et al., 2021b). Another study also reported a novel 3D composite scaffold not only triggered the ablation of osteosarcoma *via* high temperature generated by near-infrared II light, but also promoted vascularized bone regeneration *in vivo* by the controlled release of bioactive ions (Sr, Cu, and Si) (Yang et al., 2021a). The scaffold could offer the cells the 3D space, mechanical support and so on. Recently, hydrogels with a 3D network structure, high water absorption and mimicking cell microenvironment have been widely developed. It can be used for the cell encapsulation and ingrowth, thereby promoting their uniform distribution and slightly higher loading densities (Hölzl et al., 2016). Also, bone tissue engineering generally concentrates on fully elastic materials as a result of their superior mechanical strength and stiffness, whereas bone tissue is characteristically viscoelastic. viscoelastic material, which has features such as direct cell behavior and stress relaxation influence, complete with mineralized matrix deposition and osteogenic differentiation (Wang and Yeung, 2017). So, hydrogels with tunable stress-relaxation behavior tend to be a key to direct bone tissue regeneration in non-load-bearing conditions. Mechanically stable 3D constructs can be produced and an excellent biomimetic environment similar to the natural ECM can be provided, in terms of adding hydrogels to robust macroporous scaffolds, while their pores are filled with soft cell-containing hydrogels (Visser et al., 2015; Ovsianikov et al., 2018). However, the limitations of *ex vivo* tissue engineering are noteworthy. This includes donor tissue morbidity, the need for a great number of immune-acceptable cells to fill synthetic scaffold, and the challenges posed by the expansion of large numbers of cells *in vitro*, such as lack and loss of reliable, reproducible cell sources and cellular phenotype (Gaharwar et al., 2020).

Recently, a novel method called *in-situ* tissue regeneration, which leverages the body's innate regenerative potential, as well as eliminates the need for *ex vivo* cell manipulation, was introduced in (**Figure 1B**). It has several ways in *in-situ* tissue engineering, such as bioactive cues can be incorporated into biomaterials, to repair the place of injury. *In situ* tissue engineering has advantages over *ex vivo* tissue engineering, because it does not need the process of harvesting cells, thus, reducing regulatory hurdles. In addition, *ex vivo* ways need complex cell culture conditions to obtain functional tissues but *in situ* approaches don't. Finally, the shelf life of synthetic scaffolds over the cell-laden scaffolds. Therefore, the *in situ* methods have an excellent performance than *ex situ* methods for clinical application (Gaharwar et al., 2020).

In this review, we aim to outline the recent advances of exosome-laden hydrogels for *in-situ* bone tissue regeneration. The advantages of *in-situ* bone tissue engineering compared with traditional tissue engineering were summarized. Moreover, the development and challenges of hydrogels and exosomes for tissue regeneration was elaborated. Besides, the encapsulation strategies of exosome-laden hydrogels are listed, and the research progress and prospects of bioactive hydrogel composite system for continuous delivery of exosomes for *in-situ* bone repair are also discussed in this review.

# HYDROGELS USED FOR *IN-SITU* BONE TISSUE REGENERATION

## Types and Development of Hydrogels

Hydrogelsare three-dimensional (3D) structures formed by physical or chemical cross-linking between hydrophilic polymer chains. It is well known that hydrogels are hydrophilic polymers, with the property of highly-crosslinked water-swollen networks and the ability to swell in water without dissolving. Due to its profound biocompatibility, it could be used in numerous disease treatments as well as play an important role in tissue remodeling (Buwalda et al., 2014). During the biomimetic systems, the hydrogel is a soft material similar to the extracellular matrix, which could generate artificial organs. The material sources of hydrogels can be divided into natural hydrogels and synthetic hydrogels (Zhu and Marchant, 2011). There are four main types of natural polymers including proteins, polysaccharides, protein/polysaccharide hybrid polymers and DNA, could be used to fabricate natural hydrogels. While the polymer types made of synthetic hydrogels were divided into non-biodegradable, biodegradable, and bioactive polymers (Zhu and Marchant, 2011). Natural materials including chitosan, alginate, hyaluronic acid (HA), collagen and gelatin, with the inherent performance of biodegradable and always have integrin binding sites to adhere and coordinate cell responses (Dimatteo et al., 2018). The natural polymers or synthetic polymers used in hydrogels could determine some properties and application of hydrogels. Natural protein polymers are suitable for the preparation of biocompatible hydrogels, while synthetic hydrogels are suitable for various biomedical applications, such as controlled drug release. Moreover, the mechanical property of synthetic hydrogels could be adjustable (Gyles et al., 2017).

## Requirement and Characterization of Hydrogels for Bone Tissue Regeneration

For bone tissue regeneration, hydrogels can be considered as very attractive scaffolds and very promising alternative materials (Bai et al., 2018). And the marked advantage of injectable hydrogels is that they can be implanted in the desired area of tissue through minimally invasive techniques (Staruch et al., 2017). This is because of their suitable properties, including their excellent elasticity, biocompatibility, biodegradability and mechanical properties (Huang et al., 2017; Pishavar et al., 2021). Injectable hydrogels can promote *in situ* tissue regeneration by the way of filling irregular defects.

Also, the different characteristics of hydrogels can be gained through changing the chemical feature of bonds, degree of cross-linking and molecular weight of the polymer (Xue et al., 2022). Moreover, we are facing a huge challenge, for example, the need to combine with the desired characteristics of hydrogels. Because the hydrogel functions explored are sometimes interdependent and sometimes mutually exclusive. For instance, increasing the degree of chemical cross-linking can gain higher stiffness hydrogels. On the contrary, hydrogels with the potential to heal by themselves can be obtained through introducing dynamic cross-linking. Apart from hydrogel structure is required to be adjusted, adding appropriate fillers becomes a strategy to control and manipulate the nano and macro properties of materials (Piantanida et al., 2019). Another factor that should take into consideration is the degradation of hydrogels while designing tissue regeneration scaffolds.

In terms of injectable hydrogels, which have highly concentrated structures including nano-sized pores, micron-level proliferating cells cannot penetrate them without degrading the covalent bonds that bind them together. Therefore, the regeneration of damaged tissue needs to maintain an accurate balance between tissue integration rate and scaffold degradation rate (Deng et al., 2019). On the one hand, slow degradation of materials always leads to an increase in the inflammatory response and can promote fibrosis (Alijotas-Reig et al., 2013). On the other hand, materials that degrade too fast provide insufficient scaffolds to maintain the infiltration and batch arrangement of proliferating cells. To solve these problems, the injectable microporous scaffolds have been designed by some research groups (Bencherif et al., 2012; Griffin et al., 2015), which not only adapt to tissue regeneration but also keep bulk stability. These systems' widely adoption, provides an ideal design method with scaffold adjustability so that the scaffold can meet the precise physical and chemical requirements of the wound site (Dimatteo et al., 2018; Wu et al., 2021). Moreover, tissue regeneration is closely associated with biomaterials *in situ* degradation. The rate of tissue generation for optimal tissue growth is the same as the biomaterials degradation rate (Gaharwar et al., 2020).

## Application and Prospect of *In-Situ* Bone Tissue Regeneration

Zhang and his group fabricated a bioactive nanocomposite hydrogel to regulate the delivery in the local and regeneration-specific release of dexamethasone (Dex). The nanocomposite hydrogel with excellent injection performance and efficient stress relaxation, so it can be easily injected and adapted to irregular bone defects. The release of $Mg^{2+}$ from hydrogel can promote osteogenic differentiation, encapsulate human mesenchymal stem cells (hMSCs), and activate alkaline

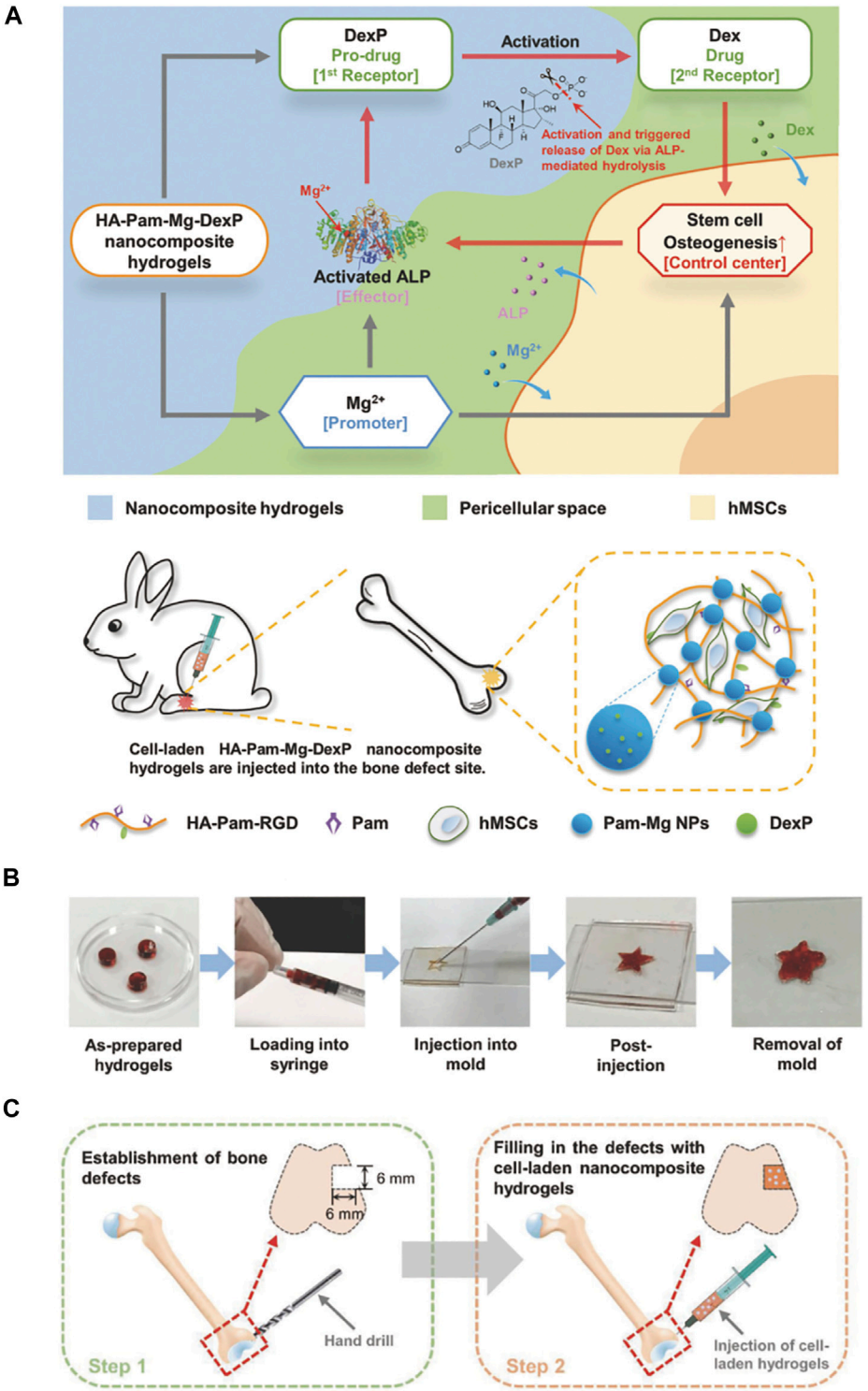


**FIGURE 2 |** Injectable HA-Pam-Mg nanocomposite hydrogel promotes the healing of bone defects. **(A)** Schematic representation of "smart" hydrogels and injections of hMSC-laden nanocomposite hydrogels promote *in situ* bone regeneration. **(B)** Demonstration of the injectability and formability of nanocomposite hydrogels. **(C)** HA-Pam-Mg nanocomposite hydrogels encapsulating MSCs promote healing of rabbit femur defects (Zhang et al., 2018b). Copyright 2018, WILEY-VCH Verlag GmbH & Co. KGaA, Weinheim.

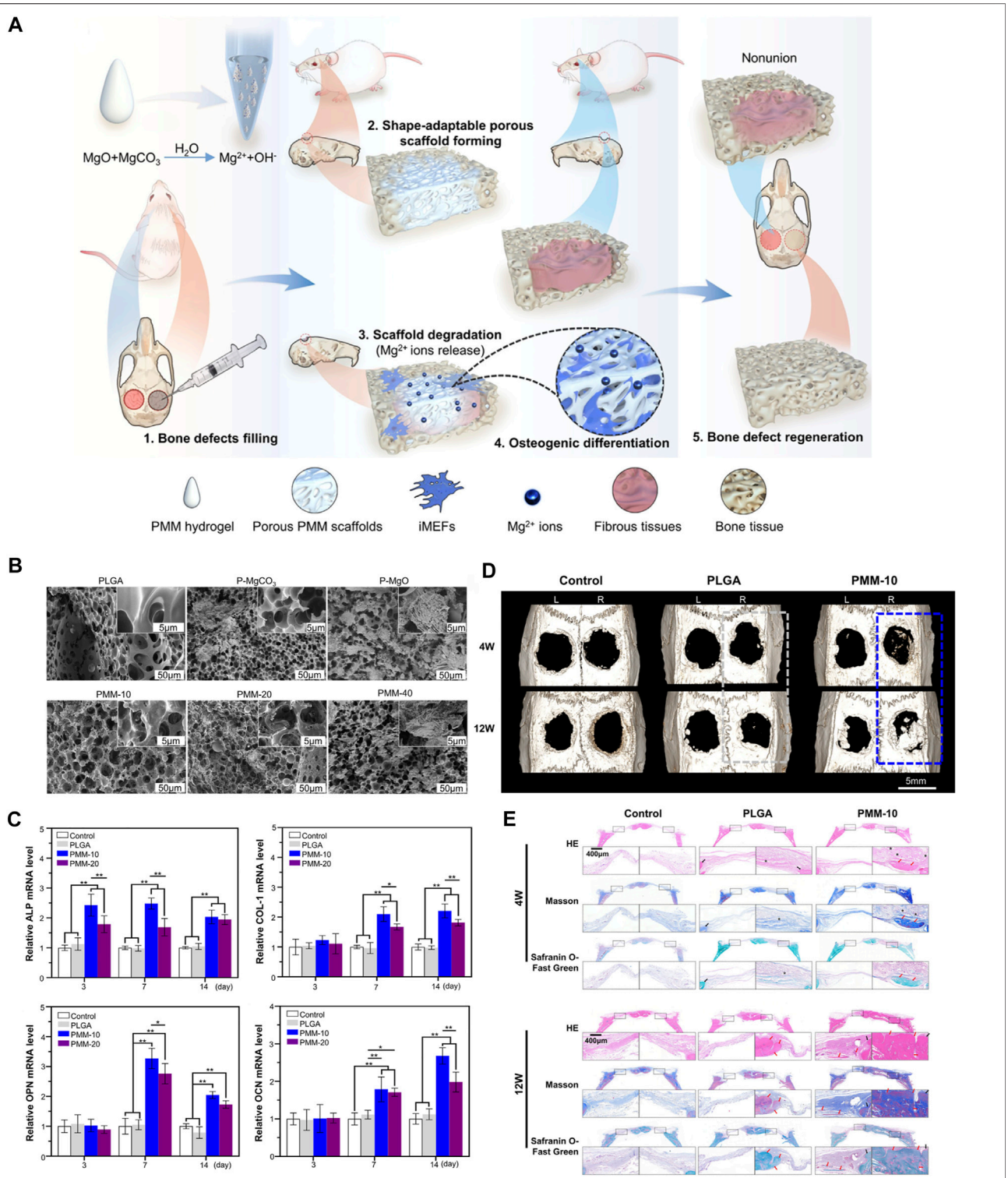


**FIGURE 3 |** Schematic diagram of MgO/MgCO3@PLGA(PMM) hydrogel promoting bone defect repair. **(A)** Schematic diagram of the mechanism of injectable PMM hydrogel promoting bone defect regeneration. **(B)** SEM images of PLGA and PM scaffolds loaded with MgO/MgCO particles with different weight ratios. **(C)** The relative expression levels of marker genes related to osteogenic differentiation were analyzed. **(D)** Reconstructed 3D micro-CT images of rat crania with the treated defects labeled with rectangular box (gray: PLGA, blue: PMM). **(E)** Histological evaluation of bone defect regeneration using H&E, Masson's trichrome, and Safranin O-Fast Green staining (*represents residual materials showing the blank area; red arrows indicate new bone, and black arrows indicate host bone) (Zhou et al., 2021). Copyright 2021, American Chemical Society.

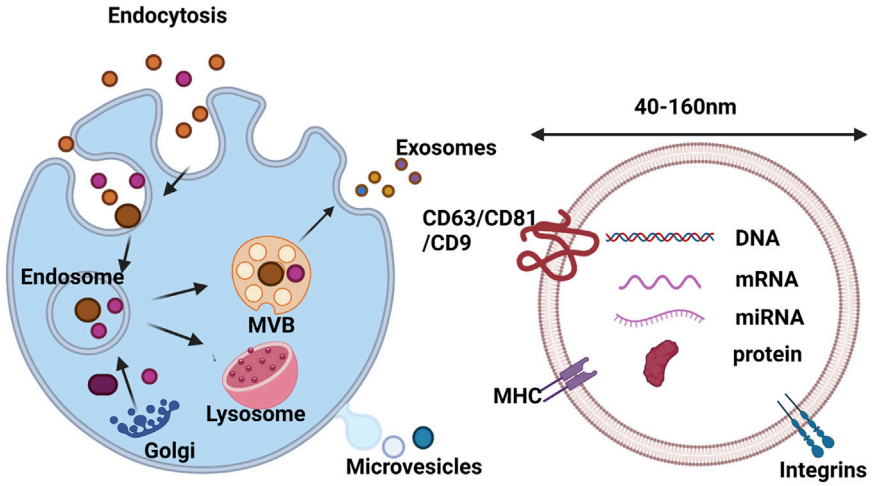


**FIGURE 4 |** Biogenesis and composition of exosomes. Exosome formation is initiated by invagination of the plasma membrane to form EEs, which fuse to form MVBs. Then, MVBs fuse with the plasma membrane to release exosomes into the extracellular matrix, or fuse with lysosomes for degradation. The composition of exosomes includes lipids, DNA, RNA and proteins (Huang et al., 2021). Copyright 2021, The Royal Society of Chemistry.

phosphatase (ALP) (**Figure 2**). For the sake of promoting hMSCs osteogenesis further, the activated ALP catalyzes the dephosphorylation of Dex phosphate results in releasing Dex from hydrogel quickly. With an emphasis on the bone regeneration rate is better than previous in terms of the positive feedback circuit controlling the activation and release of Dex at the hydrogel implantation sites. The report reveals that injectable nanocomposite hydrogel regulates diverse therapeutic cargoes released in an optimization way and promotes *in situ* bone regeneration through minimally invasive surgery (Zhang et al., 2018b).

Hang reported an excellent injectable MgO/MgCO3@PLGA (PMM) hydrogel to improve bone regeneration. PMM hydrogel not only has good injectable properties, but also can form porous scaffolds *in situ* by solid-liquid transformation, and fill irregular bone defects through its huge shape adaptability. As shown in **Figure 3**, the injectable PMM hydrogel was investigated for rat calvarial defect repair. Injectable PMM hydrogels can form porous scaffolds *in situ*, through controlled release of $Mg^{2+}$, can meaningfully promote bone regeneration (Zhou et al., 2021). Another study reported an in situ-forming biomaterial, which mixed montmorillonite (MMT) with photopolymerizable methacrylated glycol chitosan (MeGC) hydrogel, could promote bone regeneration. And the nanocomposite hydrogels have great potential to recruit native cells and promote bone formation. Nanosilicate-loaded MeGC hydrogel, which provides a new material design strategy with cell-free and free of growth factors (Cui et al., 2019).

To exploit the potential of hydrogels in various bone regeneration strategies, further research should also focus on developing better compatible nanoparticles (Mehrali et al., 2017). Additionally, one of the biggest challenges still facing bone tissue engineering is that, unlike natural tissues, biomaterials lack the ability to repair themselves (Koons et al., 2020).

# EXOSOMES: A CELL-FREE TISSUE ENGINEERING STRATEGY FOR BONE REGENERATION

## Biogenesis and Composition of Exosomes

Extracellular vehicle (EV) is a phospholipid bilayer spherical structure with substantial dynamic heterogeneity, which is released by almost all mammalian cells and plays a vital role in cell-to-cell communication (Robbins and Morelli, 2014). The exosome is a saucer-shaped vesicle with a diameter of 40–160 nm (**Figure 4**), which can float in sucrose gradients with a density of 1.13–1.19 g $ml^{-1}$. Plenty of cell types can secret and absorb exosomes, such as endothelial cells, immune cells, tumor cells and mesenchymal stem cells (MSCs) (Huang et al., 2021). Since diverse cells with different characteristic exosomes, this reflects the sorting process of exosomes not just related to the donor cells (van Niel et al., 2006). Some studies have found that both inside and surfaces of exosomes contain cargo, which refers to various proteins and nucleic acids, including DNA, mRNA, miRNA, lipids and small molecules (Mathivanan et al., 2010; D'Asti et al., 2012). It has been demonstrated that some proteins originate from cells or tissue while others are existing in all exosomes by proteomic analysis (Valadi et al., 2007). Generally, the various function of proteins are contained by exosomes such as heat shock proteins (HSP70 and HSP90) not only take part in the stress response but also connect with antigen binding and delivery; tetraspanins such as CD9, CD63, CD81 and CD82, which are involved in cell penetration, fusion and invasion. In addition, in exosome secretion, MVB (Multivesicularbody) formation proteins (Alix, TSG101) and proteins (Annexin and Rab) were found to possess the capacity of membrane transplantation and fusion (Cordonnier et al., 2017). Among the above proteins, some of them are involved in exosome biogenesis, such as fotilin, TSG101 and Alix. These proteins

**TABLE 1 |** Current strategies for exosome separation (Yang et al., 2020).

| Isolation technique | Advantages | Disadvantages |
|---|---|---|
| Sequential ultracentrifugation | • Low cost and<br>• Low contamination risk with extra isolation reagents<br>• Suitable for large volume preparation | • High equipment requirement<br>• Time consuming<br>• Labor intensive<br>• Protein aggregation<br>• Low portability |
| Ultrafiltration | • Low equipment cost<br>• Fast procedure<br>• good portability | • Moderate purity<br>• Possible loss due to clogging and membrane trapping |
| Gradient ultracentrifugation | • High purity of products<br>• Allowing separation of subpopulation of exosomes | • Lower volume process ability<br>• High equipment requirement<br>• Time consuming<br>• Labor intensive<br>• Low portability |
| Size-exclusion chromatography | • High purity<br>• Fast preparation<br>• Keep native state of exosomes<br>• Good reproducibility<br>• Potential for both small and large sample capacity | • High device costs<br>• Additional method for exosome enrichment is required |
| Immunoaffinity capture | • Suitable for separating exosomes of specific origin<br>• High-purity exosomes<br>• Easy to use<br>• No chemical contamination | • High-cost antibodies<br>• Exosome markers must be optimized<br>• Low processing volume and yields |
| Microfluidics-based techniques | • Highly efficient<br>• Cost-effective<br>• Portable<br>• Easily automated and integrated with diagnosis | • Low sample capacity |
| Polymer Precipitation | • Easy to use<br>• Using ordinary equipment<br>• Suitable for both small and large sample volume<br>• High efficiency | • Contaminants of protein aggregates, other extracellular vesicles and polymeric contaminants<br>• Extended processing time<br>• Require complicated clean-up steps |

are secreted during plasma membrane spillage, while others exist specifically in exosomes and can be regarded as exosome marker proteins, such as HSP70, TSG101, CD63 and CD81 (Cordonnier et al., 2017; Elkhoury et al., 2020).

Exosomes are involved in the regulation of different signaling pathways in neighboring and distant recipient cells by delivering kinds of biomolecules, including mRNAs, miRNAs, proteins and lipids (Akbari et al., 2020; Hu et al., 2021). As a cell-free biomaterial, exosomes can solve some problems encountered in the clinical application of regenerative medicine, such as the source, quantity and immune rejection of seed cells. Thus, combining exosomes with tissue engineering scaffolds can provide a new generation of scaffold biomaterials that are more suitable for tissue repair (Huang et al., 2021).

## Separation and Extraction Strategies for Exosomes

The limitation of nano-sized and distributing in complex body fluids leads to difficulty to isolate exosomes in high yield (Willms et al., 2018). At the moment, ultracentrifugation is one of the most feasible strategies for exosome isolation due to its high yield, but the high levels of protein aggregates and lipoprotein contamination present in exosome samples prepared by this method are critical for quantitative and functional analysis have a large impact (Li et al., 2017). Since it is impossible for a single way to adapt to diverse sample sources, efforts have been made to explore the different physicochemical and biochemical properties of exosomes. At present, six kinds of methods have been used in exosome separation (**Table1**), including ultracentrifugation, immunoaffinity capture, ultrafiltration, charge neutralization polymer precipitation, microfluidic technology and size exclusion chromatography. Each method has its unique special advantages and disadvantages (Yang et al., 2020). Exosomes isolated by different methods can usually be identified by detecting their surface morphology, particle size, and surface markers. Commonly used morphological-based identification methods include transmission electron microscopy (TEM) (Manda et al., 2018), scanning electron microscopy (SEM) (Singh et al., 2014), cryo-electron microscopy, and atomic force microscopy (AFM) (Misumi et al., 2018). Identification methods based on exosome size include nanoparticle tracking analysis (NTA) and dynamic light scattering (DLS) (Sitar et al., 2015). Exosome-based identification of various specific or non-specific markers. They contain the same fusion proteins and membrane transport proteins (Annexins, Flotillin, GTPases), Tetraspannins (CD9, CD82, CD81 and CD63) (Zhang et al., 2012). Exosomes

derived from MSCs could be stored at −20°C or −70°C, and can maintain biological activity for a long time (Sokolova et al., 2011; Lee et al., 2016).

## Recent Advances of Exosomes for Bone Tissue Regeneration

Recently, compared with other cell-based therapies, the secretion of MSCs have received considerable attention as a regeneration tool (Liu et al., 2017). First discovered in the 1960s, MSCs were originally described as spindle cells derived from bone marrow, which regulate the quiescence and self-renewal of hematopoietic stem cells *via* the release of paracrine factor (Pluchino and Smith, 2019). These cells with the feature of heterogeneous, apart from bone marrow, have been successfully isolated from the placenta, amniotic fluid, adipose and other tissues. Exosomes, which are derived from MSCs, have a vital influence on the function of endothelial cells and promote tube formation and thus play a role in angiogenesis and vascular network maturation (Li et al., 2016). It is easy to isolate bone marrow mesenchymal stem cells from adult tissues and have great expansion ability *in vitro*. Several evidence has been shown that MSCs with an outstanding therapeutic role in plenty of diseases (Khayambashi et al., 2021).

There is no doubt that the MSC-based tissue engineering method is an innovative strategy for clinical treatment (Lin et al., 2017). Nevertheless, it has been found that they are instability and with the potential to form cancer (Carson et al., 2006). These findings lead the research community to reconsider the biosafety of stem cell therapy. With the development of cell-free therapies, exosome has gradually become a tool for tissue repair, which is better than traditional stem cell therapy because it conquers risks and limitations.

Zhang et al. (Zhang S. et al., 2018) reported that MSC-derived exosomes with the potential to repair osteochondral defects through a way that contains increased migration, matrix synthesis and proliferation, decreased apoptosis and regulated immunoreaction. Cui et al. (Cui et al., 2016) reported that mineralized osteoblasts derived exosomes affected the miRNA profile of recipient bone marrow cells, thus promoting differentiation into osteoblasts. Owing to a change in miRNA profile, the expression of Axin 1 was inhibited, whereas the expression of ß-catenin was increased as well as the Wnt signaling pathway was activated (Gu et al., 2021).

Studies have shown that exosomes from MSCs with similar functions to MSCs, including tissue regeneration and repair, inhibition of inflammation, regulation of immunity and so on (Askenase, 2020). Some advantages of using exosomes for tissue regeneration rather than MSCs are as follows. First of all, the immune risks associated with stem cell transplantation are avoidable. And exosomes cannot self-replication without the potential to form endogenous tumors (Lener et al., 2015). A report showed that a spinal cord–injured patient, who transplanted olfactory mucosal stem cells, formed tumors at the injured site (Dlouhy et al., 2014), emphasizing stem cell therapy with potential risks. Second, compared with MSCs, exosomes can be stored for a longer time and can be used more conveniently. Third, differ from exosomes, MSCs are too big to circulate through capillaries. Especially, exosomes can promote lung repair by entering the lungs after infecting Corona Virus Disease 2019 (COVID-19) (Askenase, 2020). Finally, in contrast with MSCs, the biogenesis and functional characteristics of exosomes can be defined more correctly. The function of MSCs can be reprogrammed by environmental factors, but not exosomes (Lener et al., 2015). All of these advantages make MSC exosomes can be administered easily and treat kinds of diseases safe (Shiue et al., 2019).

A study reported that exosomes secreted by human mesenchymal stem cells (hMSCs) could induce osteogenesis of hMSCs through osteogenic pre-differentiation at different times, and the extracted exosomes were combined with 3D printed titanium alloy scaffolds for cell-free bone regeneration (**Figure 5**). The results showd that the bone tissue regeneration efficiency of cell-free exosome scaffolds was comparable to that of hMSC-seeded scaffolds, so replacing stem cells with osteogenic exosomes secreted by pre-differentiated stem cells was expected to become a new cell-free bone regeneration pathway (Zhai et al., 2020).

## Limitation and Prospect of Exosomes for *In-Situ* Bone Regeneration

Although we all know the benefits of exosomes, the shortcomings of delivering a therapeutic dosage of exosomes, peculiarly *via* systemic injections, may over their advantages (Riau et al., 2019). The common ways to administer exosomes are intravenous, subcutaneous, and intraperitoneal injections. When it comes to the exosomes' biological effects, the crucial factor that must be considered is the target cell, which could internalize exosomes through endocytosis, if not, exosomes will enter the blood circulation and be quickly removed. Since the short half-life exosomes possess, which exist only 2–4 min (Saunderson et al., 2014), and will be quickly removed from the blood vessels. Then exosomes will enter the organs (Schiffelers et al., 2000). For example, exosomes isolated from B16-BL6 mouse melanoma cells rapidly disappeared after intravenous injection with a half-life of 2 min (Takahashi et al., 2013). Further study has been demonstrated that after 2 h systemic injection, exosomes can be found in the liver, lung, spleen and gastrointestinal significantly (Takahashi et al., 2013; György et al., 2015). Generally, these exosomes are mainly phagocytosed by macrophages in the spleen or liver (Huang et al., 2021). On the one hand, the injection ways of exosomes like direct intravenous, subcutaneous and intraperitoneal injection, can cause a macrophages response in the reticuloendothelial system, leading to rejection. When applied systemically or locally (skin or eye), exosomes have shown a short half-life after interacting with sweat, tears and the epithelial barrier (Riau et al., 2019). On the other hand, it is difficult to purify and produce exosomes on a large scale due to the demand for consistency of nanometer-sized exosomes by the costly protocols (Riau et al., 2019).

To solve this problem, the exosome therapy research with emphasis on the combination of exosomes and biomaterials. The durability and stability of exosomes can increase significantly while combined with diverse biomaterials as scaffolds.

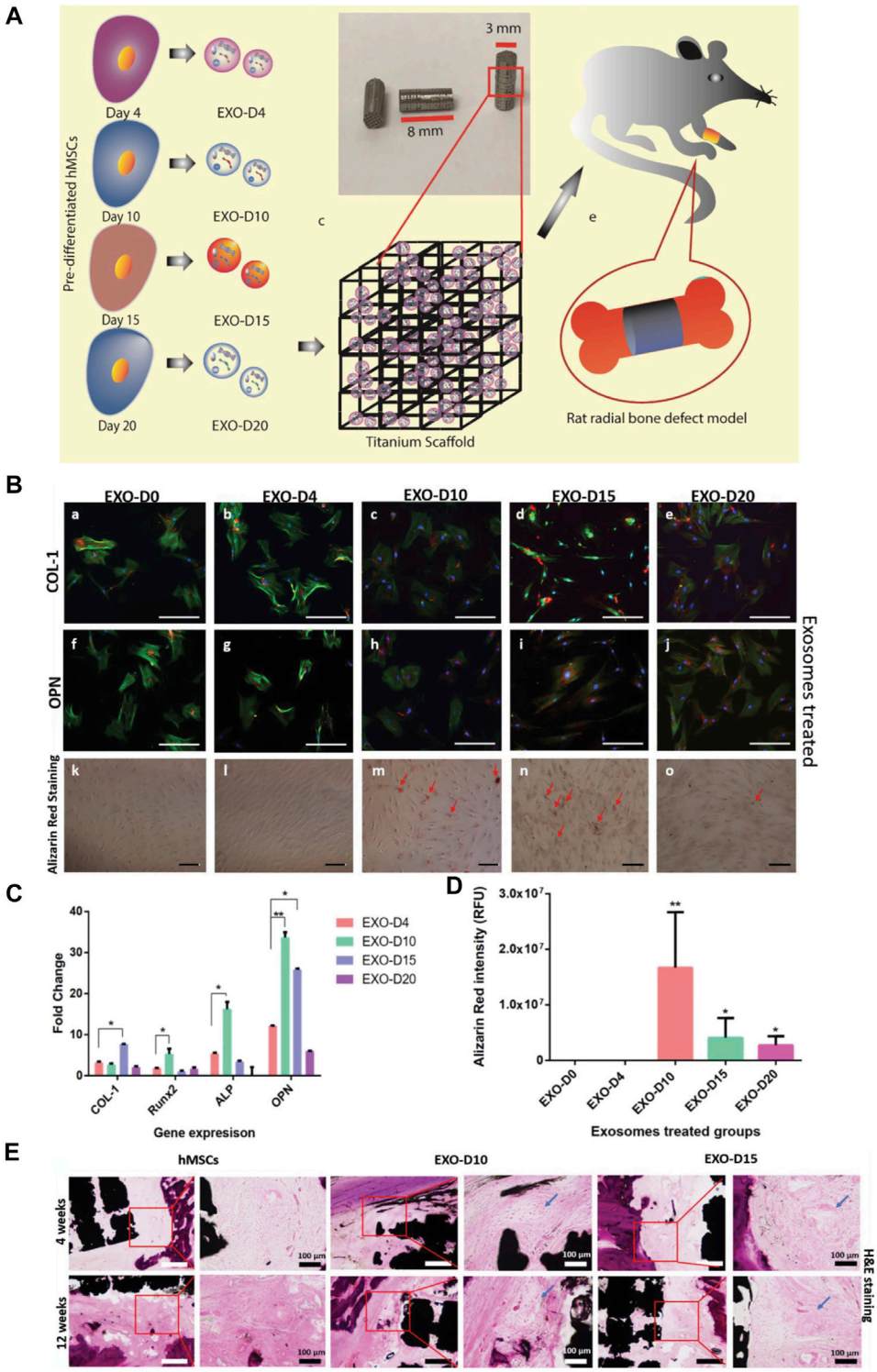


**FIGURE 5 |** Overview of stem cell-derived exosomes for bone tissue regeneration. **(A)** Exosomes from hMSCs were isolated and complexed with Ti scaffolds and implanted into the radial defect of the rat. **(B)** Immunofluorescence staining of osteogenic markers (COL-1[a-e]; OPN[f-j]) in hMSCs showing osteogenic exosome-induced osteogenic differentiation. **(C)** Real-time PCR of osteogenic markers (COL-1, Runx2, ALP, and OPN) showed exosome-induced osteogenesis of hMSCs. **(D)** Intensity of Alizarin Red after induction in various exosomes. **(E)** H&E staining demonstrated new bone formation *in vivo* (Zhai et al., 2020). Copyright 2020 The Authors. Published by Wiley-VCH GmbH.

Furthermore, the ideal biomaterial should with the capacity of maintaining the bioactivity of exosomes and controlling the release kinetics of exosomes in terms of the expected release schedule. In addition, the characteristic of biomaterials must be taken into consideration, which can influence the efficiency of loading or releasing exosomes. Thus, when it comes to materials design, porosity is a fundamental element that needs to be emphasized, which can promote substance transport in the injured tissue owing to highly connected porous networks. Through the micro or nanoscale porosity can release bioactive agents, move gasses, nutrients, and waste products better than materials of other sizes. Tissue engineering biomaterials as similar to the natural ECM, which can supply migration, growth and survival of MSCs with a scaffold. As biomaterials for bone tissue repair, with proper stability and integrity, and have appropriate stiffness and mechanical properties like bone tissue look necessary. Undoubtedly, the scaffold needs the potential to be biodegradable, and the degradation rate should match the regeneration of new tissue so that the scaffold could be replaced. When cleavable groups need to incorporate into the scaffold, the rate of degradation should be controlled primarily. What important most is the biocompatibility of biomaterial, the potential to perform without causing adverse host reactions, and it should not accumulate in the body, thus the biomaterial and degradation products should be bio-absorbable (Safari et al., 2021).

As we all know, natural ingredients obtained from biological sources with inherent biocompatibility can be well applied in the body and can also be degraded by enzymatic cleavage easily. However, synthetic biomaterial with more fantastic functions and structures. The biomaterials will be more universal if change the molecular composition gain new properties and optimize the existing properties and so on. Beyond that, kinds of membranes, nanoparticles and hydrogels have been used to promote the controlled release of bioactive molecules in tissue repair (Ding et al., 2014; Xu et al., 2015; Liang et al., 2019; Safari et al., 2021).

Without encapsulation, exosomes can be cleared from the body through fluids at a quick speed (Riau et al., 2019). Thus, delivering exosomes needs a more powerful way to avoid clearance by the host (Khayambashi et al., 2021).

# EXOSOMES LADEN HYDROGELS FOR INDUCING *IN-SITU* BONE REGENERATION

## Hydrogel as a Vehicle for Exosome Delivery

It is a popular choice to apply hydrogels as a delivery system and scaffold materials owing to hemostatic ability, antibacterial activity, injectability, tissue adhesion, self-healing and so on (Li et al., 2015; Huang W. et al., 2016; Lokhande et al., 2018; Safari et al., 2021). Hydrogel encapsulated exosomes can protect them without degradation and supply therapeutic effects with persistent exosomes delivery (Riau et al., 2019). Currently, the local continuous drug delivery of exosomes is available through hydrogels as carriers. For instance, previous studies reported that the MSC-EVs combined with chitosan and silk fibrin-synthesized hydrogels showed a sustained release and long-term wounding healing for up to 2 weeks (Shi et al., 2017). The property of hydrogels, such as hydrophilic and cross-linking behavior, have promoted the capability of controlled drug release. Besides, it has demonstrated that hydrogels with important effects on the fields of bone formation, angiogenesis, immunology and oncology (Mantha et al., 2019). It has been studied that the purified, unformulated exosomes biodistribution in animal models. The vary of administrations including intravenous, subcutaneous, intraperitoneal, intranasal and retro-orbital, were used to evaluate disposal and exosome kinetics *in vivo* (Zhang et al., 2018a).

In comparison with stem cells, exosomes with more advantages in tissue regeneration can maintain biological activity and are highly stable for some time. Additionally, exosomes have the capability for targeting organs, initiating tissue regeneration, and protecting plenty of bioactive ingredients without degradation (Lou et al., 2017). Owing to exosomes do not have self-replicating characteristics, exosomes can reduce the danger of iatrogenic tumor formation and can reduce the formation of embolism when MSCs are injected. However, purified unformed exosomes can be cleared from the host at a short period after being absorbed by the reticuloendothelial system (Conlan et al., 2017). To conquer these limitations, hydrogels with the property of degradation can play a crucial role in protecting exosomes and take for a carrier and delivery depots of exosomes in the entry site so that a more durable therapeutic effect will obtain.

In addition, the high concentration of therapeutic molecules involved in exosomes can be delivered locally when exosomes are combined with hydrogels and applied near or in the target tissue site (Riau et al., 2019). Because of the structural or physicochemical characteristics of the hydrogel, the degradation rate of the hydrogel matrix can be adjusted, and the release and functional characteristics of the embedded exosomes can be controlled.

Furthermore, biodegradable hydrogel should be taken into consideration as an outstanding candidate for exosomes encapsulation in plenty of treatments, because they have the ability of biocompatible and are similar to the intracellular matrix. These advanced hydrogel-exosome formulation platforms could offer special formations to tissue engineering, for example, bone repair (Liu et al., 2019). To a certain degree, the treatment effect of exosomes depends on the design and function of hydrogels (Pishavar et al., 2021).

## Approaches of Hydrogel-Exosome Encapsulation

At present, there are several methods to transport exosomes to target tissues and organs, which can be divided into systematic and local. Systemic ways of administration include intravenous, oral, intranasal, intraperitoneal, and subcutaneous, while local administration can be realized by directly loading exosomes suspension or loading exosomes into biomaterials (Pinheiro et al., 2018; Alqurashi et al., 2021). The therapeutic benefit process of using exosomes is enhanced by the use of hydrogels

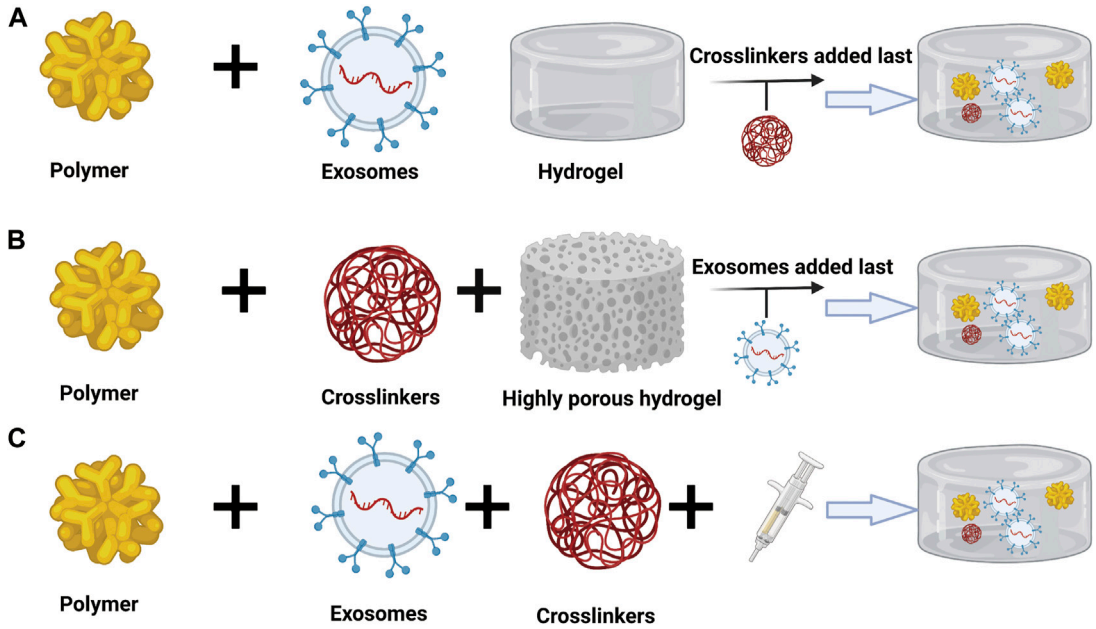


**FIGURE 6 |** Approaches to encapsulate exosomes in hydrogels: **(A)** Combining the exosomes with polymers followed by the addition of crosslinkers to induce gelation. **(B)** Physical incorporation of the hydrogels, or the "breathing" technique. **(C)** Mixing of the exosomes with both the polymers in solution and crosslinkers simultaneously (Khayambashi et al., 2021). Copyright 2021, MDPI, Basel, Switzerland.

in bone tissue engineering. Generally, there are three ways to encapsulate exosomes into a hydrogel matrix (Riau et al., 2019).

The first means is that exosomes are combined with the polymer, and then a cross-linking agent is added to induce gelation (**Figure 6A**). Studies have reported this method, which uses hyaluronic acid (HA), gelatin and heparin to form a polymer. Exosomes derived from bone marrow stem cells are incorporated into this polymer, and polyethylene glycol diacrylate (PEGDA) is used as the gelling agent of the system (Ghosh et al., 2005; Qin et al., 2016). This method is based on the active precursor for covalent cross-linking. Since this technology provides hydrogels with adjustable properties, controllable mechanical properties and degradation rates, it is an attractive strategy for exosomes and cell encapsulation (Nicodemus and Bryant, 2008). Nevertheless, a universal problem that exists is that when new compounds are added, such as cross-linking agents, they may be potentially cytotoxic to biomolecules. The advantage of this method is the use of macromonomers, which are usually derived from biocompatible polymers (Khayambashi et al., 2021).

The second way is the physical combination of hydrogel or "breathing" technology (**Figure 6B**). This technique has two main steps. First, the water in the hydrogel is removed by putting the swollen hydrogel in a solvent. The second step is to put the hydrogel in an aqueous solution containing exosomes so that the porous hydrogel is absorbed into the exosomes (Thomas et al., 2009). According to the principles of smart hydrogels, the method has been developed. That is, the hydrogel will form a swelling structure when in water, and the hydrogel will even collapse and undergo a phase change in a low-polar solvent (Shipway and Willner, 2001). Nevertheless, to use the method, the pore size of the hydrogel needs to be adjustable, and there is no doubt that the pore size needs to be larger than the encapsulated exosomes. Once inside the cell, loosely attached exosomes will effusion when exposed to the target (Thomas et al., 2009).

The last method is to mix the polymer and the crosslinker in the solution with the exosomes at the same time (**Figure 6C**). A study used this method, which resulted in situ gelation, enabling targeted delivery of exosomes to the site of action. They used fat-derived exosomes and peptides for wound healing (Wang et al., 2019). In general, this strategy requires the use of a dual-cavity syringe, which has the ability to inject the hydrogel with exosomes directly into the defect site (Ghosh et al., 2005; Riau et al., 2019). There are a variety of mechanisms that can be used for *in-situ* gelation, such as ultraviolet radiation, ion exchange, pH changes, and temperature changes (Ruel-Gariépy and Leroux, 2004). This strategy is very significant in filling the critical size defects of complex shapes, allowing the combined biomolecules to have good viability. This type of injectable scaffold has the required inherent tissue properties, so it can work alone without external induction (Sargeant et al., 2012; Khayambashi et al., 2021).

## Advances and Development of Exosome-Laden Hydrogels for *In-Situ* Bone Regeneration

The interaction between exosomes and biological materials determines the effective concentration of exosomes in biological materials. Electrostatic interaction and biologically active adhesion are the main ways to combine exosomes with biological materials. The mutual attraction or repulsion between

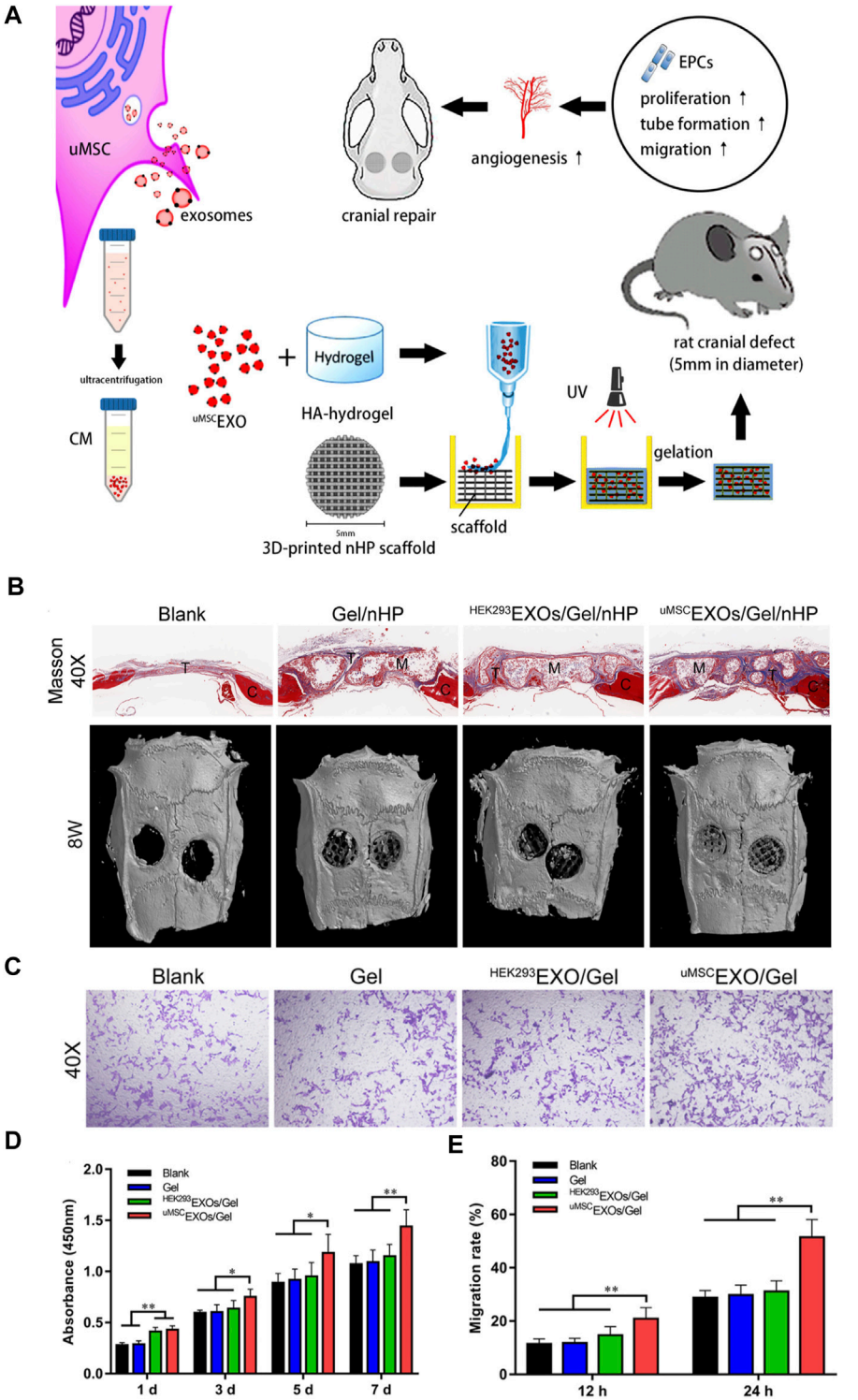


**FIGURE 7 |** Schematic diagram of $^{uMSC}$EXOs combined with HA-Gel and nHP scaffolds to promote the repair of skull defects. **(A)** Hydrogel composite exosomes scaffold promotes angiogenesis to repair critical size skull defects in rats. **(B)** The micro-CT scan image and quantitative analysis of the Masson's trichrome (40 × ) image after 8 weeks of repairing the critical size skull defect *in vivo* in the rat, showing the skull defect area. **(C)** Transwell migration analysis of endothelial progenitor cells in different treatments. **(D)** CCK-8 shows that $^{uMSC}$EXOs can promote EPCs proliferation. **(E)** Quantitative analysis of the migration rate (Zhang et al., 2021). Copyright 2021, American Chemical Society.

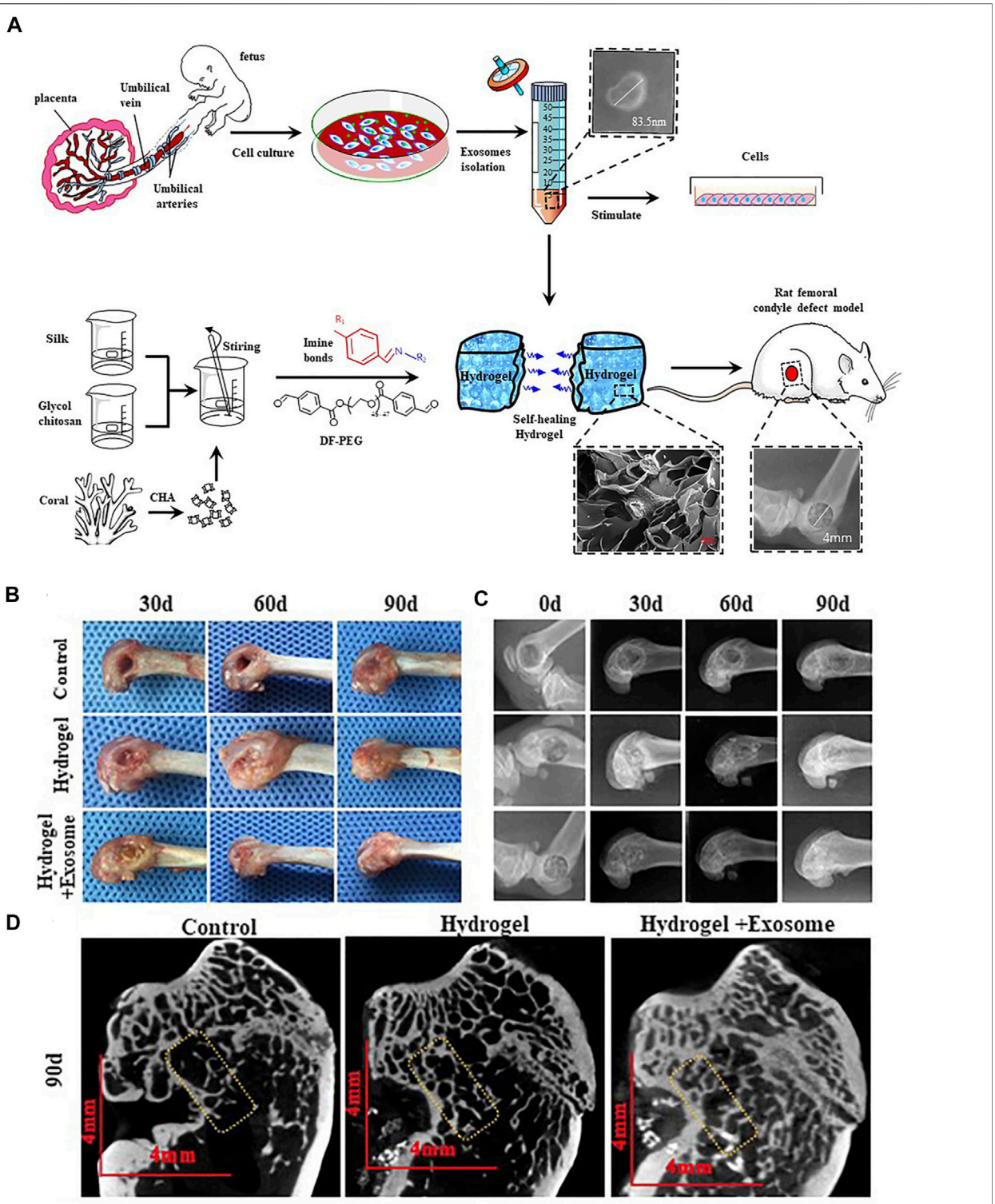


**FIGURE 8 |** HucMSC-derived exosomes combined with CHA/SF/GCS/DF-PEG hydrogel for the treatment of femoral condyle defects in rats. **(A)** The separation and identification of HucMSC-derived exosomes and the preparation of CHA/SF/GCS/DF-PEG hydrogel are used for testing on SD rats with induced femoral condyle defects. **(B)** 0, 30 and 90 days after implantation of CHA/SF/GCS/DF-PEG hydrogel or CHA/SF/GCS/DF-PEG hydrogel combined with hucMSC-derived exosomes, gross observation **(C)** X-ray **(D)** Micro-CT imaging results (Wang et al., 2020). Copyright 2020, Frontiers in Bioengineering and Biotechnology.

exosomes and biological materials depends on the negatively charged phospholipid membrane of exosomes and the charged residues of glycocalyx (Gerlach and Griffin, 2016). For example, a cation delivery system containing chitosan hydrogel retains exosomes through electrostatic force. The exosomes derived from MSC express adhesion molecules, for example, CD44 and *a* integrins. Therefore, exosomes have biological activity on extracellular matrix ingredients, for instance, type I collagen, fibronectin and hyaluronic acid and so on (Huang C.-C. et al., 2016; Brennan et al., 2020; Safari et al., 2021).

Zhang has reported that a nanoparticle composite was prepared by encapsulating umbilical MSC-derived exosomes ($^{uMSC}$EXOs) in hyaluronic acid hydrogel (HA-Gel), and combining them with nanohydroxyapatite/poly-ε -caprolactone (nHP) scaffold combined to repair rat skull defects (**Figure 7**). The methods of imaging and histological evaluation have shown that the $^{uMSC}$EXOs/Gel/nHP composite material significantly promotes bone regeneration *in vivo*, and $^{uMSC}$EXOs may be essential in the bone repair pathway. In addition, *in vitro* experiments have shown that $^{uMSC}$EXOs have the potential to make endothelial progenitor cells (EPCs) proliferate, migrate, and angiogenesis, but have little effect on the osteogenic differentiation of bone marrow mesenchymal stem cells. It cannot be ignored that mechanism studies have shown that exosomal miR-21 is a potential intercellular messenger, which promotes angiogenesis by up-regulating the NOTCH1/DLL4 pathway. In summary, the results of the study show a way to use exosomes to repair bone defects, which may be regulated by the miR-21/NOTCH1/DLL4 signal axis (Zhang et al., 2021).

Another research has been reported that a self-healing coralline hydroxyapatite (CHA)/silk fibroin (SF)/glycol chitosan (GCS)/difunctionalized polyethylene glycol (DF-PEG) hydrogel was successfully prepared (**Figure 8**), which has perfect comprehensive properties. Moreover, it is expected to be an excellent material that will be used in bone graft. The better bone repair effect will be if add hucMSC-derived exosomes to this hydrogel (Wang et al., 2020).

## FUTURE AND PROSPECTS

In the past few decades, bone tissue engineering has gradually developed, especially in the past few years due to the rise of *in-situ* tissue engineering. In this context, the composite of various types of hydrogels and nanoparticles that are similar to natural extracellular matrixes has obvious advantages in the treatment of bone tissue repair. There is no doubt that the evaluation of the main properties of hydrogel composite nanoparticles, such as biocompatibility and biodegradability, is necessary. In addition, their interaction with surrounding tissues is also an important factor that must be considered. Seed cells are widely used as a key element in regenerative medicine. For example, mesenchymal stem cells (MSCs) derived from various sources have good prospects in clinical research as cell-based therapies. As the core of tissue repair, seed cells are widely used in various fields of regenerative medicine. However, the use of stem cells for treatment always has problems such as low cell survival rate and immune rejection. Therefore, the use of stem cells for tissue regeneration has safety issues that cannot be ignored (Hofer and Tuan, 2016). And most of the therapeutic benefits of MSCs come from the release of paracrine factor exosomes with anti-inflammatory activity. The exciting discovery of exosomes contributes to cell-free therapy in tissue regeneration. Exosomes are nanoscale extracellular vesicles that contain biologically active molecules such as RNA and proteins; therefore, exosomes have similar functions to parent cells. Although the size of exosomes is similar to liposomes, naturally derived exosomes have many natural advantages over other nanoparticles. Naturally derived exosomes have outstanding biocompatibility, biodegradability, low toxicity and immunogenicity. The major limitations of exosome extraction was the purity and mass production, which restricted the wide clinical application (Aheget et al., 2020). Moreover, exosomes had their own inherent limitations including low targeting capacity, low circulating half-life and low concentration of functional molecules, which affected the clinical effectiveness (Jafari et al., 2020). The separation of exosomes is also a key issue. At present, ultracentrifugation is the most common method for extracting exosomes, but it also has disadvantages such as lipoprotein contamination. If we want to make progress in the field of exosomes research, we must develop efficient exosomes separation technology. A large number of studies have shown that the compounding of exosomes and hydrogel can improve the stability of exosomes and provide a continuous treatment environment for tissue defects. In addition, it contributes to maintaining the content of exosomal protein and miRNA in the body. However, many current treatment strategies to promote bone tissue repair also have shortcomings. These limitations include how the biomimetic scaffold is optimized to be like natural tissues and how bioactive molecules can deliver and maintain activity more efficiently. With the comprehensive disclosure of exosomes and their functions, the combination of exosomes and hydrogels will have more applications that cannot be ignored in clinical practice.

## AUTHOR CONTRIBUTIONS

JnS and ZY contributed equally to this work. JnS and ZY collected the literature and manuscript writing. XW and JaS conceived the idea, supervised the writing and reviewed the manuscript.

## FUNDING

This work was financially supported by National Key R&D Program of China (2018YFC2001500), National Natural Science Foundation of China (82172098 and 82001968), Shanghai Pujiang Program (20PJ1403800).

## REFERENCES


Aheget, H., Tristán-Manzano, M., Mazini, L., Cortijo-Gutierrez, M., Galindo-Moreno, P., Herrera, C., et al. (2020). Exosome: A New Player in Translational Nanomedicine. *Jcm* 9 (8), 2380. doi:10.3390/jcm9082380

Akbari, A., Jabbari, N., Sharifi, R., Ahmadi, M., Vahhabi, A., Seyedzadeh, S. J., et al. (2020). Free and Hydrogel Encapsulated Exosome-Based Therapies in Regenerative Medicine. *Life Sci.* 249, 117447. doi:10.1016/j.lfs.2020.117447

Alijotas-Reig, J., Fernández-Figueras, M. T., and Puig, L. (2013). Late-Onset Inflammatory Adverse Reactions Related to Soft Tissue Filler Injections. *Clinic Rev. Allerg Immunol.* 45 (1), 97–108. doi:10.1007/s12016-012-8348-5

Alqurashi, H., Ortega Asencio, I., and Lambert, D. W. (2021). The Emerging Potential of Extracellular Vesicles in Cell-free Tissue Engineering and Regenerative Medicine. *Tissue Eng. B: Rev.* 27 (5), 530–538. doi:10.1089/ten.TEB.2020.0222

Askenase, P. W. (2020). COVID-19 Therapy with Mesenchymal Stromal Cells (MSC) and Convalescent Plasma Must Consider Exosome Involvement: Do the Exosomes in Convalescent Plasma Antagonize the Weak Immune Antibodies? *J. Extracellular Vesicles* 10 (1), e12004. doi:10.1002/jev2.12004

Bai, X., Gao, M., Syed, S., Zhuang, J., Xu, X., and Zhang, X.-Q. (2018). Bioactive Hydrogels for Bone Regeneration. *Bioactive Mater.* 3 (4), 401–417. doi:10.1016/j.bioactmat.2018.05.006

Bencherif, S. A., Sands, R. W., Bhatta, D., Arany, P., Verbeke, C. S., Edwards, D. A., et al. (2012). Injectable Preformed Scaffolds with Shape-Memory Properties. *Proc. Natl. Acad. Sci. U.S.A.* 109 (48), 19590–19595. doi:10.1073/pnas.1211516109

Brennan, M. Á., Layrolle, P., and Mooney, D. J. (2020). Biomaterials Functionalized with MSC Secreted Extracellular Vesicles and Soluble Factors for Tissue Regeneration. *Adv. Funct. Mater.* 30 (37), 1909125. doi:10.1002/adfm.201909125

Buwalda, S. J., Boere, K. W. M., Dijkstra, P. J., Feijen, J., Vermonden, T., and Hennink, W. E. (2014). Hydrogels in a Historical Perspective: From Simple Networks to Smart Materials. *J. Controlled Release* 190, 254–273. doi:10.1016/j.jconrel.2014.03.052

Campana, V., Milano, G., Pagano, E., Barba, M., Cicione, C., Salonna, G., et al. (2014). Bone Substitutes in Orthopaedic Surgery: from Basic Science to Clinical Practice. *J. Mater. Sci. Mater. Med.* 25 (10), 2445–2461. doi:10.1007/s10856-014-5240-2

Carson, C. T., Aigner, S., and Gage, F. H. (2006). Stem Cells: the Good, Bad and Barely in Control. *Nat. Med.* 12 (11), 1237–1238. doi:10.1038/nm1106-1237

Conlan, R. S., Pisano, S., Oliveira, M. I., Ferrari, M., and Mendes Pinto, I. (2017). Exosomes as Reconfigurable Therapeutic Systems. *Trends Mol. Med.* 23 (7), 636–650. doi:10.1016/j.molmed.2017.05.003

Cordonnier, M., Chanteloup, G., Isambert, N., Seigneuric, R., Fumoleau, P., Garrido, C., et al. (2017). Exosomes in Cancer Theranostic: Diamonds in the Rough. *Cell Adhes. Migration* 11 (2), 151–163. doi:10.1080/19336918.2016.1250999

Cui, Y., Luan, J., Li, H., Zhou, X., and Han, J. (2016). Exosomes Derived from Mineralizing Osteoblasts Promote ST2 Cell Osteogenic Differentiation by Alteration of microRNA Expression. *FEBS Lett.* 590 (1), 185–192. doi:10.1002/1873-3468.12024

Cui, Z.-K., Kim, S., Baljon, J. J., Wu, B. M., Aghaloo, T., and Lee, M. (2019). Microporous Methacrylated Glycol Chitosan-Montmorillonite Nanocomposite Hydrogel for Bone Tissue Engineering. *Nat. Commun.* 10, 10. doi:10.1038/s41467-019-11511-3

D'Asti, E., Garnier, D., Lee, T. H., Montermini, L., Meehan, B., and Rak, J. (2012). Oncogenic Extracellular Vesicles in Brain Tumor Progression. *Front. Physio.* 3, 294. doi:10.3389/fphys.2012.00294

De Witte, T.-M., Fratila-Apachitei, L. E., Zadpoor, A. A., and Peppas, N. A. (2018). Bone Tissue Engineering *via* Growth Factor Delivery: from Scaffolds to Complex Matrices. *Regenerative Biomater.* 5 (4), 197–211. doi:10.1093/rb/rby013

Deng, C., Chang, J., and Wu, C. (2019). Bioactive Scaffolds for Osteochondral Regeneration. *J. Orthopaedic Translation* 17, 15–25. doi:10.1016/j.jot.2018.11.006

Dimatteo, R., Darling, N. J., and Segura, T. (2018). *In Situ* forming Injectable Hydrogels for Drug Delivery and Wound Repair. *Adv. Drug Deliv. Rev.* 127, 167–184. doi:10.1016/j.addr.2018.03.007

Dimitriou, R., Jones, E., McGonagle, D., and Giannoudis, P. V. (2011). Bone Regeneration: Current Concepts and Future Directions. *BMC Med.* 9 (1), 66. doi:10.1186/1741-7015-9-66

Ding, F., Deng, H., Du, Y., Shi, X., and Wang, Q. (2014). Emerging Chitin and Chitosan Nanofibrous Materials for Biomedical Applications. *Nanoscale* 6 (16), 9477–9493. doi:10.1039/c4nr02814g

Dlouhy, B. J., Awe, O., Rao, R. C., Kirby, P. A., and Hitchon, P. W. (2014). Autograft-derived Spinal Cord Mass Following Olfactory Mucosal Cell Transplantation in a Spinal Cord Injury Patient. *Spi* 21 (4), 618–622. doi:10.3171/2014.5.Spine13992

Elkhoury, K., Koçak, P., Kang, A., Arab-Tehrany, E., Ellis Ward, J., and Shin, S. R. (2020). Engineering Smart Targeting Nanovesicles and Their Combination with Hydrogels for Controlled Drug Delivery. *Pharmaceutics* 12 (9), 849. doi:10.3390/pharmaceutics12090849

Gaharwar, A. K., Singh, I., and Khademhosseini, A. (2020). Engineered Biomaterials for *In Situ* Tissue Regeneration. *Nat. Rev. Mater.* 5 (9), 686–705. doi:10.1038/s41578-020-0209-x

Gerlach, J. Q., and Griffin, M. D. (2016). Getting to Know the Extracellular Vesicle Glycome. *Mol. Biosyst.* 12 (4), 1071–1081. doi:10.1039/c5mb00835b

Ghosh, K., Shu, X. Z., Mou, R., Lombardi, J., Prestwich, G. D., Rafailovich, M. H., et al. (2005). Rheological Characterization of *In Situ* Cross-Linkable Hyaluronan Hydrogels. *Biomacromolecules* 6 (5), 2857–2865. doi:10.1021/bm050361c

Griffin, D. R., Weaver, W. M., Scumpia, P. O., Di Carlo, D., and Segura, T. (2015). Accelerated Wound Healing by Injectable Microporous Gel Scaffolds Assembled from Annealed Building Blocks. *Nat. Mater* 14 (7), 737–744. doi:10.1038/nmat4294

Gu, C., Feng, J., Waqas, A., Deng, Y., Zhang, Y., Chen, W., et al. (2021). Technological Advances of 3D Scaffold-Based Stem Cell/Exosome Therapy in Tissues and Organs. *Front. Cel Dev. Biol.* 9, 709204. doi:10.3389/fcell.2021.709204

Gyles, D. A., Castro, L. D., Silva, J. O. C., and Ribeiro-Costa, R. M. (2017). A Review of the Designs and Prominent Biomedical Advances of Natural and Synthetic Hydrogel Formulations. *Eur. Polym. J.* 88, 373–392. doi:10.1016/j.eurpolymj.2017.01.027

György, B., Hung, M. E., Breakefield, X. O., and Leonard, J. N. (2015). Therapeutic Applications of Extracellular Vesicles: Clinical Promise and Open Questions. *Annu. Rev. Pharmacol. Toxicol.* 55, 439–464. doi:10.1146/annurev-pharmtox-010814-124630

Ho-Shui-Ling, A., Bolander, J., Rustom, L. E., Johnson, A. W., Luyten, F. P., and Picart, C. (2018). Bone Regeneration Strategies: Engineered Scaffolds, Bioactive Molecules and Stem Cells Current Stage and Future Perspectives. *Biomaterials* 180, 143–162. doi:10.1016/j.biomaterials.2018.07.017

Hofer, H. R., and Tuan, R. S. (2016). Secreted Trophic Factors of Mesenchymal Stem Cells Support Neurovascular and Musculoskeletal Therapies. *Stem Cel Res Ther* 7, 14. doi:10.1186/s13287-016-0394-0

Hölzl, K., Lin, S., Tytgat, L., Van Vlierberghe, S., Gu, L., and Ovsianikov, A. (2016). Bioink Properties before, during and after 3D Bioprinting. *Biofabrication* 8 (3), 032002. doi:10.1088/1758-5090/8/3/032002

Hu, Y., Li, X., Zhang, Q., Gu, Z., Luo, Y., Guo, J., et al. (2021). Exosome-guided Bone Targeted Delivery of Antagomir-188 as an Anabolic Therapy for Bone Loss. *Bioactive Mater.* 6 (9), 2905–2913. doi:10.1016/j.bioactmat.2021.02.014

Huang, C.-C., Narayanan, R., Alapati, S., and Ravindran, S. (2016a). Exosomes as Biomimetic Tools for Stem Cell Differentiation: Applications in Dental Pulp Tissue Regeneration. *Biomaterials* 111, 103–115. doi:10.1016/j.biomaterials.2016.09.029

Huang, J., Xiong, J., Yang, L., Zhang, J., Sun, S., and Liang, Y. (2021). Cell-free Exosome-Laden Scaffolds for Tissue Repair. *Nanoscale* 13 (19), 8740–8750. doi:10.1039/d1nr01314a

Huang, Q., Zou, Y., Arno, M. C., Chen, S., Wang, T., Gao, J., et al. (2017). Hydrogel Scaffolds for Differentiation of Adipose-Derived Stem Cells. *Chem. Soc. Rev.* 46 (20), 6255–6275. doi:10.1039/c6cs00052e

Huang, W., Wang, Y., Chen, Y., Zhao, Y., Zhang, Q., Zheng, X., et al. (2016b). Strong and Rapidly Self-Healing Hydrogels: Potential Hemostatic Materials. *Adv. Healthc. Mater.* 5 (21), 2813–2822. doi:10.1002/adhm.201600720

Jafari, D., Shajari, S., Jafari, R., Mardi, N., Gomari, H., Ganji, F., et al. (2020). Designer Exosomes: A New Platform for Biotechnology Therapeutics. *Biodrugs* 34 (5), 567–586. doi:10.1007/s40259-020-00434-x

Kempen, D. H. R., Lu, L., Heijink, A., Hefferan, T. E., Creemers, L. B., Maran, A., et al. (2009). Effect of Local Sequential VEGF and BMP-2 Delivery on Ectopic and Orthotopic Bone Regeneration. *Biomaterials* 30 (14), 2816–2825. doi:10.1016/j.biomaterials.2009.01.031

Khayambashi, P., Iyer, J., Pillai, S., Upadhyay, A., Zhang, Y., and Tran, S. (2021). Hydrogel Encapsulation of Mesenchymal Stem Cells and Their Derived Exosomes for Tissue Engineering. *Ijms* 22 (2), 684. doi:10.3390/ijms22020684

Koons, G. L., Diba, M., and Mikos, A. G. (2020). Materials Design for Bone-Tissue Engineering. *Nat. Rev. Mater.* 5 (8), 584–603. doi:10.1038/s41578-020-0204-2

Laurencin, C., Khan, Y., and El-Amin, S. F. (2006). Bone Graft Substitutes. *Expert Rev. Med. Devices* 3 (1), 49–57. doi:10.1586/17434440.3.1.49

Lee, M., Ban, J.-J., Im, W., and Kim, M. (2016). Influence of Storage Condition on Exosome Recovery. *Biotechnol. Bioproc. E* 21 (2), 299–304. doi:10.1007/s12257-015-0781-x

Lener, T., Gimona, M., Aigner, L., Börger, V., Buzas, E., Camussi, G., et al. (2015). Applying Extracellular Vesicles Based Therapeutics in Clinical Trials - an ISEV Position Paper. *J. Extracellular Vesicles* 4, 30087. doi:10.3402/jev.v4.30087

Li, L., Yan, B., Yang, J., Chen, L., and Zeng, H. (2015). Novel Mussel-Inspired Injectable Self-Healing Hydrogel with Anti-biofouling Property. *Adv. Mater.* 27 (7), 1294–1299. doi:10.1002/adma.201405166

Li, P., Kaslan, M., Lee, S. H., Yao, J., and Gao, Z. (2017). Progress in Exosome Isolation Techniques. *Theranostics* 7 (3), 789–804. doi:10.7150/thno.18133

Li, X., Jiang, C., and Zhao, J. (2016). Human Endothelial Progenitor Cells-Derived Exosomes Accelerate Cutaneous Wound Healing in Diabetic Rats by Promoting Endothelial Function. *J. Diabetes its Complications* 30 (6), 986–992. doi:10.1016/j.jdiacomp.2016.05.009

Liang, Y., Zhao, X., Hu, T., Chen, B., Yin, Z., Ma, P. X., et al. (2019). Adhesive Hemostatic Conducting Injectable Composite Hydrogels with Sustained Drug Release and Photothermal Antibacterial Activity to Promote Full-Thickness Skin Regeneration during Wound Healing. *Small* 15 (12), 1900046. doi:10.1002/smll.201900046

Lin, W., Xu, L., Zwingenberger, S., Gibon, E., Goodman, S. B., and Li, G. (2017). Mesenchymal Stem Cells Homing to Improve Bone Healing. *J. Orthopaedic Translation* 9, 19–27. doi:10.1016/j.jot.2017.03.002

Liu, X., Yang, Y., Li, Y., Niu, X., Zhao, B., Wang, Y., et al. (2017). Integration of Stem Cell-Derived Exosomes with *In Situ* Hydrogel Glue as a Promising Tissue Patch for Articular Cartilage Regeneration. *Nanoscale* 9 (13), 4430–4438. doi:10.1039/c7nr00352h

Liu, Y., Ma, Y., Zhang, J., Yuan, Y., and Wang, J. (2019). Exosomes: A Novel Therapeutic Agent for Cartilage and Bone Tissue Regeneration. *Dose-Response* 17 (4), 155932581989270. doi:10.1177/1559325819892702

Lokhande, G., Carrow, J. K., Thakur, T., Xavier, J. R., Parani, M., Bayless, K. J., et al. (2018). Nanoengineered Injectable Hydrogels for Wound Healing Application. *Acta Biomater.* 70, 35–47. doi:10.1016/j.actbio.2018.01.045

Lou, G., Chen, Z., Zheng, M., and Liu, Y. (2017). Mesenchymal Stem Cell-Derived Exosomes as a New Therapeutic Strategy for Liver Diseases. *Exp. Mol. Med.* 49 (6), e346. doi:10.1038/emm.2017.63

Manda, S. V., Kataria, Y., Tatireddy, B. R., Ramakrishnan, B., Ratnam, B. G., Lath, R., et al. (2018). Exosomes as a Biomarker Platform for Detecting Epidermal Growth Factor Receptor-Positive High-Grade Gliomas. *J. Neurosurg.* 128 (4), 1091–1101. doi:10.3171/2016.11.Jns161187

Mantha, S., Pillai, S., Khayambashi, P., Upadhyay, A., Zhang, Y., Tao, O., et al. (2019). Smart Hydrogels in Tissue Engineering and Regenerative Medicine. *Materials* 12 (20), 3323. doi:10.3390/ma12203323

Mathivanan, S., Ji, H., and Simpson, R. J. (2010). Exosomes: Extracellular Organelles Important in Intercellular Communication. *J. Proteomics* 73 (10), 1907–1920. doi:10.1016/j.jprot.2010.06.006

Mehrali, M., Thakur, A., Pennisi, C. P., Talebian, S., Arpanaei, A., Nikkhah, M., et al. (2017). Nanoreinforced Hydrogels for Tissue Engineering: Biomaterials that Are Compatible with Load-Bearing and Electroactive Tissues. *Adv. Mater.* 29 (8), 1603612. doi:10.1002/adma.201603612

Misumi, I., Sugawara, K., Takahata, K., Takahashi, K., and Ehara, K. (2018). Size Measurements of Standard Nanoparticles Using Metrological Atomic Force Microscope and Evaluation of Their Uncertainties. *Precision Eng.* 51, 691–701. doi:10.1016/j.precisioneng.2017.11.013

Nicodemus, G. D., and Bryant, S. J. (2008). Cell Encapsulation in Biodegradable Hydrogels for Tissue Engineering Applications. *Tissue Eng. Part B: Rev.* 14 (2), 149–165. doi:10.1089/ten.teb.2007.0332

Ovsianikov, A., Khademhosseini, A., and Mironov, V. (2018). The Synergy of Scaffold-Based and Scaffold-free Tissue Engineering Strategies. *Trends Biotechnol.* 36 (4), 348–357. doi:10.1016/j.tibtech.2018.01.005

Petta, D., Fussell, G., Hughes, L., Buechter, D. D., Sprecher, C. M., Alini, M., et al. (2016). Calcium Phosphate/thermoresponsive Hyaluronan Hydrogel Composite Delivering Hydrophilic and Hydrophobic Drugs. *J. Orthopaedic Translation* 5, 57–68. doi:10.1016/j.jot.2015.11.001

Piantanida, E., Alonci, G., Bertucci, A., and De Cola, L. (2019). Design of Nanocomposite Injectable Hydrogels for Minimally Invasive Surgery. *Acc. Chem. Res.* 52 (8), 2101–2112. doi:10.1021/acs.accounts.9b00114

Pinheiro, A., Silva, A. M., Teixeira, J. H., Gonçalves, R. M., Almeida, M. I., Barbosa, M. A., et al. (2018). Extracellular Vesicles: Intelligent Delivery Strategies for Therapeutic Applications. *J. Controlled Release* 289, 56–69. doi:10.1016/j.jconrel.2018.09.019

Pishavar, E., Luo, H., Naserifar, M., Hashemi, M., Toosi, S., Atala, A., et al. (2021). Advanced Hydrogels as Exosome Delivery Systems for Osteogenic Differentiation of MSCs: Application in Bone Regeneration. *Ijms* 22 (12), 6203. doi:10.3390/ijms22126203

Pluchino, S., and Smith, J. A. (2019). Explicating Exosomes: Reclassifying the Rising Stars of Intercellular Communication. *Cell* 177 (2), 225–227. doi:10.1016/j.cell.2019.03.020

Qin, Y., Wang, L., Gao, Z., Chen, G., and Zhang, C. (2016). Bone Marrow Stromal/stem Cell-Derived Extracellular Vesicles Regulate Osteoblast Activity and Differentiation *In Vitro* and Promote Bone Regeneration *In Vivo*. *Sci. Rep.* 6, 21961. doi:10.1038/srep21961

Riau, A. K., Ong, H. S., Yam, G. H. F., and Mehta, J. S. (2019). Sustained Delivery System for Stem Cell-Derived Exosomes. *Front. Pharmacol.* 10, 1368. doi:10.3389/fphar.2019.01368

Robbins, P. D., and Morelli, A. E. (2014). Regulation of Immune Responses by Extracellular Vesicles. *Nat. Rev. Immunol.* 14 (3), 195–208. doi:10.1038/nri3622

Ruel-Gariépy, E., and Leroux, J.-C. (2004). In Situ-forming Hydrogels-Review of Temperature-Sensitive Systems. *Eur. J. Pharmaceutics Biopharmaceutics* 58 (2), 409–426. doi:10.1016/j.ejpb.2004.03.019

Safari, B., Aghazadeh, M., Davaran, S., and Roshangar, L. (2022). Exosome-loaded Hydrogels: a New Cell-free Therapeutic Approach for Skin Regeneration. *Eur. J. Pharmaceutics Biopharmaceutics* 171, 50–59. doi:10.1016/j.ejpb.2021.11.002

Sargeant, T. D., Desai, A. P., Banerjee, S., Agawu, A., and Stopek, J. B. (2012). An *In Situ* Forming Collagen-PEG Hydrogel for Tissue Regeneration. *Acta Biomater.* 8 (1), 124–132. doi:10.1016/j.actbio.2011.07.028

Saunderson, S. C., Dunn, A. C., Crocker, P. R., and McLellan, A. D. (2014). CD169 Mediates the Capture of Exosomes in Spleen and Lymph Node. *Blood* 123 (2), 208–216. doi:10.1182/blood-2013-03-489732

Schiffelers, R. M., Bakker-Woudenberg, I. A., and Storm, G. (2000). Localization of Sterically Stabilized Liposomes in Experimental Rat *Klebsiella pneumoniae* Pneumonia: Dependence on Circulation Kinetics and Presence of Poly(ethylene)glycol Coating. *Biochim. Biophys. Acta* 1468 (1-2), 253–261. doi:10.1016/s0005-2736(00)00265-0

Shi, Q., Qian, Z., Liu, D., Sun, J., Wang, X., Liu, H., et al. (2017). GMSC-derived Exosomes Combined with a Chitosan/Silk Hydrogel Sponge Accelerates Wound Healing in a Diabetic Rat Skin Defect Model. *Front. Physiol.* 8, 904. doi:10.3389/fphys.2017.00904

Shipway, A. N., and Willner, I. (2001). Nanoparticles as Structural and Functional Units in Surface-Confined Architectures. *Chem. Commun.* (20), 2035–2045. doi:10.1039/B105164B

Shiue, S.-J., Rau, R.-H., Shiue, H.-S., Hung, Y.-W., Li, Z.-X., Yang, K. D., et al. (2019). Mesenchymal Stem Cell Exosomes as a Cell-free Therapy for Nerve Injury-Induced Pain in Rats. *Pain* 160 (1), 210–223. doi:10.1097/j.pain.0000000000001395

Singh, R., Pochampally, R., Watabe, K., Lu, Z., and Mo, Y.-Y. (2014). Exosome-mediated Transfer of miR-10b Promotes Cell Invasion in Breast Cancer. *Mol. Cancer* 13, 256. doi:10.1186/1476-4598-13-256

Sitar, S., Kejžar, A., Pahovnik, D., Kogej, K., Tušek-Žnidarič, M., Lenassi, M., et al. (2015). Size Characterization and Quantification of Exosomes by

Asymmetrical-Flow Field-Flow Fractionation. *Anal. Chem.* 87 (18), 9225–9233. doi:10.1021/acs.analchem.5b01636

Sokolova, V., Ludwig, A.-K., Hornung, S., Rotan, O., Horn, P. A., Epple, M., et al. (2011). Characterisation of Exosomes Derived from Human Cells by Nanoparticle Tracking Analysis and Scanning Electron Microscopy. *Colloids Surf. B: Biointerfaces* 87 (1), 146–150. doi:10.1016/j.colsurfb.2011.05.013

Staruch, R. M. T., Glass, G. E., Rickard, R., Hettiaratchy, S. P., and Butler, P. E. M. (2017). Injectable Pore-Forming Hydrogel Scaffolds for Complex Wound Tissue Engineering: Designing and Controlling Their Porosity and Mechanical Properties. *Tissue Eng. Part B: Rev.* 23 (2), 183–198. doi:10.1089/ten.TEB.2016.0305

Takahashi, Y., Nishikawa, M., Shinotsuka, H., Matsui, Y., Ohara, S., Imai, T., et al. (2013). Visualization and *In Vivo* Tracking of the Exosomes of Murine Melanoma B16-BL6 Cells in Mice after Intravenous Injection. *J. Biotechnol.* 165 (2), 77–84. doi:10.1016/j.jbiotec.2013.03.013

Thomas, V., Yallapu, M. M., Sreedhar, B., and Bajpai, S. K. (2008). Breathing-in/breathing-out Approach to Preparing Nanosilver-Loaded Hydrogels: Highly Efficient Antibacterial Nanocomposites. *J. Appl. Polym. Sci.* 111 (2), NA. doi:10.1002/app.29018

Valadi, H., Ekström, K., Bossios, A., Sjöstrand, M., Lee, J. J., and Lötvall, J. O. (2007). Exosome-mediated Transfer of mRNAs and microRNAs Is a Novel Mechanism of Genetic Exchange between Cells. *Nat. Cel Biol* 9 (6), 654–659. doi:10.1038/ncb1596

van Niel, G., Porto-Carreiro, I., Simoes, S., and Raposo, G. (2006). Exosomes: a Common Pathway for a Specialized Function. *J. Biochem.* 140 (1), 13–21. doi:10.1093/jb/mvj128

Vanderstappen, J., Lammens, J., Berger, P., and Laumen, A. (2015). Ilizarov Bone Transport as a Treatment of Congenital Pseudarthrosis of the Tibia: a Long-Term Follow-Up Study. *J. Children's Orthopaedics* 9 (4), 319–324. doi:10.1007/s11832-015-0675-7

Visser, J., Melchels, F. P. W., Jeon, J. E., van Bussel, E. M., Kimpton, L. S., Byrne, H. M., et al. (2015). Reinforcement of Hydrogels Using Three-Dimensionally Printed Microfibres. *Nat. Commun.* 6 (1), 6933. doi:10.1038/ncomms7933

Wang, C., Wang, M., Xu, T., Zhang, X., Lin, C., Gao, W., et al. (2019). Engineering Bioactive Self-Healing Antibacterial Exosomes Hydrogel for Promoting Chronic Diabetic Wound Healing and Complete Skin Regeneration. *Theranostics* 9 (1), 65–76. doi:10.7150/thno.29766

Wang, L., Wang, J., Zhou, X., Sun, J., Zhu, B., Duan, C., et al. (2020). A New Self-Healing Hydrogel Containing hucMSC-Derived Exosomes Promotes Bone Regeneration. *Front. Bioeng. Biotechnol.* 8 (1047), 564731. doi:10.3389/fbioe.2020.564731

Wang, W., and Yeung, K. W. K. (2017). Bone Grafts and Biomaterials Substitutes for Bone Defect Repair: A Review. *Bioactive Mater.* 2 (4), 224–247. doi:10.1016/j.bioactmat.2017.05.007

Wei, H., Cui, J., Lin, K., Xie, J., and Wang, X. (2022). Recent Advances in Smart Stimuli-Responsive Biomaterials for Bone Therapeutics and Regeneration. *Bone Res.* 10 (1), 17. doi:10.1038/s41413-021-00180-y

Willms, E., Cabañas, C., Mäger, I., Wood, M. J. A., and Vader, P. (2018). Extracellular Vesicle Heterogeneity: Subpopulations, Isolation Techniques, and Diverse Functions in Cancer Progression. *Front. Immunol.* 9, 17. doi:10.3389/fimmu.2018.00738

Wu, R., Li, Y., Shen, M., Yang, X., Zhang, L., Ke, X., et al. (2021). Bone Tissue Regeneration: The Role of Finely Tuned Pore Architecture of Bioactive Scaffolds before Clinical Translation. *Bioactive Mater.* 6 (5), 1242–1254. doi:10.1016/j.bioactmat.2020.11.003

Xu, R., Luo, G., Xia, H., He, W., Zhao, J., Liu, B., et al. (2015). Novel Bilayer Wound Dressing Composed of Silicone Rubber with Particular Micropores Enhanced Wound Re-epithelialization and Contraction. *Biomaterials* 40, 1–11. doi:10.1016/j.biomaterials.2014.10.077

Xue, X., Hu, Y., Wang, S., Chen, X., Jiang, Y., and Su, J. (2022). Fabrication of Physical and Chemical Crosslinked Hydrogels for Bone Tissue Engineering. *Bioactive Mater.* 12, 327–339. doi:10.1016/j.bioactmat.2021.10.029

Yan, Q., Dong, H., Su, J., Han, J., Song, B., Wei, Q., et al. (2018). A Review of 3D Printing Technology for Medical Applications. *Engineering* 4 (5), 729–742. doi:10.1016/j.eng.2018.07.021

Yang, C., Ma, H., Wang, Z., Younis, M. R., Liu, C., Wu, C., et al. (2021a). 3D Printed Wesselsite Nanosheets Functionalized Scaffold Facilitates NIR-II Photothermal Therapy and Vascularized Bone Regeneration. *Adv. Sci.* 8 (20), 2100894. doi:10.1002/advs.202100894

Yang, C., Zheng, Z., Younis, M. R., Dong, C., Chen, Y., Lei, S., et al. (2021b). 3D Printed Enzyme-Functionalized Scaffold Facilitates Diabetic Bone Regeneration. *Adv. Funct. Mater.* 31 (20), 2101372. doi:10.1002/adfm.202101372

Yang, D., Zhang, W., Zhang, H., Zhang, F., Chen, L., Ma, L., et al. (2020). Progress, Opportunity, and Perspective on Exosome Isolation - Efforts for Efficient Exosome-Based Theranostics. *Theranostics* 10 (8), 3684–3707. doi:10.7150/thno.41580

Yu, J., Xia, H., and Ni, Q.-Q. (2018). A Three-Dimensional Porous Hydroxyapatite Nanocomposite Scaffold with Shape Memory Effect for Bone Tissue Engineering. *J. Mater. Sci.* 53 (7), 4734–4744. doi:10.1007/s10853-017-1807-x

Zhai, M., Zhu, Y., Yang, M., and Mao, C. (2020). Human Mesenchymal Stem Cell Derived Exosomes Enhance Cell-Free Bone Regeneration by Altering Their miRNAs Profiles. *Adv. Sci.* 7 (19), 2001334. doi:10.1002/advs.202001334

Zhang, K., Jia, Z., Yang, B., Feng, Q., Xu, X., Yuan, W., et al. (2018b). Adaptable Hydrogels Mediate Cofactor-Assisted Activation of Biomarker-Responsive Drug Delivery *via* Positive Feedback for Enhanced Tissue Regeneration. *Adv. Sci.* 5 (12), 1800875. doi:10.1002/advs.201800875

Zhang, K., Zhao, X., Chen, X., Wei, Y., Du, W., Wang, Y., et al. (2018a). Enhanced Therapeutic Effects of Mesenchymal Stem Cell-Derived Exosomes with an Injectable Hydrogel for Hindlimb Ischemia Treatment. *ACS Appl. Mater. Inter.* 10 (36), 30081–30091. doi:10.1021/acsami.8b08449

Zhang, L., Yang, G., Johnson, B. N., and Jia, X. (2019). Three-dimensional (3D) Printed Scaffold and Material Selection for Bone Repair. *Acta Biomater.* 84, 16–33. doi:10.1016/j.actbio.2018.11.039

Zhang, S., Chuah, S. J., Lai, R. C., Hui, J. H. P., Lim, S. K., and Toh, W. S. (2018c). MSC Exosomes Mediate Cartilage Repair by Enhancing Proliferation, Attenuating Apoptosis and Modulating Immune Reactivity. *Biomaterials* 156, 16–27. doi:10.1016/j.biomaterials.2017.11.028

Zhang, X., Wang, X., Zhu, H., Kranias, E. G., Tang, Y., Peng, T., et al. (2012). Hsp20 Functions as a Novel Cardiokine in Promoting Angiogenesis *via* Activation of VEGFR2. *Plos One* 7 (3), e32765. doi:10.1371/journal.pone.0032765

Zhang, Y., Wu, C., Friis, T., and Xiao, Y. (2010). The Osteogenic Properties of CaP/silk Composite Scaffolds. *Biomaterials* 31 (10), 2848–2856. doi:10.1016/j.biomaterials.2009.12.049

Zhang, Y., Xie, Y., Hao, Z., Zhou, P., Wang, P., Fang, S., et al. (2021). Umbilical Mesenchymal Stem Cell-Derived Exosome-Encapsulated Hydrogels Accelerate Bone Repair by Enhancing Angiogenesis. *ACS Appl. Mater. Inter.* 13 (16), 18472–18487. doi:10.1021/acsami.0c22671

Zhou, H., Yu, K., Jiang, H., Deng, R., Chu, L., Cao, Y., et al. (2021). A Three-In-One Strategy: Injectable Biomimetic Porous Hydrogels for Accelerating Bone Regeneration *via* Shape-Adaptable Scaffolds, Controllable Magnesium Ion Release, and Enhanced Osteogenic Differentiation. *Biomacromolecules* 22 (11), 4552–4568. doi:10.1021/acs.biomac.1c00842

Zhu, G., Zhang, T., Chen, M., Yao, K., Huang, X., Zhang, B., et al. (2021). Bone Physiological Microenvironment and Healing Mechanism: Basis for Future Bone-Tissue Engineering Scaffolds. *Bioactive Mater.* 6 (11), 4110–4140. doi:10.1016/j.bioactmat.2021.03.043

Zhu, J., and Marchant, R. E. (2011). Design Properties of Hydrogel Tissue-Engineering Scaffolds. *Expert Rev. Med. Devices* 8 (5), 607–626. doi:10.1586/erd.11.27

**Conflict of Interest:** The authors declare that the research was conducted in the absence of any commercial or financial relationships that could be construed as a potential conflict of interest.

**Publisher's Note:** All claims expressed in this article are solely those of the authors and do not necessarily represent those of their affiliated organizations, or those of the publisher, the editors and the reviewers. Any product that may be evaluated in this article, or claim that may be made by its manufacturer, is not guaranteed or endorsed by the publisher.

frontiers | Frontiers in Bioengineering and Biotechnology

REVIEW
published: 01 April 2022
doi: 10.3389/fbioe.2022.845342

# 3D-Printed Hydrogels in Orthopedics: Developments, Limitations, and Perspectives

*Zhen Liu[1†], Weiwei Xin[1†], Jindou Ji[2†], Jialian Xu[1], Liangjun Zheng[1], Xinhua Qu[1]* and Bing Yue[1]**

[1]Department of Bone and Joint Surgery, Department of Orthopedics, Renji Hospital, School of Medicine, Shanghai Jiao Tong University, Shanghai, China, [2]The First Clinical Medical College, Shandong University of Traditional Chinese Medicine, Jinan, China

OPEN ACCESS

**Edited by:**
*Di Huang,*
*Taiyuan University of Technology, China*

**Reviewed by:**
*Wenguo Cui,*
*Shanghai Jiao Tong University, China*
*Xiaobo Huang,*
*Taiyuan University of Technology, China*
*Wei Luo,*
*Donghua University, China*

***Correspondence:**
*Xinhua Qu*
*xinhua_qu@126.com*
*Bing Yue*
*advbmp2@163.com*

[†]*These authors have contributed equally to this work*

**Specialty section:**
*This article was submitted to Biomaterials, a section of the journal Frontiers in Bioengineering and Biotechnology*

**Received:** *29 December 2021*
**Accepted:** *24 February 2022*
**Published:** *01 April 2022*

**Citation:**
*Liu Z, Xin W, Ji J, Xu J, Zheng L, Qu X and Yue B (2022) 3D-Printed Hydrogels in Orthopedics: Developments, Limitations, and Perspectives. Front. Bioeng. Biotechnol. 10:845342. doi: 10.3389/fbioe.2022.845342*

Three-dimensional (3D) printing has been used in medical research and practice for several years. Various aspects can affect the finished product of 3D printing, and it has been observed that the impact of the raw materials used for 3D printing is unique. Currently, hydrogels, including various natural and synthetic materials, are the most biologically and physically advantageous biological raw materials, and their use in orthopedics has increased considerably in recent years. 3D-printed hydrogels can be used in the construction of extracellular matrix during 3D printing processes. In addition to providing sufficient space structure for osteogenesis and chondrogenesis, hydrogels have shown positive effects on osteogenic and chondrogenic signaling pathways, promoting tissue repair in various dimensions. 3D-printed hydrogels are currently attracting extensive attention for the treatment of bone and joint injuries owing to the above-mentioned significant advantages. Furthermore, hydrogels have been recently used in infection prevention because of their antiseptic impact during the perioperative period. However, there are a few shortcomings associated with hydrogels including difficulty in getting rid of the constraints of the frame, poor mechanical strength, and burst release of loadings. These drawbacks could be overcome by combining 3D printing technology and novel hydrogel material through a multi-disciplinary approach. In this review, we provide a brief description and summary of the unique advantages of 3D printing technology in the field of orthopedics. In addition, some 3D printable hydrogels possessing prominent features, along with the key scope for their applications in bone joint repair, reconstruction, and antibacterial performance, are discussed to highlight the considerable prospects of hydrogels in the field of orthopedics.

**Keywords: bone joint repair, reconstructive implant, antibacterial and anti-infection characteristics, 3D printing, hydrogel**

## 1 INTRODUCTION

Without effective intervention and treatment, existing injuries and defects can lead to new complications, such as severe infections, which can subsequently result in severe necrosis of the bone and joint, and ultimately the complete loss of bone and joint function. Existing clinical approaches to bone and joint surgery include allogeneic and autologous bone grafts and metal substitute grafts (Levato et al., 2017), with autologous bone grafts being limited by the scarcity of

donors; allogeneic bone grafts are limited in that they may lead to immune rejection. A significant issue associated with metal substitute grafts is that they are prone to wear and tear. Therefore, the life span of metal substitutes is generally short and there is a possibility that the individual may have to undergo secondary surgery. In fact, according to the literature (Canovas and Dagneaux, 2018), a survey showed that up to 30% of patients were dissatisfied after total knee arthroplasty.

Hydrogel-based three-dimensional (3D) printing technology has emerged as an effective treatment option for bone and joint injury problems, and its comprehensive advantages are being gradually unfolded. 3D-printed hydrogel materials not only possess most repair properties of existing repair materials (Perera et al., 2021), but also have unique ductility, hydrophilicity, and histocompatibility; moreover, there are extensive material choices as a considerable number of 3D-printed hydrogel materials have been discovered. Thus, owing to their unique advantages, hydrogels hold a huge potential in bone and joint tissue repair, anti-infection, and even tumor treatment.

From the 1990s to the 2010s, researchers experimented with various properties of 3D-printed hydrogels in the laboratory; thus, there has been significant progress in hydrogel-based 3D printing technology. In this paper, we will briefly introduce 3D-printed hydrogels and summarize the main and latest scientific findings in the field of 3D hydrogels in orthopedics to help gain a holistic and intuitive understanding of all aspects of 3D-printed hydrogels. The existing 3D printing technologies applicable to hydrogel materials are also presented. This review not only demonstrates the progress and technologies that have been achieved but also reflects on the problems that exist in order to promote the advancement of hydrogel-based 3D printing technology in the field of orthopedics and its early application in the practical treatment of bone and joint tissue repair.

# 2 HYDROGELS

## 2.1 Introduction to Hydrogels

Currently, hydrogels are popular biomaterials for 3D printing and are considered to be the core of 3D bioprinting. They are 3D mesh structures that are composed of highly absorbent cross-linked polymer chains, which swell rapidly in water and retain a large amount of water without dissolving in the swollen state (Abdollahiyan et al., 2020). They are cross-linked by physicochemical means, and the degree of cross-linking determines the water absorption; the higher the degree of cross-linking, the lower the water absorption. Therefore, the water content of hydrogels can vary considerably, from less than 10% to more than 95%, which makes it possible for hydrogels to exhibit both solid and liquid behavior (Gungor-Ozkerim et al., 2018). The solid nature of the hydrogel allows it to maintain a certain volume and form under certain conditions, whereas the liquid nature refers to its ability to allow solutes to diffuse and permeate through the hydrogel. The ability to maintain a certain volume and morphology ensures the feasibility of hydrogels as 3D printing scaffold materials (Turnbull et al., 2018), whereas the ability to allow solutes to diffuse within it makes it possible to add various inorganic and organic solutes to hydrogels.

## 2.2 Hydrogel Classification

### 2.2.1 Macro and Micro Hydrogels

Hydrogels can be classified according to their size and shape into macroscopic and microscopic gels (microspheres) (Nikolova and Chavali, 2019). Macroscopic hydrogels can be further classified into columnar, porous sponge, fibrous, membrane, spherical, etc. according to their shapes, while microscopic hydrogels can be classified into micron and nanoscale gels according to their diameters.

Nanocomposite biomaterials are a relatively new class of materials that combine biopolymers and biodegradable matrix structures with nanoscale bioactive and easily absorbed fillers (Bharadwaz and Jayasuriya, 2020). The nanofillers induced into polymeric matrices present important physical and chemical properties, such as large surface area, improved mechanical strength and stability, improved cell adhesion, proliferation and differentiation, and tissue regeneration compatibility for biomaterials (Zhai et al., 2017).

### 2.2.2 External Stimulation

Hydrogels can be divided into two categories according to their response to external stimuli: conventional and environment-sensitive hydrogels. Conventional hydrogels are insensitive to changes in the environment, such as temperature or pH. Environment-sensitive hydrogels are a class of polymer gels that can sense small changes or stimuli in the external environment (such as temperature, pH, light, electricity, pressure, etc.) and produce corresponding changes in physical structure and chemical properties or even mutations (Zhang et al., 2021). An impressive feature of such hydrogels is that their solvation behavior changes significantly during the response to the environment; this stimulus response property enables these hydrogels to be used as sensors, controlled release switches, etc., which is the focus of considerable current research (Jing et al., 2021).

An example is a hydrogel with a photothermal agent as its component, which converts light energy into heat under near infrared (NIR) irradiation. Its target temperature can be adjusted by changing the concentration and ratio of the photothermal agent, the irradiation time, and the laser intensity (Zhang et al., 2021). Mild local heat (41–43 °C) promotes cell proliferation, angiogenesis, wound healing, and bone regeneration, while higher temperatures (>50 °C) can effectively inhibit bacterial proliferation in infected wounds (Ji et al., 2020). Therefore, the photothermal effect can be adapted to different applications by using different temperatures.

### 2.2.3 Constituent Materials

Based on materials, hydrogels can be divided into natural polymeric hydrogels and synthetic polymeric hydrogels. The primary natural materials are currently agarose, alginate, gelatin, hyaluronic acid, and fibrin, and the main artificial materials are polyvinyl alcohol and polyethylene glycol (Naranda et al., 2021).

**TABLE 1 |** Properties of typical composite 3D-printed hydrogels.

| Hydrogel composition | Cross-linking method | 3D printing method | Generating organizations | Advantages | Limitations | References |
|---|---|---|---|---|---|---|
| Hyaluronic acid (HA)/alginate/polylactic acid (PLA) | Physical cross-linking | Extrusion-based printing method/droplet-based printing | Cartilage | Biocompatibility | Low mechanical strength | Bio-inspired hydrogel composed of hyaluronic acid and alginate as a potential bioink for 3D bioprinting of articular cartilage engineering constructs. Acta Biomater. 2020 Apr |
| Methacrylated poly [N-(2-hydroxypropyl)methacrylamide mono/diacrylate] (pHPMA-lac)/polyethylene glycol (PEG)/methacrylated hyaluronic acid (HAMA)/polycaprolactone (PCL) co-printing | Chemical cross-linking | Extrusion-based printing | Cartilage | Biocompatibility | Higher HAMA concentrations are detrimental to chondrogenesis | Development of a thermosensitive HAMA-containing bio-ink for the fabrication of composite cartilage repair constructs. Biofabrication. 2017 Mar |
| Alginate/Gelatin/Chondroitin Sulfate/Graphene Oxide Nano | Physical cross-linking, chemical cross-linking | Extrusion-based printing (micro-extrusion) | Cartilage | Printability | High preparation cost | Chondroinductive Alginate-Based Hydrogels Having Graphene Oxide for 3D-Printed Scaffold Fabrication. ACS Appl Mater Interfaces. 2020 Jan |
| Gelatin/alginate/nanosilicate | Physical cross-linking | Extrusion-based printing | Bone | Mechanical strength | -- | 3D-bioprinted functional and biomimetic hydrogel scaffolds incorporated with nanosilicates to promote bone healing in rat calvarial defect model. Mater Sci Eng C Mater Biol Appl. 2020 Ju |
| Gelatin methacrylate (GelMA)/vascular endothelial generating factor (VEGF)/silicate nanosheets | Chemical cross-linking | Extrusion-based printing (stitching of cylindrical structures) | Bone | Promotes bone tissue production capacity | Complex printing process | Bioprinted Osteogenic and Vasculogenic Patterns for Engineering 3D Bone Tissue. adv Healthc Mater. 2017 |
| Silk protein/nano hydroxyapatite/nano silver ion/nano gold ion | Chemical cross-linking | Extrusion-based printing | Bone | Antibacterial activity | Higher cost of raw materials | Antibacterial silk fibroin/nanohydroxyapatite hydrogels with silver and gold nanoparticles for bone regeneration. nanomedicine. 2017 Jan |
| Hydroxyapatite (HA)/polydopamine (PDA)/carboxymethyl chitosan (CMCS) | Chemical cross-linking | Extrusion-based printing | Bone | Osteogenesis | -- | Bifunctional scaffolds of hydroxyapatite/poly (dopamine)/carboxymethyl chitosan with osteogenesis and anti-osteosarcoma effect. Biomater Sci. 2021 May |
| Alginate/Methylcellulose/Magnesium silicate clay (Laponite) | Physical cross-linking | Extrusion-based printing | Bone/Cartilage | Drug release effect | -- | Development of a clay based bioink for 3D cell printing for skeletal application. Biofabrication. 2017 Jul |
| Chondroitin methacrylate-sulfate (CSMA)/thermosensitive poly (N-(2-hydroxypropyl)methacrylate-mono/diacrylate)/polyethylene glycol triblock copolymer (MP) | Chemical cross-linking | Extrusion-based printing (microvalve) | Cartilage | Thermal Controllability | Difficult to apply clinically | A thermo-responsive and photo-polymerizable chondroitin sulfate-based hydrogel for 3D printing applications. Carbohydr Polym. 2016 Sep |

Polysaccharide hydrogel materials (Sahai et al., 2021) are carbohydrate macromolecules that are constructed by repeating monosaccharide units linked by glycosidic bonds. The family of polysaccharide hydrogels is extremely large; it includes agarose, chitin (Demirtas et al., 2017; Yadav et al., 2021), heparin, chondroitin sulfate, etc. Gelatin is a product of collagen degradation. It is cost-effective and promotes cartilage and bone regeneration. Hyaluronic acid is an important

component of the extracellular matrix of cartilage, and it effectively activates signaling pathways that promote cell differentiation and proliferation, thus enabling efficient cartilage or bone repair and reconstruction (Haung et al., 2021).

Natural polymers have better biocompatibility and environmental sensitivity, and they are abundantly available and inexpensive compared to artificial materials (Wang et al., 2019). However, natural polymers have lesser stability and are prone to degradation. Synthetic polymer hydrogels, conversely, have relatively better stability and mechanical strength. We have summarized the emerging 3D-printed composite hydrogels enlisted in this paper in **Table 1**.

Hydrogel materials composed of decellularized extracellular matrix have recently attracted significant attention in the experimental field. The decellularized extracellular matrix contains almost all the natural materials for the microenvironment required for cell growth (Kabirian and Mozafari, 2020). Furthermore, the matrix is loose and porous with extremely superior biocompatibility and degradability. Qiu et al. investigated decellularized extracellular matrix hydrogel materials based on the periosteal matrix (PEM) (Qiu et al., 2020). This matrix is a highly vascularized tissue that is deeply involved in the bone healing process; previous studies have shown that bio-scaffolds composed of periosteal matrix undergo spontaneous biomineralization and play an active role in bone defect repair. Hydrogels derived from a porcine decellularized periosteum were generated and characterized. The experimental results indicate that this hydrogel material promoted macrophage chemotaxis and M2 polarization associated with constructive bone remodeling and did not trigger adverse immune responses. It also promotes vascular formation and migration, osteogenic differentiation, and bone biomineralization. This illustrates the dynamic involvement of PEM hydrogels in all phases of the fracture repair process, thereby promoting bone regeneration *in vivo*.

### 2.2.1 Cross-Linking Methods

Hydrogels can be classified into physical and chemical gels based on the cross-linking method of the hydrogel. Physical gels are hydrogels that are formed by cross-linking through physical forces such as electrostatic interactions, hydrogen bonding, hydrophobic interactions, and other non-covalent bonds (Unagolla and Jayasuriya, 2020), which are non-permanent and mostly reversible. Thus, they are also known as pseudogels. However, many natural polymers, such as agar, can permanently maintain this gel state at room temperature. Among synthetic polymers, polyvinyl alcohol (PVA) also possesses such characteristics After the freeze–thaw treatment, PVA hydrogels that remain stable below 60°C can be obtained (Suzuki and Sasaki, 2015) (**Figure 1**).

Chemical cross-linking occurs mainly through covalent bonding and free-radical polymerization to form the 3D structure of the hydrogels. The cross-linking methods mainly include free radical polymerization, thiol-based Michael reactions, Schiff base reactions, and enzymatic cross-linking reactions. All these cross-linking methods are permanent (Unagolla and Jayasuriya, 2020), and thus, chemically cross-linked hydrogels are also called true gels.

Currently, the cross-linking methods most commonly used in printing go beyond the above-mentioned methods (Zhao et al., 2021). For example, methylated hydrogels with photosensitizers can rapidly form cross-links under blue light and UV light and thus gelatinize. Furthermore, sodium alginate can swiftly be cross-linked and gelatinized in a calcium chloride solution. Environmentally sensitive hydrogels are also capable of self-crosslinking in response to changes in external conditions. For instance, a temperature-sensitive hydrogel that is in a liquid state when the temperature is above 25 °C and rapidly gelatinizes when the temperature falls below 25 °C, has been reported.

Currently, the trendy research direction is composite hydrogel materials, which usually involve multiple types of crosslinking mechanisms. In this way, hydrogels can be fabricated with the desired properties. For example, the crosslinking of GelMA/alginate bioinks involves free radical polymerization of GelMA and electrostatic interactions of alginate (Stanco et al., 2020)to form interpenetrating networks.

## 2.3 Basic Properties of Hydrogels

### 2.3.1 Biocompatibility and Degradability

Biocompatibility is a significant factor for 3D bioprinting materials. It refers to the functional capabilities of a hydrogel material *in vivo* and *in vitro* without causing any adverse biological reactions (You et al., 2017). Specifically, a biocompatible material does not produce any toxic side effects on the cells and the body, does not cause hypersensitivity in the body, and does not produce toxic by-products when degraded *in vivo* and *in vitro*. Some properties of the 3D-printed hydrogels such as material temperature could be changed throughout the entire 3D printing process (Hölzl et al., 2016); the biocompatibility of the material during the entire process under different conditions is another important criterion to consider. Under the modulation of the experimental means of the experimental staff, it is desirable that the 3D-printed hydrogels are decomposed and reabsorbed *in vivo*. Degradation depends mainly on volumetric dissolution based on several mechanisms, such as hydrolysis (ester or enzyme), photolysis, untwisting, and combinations of these mechanisms. The degradation of 3D-printed hydrogel materials creates more space for cell proliferation (Ouyang et al., 2016), migration, and vascular infiltration.

### 2.3.2 Mechanical Strength

The mechanical strengths of hydrogels can be considered based on many different perspectives. In some cases, tissue formation mainly depends on the mechanical properties of the hydrogel. Hydrogel materials should ideally possess good mechanical strength throughout the 3D printing process. The rheological properties in printing will be discussed specifically in the next section. The mechanical strength here refers mainly to the ability to maintain its own structure after printing (Gómez et al., 2016). Hydrogel materials are exposed to pressures and stresses from all angles, whether they are *in vitro* or later implanted in the body, and therefore, they need to have good resistance to compression. In addition to the compressive capacity, tensile resistance is essential (Yue et al., 2020).

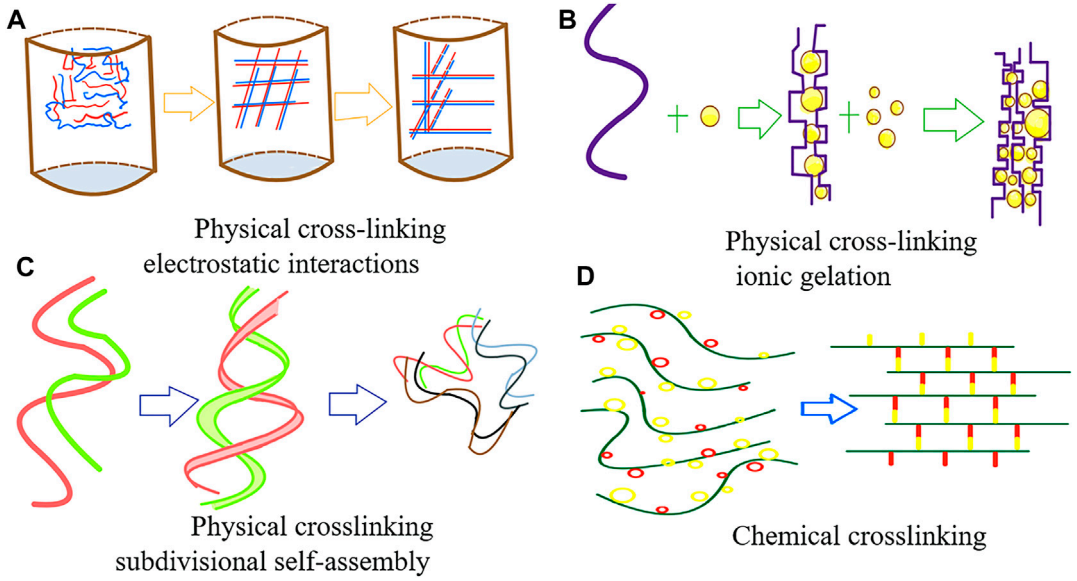


**FIGURE 1 |** Cross-linking methods for hydrogels.

For example, the human knee joint cartilage–bone interface can bear compressive stresses of 1 MPa and an interfacial toughness of approximately 800 J $m^{-2}$ over 1 million cycles of loads per year (Zhao et al., 2021). In order for the hydrogel structure to attain this strength, a few methods have been used, including supplementing the hydrogel with mineral particles such as hydroxyapatite to produce a composite hydrogel, co-printing by combining printed polycaprolactone (PCL) scaffolds (Mouser et al., 2017), and exploiting cross-linking mechanisms (Bi et al., 2019). For example, alginate hydrogels are cross-linked using a three-step process to improve elastic stiffness.

### 2.3.3 Viscosity

Viscosity refers to the intrinsic resistance of a fluid to flow in response to an external force. The molecular weight, concentration, and prevailing temperature of a hydrogel together determine its viscosity. In general, the higher the molecular weight and concentration, the higher is the corresponding viscosity (Han et al., 2021). Particularly, in extrusion-based 3D bioprinting, the hydrogel should possess a high viscosity, because it will help counteract the surface tension of the hydrogel. Further, the hydrogel droplets can be extruded more smoothly from the nozzle and further form continuous lines (Daly et al., 2017), which ensures that the two adjacent hydrogel chains do not bond together. However, high concentrations of hydrogels cannot form a good extracellular microenvironment, and thus, low concentrations of high-molecular-weight hydrogels are preferable.

### 2.3.4 Shear Dilution

Shear dilution refers to the ability to decrease viscosity as the shear rate increases. Normally, the higher the concentration of the hydrogel system, the more pronounced is the shear dilution. Hydrogels are exposed to high shear rates from within the device during 3D bioprinting, and the viscosity decreases, which ensures the survival of cells and therefore, the adaptability of 3D bioprinting.

### 2.3.5 Printability

Most existing 3D bioprinting techniques adopt a layer-by-layer approach, and thus, it is necessary that hydrogel materials maintain their original structure and morphology during the entire process of 3D printing (Kyle et al., 2017). This means that they need to have structural fidelity and integrity. This property may be related to the viscosity, surface tension, rheological properties, and cross-linking mechanisms of the hydrogels; it can be measured quantitatively using standardized tests. The primary method for assessing printability is to analyze the fiber diameter and pore size exhibited by 3D-printed hydrogel materials under varying printing pressures, printing speeds, and programmed fiber spacing.

Currently, the main method for enhancing the printability of hydrogels is to add easy-to-print components to the hydrogel to form a composite hydrogel (Chen et al., 2020). For example, nano-inorganic salt materials such as alginate are evenly incorporated into the hydrogel so that its overall microstructure remains stable and printable.

The first layer formation is a special consideration for hydrogel 3D bioprinting. It plays a crucial role in the formation and refinement of the overall 3D-printed structure. The first layer of printed bioink and the underlying structure maintain a larger contact angle, which is conducive to maintaining the upright and stable state of the bioink hydrogel material (Abdulghani and Morouco, 2019). The organic interaction between the 3D-printed hydrogel and the substrate facilitates both the overall positional

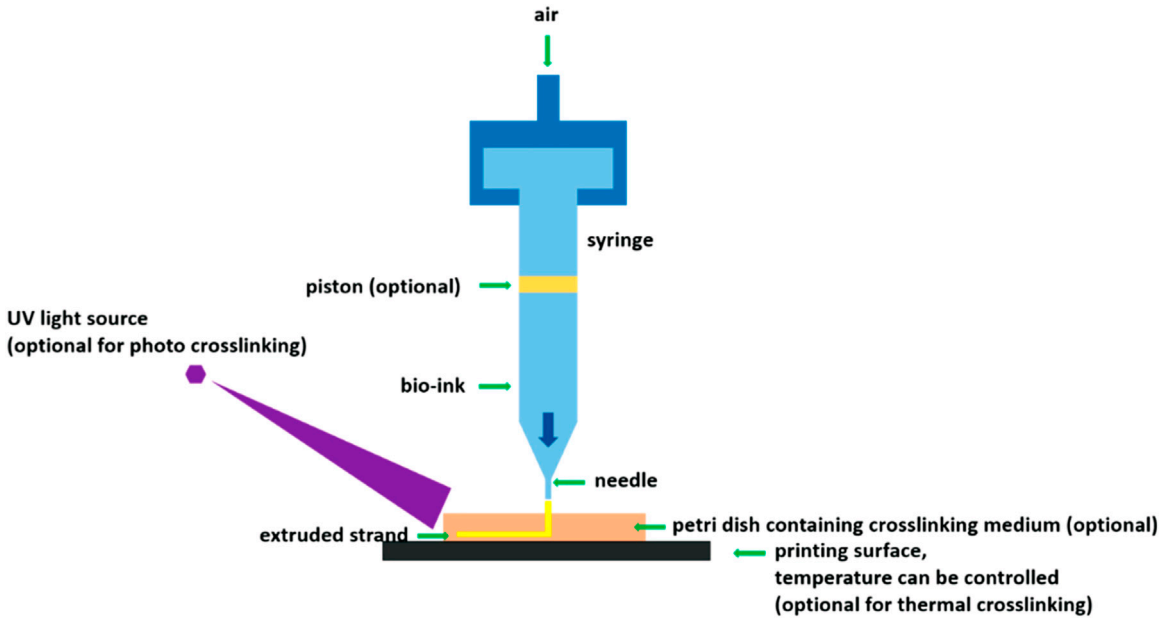


**FIGURE 2 |** Extrusion-based 3D printing schematic. (Schematic of extrusion-based bioprinting using various crosslinking mechanisms (You et al., 2017). Reproduced from (You et al., 2017) with permission from Copyright 2021 MDPI).

anchoring of the 3D-printed structure and the effective avoidance of abnormal deformation and movement during the subsequent layer-by-layer printing process.

## 3 3D BIOPRINTING

The 3D bioprinting technology has become an extremely popular research direction in the field of medical tissue repair. This approach maximizes multiple biomaterials for tissue fabrication (Zamborsky et al., 2019). Bioprinting technology can also be described as the spatial patterning of living cells using bioinks. It involves three main components: a polymer solution, living cells, and a 3D printer. Bioprinting is known to be an additive manufacturing technique that assembles materials layer by layer and is, therefore, cost-effective. The popular 3D bioprinting techniques in orthopedics include extrusion, droplet/inkjet, and laser printing techniques, as well as other techniques such as printing based on stereoscopic laser scales such as UV (Huang J. et al., 2021). Other 3D scaffold manufacturing methods that are widely used in the field of tissue engineering include fused deposition modeling (FDM) and direct ink writing (DIW).

### 3.1 Extrusion-Based 3D Printing

Extrusion-based 3D printing is mainly based on the intrinsic pressure of the 3D printer; it uses nozzles to eject the hydrogel adhesive strips and arrange them on a 3D structure according to a computer-aided design model, relying mainly on the shear dilution of the bioink in this process (Dhawan et al., 2019). This technique can be driven in various ways, such as pneumatic, electromagnetic, or mechanical drives (**Figure 2**). This is achieved by using screws, pneumatic pumps, and pistons to distribute long filaments of hydrogel onto the substrate through nozzles, which become the skeletal structure of the bone or cartilage tissue. Subsequently, the stem cells encased in the hydrogel materials proliferate and differentiate in the 3D-printed structure, thereby generating an appropriate graft replacement.

Such techniques have high printing speeds and are also more conducive to the formation of porous structures such as hydrogels (Zhang et al., 2019). This 3D printing approach also offers unique advantages in printing high-cell-density bioinks and has the ability to build complex 3D structures with multiple cell types and materials. Nevertheless, the high shear force used during the printing process can easily damage and kill the cells (Zhang et al., 2019), which causes the elimination of more stem cells during the printing process and may impair viability of the surviving cells. Hence, the subsequent proliferation and differentiation processes may take more time or even fail to achieve the desired results (Cui et al., 2020). Furthermore, this 3D printing technology still has a low printing accuracy; therefore, the 3D graphics printed in this way may not precisely generate the desired bone and cartilage structures.

### 3.2 Droplet-Based 3D Printing

The droplet-based bioprinting method involves inkjet, acoustic droplet jetting, and microvalve bioprinting. It is mainly based on a traditional 2D bioprinter with a modified print head and print head control. This type of printing achieves a certain degree of control of the droplets produced by the printer, mainly by means

of electric and ultrasonic energy, to eject droplets from the prepolymer solution onto the platform in a predefined pattern (Mora-Boza and Lopez-Donaire, 2018).

For example, thermal inkjet printers mainly use heat to generate pressure pulses in the print head in a short time, thus resulting in the ejection of bioink droplets (Turnbull et al., 2018). Other inkjet printing systems rely on piezoelectric crystals, which are mechanically stressed by the application of a voltage, which subsequently results in a change in shape. This approach further generates an acoustic wave, which creates sufficient pressure to eject the droplets from the nozzle.

This 3D printing technology has high printing accuracy and controllability because very small droplets can be manipulated as printing units. However, it also has apparent disadvantages in that the form of the bioink is severely restricted and must be in liquid form (Mora-Boza and Lopez-Donaire, 2018); additionally, it is difficult to control the droplet size consistently, there is uneven dispersion of cells in the droplet, and printer nozzles are prone to clogging.

## 3.3 Laser-Assisted 3D Printing

The laser printing approach, which is a relatively new technology, initiates the release of droplets mainly through the guidance of a laser. The main mode involves a two-layer approach, where the top layer is the energy-absorbing donor layer and the bottom layer is the bioink layer. When the top layer receives the laser pulse wave, bubbles are generated at the interface, thus pushing the droplets onto the substrate to achieve the release of the bioink. Using the high energy of the laser, the printer can operate without any direct contact with the model. This printing technology, similarly to the droplet-based printing technology, encompasses different modalities, including the Stereo Lithography Apparatus (SLA), Digital Light Processing (DLP), and two-photon polymerization (2 PP).

The SLA technology involves focusing a specific-wavelength and -intensity laser on the surface of a light-cured material, causing its sequential solidification from point to line and from line to surface, printing one layer, and then moving the lift table in the vertical direction by the height of that layer and subsequently curing another layer (Huang J. et al., 2021). The layers are thus stacked to form a three-dimensional structure. This technology displays high precision and speed and is already popular among laser-based 3D printing technologies.

The DLP modality is a variant of SLA. In this process, digital micromirror elements are used to project product cross-sectional shapes onto the surface of a liquid bright resin (Turnbull et al., 2018), light-curing it layer by layer. DLP 3D printing is faster than SLA owing to the slide/sheet-like curing of each layer. This technology is ideal for high-resolution molding.

Meanwhile, the 2 PP technology is a "nano-optics" application. This technology is similar to light-curing additive manufacturing, but 2 PP can achieve thinner layer thicknesses and $X$ and $Y$ axis resolutions between 100 and 200 nm (Mora-Boza and Lopez-Donaire, 2018). In contrast to the ordinary 3D printing optical polymerization with an ultraviolet laser, 2 PP uses a near-infrared long laser. As near-infrared wavelength photon energy, linear absorption, and Rayleigh scattering are low, and penetration in the medium is high, 2 PP enables the production of a wider variety of bone and cartilage replacement implants.

Laser-assisted 3D printing is highly effective for the utilization of bioinks with low viscosity. As a result, it only prints relatively thin structures. Although this printing method has high accuracy and resolution, its high cost and demanding requirements for bioinks limit its wide application.

# 4 CARTILAGE REPAIR AND RECONSTRUCTION

3D printing based on hydrogels can solve many of the problems and shortcomings of the restorative treatment of articular cartilage injury that is currently used in mainstream clinical practice. First, bone marrow mesenchymal stem cells or cell clusters with differentiation capacity are added into hydrogels, such as chondrogenic cells (ACPCs), whose differentiation capacity and characteristics have been demonstrated by Riccardo et al. (Levato et al., 2017). These differentiated cell tissues are added into the biocarrier hydrogel, and then the hydrogel units that are wrapped with cell clusters are deposited into the already constructed cartilage design model. In this case, the initial skeletal shape and volume of the 3D-printed implant material are fixed at the beginning. These hydrogel materials basically mimic the extracellular matrix and microenvironment in the human body, wherein the stem cell clusters can naturally and rapidly divide and differentiate. Eventually, the cells constitute the volume and morphology of the scaffold by continuously differentiating and proliferating and eventually migrating to the various components of the scaffold (Vega et al., 2017), at which point the ideal hydrogel material will begin to degrade naturally. In order to better promote cell differentiation and proliferation, a series of cytokines, such as BMPs and TGF, can be added based on the liquid behavior of the hydrogel (Gibbs et al., 2016), in addition to suitable nutritional conditions, to further promote the differentiation and growth of cartilage tissue.

## 4.1 Single Material Hydrogels

Some natural hydrogel materials inherently have the ability to promote chondrogenesis, such as collagen; Wincent et al. showed that mesenchymal stem cells, articular chondrocytes, etc. can undergo specific chemical reactions with collagen, microcurrent change sensing, etc. (Maisani et al., 2018), thus promoting cellular differentiation and regeneration. In addition to alginate and collagen, there are a series of natural materials with high biocompatibility, such as agarose, fibrin (Noori et al., 2017), and hyaluronic acid (Noori et al., 2017).

Polysaccharide hydrogel materials (Sahai et al., 2021) play a crucial role in living systems. These abundant polysaccharides inherently possess ideal properties such as biocompatibility, biodegradability, and functional groups that contribute to simple chemical modifications for customizability, cytocompatibility, and organized macrostructural features,

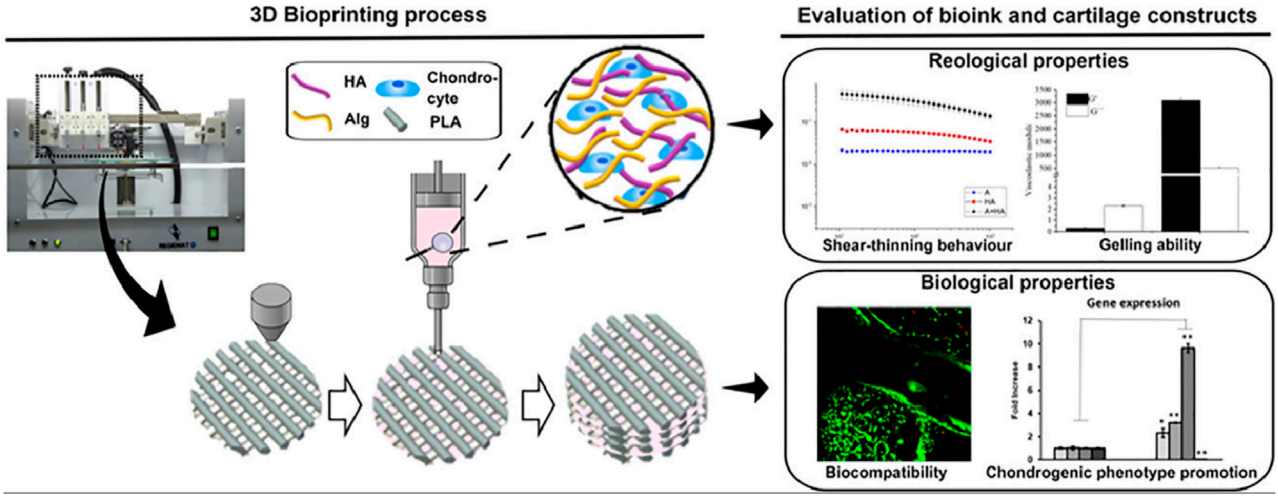


**FIGURE 3 |** A new composite hydrogel material for the 3D printing of articular cartilage repair (Antich et al., 2020) (Reproduced from Creative Commons license).

which makes them promising biomaterials (Radhakrishnan et al., 2017). Alginate is also a type of polysaccharide; specifically, alginate, or sodium alginate (in its original form) is an anionic polysaccharide of algal origin, consisting of mannoglycan aldehyde and gulonate units. The structure of alginate is similar to that of natural ECM, and properties such as good biocompatibility, high viscosity, and easy gelation make it an ideal material for 3D bioprinting (Radhakrishnan et al., 2017). Polysaccharide-based hydrogel materials are widely used in 3D hydrogel printing of cartilage and bone.

The biocompatibility of gelatin itself is due to the fact that the Arg-Gly-Asp (RGD) sequence in collagen is better preserved in gelatin (Gu et al., 2018), which allows gelatin to effectively promote cartilage tissue cell generation and migration.

Hyaluronic acid not only possesses excellent biocompatibility and the ability to promote chondrocyte differentiation and proliferation but also has good adhesion and ductility (Antich et al., 2020). Therefore, it is also used extensively in hydrogel-based 3D-printed cartilage repair techniques.

Apart from natural hydrogel materials, an increasing number of synthetic hydrogels are being used in large quantities for 3D printing of cartilage repair and reconstruction (Kundu et al., 2015). The utilization of synthetic hydrogel materials in cartilage repair and reconstruction has unique advantages (Lin et al., 2017; Yang et al., 2021).

## 4.2 Emerging Composite Hydrogels

To obtain more ideal bioprinting materials, researchers have combined different hydrogel materials to create composite hydrogel materials with more comprehensive characteristics and have made progress in 3D-printed cartilage repair engineering.

Antich et al. combined hyaluronic acid with alginate to obtain a new composite hydrogel material for the 3D printing of articular cartilage repair (Antich et al., 2020). The authors analyzed the properties of these HA/PLA composite hydrogels, such as viscosity, degradability, cell viability; moreover, they performed the karyotype analysis of new cartilage formation, by combining hyaluronic acid with alginate in the presence of calcium ions to form physical cross-links (**Figure 3**).

Cartilage formation in hybrid 3D-bioprinted constructs after 1 month in culture. Quantitative analysis of type II collagen 1) and GAG 2) in the total extract per scaffold (in 1 ml). 3) Gene expression levels of hyaline-specific chondrogenic marker genes (COL2A1, ACAN, and SOX9), fibrotic maker (COL1A1) and hypertrophic marker (COL10A1) in bioprinted 3D hybrid construct (mean ± SD, $n = 3$, Student's t-test, $^{*}p < 0.05$, $^{**}p < 0.01$). Reproduced from Creative Commons license.

Similar experiments for the development of bioinks were carried out by Mouser et al. They added methacrylated hyaluronic acid (HAMA) to a thermosensitive hydrogel composed of methacrylated poly [N-(2-hydroxypropyl) methacrylamide mono/diacrylate] (pHPMA-lac)/polyethylene glycol (PEG) triblock copolymer, to improve the printability of the bioink and guarantee the shape and volume of the generated cartilage tissue (Mouser et al., 2017). Moreover, they co-printed the bioink with polycaprolactone (PCL) to improve the mechanical stability of the bioink. Finally, the performance of the formulations was evaluated by *in vitro* incubation. The experimental results showed that the concentration of HAMA has a significant impact on the ability of chondrocytes to produce cartilage matrix, which shows a positive correlation at a certain concentration. However, an extremely high concentration can also lead to poor fibrocartilage formation. The final results of the experiment showed that the concentration of HAMA between 0.25 and 0.5% was the most favorable for the formation of the cartilage matrix. Moreover, the experimental results also showed that the synergistic printing of this triblock copolymer composed of thermosensitive hydrogel and PCL could produce 3D structures with mechanical strength almost identical to that of natural cartilage.

These studies mainly focused on improving the biocompatibility of 3D-printed hydrogels. Studies have also considered improving the physical properties of 3D-printed hydrogels to make them more suitable as printed bioinks. For example, Olate-Moya et al. intended to improve the mechanical properties and processability of hydrogels by compounding them. For this purpose, they combined the nanoparticle material graphene oxide with alginate (Olate-Moya et al., 2020) and added chondroitin sulfate from glycosaminoglycans to ensure the histocompatibility of the hydrogel material. The study and analysis of the characterization of the newly synthesized bioink, the water content and swelling rate of the 3D-printed scaffold, the rheological properties of the ink, the mechanical properties of the hydrogel, the biological interaction between the scaffold and BMSCs, and the histological and cytological studies of the new cartilage revealed several benefits. They showed that the new hydrogel material has enhanced printability, superior rheological properties, and a robust scaffold morphology retention. In addition, the new material also has good histocompatibility owing to the addition of chondroitin sulfate.

Most of the current trials and studies are based on this model. When natural or artificial hydrogel materials with different properties are combined through different cross-linking methods, a composite hydrogel material with all the superior properties of its components is obtained. Therefore, this model has the potential to create hydrogel materials with good biocompatibility, good mechanical properties and printability, and the ability to promote the proliferation and differentiation of cartilage.

You et al. targeted calcified cartilage in the deeper layers of articular cartilage, which is an important transition location for the repair of calcified cartilage; repair of this damage is difficult to achieve with most current regenerative engineering as the osteochondral interface is critical for maintaining the structural integrity of the joint (Yang et al., 2017). Therefore, in order to fully mimic the structure and generation process of calcified cartilage, homogeneous hydroxyapatite was mixed with alginate hydrogel, the resulting hydrogel was used for 3D bioprinting, and the printed material implanted subcutaneously in mice (You et al., 2018). The cellular activity, proliferation, and secretion of cartilage matrix were evaluated in the experiment, and the potential for cartilage tissue mineralization was quantified by assaying alkaline phosphatase activity. The rheology and print fidelity of the composite formed hydrogels were also considered. The final experimental results showed that the addition of HAP to the alginate hydrogel did not impair the activity and proliferation capacity of the cells, and it did not affect their secretion of cartilage matrix. Furthermore, it stimulated the secretion of mineralized matrix by chondrocytes, thus promoting mineral deposition *in vivo*, provided that the HAP particles were well dispersed. This experimental result illustrates the promising application and characteristics of this material in promoting calcified cartilage formation and ensuring the integrity of bone and joint repair.

Once the articular cartilage generated by hydrogel-based 3D bioprinting has been printed, its clinical application is another significant challenge. Only a few are currently used for humans. Preliminary tests have been performed in small animals, and very few preliminary applications have been performed *in vivo* in large organisms. In a more recent study by Shim et al., 3D-printed chondrocytes were implanted into the knee joints of rabbits, where evidence of fusion of bone and cartilage growth, the generation of new joints, and the production of cartilage surface membranes was observed (Ge et al., 2009). Zhang et al. conducted an *in vivo* study in rhesus monkeys, where electron beam melting was used to develop a porous titanium cage filled with simvastatin/poloxam 407 hydrogel and bone inward growth and spinal fusion were evaluated. This experiment was performed in larger animals (monkeys), providing a preliminary lead for experiments in humans (Zhang et al., 2020). These experiments and studies illustrate the massive potential of hydrogel-based 3D-printed cartilage structures implanted *in vivo* as a replacement therapy for bone joints, thus offering a new approach to articular cartilage repair.

# 5 BONE REPAIR AND RECONSTRUCTION

## 5.1 Special Nature of Bone Requirements

Infections caused by bone and joint injuries not only damage the articular cartilage but also inevitably affect the bone when the lesions have progressed to a certain level or when they are in a very specific location. Osteoarthritis, fractures, traumatic bone tumors, and other conditions directly affect the quality of long bones. Therefore, 3D-printed hydrogels have been extensively investigated, and to some extent, used for the repair and reconstruction of bone tissue (Feng et al., 2021).

The bone has unique characteristics compared to cartilage, and therefore also has some unique requirements for 3D-printed hydrogel materials, including some functions and characteristics of higher standards (Hernandez et al., 2017). First, 3D-printed hydrogels for bone tissue repair and reconstruction need to possess higher strength and hardness compared to that used for cartilage (Chen C. Y. et al., 2021). 3D-printed hydrogels have sufficient mechanical strength not only for maintaining human mechanics but also for maintaining the mechanical stability of the 3D-printed structure itself (Huang K.-H. et al., 2021). The angiogenesis of bone tissue is more important than the cartilage tissue (Son et al., 2015). The structure of bone tissue is complex, and it is mainly composed of various skeletal cells and blood vessels that penetrate them. The blood vessels provide the necessary oxygen and nutrition for bone tissue cells. Therefore, it is essential for 3D-printed hydrogels to possess pro-angiogenic properties in bone tissue.

## 5.2 Composite 3D-Printed Hydrogels

By organically combining different hydrogel materials, hydrogel materials can possess good mechanical strength while combining the original biocompatibility and viscosity properties. The current mainstream approach to increase the mechanical strength of hydrogels is to add inorganic molecules, such as silicates, to the hydrogels. Liu et al. developed a composite hydrogel material based on gelatin and alginate and further added nanoscale silicate materials to the original composite

hydrogel material (Liu et al., 2020), with the aim of retaining the original properties of the composite hydrogel and further increasing the mechanical strength. Hydration tests, microstructural and elemental analyses, rheological analyses, and uniaxial compression tests were performed to evaluate the newly synthesized hydrogel materials, and cryo-transmission electron microscopy and Fourier transform infrared spectroscopy (FT-IR) were used specifically for mechanical strength and cell proliferation assays and *in vitro* osteogenesis analyses. An *in vivo* model of cranial defects in rats was also established to evaluate the *in vivo* experimental effects of this hydrogel material. The final results showed that the mechanical strength of the hydrogel material was significantly enhanced by the addition of nanosilicate to the composite hydrogel material, and the excellent properties of the hydrogel were retained.

Besides silicates, research has been conducted on carbon materials (Cheng et al., 2018); graphene oxide materials are of great use in bone and cartilage repair (Cheng et al., 2020). For example, Dr. Qi Zhao's team prepared a new composite hydrogel material by preparing serine as a methacrylate hydrogel material and then combining it with graphene oxide. This hydrogel material was used for the repair of rat cranial bone in certain *in vivo* experiments. During the experiments, the density of the generated bone was assessed by X-ray, histological, and cytological analyses, and finally, RNA sequencing analysis was performed for a deeper assessment (Qi et al., 2020). The experimental results showed that the addition of graphene oxide to the hydrogel material significantly increased the mechanical strength of the hydrogel structure; moreover, the addition had no impact on the biocompatibility of the hydrogel. However, the addition of graphene oxide reduced the degradability of the hydrogel material to some extent. In a comparative analysis with the control group, the effectiveness of the hydrogel for osteogenic treatment was demonstrated by measuring bone density and analyzing bone tissue histology. A further RNA sequencing was performed to analyze the activation of the relevant osteogenic cytokine signaling pathways in the context of the hydrogel treatment. In the experimental results, it was observed that the relevant signaling pathways such as BMP showed more activities, thus reinforcing the potential of the new composite 3D-printed hydrogel as a bone tissue repair material. There are many other compounds that can be used to enhance the mechanical strength of hydrogels, and many similar hydrogel materials have been explored and fabricated based on these compounds (Pathmanapan et al., 2020).

In addition to the pressure resistance, the mechanical strength of hydrogel materials also includes tensile resistance. It is important that the hydrogel structure maintains its original physical structure and morphology in the face of external pressure and possess good tensile resistance against stretching (Bouler et al., 2017). Therefore, double network gels (DN gels), which are composite hydrogels formed by combining two polymers with different physical properties, have been studied and developed. Here, one is a rigid network and the other is a flexible network; such a structure ensures that the hydrogel material maintains its structural resistance to pressure and also ensures its resistance to stretching. Bi et al. combined two materials, chitosan and polyvinyl alcohol (PVA), to form a double network hydrogel material; to further enhance its mechanical strength and osteogenic differentiation, hydrogel surface mineralization was introduced, and based on this, the hydrogel material was combined with inorganic compounds. This was done by repeatedly soaking the double-mesh hydrogel in aqueous solutions of calcium chloride and potassium hydrogen phosphate alternately, which yielded mineralized crystals on the surface of the hydrogel (Bi et al., 2019). The surface mineralized double-network hydrogel material obtained through this process was evaluated under several physical conditions, along with its histological and cytological analyses. These analyses demonstrated that this material clearly possesses a certain degree of enhanced physical and mechanical strength and better histocompatibility and osteogenic differentiation induction.

The rheological properties of hydrogels have also been a significant challenge in the field of 3D-printed bone tissue engineering. An ideal hydrogel material ensures that the encapsulated cells can be uniformly distributed and should migrate efficiently for growth during the 3D printing process. To address this challenge, Bendtsen et al. explored novel hydrogel composites by experimenting with two natural and synthetic materials, alginate and polyvinyl alcohol, to form a base composite hydrogel, and then adding hydroxyapatite to the hydrogel material as a base (Bendtsen et al., 2017). Hydroxyapatite (HA) is the main inorganic component of natural bone (Yao et al., 2021), and its incorporation into polyvinyl alcohol (PVA) suspensions was used to increase the viscosity of the hydrogel formulation and increase the biocompatibility and osteoconductivity of the printed scaffold. A variety of solution formulations was also used for the study to identify an optimal formulation system. The final results confirmed that the composite hydrogel material incorporating calcium hydroxyphosphate has good viscoelasticity at the appropriate concentration and is fully adaptable to the extrusion process in 3D printing and can later form a high-fidelity scaffold structure. The hydrogel provides favorable conditions for the regeneration of bone structures and has the ability to promote bone tissue generation *in vitro*.

Therefore, it can be seen that combining organic hydrogel materials with good biocompatibility and inorganic compounds with certain mechanical strength in an appropriate way (Heid and Boccaccini, 2020) can effectively combine the advantages of both materials and create hydrogel materials with more promising applications in the field of bone tissue repair and reconstruction. These inorganic compounds are mainly the aforementioned silicate-based inorganic materials, calcium phosphate-based inorganic materials (Dhivya et al., 2015), and newly discovered inorganic materials containing metallic strontium. The inorganic materials containing metallic strontium can integrate with bone hydroxyapatite and reduce bone resorption by increasing the number of bone formation sites and decreasing the number of active osteoclasts. Therefore, strontium-doped bioactive glasses, hydroxyapatite, and calcium phosphate (scaffolds) show great promise as bone graft replacement materials.

The microscopic hydrogel materials (Chen et al., 2020) have also been used extensively in hydrogel-based 3D-printed bone repair and reconstruction experiments. The charged properties of the hydrogel microstructure, volume size, and shape of the microstructure are important determinants of bone tissue generation. Prof. Cui Zhang's group focused on studying composite hydrogels with nanomaterials, starting with chitosan as the most primitive raw material, and used methylated polyethylene glycol chitosan as the base plate material, wherein they introduced montmorillonite (MMT). The MMT particles are usually plate-shaped with a thickness of approximately 1 nm and a diameter of approximately 0.2–2 μm; the repeating structural unit of MMT consists of an alumina octahedral plate sandwiched between two silica tetrahedral layers (Cui et al., 2019). Because the surface of MMT is dominated by oxide anions, its overall surface charge is shallowly negative, which facilitates the mixing of this nanohydrogel material with cationic agents. Therefore, the introduction of this material into the hydrogel enables the nanostructure of the composite hydrogel to be cross-linked and sparsely porous. This porous structure can mimic the microenvironment of bone proliferation and differentiation in a highly reductive manner; this ensures that the composite 3D-printed hydrogel nanomaterial is highly induced by osteogenic differentiation. Therefore, by focusing on the development of 3D-printed hydrogel microstructures, the improved hydrogel materials from the molecular and cellular levels of osteogenic differentiation could be used in a large number of bone tissue engineering applications in the future.

Another major challenge in the field of bone tissue repair is the repair of large segmental bone defects that exceed a critical size (Chen et al., 2019). Yu et al. have made some attempts in this field by applying 3D printing hydrogel technology. The primary materials that were used included preosteoblast-derived matrix (Yu et al., 2020) (a special decellularized extracellular matrix material) and gelatin methacrylate (GelMA) hydrogel. Bone marrow mesenchymal stem cells (BMSCs) were inoculated to grow on the prepared composite hydrogel material to study properties for *in vitro* experiments. *in vivo* experiments were also performed on rabbits by artificially creating large-stage bone defects of 15 mm and using the implants generated from this hydrogel material for *in vivo* experiments. Their experimental results showed that *in vitro*, pODM exhibited some degree of chemotaxis and osteogenic induction of bone marrow mesenchymal stem cells (BMSCs). The implantation of pODM/gelatin methacrylate (GelMA) structures as engineered periosteal bone substitutes effectively repaired critical-sized segmental bone defects in the radius of rabbits. What's more, the hydrogel material of the extracellular matrix we have already mentioned in the previous introduction of hydrogel material itself is very loose and porous, which facilitates cell growth and migration.

### 5.3 Angiogenesis

An additional feature required for hydrogel materials for bone tissue reconstruction and repair is the ability of angiogenesis, as blood supply is the primary factor for the survival of new bone tissue without necrosis (Kuss et al., 2018). Current research has proposed two main strategies for generating vascular tissue; one is the artificial creation of vascular tissue through the distribution of vascular endothelial cells and the other is the formation of neovascularization through the self-assembly of the organism itself (Koç et al., 2014; Deng et al., 2017; Lin et al., 2019). Professor Batzaya Byambaa's group has studied and explored several levels and dimensions of angiogenesis in bone tissue engineering. First, to study the structure of the microenvironment, they created cylindrical bio-skeletal units of hypomethacrylic gelatin hydrogels and combined the hydrogel material with vascular endothelial generating factor (VEGF) to form gels of conjugated compounds (Byambaa et al., 2017). This hydrogel was then applied to bone tissue engineering, and its osteogenic induction and angiogenic ability were evaluated by cytological and histological methods. The results showed that after microenvironmental modifications and the addition of VEGF, this particular hydrogel had a good angiogenic effect, which improved bone tissue recovery and reconstruction, resulting in a more complete and comprehensive bone tissue repair. In addition, the hydrogel material with photothermal effect, which was mentioned before, has good potential in angiogenesis by quantitatively regulating the temperature of the hydrogel and thus controlling the physical state, microenvironmental temperature, and release of embedded cytokines.

## 6 ANTI-INFECTION PROPERTIES OF 3D-PRINTED HYDROGELS

Currently, 3D-printed hydrogels are one of the most popular materials for bone tissue engineering, and their antibacterial and anti-infection effects are excellent properties. Furthermore, studies on the antimicrobial properties of hydrogels are also one of the most popular research directions today. A significant portion of articular cartilage and bone damage is caused by infection and inflammation, and severe infection can cause irreversible damage to the bone and joint. Other causes of osteoarthritic injury, such as external mechanical violence, inevitably cause secondary infections. There are also a large number of medical operations, cartilage and bone repair and reconstruction, and the implants themselves may cause infection, and thus, the problem of infection will continue throughout the process of bone and joint repair and reconstruction. The hydrogel materials currently studied in the laboratory have shown good potential in terms of antibacterial and anti-infective properties (Li et al., 2017).

The hydrogel materials with antimicrobial activity are divided into three main categories. The first category is hydrogel materials containing inorganic antimicrobial metal ions or metal oxide nanoparticles, such as silver (Lu et al., 2016), copper and other metal ions, zinc oxide, nickel oxide, and other metal oxides. The second category is hydrogel materials containing antibiotic antimicrobial agent drugs, which are mainly combined with hydrogel and wrapped inside the hydrogel material, relying on the liquid behavior of the hydrogel, which is released at the

appropriate time to play an antibacterial and anti-infective role (Chen Z.-Y. et al., 2021). The last category is the hydrogel whose material itself has antibacterial and anti-infective ability, which is rare. It also has very obvious advantages; it is bactericidal and effective with almost no toxic side effects.

## 6.1 Addition of Antimicrobial Inorganic Metals

The antibacterial ability of silver-containing materials has been widely demonstrated in clinical practice, and silver-containing dressings are now commonly used in clinical surgery to treat wounds and prevent infection. Thus, biohydrogel materials containing silver ions in nanoparticles (Xu et al., 2018) are a common combination of anti-infective metal ions and hydrogel materials, and nanoparticles of silver ions can bind to natural hydrogel materials such as polysaccharides. Furthermore, they possess the ability to bind to many synthetic hydrogel materials. Silver ions have good efficacy in dealing with the anti-infective effects of Gram-negative bacteria. In a recent study (Ribeiro et al., 2017), Marta Ribeiro et al. incorporated particles of silver and gold nanoparticles into filamentous protein/hydroxyapatite nanogels to synthesize 3D-printed hydrogel materials with good antibacterial properties and the ability to promote bone tissue repair. During their experiments, they characterized the presence of AgNPs and AuNPs in the hydrogels using UV spectrophotometry, transmission electron microscopy, and thermogravimetric analysis. The *in vitro* antibacterial studies showed that hydrogels containing AgNPs and AuNPs exhibited significant inhibition of both Gram-positive and Gram-negative bacteria. The cytocompatibility studies using osteoblasts showed that the hydrogels had a significant effective antibacterial ability at a concentration of 0.5% for AgNPs, but for AuNPs and the hydrogels containing AuNPs were effective as antibacterial materials at almost all concentrations within the normal range without affecting cell behavior. In this experiment, it can be seen that besides silver ions, gold ions also have good antimicrobial properties. Some other experiments demonstrated that copper ions can also be added to 3D-printed hydrogel materials for antimicrobial activity (Zou et al., 2020).

In addition to these metal ions, researchers have also explored emerging rare metal ion materials, such as strontium metal (Tommasi et al., 2016) and lanthanum metal, which may possess a greater antibacterial potential and may also have more osteogenic activity. Moreover, when these metal ions are compounded with other hydrogel materials, the newly generated hydrogel materials may have a better ability to promote bone and cartilage tissue production in addition to antibacterial properties. For example, Professor Chen et al. introduced lanthanum metal ions into double-physical cross-linked hydrogel materials. In the experiments, the experimentalists created a network of dual physically cross-linked hydrogel materials from two materials, alginate, a natural hydrogel material, and polyvinyl alcohol, a synthetic material, and then added lanthanum metal (Hu et al., 2017). The mechanical properties, luminescence properties, biocompatibility, and antibacterial activity of this composite hydrogel were comprehensively evaluated in the experiments. It was found that this hydrogel material has excellent compressive and tensile resistance and excellent biocompatibility due to the double physical cross-linked structure, and most importantly owing to the introduction of lanthanum metal ions. These ions not only possess good photosensitive properties but also facilitate the detection and regulation of the hydrogel material in various biological microenvironmental situations; they also have a good antibacterial effect (Yang et al., 2016). Compared to silver ion materials, lanthanum metal ions showed good inhibitory effects on *Staphylococcus aureus* and *Escherichia coli* in the experiments. The discovery of this unexpected antibacterial effect may be of great reference value for the development of antibacterial hydrogels containing metal ion nanoparticles.

In addition, inorganic materials and metal oxide particles possess good bactericidal effects, mainly through the mechanism of photocatalytic reaction to kill microorganisms in a relatively short period of time, and zinc oxide is currently the most widely used metal oxide. It has shown good bactericidal activity in experiments and has almost no cytotoxicity. The antimicrobial properties of the material were investigated by experimentalists who formed ZnO nanorods *in situ* in a cross-linked carboxymethyl chitosan (CMCh) matrix, treated the CMCh hydrogels with zinc nitrate solution, and then oxidized the zinc ions with an alkaline solution to successfully prepare antimicrobial carboxymethyl chitosan/ZnO nanocomposite hydrogels (Wahid et al., 2016). We focused on the point where the researchers investigated the antibacterial activity of CMCh/ZnO hydrogels against *Escherichia coli* and *Staphylococcus aureus* by CFU assay. The experimental results showed that the synthesized CMCh/ZnO nanocomposite hydrogels exhibited excellent antibacterial activity.

## 6.2 Addition of Antibiotics

The incorporation of antibiotics into hydrogel materials is also a common method used. Currently, the primary methods include the use of hydrogel material as a carrier for antibiotic drugs. Here, antibiotics are added to the microstructural units of the hydrogel to be released at the right time, and also by surface nanomaterial engineering, wherein the antibiotic drugs are infiltrated on the surface of the hydrogel. Some of the antibiotics that are often incorporated into hydrogel materials in research include ciprofloxacin and vancomycin (Jung et al., 2019). Salma et al. constructed a nano-hydrogel material containing doxycycline with the aim of enhancing its anti-infective ability by using 3D-printed hydrogels for drug delivery. The base material of this hydrogel material is a composite of three materials: gelatin, polyvinyl alcohol, and hyaluronic acid. The specific method used was to first prepare doxycycline/hydroxyapatite nanoparticles (DX/HAp) by mixing followed by solution centrifugation, etc., and then by mixing the manufactured particles into polycaprolactone (El-Habashy et al., 2021), and finally, fusing them with gelatin and hyaluronic acid materials to form doxycycline 3D-printed composite hydrogel material with relatively uniform dispersion. The *in vitro* experiments performed on this hydrogel material were aimed at determining the physicochemical characterization and *in vitro*

drug release ability of the hydrogel material. The *in vivo* experiments were conducted to construct a rabbit injury model and to repair and reconstruct bone tissue using this 3D-printed hydrogel material, which was eventually analyzed by histological and cytological measurements of the repaired tissue. The experimental results also largely met the expectations because this newly synthesized hydrogel material not only has good rheological properties and biocompatibility, but most importantly, it can release doxycycline both *in vivo* and *in vitro*.

In addition to inorganic metal ion oxidation and antimicrobial agents, scientists have also explored other substances added to hydrogel materials to play a certain antimicrobial role. For example, some biological extracts with special antibacterial effects, such as curcumin, honey, and lignin (Yang et al., 2018), as well as carbon materials and lysozyme (Wu et al., 2018), have shown some degree of antibacterial and antimicrobial effects against both *S. aureus* and *E. coli* when added to 3D-printed hydrogels.

### 6.3 Inherent Antibacterial Activity

The main hydrogel materials with inherent antimicrobial activity are synthetic polymeric antimicrobial materials (Chang et al., 2021), for example, redox-generated iron-based silane macromolecular hydrogels and some materials containing antimicrobial peptides, which are still relatively rare and have not been widely studied or applied in the field of orthopedics.

## 7 CURRENT SHORTCOMINGS OF 3D-PRINTED HYDROGELS

Hydrogel-based 3D printing technology has been extensively explored, and impressive results have been achieved in experimental research. However, there are still several shortcomings in this technology that need to be addressed.

### 7.1 Insufficient Mechanical Strength

In addition to the diversity of hydrogel properties and the mechanical strength of hydrogels alone, there are a few other problems that need to be overcome. The mechanical strength of hydrogels includes resistance to compression, tensile properties, and shear dilution capabilities. Firstly, the 3D-printed hydrogel bio-skeleton should possess the ability to retain its own morphology and structure and resist pressure from outside. Moreover, the hydrogel could also be stretched and pulled during the process of 3D printing, and the ductility of the material with compressive ability may not be as ideal as the compressive ability. A hydrogel material with sufficient and comprehensive capabilities to cope with various experimental and clinical environments is needed for practical clinical applications.

### 7.2 Angiogenic Capacity

The 3D-printed bone tissue engineering using hydrogels needs to be further investigated and solved by establishing vascular networks in the generated bone and cartilage replacement tissues. The survival and long-term maintenance of new tissues can only be ensured by establishing a vascular network in new tissues and structures to maintain the blood supply to the new tissues. Currently, there are relatively poor coping strategies to solve the problem of vascular network generation and establishment, and it is still in the preliminary experimental and testing stage (Chen et al., 2018). Therefore, a certain volume and scale of 3D-printed bone tissue replacement have hardly been tested because this problem of vascular generation and vascular network establishment needs to be solved before we can further consider a certain scale of regenerated tissues and structures.

### 7.3 Insufficient Intrinsic Antibacterial Activity

The sterility and antibacterial ability mentioned previously are also worthy of attention. Several existing materials with antimicrobial activity are not satisfactory in other aspects of performance and have not received widespread attention. Therefore, the main approach taken to solve the antimicrobial problem is the addition of metallic substances or antibiotics, which are antimicrobial substances in hydrogel materials; because they are added substances, they have to consider the problem of uniform dispersion and long-term release similar to the cytokines mentioned previously. In addition to the antimicrobial properties, we must also ensure the sterility of the 3D-printed hydrogel material itself during the whole process and not only in the experimental environment. For practical applications, the process flow of the production and the surgical self-contained whole process to ensure the sterility of the 3D-printed implant material needs to be chosen according to the hydrogel's own characteristics.

### 7.4 Degradability and Cytotoxicity of Degradation Products

The degradability and cytotoxicity of hydrogels are major criteria for consideration of hydrogels, and are one of the current shortcomings. Once the hydrogel material constitutes the 3D-bioprinted biological skeleton, the real need for clinical treatment is to implant the new bone and cartilage tissues formed into the human body to achieve clinically effective bone and cartilage tissue repair and reconstruction (Ma et al., 2018). However, whether and when the hydrogel material will eventually need to be degraded in this process (Gao et al., 2019), and whether the material generated after degradation is cytotoxic are questions that must be considered. If we create a repair material that is implanted in the human body for a long time together with the hydrogel, then we need to consider the maintenance of the hydrogel in the body. When the cartilage and bone cells have proliferated and migrated sufficiently in the bio-scaffold material to constitute the whole tissue, the hydrogel is no longer needed to maintain the structure. Further concerns include the degradation of hydrogels and how we should regulate the time of its degradation in order to avoid degradation before tissue repair is generated (Gao et al., 2019) or a delayed

degradation occurs. It is also important to note that even though most hydrogels are biocompatible and almost non-cytotoxic, once decomposed, whether the decomposition products can be guaranteed to be absolutely non-cytotoxic and persistent in the human body are issues that need to be further explored and considered.

### 7.5 Lack of Adequate *in Vivo* Experiments

There have not been sufficient *in vivo* experiments, and most existing ones do not involve 3D-printed implants. Most of these *in vivo* experiments have been performed on small animals such as mice and rats, with some degree of implantation on the surface of the body, and there have been no real cases of repair and replacement of a section of bone or a specific joint. One of the main *in vivo* experimental models used is the repair of cranial defects in mice; however, there is a difference between the repair and reconstruction of cranial bones and the repair of knee and hip injuries. In addition to the lack of further experiments on large animals, in addition to mice, we can also see the establishment of *in vivo* models of rabbits (Jiang et al., 2021), lack of *in vivo* experiments, and models of large mammals such as pigs and cattle, and thus, the practical application of 3D-printed hydrogel *in vivo* still should be comprehensively studied.

### 7.6 Lack of Systematic Scientific Consideration and Evaluation Criteria

The use of 3D-printed hydrogel materials in clinical applications also requires technical, regulatory, and ethical considerations and justifications. First, a set of strict manufacturing and use standards must be established for 3D-printed hydrogel materials to ensure the reliability and safety of the materials and implants themselves. The safety of the implant during implantation and the certainty of its repair ability need to be ensured. The use of this technology in the clinical setting will certainly be challenged by ethical considerations (Abbadessa et al., 2016b). In addition to a rigorous ethical review, we need to strictly regulate and review the scope of use of hydrogel 3D printing as a technology.

## 8 OUTLOOK AND CONCLUSION

The combination of bioprinting and (Kang et al., 2015) computer-aided algorithms, which allows the computer to recognize and analyze the CT, MRI, and other examination results by inputting them into the computer, and eventually generate a personalized design that fits the patient's actual situation through built-in algorithms, is a key focus area in hydrogel-based 3D printing technology. Such a combination can effectively screen and select a suitable hydrogel material for the case and use it for appropriate reconstruction. The computer recognizes and analyzes the results of CT and MRI examinations, and eventually generates a personalized design that is tailored to the patient's situation through built-in algorithms.

The 3D bioprinting with electronic computers combined with various control systems to achieve high precision is a popular future direction for the use of 3D-printed hydrogel materials at the micron or even nanometer level (Xu et al., 2018), thereby allowing a more favorable formation microenvironment for bone tissue.

In the future, it is almost certain that 3D bioprinting will transition into 4D bioprinting, which would involve the addition of a new dimension to the original one, that is, time. The shape and function of hydrogels can follow time, mainly referring to the hydrogel materials that are sensitive to the response to external stimuli. Control of hydrogel materials by changing external conditions such as light intensity, temperature (Ji et al., 2020), pH value, magnetic field, and electric field (Mei et al., 2021) has been achieved. Based on further in-depth research on this aspect, future hydrogel materials could possess memory functions (Abbadessa et al., 2016a); they could be able to adjust their physicochemical properties on their own, following the external environment and our objective needs.

However, there are many shortcomings that need to be addressed, such as more comprehensive and stable mechanical strength. Single hydrogel materials have distinctive qualities, but they are not sufficiently comprehensive; for example, gelatin, hyaluronic acid, and other materials with high biocompatibility and osteogenic–chondrogenic induction (Daly et al., 2016) have low mechanical strength (Ahlfeld et al., 2017). Furthermore, materials such as alginate and polyvinyl alcohol lack the ability to induce cell proliferation and differentiation as much as gelatin and hyaluronic acid; hence, certain cytokines and other substances need to be added to simulate the extracellular microenvironment to the possible extent. Furthermore, hydrogel materials with good intrinsic antibacterial ability are still very rare, and the antibacterial properties of the few existing ones are yet to be fully evaluated. Finally, the composite hydrogel preparation process is sophisticated and expensive. Although there is a wide variety of composite hydrogels, none of them have been widely accepted because they do not meet the standards specified for clinical use.

Therefore, we can see that 3D-printed hydrogel materials in orthopedics, especially in the field of bone and joint repair, possess a very wide range of potential applications and prospects, and a considerable part of the results have been achieved in experiments. Some researchers have also explored the clinical applications. Many materials have the ability to induce cellular osteogenesis into cartilage differentiation and proliferation; after a certain degree of improvement, they possess a certain degree of mechanical strength and antibacterial activity. Thus, it is bound to be a popular focus of future research. It is believed that after more research and future discoveries, 3D-printed hydrogel materials will be applied in the near future in osteochondral tissue repair and reconstruction to solve bone and joint injury problems.

## AUTHOR CONTRIBUTIONS

ZL, WX, and JJ wrote the draft manuscript. LZ, WX, JJ, JX, and LZ performed the literature review and data collection. BY and XQ conceived the general idea and revised the manuscript. All authors contributed to the article and approved the submitted version.

## FUNDING

This work was supported by the National Natural Science Foundation of China (Grant Nos 82172464, 82172453, and 81972086); National Key Research and Development Project of China (Grant Nos 2020YFC1107500 and 2020YFC1107503); The Shanghai Rising-Star Program (21QA1405500); Shanghai "Rising Stars of Medical Talent" Youth Development Program (Youth Medical Talents - Specialist Program) (Grant No. 2019-72); "Technology Innovation Action Plan" Key Project of Shanghai Science and Technology Commission (Grant No. 19411962800); Shanghai municipal education commission—Gaofeng clinical medicine grant support (Grant No. 20161423); NSFC Advancing Targeted Projects (RJTJ-JX-005 and RJTJ22-RC-011).

## REFERENCES

Abbadessa, A., Blokzijl, M. M., Mouser, V. H. M., Marica, P., Malda, J., Hennink, W. E., et al. (2016a). A Thermo-Responsive and Photo-Polymerizable Chondroitin Sulfate-Based Hydrogel for 3D Printing Applications. *Carbohydr. Polym.* 149, 163–174. doi:10.1016/j.carbpol.2016.04.080

Abbadessa, A., Mouser, V. H. M., Blokzijl, M. M., Gawlitta, D., Dhert, W. J. A., Hennink, W. E., et al. (2016b). A Synthetic Thermosensitive Hydrogel for Cartilage Bioprinting and its Biofunctionalization with Polysaccharides. *Biomacromolecules* 17, 2137–2147. doi:10.1021/acs.biomac.6b00366

Abdollahiyan, P., Oroojalian, F., Mokhtarzadeh, A., and De La Guardia, M. (2020). Hydrogel-Based 3D Bioprinting for Bone and Cartilage Tissue Engineering. *Biotechnol. J.* 15, e2000095. doi:10.1002/biot.202000095

Abdulghani, S., and Morouco, P. G. (2019). Biofabrication for Osteochondral Tissue Regeneration: Bioink Printability Requirements. *J. Mater. Sci. Mater. Med.* 30, 20. doi:10.1007/s10856-019-6218-x

Ahlfeld, T., Cidonio, G., Kilian, D., Duin, S., Akkineni, A. R., Dawson, J. I., et al. (2017). Development of a clay Based Bioink for 3D Cell Printing for Skeletal Application. *Biofabrication* 9, 034103. doi:10.1088/1758-5090/aa7e96

Antich, C., De Vicente, J., Jiménez, G., Chocarro, C., Carrillo, E., Montañez, E., et al. (2020). Bio-inspired Hydrogel Composed of Hyaluronic Acid and Alginate as a Potential Bioink for 3D Bioprinting of Articular Cartilage Engineering Constructs. *Acta Biomater.* 106, 114–123. doi:10.1016/j.actbio.2020.01.046

Bendtsen, S. T., Quinnell, S. P., and Wei, M. (2017). Development of a Novel Alginate-polyvinyl Alcohol-hydroxyapatite Hydrogel for 3D Bioprinting Bone Tissue Engineered Scaffolds. *J. Biomed. Mater. Res.* 105, 1457–1468. doi:10.1002/jbm.a.36036

Bharadwaz, A., and Jayasuriya, A. C. (2020). Recent Trends in the Application of Widely Used Natural and Synthetic Polymer Nanocomposites in Bone Tissue Regeneration. *Mater. Sci. Eng. C* 110, 110698. doi:10.1016/j.msec.2020.110698

Bi, S., Wang, P., Hu, S., Li, S., Pang, J., Zhou, Z., et al. (2019). Construction of Physical-Crosslink Chitosan/PVA Double-Network Hydrogel with Surface Mineralization for Bone Repair. *Carbohydr. Polym.* 224, 115176. doi:10.1016/j.carbpol.2019.115176

Bouler, J. M., Pilet, P., Gauthier, O., and Verron, E. (2017). Biphasic Calcium Phosphate Ceramics for Bone Reconstruction: A Review of Biological Response. *Acta Biomater.* 53, 1–12. doi:10.1016/j.actbio.2017.01.076

Byambaa, B., Annabi, N., Yue, K., Trujillo-De Santiago, G., Alvarez, M. M., Jia, W., et al. (2017). Bioprinted Osteogenic and Vasculogenic Patterns for Engineering 3D Bone Tissue. *Adv. Healthc. Mater.* 6 (16). doi:10.1002/adhm.201700015

Canovas, F., and Dagneaux, L. (2018). Quality of Life after Total Knee Arthroplasty. *Orthop. Traumatol. Surg. Res.* 104 (1S), S41–S46. doi:10.1016/j.otsr.2017.04.017

Chang, K.-C., Chen, W.-C., Chen, C.-H., Ko, C.-L., Liu, S.-M., and Chen, J.-C. (2021). Chemical Cross-Linking on Gelatin-Hyaluronan Loaded with Hinokitiol for the Preparation of Guided Tissue Regeneration Hydrogel Membranes with Antibacterial and Biocompatible Properties. *Mater. Sci. Eng. C* 119, 111576. doi:10.1016/j.msec.2020.111576

Chen, Y.-W., Shen, Y.-F., Ho, C.-C., Yu, J., Wu, Y.-H. A., Wang, K., et al. (2018). Osteogenic and Angiogenic Potentials of the Cell-Laden Hydrogel/mussel-Inspired Calcium Silicate Complex Hierarchical Porous Scaffold Fabricated by 3D Bioprinting. *Mater. Sci. Eng. C* 91, 679–687. doi:10.1016/j.msec.2018.06.005

Chen, X., Gao, C., Jiang, J., Wu, Y., Zhu, P., and Chen, G. (2019). 3D Printed Porous PLA/nHA Composite Scaffolds with Enhanced Osteogenesis and Osteoconductivity *In Vivo* for Bone Regeneration. *Biomed. Mater.* 14, 065003. doi:10.1088/1748-605x/ab388d

Chen, T., Zou, Q., Du, C., Wang, C., Li, Y., and Fu, B. (2020). Biodegradable 3D Printed HA/CMCS/PDA Scaffold for Repairing Lacunar Bone Defect. *Mater. Sci. Eng. C* 116, 111148. doi:10.1016/j.msec.2020.111148

Chen, C. Y., Shie, M. Y., Lee, A. K., Chou, Y. T., Chiang, C., and Lin, C. P. (2021a). 3D-Printed Ginsenoside Rb1-Loaded Mesoporous Calcium Silicate/Calcium Sulfate Scaffolds for Inflammation Inhibition and Bone Regeneration. *Biomedicines* 9, 907. doi:10.3390/biomedicines9080907

Chen, Z.-Y., Gao, S., Zhang, Y.-W., Zhou, R.-B., and Zhou, F. (2021b). Antibacterial Biomaterials in Bone Tissue Engineering. *J. Mater. Chem. B* 9, 2594–2612. doi:10.1039/d0tb02983a

Cheng, Z., Landish, B., Chi, Z., Nannan, C., Jingyu, D., Sen, L., et al. (2018). 3D Printing Hydrogel with Graphene Oxide Is Functional in Cartilage protection by Influencing the Signal Pathway of Rank/Rankl/OPG. *Mater. Sci. Eng. C* 82, 244–252. doi:10.1016/j.msec.2017.08.069

Cheng, Z., Xigong, L., Weiyi, D., Jingen, H., Shuo, W., Xiangjin, L., et al. (2020). Potential Use of 3D-Printed Graphene Oxide Scaffold for Construction of the Cartilage Layer. *J. Nanobiotechnol.* 18, 97. doi:10.1186/s12951-020-00655-w

Cui, Z.-K., Kim, S., Baljon, J. J., Wu, B. M., Aghaloo, T., and Lee, M. (2019). Microporous Methacrylated Glycol Chitosan-Montmorillonite Nanocomposite Hydrogel for Bone Tissue Engineering. *Nat. Commun.* 10, 3523. doi:10.1038/s41467-019-11511-3

Cui, X., Li, J., Hartanto, Y., Durham, M., Tang, J., Zhang, H., et al. (2020). Advances in Extrusion 3D Bioprinting: A Focus on Multicomponent Hydrogel-Based Bioinks. *Adv. Healthc. Mater.* 9, e1901648. doi:10.1002/adhm.201901648

Daly, A. C., Critchley, S. E., Rencsok, E. M., and Kelly, D. J. (2016). A Comparison of Different Bioinks for 3D Bioprinting of Fibrocartilage and Hyaline Cartilage. *Biofabrication* 8, 045002. doi:10.1088/1758-5090/8/4/045002

Daly, A. C., Freeman, F. E., Gonzalez-Fernandez, T., Critchley, S. E., Nulty, J., and Kelly, D. J. (2017). 3D Bioprinting for Cartilage and Osteochondral Tissue Engineering. *Adv. Healthc. Mater.* 6. doi:10.1002/adhm.201700298

Demirtas, T. T., Irmak, G., and Gumusderelioglu, M. (2017). A Bioprintable Form of Chitosan Hydrogel for Bone Tissue Engineering. *Biofabrication* 9, 035003. doi:10.1088/1758-5090/aa7b1d

Deng, Y., Jiang, C., Li, C., Li, T., Peng, M., Wang, J., et al. (2017). 3D Printed Scaffolds of Calcium Silicate-Doped β-TCP Synergize with Co-cultured Endothelial and Stromal Cells to Promote Vascularization and Bone Formation. *Sci. Rep.* 7, 5588. doi:10.1038/s41598-017-05196-1

Dhawan, A., Kennedy, P. M., Rizk, E. B., and Ozbolat, I. T. (2019). Three-dimensional Bioprinting for Bone and Cartilage Restoration in Orthopaedic Surgery. *J. Am. Acad. Orthop. Surg.* 27, e215–e226. doi:10.5435/jaaos-d-17-00632

Dhivya, S., Saravanan, S., Sastry, T. P., and Selvamurugan, N. (2015). Nanohydroxyapatite-reinforced Chitosan Composite Hydrogel for Bone Tissue Repair *In Vitro* and *In Vivo*. *J. Nanobiotechnol.* 13, 40. doi:10.1186/s12951-015-0099-z

El-Habashy, S. E., El-Kamel, A. H., Essawy, M. M., Abdelfattah, E.-Z. A., and Eltaher, H. M. (2021). 3D Printed Bioinspired Scaffolds Integrating Doxycycline Nanoparticles: Customizable Implants for *In Vivo*

Osteoregeneration. *Int. J. Pharmaceutics* 607, 121002. doi:10.1016/j.ijpharm.2021.121002

Feng, Y., Zhu, S., Mei, D., Li, J., Zhang, J., Yang, S., et al. (2021). Application of 3D Printing Technology in Bone Tissue Engineering: A Review. *Curr. Drug Deliv.* 18, 847–861. doi:10.2174/1567201817999201113100322

Gao, F., Xu, Z., Liang, Q., Li, H., Peng, L., Wu, M., et al. (2019). Osteochondral Regeneration with 3D-Printed Biodegradable High-Strength Supramolecular Polymer Reinforced-Gelatin Hydrogel Scaffolds. *Adv. Sci.* 6, 1900867. doi:10.1002/advs.201900867

Ge, Z., Tian, X., Heng, B. C., Fan, V., Yeo, J. F., and Cao, T. (2009). Histological Evaluation of Osteogenesis of 3D-Printed Poly-Lactic-Co-Glycolic Acid (PLGA) Scaffolds in a Rabbit Model. *Biomed. Mater.* 4, 021001. doi:10.1088/1748-6041/4/2/021001

Gibbs, D. M. R., Black, C. R. M., Dawson, J. I., and Oreffo, R. O. C. (2016). A Review of Hydrogel Use in Fracture Healing and Bone Regeneration. *J. Tissue Eng. Regen. Med.* 10, 187–198. doi:10.1002/term.1968

Gómez, S., Vlad, M. D., López, J., and Fernández, E. (2016). Design and Properties of 3D Scaffolds for Bone Tissue Engineering. *Acta Biomater.* 42, 341–350. doi:10.1016/j.actbio.2016.06.032

Gu, Y., Zhang, L., Du, X., Fan, Z., Wang, L., Sun, W., et al. (2018). Reversible Physical Crosslinking Strategy with Optimal Temperature for 3D Bioprinting of Human Chondrocyte-Laden Gelatin Methacryloyl Bioink. *J. Biomater. Appl.* 33, 609–618. doi:10.1177/0885328218805864

Gungor-Ozkerim, P. S., Inci, I., Zhang, Y. S., Khademhosseini, A., and Dokmeci, M. R. (2018). Bioinks for 3D Bioprinting: an Overview. *Biomater. Sci.* 6, 915–946. doi:10.1039/c7bm00765e

Han, X., Chang, S., Zhang, M., Bian, X., Li, C., and Li, D. (2021). Advances of Hydrogel-Based Bioprinting for Cartilage Tissue Engineering. *Front. Bioeng. Biotechnol.* 9, 746564. doi:10.3389/fbioe.2021.746564

Haung, S. M., Lin, Y. T., Liu, S. M., Chen, J. C., and Chen, W. C. (2021). *In Vitro* Evaluation of a Composite Gelatin-Hyaluronic Acid-Alginate Porous Scaffold with Different Pore Distributions for Cartilage Regeneration. *Gels* 7, 165. doi:10.3390/gels7040165

Heid, S., and Boccaccini, A. R. (2020). Advancing Bioinks for 3D Bioprinting Using Reactive Fillers: A Review. *Acta Biomater.* 113, 1–22. doi:10.1016/j.actbio.2020.06.040

Hernandez, I., Kumar, A., and Joddar, B. (2017). A Bioactive Hydrogel and 3D Printed Polycaprolactone System for Bone Tissue Engineering. *Gels* 3, 26. doi:10.3390/gels3030026

Hölzl, K., Lin, S., Tytgat, L., Van Vlierberghe, S., Gu, L., and Ovsianikov, A. (2016). Bioink Properties before, during and after 3D Bioprinting. *Biofabrication* 8, 032002. doi:10.1088/1758-5090/8/3/032002

Hu, C., Wang, M. X., Sun, L., Yang, J. H., Zrínyi, M., and Chen, Y. M. (2017). Dual-Physical Cross-Linked Tough and Photoluminescent Hydrogels with Good Biocompatibility and Antibacterial Activity. *Macromol. Rapid Commun.* 38. doi:10.1002/marc.201600788

Huang, J., Xiong, J., Wang, D., Zhang, J., Yang, L., Sun, S., et al. (2021a). 3D Bioprinting of Hydrogels for Cartilage Tissue Engineering. *Gels* 7. doi:10.3390/gels7030144

Huang, K.-H., Chen, C.-Y., Chang, C.-Y., Chen, Y.-W., and Lin, C.-P. (2021b). The Synergistic Effects of Quercetin-Containing 3D-Printed Mesoporous Calcium Silicate/calcium Sulfate/poly-ε-Caprolactone Scaffolds for the Promotion of Osteogenesis in Mesenchymal Stem Cells. *J. Formos. Med. Assoc.* 120, 1627–1634. doi:10.1016/j.jfma.2021.01.024

Ji, X., Yuan, X., Ma, L., Bi, B., Zhu, H., Lei, Z., et al. (2020). Mesenchymal Stem Cell-Loaded Thermosensitive Hydroxypropyl Chitin Hydrogel Combined with a Three-Dimensional-Printed Poly(ε-Caprolactone)/nano-Hydroxyapatite Scaffold to Repair Bone Defects via Osteogenesis, Angiogenesis and Immunomodulation. *Theranostics* 10, 725–740. doi:10.7150/thno.39167

Jiang, G., Li, S., Yu, K., He, B., Hong, J., Xu, T., et al. (2021). A 3D-Printed PRP-GelMA Hydrogel Promotes Osteochondral Regeneration through M2 Macrophage Polarization in a Rabbit Model. *Acta Biomater.* 128, 150–162. doi:10.1016/j.actbio.2021.04.010

Jing, Z., Ni, R., Wang, J., Lin, X., Fan, D., Wei, Q., et al. (2021). Practical Strategy to Construct Anti-osteosarcoma Bone Substitutes by Loading Cisplatin into 3D-Printed Titanium alloy Implants Using a Thermosensitive Hydrogel. *Bioactive Mater.* 6, 4542–4557. doi:10.1016/j.bioactmat.2021.05.007

Jung, S. W., Oh, S. H., Lee, I. S., Byun, J.-H., and Lee, J. H. (2019). *In Situ* Gelling Hydrogel with Anti-Bacterial Activity and Bone Healing Property for Treatment of Osteomyelitis. *Tissue Eng. Regen. Med.* 16, 479–490. doi:10.1007/s13770-019-00206-x

Kabirian, F., and Mozafari, M. (2020). Decellularized ECM-Derived Bioinks: Prospects for the Future. *Methods* 171, 108–118. doi:10.1016/j.ymeth.2019.04.019

Kang, H.-W., Yoo, J. J., and Atala, A. (2015). Bioprinted Scaffolds for Cartilage Tissue Engineering. *Methods Mol. Biol.* 1340, 161–169. doi:10.1007/978-1-4939-2938-2_11

Koç, A., Finkenzeller, G., Elçin, A. E., Stark, G. B., and Elçin, Y. M. (2014). Evaluation of Adenoviral Vascular Endothelial Growth Factor-Activated Chitosan/hydroxyapatite Scaffold for Engineering Vascularized Bone Tissue Using Human Osteoblasts: *In Vitro* and *In Vivo* Studies. *J. Biomater. Appl.* 29, 748–760. doi:10.1177/0885328214544769

Kundu, J., Shim, J.-H., Jang, J., Kim, S.-W., and Cho, D.-W. (2015). An Additive Manufacturing-Based PCL-Alginate-Chondrocyte Bioprinted Scaffold for Cartilage Tissue Engineering. *J. Tissue Eng. Regen. Med.* 9, 1286–1297. doi:10.1002/term.1682

Kuss, M. A., Wu, S., Wang, Y., Untrauer, J. B., Li, W., Lim, J. Y., et al. (2018). Prevascularization of 3D Printed Bone Scaffolds by Bioactive Hydrogels and Cell Co-culture. *J. Biomed. Mater. Res.* 106, 1788–1798. doi:10.1002/jbm.b.33994

Kyle, S., Jessop, Z. M., Al-Sabah, A., and Whitaker, I. S. (2017). 'Printability' of Candidate Biomaterials for Extrusion Based 3D Printing: State-Of-The-Art. *Adv. Healthc. Mater.* 6. doi:10.1002/adhm.201700264

Levato, R., Webb, W. R., Otto, I. A., Mensinga, A., Zhang, Y., Van Rijen, M., et al. (2017). The Bio in the Ink: Cartilage Regeneration with Bioprintable Hydrogels and Articular Cartilage-Derived Progenitor Cells. *Acta Biomater.* 61, 41–53. doi:10.1016/j.actbio.2017.08.005

Li, P., Zhao, J., Chen, Y., Cheng, B., Yu, Z., Zhao, Y., et al. (2017). Preparation and Characterization of Chitosan Physical Hydrogels with Enhanced Mechanical and Antibacterial Properties. *Carbohydr. Polym.* 157, 1383–1392. doi:10.1016/j.carbpol.2016.11.016

Lin, Y.-H., Chiu, Y.-C., Shen, Y.-F., Wu, Y.-H. A., and Shie, M.-Y. (2017). Bioactive Calcium Silicate/poly-ε-Caprolactone Composite Scaffolds 3D Printed under Mild Conditions for Bone Tissue Engineering. *J. Mater. Sci. Mater. Med.* 29, 11. doi:10.1007/s10856-017-6020-6

Lin, Y.-H., Chuang, T.-Y., Chiang, W.-H., Chen, I.-W. P., Wang, K., Shie, M.-Y., et al. (2019). The Synergistic Effects of Graphene-Contained 3D-Printed Calcium Silicate/poly-ε-Caprolactone Scaffolds Promote FGFR-Induced Osteogenic/angiogenic Differentiation of Mesenchymal Stem Cells. *Mater. Sci. Eng. C* 104, 109887. doi:10.1016/j.msec.2019.109887

Liu, B., Li, J., Lei, X., Cheng, P., Song, Y., Gao, Y., et al. (2020). 3D-bioprinted Functional and Biomimetic Hydrogel Scaffolds Incorporated with Nanosilicates to Promote Bone Healing in Rat Calvarial Defect Model. *Mater. Sci. Eng. C* 112, 110905. doi:10.1016/j.msec.2020.110905

Lu, H., Liu, Y., Guo, J., Wu, H., Wang, J., and Wu, G. (2016). Biomaterials with Antibacterial and Osteoinductive Properties to Repair Infected Bone Defects. *Int. J. Mol. Sci.* 17, 334. doi:10.3390/ijms17030334

Ma, H., Feng, C., Chang, J., and Wu, C. (2018). 3D-printed Bioceramic Scaffolds: From Bone Tissue Engineering to Tumor Therapy. *Acta Biomater.* 79, 37–59. doi:10.1016/j.actbio.2018.08.026

Maisani, M., Ziane, S., Ehret, C., Levesque, L., Siadous, R., Le Meins, J. F., et al. (2018). A New Composite Hydrogel Combining the Biological Properties of Collagen with the Mechanical Properties of a Supramolecular Scaffold for Bone Tissue Engineering. *J. Tissue Eng. Regen. Med.* 12, e1489–e1500. doi:10.1002/term.2569

Mei, Q., Rao, J., Bei, H. P., Liu, Y., and Zhao, X. (2021). 3D Bioprinting Photo-Crosslinkable Hydrogels for Bone and Cartilage Repair. *Int. J. Bioprint* 7, 367. doi:10.18063/ijb.v7i3.367

Mora-Boza, A., and Lopez-Donaire, M. L. (2018). Preparation of Polymeric and Composite Scaffolds by 3D Bioprinting. *Adv. Exp. Med. Biol.* 1058, 221–245. doi:10.1007/978-3-319-76711-6_10

Mouser, V. H. M., Abbadessa, A., Levato, R., Hennink, W. E., Vermonden, T., Gawlitta, D., et al. (2017). Development of a Thermosensitive HAMA-Containing Bio-Ink for the Fabrication of Composite Cartilage Repair Constructs. *Biofabrication* 9, 015026. doi:10.1088/1758-5090/aa6265

Naranda, J., Bračič, M., Vogrin, M., and Maver, U. (2021). Recent Advancements in 3D Printing of Polysaccharide Hydrogels in Cartilage Tissue Engineering. *Materials (Basel)* 14. doi:10.3390/ma14143977

Nikolova, M. P., and Chavali, M. S. (2019). Recent Advances in Biomaterials for 3D Scaffolds: A Review. *Bioactive Mater.* 4, 271–292. doi:10.1016/j.bioactmat.2019.10.005

Noori, A., Ashrafi, S. J., Vaez-Ghaemi, R., Hatamian-Zaremi, A., and Webster, T. J. (2017). A Review of Fibrin and Fibrin Composites for Bone Tissue Engineering. *Int. J. Nanomedicine* 12, 4937–4961. doi:10.2147/ijn.s124671

Olate-Moya, F., Arens, L., Wilhelm, M., Mateos-Timoneda, M. A., Engel, E., and Palza, H. (2020). Chondroinductive Alginate-Based Hydrogels Having Graphene Oxide for 3D Printed Scaffold Fabrication. *ACS Appl. Mater. Inter.* 12, 4343–4357. doi:10.1021/acsami.9b22062

Ouyang, L., Yao, R., Zhao, Y., and Sun, W. (2016). Effect of Bioink Properties on Printability and Cell Viability for 3D Bioplotting of Embryonic Stem Cells. *Biofabrication* 8, 035020. doi:10.1088/1758-5090/8/3/035020

Pathmanapan, S., Periyathambi, P., and Anandasadagopan, S. K. (2020). Fibrin Hydrogel Incorporated with Graphene Oxide Functionalized Nanocomposite Scaffolds for Bone Repair - *In Vitro* and *In Vivo* Study. *Nanomedicine Nanotechn. Biol. Med.* 29, 102251. doi:10.1016/j.nano.2020.102251

Perera, K., Ivone, R., Natekin, E., Wilga, C. A., Shen, J., and Menon, J. U. (2021). 3D Bioprinted Implants for Cartilage Repair in Intervertebral Discs and Knee Menisci. *Front. Bioeng. Biotechnol.* 9, 754113. doi:10.3389/fbioe.2021.754113

Qi, C., Deng, Y., Xu, L., Yang, C., Zhu, Y., Wang, G., et al. (2020). A Sericin/Graphene Oxide Composite Scaffold as a Biomimetic Extracellular Matrix for Structural and Functional Repair of Calvarial Bone. *Theranostics* 10, 741–756. doi:10.7150/thno.39502

Qiu, P., Li, M., Chen, K., Fang, B., Chen, P., Tang, Z., et al. (2020). Periosteal Matrix-Derived Hydrogel Promotes Bone Repair through an Early Immune Regulation Coupled with Enhanced Angio- and Osteogenesis. *Biomaterials* 227, 119552. doi:10.1016/j.biomaterials.2019.119552

Radhakrishnan, J., Subramanian, A., Krishnan, U. M., and Sethuraman, S. (2017). Injectable and 3D Bioprinted Polysaccharide Hydrogels: From Cartilage to Osteochondral Tissue Engineering. *Biomacromolecules* 18, 1–26. doi:10.1021/acs.biomac.6b01619

Ribeiro, M., Ferraz, M. P., Monteiro, F. J., Fernandes, M. H., Beppu, M. M., Mantione, D., et al. (2017). Antibacterial Silk Fibroin/nanohydroxyapatite Hydrogels with Silver and Gold Nanoparticles for Bone Regeneration. *Nanomedicine Nanotechn. Biol. Med.* 13, 231–239. doi:10.1016/j.nano.2016.08.026

Sahai, N., Gogoi, M., and Tewari, R. P. (2021). 3D Printed Chitosan Composite Scaffold for Chondrocytes Differentiation. *Curr. Med. Imaging* 17, 832–842. doi:10.2174/1573405616666201217112939

Son, S.-R., Sarkar, S. K., Linh, N.-T. B., Padalhin, A. R., Kim, B. R., Jung, H. I., et al. (2015). Platelet-rich Plasma Encapsulation in Hyaluronic Acid/gelatin-BCP Hydrogel for Growth Factor Delivery in BCP Sponge Scaffold for Bone Regeneration. *J. Biomater. Appl.* 29, 988–1002. doi:10.1177/0885328214551373

Stanco, D., Urban, P., Tirendi, S., Ciardelli, G., and Barrero, J. (2020). 3D Bioprinting for Orthopaedic Applications: Current Advances, Challenges and Regulatory Considerations. *Bioprinting* 20, e00103. doi:10.1016/j.bprint.2020.e00103

Suzuki, A., and Sasaki, S. (2015). Swelling and Mechanical Properties of Physically Crosslinked Poly(vinyl Alcohol) Hydrogels. *Proc. Inst. Mech. Eng. H* 229, 828–844. doi:10.1177/0954411915615469

Tommasi, G., Perni, S., and Prokopovich, P. (2016). An Injectable Hydrogel as Bone Graft Material with Added Antimicrobial Properties. *Tissue Eng. A* 22, 862–872. doi:10.1089/ten.tea.2016.0014

Turnbull, G., Clarke, J., Picard, F., Riches, P., Jia, L., Han, F., et al. (2018). 3D Bioactive Composite Scaffolds for Bone Tissue Engineering. *Bioactive Mater.* 3, 278–314. doi:10.1016/j.bioactmat.2017.10.001

Unagolla, J. M., and Jayasuriya, A. C. (2020). Hydrogel-based 3D Bioprinting: A Comprehensive Review on Cell-Laden Hydrogels, Bioink Formulations, and Future Perspectives. *Appl. Mater. Today* 18. doi:10.1016/j.apmt.2019.100479

Vega, S., Kwon, M. Y., Kwon, M., and Burdick, J. (2017). Recent Advances in Hydrogels for Cartilage Tissue Engineering. *eCM* 33, 59–75. doi:10.22203/ecm.v033a05

Wahid, F., Yin, J.-J., Xue, D.-D., Xue, H., Lu, Y.-S., Zhong, C., et al. (2016). Synthesis and Characterization of Antibacterial Carboxymethyl Chitosan/ZnO Nanocomposite Hydrogels. *Int. J. Biol. Macromol.* 88, 273–279. doi:10.1016/j.ijbiomac.2016.03.044

Wang, W., Junior, J. R. P., Nalesso, P. R. L., Musson, D., Cornish, J., Mendonça, F., et al. (2019). Engineered 3D Printed Poly(ε-Caprolactone)/graphene Scaffolds for Bone Tissue Engineering. *Mater. Sci. Eng. C* 100, 759–770. doi:10.1016/j.msec.2019.03.047

Wu, T., Huang, J., Jiang, Y., Hu, Y., Ye, X., Liu, D., et al. (2018). Formation of Hydrogels Based on Chitosan/alginate for the Delivery of Lysozyme and Their Antibacterial Activity. *Food Chem.* 240, 361–369. doi:10.1016/j.foodchem.2017.07.052

Xu, H., Zhang, G., Xu, K., Wang, L., Yu, L., Xing, M. M. Q., et al. (2018). Mussel-inspired Dual-Functional PEG Hydrogel Inducing Mineralization and Inhibiting Infection in Maxillary Bone Reconstruction. *Mater. Sci. Eng. C* 90, 379–386. doi:10.1016/j.msec.2018.04.066

Yadav, L. R., Chandran, S. V., Lavanya, K., and Selvamurugan, N. (2021). Chitosan-based 3D-Printed Scaffolds for Bone Tissue Engineering. *Int. J. Biol. Macromol.* 183, 1925–1938. doi:10.1016/j.ijbiomac.2021.05.215

Yang, Y., Yang, S., Wang, Y., Yu, Z., Ao, H., Zhang, H., et al. (2016). Anti-infective Efficacy, Cytocompatibility and Biocompatibility of a 3D-Printed Osteoconductive Composite Scaffold Functionalized with Quaternized Chitosan. *Acta Biomater.* 46, 112–128. doi:10.1016/j.actbio.2016.09.035

Yang, J., Zhang, Y. S., Yue, K., and Khademhosseini, A. (2017). Cell-laden Hydrogels for Osteochondral and Cartilage Tissue Engineering. *Acta Biomater.* 57, 1–25. doi:10.1016/j.actbio.2017.01.036

Yang, W., Fortunati, E., Bertoglio, F., Owczarek, J. S., Bruni, G., Kozanecki, M., et al. (2018). Polyvinyl Alcohol/chitosan Hydrogels with Enhanced Antioxidant and Antibacterial Properties Induced by Lignin Nanoparticles. *Carbohydr. Polym.* 181, 275–284. doi:10.1016/j.carbpol.2017.10.084

Yang, X., Wang, Y., Zhou, Y., Chen, J., and Wan, Q. (2021). The Application of Polycaprolactone in Three-Dimensional Printing Scaffolds for Bone Tissue Engineering. *Polymers (Basel)* 13, 2754. doi:10.3390/polym13162754

Yao, M., Zou, Q., Zou, W., Xie, Z., Li, Z., Zhao, X., et al. (2021). Bifunctional Scaffolds of Hydroxyapatite/poly(dopamine)/carboxymethyl Chitosan with Osteogenesis and Anti-osteosarcoma Effect. *Biomater. Sci.* 9, 3319–3333. doi:10.1039/d0bm01785j

You, F., Eames, B. F., and Chen, X. (2017). Application of Extrusion-Based Hydrogel Bioprinting for Cartilage Tissue Engineering. *Int. J. Mol. Sci.* 18, 1597. doi:10.3390/ijms18071597

You, F., Chen, X., Cooper, D. M. L., Chang, T., and Eames, B. F. (2018). Homogeneous Hydroxyapatite/alginate Composite Hydrogel Promotes Calcified Cartilage Matrix Deposition with Potential for Three-Dimensional Bioprinting. *Biofabrication* 11, 015015. doi:10.1088/1758-5090/aaf44a

Yu, Y., Wang, Y., Zhang, W., Wang, H., Li, J., Pan, L., et al. (2020). Biomimetic Periosteum-Bone Substitute Composed of Preosteoblast-Derived Matrix and Hydrogel for Large Segmental Bone Defect Repair. *Acta Biomater.* 113, 317–327. doi:10.1016/j.actbio.2020.06.030

Yue, S., He, H., Li, B., and Hou, T. (2020). Hydrogel as a Biomaterial for Bone Tissue Engineering: A Review. *Nanomaterials (Basel)* 10, 1511. doi:10.3390/nano10081511

Zamborsky, R., Kilian, M., Jacko, P., Bernadic, M., and Hudak, R. (2019). Perspectives of 3D Printing Technology in Orthopaedic Surgery. *BLL* 120, 498–504. doi:10.4149/bll_2019_079

Zhai, X., Ma, Y., Hou, C., Gao, F., Zhang, Y., Ruan, C., et al. (2017). 3D-Printed High Strength Bioactive Supramolecular Polymer/Clay Nanocomposite Hydrogel Scaffold for Bone Regeneration. *ACS Biomater. Sci. Eng.* 3, 1109–1118. doi:10.1021/acsbiomaterials.7b00224

Zhang, L., Yang, G., Johnson, B. N., and Jia, X. (2019). Three-dimensional (3D) Printed Scaffold and Material Selection for Bone Repair. *Acta Biomater.* 84, 16–33. doi:10.1016/j.actbio.2018.11.039

Zhang, W., Sun, C., Zhu, J., Zhang, W., Leng, H., and Song, C. (2020). 3D Printed Porous Titanium Cages Filled with Simvastatin Hydrogel Promotes Bone Ingrowth and Spinal Fusion in Rhesus Macaques. *Biomater. Sci.* 8, 4147–4156. doi:10.1039/d0bm00361a

Zhang, X., Tan, B., Wu, Y., Zhang, M., and Liao, J. (2021). A Review on Hydrogels with Photothermal Effect in Wound Healing and Bone Tissue Engineering. *Polymers (Basel)* 13, 2100. doi:10.3390/polym13132100

Zhao, X., Chen, X., Yuk, H., Lin, S., Liu, X., and Parada, G. (2021). Soft Materials by Design: Unconventional Polymer Networks Give Extreme Properties. *Chem. Rev.* 121 (8), 4309–4372. doi:10.1021/acs.chemrev.0c01088

Zou, F., Jiang, J., Lv, F., Xia, X., and Ma, X. (2020). Preparation of Antibacterial and Osteoconductive 3D-Printed PLGA/Cu(I)@ZIF-8 Nanocomposite Scaffolds for Infected Bone Repair. *J. Nanobiotechnol.* 18, 39. doi:10.1186/s12951-020-00594-6

**Conflict of Interest:** The authors declare that the research was conducted in the absence of any commercial or financial relationships that could be construed as a potential conflict of interest.

The reviewer WC declared a shared affiliation, with no collaboration, with several of the authors ZL, JX, XQ, and BY to the handling editor at the time of the review.

**Publisher's Note:** All claims expressed in this article are solely those of the authors and do not necessarily represent those of their affiliated organizations, or those of the publisher, the editors, and the reviewers. Any product that may be evaluated in this article, or claim that may be made by its manufacturer, is not guaranteed or endorsed by the publisher.

frontiers | Frontiers in Bioengineering and Biotechnology

REVIEW
published: 25 April 2022
doi: 10.3389/fbioe.2022.865250

# Recent Advances in Multifunctional Hydrogels for the Treatment of Osteomyelitis

*Weiwei Xin, Yingjian Gao and Bing Yue**

*Department of Orthopedics, Renji Hospital, School of Medicine, Shanghai Jiao Tong University, Shanghai, China*

Osteomyelitis (OM), a devastating disease caused by microbial infection of bones, remains a major challenge for orthopedic surgeons. Conventional approaches for prevention and treatment of OM are unsatisfactory. Various alternative strategies have been proposed, among which, hydrogel-based strategies have demonstrated potential due to their unique properties, including loadable, implantable, injectable, printable, degradable, and responsive to stimuli. Several protocols, including different hydrogel designs, selection of antimicrobial agent, co-administration of bone morphogenetic protein 2 (BMP 2), and nanoparticles, have been shown to improve the biological properties, including antimicrobial effects, osteo-induction, and controlled drug delivery. In this review, we describe the current and future directions for designing hydrogels and their applications to improve the biological response to OM *in vivo*.

**Keywords: hydrogel, osteomyelitis, infection, drug-loaded materials, *in vivo***

OPEN ACCESS

***Edited by:***
*Di Huang,*
*Taiyuan University of Technology, China*

***Reviewed by:***
*Jochen Salber,*
*Ruhr-University Bochum, Germany*
*Congqin Ning,*
*Shanghai Normal University, China*

****Correspondence:***
*Bing Yue*
*advbmp2@163.com*

***Specialty section:***
*This article was submitted to Biomaterials, a section of the journal Frontiers in Bioengineering and Biotechnology*

***Received:*** *29 January 2022*
***Accepted:*** *04 April 2022*
***Published:*** *25 April 2022*

***Citation:***
*Xin W, Gao Y and Yue B (2022) Recent Advances in Multifunctional Hydrogels for the Treatment of Osteomyelitis. Front. Bioeng. Biotechnol. 10:865250. doi: 10.3389/fbioe.2022.865250*

## 1 INTRODUCTION

### 1.1 Osteomyelitis

Osteomyelitis (OM) is a catastrophic disease caused by a pathogen infection. The incidence of OM varies from 0.1 to 30% in different subspecialties, costing the health care system between $15,000–$17,000 per patient (Schwarz et al., 2019). Staphylococcal infections account for 75% of cases (Arciola et al., 2005; Walter et al., 2012). The most common pathogen is *Staphylococcus aureus* (*S. aureus*) (Darouiche, 2004; Arciola et al., 2005; Pulido et al., 2008), and over 50% of the infections are caused by methicillin-resistant *Staphylococcus aureus* (MRSA) (Kaplan, 2014). The invasive capability of *S. aureus* is attributed to its virulence factors and resistance mechanisms, including toxin secretion (Otto, 2014), adherence (Otto, 2008), the slow-growing small colony variant (SCV) subpopulation (Sendi et al., 2006; Tuchscherr et al., 2010), intracellular persistence in bone cells (Masters et al., 2019), the development of antimicrobial resistance (Kaplan, 2014), and biofilm formation (de Mesy Bentley et al., 2017; de Mesy Bentley et al., 2018; Ricciardi et al., 2018; Masters et al., 2019). These mechanisms enable bacteria to endure in hostile environments (Mah and O'Toole, 2001; Savage et al., 2013; de Mesy Bentley et al., 2017; de Mesy Bentley et al., 2018) and cause damage to the surrounding host tissue *via* various mechanism (Redlich and Smolen, 2012; Junka et al., 2017; Putnam et al., 2019).

Currently, no ideal classification and treatment strategies for OM are available. Due to the refractory nature of OM, its costly and long-term treatment, and high rate of disability, improved treatment strategies are urgently needed. Although some therapeutic strategies have been investigated, such as vaccines and monoclonal antibodies (mAbs) (Fowler and Proctor, 2014; Rouha et al., 2015; Thammavongsa et al., 2015; Varshney et al., 2018), the identification of bacterial

species and sensitive antibiotics, removal of the implants, extensive debridement, and systemic antibiotic administration for 4–6 weeks remain the standard treatment strategies for OM. Irrigation with antiseptic and implantation of antibiotic-laden spacers in the dead space are adjuncts to this standard procedure (Peng et al., 2010).

Under all treatment scenarios, the key to success is the thorough debridement of infected and necrotic tissue, and eliminating patient risk factors (such as smoking, diabetes mellitus, and immunosuppressants). Unfortunately, it is not possible to completely debride the infectious tissues (Varshney et al., 2018). Clinically, bone debridement is performed by visually distinguishing necrotic "white" bone from healthy "red" bone. In this way, bacteria colonized in biofilms, especially in the osteocyte-lacuno canalicular network (OLCN) (de Mesy Bentley et al., 2017; de Mesy Bentley et al., 2018), remain in the "red" bone, thereby causing a recurrence of infection following multiple extensive debridement. The rate of failure for the staged revision approach against MRSA orthopedic device-related infections (ODRI) ranges between 11% and 52% (Parry and Duncan, 2014), which indicates the necessity for research on novel treatment strategies (Varshney et al., 2018).

Moreover, the effectiveness of the current treatments against *S. aureus* colonized in the bone matrix are currently unknown, although long-term use of systemic antibiotics is the current standard of care. Impaired local blood supply and multiple bacterial resistance mechanisms result in insufficient local concentrations of antibiotics following systemic administration. Meanwhile, a high dose of systemic antibiotic administration over an extended period is not recommended due to the potential systemic toxicity, including ototoxicity and nephrotoxicit (Naughton, 2008; Elyasi et al., 2012; Kubin et al., 2012).

To address these issues, topical antibiotic delivery, which can offer higher concentrations at the target site with fewer side effects compared to systemic administration (Hake et al., 2015), is a promising approach to manage the dead space due to the local drug infusion and its barrier effect on preventing biofilm formation (Pan et al., 2018).

## 1.2 Polymethylmethacrylate Antibiotic-Laden Bone Cement

As an antibiotic carrier, polymethylmethacrylate (PMMA) bone cement has been used to treat OM and ODRI. Implanted in the dead space, antibiotic-laden bone cement (ALBC) delivers a high concentration of antibiotics locally to the infection site without off-target systemic toxicity. However, as a local antibiotic vehicle, PMMA also has several drawbacks.

One limitation of PMMA is its poor drug-release kinetics. The molecular structure of PMMA and its tight packing influence the diffusion of drugs, and hence the release rate of the laden antibiotics. A large amount remains encapsulated within the polymer and is not released (Frutos Cabanillas et al., 2000; Kuehn et al., 2005). *In vitro* and *in vivo* findings have demonstrated that only 5%–18% of the incorporated drug is eluted from PMMA (Masters et al., 2019). Furthermore, the antibiotic release from PMMA presents a burst pattern within the first 24 h followed by a rapid decrease in release that lowers drug concentrations to below the minimum inhibitory concentration (MIC) (Guelcher et al., 2011). Clinically, cement spacers remain *in situ* for up to 6 weeks. The sustained elution of antibiotics at such low concentrations can induce the formation of antibiotic resistance and small colony variants (SCVs) (Sendi et al., 2006; Masters et al., 2019). Additionally, the non-eluting surface of spacers and beads provides a site for pathogen colonization and biofilm formation (Barth et al., 2011; Ma et al., 2018). Weber and Lautenbach (1986) showed that gentamicin ALBC increased the percentage of drug-resistant bacteria from 29% preoperatively to 41% postoperatively. Furthermore, the exothermic reaction inactivates heat-sensitive antibiotics during polymerization of bone cement (Boot et al., 2021). The limited antibiotics that can be loaded in PMMA are not fully effective against the microorganisms. Moreover, unreacted methacrylate monomers can induce toxicity issues (Yoshii, 1997). Finally, beads and spacers require additional surgeries for removal.

These drawbacks of PMMA bone cements have prompted the development of novel vehicles for topical drug delivery and dead space management, with the following criteria: 1) biocompatibility, 2) biodegradability, 3) suitable drug elution kinetics (i.e., burst release followed by sustained release at concentrations higher than the MIC), and 4) osteo-conductivity (Sarigol-Calamak and Hascicek, 2018). Various materials have potential for delivering antibiotics directly to complex microenvironments at desired concentrations, including calcium sulfates or phosphates, demineralized bone matrix, natural polymers, and synthetic polymers (Bibbo and Patel, 2006; Rupprecht et al., 2007; Borkhuu et al., 2008; Ferguson et al., 2014; Romano et al., 2014; Cho et al., 2018; Masters et al., 2019; Li et al., 2020b; Boot et al., 2020; Boot et al., 2021; Eltawila et al., 2021; Sun et al., 2021). Furthermore, studies have also investigated the delivery of alternative antimicrobial agents, combinations of antimicrobial agents, and osteoinductive adjuvants that are not effectively carried or eluted by PMMA (Inzana et al., 2016). Hydrogel-based release system have demonstrated potential due to their unique properties, such as high water absorption capacity, high porosity, almost free diffusible interconnectivity, and stimulus-responsive. Different agents or techniques have been evaluated in the complex microenvironment of OM. However, the *in vivo* data on hydrogels for the treatment of OM are limited. In this review, we describe the current and future directions for the design of hydrogels and their applications *in vivo* to improve the treatment of OM (**Figure 1**).

# 2 HYDROGELS

Hydrogels are water-swollen polymer networks. For drug delivery, hydrogels combine the advantages of minimally invasive application, *in situ* polymerization, inherently adhesiveness, and sustained drug release (De Witte et al., 2018). Moreover, the protease-degradable nature of hydrogels, suitable for bone biological engineering, such as collagen,

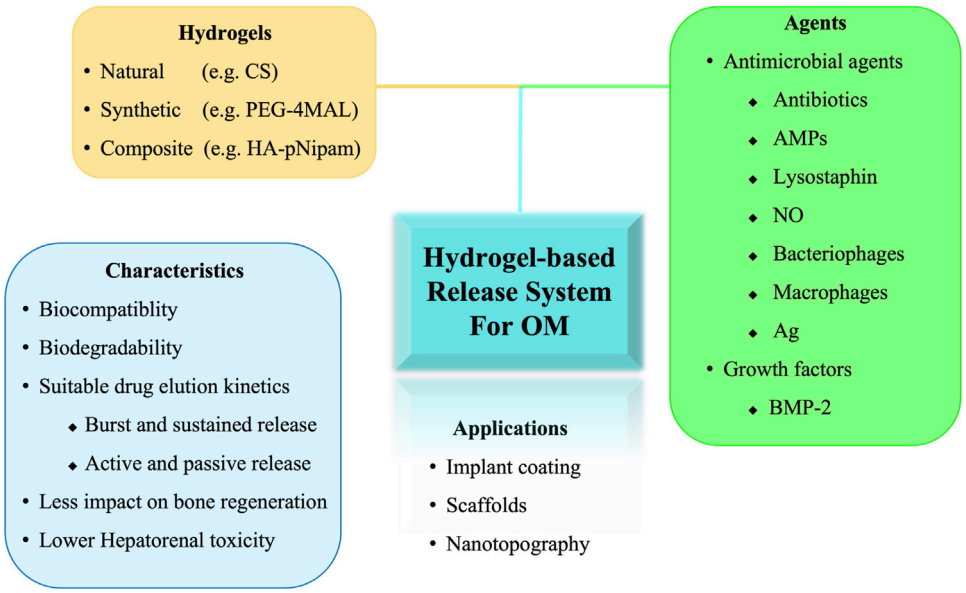


**FIGURE 1 |** Schematic illustration of hydrogel-based release system for the treatment of osteomyelitis. OM, osteomyelitis; CS, Chitosan; PEG-4MAL, four-arm poly (ethylene glycol)-maleimide; HA-pNipam, Hyaluronic acid -poly (N-isopropylacrylamide); AMPs, Antimicrobial peptides; Ag, Silver; BMP, bone morphogenetic protein.

hyaluronic acid (HyA), also allows the host to degrade and replace them with repair tissue. Additional surgeries are not required to remove hydrogels, as is the case for non-degradable scaffolds (Johnson et al., 2018). These properties confer the significant therapeutic versatility of hydrogels for topical drugs delivery in heterogeneous and anatomically complex conditions, such as OM (Slaughter et al., 2009). Natural polymers, synthetic polymers, and the composite biomaterials have been used as drug vehicles in *in vivo* studies on OM (**Supplementary Table S1**).

## 2.1 Natural Polymers

Natural polymer-based hydrogels, such as collagen, HyA, and chitosan (CS), are both biocompatible and biodegradable, making them suitable for drug delivery (Liu et al., 2020).

### 2.1.1 Collagen

Collagen is the most widely used natural polymer in orthopedic applications, among which Type I collagen is the most abundant structural protein in the body. As an important extracellular matrix protein of bone, Type I collagen can induce tissue regeneration. The early deposition of collagen matrix is essential for bone repair and remodeling, which forms a guiding structure for regeneration process. The interaction of collagen matrix with heterodimeric integrin receptors activates intracellular signal transduction pathways to induce various cellular proliferation, differentiation, and other functions. Thus, osteoblastic phenotypes are affected by collagen; cells migrate to collagen, where they organize and remodel the cytoskeleton (Rupprecht et al., 2007). For most local drug delivery systems using collagen, the collagen products are impregnated with an antibiotic solution, and the drugs are absorbed by the hydrophilic matrix (Inzana et al., 2016).

In a rabbit mandibular OM model with spontaneous oral bacterial contamination induced by arsenic trioxide, a single intra-lesion injection of gentamicin-collagen (GNT-COLL) hydrogels was more efficient at suppressing of OM than multidose systemic gentamicin. The OM was successfully halted, without recurrence for up to 12 weeks, where a significant increase in ridge length preservation percentage (RLP%) in the GNT-COLL hydrogel group was observed. These results showed up clinically as a slight displacement of the adjacent incisors. This regeneration phenomenon was enhanced by the mixture of hydroxyapatite nanoparticles (NPs) in the hydrogel (Eltawila et al., 2021).

### 2.1.2 Hyaluronic Acid

Hyaluronic acid (HyA), also known as hyaluronan, is a natural polysaccharide found in the body with excellent biocompatibility, biodegradability, and gelling features due to its ability to rapidly bind to water. Some aqueous formulations based on HyA or its derivatives can be injected and subsequently gelate *in situ*, according to their molecular weight and local microenviroment. HyA can cross-link or conjugate with various biomacromolecules and efficiently load various drugs, even nanoparticles. As such, it is widely used in biomedical applications, and has high potential as a controlled drug-delivery material (Kartika et al., 2021; Zhang et al., 2022). The cytocompatibility of HyA has been confirmed in an *in vitro* study using human dermal fibroblasts. After autoclaving, the chemical derivatization of HyA with poly lactic acid retains its chemical structure of the starting copolymers, rheological characteristics, and drug-release properties (Pitarresi et al., 2013). The

rheological features ensure that hydrogel is mostly retained on the roughness titanium prosthesis surface, despite the intense shear stress experienced during insertion (Pitarresi et al., 2013; Drago et al., 2014). These illustrate its potential use in orthopedics, especially for the antimicrobial coatings of orthopedic devices for the prevention and/or treatment of OM (Boot et al., 2017; Boot et al., 2020).

Disposable Antibacterial Coating (DAC®) (Novagenit Srl, Mezzolombardo, Italy) hydrogel consists of hyaluronan and poly D, L-lactide via covalent linkage. It is used as a disposable, rapidly bioresorbable antimicrobial coating for orthopedic implants. In 2014, a study addressed the following concerns regarding this HyA hydrogel: 1) Can it be used for the controlled release of antimicrobial agents *in vitro*? 2) Can this hydrogel (alone or antimicrobial-laden) coating reduce pathogen colonization on implants? And 3) what is the feasibility of intraoperative manufacture of coating and its resistance to the intense stress generated during the insertion? (Drago et al., 2014). The authors showed that all tested antibacterial compounds (gentamicin, vancomycin, amikacin, tobramycin, N-acetylcysteine, and sodium salicylate) were completely released in less than 96 h. The drug-laden DAC® hydrogel presented bactericidal and antibiofilm effects *in vitro* [against MRSA, methicillin resistant *Staphylococcus epidermidis* (MRSE), *E. coli*, *Pseudomonas aeruginosa*, *Acinetobacter baumannii,* and vancomycin-resistant *Enterococcus faecalis*]. Intraoperative preparation of hydrogel prosthesis coating is feasible. Almost 80% of the hydrogels are retained on the surface of the implants, after the press-fit insertion of the coated implants in rabbit tibias or human femurs (Drago et al., 2014). *In vivo*, loaded or unloaded with 2% (w/v) vancomycin, the hydrogel coating on titanium rods implanted into rabbit tibias had no effect on the volume or timing of bone apposition. In addition, no inflammation was observed (Boot et al., 2017). Meanwhile, Vancomycin-laden DAC® reduced the local bacterial burden (MRAS or MRSE) with more bone implant contact (Lovati et al., 2016; Boot et al., 2020). Recently, a multi-center matched case–control study revealed no infection or adverse events (0/43) in a mega-prosthesis treatment group with antimicrobial-laden DAC® hydrogel coating, compared with the infection rate of 14% (6/43) in a control group without coating, at a mean follow-up of 2 years (Zoccali et al., 2021). Those findings suggest that this treatment strategy could be used safely to prevent early surgical site infections of arthroplasty.

HyA-poly (*N*-isopropylacrylamide) (HA-pNipam) hydrogel is another common delivery system used in OM research. Gentamicin and vancomycin can be loaded into this thermo-responsive HyA-based hydrogel, and are subsequently released in an initial burst followed by a more sustained release pattern. The drugs could be detected for more than 14 days *in vitro* and 10 days *in vivo* (Boot et al., 2021; Foster et al., 2021). This sustained antibiotic-release system markedly increases treatment efficacy (Ter Boo et al., 2016; Ter Boo et al., 2018; Vallejo Diaz et al., 2020; Boot et al., 2021; Foster et al., 2021) without hepatorenal toxicity (Foster et al., 2021).

### 2.1.3 Chitosan

Chitosan (CS), another polysaccharide biopolymer produced by chitin deacetylation, mainly exists in the shells of crustaceans, insects, and fungal cell walls (Bakshi et al., 2020). Multiple special properties of CS have been reported, including biocompatibility, biodegradability, bioadhesion, low toxicity and immunogenicity, plasticity, modifiability, and printability (Tao F. et al., 2020; Tao et al., 2021). The polycationic nature allows CS to interact with the polyanionic molecules on the bacterial surface to alter bacterial permeability (Raafat et al., 2008). In addition, active amino groups in CS can disrupt RNA and protein synthesis by interfering with DNA (Tao et al., 2021). These molecular structure-related peculiarities attribute to the broad spectrum antibacterial properties of CS (Tan et al., 2013).

Due to the special biological and physicochemical characteristics of CS, CS-based biomaterials are used to simulate the natural extracellular matrix (ECM) and as a drug vehicle. CS has attracted considerable attention in bone tissue engineering, owing to its innate antimicrobial, osteo-inductive, and mechanical properties. CS-based topical drug delivery systems can promote bone regeneration and treat bone diseases, with CS showing promising efficacy in OM treatment (Kazimierczak et al., 2019; Kimna et al., 2019; Tao J. et al., 2020). In addition to antibiotics (Li et al., 2020a; Tao J. et al., 2020), silver can also be released in a sustained manner from CS hydrogel *in vivo* (Croes et al., 2018).

Other natural polymers such as gelatin and alginate (ALG), which have also been studied *in vivo* as vehicles for local drug delivery for the treatment of OM (Wu et al., 2013; Aldrich et al., 2019; Cobb et al., 2019; Sun et al., 2021) (**Supplementary Table S1**), have been illuminated previously (You et al., 2017; Pedroza-Gonzalez et al., 2021). Although the cell behavior and tissue formation can be significantly affected by changing the properties (such as viscosity and stiffness) of the natural polymers (Daly et al., 2016), the local antibiotic release (including release amount and rate) of these polymers remains unsatisfactory (Wang and Tang, 2019). Some techniques have been designed to control release kinetics, degradation rates, predictability of behavior and quality, and mechanical properties. Synthetic polymers are one such approach.

## 2.2 Synthetic Polymers

PEG-based hydrogels are common synthetic local delivery systems for OM used in *in vivo* studies. Mixing of hydrogels with crosslinked starch (CSt) can inhibit PEG-based hydrogel swelling, thereby reducing the rate of drug release. Covered by a PEG-poly (lactic-co-caprolactone) (PEG-PLCL) membrane, this PEG-based hydrogel coating system allows a sustained vancomycin release, without initial burst release, for approximately 3 weeks *in vitro* and over 4 weeks *in vivo*, and demonstrates a promising antimicrobial activity against *S. aureus*. Additionally, drug loading and the coating thickness regulate the release profile of the hydrogel coating (Li et al., 2017).

Another PEG-based synthetic polymer, four-arm PEG macromers (PEG-4MAL), functionalized with terminal maleimide groups that react specifically with thiols, are functionalized with cell adhesive peptides and cross-linked into a network using thiolated molecules such as protease-degradable peptides with terminal cysteines. The physically encapsulated drugs are released as the hydrogel is degraded, or

*via* direct diffusion. This implies that the release of its payload can be tuned with respect to the local microenvironment. Hydrogel-mediated lysostaphin and bacteriophage delivery systems have been shown to eliminate MRSA and *P. aeruginosa* infection in mice models of OM (Johnson et al., 2018; Johnson et al., 2019; Wroe et al., 2020), and release bone morphogenetic protein 2 (BMP-2) in a sustained pattern as well (Johnson et al., 2019). BMP-2-laden PEG-4MAL demonstrated higher osteo-regeneration ability compared to BMP-2-soaked collagen sponges (Shekaran et al., 2014). Moreover, the degradation products of PEG-4MAL hydrogel are excreted via the urine with low toxicity (Johnson et al., 2018).

# 3 AGENTS

## 3.1 Antimicrobial Agents

Antimicrobial agents are essential for the treatment of OM. Different agents based on hydrogel drug delivery systems have been investigated *in vivo* (**Supplementary Table S1**).

### 3.1.1 Antibiotics

Unlike ALBC, using hydrogels as drug carriers greatly expands the selection of antibiotics. Although these drugs can decrease the lower critical solution temperature (LCST) of thermo-responsive hydrogels, such as the HA-pNipam hydrogel, known as the Hoffmeister effect (Ter Boo et al., 2016), the drug-loaded hydrogel remains injectable and gellable, and its payload delivery and applicability are not impacted. Therefore, it is possible to load a wide spectrum of antimicrobial agents into hydrogels (Boot et al., 2021). However, in *in vivo* studies on OM, the most common antibiotics loaded in the hydrogels are gentamicin and vancomycin.

Depending on the different vehicle system designs, gentamicin and vancomycin, the most effective antibiotics against OM, can be released in different patterns (burst, sustained, and burst and sustained). For example, the direct release of vancomycin can be disrupted because its positive charge can interact with the negatively charged ALG chains (Jung et al., 2019). *In vitro*, the duration of antibiotic-release has been shown to last from less than 96 h to more than 6 weeks (Drago et al., 2014; Ter Boo et al., 2016; Li et al., 2017; Jung et al., 2019; Li et al., 2020a; Boot et al., 2021). However, the release time *in vivo* has rarely been reported, but the available data suggest a range of 72 h to more than 6 weeks (Changez et al., 2005; Li et al., 2017; Overstreet et al., 2019; Li et al., 2020a; Foster et al., 2021). After covering with a PEG-PLCL membrane, the CSt-mixed PEG-based vehicle system, coated on a Ti implant by covalently bound, sustainedly released vancomycin for over 4 weeks *in vivo*, without an initial burst release, thereby showing good antimicrobial activity against *S. aureus* (Li et al., 2017). Foster et al. (2021) reported that antibiotics can be released from HA-pNipam hydrogel for over 10 days, with local concentrations higher than the MIC. Increasing the concentration of gentamicin or vancomycin to 44% (w/w) in a composite hydrogel, which consisted of poly (acrylic acid) and gelatin, maintains the local antibiotics concentration at levels higher than MIC for more than 6 weeks (Changez et al., 2005).

*In vivo* use of other antibiotics, such as colistin, tobramycin, daptomycin, and isoniazid, in combination with hydrogels has been reported only sporadically (Spicer et al., 2013; Aldrich et al., 2019; Liu et al., 2019; Overstreet et al., 2019). Recently, daunorubicin, ketoconazole, rifapentine, and sitafloxacin have been demonstrated bactericidal activity against *S. aureus* SCVs. Sitafloxacin can also be used to eliminate methicillin-susceptible and -resistant *S. aureus*, as well as *S. aureus* within an established biofilm (Trombetta et al., 2018). Designing optimal hydrogel delivery systems for these drugs will offer novel treatment strategies for patients with OM.

The widespread emergence of antibiotic-resistant bacteria, which has heralded in a post-antibiotic era (Roca et al., 2015), has prompted the development of strategies other than traditional antibiotic therapy. Some antimicrobial agents, such as bacteriophages, antimicrobial peptides (AMPs), nitric oxide (NO), and silver (Ag), have been applied to the hydrogel local drug delivery system; therefore, these strategies open new avenues for the treatment of OM (**Table 1**; **Supplementary Table S1**).

### 3.1.2 Antimicrobial Peptides

AMPs, usually short positively charged peptide sequences (Ter Boo et al., 2015), target a specific features of microbial cell membranes, which distinguishes the broad range of pathogen species from multicellular plants and animals (Zasloff, 2002). The amphipathic structure of cationic AMPs confers their ability to bind to and disturb the pathogen cellular membrane, and induce the cell death (Epand and Vogel, 1999). In contrast to antibiotics, it is not possible to develop acquired resistance toward AMPs for sensitive bacterial strains, despite the inherent resistance in some bacterial species (Zasloff, 2002). The use of AMPs in OM is quite limited. Yang G. et al. (2018) used RADA16 to form a stable hydrogel scaffold that controlled the release of Tet213, a kind of cationic AMPs. The release of Tet213 was sustained for up to 28 days. *In vitro*, the growth of *S. aureus* was inhibited by this AMPs-laden hydrogel, while the proliferation of bone mesenchymal stem cells (BMSCs) was promoted. *In vivo*, RADA16-AMP self-assembling peptide has demonstrated a promising effect on bone formation.

### 3.1.3 Lysostaphin

Lysostaphin is a metallo-endopeptidase produced by *S. simulans* (Schindler and Schuhardt, 1964). The bacteriolytic enzyme exhibits a highly specific anti-staphylococcal activity (Kumar, 2008). Notably, this bacteriolytic enzyme, which possesses high anti-staphylococcal activity, exhibits antimicrobial activity against resistant strains, including MRSA, vancomycin-intermediate *S. aureus*, vancomycin resistant *S. aureus* and *S. epidermidis* (Climo et al., 1998; Patron et al., 1999; Mohamed et al., 2014). In contrast to most small-molecule antibiotics, the antimicrobial activity of lysostaphin is not dependent on the bacterial metabolic state; hence, it is active against bacteria in biofilms (Patron et al., 1999), and effectively kills bacteria at lower concentrations (Wu et al., 2003). Furthermore, lysostaphin does not impact the osteogenic differentiation of human cells (Johnson et al., 2018). Unlike systemic use of antibiotics, the species-specific nature of lysostaphin does not perturb the gut

**TABLE 1 |** Summary of advantages and limitations of different agents in hydrogels for OM.

| Agents | | Advantages | Limitations | References |
|---|---|---|---|---|
| Antimicrobial agents | Antibiotics | A wide variety of selection; broad clinical application; easy to manipulate | Resistance species | Overstreet et al. (2019), Eltawila et al. (2021), Foster et al. (2021), Sun et al. (2021) |
| | AMPs | A wide variety of selection; no resistance | Cytotoxicity | Guoli Yang et al. (2018) |
| | Lysostaphin | Highly specific anti-staphylococcal activity; synergistic effects with β-lactam antibiotics | Narrow antibacterial spectrum; the development of neutralizing antibodies; resistance species | Johnson et al. (2018), Johnson et al. (2019), Johnson et al. (2019) |
| | NO | Multifunctional (antibacterial, promotion of osteogenic differentiation, inflammation regulation) | The NO release is irreversible and difficult to be controlled | Li et al. (2020b) |
| | Bacteriophages | Extremely pervasive, sustained antimicrobial effect; synergistic effects antibiotics | Resistance species | Cobb et al. (2019), Ferry et al. (2020), Wroe et al. (2020) |
| | MΦs | MΦs are presumed to mediate biofilm clearance, which transform the bacteria from the dormant state into the active planktonic state, sensitizing them to antibiotics | Limited half-life; no prophylactic efficacy | Aldrich et al. (2019) |
| | Sliver | Being widely used in clinic | The efficacy and safety remain controversial in orthopedic application | Croes et al. (2018), Xu et al. (2018) |
| BMP-2 | | Osteo-generation effect; co-delivery with other agents | — | Aldrich et al. (2019), Johnson et al. (2019) |
| PDA | | Multifunctional (good adhesion and reducing capability to deposit bioactive molecules and synthesize antimicrobial agents, inducing the mineralization of hydroxyapatite, excellent photothermal properties) | — | Xu et al. (2018), Li et al. (2020b) |

*AMP, Antimicrobial Peptide; MΦs, Macrophages; BMP, Bone Morphogenetic Protein; OM, Osteomyelitis; —, not mentioned.*

microbiota. These features make lysostaphin an potential candidate for the treatment of staphylococcal OM.

Johnson et al. (2018) engineered a low-toxicity, injectable PEG-4MAL hydrogel. The elastic and adhesive features of the hydrogel were not affected by the addition of lysostaphin; meanwhile, the release of lysostaphin could be controlled by tuning the mesh structure of the hydrogel. Also, due to the protease-degradable peptide cross-linked in the hydrogel, lysostaphin release is influenced by local protease activity, which is elevated in the inflammatory microenvironment triggered by bacterial infection (Wolcott et al., 2008). This design maintains the activity of lysostaphin over 14 days (Johnson et al., 2018; Johnson et al., 2019). In a murine model, the lysostaphin-loaden PEG-4MAL hydrogel was shown to clear the infections and supported fracture cure or defect repair (Johnson et al., 2018; Johnson et al., 2019). Seven days post-infection, a multiplexed cytokine array assay revealed a sterile state had been restored in mice in the lysostaphin-laden hydrogel group, and after 5 weeks, bacterial counts revealed persistent infection in mice in the control group; however, animals in the trial group remained sterile, confirming the results at 1-week post-surgery. The group treated with the sustained lysostaphin topical release system showed comparable bone regeneration and mechanical properties to the uninfected group. Notably, sustained release of lysostaphin from hydrogel presented efficient anti-biofilm activity, while the soluble lysostaphin (no hydrogel) did not.

Despite this, there remain two concerns regarding the use of lysostaphin namely the development of neutralizing antibodies (Johnson et al., 2018; Johnson et al., 2019), and the potential resistance to the enzyme (Boyle-Vavra et al., 2001; Climo et al., 2001). Interestingly, lysostaphin synergizes with β-lactam antibiotics, and lysostaphin can render the resistant strains susceptible to the antibiotics (Climo et al., 2001; Kiri et al., 2002). The *in vivo* effects of the combined delivery of lysostaphin and antibiotics warrant further investigations.

### 3.1.4 Nitric Oxide

NO exerts various important physiological functions. In addition to its role as a signaling molecule, NO is involved in immune regulation and wound healing (Hoang Thi et al., 2018; Li et al., 2020b). Low concentrations of exogenous NO can enter pathogens and provide a degree of antibacterial activity. Additionally, upon reaction with superoxide (·O2–), NO produces peroxynitrite (·ONOO–), which possesses tremendous virulence against bacteria. However, the NO release is irreversible and difficult to be controlled (Yang T. et al., 2018).

To use NO more effectively, Li et al. (2020b) have engineered a hydrogel system, PCP/RSNO, comprising a polyvinyl alcohol (PVA) hydrogel modified with CS, polydopamine (PDA), and a NO-release donor (**Figure 2**). By coating the hydrogel with a red phosphorous (RP) nanofilm, deposited on a titanium implant (Ti-RP/PCP/RSNO), the release of NO and ·O2– could be controlled using near-infrared (NIR) light, which subsequently formed ·ONOO-. Synergism between ·ONOO–, ·O2–, and hyperthermia at 808 nm NIR irradiation destroyed over 93.1% of an MRSA biofilm *in vitro*, demonstrating greater effectiveness than vancomycin (76.2%). Furthermore, the anti-biofilm efficiency was approximately 91.9%. In addition to the antibacterial mechanism against MRSA biofilms, the released NO promoted the osteogenic differentiation and regulated

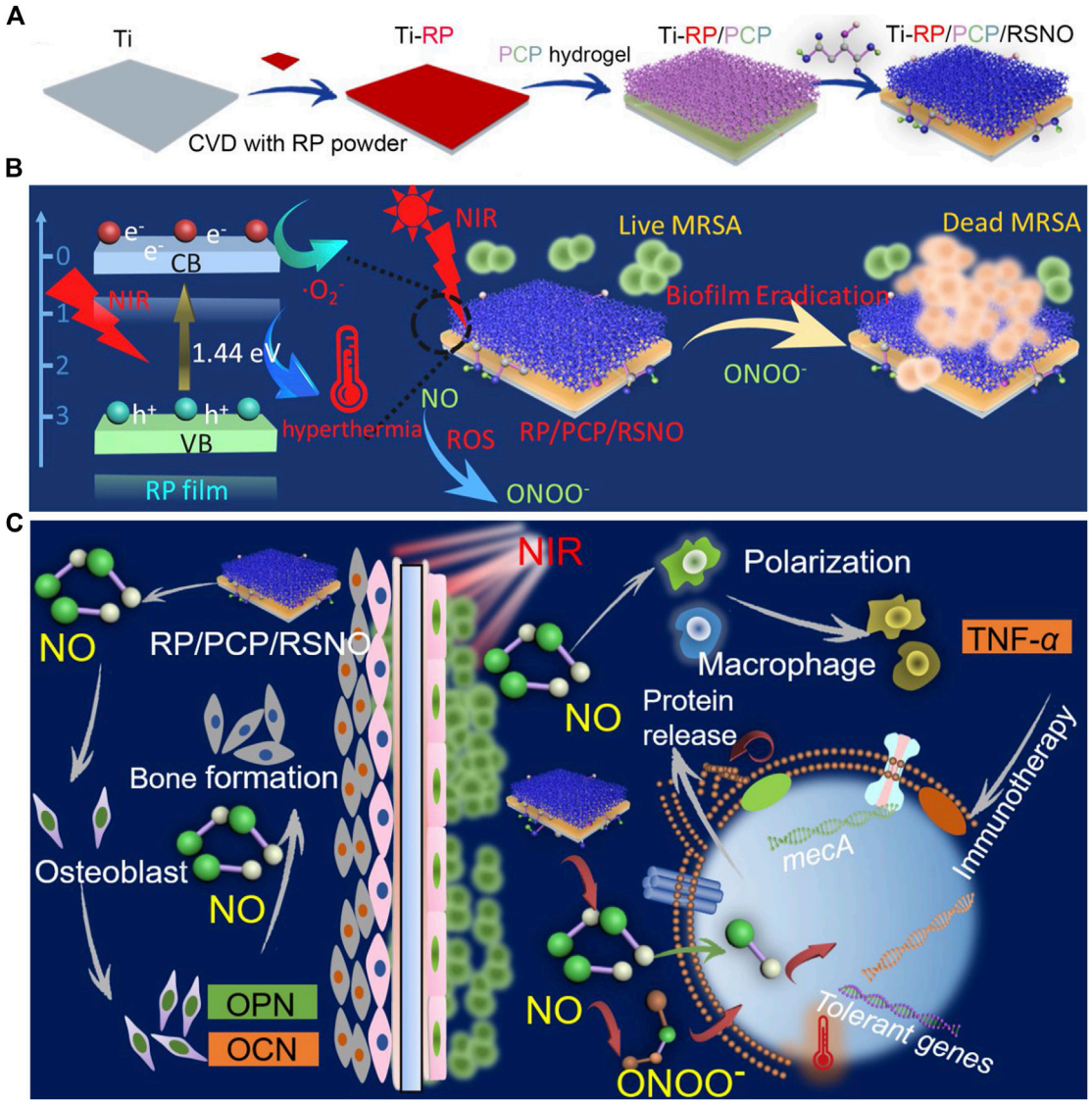


**FIGURE 2 | (A)** Schematic representation of the Ti-RP/PCP/RSNO hydrogel coating system preparation process. **(B)** Schematic representation of NIR triggered biofilm eradication. **(C)** Schematic representation of the mechanism of promoted bone formation and MRSA biofilm eradication. Ti, titanium; CVD, chemical vapor deposition; RP, red phosphorous; PCP, polyvinyl alcohol hydrogel modified with chitosan and polydopamine; RSNO, NO donor of S-nitrosuccinic acid; NIR, near-infrared; MRSA, methicillin-resistant *Staphylococcus aureus*; NO, Nitric oxide. Reprinted with permission from Li et al. (2020b). Copyright: 2020 American Chemical Society.

inflammatory polarization by upregulating the expression of *Alp*, *Opn*, *Ocn*, and *Tnf*-α. The efficient biofilm eradication (99.2%) and bone formation induced by NO released from this coating system under NIR irradiation have also been confirmed *in vivo*.

### 3.1.5 Bacteriophages

Bacteriophages exert a sustained antimicrobial effect and have potential to prevent and control bacterial biofilms (Sarker et al., 2012; Geredew Kifelew et al., 2019). Bacteriophages are associated with most known species of bacteria. The high specificity prevents side effects associated with the human microbiome (Rhoads et al., 2009; Petrovic Fabijan et al., 2020). Recently, a clinical trial reported the safety and tolerability of adjunctive bacteriophage approach for the treatment of severe *S. aureus* infection (Petrovic Fabijan et al., 2020).

Wroe et al. (2020) have engineered an injectable PEG-4MAL based hydrogel that encapsulate and delivered *P. aeruginosa* bacteriophages to the site of OM. Bacteriophages were released in a controlled manner with a retained bacteriolytic activity. *In vitro*, both planktonic and biofilm pathogens were effectively eliminated using this phage delivery system. Furthermore, the metabolic activity of human mesenchymal stromal cells was not disturbed. Seven-days following implantation in murine radial infectious defects, live *P. aeruginosa* counts were reduced 4.7-fold

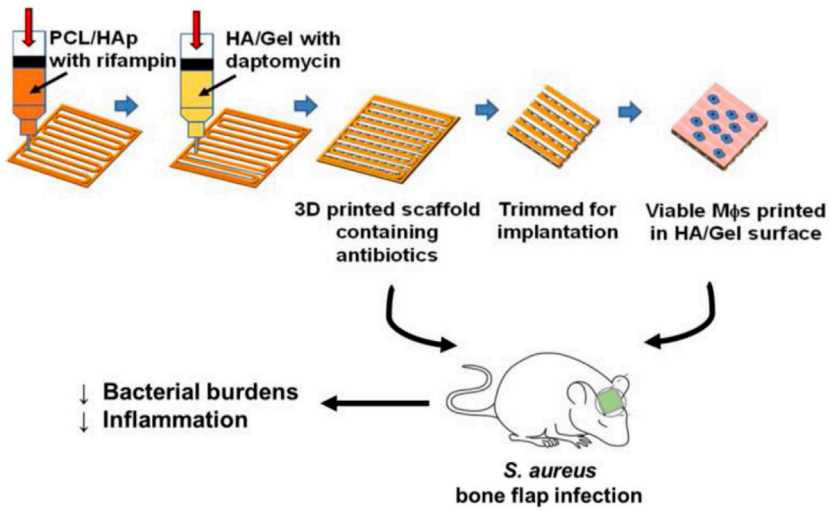


**FIGURE 3 |** Schematic representation of 3D bioprinted scaffolds containing viable macrophages and antibiotics, and reduction of bacterial burdens in a mouse model of *S. aureus* craniotomy-associated biofilm infection. PCL, polycaprolactone; HAp, hydroxyapatite; HA, hyaluronic acid. Reprinted with permission from Aldrich et al. (2019). Copyright: 2019 American Chemical Society.

in the bacteriophage-laden hydrogel group, compared with that in the bacteriophage-free hydrogel group.

Ferry et al. (2020) reported a case of recurrent *S. aureus* knee mega-prosthesis infection treated with a bacteriophage-laden DAC® hydrogel. Unfortunately, the patient suffered a myocardial infarction and underwent emergency stenting and received dual antiplatelet therapy 5-days later. Consequently, bleeding persisted at the surgical site and led to another prosthesis exposition for debridement. No *S. aureus* was found in culture, although three other bacteria strains were identified.

These results support the development of bacteriophage-delivery hydrogels, and provide new therapeutic frontiers for OM. To improve the safety of phage therapy, Cobb et al. (2019) modified the bacteriophages with CRISPR-Cas9 to remove all staphylococcal cytotoxin and enterotoxin genes, thereby preventing toxin contamination in the phage solution. However, the phage-delivery alginate hydrogel was efficacious against soft tissue infections *in vivo*, but not for bone infections.

Resistance is another obstacle hindering the use of bacteriophages. Phages depend on specific proteins to adhere to and infect bacteria. Thus, it is possible to develop resistance to phages, like antibiotics (Yilmaz et al., 2013). Although this might be limited due to the coevolution of bacteriophages and their hosts (Sweere et al., 2019). The co-delivery of bacteriophages and antibiotics could be a potential approach. Synergism upon dissolving the biofilm of MRSA and *P. aeruginosa* has been demonstrated (Yilmaz et al., 2013).

### 3.1.6 Macrophages

Activated macrophages (MΦs) significantly limit *S. aureus* biofilm growth and colonization (Hanke et al., 2013). It is also presumed that activated MΦs facilitate biofilm clearance, which transform the dormant bacteria within the biofilm into a metabolically active planktonic state and sensitive to antibiotics (Hanke et al., 2013; Aldrich et al., 2019). In a proof-of-concept study, Aldrich et al. (2019) demonstrated the synergistic effects of MΦs and antibiotics in a 3D bio-printed antibiotic-loaded bone scaffold, which promoted *S. aureus* clearance in a craniotomy-associated infection in mice (**Figure 3**). For treatment, the scaffolds were placed in the defect area at day 7 post-infection, and the incorporation of MΦs further reduced bacterial burden compared to antibiotics alone. The exact antimicrobial mechanism remains to be determined. It is possible that the direct antimicrobial effect of MΦs, and cytokines/chemokines secreted by activated MΦs enhanced the antibacterial activity of other glia/leukocytes. However, the synergistic effects were detected only in the treatment paradigm, but not in the prevention paradigm in which the scaffolds were inserted 1 day prior to *S. aureus* inoculation. One possibility reason is lack of some signals, which are present in an established biofilm, to activate MΦs. Meanwhile, the authors found that the beneficial effect of MΦs was transient. No more decrease of bacterial titers was observed 7 days after treatment. This was likely attributed to the limited half-life of MΦs when exposed to the large number of bacteria in the biofilm that produced lytic toxins. Although the authors observed bacterial burden only in Galea and Brain, but not in bone tissue. The study presents an immune-based 3D bioprinting approach to promote biofilm clearance.

### 3.1.7 Silver

Before the discovery of penicillin, silver (Ag) was used clinically as a bactericidal agent (Chopra, 2007). Due to the nucleophilic functions of proteins, enzymes, and cell membrane components in bacteria, they react with Ag cations ($Ag^{+}$), which then disrupt their function and displace metal ions, such as $Zn^{2+}$ and $Ca^{2+}$. These subsequently induce the bacterial death (Hetrick and Schoenfisch, 2006). Silver

nanoparticles (AgNP) can be synthesized *in situ* using polydopamine (PDA) and mineralized on PEG diacrylate (PEGda) hydrogels. Therefore, the so-called AgNPs/PDA-coated PEGda hydrogels were designed for the treatment of anti-infection (Xu et al., 2018). Controlled Ag delivery inhibits the growth of *S. aureus* and *E. coli*; *in vivo*, the AgNP/PDA gel efficiently repaired maxillary defects without infection.

To our knowledge, Ag-loaded hydrogels have been rarely studied for the treatment of OM. Croes et al. (2018) have developed a CS-based coating with AgNPs, which showed burst and sustained drug release properties. However, no antimicrobial effects were found *in vivo*. Furthermore, radiological signs of aggravated OM were observed. The authors attributed the poor antibacterial property to the cytotoxicity for neutrophils at antimicrobial Ag concentrations, and the diminished phagocytic effect at nontoxic concentrations. In orthopedic applications, the true efficacy and safety of Ag remains controversial (Prokopovich et al., 2013; Wafa et al., 2015; Masters et al., 2019). Future research should investigate the ideal formulation and concentration of Ag or AgNPs for safe clinical use.

## 3.2 Bone Morphogenetic Protein 2

Recombinant BMPs have been developed to address the challenge of segmental bone defects. BMP-2 promotes cell proliferation, alkaline phosphatase activity, differentiation, and mineralization *in vitro* and *in vivo* (Tao et al., 2021). The US FDA has approved the use of BMP-2 to facilitate bone formation (Burkus et al., 2002). However, its use is limited by adverse events associated with supraphysiological doses, including inflammation and heterotopic bone formation (Hustedt and Blizzard, 2014). Carriers with controlled BMP-2 release have been developed to promote bone regeneration and reduce the incidence of adverse effects (Hustedt and Blizzard, 2014; Shekaran et al., 2014; Huang et al., 2017; Han et al., 2020; Sun et al., 2020; Tao et al., 2021). A BMP-2-loaded PEG-4MAL hydrogel has been shown to generate better quality bone compared to a BMP-2-laden collagen sponge (Shekaran et al., 2014).

Interventions that promote bone growth while fighting bone infections have the potential to significantly reduce the incidence of non-union and improve patient prognosis. BMP-2 encapsulated in hydrogels with antibiotics can be released in an initial burst manner followed by a sustained release pattern (Jung et al., 2019). Previous studies demonstrated that vancomycin incorporated into the hydrogels did not significantly interfere with the release of BMP-2 (Jung et al., 2019), and that the loaded antibiotics, including ampicillin, cefazolin, dibekacin, vancomycin, teicoplanin, and minocycline, did not inhibit the ability of rhBMP-2 to repair cranial defects (Suzuki et al., 2006). The sustained release of BMP-2 led to prolonged activity, and resulted in effective osteogenic differentiation and bone reconstruction (Kim et al., 2018; Jung et al., 2019). *In vivo*, BMP-2 and antibiotic-co-encapsulated hydrogel group increased bone reconstruction (Suzuki et al., 2006) and significantly improved biomechanical features compared to the other groups (Suzuki et al., 2006; Jung et al., 2019). The rationale for this strategy was that the co-administration of antibiotics and BMP-2 preserved their own functionality. Moreover, co-administration showed more effective suppression of bacteria compared to the antibiotic alone; this result could be attributed to the rapid proliferation of bone marrow stromal cells induced by BMP-2 outpacing the infectivity and proliferation of pathogen (Jung et al., 2019).

In a study investigating a bifunctional hydrogel, Johnson et al. (2019) also showed that BMP-2 and lysostaphin-co-encapsulated PEG-4MAL hydrogels prevented *S. aureus* infection and promoted segmental bone defect regeneration. The co-encapsulated hydrogel with *S. aureus* group showed equal amounts of new bone formation as the sterile hydrogel alone group.

## 3.3 Polydopamine

Due to its excellent biocompatibility, hydrophilicity and adhesion reactions with various molecules, PDA has been used pervasively in tissue engineering. In addition to being a crosslinking agent, PDA has been shown to induce the mineralization of hydroxyapatite on demineralized dentin (Zhou et al., 2012), and presents good adhesion and reducing capabilities to deposit bioactive molecules (Sileika et al., 2011; Xu et al., 2018).

PDA has been used to synthesize AgNPs *in situ* on a PEGda scaffold to construct an AgNPs/PDA-coated PEGda hydrogel (Xu et al., 2018). This hydrogel delivery system exhibited excellent cytocompatibility with strong antimicrobial effects against *S. aureus* and *E. coli*, and simultaneously promoted bone generation, due to dual functions of anti-bacterial activity of AgNPs and graft mineralization of PDA. The expression of some osteogenic genes was upregulated *in vitro*, including osteocalcin, runt-related transcription factor 2, bone sialoprotein, and alkaline phosphatase. The rat maxillary bone defects were efficiently repaired (Xu et al., 2018).

In addition, PDA present excellent photothermal properties. NIR irradiation activates photothermal PDA in the hydrogel, and local hyperthermia destroies the integrity of bacteria, leading to bacterial inactivation in a synergistic manner (Gao et al., 2019; Li et al., 2020b). In the Ti-RP/PCP/RSNO system, PDA in the hydrogel increases the bonding strength between the hydrogel and RP-modified implants (Li et al., 2020b). Meanwhile, NIR irradiation activated the photothermal effect of PDA. The generated local hyperthermia disrupted bacterial integrity and eliminated the MRSA burden in a synergistic manner with the simultaneous generation of ·ONOO− and ·O2−.

# 4 METHODS TO CONTROL DRUG RELEASE

## 4.1 Extending Drug Release

Treatment duration is an important factor affecting the success of antibiotic therapy for OM. Thus, in addition to mechanical strength, degradability and histocompatibility, drug elution kinetics are important for vehicle choice. For most hydrogels, the loaded drugs are released in a burst manner, driven by diffusion. *In vitro*, >90% of antibiotics are released within the first day, while the remaining are released within the following 4 days. However, *in vivo*, the release time may be extended due to

the potentially limited fluid volume and mass transfer at the infectious site (Ruan et al., 2016; Li et al., 2017; Haider et al., 2018; Johnson et al., 2018). Extending or controlling the effective duration of drug release can be achieved by successive injections (Boot et al., 2021) or modification of the hydrogel (Sun et al., 2021).

### 4.1.1 Composite Materials

The development of composite materials can overcome the shortcomings of the individual constituents. The HA-pNipam hydrogel and CSt-mixed PEG hydrogels are composite polymers derived from natural and synthetic materials, respectively. Gentamicin and vancomycin loaded in the HA-pNipam hydrogel were released for more than 336 h *in vitro* and 10 days *in vivo* (Boot et al., 2021; Foster et al., 2021). Drugs release was delayed in a PEG-based hydrogel mixed with CSt, to 3 weeks *in vitro* and 4 weeks *in vivo* without an initial burst release (Li et al., 2017).

An *in situ* gelling alginate/HyA hydrogel, designed by Jung et al. (2019), continuously released both vancomycin and BMP-2 for 6 weeks *in vitro* without significant cytotoxicity. The results of the *in vivo* study demonstrated that this vancomycin/BMP-2-laden-alginate/HyA hydrogel could efficiently inhibit *S. aureus* proliferation and promote bone regeneration. Another example of a PEG composites, a triblock PLA-DX-PEG hydrogel (PDLLA-p-dioxane-PEG) composed of PLA:DX:PEG at a molar ratio of 5: 1:3. *In vitro*, almost 40% of the laden teicoplanin was released within the first 24 h, and the concentrations above the MIC 90% for *S. aureus* were maintained for 2 weeks (Suzuki et al., 2006).

### 4.1.2 Transglutaminase

Transglutaminase (TGase) can produce conjugates derivatized at the level of Gln and/or Lys residues, and has been used successfully in various biotechnological applications (Duarte et al., 2020; Dell'Olmo et al., 2021; Sun et al., 2021). The hydrogels, crosslinked by TGase, can control the release of loaded drugs at the targeted site, acting as "smart" delivery systems. In a novel vancomycin-impregnated gelatin/alginate hydrogel crosslinked by TGase, over 90% crosslinking was achieved (Sun et al., 2021). The release time of the encapsulated antibiotics increased with increasing TGase concentrations, from approximately 20 min without TGase to more than 120 h with 1% TGase. In an *in vivo* study of implant-associated infection in rat, the vancomycin-treated group showed reduced biofilm formation and inflammation, and significant bone regeneration, even after inoculation with a high dose of MRSA. Notably, these beneficial effects were observed with the vancomycin-laden hydrogel, but not with the gentamicin-loaded hydrogel.

### 4.1.3 Nanoparticles

NP-based anti-infection strategies have promising for biomedical applications. This can be attributed to the large surface area to volume ratio and the flexibility in tuning their charactristics (Zhang et al., 2008). Many biocompatible and biodegradable NPs, such as liposomes and polymeric NPs, have been used as vehicles to control antimicrobial delivery (Forier et al., 2014; Ma et al., 2019; Tao J. et al., 2020). Using this approach, the limitations of antibiotic treatment can be overcome, including inefficient drug release, enzymatic inactivation of drugs, and cytotoxicity (Meers et al., 2008). Compared to free drugs, the encapsulated antibiotics can efficiently penetrate extracellular polymeric substances, resulting in the delivery of therapeutic doses at the target site.

CS-based NPs are used as drug vehicles due to their ideal biological characteristics, such as biocompatibility, antimicrobial properties, and low toxicity. Tao J. et al. (2020) hypothesized that the positive charge of quaternary ammonium CS (QCA) and negative charge of carboxylated CS (CC) drive the electrostatic adsorption-driven assembly of NPs, which can efficiently load the water-soluble antibiotics. Based on the hypothesis, they engineered vancomycin-NPs incorporated in CS-gel to construct an injectable thermosensitive vancomycin-NPs/gel drug delivery system. From CS hydrogel alone, vancomycin was released within 1–5 days (Ruan et al., 2016; Haider et al., 2018). In contrast, vancomycin release was extended over 26 days, and 65% of the laden antibiotic was released from the vancomycin-NPs/gel *in vitro*; this meets the clinical demand for OM treatment. In a rabbit tibia *S. aureus* OM model, the sustained release of vancomycin reduced the white blood cell (WBC) count and C-reactive protein (CRP) levels at 4–8 weeks. Radiological and histological analyses showed that the vancomycin-NPs/gel accelerated bone repair under OM conditions (Tao J. et al., 2020).

Liposome-NPs are also commonly applied as drug delivery polymers, since their phospholipid bilayer structure that mimics the cell membrane, enabling fusion with pathogen cell membrane (Allen and Cullis, 2013; Zununi Vahed et al., 2017). Subsequently, the loaded drugs are released to the cellular membrane or cytoplasm of the pathogens (Malam et al., 2009). Studies have demonstrated that encapsulating liposome NPs into hydrogels further extends drug release, since the loaded drugs meet two barriers during release: the liposome and hydrogel networks (O'Neill et al., 2017; Liu et al., 2019). As an excellent vehicle for N′-dodecanoylisonicotinohydrazide (DINH), the drug-laden NPs can be easily prepared and encapsulated into a PLGA-PEG-PLGA hydrogel by simple mixing. The incorporation of liposome NPs does not interfere with the properties of the hydrogel. An *in vivo* pharmacokinetics analysis showed that, compared with the liposome-free hydrogel, a liposome-NPs-hydrogel DINH delivery system released drugs at target sites over a longer duration, with stable drug concentrations. These properties suggest that this system may have potential for localized bone tuberculosis (Liu et al., 2019).

Ag-based NPs have received considerable attention with satisfactory efficacy in wound care. Because the bioavailability and antimicrobial activity of free Ag ions is reduced due to the rapid sequestration by proteins and other cellular components in the wound (Xiu et al., 2011). Despite their sustained release property, AgNPs in the CS gel coating did not show the expected antibacterial efficacy, and even showed signs of aggravating the infection due to its cytotoxicity (Croes et al., 2018). Identifying the ideal formulation and concentration of AgNPs is a theme for future research.

## 4.2 Passive and Active Release

Most sustained drug-release systems prolong the release of agents through passive mechanisms, including diffusion, swelling, and erosion (Ter Boo et al., 2015). Drug diffusion depends on the difference in concentration between the inside and outside of the gel and the length of the diffusion path. Swelling of the hydrogel promotes diffusion of the encapsulated drugs. Bulk erosion of the hydrogel reduces the path length and facilitates drug release with the eroded portion.

Studies have investigated stimulus-sensitive hydrogels, which adapt their physical features and cleave attached chemical groups in response to various stimuli (Li et al., 2020a; Li et al., 2020b; McCarthy et al., 2021). For example, hyaluronidase is an *S. aureus* metabolite related to species spreading (Gu et al., 2015). The acidic nature of *S. aureus* infectious lesions could be enhanced by hyaluronidase activity (Radovic-Moreno et al., 2012; Wang et al., 2017). Therefore, HyA has been selected as a trigger to release agents on demand. In addition to passive release, drugs can be released based on the concentration of bacteria or their metabolites. Li et al. (2020a) developed a HyA-CS/β-glycerophosphate (β-GP)-based thermosensitive hydrogel. Using this intelligent drug-delivery system, which was triggered by HyA, vancomycin hydrochloride was released in a burst or burst-sustained pattern. As the concentration of hyaluronidase increased, the active release pattern was enhanced. *In vitro*, vancomycin concentrations were much higher than the MIC after 25 days, whereas *in vivo*, the drug was completely released and detected for up to 30 days, which was sufficient for preventing or treating infection.

In the smart delivery system designed by Johnson et al. (2018), protease-degradable cross-linking peptide GCRDVPMSMRGGDRCG (VPM) was covalently incorporated into a PEG-4MAL network. In addition to a passive sustained release pattern, due to the inclusion of VPM, the encapsulated drugs could be actively released depending on the local protease levels. These are often elevated in the inflammatory microenvironment triggered by bacterial infection (Wolcott et al., 2008).

# 5 APPLICATIONS

## 5.1 Implant Coating

In addition to filling dead space directly, drug-laden hydrogels are mainly used to coat orthopedic implants (Li et al., 2017; Boot et al., 2020; Li et al., 2020b; Boot et al., 2021; Foster et al., 2021; Sun et al., 2021). Almost 80% of the hydrogel coated on the implants was found to remain after press-fit insertion (Drago et al., 2014). These drug-laden hydrogel coatings have the following advantages: 1) inhibition of bacterial colonization on the implant in the early postoperative phase, to win the "race to the surface" (**Figure 4**); 2) a favorable safety profile, since high local concentrations and complete controlled drug release over a relatively short period may prevent antibiotic resistance and possible side effects on bone healing; 3) versatility, as different antimicrobial agents can be selected for mixing during the procedure; 4) ease of handling; 5) low costs (Drago et al., 2014). The hydrogel coatings for OM have been primarily studied in rats, rabbits, and sheep, to investigate their prophylactic efficacy (Li et al., 2017; Li et al., 2020b; Boot et al., 2020; Boot et al., 2021; Foster et al., 2021; Sun et al., 2021). The release of agents in a burst and sustained manner reduces the inflammatory response and optimizes the antibacterial effect, demonstrating efficacy towards preventing or treating implant-associated infections.

## 5.2 Scaffolds

An optimal bone graft to treat bone defects induced by infection should possess the following properties: 1) a biphasic drug-release profile with enhanced drug elution kinetics; 2) biodegradability; and 3) osteo-conductivity (Masters et al., 2019). Research is ongoing to improve the properties of bio-scaffolds by loading hydrogels with different frames.

### 5.2.1 Tricalcium Phosphate Scaffold

Tricalcium phosphate (TCP) is biodegradable, biocompatible, and osteoconductive. TCP cements have inherent porosity and high pore interconnectivity, which enhance the adsorption ability and release of loaded drugs, thus has been used widely as a bone graft (Almirall et al., 2004; Kondo et al., 2005; Silverman et al., 2007; Giavaresi et al., 2012; Wu et al., 2013). However, TCP cements rapidly release the impregnated drugs. Approximately 80% of laden antibiotics are released within 4 days (Teo et al., 2011; Wu et al., 2013).

To engineer an optimal antimicrobial delivery system for the treatment of OM that is easy to handle, biodegradable, and ensures a constant drug release at an effective concentration for a long period, antibiotic-laden hydrogels were introduced into a TCP scaffold (Wu et al., 2013; Li et al., 2020a). Following vacuum adsorption in the hydrogel solution to form the coatings, the TCP scaffold maintained its polyporous structure. This antibiotic delivery system presented elution kinetics characterized by an initial burst followed by zero-order release sustained for more than 25 days *in vitro* and 30 days *in vivo* (Wu et al., 2013; Li et al., 2020a), with higher concentration than the MIC over 25 days *in vivo* (Li et al., 2020a). Following implantation in a rabbit femur condyle OM defect model, the antibacterial and osteogenic effects of these delivery systems were enhanced compared to those of intramuscular antibiotic injection or TCP scaffold alone, which are routine approaches (Wu et al., 2013; Li et al., 2020a).

### 5.2.2 The 3D-Bioprinting Approach

3D bioprinting has demonstrated excellent potential in bone tissue engineering. Using different strategies, material containing living cells is deposited to fabricate living volumetric constructs in a layer-by-layer manner, such as vascularized bone-like fragment (Byambaa et al., 2017; Ashammakhi et al., 2019). However, studies on the use of 3D bioprinting for OM are rare. Aldrich et al. (2019) have developed a 3D bioprinting bone scaffold engineered for sustained local antibiotic release, in combination with the incorporation of MΦs that possessed potent antimicrobial activity. This 3D-printed scaffold was constructed with methacrylated hyaluronic acid

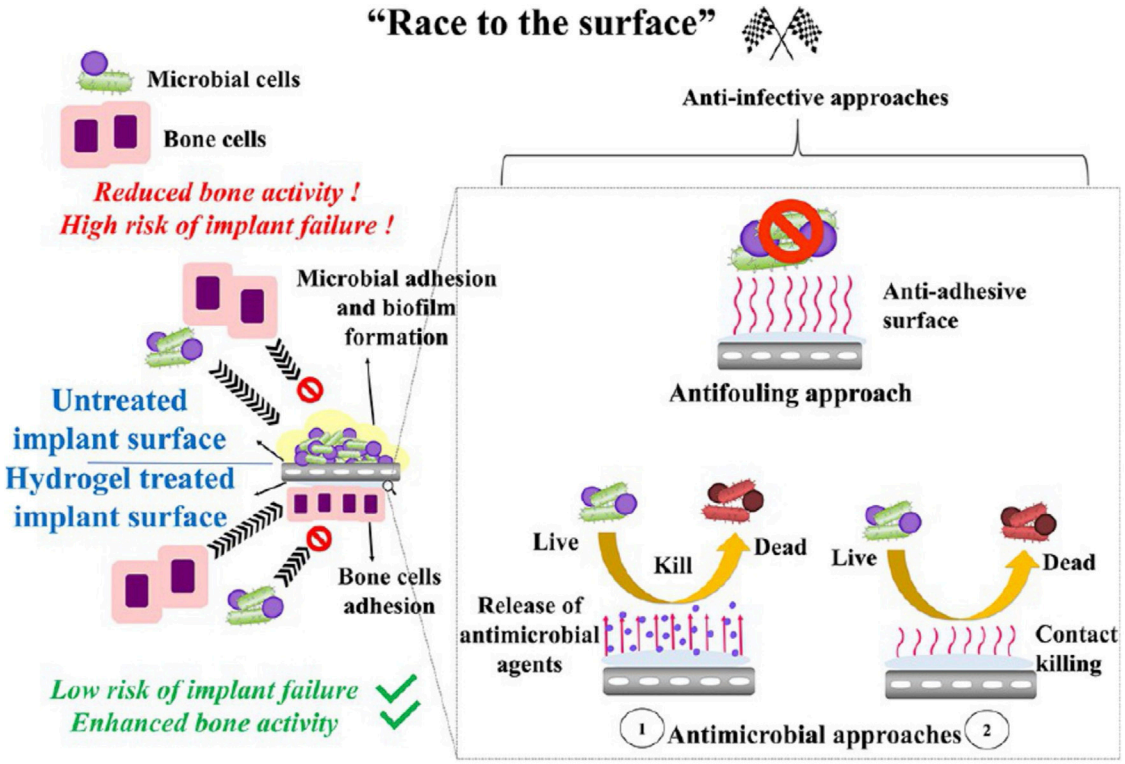


**FIGURE 4 |** Schematic illustration of the winning "race of the surface" of anti-infective hydrogels. Reprinted with permission from Garg et al. (2021). Copyright: 2021 American Chemical Society.

(Me-HyA)- and methacrylated gelatin (Me-Gel)-based hydrogels encapsulating daptomycin between a polycaprolactone/hydroxyapatite frame incorporated with rifampin. MΦs were printed on the surface of the HyA/gel hydrogel matrix in L929 solution to maximize cell viability. In an *S. aureus* craniotomy-associated biofilm mouse model, antibiotic scaffolds with MΦs reduced the bacterial burden (**Figure 3**); however, infection in the bone defect was not investigated. Due to the short life span of MΦs, this strategy only demonstrated an early therapeutic effect, which was lost at 7 days, with no preventive effects were observed. This proof-of-concept study provides an insight into 3D bioprinting technology in the OM field.

## 5.3 Nanotopography

Stem cell proliferation and differentiation can be modulated by the external microenvironments and specific biophysical cues. As a stream of stem research, nanotography, with diverse biomaterials and different surface geometries, can precisely and efficiently regulate the behavior of stem cells and enhance their abilities through specific cell-surface interaction (Kim et al., 2017; Thomas et al., 2018). Vertically aligned 1D nanomaterials have been used in advanced biomedical applications (Kwak et al., 2015; Poudineh et al., 2018). Living cells and tissues can interface on these efficient platforms. Due to the nanoscale diameters and sharp tips, they can pierce cell membrane, impacting cell viability. The volumes of mammalian and bacterial cells differ. By tuning their physical features (i.e., the relative size of the nanoneedles compared to the cells), these nanomaterials can pierce the pathogen cell membrane without disturbing the integrity of mammalian cell membranes (Mas-Moruno et al., 2019). Furthermore, the long 1D structure facilitates cellular interfacing with the external microenvironments, and the high-aspect-ratio feature of their sharp tip structure effectively prevents biofilm formation via mechanical lysis (Pogodin et al., 2013; May et al., 2016).

Based on these advantages of 1D nanomaterials, Park et al. (2019) designed a biocompatible PEG dimethacrylate-based hydrogel patch (**Figure 5**). This patch possessed a nanospike (hSPIKE) arrays with tapered tips. This transplantable platform promoted the osteogenic, chondrogenic, and adipogenic differentiation of dental pulp stem cells *in vitro* without altering cell viability. Furthermore, the hSPIKE arrays exhibited efficient bactericidal effects against both Gram-positive and -negative bacteria. Compared with a flat patch, the hSPIKE patch significantly promoted the healing of mouse cranial bone defect while preventing bacterial infections.

# 6 EFFECT ON BONE HEALING

The impact of any antibiotic-laden-biomaterial (ALB) implanted in a fracture or bone defect on bone regeneration

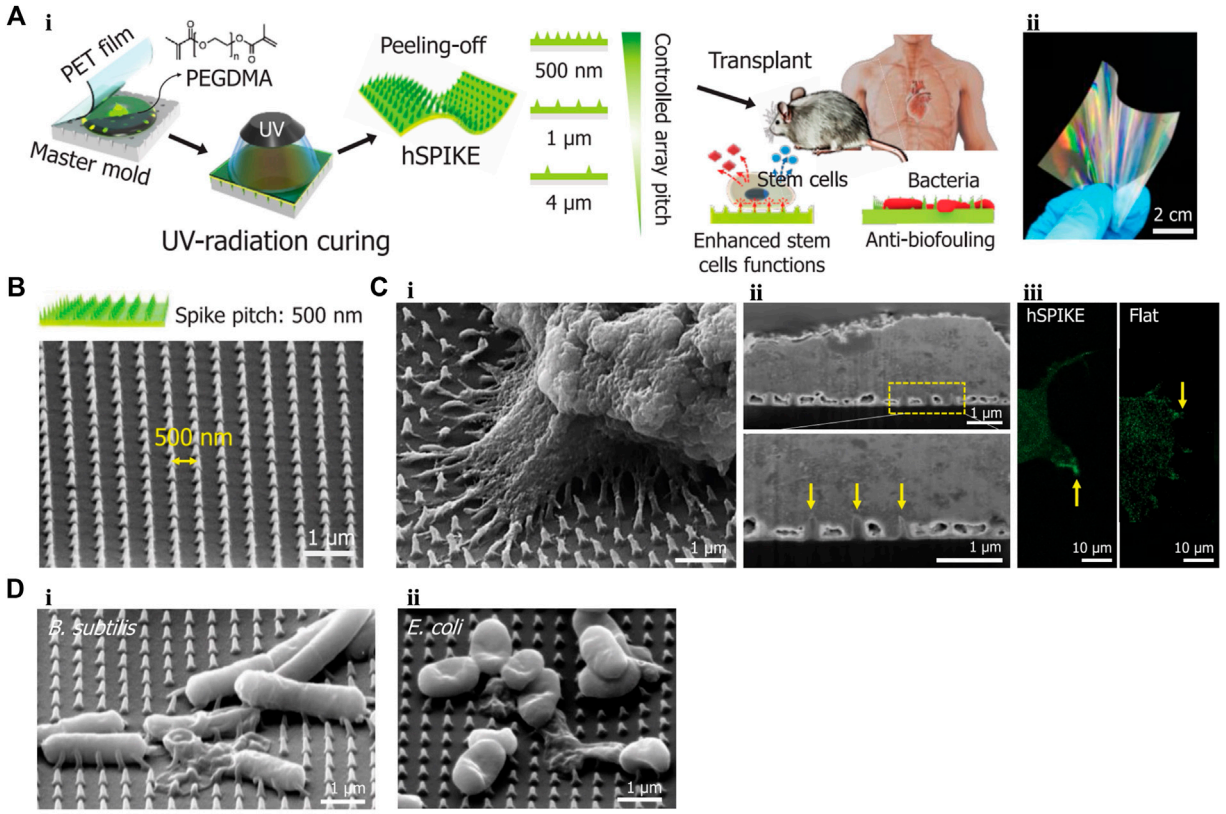


**FIGURE 5 | (A) (i)** Schematic representation of fabrication process of the hSPIKE patch. **(ii)** Photograph of the hSPIKE patch. **(B)** Scanning electron micrograph (SEM) image of the hSPIKE. **(C) (i)** SEM of Dental pulp stem cells (DPSCs) cultured on the hSPIKE, **(ii)** focused ion beam (FIB)-SEM cross-section of DPSCs cultured on the hSPIKE, and **(iii)** fluorescence microscopy images of DPSCs cultured on the hSPIKE (left) and flat substrates (right). **(D)** SEM of **(i)** *B. subtilis* and **(ii)** *E. coli* cultured on the hSPIKE. PET, polyethylene terephthalate; hSPIKE, hydrogel nanospike array; *B. sutilis, Bacillus subtilis*; *E. coli, Escherichia coli*. Reprinted with permission from Park et al. (2019). Copyright: 2019 American Chemical Society.

must be addressed. Hydrogels themselves, as foreign materials, and high local concentrations of antimicrobial agents may influence tissue healing (Ter Boo et al., 2018). Studies have investigated bone regeneration following ABL implantation *in vitro* (Ter Boo et al., 2018; Li et al., 2020a; Boot et al., 2020; Tao J. et al., 2020; Vallejo Diaz et al., 2020; Eltawila et al., 2021; Foster et al., 2021; Sun et al., 2021). However, to our knowledge, limited *in vivo* studies have evaluated the influence of hydrogels on bone healing.

Ter Boo et al. (2018) observed fracture healing in groups treated with HA-pNipam hydrogel alone in the absence of bacterial contamination using a rabbit humeral fracture model. Implantation of HA-pNipam hydrogel showed no significant effect on clinical or biological responses, including weight, CRP levels, and WBC count. No significant differences in relative stiffness were observed 4 weeks after hydrogel application. Compared with contralateral non-fractured humerus, the mean relative stiffness values with and without HA-pNipam hydrogel were 49%–67%, respectively. Contact radiographs and histopathological analyses in both groups revealed callus formation at both the *cis* and *trans* sides of the humerus, and at the interface between the screws and intramedullary cavity. Compared to the control group, the HA-pNipam group presented less bone callus formation only at the *cis* side, where the HA-pNipam hydrogel was injected. Another study investigating the effects of a DAC® hydrogel coating on bone apposition at a titanium implant surface *in vivo*, showed that, compared with the group without coating, the hydrogel coating loaded or unloaded with 2% vancomycin neither affected the volume and timing of bone apposition, nor induced an inflammatory response (Boot et al., 2017). The results of these two studies showed that HA-pNipam and DAC® hydrogels did not affect bone regeneration. In future, more research is needed on other hydrogels.

## 7 HEPATORENAL TOXICITY

Hepatorenal side effects of hydrogels in bone infection have been reported (Changez et al., 2005; Overstreet et al., 2015; Johnson et al., 2018; Johnson et al., 2019; Li et al., 2020b; Foster et al., 2021). In rabbits, Li et al. (2020a) have found that, compared with the

blank group, those treated with a VH-HyA-CS/β-GP hydrogel-laden TCP scaffold showed no significant difference in aspartate aminotransferase (AST) and blood urea nitrogen (BUN) levels at 1, 4, and 7 days, whereas alanine aminotransferase and serum creatinine (SCr) levels increased slightly at 4–7 days. In rats, no differences in BUN, SCr, and uric acid (UA) levels were found between the Ti-RP/PCP/RSNO and control groups, while systemic vancomycin treatment increased SCr and UA levels and induced renal toxicity (Li et al., 2020b). Additionally, liver enzyme tests and histological analyses of the liver and kidneys supported the safety of lysostaphin-delivering PEG hydrogels designed by Johnson et al. (2018). These results support the safety of the application of these local antimicrobial agent delivery hydrogel systems.

## 8 OUTLOOKS

Collectively, available hydrogel designs have demonstrated the superior ability to prevent or treat OM, compared to the clinical gold standard of ALBC. However, there remains several challenges in the clinical applications. First, potential resistance to present agents remains a concern. Co-delivery of different agents may represent a suitable approach to overcome this challenge. Alternative strategies, such as mAb treatment and conjugation of bisphosphonates to conventional antibiotics, are increasingly attractive for the treatment of OM (Sedghizadeh et al., 2017; Masters et al., 2019). Hydrogel loading with these agents would increase the number of therapeutic strategies. Second, whether the hydrogel can be applied once in a one-stage exchange procedure remains to be determined. Eliminating the need for a second revision surgery would be an attractive prospect (Boot et al., 2021). Thus, future work should focus on engineering smart or intelligent hydrogel delivery systems that are responsive to multiple stimuli, and outstanding breakthroughs in 4D printing (Chu et al., 2020). Third, present studies have focused on the OM induced by *S. aureus*. Different hydrogel antimicrobial approaches should be investigated for infections by a diverse range of species. Fourth, to date, only a few drug-laden hydrogels have been used successfully in the clinic. More studies are needed to develop an optimal hydrogel system for OM.

## 9 CONCLUSION

OM remains a major challenge due to its complicated microenvironment. An in-depth understanding the mechanism of OM will help to develop better treatment strategies. Loading antimicrobial agents into hydrogels, even co-incorporating osteo-inductive materials and other adjuvants, is a promise strategy. This review discussed current hydrogel designs and their applications to improve the biological response to OM *in vivo*, thereby providing insights into the development of novel prevention and treatment options for OM.

## AUTHOR CONTRIBUTIONS

BY conceived the general idea and provided critical revision and final approval of the manuscript. WX and YG conducted the literature study and wrote the draft manuscript. All authors contributed to the article and approved the submitted version.

## FUNDING

This work was supported by the National Natural Science Foundation of China (Grant nos. 81972086 and 81672196); Shanghai "Rising Stars of Medical Talent" Youth Development Program (Youth Medical Talents—Specialist Program) (Grant no. 2019-72); National Key Research and Development Project of China (Grant nos. 2020YFC1107500, and 2020YFC1107503); "Technology Innovation Action Plan" Key Project of Shanghai Science and Technology Commission (Grant no. 19411962800); Clinical Scientific innovation and Cultivation Fund of Renji Hospital Affiliated School of Medicine, Shanghai Jiaotong University (Grant no. PY2018-I-02); RENJI-NSFC Advancing Targeted Projects (RJTJ-JX-005).

## SUPPLEMENTARY MATERIAL

The Supplementary Material for this article can be found online at: https://www.frontiersin.org/articles/10.3389/fbioe.2022.865250/full#supplementary-material

## REFERENCES

Aldrich, A., Kuss, M. A., Duan, B., and Kielian, T. (2019). 3D Bioprinted Scaffolds Containing Viable Macrophages and Antibiotics Promote Clearance of *Staphylococcus aureus* Craniotomy-Associated Biofilm Infection. *ACS Appl. Mater. Inter.* 11 (13), 12298–12307. doi:10.1021/acsami.9b00264

Allen, T. M., and Cullis, P. R. (2013). Liposomal Drug Delivery Systems: from Concept to Clinical Applications. *Adv. Drug Deliv. Rev.* 65 (1), 36–48. doi:10.1016/j.addr.2012.09.037

Almirall, A., Larrecq, G., Delgado, J. A., Martı´nez, S., Planell, J. A., and Ginebra, M. P. (2004). Fabrication of Low Temperature Macroporous Hydroxyapatite Scaffolds by Foaming and Hydrolysis of an α-TCP Paste. *Biomaterials* 25 (17), 3671–3680. doi:10.1016/j.biomaterials.2003.10.066

Arciola, C. R., An, Y. H., Campoccia, D., Donati, M. E., and Montanaro, L. (2005). Etiology of Implant Orthopedic Infections: a Survey on 1027 Clinical Isolates. *Int. J. Artif. Organs* 28 (11), 1091–1100. doi:10.1177/039139880502801106

Ashammakhi, N., Hasan, A., Kaarela, O., Byambaa, B., Sheikhi, A., Gaharwar, A. K., et al. (2019). Advancing Frontiers in Bone Bioprinting. *Adv. Healthc. Mater.* 8 (7), 1801048. doi:10.1002/adhm.201801048

Bakshi, P. S., Selvakumar, D., Kadirvelu, K., and Kumar, N. S. (2020). Chitosan as an Environment Friendly Biomaterial - a Review on Recent Modifications and Applications. *Int. J. Biol. Macromolecules* 150, 1072–1083. doi:10.1016/j.ijbiomac.2019.10.113

Barth, R. E., Vogely, H. C., Hoepelman, A. I. M., and Peters, E. J. G. (2011). 'To Bead or Not to Bead?' Treatment of Osteomyelitis and Prosthetic Joint-Associated Infections with Gentamicin Bead Chains. *Int. J. Antimicrob. Agents* 38 (5), 371–375. doi:10.1016/j.ijantimicag.2011.03.008

Bibbo, C., and Patel, D. V. (2006). The Effect of Demineralized Bone Matrix-Calcium Sulfate with Vancomycin on Calcaneal Fracture Healing and Infection Rates: a Prospective Study. *Foot Ankle Int.* 27 (7), 487–493. doi:10.1177/107110070602700702

Boot, W., Gawlitta, D., Nikkels, P. G. J., Pouran, B., van Rijen, M. H. P., Dhert, W. J. A., et al. (2017). Hyaluronic Acid-Based Hydrogel Coating Does Not Affect Bone Apposition at the Implant Surface in a Rabbit Model. *Clin. Orthop. Relat. Res.* 475 (7), 1911–1919. doi:10.1007/s11999-017-5310-0

Boot, W., Schmid, T., D'Este, M., Guillaume, O., Foster, A., Decosterd, L., et al. (2021). A Hyaluronic Acid Hydrogel Loaded with Gentamicin and Vancomycin Successfully Eradicates Chronic Methicillin-Resistant *Staphylococcus aureus* Orthopedic Infection in a Sheep Model. *Antimicrob. Agents Chemother.* 65 (4), e01840–20. doi:10.1128/AAC.01840-20

Boot, W., Vogely, H. C., Vogely, H., Nikkels, P., Pouran, B., van Rijen, M., et al. (2020). Prophylaxis of Implant-Related Infections by Local Release of Vancomycin from a Hydrogel in Rabbits. *eCM* 39, 108–120. doi:10.22203/eCM.v039a07

Borkhuu, B., Borowski, A., Shah, S. A., Littleton, A. G., Dabney, K. W., and Miller, F. (2008). Antibiotic-loaded Allograft Decreases the Rate of Acute Deep Wound Infection after Spinal Fusion in Cerebral Palsy. *Spine* 33 (21), 2300–2304. doi:10.1097/BRS.0b013e31818786ff

Boyle-Vavra, S., Carey, R. B., and Daum, R. S. (2001). Development of Vancomycin and Lysostaphin Resistance in a Methicillin-Resistant *Staphylococcus aureus* Isolate. *J. Antimicrob. Chemother.* 48 (5), 617–625. doi:10.1093/jac/48.5.617

Burkus, J. K., Gornet, M. F., Dickman, C. A., and Zdeblick, T. A. (2002). Anterior Lumbar Interbody Fusion Using rhBMP-2 with Tapered Interbody Cages. *J. Spinal Disord. Tech.* 15 (5), 337–349. doi:10.1097/00024720-200210000-00001

Byambaa, B., Annabi, N., Yue, K., Trujillo-de Santiago, G., Alvarez, M. M., Jia, W., et al. (2017). Bioprinted Osteogenic and Vasculogenic Patterns for Engineering 3D Bone Tissue. *Adv. Healthc. Mater.* 6 (16), 1700015. doi:10.1002/adhm.201700015

Changez, M., Koul, V., and Dinda, A. K. (2005). Efficacy of Antibiotics-Loaded Interpenetrating Network (IPNs) Hydrogel Based on Poly(acrylic Acid) and Gelatin for Treatment of Experimental Osteomyelitis: *In Vivo* Study. *Biomaterials* 26 (14), 2095–2104. doi:10.1016/j.biomaterials.2004.06.008

Cho, J.-W., Kim, J., Cho, W.-T., Kent, W. T., Kim, H.-J., and Oh, J.-K. (2018). Antibiotic Coated Hinged Threaded Rods in the Treatment of Infected Nonunions and Intramedullary Long Bone Infections. *Injury* 49 (10), 1912–1921. doi:10.1016/j.injury.2018.07.016

Chopra, I. (2007). The Increasing Use of Silver-Based Products as Antimicrobial Agents: a Useful Development or a Cause for Concern? *J. Antimicrob. Chemother.* 59 (4), 587–590. doi:10.1093/jac/dkm006

Chu, H., Yang, W., Sun, L., Cai, S., Yang, R., Liang, W., et al. (2020). 4D Printing: A Review on Recent Progresses. *Micromachines* 11 (9), 796. doi:10.3390/mi11090796

Climo, M. W., Ehlert, K., and Archer, G. L. (2001). Mechanism and Suppression of Lysostaphin Resistance in Oxacillin-Resistant *Staphylococcus aureus*. *Antimicrob. Agents Chemother.* 45 (5), 1431–1437. doi:10.1128/AAC.45.5.1431-1437.2001

Climo, M. W., Patron, R. L., Goldstein, B. P., and Archer, G. L. (1998). Lysostaphin Treatment of Experimental Methicillin-Resistant *Staphylococcus aureus* Aortic Valve Endocarditis. *Antimicrob. Agents Chemother.* 42 (6), 1355–1360. doi:10.1128/AAC.42.6.1355

Cobb, L. H., Park, J., Swanson, E. A., Beard, M. C., McCabe, E. M., Rourke, A. S., et al. (2019). CRISPR-Cas9 Modified Bacteriophage for Treatment of *Staphylococcus aureus* Induced Osteomyelitis and Soft Tissue Infection. *PLoS One* 14 (11), e0220421. doi:10.1371/journal.pone.0220421

Croes, M., Bakhshandeh, S., van Hengel, I. A. J., Lietaert, K., van Kessel, K. P. M., Pouran, B., et al. (2018). Antibacterial and Immunogenic Behavior of Silver Coatings on Additively Manufactured Porous Titanium. *Acta Biomater.* 81, 315–327. doi:10.1016/j.actbio.2018.09.051

Daly, A. C., Critchley, S. E., Rencsok, E. M., and Kelly, D. J. (2016). A Comparison of Different Bioinks for 3D Bioprinting of Fibrocartilage and Hyaline Cartilage. *Biofabrication* 8 (4), 045002. doi:10.1088/1758-5090/8/4/045002

Darouiche, R. O. (2004). Treatment of Infections Associated with Surgical Implants. *N. Engl. J. Med.* 350 (14), 1422–1429. doi:10.1056/NEJMra035415

de Mesy Bentley, K. L., MacDonald, A., Schwarz, E. M., and Oh, I. (2018). Chronic Osteomyelitis with *Staphylococcus aureus* Deformation in Submicron Canaliculi of Osteocytes. *JBJS Case Connector* 8 (1), e8. doi:10.2106/JBJS.CC.17.00154

de Mesy Bentley, K. L., Trombetta, R., Nishitani, K., Bello-Irizarry, S. N., Ninomiya, M., Zhang, L., et al. (2017). Evidence ofStaphylococcus AureusDeformation, Proliferation, and Migration in Canaliculi of Live Cortical Bone in Murine Models of Osteomyelitis. *J. Bone Miner Res.* 32 (5), 985–990. doi:10.1002/jbmr.3055

De Witte, T.-M., Fratila-Apachitei, L. E., Zadpoor, A. A., and Peppas, N. A. (2018). Bone Tissue Engineering via Growth Factor Delivery: from Scaffolds to Complex Matrices. *Regen. Biomater.* 5 (4), 197–211. doi:10.1093/rb/rby013

Dell'Olmo, E., Gaglione, R., Arciello, A., Piccoli, R., Cafaro, V., Di Maro, A., et al. (2021). Transglutaminase-mediated Crosslinking of a Host Defence Peptide Derived from Human Apolipoprotein B and its Effect on the Peptide Antimicrobial Activity. *Biochim. Biophys. Acta (Bba) - Gen. Subjects* 1865 (2), 129803. doi:10.1016/j.bbagen.2020.129803

Drago, L., Boot, W., Dimas, K., Malizos, K., Hänsch, G. M., Stuyck, J., et al. (2014). Does Implant Coating with Antibacterial-Loaded Hydrogel Reduce Bacterial Colonization and Biofilm Formation *In Vitro*? *Clin. Orthop. Relat. Res.* 472 (11), 3311–3323. doi:10.1007/s11999-014-3558-1

Duarte, L., Matte, C. R., Bizarro, C. V., and Ayub, M. A. Z. (2020). Transglutaminases: Part I-Origins, Sources, and Biotechnological Characteristics. *World J. Microbiol. Biotechnol.* 36 (1), 15. doi:10.1007/s11274-019-2791-x

Eltawila, A. M., Hassan, M. N., Safaan, S. M., Abd El-Fattah, A., Zakaria, O., El-Khordagui, L. K., et al. (2021). Local Treatment of Experimental Mandibular Osteomyelitis with an Injectable Biomimetic Gentamicin Hydrogel Using a New Rabbit Model. *J. Biomed. Mater. Res.* 109 (11), 1677–1688. doi:10.1002/jbm.b.34824

Elyasi, S., Khalili, H., Dashti-Khavidaki, S., and Mohammadpour, A. (2012). Vancomycin-induced Nephrotoxicity: Mechanism, Incidence, Risk Factors and Special Populations. A Literature Review. *Eur. J. Clin. Pharmacol.* 68 (9), 1243–1255. doi:10.1007/s00228-012-1259-9

Epand, R. M., and Vogel, H. J. (1999). Diversity of Antimicrobial Peptides and Their Mechanisms of Action. *Biochim. Biophys. Acta* 1462 (1-2), 11–28. doi:10.1016/s0005-2736(99)00198-4

Ferguson, J. Y., Dudareva, M., Riley, N. D., Stubbs, D., Atkins, B. L., and McNally, M. A. (2014). The Use of a Biodegradable Antibiotic-Loaded Calcium Sulphate Carrier Containing Tobramycin for the Treatment of Chronic Osteomyelitis. *Bone Jt. J.* 96-B (6), 829–836. doi:10.1302/0301-620X.96B6.32756

Ferry, T., Batailler, C., Petitjean, C., Chateau, J., Fevre, C., Forestier, E., et al. (2020). The Potential Innovative Use of Bacteriophages within the DAC Hydrogel to Treat Patients with Knee Megaprosthesis Infection Requiring "Debridement Antibiotics and Implant Retention" and Soft Tissue Coverage as Salvage Therapy. *Front. Med.* 7, 342. doi:10.3389/fmed.2020.00342

Forier, K., Raemdonck, K., De Smedt, S. C., Demeester, J., Coenye, T., and Braeckmans, K. (2014). Lipid and Polymer Nanoparticles for Drug Delivery to Bacterial Biofilms. *J. Controlled Release* 190, 607–623. doi:10.1016/j.jconrel.2014.03.055

Foster, A. L., Boot, W., Stenger, V., D'Este, M., Jaiprakash, A., Eglin, D., et al. (2021). Single-stage Revision of MRSA Orthopedic Device-related Infection in Sheep with an Antibiotic-loaded Hydrogel. *J. Orthop. Res.* 39 (2), 438–448. doi:10.1002/jor.24949

Fowler, V. G., Jr., and Proctor, R. A. (2014). Where Does a *Staphylococcus aureus* Vaccine Stand? *Clin. Microbiol. Infect.* 20 (Suppl. 5), 66–75. doi:10.1111/1469-0691.12570

Frutos Cabanillas, P., Díez Peña, E., Barrales-Rienda, J. M., and Frutos, G. (2000). Validation and *In Vitro* Characterization of Antibiotic-Loaded Bone Cement Release. *Int. J. Pharm.* 209 (1-2), 15–26. doi:10.1016/s0378-5173(00)00520-2

Gao, G., Jiang, Y.-W., Jia, H.-R., and Wu, F.-G. (2019). Near-infrared Light-Controllable On-Demand Antibiotics Release Using Thermo-Sensitive Hydrogel-Based Drug Reservoir for Combating Bacterial Infection. *Biomaterials* 188, 83–95. doi:10.1016/j.biomaterials.2018.09.045

Garg, D., Matai, I., and Sachdev, A. (2021). Toward Designing of Anti-infective Hydrogels for Orthopedic Implants: From Lab to Clinic. *ACS Biomater. Sci. Eng.* 7 (6), 1933–1961. doi:10.1021/acsbiomaterials.0c01408

Geredew Kifelew, L., Mitchell, J. G., and Speck, P. (2019). Mini-review: Efficacy of Lytic Bacteriophages on Multispecies Biofilms. *Biofouling* 35 (4), 472–481. doi:10.1080/08927014.2019.1613525

Giavaresi, G., Bertazzoni Minelli, E., Sartori, M., Benini, A., Della Bora, T., Sambri, V., et al. (2012). Microbiological and Pharmacological Tests on New Antibiotic-Loaded PMMA-Based Composites for the Treatment of Osteomyelitis. *J. Orthop. Res.* 30 (3), 348–355. doi:10.1002/jor.21531

Giavaresi, G., Meani, E., Sartori, M., Ferrari, A., Bellini, D., Sacchetta, A. C., et al. (2014). Efficacy of Antibacterial-Loaded Coating in an *In Vivo* Model of Acutely Highly Contaminated Implant. *Int. Orthopaedics (Sicot)* 38 (7), 1505–1512. doi:10.1007/s00264-013-2237-2

Gu, F.-F., Han, L.-Z., Chen, X., Wang, Y.-C., Shen, H., Wang, J.-Q., et al. (2015). Molecular Characterization ofStaphylococcus Aureusfrom Surgical Site Infections in Orthopedic Patients in an Orthopedic Trauma Clinical Medical Center in Shanghai. *Surg. Infections* 16 (1), 97–104. doi:10.1089/sur.2014.027

Guelcher, S. A., Brown, K. V., Li, B., Guda, T., Lee, B.-H., and Wenke, J. C. (2011). Dual-purpose Bone Grafts Improve Healing and Reduce Infection. *J. Orthop. Trauma* 25 (8), 477–482. doi:10.1097/BOT.0b013e31821f624c

Haider, M., Hassan, M. A., Ahmed, I. S., and Shamma, R. (2018). Thermogelling Platform for Baicalin Delivery for Versatile Biomedical Applications. *Mol. Pharmaceutics* 15 (8), 3478–3488. doi:10.1021/acs.molpharmaceut.8b00480

Hake, M. E., Young, H., Hak, D. J., Stahel, P. F., Hammerberg, E. M., and Mauffrey, C. (2015). Local Antibiotic Therapy Strategies in Orthopaedic Trauma: Practical Tips and Tricks and Review of the Literature. *Injury* 46 (8), 1447–1456. doi:10.1016/j.injury.2015.05.008

Han, S. H., Cha, M., Jin, Y.-Z., Lee, K.-M., and Lee, J. H. (2020). BMP-2 and hMSC Dual Delivery onto 3D Printed PLA-Biogel Scaffold for Critical-Size Bone Defect Regeneration in Rabbit Tibia. *Biomed. Mater.* 16 (1), 015019. doi:10.1088/1748-605X/aba879

Hanke, M. L., Heim, C. E., Angle, A., Sanderson, S. D., and Kielian, T. (2013). Targeting Macrophage Activation for the Prevention and Treatment ofStaphylococcus aureusBiofilm Infections. *J.I.* 190 (5), 2159–2168. doi:10.4049/jimmunol.1202348

Hetrick, E. M., and Schoenfisch, M. H. (2006). Reducing Implant-Related Infections: Active Release Strategies. *Chem. Soc. Rev.* 35 (9), 780–789. doi:10.1039/b515219b

Hoang Thi, T. T., Lee, Y., Le Thi, P., and Park, K. D. (2018). Nitric Oxide-Releasing Injectable Hydrogels with High Antibacterial Activity through *In Situ* Formation of Peroxynitrite. *Acta Biomater.* 67, 66–78. doi:10.1016/j.actbio.2017.12.005

Huang, H., Feng, J., Wismeijer, D., Wu, G., and Hunziker, E. (2017). Hyaluronic Acid Promotes the Osteogenesis of BMP-2 in an Absorbable Collagen Sponge. *Polymers* 9 (8), 339. doi:10.3390/polym9080339

Hustedt, J. W., and Blizzard, D. J. (2014). The Controversy Surrounding Bone Morphogenetic Proteins in the Spine: a Review of Current Research. *Yale J. Biol. Med.* 87 (4), 549–561.

Inzana, J. A., Schwarz, E. M., Kates, S. L., and Awad, H. A. (2016). Biomaterials Approaches to Treating Implant-Associated Osteomyelitis. *Biomaterials* 81, 58–71. doi:10.1016/j.biomaterials.2015.12.012

Johnson, C. T., Sok, M. C. P., Martin, K. E., Kalelkar, P. P., Caplin, J. D., Botchwey, E. A., et al. (2019). Lysostaphin and BMP-2 Co-delivery Reduces *S. aureus* Infection and Regenerates Critical-Sized Segmental Bone Defects. *Sci. Adv.* 5 (5), eaaw1228. doi:10.1126/sciadv.aaw1228

Johnson, C. T., Wroe, J. A., Agarwal, R., Martin, K. E., Guldberg, R. E., Donlan, R. M., et al. (2018). Hydrogel Delivery of Lysostaphin Eliminates Orthopedic Implant Infection by *Staphylococcus aureus* and Supports Fracture Healing. *Proc. Natl. Acad. Sci. U.S.A.* 115 (22), E4960–E4969. doi:10.1073/pnas.1801013115

Jung, S. W., Oh, S. H., Lee, I. S., Byun, J.-H., and Lee, J. H. (2019). *In Situ* Gelling Hydrogel with Anti-bacterial Activity and Bone Healing Property for Treatment of Osteomyelitis. *Tissue Eng. Regen. Med.* 16 (5), 479–490. doi:10.1007/s13770-019-00206-x

Junka, A., Szymczyk, P., Ziółkowski, G., Karuga-Kuzniewska, E., Smutnicka, D., Bil-Lula, I., et al. (2017). Bad to the Bone: On *In Vitro* and *Ex Vivo* Microbial Biofilm Ability to Directly Destroy Colonized Bone Surfaces without Participation of Host Immunity or Osteoclastogenesis. *PLoS One* 12 (1), e0169565. doi:10.1371/journal.pone.0169565

Kaplan, S. L. (2014). Recent Lessons for the Management of Bone and Joint Infections. *J. Infect.* 68 (Suppl. 1), S51–S56. doi:10.1016/j.jinf.2013.09.014

Kartika, R. W., Alwi, I., Suyatna, F. D., Yunir, E., Waspadji, S., Immanuel, S., et al. (2021). Wound Healing in Diabetic Foot Ulcer Patients Using Combined Use of Platelet Rich Fibrin and Hyaluronic Acid, Platelet Rich Fibrin and Placebo: An Open Label, Randomized Controlled Trial. *Acta Med. Indones* 53 (3), 268–275.

Kazimierczak, P., Kolmas, J., and Przekora, A. (2019). Biological Response to Macroporous Chitosan-Agarose Bone Scaffolds Comprising Mg- and Zn-Doped Nano-Hydroxyapatite. *Ijms* 20 (15), 3835. doi:10.3390/ijms20153835

Kim, H. N., Jang, K.-J., Shin, J.-Y., Kang, D., Kim, S. M., Koh, I., et al. (2017). Artificial Slanted Nanocilia Array as a Mechanotransducer for Controlling Cell Polarity. *ACS Nano* 11 (1), 730–741. doi:10.1021/acsnano.6b07134

Kim, H. Y., Lee, J. H., Lee, H. A. R., Park, J.-S., Woo, D. K., Lee, H.-C., et al. (2018). Sustained Release of BMP-2 from Porous Particles with Leaf-Stacked Structure for Bone Regeneration. *ACS Appl. Mater. Inter.* 10 (25), 21091–21102. doi:10.1021/acsami.8b02141

Kimna, C., Deger, S., Tamburaci, S., and Tihminlioglu, F. (2019). Chitosan/montmorillonite Composite Nanospheres for Sustained Antibiotic Delivery at post-implantation Bone Infection Treatment. *Biomed. Mater.* 14 (4), 044101. doi:10.1088/1748-605X/ab1a04

Kiri, N., Archer, G., and Climo, M. W. (2002). Combinations of Lysostaphin with β-Lactams Are Synergistic against Oxacillin-Resistant Staphylococcus Epidermidis. *Antimicrob. Agents Chemother.* 46 (6), 2017–2020. doi:10.1128/AAC.46.6.2017-2020.2002

Kondo, N., Ogose, A., Tokunaga, K., Ito, T., Arai, K., Kudo, N., et al. (2005). Bone Formation and Resorption of Highly Purified β-tricalcium Phosphate in the Rat Femoral Condyle. *Biomaterials* 26 (28), 5600–5608. doi:10.1016/j.biomaterials.2005.02.026

Kubin, C. J., Ellman, T. M., Phadke, V., Haynes, L. J., Calfee, D. P., and Yin, M. T. (2012). Incidence and Predictors of Acute Kidney Injury Associated with Intravenous Polymyxin B Therapy. *J. Infect.* 65 (1), 80–87. doi:10.1016/j.jinf.2012.01.015

Kuehn, K.-D., Ege, W., and Gopp, U. (2005). Acrylic Bone Cements: Composition and Properties. *Orthop. Clin. North America* 36 (1), 17–28. doi:10.1016/j.ocl.2004.06.010

Kumar, J. K. (2008). Lysostaphin: an Antistaphylococcal Agent. *Appl. Microbiol. Biotechnol.* 80 (4), 555–561. doi:10.1007/s00253-008-1579-y

Kwak, M., Han, L., Chen, J. J., and Fan, R. (2015). Interfacing Inorganic Nanowire Arrays and Living Cells for Cellular Function Analysis. *Small* 11 (42), 5600–5610. doi:10.1002/smll.201501236

Li, D., Lv, P., Fan, L., Huang, Y., Yang, F., Mei, X., et al. (2017). The Immobilization of Antibiotic-Loaded Polymeric Coatings on Osteoarticular Ti Implants for the Prevention of Bone Infections. *Biomater. Sci.* 5 (11), 2337–2346. doi:10.1039/c7bm00693d

Li, Y., Li, G., Sha, X., Li, L., Zhang, K., Liu, D., et al. (2020a). An Intelligent Vancomycin Release System for Preventing Surgical Site Infections of Bone Tissues. *Biomater. Sci.* 8 (11), 3202–3211. doi:10.1039/d0bm00255k

Li, Y., Liu, X., Li, B., Zheng, Y., Han, Y., Chen, D.-f., et al. (2020b). Near-Infrared Light Triggered Phototherapy and Immunotherapy for Elimination of Methicillin-Resistant *Staphylococcus aureus* Biofilm Infection on Bone Implant. *ACS Nano* 14 (7), 8157–8170. doi:10.1021/acsnano.0c01486

Liu, P., Guo, B., Wang, S., Ding, J., and Zhou, W. (2019). A Thermo-Responsive and Self-Healing Liposome-In-Hydrogel System as an Antitubercular Drug Carrier for Localized Bone Tuberculosis Therapy. *Int. J. Pharmaceutics* 558, 101–109. doi:10.1016/j.ijpharm.2018.12.083

Liu, S., Ji, X.-X., and Zhu, J.-F. (2021). Recent Progress in the Synthesis and Biomedical Properties of Natural Biopolymer Composites. *Cmc* 28, 8243–8266. doi:10.2174/0929867328666201217104038

Lovati, A. B., Drago, L., Bottagisio, M., Bongio, M., Ferrario, M., Perego, S., et al. (20162016). Systemic and Local Administration of Antimicrobial and Cell Therapies to Prevent Methicillin-ResistantStaphylococcus Epidermidis-Induced Femoral Nonunions in a Rat Model. *Mediators Inflamm.* 2016, 1–12. doi:10.1155/2016/9595706

Ma, D., Shanks, R. M. Q., Davis, C. M., 3rd, Craft, D. W., Wood, T. K., Hamlin, B. R., et al. (2018). Viable Bacteria Persist on Antibiotic Spacers Following Two-Stage Revision for Periprosthetic Joint Infection. *J. Orthop. Res.* 36 (1), 452–458. doi:10.1002/jor.23611

Ma, Y., Cortez-Jugo, C., Li, J., Lin, Z., Richardson, R. T., Han, Y., et al. (2019). Engineering Biocoatings to Prolong Drug Release from Supraparticles. *Biomacromolecules* 20 (9), 3425–3434. doi:10.1021/acs.biomac.9b00710

Mah, T.-F. C., and O'Toole, G. A. (2001). Mechanisms of Biofilm Resistance to Antimicrobial Agents. *Trends Microbiol.* 9 (1), 34–39. doi:10.1016/s0966-842x(00)01913-2

Malam, Y., Loizidou, M., and Seifalian, A. M. (2009). Liposomes and Nanoparticles: Nanosized Vehicles for Drug Delivery in Cancer. *Trends Pharmacol. Sci.* 30 (11), 592–599. doi:10.1016/j.tips.2009.08.004

Mas-Moruno, C., Su, B., and Dalby, M. J. (2019). Multifunctional Coatings and Nanotopographies: Toward Cell Instructive and Antibacterial Implants. *Adv. Healthc. Mater.* 8 (1), 1801103. doi:10.1002/adhm.201801103

Masters, E. A., Trombetta, R. P., de Mesy Bentley, K. L., Boyce, B. F., Gill, A. L., Gill, S. R., et al. (2019). Evolving Concepts in Bone Infection: Redefining "biofilm", "acute vs. Chronic Osteomyelitis", "the Immune Proteome" and "local Antibiotic Therapy". *Bone Res.* 7, 20. doi:10.1038/s41413-019-0061-z

May, P. W., Clegg, M., Silva, T. A., Zanin, H., Fatibello-Filho, O., Celorrio, V., et al. (2016). Diamond-coated 'black Silicon' as a Promising Material for High-Surface-Area Electrochemical Electrodes and Antibacterial Surfaces. *J. Mater. Chem. B* 4 (34), 5737–5746. doi:10.1039/c6tb01774f

McCarthy, P. C., Zhang, Y., and Abebe, F. (2021). Recent Applications of Dual-Stimuli Responsive Chitosan Hydrogel Nanocomposites as Drug Delivery Tools. *Molecules* 26 (16), 4735. doi:10.3390/molecules26164735

Meers, P., Neville, M., Malinin, V., Scotto, A. W., Sardaryan, G., Kurumunda, R., et al. (2008). Biofilm Penetration, Triggered Release and *In Vivo* Activity of Inhaled Liposomal Amikacin in Chronic *Pseudomonas aeruginosa* Lung Infections. *J. Antimicrob. Chemother.* 61 (4), 859–868. doi:10.1093/jac/dkn059

Mohamed, M. F., Hamed, M. I., Panitch, A., and Seleem, M. N. (2014). Targeting Methicillin-Resistant *Staphylococcus aureus* with Short Salt-Resistant Synthetic Peptides. *Antimicrob. Agents Chemother.* 58 (7), 4113–4122. doi:10.1128/AAC.02578-14

Naughton, C. A. (2008). Drug-induced Nephrotoxicity. *Am. Fam. Physician* 78 (6), 743–750.

O'Neill, H. S., Herron, C. C., Hastings, C. L., Deckers, R., Lopez Noriega, A., Kelly, H. M., et al. (2017). A Stimuli Responsive Liposome Loaded Hydrogel Provides Flexible On-Demand Release of Therapeutic Agents. *Acta Biomater.* 48, 110–119. doi:10.1016/j.actbio.2016.10.001

Otto, M. (2014). *Staphylococcus aureus* Toxins. *Curr. Opin. Microbiol.* 17, 32–37. doi:10.1016/j.mib.2013.11.004

Otto, M. (2008). Targeted Immunotherapy for Staphylococcal Infections. *BioDrugs* 22 (1), 27–36. doi:10.2165/00063030-200822010-00003

Overstreet, D. J., Badha, V. S., Heffernan, J. M., Childers, E. P., Moore, R. C., Vernon, B. L., et al. (2019). Temperature-responsive PNDJ Hydrogels Provide High and Sustained Antimicrobial Concentrations in Surgical Sites. *Drug Deliv. Transl. Res.* 9 (4), 802–815. doi:10.1007/s13346-019-00630-5

Overstreet, D., McLaren, A., Calara, F., Vernon, B., and McLemore, R. (2015). Local Gentamicin Delivery from Resorbable Viscous Hydrogels Is Therapeutically Effective. *Clin. Orthop. Relat. Res.* 473 (1), 337–347. doi:10.1007/s11999-014-3935-9

Pan, C., Zhou, Z., and Yu, X. (2018). Coatings as the Useful Drug Delivery System for the Prevention of Implant-Related Infections. *J. Orthop. Surg. Res.* 13 (1), 220. doi:10.1186/s13018-018-0930-y

Park, S., Park, H.-H., Sun, K., Gwon, Y., Seong, M., Kim, S., et al. (2019). Hydrogel Nanospike Patch as a Flexible Anti-pathogenic Scaffold for Regulating Stem Cell Behavior. *ACS Nano* 13 (10), 11181–11193. doi:10.1021/acsnano.9b04109

Parry, M. C., and Duncan, C. P. (2014). The challenge of Methicillin Resistant Staphylococcal Infection after Total Hip Replacement. *Bone Jt. J.* 96-B (11 Suppl. A), 60–65. doi:10.1302/0301-620X.96B11.34333

Patron, R. L., Climo, M. W., Goldstein, B. P., and Archer, G. L. (1999). Lysostaphin Treatment of Experimental Aortic Valve Endocarditis Caused by a *Staphylococcus aureus* Isolate with Reduced Susceptibility to Vancomycin. *Antimicrob. Agents Chemother.* 43 (7), 1754–1755. doi:10.1128/AAC.43.7.1754

Pedroza-González, S. C., Rodriguez-Salvador, M., Pérez Benítez, B. E., Alvarez, M. M., and Trujillo-de Santiago, G. (2021). Bioinks for 3D Bioprinting: A Scientometric Analysis of Two Decades of Progress. *Int. J. Bioprint* 7 (2), 333. doi:10.18063/ijb.v7i2.337

Peng, K.-T., Chen, C.-F., Chu, I.-M., Li, Y.-M., Hsu, W.-H., Hsu, R. W.-W., et al. (2010). Treatment of Osteomyelitis with Teicoplanin-Encapsulated Biodegradable Thermosensitive Hydrogel Nanoparticles. *Biomaterials* 31 (19), 5227–5236. doi:10.1016/j.biomaterials.2010.03.027

Penn-Barwell, J. G., Baker, B., and Wenke, J. C. (2015). Local Bismuth Thiols Potentiate Antibiotics and Reduce Infection in a Contaminated Open Fracture Model. *J. Orthop. Trauma* 29 (2), e73–e78. doi:10.1097/BOT.0000000000000171

Petrovic Fabijan, A., Lin, R. C. Y., Ho, J., Maddocks, S., Ben Zakour, N. L., Iredell, J. R., et al. (2020). Safety of Bacteriophage Therapy in Severe *Staphylococcus aureus* Infection. *Nat. Microbiol.* 5 (3), 465–472. doi:10.1038/s41564-019-0634-z

Pitarresi, G., Palumbo, F. S., Calascibetta, F., Fiorica, C., Di Stefano, M., and Giammona, G. (2013). Medicated Hydrogels of Hyaluronic Acid Derivatives for Use in Orthopedic Field. *Int. J. Pharmaceutics* 449 (1-2), 84–94. doi:10.1016/j.ijpharm.2013.03.059

Pogodin, S., Hasan, J., Baulin, V. A., Webb, H. K., Truong, V. K., Phong Nguyen, T. H., et al. (2013). Biophysical Model of Bacterial Cell Interactions with Nanopatterned Cicada wing Surfaces. *Biophysical J.* 104 (4), 835–840. doi:10.1016/j.bpj.2012.12.046

Poudineh, M., Wang, Z., Labib, M., Ahmadi, M., Zhang, L., Das, J., et al. (2018). Three-Dimensional Nanostructured Architectures Enable Efficient Neural Differentiation of Mesenchymal Stem Cells via Mechanotransduction. *Nano Lett.* 18 (11), 7188–7193. doi:10.1021/acs.nanolett.8b03313

Prokopovich, P., Perni, R., Leech, R., Carmalt, I. P., and Parkin, S. (2013). A Novel Bone Cement Impregnated with Silver–tiopronin Nanoparticles: its Antimicrobial, Cytotoxic, and Mechanical Properties. *Ijn* 8, 2227–2237. doi:10.2147/IJN.S42822

Pulido, L., Ghanem, E., Joshi, A., Purtill, J. J., and Parvizi, J. (2008). Periprosthetic Joint Infection: the Incidence, Timing, and Predisposing Factors. *Clin. Orthop. Relat. Res.* 466 (7), 1710–1715. doi:10.1007/s11999-008-0209-4

Putnam, N. E., Fulbright, L. E., Curry, J. M., Ford, C. A., Petronglo, J. R., Hendrix, A. S., et al. (2019). MyD88 and IL-1R Signaling Drive Antibacterial Immunity and Osteoclast-Driven Bone Loss during *Staphylococcus aureus* Osteomyelitis. *Plos Pathog.* 15 (4), e1007744. doi:10.1371/journal.ppat.1007744

Raafat, D., von Bargen, K., Haas, A., and Sahl, H.-G. (2008). Insights into the Mode of Action of Chitosan as an Antibacterial Compound. *Appl. Environ. Microbiol.* 74 (12), 3764–3773. doi:10.1128/AEM.00453-08

Radovic-Moreno, A. F., Lu, T. K., Puscasu, V. A., Yoon, C. J., Langer, R., and Farokhzad, O. C. (2012). Surface Charge-Switching Polymeric Nanoparticles for Bacterial Cell wall-targeted Delivery of Antibiotics. *ACS Nano* 6 (5), 4279–4287. doi:10.1021/nn3008383

Redlich, K., and Smolen, J. S. (2012). Inflammatory Bone Loss: Pathogenesis and Therapeutic Intervention. *Nat. Rev. Drug Discov.* 11 (3), 234–250. doi:10.1038/nrd3669

Rhoads, D. D., Wolcott, R. D., Kuskowski, M. A., Wolcott, B. M., Ward, L. S., and Sulakvelidze, A. (2009). Bacteriophage Therapy of Venous Leg Ulcers in Humans: Results of a Phase I Safety Trial. *J. Wound Care* 18 (6), 237–243. doi:10.12968/jowc.2009.18.6.42801

Ricciardi, B. F., Muthukrishnan, G., Masters, E., Ninomiya, M., Lee, C. C., and Schwarz, E. M. (2018). *Staphylococcus aureus* Evasion of Host Immunity in the Setting of Prosthetic Joint Infection: Biofilm and beyond. *Curr. Rev. Musculoskelet. Med.* 11 (3), 389–400. doi:10.1007/s12178-018-9501-4

Roca, I., Akova, M., Baquero, F., Carlet, J., Cavaleri, M., Coenen, S., et al. (2015). The Global Threat of Antimicrobial Resistance: Science for Intervention. *New Microbes and New Infections* 6, 22–29. doi:10.1016/j.nmni.2015.02.007

Romanò, C. L., Logoluso, N., Meani, E., Romanò, D., De Vecchi, E., Vassena, C., et al. (2014). A Comparative Study of the Use of Bioactive Glass S53P4 and Antibiotic-Loaded Calcium-Based Bone Substitutes in the Treatment of Chronic Osteomyelitis. *Bone Jt. J.* 96-B (6), 845–850. doi:10.1302/0301-620X.96B6.33014

Rouha, H., Badarau, A., Visram, Z. C., Battles, M. B., Prinz, B., Magyarics, Z., et al. (2015). Five Birds, One Stone: Neutralization of α-hemolysin and 4 Bi-component Leukocidins of *Staphylococcus aureus* with a Single Human Monoclonal Antibody. *MAbs* 7 (1), 243–254. doi:10.4161/19420862.2014.985132

Ruan, H., Yu, Y., Liu, Y., Ding, X., Guo, X., and Jiang, Q. (2016). Preparation and Characteristics of Thermoresponsive Gel of Minocycline Hydrochloride and Evaluation of its Effect on Experimental Periodontitis Models. *Drug Deliv.* 23 (2), 525–531. doi:10.3109/10717544.2014.929195

Rupprecht, S., Petrovic, L., Burchhardt, B., Wiltfang, J., Neukam, F. W., and Schlegel, K. A. (2007). Antibiotic-containing Collagen for the Treatment of Bone Defects. *J. Biomed. Mater. Res.* 83B (2), 314–319. doi:10.1002/jbm.b.30797

Sarigol-Calamak, E., and Hascicek, C. (2018). Tissue Scaffolds as a Local Drug Delivery System for Bone Regeneration. *Adv. Exp. Med. Biol.* 1078, 475–493. doi:10.1007/978-981-13-0950-2_25

Sarker, S. A., McCallin, S., Barretto, C., Berger, B., Pittet, A.-C., Sultana, S., et al. (2012). Oral T4-like Phage Cocktail Application to Healthy Adult Volunteers from Bangladesh. *Virology* 434 (2), 222–232. doi:10.1016/j.virol.2012.09.002

Savage, V. J., Chopra, I., and O'Neill, A. J. (2013). *Staphylococcus aureus* Biofilms Promote Horizontal Transfer of Antibiotic Resistance. *Antimicrob. Agents Chemother.* 57 (4), 1968–1970. doi:10.1128/AAC.02008-12

Schindler, C. A., and Schuhardt, V. T. (1964). Lysostaphin: A New Bacteriolytic Agent for the Staphylococcus. *Proc. Natl. Acad. Sci. U.S.A.* 51, 414–421. doi:10.1073/pnas.51.3.414

Schwarz, E. M., Parvizi, J., Gehrke, T., Aiyer, A., Battenberg, A., Brown, S. A., et al. (2019). 2018 International Consensus Meeting on Musculoskeletal Infection: Research Priorities from the General Assembly Questions. *J. Orthop. Res.* 37 (5), 997–1006. doi:10.1002/jor.24293

Sedghizadeh, P. P., Sun, S., Junka, A. F., Richard, E., Sadrerafi, K., Mahabady, S., et al. (2017). Design, Synthesis, and Antimicrobial Evaluation of a Novel Bone-Targeting Bisphosphonate-Ciprofloxacin Conjugate for the Treatment of Osteomyelitis Biofilms. *J. Med. Chem.* 60 (6), 2326–2343. doi:10.1021/acs.jmedchem.6b01615

Sendi, P., Rohrbach, M., Graber, P., Frei, R., Ochsner, P. E., and Zimmerli, W. (2006). Staphylococcus aureusSmall Colony Variants in Prosthetic Joint Infection. *Clin. Infect. Dis.* 43 (8), 961–967. doi:10.1086/507633

Shekaran, A., García, J. R., Clark, A. Y., Kavanaugh, T. E., Lin, A. S., Guldberg, R. E., et al. (2014). Bone Regeneration Using an Alpha 2 Beta 1 Integrin-specific Hydrogel as a BMP-2 Delivery Vehicle. *Biomaterials* 35 (21), 5453–5461. doi:10.1016/j.biomaterials.2014.03.055

Sileika, T. S., Kim, H.-D., Maniak, P., and Messersmith, P. B. (2011). Antibacterial Performance of Polydopamine-Modified Polymer Surfaces Containing Passive and Active Components. *ACS Appl. Mater. Inter.* 3 (12), 4602–4610. doi:10.1021/am200978h

Silverman, L. D., Lukashova, L., Herman, O. T., Lane, J. M., and Boskey, A. L. (2007). Release of Gentamicin from a Tricalcium Phosphate Bone Implant. *J. Orthop. Res.* 25 (1), 23–29. doi:10.1002/jor.20284

Slaughter, B. V., Khurshid, S. S., Fisher, O. Z., Khademhosseini, A., and Peppas, N. A. (2009). Hydrogels in Regenerative Medicine. *Adv. Mater.* 21 (32-33), 3307–3329. doi:10.1002/adma.200802106

Spicer, P. P., Shah, S. R., Henslee, A. M., Watson, B. M., Kinard, L. A., Kretlow, J. D., et al. (2013). Evaluation of Antibiotic Releasing Porous Polymethylmethacrylate Space Maintainers in an Infected Composite Tissue Defect Model. *Acta Biomater.* 9 (11), 8832–8839. doi:10.1016/j.actbio.2013.07.018

Sun, C.-K., Ke, C.-J., Lin, Y.-W., Lin, F.-H., Tsai, T.-H., and Sun, J.-S. (2021). Transglutaminase Cross-Linked Gelatin-Alginate-Antibacterial Hydrogel as the Drug Delivery-Coatings for Implant-Related Infections. *Polymers* 13 (3), 414. doi:10.3390/polym13030414

Sun, K., Lin, H., Tang, Y., Xiang, S., Xue, J., Yin, W., et al. (2020). Injectable BMP-2 Gene-Activated Scaffold for the Repair of Cranial Bone Defect in Mice. *Stem Cell Transl Med* 9 (12), 1631–1642. doi:10.1002/sctm.19-0315

Suzuki, A., Terai, H., Toyoda, H., Namikawa, T., Yokota, Y., Tsunoda, T., et al. (2006). A Biodegradable Delivery System for Antibiotics and Recombinant Human Bone Morphogenetic Protein-2: A Potential Treatment for Infected Bone Defects. *J. Orthop. Res.* 24 (3), 327–332. doi:10.1002/jor.20049

Sweere, J. M., Van Belleghem, J. D., Ishak, H., Bach, M. S., Popescu, M., Sunkari, V., et al. (2019). Bacteriophage Trigger Antiviral Immunity and Prevent Clearance of Bacterial Infection. *Science* 363 (6434). doi:10.1126/science.aat9691

Tan, H., Ma, R., Lin, C., Liu, Z., and Tang, T. (2013). Quaternized Chitosan as an Antimicrobial Agent: Antimicrobial Activity, Mechanism of Action and Biomedical Applications in Orthopedics. *Ijms* 14 (1), 1854–1869. doi:10.3390/ijms14011854

Tao, F., Cheng, Y., Shi, X., Zheng, H., Du, Y., Xiang, W., et al. (2020). Applications of Chitin and Chitosan Nanofibers in Bone Regenerative Engineering. *Carbohydr. Polym.* 230, 115658. doi:10.1016/j.carbpol.2019.115658

Tao, F., Ma, S., Tao, H., Jin, L., Luo, Y., Zheng, J., et al. (2021). Chitosan-based Drug Delivery Systems: From Synthesis Strategy to Osteomyelitis Treatment - A Review. *Carbohydr. Polym.* 251, 117063. doi:10.1016/j.carbpol.2020.117063

Tao, J., Zhang, Y., Shen, A., Yang, Y., Diao, L., Wang, L., et al. (2020). Injectable Chitosan-Based Thermosensitive Hydrogel/Nanoparticle-Loaded System for Local Delivery of Vancomycin in the Treatment of Osteomyelitis. *Ijn* Vol. 15, 5855–5871. doi:10.2147/IJN.S247088

Teo, E. Y., Ong, S.-Y., Khoon Chong, M. S., Zhang, Z., Lu, J., Moochhala, S., et al. (2011). Polycaprolactone-based Fused Deposition Modeled Mesh for Delivery of Antibacterial Agents to Infected Wounds. *Biomaterials* 32 (1), 279–287. doi:10.1016/j.biomaterials.2010.08.089

Ter Boo, G.-J. A., Arens, D., Metsemakers, W.-J., Zeiter, S., Richards, R. G., Grijpma, D. W., et al. (2016). Injectable Gentamicin-Loaded Thermo-Responsive Hyaluronic Acid Derivative Prevents Infection in a Rabbit Model. *Acta Biomater.* 43, 185–194. doi:10.1016/j.actbio.2016.07.029

Ter Boo, G.-J. A., Grijpma, D. W., Moriarty, T. F., Richards, R. G., and Eglin, D. (2015). Antimicrobial Delivery Systems for Local Infection Prophylaxis in Orthopedic- and Trauma Surgery. *Biomaterials* 52, 113–125. doi:10.1016/j.biomaterials.2015.02.020

Ter Boo, G.-J., Schmid, T., Schmid, T., Zderic, I., Nehrbass, D., Camenisch, K., et al. (2018). Local Application of a Gentamicin-Loaded Thermo-Responsive Hydrogel Allows for Fracture Healing upon Clearance of a High *Staphylococcus aureus* Load in a Rabbit Model. *eCM* 35, 151–164. doi:10.22203/eCM.v035a11

Thammavongsa, V., Rauch, S., Kim, H. K., Missiakas, D. M., and Schneewind, O. (2015). Protein A-Neutralizing Monoclonal Antibody Protects Neonatal Mice against *Staphylococcus aureus*. *Vaccine* 33 (4), 523–526. doi:10.1016/j.vaccine.2014.11.051

Thomas, D., O'Brien, T., and Pandit, A. (2018). Toward Customized Extracellular Niche Engineering: Progress in Cell-Entrapment Technologies. *Adv. Mater.* 30 (1), 1703948. doi:10.1002/adma.201703948

Trombetta, R. P., Dunman, P. M., Schwarz, E. M., Kates, S. L., and Awad, H. A. (2018). A High-Throughput Screening Approach to Repurpose FDA-Approved Drugs for Bactericidal Applications against *Staphylococcus aureus* Small-Colony Variants. *mSphere* 3 (5), e00422–18. doi:10.1128/mSphere.00422-18

Tuchscherr, L., Heitmann, V., Hussain, M., Viemann, D., Roth, J., von Eiff, C., et al. (2010). Staphylococcus aureusSmall-Colony Variants Are Adapted Phenotypes for Intracellular Persistence. *J. Infect. Dis.* 202 (7), 1031–1040. doi:10.1086/656047

Vallejo Diaz, A., Deimling, C., Morgenstern, M., D'Este, M., Puetzler, J., Zeiter, S., et al. (2020). Local Application of a Gentamicin-Loaded Hydrogel Early after Injury Is Superior to Perioperative Systemic Prophylaxis in a Rabbit Open Fracture Model. *J. Orthop. Trauma* 34 (5), 231–237. doi:10.1097/BOT.0000000000001707

Varshney, A. K., Kuzmicheva, G. A., Lin, J., Sunley, K. M., Bowling, R. A., Jr., Kwan, T.-Y., et al. (2018). A Natural Human Monoclonal Antibody Targeting Staphylococcus Protein A Protects against *Staphylococcus aureus* Bacteremia. *PLoS One* 13 (1), e0190537. doi:10.1371/journal.pone.0190537

Wafa, H., Grimer, R. J., Reddy, K., Jeys, L., Abudu, A., Carter, S. R., et al. (2015). Retrospective Evaluation of the Incidence of Early Periprosthetic Infection with Silver-Treated Endoprostheses in High-Risk Patients. *Bone Jt. J.* 97-B (2), 252–257. doi:10.1302/0301-620X.97B2.34554

Walter, G., Kemmerer, M., Kappler, C., and Hoffmann, R. (2012). Treatment Algorithms for Chronic Osteomyelitis. *Dtsch Arztebl Int.* 109 (14), 257–264. doi:10.3238/arztebl.2012.0257

Wang, M., and Tang, T. (2019). Surface Treatment Strategies to Combat Implant-Related Infection from the Beginning. *J. Orthopaedic Translation* 17, 42–54. doi:10.1016/j.jot.2018.09.001

Wang, T., Liu, X., Zhu, Y., Cui, Z. D., Yang, X. J., Pan, H., et al. (2017). Metal Ion Coordination Polymer-Capped pH-Triggered Drug Release System on Titania Nanotubes for Enhancing Self-Antibacterial Capability of Ti Implants. *ACS Biomater. Sci. Eng.* 3 (5), 816–825. doi:10.1021/acsbiomaterials.7b00103

Weber, F. A., and Lautenbach, E. E. G. (1986). Revision of Infected Total Hip Arthroplasty. *Clin. Orthopaedics Relat. Res.* 211, 108–115. doi:10.1097/00003086-198610000-00015

Wolcott, R. D., Rhoads, D. D., and Dowd, S. E. (2008). Biofilms and Chronic Wound Inflammation. *J. Wound Care* 17 (8), 333–341. doi:10.12968/jowc.2008.17.8.30796

Wroe, J. A., Johnson, C. T., and García, A. J. (2020). Bacteriophage Delivering Hydrogels Reduce Biofilm Formation *In Vitro* and Infection *In Vivo*. *J. Biomed. Mater. Res.* 108 (1), 39–49. doi:10.1002/jbm.a.36790

Wu, J. A., Kusuma, C., Mond, J. J., and Kokai-Kun, J. F. (2003). Lysostaphin Disrupts *Staphylococcus aureus* and Staphylococcus Epidermidis Biofilms on Artificial Surfaces. *Antimicrob. Agents Chemother.* 47 (11), 3407–3414. doi:10.1128/AAC.47.11.3407-3414.2003

Wu, T., Zhang, Q., Ren, W., Yi, X., Zhou, Z., Peng, X., et al. (2013). Controlled Release of Gentamicin from Gelatin/genipin Reinforced Beta-Tricalcium Phosphate Scaffold for the Treatment of Osteomyelitis. *J. Mater. Chem. B* 1 (26), 3304–3313. doi:10.1039/c3tb20261e

Xiu, Z.-M., Ma, J., and Alvarez, P. J. J. (2011). Differential Effect of Common Ligands and Molecular Oxygen on Antimicrobial Activity of Silver Nanoparticles versus Silver Ions. *Environ. Sci. Technol.* 45 (20), 9003–9008. doi:10.1021/es201918f

Xu, H., Zhang, G., Xu, K., Wang, L., Yu, L., Xing, M. M. Q., et al. (2018). Mussel-inspired Dual-Functional PEG Hydrogel Inducing Mineralization and Inhibiting Infection in Maxillary Bone Reconstruction. *Mater. Sci. Eng. C* 90, 379–386. doi:10.1016/j.msec.2018.04.066

Yang, G., Huang, T., Wang, Y., Wang, H., Li, Y., Yu, K., et al. (2018). Sustained Release of Antimicrobial Peptide from Self-Assembling Hydrogel Enhanced Osteogenesis. *J. Biomater. Sci. Polym. Edition* 29 (15), 1812–1824. doi:10.1080/09205063.2018.1504191

Yang, T., Zelikin, A. N., and Chandrawati, R. (2018). Progress and Promise of Nitric Oxide-Releasing Platforms. *Adv. Sci.* 5 (6), 1701043. doi:10.1002/advs.201701043

Yilmaz, C., Colak, M., Yilmaz, B. C., Ersoz, G., Kutateladze, M., and Gozlugol, M. (2013). Bacteriophage Therapy in Implant-Related Infections. *The J. Bone Jt. Surgery-American Volume* 95 (2), 117–125. doi:10.2106/JBJS.K.01135

Yoshii, E. (1997). Cytotoxic Effects of Acrylates and Methacrylates: Relationships of Monomer Structures and Cytotoxicity. *J. Biomed. Mater. Res.* 37 (4), 517–524. doi:10.1002/(sici)1097-4636(19971215)37:4<517::aid-jbm10>3.0.co;2-5

You, F., Eames, B. F., and Chen, X. (2017). Application of Extrusion-Based Hydrogel Bioprinting for Cartilage Tissue Engineering. *Ijms* 18 (7), 1597. doi:10.3390/ijms18071597

Zasloff, M. (2002). Antimicrobial Peptides of Multicellular Organisms. *Nature* 415 (6870), 389–395. doi:10.1038/415389a

Zhang, L., Gu, F., Chan, J., Wang, A., Langer, R., and Farokhzad, O. (2008). Nanoparticles in Medicine: Therapeutic Applications and Developments. *Clin. Pharmacol. Ther.* 83 (5), 761–769. doi:10.1038/sj.clpt.6100400

Zhang, Y., Zheng, Y., Shu, F., Zhou, R., Bao, B., Xiao, S., et al. (2022). In Situ-formed Adhesive Hyaluronic Acid Hydrogel with Prolonged Amnion-Derived Conditioned Medium Release for Diabetic Wound Repair. *Carbohydr. Polym.* 276, 118752. doi:10.1016/j.carbpol.2021.118752

Zhou, Y.-Z., Cao, Y., Liu, W., Chu, C. H., and Li, Q.-L. (2012). Polydopamine-induced Tooth Remineralization. *ACS Appl. Mater. Inter.* 4 (12), 6901–6910. doi:10.1021/am302041b

Zoccali, C., Scoccianti, G., Biagini, R., Daolio, P. A., Giardina, F. L., and Campanacci, D. A. (2021). Antibacterial Hydrogel Coating in Joint Mega-Prosthesis: Results of a Comparative Series. *Eur. J. Orthop. Surg. Traumatol.* 31 (8), 1647–1655. doi:10.1007/s00590-021-02884-7

Zununi Vahed, S., Salehi, R., Davaran, S., and Sharifi, S. (2017). Liposome-based Drug Co-delivery Systems in Cancer Cells. *Mater. Sci. Eng. C* 71, 1327–1341. doi:10.1016/j.msec.2016.11.073

**Conflict of Interest:** The authors declare that the research was conducted in the absence of any commercial or financial relationships that could be construed as a potential conflict of interest.

**Publisher's Note:** All claims expressed in this article are solely those of the authors and do not necessarily represent those of their affiliated organizations, or those of the publisher, the editors and the reviewers. Any product that may be evaluated in this article, or claim that may be made by its manufacturer, is not guaranteed or endorsed by the publisher.

frontiers | Frontiers in Bioengineering and Biotechnology

ORIGINAL RESEARCH
published: 13 May 2022
doi: 10.3389/fbioe.2022.845345

# Highly Water-Absorptive and Antibacterial Hydrogel Dressings for Rapid Postoperative Detumescence

*Yuan Fang[1,2], Haibo Li[1,2], Jingting Chen[1], Yao Xiong[1], Xu Li[2], Jianda Zhou[2], Shengli Li[1], Shoubao Wang[1]* and Binbin Sun[3,4]**

[1]Department of Plastic and Reconstructive Surgery, Shanghai Ninth People's Hospital, Shanghai Jiao Tong University School of Medicine, Shanghai, China, [2]Department of Plastic Surgery, The Third Xiangya Hospital, Central South University, Changsha, China, [3]Department of Orthopaedics, Shanghai Ninth People's Hospital, Shanghai Jiao Tong University School of Medicine, Shanghai, China, [4]Collage of Biological Science and Medical Engineering, Donghua University, Shanghai, China

Postoperative wound edema, infection, and pain burden the patient's life. Therefore, the purpose of this study is to develop an effective antibacterial, multifunctional application to prevent postoperative edema and relieve postoperative pain by making full use of the dehydrating and analgesic effects of magnesium sulfate ($MgSO_4$), magnesium oxide (MgO), sodium alginate (SA), and sodium carboxymethyl cellulose (Na-CMC) to make a composite hydrogel, which can promote postoperative detumescence. $MgSO_4$/MgO/SA/Na-CMC composite hydrogel dressings have outstanding mechanical properties, high water absorption, and good biocompatibility. MgO endows the hydrogel dressing with excellent antibacterial properties and better antibacterial activity against common bacteria and multidrug-resistant bacteria. In addition, $MgSO_4$/MgO/SA/Na-CMC hydrogel dressing shows superior dehydration and analgesic properties in the postoperative nude mice model. This study shows that the multifunctional $MgSO_4$/MgO/SA/Na-CMC composite hydrogel dressing developed as a surgical incision dressing has broad prospects in the prevention of incision infection, postoperative edema, and analgesia.

**Keywords: hydrogel, detumescence, antibacterial, $MgSO_4$, MgO**

OPEN ACCESS

***Edited by:***
*Sushila Maharjan, Brigham and Women's Hospital and Harvard Medical School, United States*

***Reviewed by:***
*Mojgan Heydari, Materials and Energy Research Center, Iran*
*Kyung Min Park, Incheon National University, South Korea*
*Ilker Bayer, Italian Institute of Technology (IIT), Italy*

****Correspondence:***
*Binbin Sun*
*sunbinbin1992@163.com*
*Shoubao Wang*
*wxldragon198418@163.com*

***Specialty section:***
*This article was submitted to Biomaterials, a section of the journal Frontiers in Bioengineering and Biotechnology*

***Received:*** *29 December 2021*
***Accepted:*** *23 March 2022*
***Published:*** *13 May 2022*

***Citation:***
*Fang Y, Li H, Chen J, Xiong Y, Li X, Zhou J, Li S, Wang S and Sun B (2022) Highly Water-Absorptive and Antibacterial Hydrogel Dressings for Rapid Postoperative Detumescence. Front. Bioeng. Biotechnol. 10:845345. doi: 10.3389/fbioe.2022.845345*

## INTRODUCTION

A postoperative incision is usually accompanied by complications such as edema and infection, which are significant problems for patients and medical staff (Maheshwer et al., 2021). Especially in plastic surgery, patients have obvious facial edema after the operation, which significantly affects their life and work. Effective incision management after the operation can not only reduce complications and human and material costs but also achieve rapid recovery and reduce unnecessary troubles to life and work caused by surgical complications (El Hosary et al., 2020).

Because of their soft texture and viscosity, hydrogels have been very popular with researchers in recent years (Singh et al., 2013; Bayer, 2021; Cheng et al., 2021; Guimaraes et al., 2021). Hydrogels are ideal dressings with biocompatibility. At the same time, it can be used and replaced according to the needs of patients. This not only reduces the inconvenience of repeated medical treatment after an operation but also reduces the workload of doctors. Because hydrogels are more commonly used as postoperative dressings, at present, many studies reported that hydrogel dressings can achieve bacteriostatic effects or provide the best pH value to promote wound healing (Cheng et al., 2021; Fan et al., 2021; Liang et al., 2021). At present, the clinical hydrogel material used for postoperative

**TABLE 1 |** The composition list of $MgSO_4$/MgO/SA/Na-CMC composite hydrogels.

| | Ctrl | Mg10 | Mg20 | Mg30 | Mg40 |
|---|---|---|---|---|---|
| $ddH_2O$ (ml) | 9.0 | 9.0 | 9.0 | 9.0 | 9.0 |
| Glycerol (ml) | 1.0 | 1.0 | 1.0 | 1.0 | 1.0 |
| Mg (%) | 0.0 | 10.0 | 20.0 | 30.0 | 40.0 |
| SA (g) | 0.5 | 0.5 | 0.5 | 0.5 | 0.5 |
| Na-CMC (g) | 0.5 | 0.5 | 0.5 | 0.5 | 0.5 |

incision edema is "cold compress." The principle of cold compress is only to promote vasoconstriction and reduce postoperative swelling. This solution has obvious limitations: first, only relying on physical cooling to reduce swelling has a limited effect; and second, the postoperative incision is still at risk of infection. Few dressings focus on the needs of plastic surgery for detumescence, anti-infection, and pain. To avoid postoperative edema and infection, the hydrogel dressings we studied should have good water absorption and antibacterial ability.

It is well known that oral magnesium sulfate ($MgSO_4$) forms a hypertonic environment in the intestine and has the function of catharsis (Krenzelok et al., 1985). Magnesium oxide (MgO) also has an antibacterial effect (Muniz Diaz et al., 2021; Wang et al., 2021). Although some researchers have added antibiotics to the dressing to achieve antibacterial effect, it will lead to bacterial resistance (Fischbach and Walsh, 2009). We may solve this issue by directly including MgO, a material with antibacterial activity, into the dressing. At present, hydrogel technology based on sodium alginate (SA) and sodium carboxymethyl cellulose (Na-CMC) has been very mature, which can carry drugs for the treatment of related diseases (Sheng et al., 2021). Therefore, it is feasible for us to add $MgSO_4$/MgO into hydrogels. In this dressing, we used $MgSO_4$ with water absorption and MgO with antibacterial effect. According to the already mature SA/Na-CMC hydrogel preparation technology, combined with $MgSO_4$ and MgO, a new dressing was prepared. This dressing had both absorptive and antibacterial hydrogel dressing and could accelerate wound detumescence after operation. It is very valuable in clinical application.

To this end, we mixed $MgSO_4$, MgO, SA, and Na-CMC in a certain proportion to prepare hydrogels with high water absorption and antibacterial effects. We evaluated the appearance of $MgSO_4$/MgO/SA/Na-CMC composite hydrogel dressings by gross characterization. The internal structure of the hydrogels was examined by scanning electron microscopy. The swelling ratio of the hydrogels was used to assess the water absorbency of hydrogel dressings. After HaCaT cells were co-cultured with the hydrogel extract for a period of time, the biocompatibility of the hydrogel dressing was evaluated by live/dead staining. The antibacterial activity of hydrogel dressings was tested by bacteriostasis experiments of *Escherichia coli* and *Staphylococcus aureus*. The surgical incision edema model was used to detect the swelling effect of hydrogels *in vivo*.

# MATERIALS AND METHODS

## Materials

Sodium alginate (SA), magnesium sulfate ($MgSO_4$), magnesium oxide (MgO), sodium carboxymethyl cellulose (Na-CMC), and glycerol were purchased from Shanghai Aladdin Biochemical Technology Co., Ltd.

## Hydrogel Preparation

We used the dosage of materials listed in **Table 1** and added each material to prepare the composite hydrogels. At room temperature, 1 ml glycerol was added to 9 ml double-distilled $H_2O$ (dd $H_2O$). At 25°C, $MgSO_4$ and MgO ($MgSO_4$: MgO = 99:1 w/w) powders of different weights were separately added to the aforementioned solution and stirred for 30 min. After adding SA and Na-CMC successively, the solution was stirred in a 65°C constant temperature water bath for 6 h. The thicker liquid was added to the abrasives and placed in the 4°C refrigerator for preservation in subsequent experiments.

## Morphological Assay

The appearance of these five groups of hydrogels was photographed with digital cameras. The prepared $MgSO_4$/MgO/SA/Na-CMC hydrogel dressings were freeze-dried for 48 h at −80°C. The samples were cut with a small blade and placed on the scaffold. The internal morphology of the hydrogels was observed by scanning electron microscopy (SEM).

## Mechanical Properties

The mechanical properties of these five groups of hydrogels were tested using the HY-940FS universal testing machine (Shanghai, China) at room temperature. The prepared $MgSO_4$/MgO/SA/Na-CMC hydrogel dressings were compressed to 50% deformation under wet conditions. The strain–stress curve was obtained and the compression modulus was calculated.

## Swelling Rate Determination

The purpose of the swelling test is to evaluate the ability of materials to absorb solvents. We used $ddH_2O$ as the experimental solvent. We calculated the swelling rate in the dry and wet states. First, the prepared hydrogel block (d = 1 cm) was freeze-dried at −80°C for 48 h. The weight of the freeze-dried sample ($W_0$) was measured. Then, the gel was soaked in 25°C $ddH_2O$ and weighed once every 5 min. Before weighing, the excess water was removed from the sample surface with a filter paper, and the recorded value was $W_t$. This was continued until the weight remained constant. Second, the swelling capacity of wet hydrogels is measured. The back skin of mice was intercepted. The prepared hydrogels with a diameter of 1 cm were weighed and recorded as $W_0$. Mice skin was placed on the cell strainer (biosharp, BS-100-CS), infiltrated in $ddH_2O$, and five groups of hydrogels were placed on the top of each

group, with three repeated experiments in each group. The weight $W_t$ was recorded every 2 h until the weight was constant.

The swelling rate (SR) was calculated by the following formula:

$$SR(\%) = \frac{W_t - W_0}{W_0} \times 100\%.$$

Among them, ($W_t$) is the weight of the swelling hydrogel at the time (T) and ($W_0$) is the initial weight of the sample. For each group of three samples, the average value and mean square error are calculated to minimize the error.

## Biocompatibility

The synthesized epidermal cells (HaCaT cells) were cultivated in the hydrogel extract, and the state of the cells was determined using live/dead staining assay to assess the hydrogel's biocompatibility. The HaCaT cells were inoculated in 24-well plates and incubated in a humidified incubator at 37°C and 5% $CO^2$ for three days. The sterilized hydrogels were soaked in sterile PBS for 48 h. Then, 100 ul of the net extract soaked for 48 h was absorbed and co-cultured with 900 ul medium for 24 h. Then, 100 ul of the net extract soaked for 48 h was absorbed, and the cells were co-cultured with 900 ul medium for 48 h. The stained cells were observed under a fluorescence microscope. Living cells absorb calcein AM and emit green fluorescence, while PI enters dead cells and emits red fluorescence after binding with DNA.

## Antibacterial Activity Evaluation

We used common *Escherichia coli* (ATCC 8739) and *Staphylococcus aureus* (ATCC 6538) to carry out the antibacterial activity on the surface of the hydrogel dressing. The hydrogel dressings were placed on an agar plate (petri dish) and incubated for 72 h at 37°C The diameter of the bacteriostasis circle on the agar plate (petri dish) was calculated. Each cycle was repeated three times and the average value was calculated.

## Animals

Male BALB/c nude mice aged 6–8 weeks were purchased from Shanghai Jie SiJieLaboratory Animal Co., Ltd. All animals involved were treated according to the protocol evaluated and approved by the Ethics Committee of the Ninth People's Hospital, affiliated to Shanghai Jiao Tong University School of Medicine. The mice were randomly divided into five groups with three mice in each group. The experiment was repeated with an intraperitoneal injection of anesthesia. Normal saline containing DAPI fluorescence staining was injected into the subcutaneous soft tissue. After soft tissue swelling of the extremities, the prepared hydrogel was clung to the skin surface. Hydrogels were extracted 4–6 h later. A fluorescent microscope was used to observe whether there was fluorescence in the hydrogel. By observing the swelling of the extremities in nude mice, we could see if the hydrogel was effective.

## Statistical Analysis

All experiments had three groups of repeated control, and the mean ± SD data ($n$ = 3) were expressed. The analysis was performed by ANOVA (one-way analysis of variance) test. Student's t-test was used to compare the two groups. $P \leq 0.05$ was considered statistically significant.

# RESULTS AND DISCUSSION

## Characterization of Prepared Hydrogels

The formulations of these five groups of hydrogels (Ctrl, Mg10, Mg20, Mg30, and Mg40) are shown in **Table 1**. $MgSO_4$/MgO/SA/Na-CMC hydrogels were successfully prepared with different $MgSO_4$ ratios. The visual examination of hydrogels showed an opaque or translucent appearance, while pure hydrogels without Mg were white (**Figures 1A–E**). The hydrogels were homogenous

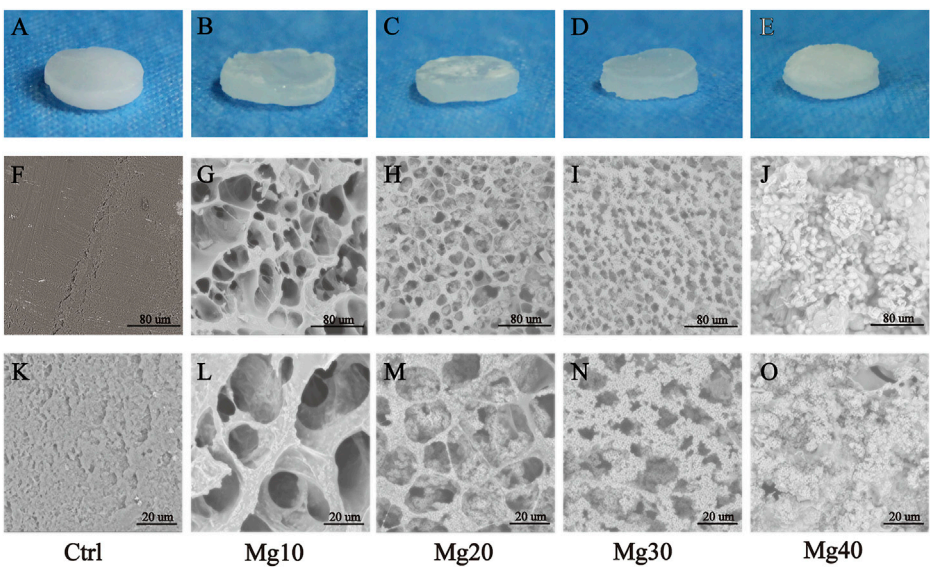


**FIGURE 1 | (A–E)** The appearance of $MgSO_4$/MgO/SA/Na-CMC composite hydrogel dressings. SEM images of the internal structure of hydrogels with low **(F–J)** and high **(K–O)** magnification.

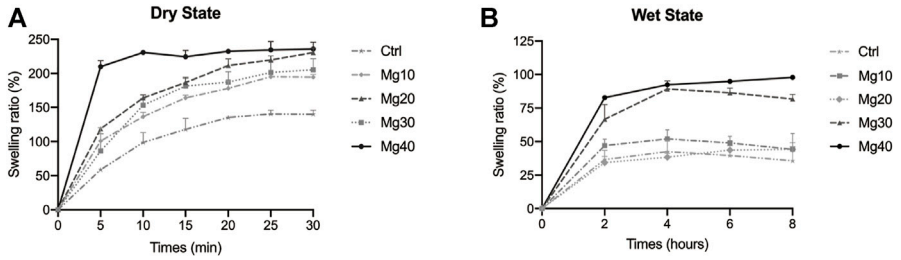


**FIGURE 2 |** The swelling ratio of different $MgSO_4$/MgO/SA/Na-CMC composite hydrogel dresssings in the dry state **(A)** and in the wet state **(B)**.

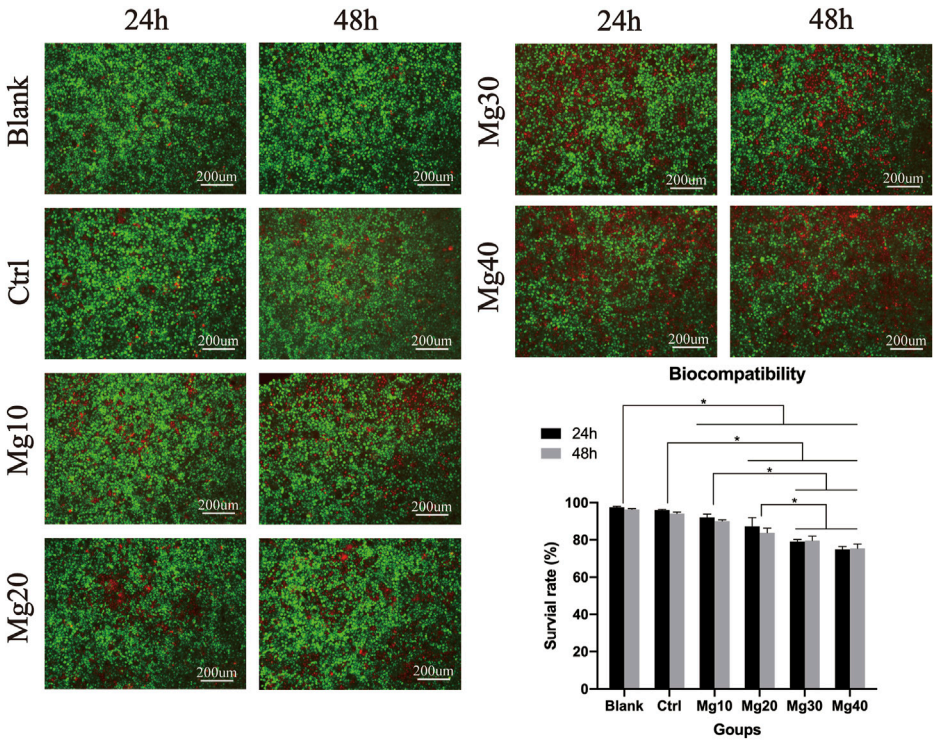


**FIGURE 3 |** Biocompatibility. $P \leq 0.05$ was considered statistically significant (*).

and soft, with a diameter of 1 cm and a thickness of about 2–3 mm.

Scanning electron microscopy (SEM) was used to examine the morphology of freeze-dried hydrogels. **Figures 1F–O** show the internal morphology of these five groups of $MgSO_4$/MgO/SA/Na-CMC hydrogels. The results showed that the pure hydrogel material (Ctrl group) was unable to maintain the porous structure because of the shrinkage of the material during the freeze-drying process (**Figures 1F,K**), while the addition of $MgSO_4$/MgO effectively maintained the porous structure of the hydrogel, which showed an interconnected and homogenous porous structure, and the pore size was about 20–100 μm (**Figures 1G,L**). However, with the increase of magnesium sulfate content, many magnesium sulfate crystals were evenly dispersed in the pores and the pore size was reduced to 20 μm approximately (**Figures 1H,L–N**). In **Figures 1J, O** the pore structures are almost invisible because most of them are filled with magnesium sulfate crystals. In **Supplementary Figure S1**, it is shown that the average pore size of groups Mg10, Mg20, and Mg30 was 34.30 ± 2.13 um, 21.32 ± 0.83 um, and 13.17 ± 0.39 um, respectively (Mean ± SEM). It indicated that the pore size decreased with the increase of the magnesium compound content of the hydrogel. Generally, a smaller pore size can improve the porosity of the hydrogel, enhancing its absorption. In addition, the mechanical properties of the five groups of hydrogels were tested and shown in **Supplementary Figure S2**. The compression modulus of the five groups was decreased with more magnesium compounds.

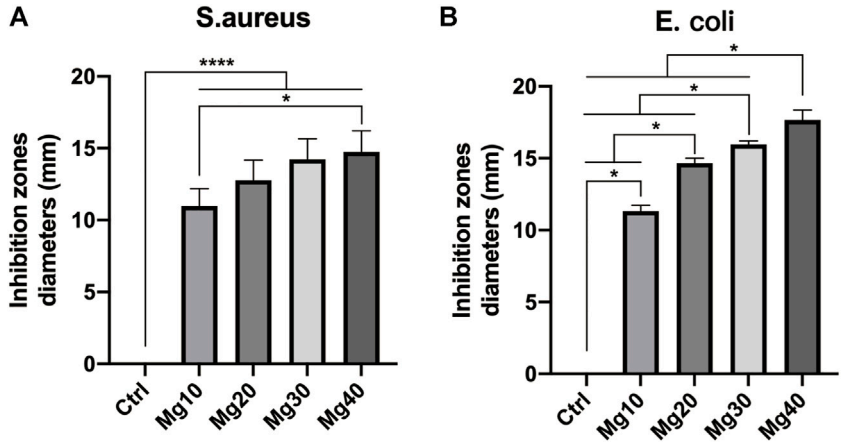


**FIGURE 4 |** The antibacterial activity of $MgSO_4$/MgO/SA/Na-CMC composite hydrogel dressings on Escherichia coli (ATCC 8739) and Staphylococcus aureus (ATCC 6538). $P \leq 0.05$ was considered statistically significant. $P \leq 0.05$ (*) $P \leq 0.0001$(****).

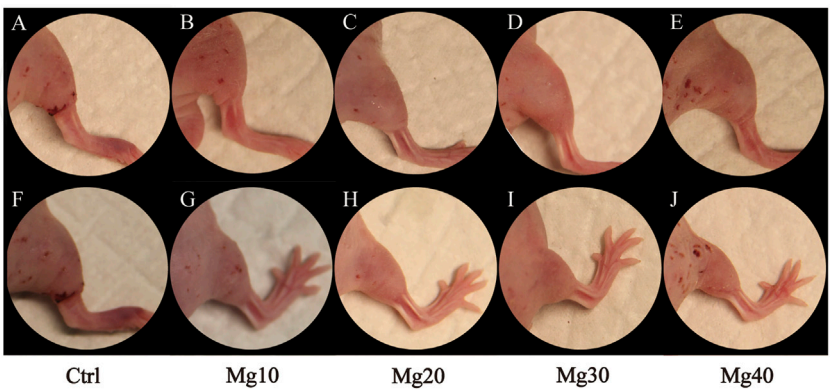


**FIGURE 5 |** Hindlimb edema model in nude mice **(A–E)**, and after treatment of $MgSO_4$/MgO/SA/Na-CMC composite hydrogel dressings **(F–J)**.

This may be due to the increase of magnesium compounds, which improves its porosity but reduces its material density; hence, it reduces its mechanical properties. We found that the mechanical properties of the group Mg40 were the worst, which may limit its application as dressing.

The past ten years have witnessed the rapid development of hydrogels. The good biocompatibility and high expansion of hydrogels have attracted the attention of many researchers (Pooresmaeil et al., 2019; Silva et al., 2019). SA is water-soluble, can effectively absorb wound secretions, and keeps the wound clean and dry, which is conducive to wound healing. In addition, SA is low-cost and easy to obtain (Gao et al., 2020). At room temperature, calcium ions ($Ca^{2+}$) were crosslinked with SA to form hydrogels to increase mechanical properties (Paudyal et al., 2013). Moreover, $Ca^{2+}$ after crosslinking could help trigger the coagulation mechanism and promote hemostasis when they were released into the wound (Afjoul et al., 2020).

## Swelling Ratio

The higher the SR value, the stronger the water absorbability of the hydrogels will be. This means that the hydrogen absorbs the exudate from the wound more strongly, thus achieving our goal of promoting incision detumescence. **Figure 2A** shows the percentage of swelling in the dry state containing different concentrations of Mg. The SR was sorted as Mg40 > Mg20 > Mg30 > Mg10 > Ctrl. All hydrogels showed swelling ability, and Mg40 or Mg20 exhibited a higher SR. As shown in **Figure 2B**, the percentage of swelling in the wet state containing different concentrations of Mg can be observed. The SR was sorted as Mg40 > Mg30 > Mg10 > Mg20 > Ctrl. The SR of the wet hydrogel was weaker than that of the dry state, but the swelling rate of Mg40 and Mg30 was still high. This was mainly due to the hypertonic effect of $MgSO_4$, which was consistent with our expectations.

$MgSO_4$ had high water absorption and is often used for catharsis (Snyder et al., 2014). We used the hypertonic effect of magnesium sulfate to solve the problem of postoperative incision

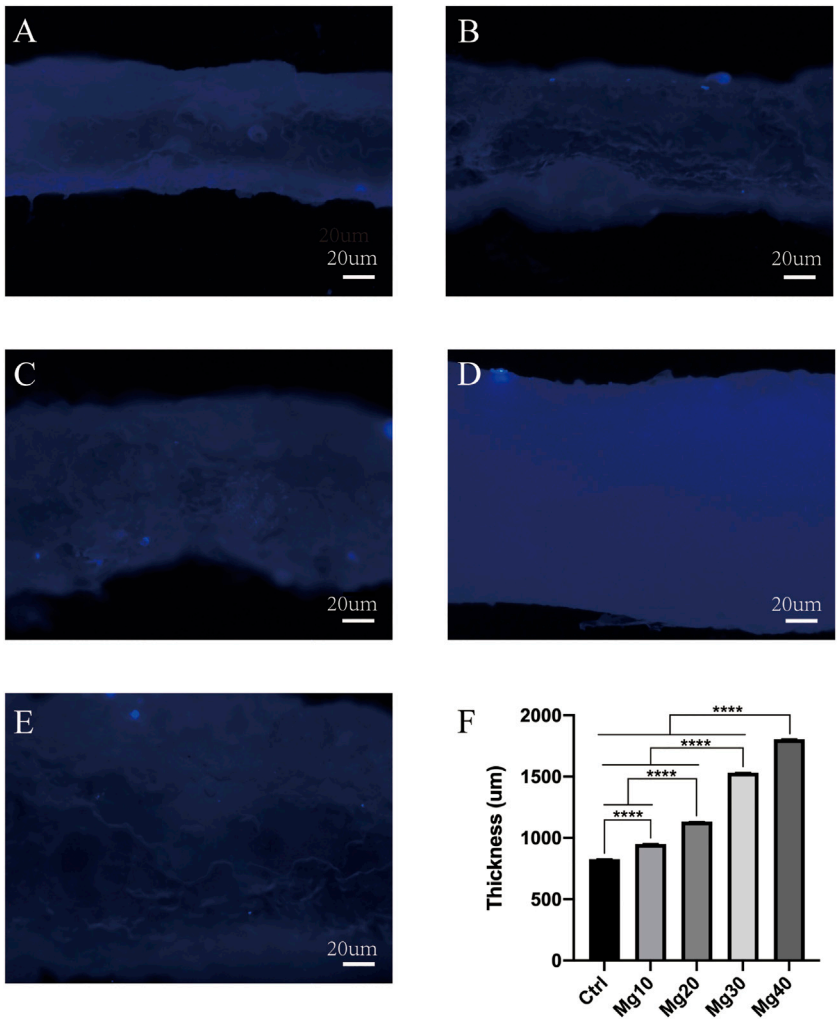


**FIGURE 6 |** The water absorption of different groups (Ctrl, Mg10, Mg20, Mg30, Mg40) of $MgSO_4$/MgO/SA/Na-CMC composite hydrogels under fluorescence microscope **(A–E)**. P ≤ 0.0001 was considered statistically significant (****).

edema. To select the appropriate concentration of $MgSO_4$, we set different $MgSO_4$ concentration gradients. Based on a comparison of water absorption in different states, we concluded that the higher the concentration, the better the water absorption effect, which corresponded to the characteristics of MgSO4's hyperosmotic action (Holland et al., 1960).

## Biocompatibility

Biocompatibility can help us identify the safety of hydrogels. Five groups of hydrogel extracts were used to culture HaCaT cells for 24 and 48 h to observe the biocompatibility of the hydrogels. After 24 h, the live/dead staining assay showed that there were many living cells (**Figure 3**). After 48 h of culture, the live/dead staining assay showed that the Mg40 hydrogel contained more than 76% dead cells than other groups. The result of fluorescence staining showed that the hydrogel had good biocompatibility and could be used for biomedical purposes.

Because the hydrogel was closely related to the epidermis, we needed to detect whether it had good biocompatibility using live/death staining detection. $Mg^{2+}$ is often used with biopharmaceuticals because of its good biocompatibility (Gao et al., 2021). As $Mg^{2+}$ is a metal ion, it can inhibit cell proliferation (Blangero and Teissie, 1985; Zhen et al., 2015). With prolonged contact time, the contact inhibition effect of hydrogels gradually showed. According to the results of live/dead staining, we chose Mg30, Mg20, Mg10, and Ctrl groups.

## Antibacterial Activity of the Hydrogels

Bacterial infection can seriously affect wound healing. The hydrogels prepared by us require anti-infection and antibacterial properties. We used two representative strains, *Escherichia coli* and *Staphylococcus aureus*, to test the antibacterial activity of hydrogels. The five groups of hydrogels were co-cultured with *Escherichia coli* and *Staphylococcus aureus*

in a 37°C incubator. After 2 days of cultivation, the diameter of the inhibition zone was measured as follows: Mg40 > Mg30 > Mg20 > Mg10 > Ctrl (**Figure 4**). All of these proved that these hydrogels had good antibacterial activity, especially the Mg40 and Mg30 groups, showing great potential for antibacterial and anti-infection properties.

Reducing the risk of infection or antibacterial effect is one of the important conditions for evaluating wound dressings. Metal ions (such as silver ions) were often used in various skin dressings to inhibit the growth of bacteria (Tao et al., 2021). However, the role of silver ions was limited and could not alleviate the problem of surgical incision edema. Therefore, we chose $Mg^{2+}$. As mentioned earlier, $MgSO_4$ had good water absorption. Moreover, some researchers have reported that $Mg^{2+}$ has antibacterial properties (Zhou et al., 2021). MgO is easily hydrated and forms a layer of magnesium hydroxide on the surface. A high concentration of reactive oxygen ions can exist on the surface of magnesium oxide. Reactive oxygen species ions are characterized by strong oxidation, which can destroy the peptide bond structure of bacterial cell membrane walls and quickly kill bacteria (Ikram et al., 2021). Therefore, the hydrogels prepared by us also showed antibacterial effects through antibacterial experiments. It is the best choice of dressing raw materials for postoperative surgical incision.

## Detumescence Effect of Hydrogels in an Edema Model

After constructing the edema model in nude mice, the detumescence effect of the hydrogel was detected by *in vivo* tests. A visual examination showed that the extremity of edema in nude mice was obvious, and the hydrogels adhered to the incision of nude mice and were removed after 6–8 h. **Figure 5** shows the contrast between the incision before and after the use of hydrogels. Visual examination between the groups showed that the detumescence effect of the four treatment groups was satisfactory, and Mg40 and Mg30 groups were significantly better than the other groups. Our hydrogels had an obvious effect on detumescence. During the experiment, neither infection nor rejection was observed, demonstrating that the hydrogels were biocompatible. The hydrogel was cut longitudinally and observed under a fluorescence microscope. It can be seen that the fluorescent bands of Mg40 and Mg30 were the widest. The order of the fluorescence bands from wide to narrow is Mg40 > Mg30 > Mg20 > Mg10 > Ctrl (**Figure 6**). This displayed that most water absorption was observed in the Mg40 and Mg30 groups. This signified that these two groups in the hydrogels had a better detumescence effect.

In the past decade, many studies were focused on the preparation of hydrogel dressing for wound healing and had achieved remarkable results (Cheng et al., 2021). These hydrogel dressings not only had antibacterial properties but also had many functions such as self-healing, hemostasis, and so on (Li et al., 2021). However, few researchers have noticed the impact of surgical incision edema on patients. We took full advantage of the hyperosmolar effect of $MgSO_4$ and added it to the hydrogel scaffold to prepare $MgSO_4$/MgO/SA/Na-CMC composite hydrogels. The model of postoperative incision edema in nude mice could show an obvious detumescence effect.

## CONCLUSION

$MgSO_4$, MgO, SA, and Na-CMC were chosen as the main components of the composite hydrogel dressings. These materials were mixed according to the proportion of each group listed in **Table 1**, and a group was selected with good biocompatibility, antibacterial activity, and detumescence effect. According to the SR, we screened Mg40 and Mg30 groups. Biocompatibility suggested that the cell mortality of Mg40 was higher than that of the other four groups, and mechanical test results indicated that Mg40 has a significantly worse compression modulus than the other four groups, so Mg40 was excluded. In the antibacterial activity, it could be seen that Mg40 and Mg30 groups had greater inhibition on *Escherichia coli* and *Staphylococcus aureus*. In animal experiments, except for the Ctrl group, Mg10, Mg20, Mg30, and Mg40 all had strong detumescence ability. In conclusion, the Mg30 group not only showed excellent antibacterial activity and detumescence effect but also had good biocompatibility. We successfully prepared $MgSO_4$/MgO/SA/Na-CMC composite hydrogel dressings with high water absorbency and antibacterial properties.

## DATA AVAILABILITY STATEMENT

The data that support the findings of this study are available on request from the corresponding author.

## ETHICS STATEMENT

The animal study was reviewed and approved by the Ethics Committee of the Ninth People's Hospital affiliated to Shanghai Jiao Tong University School of Medicine. Written informed consent was obtained from the owners for the participation of their animals in this study.

## AUTHOR CONTRIBUTIONS

YF and BS performed the research. SW and BS designed the research study. JZ, YX, and SL contributed essential reagents or tools. XL, JC, and HL helped to analyze the data. YF and BS wrote the article. SW and SL revised the article. All authors read and approved the final manuscript.

## FUNDING

This work was supported by a grant from the Natural Science Foundation of China (No. 82002065) and Postdoctoral Science Foundation (No. 2019T120347).

## ACKNOWLEDGMENTS

We thank all members of the Department of Plastic and Reconstructive Surgery and Department of Orthopaedics of Shanghai Ninth People's Hospital, Shanghai Jiao Tong University School of Medicine.

## SUPPLEMENTARY MATERIAL

The Supplementary Material for this article can be found online at: https://www.frontiersin.org/articles/10.3389/fbioe.2022.845345/full#supplementary-material

## REFERENCES

Afjoul, H., Shamloo, A., and Kamali, A. (2020). Freeze-gelled Alginate/gelatin Scaffolds for Wound Healing Applications: An *In Vitro*, *In Vivo* Study. *Mater. Sci. Eng. C* 113, 110957. doi:10.1016/j.msec.2020.110957

Bayer, I. S. (2021). A Review of Sustained Drug Release Studies from Nanofiber Hydrogels. *Biomedicines* 9 (11), 1612. doi:10.3390/biomedicines9111612

Blangero, C., and Teissié, J. (1985). Ionic Modulation of Electrically Induced Fusion of Mammalian Cells. *J. Membrain Biol.* 86 (3), 247–253. doi:10.1007/BF01870604

Cheng, H., Shi, Z., Yue, K., Huang, X., Xu, Y., and Gao, C. (2021). Sprayable Hydrogel Dressing Accelerates Wound Healing with Combined Reactive Oxygen Species-Scavenging and Antibacterial Abilities. *Acta Biomater.* 124, 219–232. doi:10.1016/j.actbio.2021.02.002

El Hosary, R., El-Mancy, S. M. S., El Deeb, K. S., Eid, H. H., El Tantawy, M. E., Shams, M. M., et al. (2020). Efficient Wound Healing Composite Hydrogel Using Egyptian Avena Sativa L. Polysaccharide Containing Beta-Glucan. *Int. J. Biol. Macromol* 149, 1331–1338. doi:10.1016/j.ijbiomac.2019.11.046

Fan, L., He, Z., Peng, X., Xie, J., Su, F., Wei, D. X., et al. (2021). Injectable, Intrinsically Antibacterial Conductive Hydrogels with Self-Healing and pH Stimulus Responsiveness for Epidermal Sensors and Wound Healing. *ACS Appl. Mater. Inter.* 13 (45), 53541–53552. doi:10.1021/acsami.1c14216

Fischbach, M. A., and Walsh, C. T. (2009). Antibiotics for Emerging Pathogens. *Science* 325 (5944), 1089–1093. doi:10.1126/science.1176667

Gao, J., Su, Y., and Qin, Y. X. (2021). Calcium Phosphate Coatings Enhance Biocompatibility and Degradation Resistance of Magnesium alloy: Correlating *In Vitro* and *In Vivo* Studies. *Bioact Mater.* 6 (5), 1223–1229. doi:10.1016/j.bioactmat.2020.10.024

Gao, X., Guo, C., Hao, J., Zhao, Z., Long, H., and Li, M. (2020). Adsorption of Heavy Metal Ions by Sodium Alginate Based Adsorbent-A Review and New Perspectives. *Int. J. Biol. Macromol* 164, 4423–4434. doi:10.1016/j.ijbiomac.2020.09.046

Guimaraes, C. F., Ahmed, R., Marques, A. P., Reis, R. L., and Demirci, U. (2021). Engineering Hydrogel-Based Biomedical Photonics: Design, Fabrication, and Applications. *Adv. Mater.* 33 (23), e2006582. doi:10.1002/adma.202006582

Holland, J. J., Hoyer, B. H., Mc, L. L., and Syverton, J. T. (1960). Enteroviral Ribonucleic Acid. I. Recovery from Virus and Assimilation by Cells. *J. Exp. Med.* 112, 821–839. doi:10.1084/jem.112.5.821

Ikram, M., Inayat, T., Haider, A., Ul-Hamid, A., Haider, J., Nabgan, W., et al. (2021). Graphene Oxide-Doped MgO Nanostructures for Highly Efficient Dye Degradation and Bactericidal Action. *Nanoscale Res. Lett.* 16 (1), 56. doi:10.1186/s11671-021-03516-z

Krenzelok, E. P., Keller, R., and Stewart, R. D. (1985). Gastrointestinal Transit Times of Cathartics Combined with Charcoal. *Ann. Emerg. Med.* 14 (12), 1152–1155. doi:10.1016/s0196-0644(85)81019-2

Li, H., Cheng, F., Wei, X., Yi, X., Tang, S., Wang, Z., et al. (2021). Injectable, Self-Healing, Antibacterial, and Hemostatic N,O-carboxymethyl Chitosan/oxidized Chondroitin Sulfate Composite Hydrogel for Wound Dressing. *Mater. Sci. Eng. C Mater. Biol. Appl.* 118, 111324. doi:10.1016/j.msec.2020.111324

Liang, Y., Li, Z., Huang, Y., Yu, R., and Guo, B. (2021). Dual-Dynamic-Bond Cross-Linked Antibacterial Adhesive Hydrogel Sealants with On-Demand Removability for Post-Wound-Closure and Infected Wound Healing. *ACS Nano* 15 (4), 7078–7093. doi:10.1021/acsnano.1c00204

Maheshwer, B., Drager, J., John, N. S., Williams, B. T., LaPrade, R. F., and Chahla, J. (2021). Incidence of Intraoperative and Postoperative Complications after Posterolateral Corner Reconstruction or Repair: A Systematic Review of the Current Literature. *Am. J. Sports Med.* 49 (12), 3443–3452. doi:10.1177/0363546520981697

Muniz Diaz, R., Cardoso-Avila, P. E., Perez Tavares, J. A., Patakfalvi, R., Villa Cruz, V., Perez Ladron de Guevara, H., et al. (2021). Two-Step Triethylamine-Based Synthesis of MgO Nanoparticles and Their Antibacterial Effect against Pathogenic Bacteria. *Nanomaterials (Basel)* 11 (2). doi:10.3390/nano11020410

Paudyal, H., Pangeni, B., Inoue, K., Kawakita, H., Ohto, K., Ghimire, K. N., et al. (2013). Preparation of Novel Alginate Based Anion Exchanger from Ulva Japonica and its Application for the Removal of Trace Concentrations of Fluoride from Water. *Bioresour. Technol.* 148, 221–227. doi:10.1016/j.biortech.2013.08.116

Pooresmaeil, M., Behzadi Nia, S., and Namazi, H. (2019). Green Encapsulation of LDH(Zn/Al)-5-Fu with Carboxymethyl Cellulose Biopolymer; New Nanovehicle for Oral Colorectal Cancer Treatment. *Int. J. Biol. Macromol* 139, 994–1001. doi:10.1016/j.ijbiomac.2019.08.060

Sheng, Y., Gao, J., Yin, Z. Z., Kang, J., and Kong, Y. (2021). Dual-drug Delivery System Based on the Hydrogels of Alginate and Sodium Carboxymethyl Cellulose for Colorectal Cancer Treatment. *Carbohydr. Polym.* 269, 118325. doi:10.1016/j.carbpol.2021.118325

Silva, K., de Carvalho, D. E. L., Valente, V. M. M., Campos Rubio, J. C., Faria, P. E., and Silva-Caldeira, P. P. (2019). Concomitant and Controlled Release of Furazolidone and Bismuth(III) Incorporated in a Cross-Linked Sodium Alginate-Carboxymethyl Cellulose Hydrogel. *Int. J. Biol. Macromol* 126, 359–366. doi:10.1016/j.ijbiomac.2018.12.136

Singh, B., Sharma, S., and Dhiman, A. (2013). Design of Antibiotic Containing Hydrogel Wound Dressings: Biomedical Properties and Histological Study of Wound Healing. *Int. J. Pharm.* 457 (1), 82–91. doi:10.1016/j.ijpharm.2013.09.028

Snyder, A., Koeller, G., Seiwert, B., Abraham, G., and Schusser, G. F. (2014). Influence of Laxatives on Gastric Emptying in Healthy Warmblood Horses Evaluated with the Acetaminophen Absorption Test. *Berl Munch Tierarztl Wochenschr* 127 (3-4), 170–175.

Tao, G., Cai, R., Wang, Y., Zuo, H., and He, H. (2021). Fabrication of Antibacterial Sericin Based Hydrogel as an Injectable and Mouldable Wound Dressing. *Mater. Sci. Eng. C Mater. Biol. Appl.* 119, 111597. doi:10.1016/j.msec.2020.111597

Wang, B., Wu, Z., Wang, S., Wang, S., Niu, Q., Wu, Y., et al. (2021). Mg/Cu-doped TiO2 Nanotube Array: A Novel Dual-Function System with Self-Antibacterial Activity and Excellent Cell Compatibility. *Mater. Sci. Eng. C Mater. Biol. Appl.* 128, 112322. doi:10.1016/j.msec.2021.112322

Zhen, Z., Liu, X., Huang, T., Xi, T., and Zheng, Y. (2015). Hemolysis and Cytotoxicity Mechanisms of Biodegradable Magnesium and its Alloys. *Mater. Sci. Eng. C Mater. Biol. Appl.* 46, 202–206. doi:10.1016/j.msec.2014.08.038

Zhou, W., Yan, J., Li, Y., Wang, L., Jing, L., Li, M., et al. (2021). Based on the Synergistic Effect of Mg(2+) and Antibacterial Peptides to Improve the Corrosion Resistance, Antibacterial Ability and Osteogenic Activity of Magnesium-Based Degradable Metals. *Biomater. Sci.* 9 (3), 807–825. doi:10.1039/d0bm01584a

**Conflict of Interest:** The authors declare that the research was conducted in the absence of any commercial or financial relationships that could be construed as a potential conflict of interest.

**Publisher's Note:** All claims expressed in this article are solely those of the authors and do not necessarily represent those of their affiliated organizations, or those of the publisher, the editors, and the reviewers. Any product that may be evaluated in this article, or claim that may be made by its manufacturer, is not guaranteed or endorsed by the publisher.

frontiers | Frontiers in Bioengineering and Biotechnology

REVIEW
published: 21 June 2022
doi: 10.3389/fbioe.2022.931800

# Hydrogels in Spinal Cord Injury Repair: A Review

*Zhenshan Lv[1], Chao Dong[2], Tianjiao Zhang[3] and Shaokun Zhang[1]**

[1]The Department of Spinal Surgery, 1st Hospital, Jilin University, Jilin Engineering Research Center for Spine and Spine Cord Injury, Changchun, China, [2]Key Laboratory of Pathobiology, Ministry of Education, College of Basic Medical Sciences, Jilin University, Changchun, China, [3]Medical Insurance Management Department, China-Japan Union Hospital of Jilin University, Changchun, China

Traffic accidents and falling objects are responsible for most spinal cord injuries (SCIs). SCI is characterized by high disability and tends to occur among the young, seriously affecting patients' lives and quality of life. The key aims of repairing SCI include preventing secondary nerve injury, inhibiting glial scarring and inflammatory response, and promoting nerve regeneration. Hydrogels have good biocompatibility and degradability, low immunogenicity, and easy-to-adjust mechanical properties. While providing structural scaffolds for tissues, hydrogels can also be used as slow-release carriers in neural tissue engineering to promote cell proliferation, migration, and differentiation, as well as accelerate the repair of damaged tissue. This review discusses the characteristics of hydrogels and their advantages as delivery vehicles, as well as expounds on the progress made in hydrogel therapy (alone or combined with cells and molecules) to repair SCI. In addition, we discuss the prospects of hydrogels in clinical research and provide new ideas for the treatment of SCI.

**Keywords: spinal cord injury, hydrogel, cells, molecular, repair, review**

OPEN ACCESS

***Edited by:***
*Di Huang,*
*Taiyuan University of Technology, China*

***Reviewed by:***
*Tianlin Gao,*
*Wageningen University and Research, Netherlands*
*Yu Sheng,*
*Beihua University, China*
*Xiang Li,*
*Max Planck Institute for Heart and Lung Research, Germany*

****Correspondence:***
*Shaokun Zhang*
*shaokun@jlu.edu.cn*

***Specialty section:***
*This article was submitted to Biomaterials, a section of the journal Frontiers in Bioengineering and Biotechnology*

***Received:*** *29 April 2022*
***Accepted:*** *26 May 2022*
***Published:*** *21 June 2022*

***Citation:***
*Lv Z, Dong C, Zhang T and Zhang S (2022) Hydrogels in Spinal Cord Injury Repair: A Review. Front. Bioeng. Biotechnol. 10:931800. doi: 10.3389/fbioe.2022.931800*

## 1 INTRODUCTION

SCI is among the most serious traumas to the nervous system. They are caused mainly by traffic accidents or violence but can also be caused by inflammation and tumors. SCI has high morbidity and disability rates and can lead to the dysfunction of various systems (including the autonomic nervous system) and multiple organs (e.g., those of the respiratory, circulatory, urinary, and digestive systems) (Baptiste and Fehlings, 2006). SCIs can be divided into primary and secondary injuries. Primary SCI is characterized by irreversible damage caused by external forces acting (directly or indirectly) on the spinal cord. Pathophysiological characteristics include edema, cellular damage (Ek et al., 2012; Chen et al., 2021; Song et al., 2021), inflammation, oxidative stress, apoptosis, and necrosis (Moon et al., 2012). Secondary injury refers to spinal cord edema caused by an external force, as well as further damage to the spinal cord caused by spinal cord compression, which may be due to fragmented intervertebral disc tissue, imbalance of gliosis, cytokine release, excessive proliferation of gliocytes, microglia and macrophage accumulation at the injury site, or the formation of astroglial scars, fibrous scars, and syringomyelia (Emmez et al., 2010; Katoh et al., 2019; Onyango et al., 2021) (**Figure 1**). Secondary injury can further lead to tissue damage and permanent loss of function (Hall and Springer, 2004), seriously affecting nerve repair and complicating synapse reconstruction.

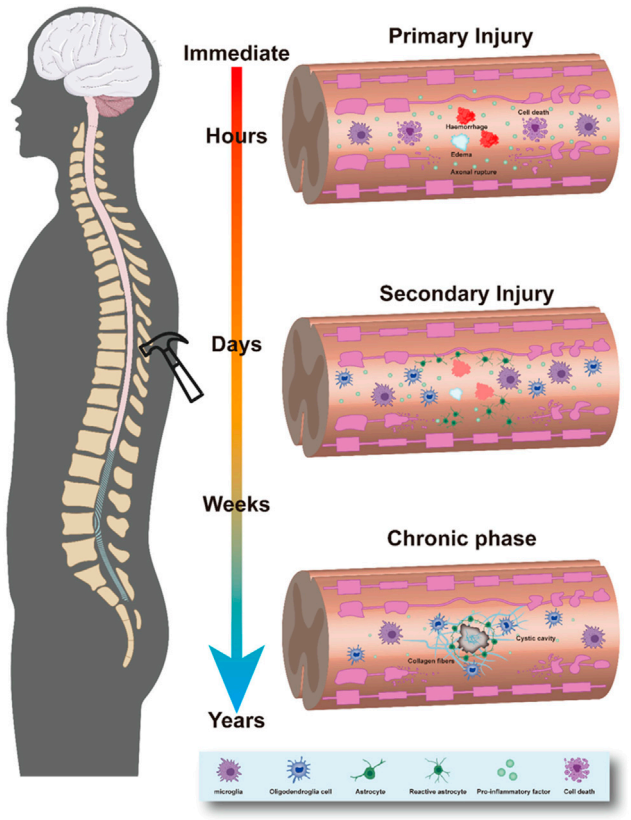


**FIGURE 1 |** Pathological process of SCI. This process consists of three phases, the primary phase, secondary phase, and chronic phase.

## 2 CURRENT TREATMENTS AND LIMITATIONS

Current treatments for SCI have nine key foci: 1) achieve spinal cord structural reconstruction, 2) inhibit astrocyte scarring, 3) promote nerve cell regeneration, 4) regulate the distribution of the extracellular matrix, 5) repair the microenvironment after injury, 6) remodel damaged neurons and axonal conduction, 7) inhibit secondary injury (Fitch et al., 1999; Choo et al., 2008; Donnelly and Popovich, 2008; Badner et al., 2017), 8) improve the microenvironment around the injury in time (Tuszynski et al., 1996; Kommareddy and Amiji, 2005), and 9) restore the nutrient supply to the spinal cord for axon regeneration (Im et al., 2010; Cregg et al., 2014). SCI treatment primarily includes surgical, pharmacological, and biological approaches (Cox et al., 2015) (**Figure 2**). The surgical method essentially decompresses the continuously compressed spine, improves the neuroprotection of the SCI, and restores the stability of the damaged spine. However, it is an invasive approach, and there is no uniform standard for the operation time. The main clinical treatments for reducing secondary injury include methylprednisolone, dexamethasone, naloxone, erythropoietin, and neuregulin (Rabchevsky et al., 2011), which improve neurological function in patients by reducing the production of inflammatory substances and inhibiting lipid peroxidation at the injury site. However, intravenous administration of large doses can trigger infection symptoms such as gastrointestinal bleeding and wound infection—such treatments remain controversial and restricted (Silva et al., 2014; Hurlbert et al., 2015). In addition, traditional administration methods, such as oral or intravenous injection (modest doses), are associated with limited crossing of the blood-spinal cord barrier, reducing direct action at the injury site. The complex pathophysiological changes of SCI and the harsh local microenvironment are not conducive to regeneration. Therefore, no single treatment method can repair damaged nerve tissue structure and function. Ideally, a nerve tissue scaffold would serve as a carrier of seed cells and active factors while also filling the lesion site, assisting seed cell survival and proliferation, promoting the reconnection of damaged spinal cord tissue, helping to bridge the gap in the lesion site and rebuild nerve conduction, and facilitating sustained drug delivery. The scaffolds most used for nerve repair include hydrogels, nanoparticles, and nanofibers (Ahmad et al., 2022). In this paper, we describe the characteristics of hydrogels and discuss their applications in SCI repair.

## 3 CHARACTERISTICS OF HYDROGELS

Hydrogels are macromolecular porous polymer network systems with a water content higher than 95%. They have viscoelasticity, high flexibility, excellent mechanical properties, strong plasticity, and good biocompatibility and biodegradability. Hydrogels can simulate the extracellular matrix environment and support the exchange of nutrients and surrounding tissues (Führmann et al., 2016). The implantation of hydrogels into injured spinal cord tissue can provide mechanical support for cells and tissues, promote cell migration, and facilitate the long-term controlled release of cellular molecules and drugs (by bridging the gap between the lesions or by providing a platform for the accumulation of neurotrophic factors in the lesion area), thereby mediating spinal cord tissue repair and regeneration (Jain et al., 2006; Toh and Loh, 2014; Assunção-Silva et al., 2015). Hydrogels can be synthesized using physical or chemical methods (**Figure 3**). Physical hydrogels are cross-linked to form a network structure under the action of non-covalent bonds. Cross-linking pathways include hydrophobic, ionic, electrostatic, and host-guest interactions, as well as hydrogen bonding and phase transitions. Physically cross-linked hydrogels will change with external conditions (e.g., temperature and pH). The preparation conditions for physically cross-linked hydrogels are relatively mild, with dynamic reversibility, self-healing, processability, and repeatability (Liu et al., 2018). Chemical hydrogels are cross-linked through chemical bonding between polymer chains, usually driven by small molecular initiators and external energy such as light and heat. Chemical cross-linking pathways include Michael addition reactions, condensation reactions, cross-linking with aldehydes, Schiff base reactions, thiol-disulfide bond exchange, free radical polymerization, photo-cross-linking, and enzyme-mediated cross-linking. Chemical hydrogels are more stable than physically cross-

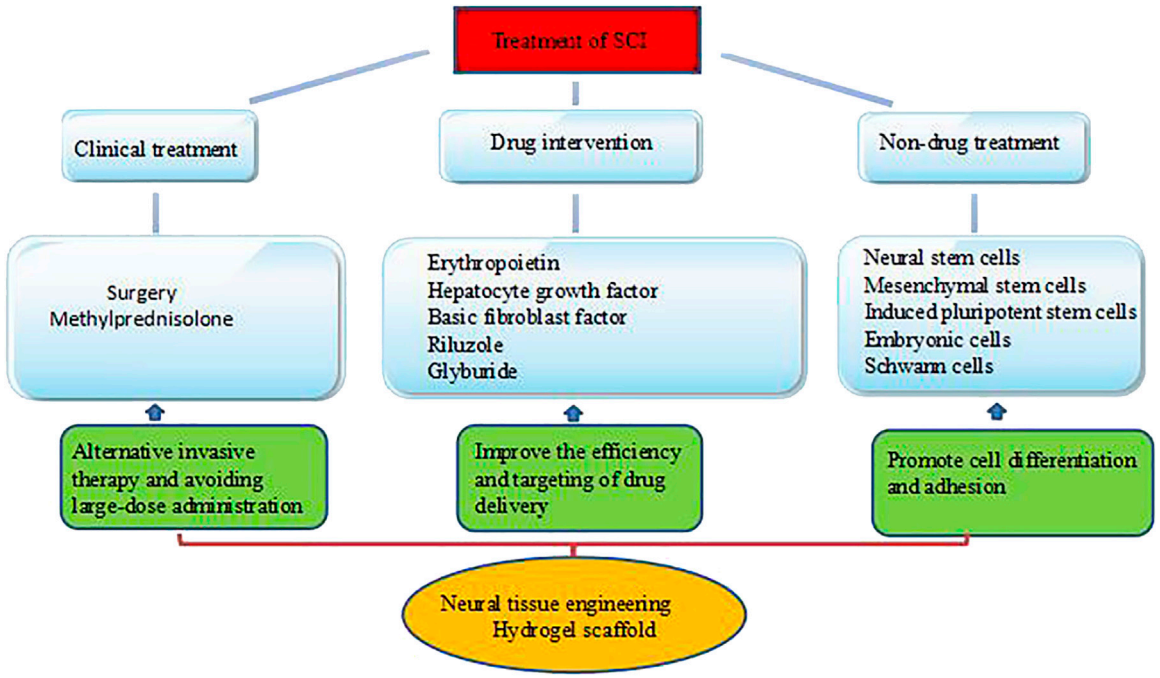


**FIGURE 2 |** Current treatment and limitations of SCI.

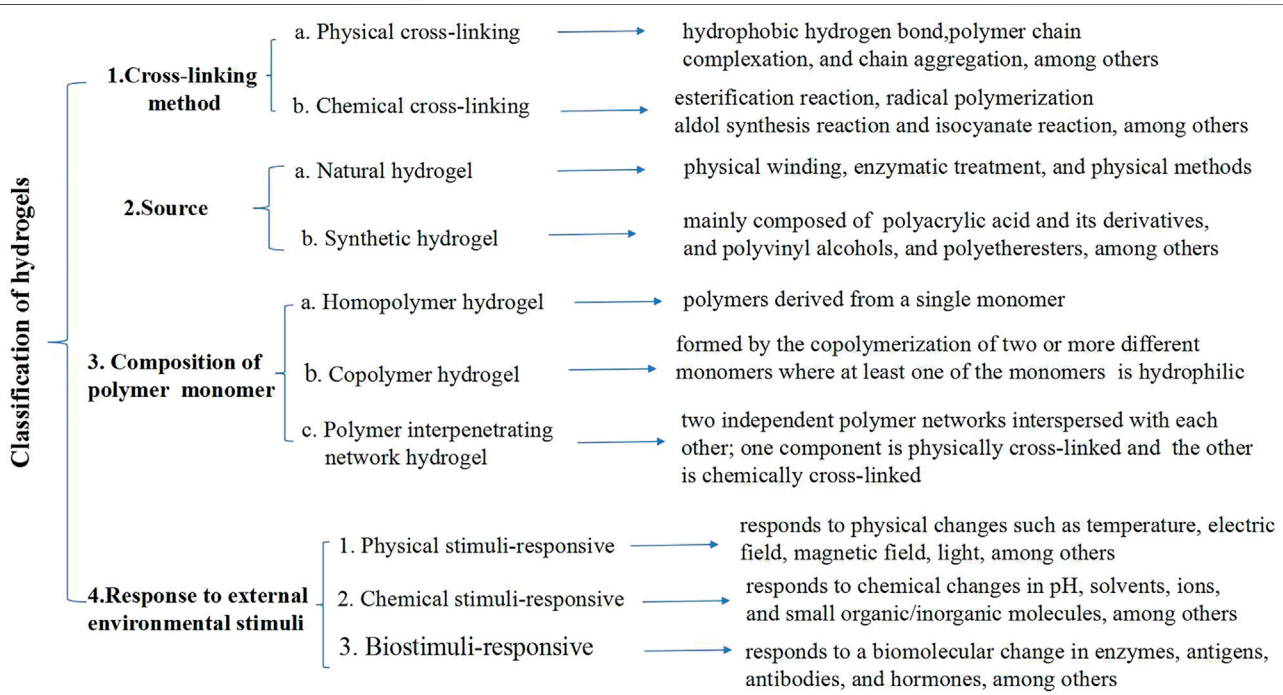


**FIGURE 3 |** Classification of hydrogels.

linked hydrogels; moreover, their structure and properties can be more precisely controlled (Hu et al., 2019). The hardness, morphology, structure, and biochemical modifications of the hydrogel materials will affect cell growth, adhesion, axon growth, proliferation, differentiation, and migration. The raw materials for synthesizing natural gels are usually proteins and

polysaccharides. Protein materials are subjected to physical or enzymatic treatments to form hydrogels, while polysaccharides such as agar and chitosan are generally synthesized *via* physical entanglement and cross-linking (Wei et al., 2015).

The uniform pores and parallel arrangement of the scaffold provide guiding channels for cells. If the pores are smaller than the size of the drug or cell, the drug and cell will be encapsulated in the hydrogel and not be released. If the pores are bigger than the drug and cell, the latter will move freely in the hydrogel network for subsequent release (Li and Mooney, 2016; Chen et al., 2018; Trombino and Cassano, 2020; Shoukat et al., 2021). Hydrogels can prevent inflammatory responses and nerve compression, as well as play an important role in controlling the release of molecules, owing to their excellent biodegradability. Controlling the degradation of hydrogels has a strong impact on improving drug and cell release; moreover, the physical and mechanical properties of the hydrogel surface will also affect cell adhesion, differentiation, and axonal growth (Lakard et al., 2004; Zhan, 2020). The smoothness and convexity of the scaffold surface can affect protein expression (Johnson et al., 2018). Animal experiments have shown that the scaffold morphology can promote cell migration and axon regeneration (Chen et al., 2020). Currently, most research on SCI repair is focused on modifying traditional hydrogels, and efforts to further strengthen the therapeutic effect of hydrogels, promote the regeneration of nerve stumps, and rebuild neural circuits should focus on modifying traditional hydrogels and developing new hydrogels with optimized mechanical properties, drug encapsulation and sustained release activities, and the ability to load cellular molecules and drugs (Xu et al., 2013; Ucar et al., 2021; Yao et al., 2021). These studies can be broadly categorized by the composition of hydrogel-based interventions for SCI, namely hydrogel therapy alone, cell-laden hydrogel therapy, drug-carrying hydrogel, or combination therapy with additional factors.

# 4 HYDROGEL THERAPY

Hydrogels are obtained from numerous sources. They are easy to process, highly flexible, and easily molded (Stegemann and Nerem, 2003). Hydrogels can carry cells in two ways. One is *via* direct injection or implantation at the site of the SCIs, filling the cavities of spinal cord lesions, bridging injury defects, and providing contact guidance for axon regeneration while self-degrading (Piantanida et al., 2019). Hydrogels can also be used as a carrier of transplanted cells or encapsulated neurotrophic factors and other drugs to complete the local enrichment and sustained release of seed cells and drugs so that the loaded molecules can be accurately delivered to the spinal cord, providing a suitable microenvironment for neural reconstruction (Liu and García, 2016; Huang et al., 2017; Dimatteo et al., 2018; Ucar et al., 2021; Yao et al., 2021). One characteristic of this approach is that the strength of the hydrogel and the degradation rate are closely related to cell survival and proliferation. The second approach involves planting seed cells after pre-preparing the scaffold, which has a specific internal structure and geometric shape, as well as the pore size, porosity, and mechanical strength. The disadvantage of this strategy is that the cells cannot be distributed uniformly or permanently in the scaffold space. In recent years, continuous advances in biomedical technology have resulted in the development of smart gels, including pH-sensitive, molecular self-loading, temperature-sensitive, and conductive hydrogels (Dadsetan et al., 2010).

## 4.1 Hydrogel Therapy Alone

Several studies have described the use of hydrogels, mainly collagen, gelatin, hyaluronic acid (HA), fibrin, chitosan, silk protein, alginate, laminin, agarose, dextran, fibronectin (FN), and their complexes for SCI repair (Hejcl et al., 2008; Gros et al., 2010; Jukes et al., 2010; King et al., 2010; Collins and Birkinshaw, 2013; Mothe et al., 2013; Meng et al., 2014) (**Figure 4**).

Collagen is the main extracellular component in the central nervous system (CNS). The cell adhesion signal peptide sequence arginine-glycine-aspartic acid (RGD) can guide cells to recognize the scaffold material, which helps maintain the cell's phenotype and activity (Hosseinkhani et al., 2013). *In vitro* experiments have shown that collagen can promote the proliferation and differentiation of nerve cells and inhibit the proliferation of neurocollagen gliosis (O'Connor et al., 2001; Ma et al., 2004). Three-dimensional collagen hydrogel scaffolds can maintain the self-renewal capacity of neural stem cells (NSCs) through the REDD1-mTOR signaling pathway (Zhang et al., 2016) and affect the differentiation of NSCs via the miR-7-Klf4 signaling pathway (Katz and Burdick, 2009). Researchers have used collagen hydrogels to repair SCI in mice and have shown that liquid collagen injected directly into the spinal cord could quickly gel and form a continuous interface in the spinal cord after inhibition and transection injury (Marchand and Woerly, 1990; Marchand et al., 1993). Furthermore, implanted collagen hydrogels could promote the migration of nerve cells, the growth and regeneration of nerve axons, and the secretion of brain-derived neurotrophic factor (BDNF) and neurotrophin-3 (NT-3) (Marchand and Woerly, 1990; Marchand et al., 1993; Yoshii et al., 2004; Klapka and Müller, 2006; Yang et al., 2010b; King et al., 2010). Collagen and chondroitin sulfate or carbodiimide composites can promote axonal regeneration in SCI (Marchand et al., 1993). In addition, the arrangement of collagen fibers is important to guide cell orientation and migration. The direction of collagen fibrils can be controlled using magnetic nanoparticles and by applying an external magnetic field (Vrana et al., 2007).

Sodium alginate hydrogel displays good biocompatibility and is often used as an injectable carrier to load drugs or cytokines targeted to the injury site (Perets et al., 2003; Grulova et al., 2015). It can be cross-linked in the presence of cations to form a reticulated alginate ion gel that promotes the osmotic diffusion of nutrients and provides three-dimensional growth space for cells (Arlov and Skjak-Braek, 2017). Sodium alginate hydrogels show better mechanical properties and cell viability and are more suitable as scaffolds for neural tissue engineering than sodium alginate + HA or sodium alginate + FN composite hydrogels (Bozza et al., 2014). Suzuki (Suzuki et al., 2002) implanted an alginate sponge into a rat

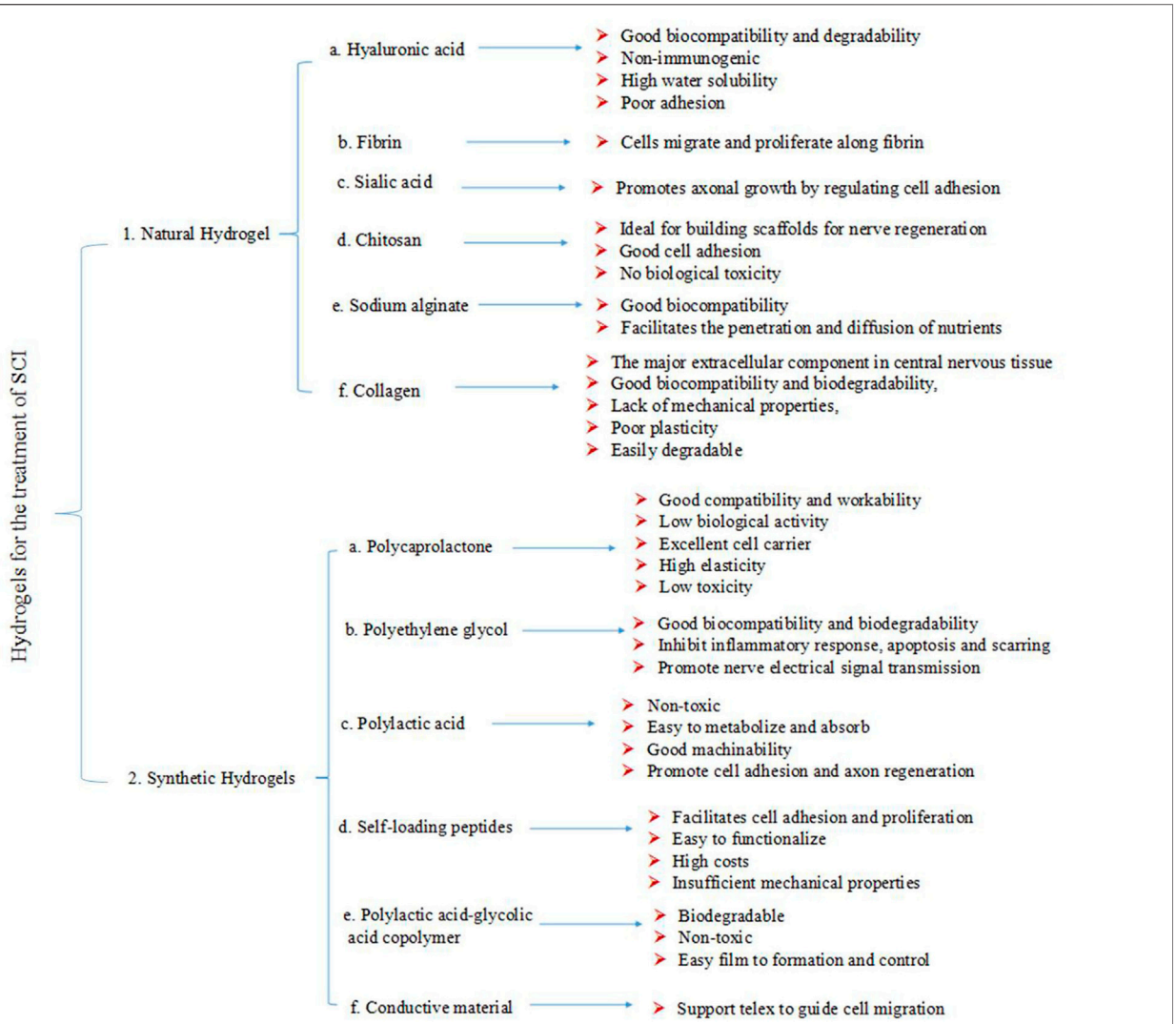


**FIGURE 4 |** Application and characteristics of hydrogels therapy.

SCI model. At 21 weeks after the operation, several fibers appeared at the injury site, and axons regenerated and formed functional synapses. Covalently cross-linked and lyophilized porous alginate gel inhibits SCI and reactive gliogenesis, as well as promotes axonal growth (Kataoka et al., 2004).

HA is the main component of the extracellular matrix of the CNS. It can reduce inflammatory injury and inhibit the formation of fibrous scars after SCI, improve nerve function recovery following injury as well as promote angiogenesis (Meng et al., 2014). HA is often combined with other materials to construct a composite hydrogel for application in neural tissue engineering, thereby optimizing HA adhesion to cells. For example, Horn used thiol-modified HA cross-linking for rat SCI repair and observed axonal regeneration (Horn et al., 2007). James et al. (Austin et al., 2012) injected a hyaluronan-methylcellulose (HAMC) hydrogel into a chronic SCI model 24 h after the latter was established. The results showed that the submembranous space gelled effectively, reduced glial fibrosis and inflammatory responses in the injured area, and promoted the recovery of axonal transmission and neural function.

Chitosan is a degradable cationic polysaccharide with excellent biocompatibility and low immune rejection. Chitosan degradation products can be metabolized (Martins et al., 2014) and easily made into hydrogels (Delmar and Bianco-Peled, 2016). Chitosan and other polymers are widely used in nerve tissue regeneration (Fang and Song, 2019). Several research groups have used chitosan catheter stents to conduct SCI *in vivo* repair experiments. Chedly et al. (2017) implanted a chitosan hydrogel into a rat spinal cord bilateral hemi-transection model; the chitosan hydrogel promoted the reconstruction of spinal cord tissue and blood vessels, reduced fibroglial scarring, regenerated numerous axons, and modulated the inflammation. Three-dimensional agarose with varying mechanical strengths has different axonal growth-promoting abilities on the dorsal root ganglion (DRG) (Balgude et al., 2001). Agarose is produced using the

directional freezing method to make directional through holes, and the regeneration of injured spinal cord axons can be induced along these holes (Stokols and Tuszynski, 2004; Stokols and Tuszynski, 2006).

FN participates in cell adhesion by binding to cell surface receptors and guiding cell differentiation, among other functions. FN has neuroprotective effects against the regulation and amelioration of ischemia-induced necrosis after CNS injury (Meng et al., 2014). As a cell carrier, it can greatly improve the survival rate of seed cells and help achieve a more uniform distribution of cells (Meng et al., 2014). Nazari et al. (2020) confirmed that FN hydrogel scaffolds could improve cell viability, induce stem cells to differentiate into oligodendrocyte precursor cells and promote SCI repair. FN hydrogel also inhibits the recruitment of reactive glial cells in the subacute phase of SCI (Johnson et al., 2010). *In vitro* studies have shown that a composite hydrogel of FN and fibrin (FB) was more effective at promoting axon growth than the single-component FN hydrogel (Meng et al., 2014).

Some synthetic hydrogels also have excellent effects on SCI repair. The polyethylene glycol (PEG) microgel scaffold can be used to delivery and secrete human bone marrow mesenchymal stem cells, and promote the repair of nerve damage (Borgens et al., 2002; Duerstock and Borgens, 2002; Laverty et al., 2004; Caldwell et al., 2020). Wang et al. (2017) prepared polymer micelles-DA/mPEG-PCL scaffolds and applied them in a spinal cord hemi-transection injury model. The results showed that the scaffold could reduce the formation of scars and cysts, as well as promote axon regeneration. In a mouse spinal cord hemisection model, conductive hydrogels (EHs) based on TA and polystyrene (PPv) can promote NSCs differentiation into neurons *in vitro*, and inhibit astrocyte differentiation. *In vivo* results demonstrated that this hydrogel promotes SCI mouseendogenous neurogenesis and functional recovery by restoring interrupted spinal cord circuits. PCL can mimic the structure of gray or white matter and promote the differentiation of NSCs to oligodendrocytes and the formation of axonal myelin sheaths, it is an ideal material in SCI tissue engineering (Donoghue et al., 2013; Patel et al., 2019). Wong et al. (2008) implanted PCL into an animal model of total transection of SCI, and its open microchannel structure facilitates axon regeneration and myelination. Babaloo et al. (2019) combined PCL with gelatin to improve cell adhesion and material degradation rate, as well as promote neuronal and myelin regeneration. The starch-PCL 3D composite scaffold can protected the injured area and promoted the recovery of behavioral function (Silva et al., 2013). Han et al. (2020) prepared an injectable hydrogel containing ursodicholic acid to inhibit inflammation, resist apoptosis, and promote the recovery of nerve function. PLLA scaffolds promoted cell migration, axon regeneration and integration with surrounding host tissues (Deng et al., 2006). Sun et al. (2020) used PLLA nanofiber multi-channel scaffolds filled with NT3-loaded gelatin sponge transplanted into a model of total transection of SCI, which reduced the deposition of collagen fibers and promoted the recovery of animal behavioral function.

## 4.2 Cell-Laden Hydrogel Therapy

The loss of neuronal tissue and the existence of cavities at the injury site make cell transplantation an effective approach to treating SCIs. The seed cells used for SCIs repair mainly include olfactory ensheathing, Schwann, neural stem (Barbour et al., 2013), embryonic stem, induced pluripotent stem, and mesenchymal stem cells (MSCs). The transplanted stem cells can differentiate into neuronal cells, and glial cells secrete various cytokines, inhibit inflammation and apoptosis, promote axon regeneration, and restore interneuron communication (Barbour et al., 2013; Tabakow et al., 2013; Doulames and Plant, 2016; Yang C. et al., 2019; Chen et al., 2019; Chu et al., 2019; Gao et al., 2020). However, single-cell therapy cannot keep the sustained concentration at the damaged spinal cord and use the combined hydrogel and cell delivery system to provide a protection system for cells and avoid apoptosis or necrosis (**Figure 5A**).

### 4.2.1 Hydrogel + Neural Stem Cells

Transplanting a mixture of hydrogel and NSCs into injured spinal cord tissue can promote differentiation into neurons, replacing dead neurons and restoring nerve conduction (Chen et al., 2010). These transplanted NSCs can also secrete various neurotrophic factors and cytokines to protect damaged nerve cells, inhibit the inflammatory response, reduce the degree of demyelination of damaged axons, and restore motor function. DNA hydrogel is a three-dimensional network structure formed by high cross-linking of DNA strands in an aqueous solution. It has shape plasticity, excellent biocompatibility and biodegradability, and accurate molecular identification. The network structure of DNA hydrogels facilitates the encapsulation of proteins and cells and regulates the release of these molecules (Patel et al., 2019; Khajouei et al., 2020; Pedersen et al., 2020). Yuan et al. (2021) loaded NSCs with DNA supramolecular hydrogel materials and injected them into the lesions of a rat SCI model with a 2-mm total transaction. The results of the study showed that 8 weeks after transplantation, the motor function of both hindlimbs in SCI rats was significantly improved, voluntary urination behavior was restored, and implanted. NSCs differentiated into neurons, oligodendrocytes, and astrocytes, achieving remyelination, forming new neural circuits, and restoring the signal transmission. Mothe et al. (2013) applied a HAMC gel encapsulated with the blood-derived growth factor rPDGF-A to load NSCs to treat SCI mice. The group receiving the combined treatment of gel and NSCs showed improved survival of neurons and oligodendrocytes in the surrounding tissue. The number of nerve cells increased, the injured area of the mice decreased, and the motor function of the lower limbs recovered better. Collagen and NSCs can form neural networks *in vitro* (Ma et al., 2004). Egawa et al. (2011) used collagen hydrogel as a carrier for NSCs. Polypeptide constructs prepared by recombinant DNA technology bind to collagen to anchor epidermal growth factor (EGF) under mild conditions, stabilizing exogenous EGF in collagen. *In vitro* experiments

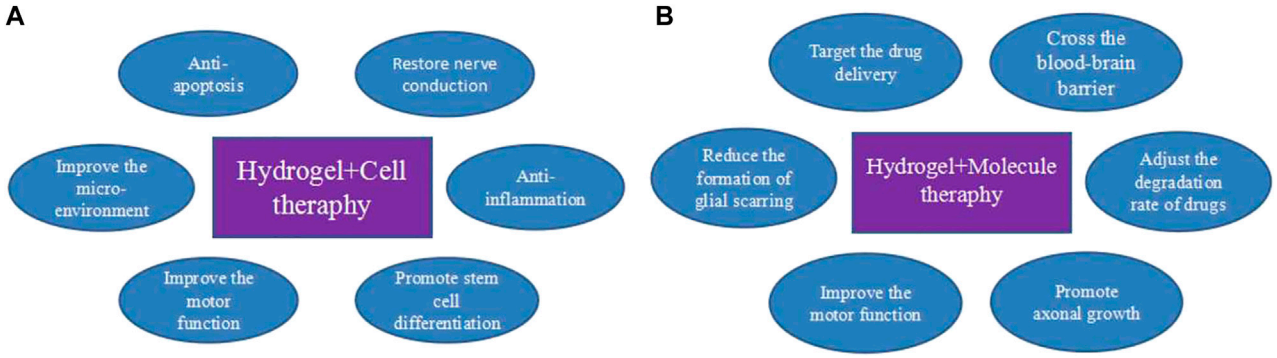


**FIGURE 5 |** Advantages of hydrogels in the treatment of SCI. **(A)** Hydrogel combined with cell therapy. **(B)** Hydrogel combined with molecular therapy.

showed that the EGF-bound collagen hydrogels have significantly increased the number of nerve cells. Yuan et al. (2014) prepared double-layer porous collagen membranes with different pore sizes as the transplant carrier for NSCs. The inner membrane layer had a large pore size that could carry many NSCs, and the outer layer structure could reduce the extension of other surrounding cells into the damaged regenerative microenvironment and glial scar, preventing platelet deposition and external compression at the injury site. This membrane design can significantly promote the differentiation of NSCs into neurons after spinal cord hemi-transection transplantation, improve the regenerative microenvironment, and facilitate the recovery of motor nerve function. The hydrogel scaffold can simulate the electrical conduction characteristics of the natural spinal cord, promoting the differentiation of NSCs and the secretion of related trophic factors (Staples et al., 2017). Hydrogels with higher conductivity can guide NSCs to promote neuron differentiation *in vitro* while inhibiting astrocyte differentiation (Zhou et al., 2018). Single-channel chitosan conduits were filled with neural stem/precursor cells (NSPCs) and photo-crosslinked chitosan hydrogel-growth factor complexes to induce stem cells to differentiate into desired cell types (Li et al., 2014).

Zarei-Kheirabadi et al. (2020) used thiol-modified HA and gel-made hydrogels to encapsulate sorted embryonic stem cell-derived NSCs, which can increase their differentiation into oligodendrocytes and reduce glial scarring, improving motor function in a mouse contusion model. *In vivo* experiments showed that chitosan tubes of composite NSCs/NSPCs could induce NSCs to differentiate into neurons and successfully connect both ends of the injured spinal cord. Sun et al. (2017) showed that IKVAV-modified silk fibroin hydrogels could promote the proliferation and differentiation of NSCs, suggesting that the hydrogels have excellent nutrient transport and signal molecule transport capabilities. Another study reported that NSC proliferation in sodium alginate hydrogels decreases with increasing mechanical properties (Banerjee et al., 2009). The degradation of the hydrogel also promotes NSC as the degraded material provides cells with more oxygen and nutrients (Ashton et al., 2007).

### 4.4.2 Hydrogel + Mesenchymal Stem Cells

Mesenchymal stem cells (MSCs) are derived from various sources. They have multi-directional differentiation potential and are easy to culture and expand *in vitro* (Parekkadan and Milwid, 2010). MSCs can migrate (chemotactic) to the injured area (Shi et al., 2012) and are ideal seed cells for tissue engineering. Syková et al. (2006) prepared macroporous hydrogels based on 2-hydroxyethyl methacrylate (HEMA) or 2-hydroxypropylmethacrylamide (HPMA) derivatives that covalently bonded with the hydrolytically degradable cross-linker N, O-dimethyl acrylamide hydroxylamide or that were modified by different surface charges, and the hydrogels carrying BM-MSCs. The gel was implanted into the spinal cord hemisection of rats, and the results showed hydrogel system loaded with BM-MSCs promoted axonal growth. Yao et al. (2020) showed that BMSCs loaded with fibrin gel could significantly improve motor function in rats. Yao et al. (2021) used a dual-enzymatically cross-linked gelatin hydrogel with hydrogen horseradish peroxidase (HRP) and galactose oxidase (GalOx) to build biocompatible HUC-MSC-loaded injectable scaffolds that showed a similar modulus to neural tissue thereby improving the survival, proliferation, and differentiation of HUC-MSCs *in vitro*. In addition, HUC-MSC-loaded hydrogels can significantly promote the recovery of hindlimb motor function in SCI mice, inhibit inflammation and apoptosis, and accelerate the repair of damaged spinal cords. Oliveira et al. (2017) showed that gellan gum, collagen, and laminin epitope-rich hydrogels all support adipose-derived mesenchymal stem cell-mediated axonal growth. The viscous hydrogel loaded with MSC-derived exosomes positively affected the efficient recovery of neural tissue (Li et al., 2020). Inoculation of fibrin gel-loaded BMSCs in a rat model of total spinal cord resection can significantly improve motor function in rats. Methacryloyl gelatin (GelMA) is synthesized from methacrylic acid *via* gelatinization. Photoinitiation occurs by introducing phenyl-2,4,6-trimethyl-benzoyl phosphonate (LAP) into GelMA. After preparation, GelMA can be quickly cross-linked and cured under blue light (at a 405-nm wavelength). The production cost of this material is low. Studies have shown that the GelMA concentration affects its pore size, swelling mechanics,

and other related physical properties (Bertlein et al., 2017; Celikkin et al., 2018). GelMA hydrogels have good biocompatibility (Fang et al., 2016; Yang D. et al., 2019) and promote BMSC growth. In addition, different concentrations of GelMA have varying effects on the cell growth state (Nichol et al., 2010)—caused by the GelMA concentration changing the degree of cross-linking in photocured GelMA hydrogels (Ren et al., 2018). Zhao et al. (2016) pointed out that the proliferation of BMSCs in photocured GelMA hydrogels might be related to pore size. Zhang et al. (2020) constructed a three-dimensional hydrogel based on HA and modified it with the laminin polypeptide PPFMLLLKGSTR. The hydrogel was loaded with human placental amniotic membrane-derived MSC exosomes and transplanted into a rat SCI model. Twenty-eight days after transplantation, the treatment of hydrogel combined with exosomes significantly promoted the motor function recovery and significantly increased the effective step rate of the rat's hindlimb. Magnetic resonance imaging showed that the fracture area at the spinal cord was significantly reduced in the hydrogel-exosome combined treatment group relative to the hydrogel-only group. Alginate hydrogels were loaded with Schwann cells combined with BDNF to treat the animal model of C5 semi-transected SCI. Schwann cells and BDNF promoted the regeneration of intact axons across the lesion site to the injured segment (Liu et al., 2017).

#### 4.2.3 Hydrogel + Embryonic Stem Cells

An injectable composite hydrogel system was developed based on a modified gelatin matrix combined with shape memory polymer fibers. This system was used to load ESC-derived motor nerves (MNs) in a directed embryonic stem cells (ESCs) differentiation and minimally invasive manner, then used to treat SCI (Wang et al., 2018). Composite hydrogels with aligned fibers enhanced cell viability and neurite outgrowth *in vitro* and enhanced ESCs differentiation into MNs *in vivo*. ESCs-loaded composite hydrogels transplanted into SCI mice *via* injection significantly enhanced tissue regeneration and angiogenesis, improved the expression of Tuj1, MAP2, and Syn, and decreased immune responses, which recovered motor function in the mice.

#### 4.2.4 Hydrogel + Induced Pluripotent Stem Cells

A dual-porous laminin-coated hydrogel seeded with induced pluripotent stem cell-derived neural progenitor cells (iPSC-NPs) in a rat model of chronic SCI was found to reduce cavitation and support iPSC-NPs survival; however, its use did not lead to a significant improvement in motor recovery (Joung et al., 2018; Ruzicka et al., 2019). Joung et al. (2018) used three-dimensional printing of iPSC-derived spinal neuronal progenitor cells (sNPCs) and oligodendrocyte progenitor cells (OPCs), and the results showed that biomarked sNPCs differentiate and extend axons throughout the microscaffold channels. Bahareh et al. (Nazari et al., 2020) determined the potential of fibrin hydrogels to enhance the differentiation of human fibroblast-induced pluripotent stem cells into oligodendrocytes. iPSCs in HA and gelatin methacrylate-based hydrogels exhibited stronger neurite elongation and spontaneously favorable neuronal differentiation (Wu et al., 2017; Fan et al., 2018). The above results confirm that iPSCs combined with hydrogels can be used to treat SCI.

### 4.3 Molecular-Carrying Hydrogel Therapy

Ordinary hydrogel as a drug delivery system mainly relies on the diffusion of the drug or the degradation of the material itself for release, which is uncontrollable and may not achieve the desired effect of drug delivery (Shoukat et al., 2021). Many drugs fail to accumulate in the CNS after systemic administration because of their inability to cross the tightly regulated blood-spinal cord barrier (Pardridge, 2011). Therefore, there is need for effective, targeted, long-term, and safe approaches for the sustained release of therapeutic substances to improve the restorative effect of SCI (Paves and Saarma, 1997; Ramer et al., 2000; La Manna et al., 2021). Drug delivery system (DDS) can effectively improve the therapeutic effect of drugs, reduce drug toxicity and improve patients' dependence on drugs. Ideally, the DDS must have good biocompatibility and must protect the drug by avoiding degradation while maintaining its stability and activity (Lagreca et al., 2020; Yang J. et al., 2021; La Manna et al., 2021). After injecting the DDS into the affected cord region, hydrogels quickly convert from liquid to gel at the injury site, bridging small gaps between the spinal cord tissue (**Figure 5B**).

#### 4.3.1 Hydrogel + Chemical Drug

Hydrogels can encapsulate drugs or drug-loaded carriers to provide sustained local drug release. Additionally, factors including the preparation method, structure, shape, pore size pH, light, magnetic field, electric field, ionic strength, and enzymatic environment of the hydrogel are closely related to drug loading and release capacity (Günther et al., 2015; Barclay et al., 2019). Local delivery can be achieved by injecting preformed hydrogels or polymer solutions gelled *in situ* into the parenchymal, intrathecal (subdural), or epidural space (Shoichet et al., 2007). Burdick et al. (2006) noted slower drug release from gels with high cross-link density, and Lindsey et al. (2015) showed that drug or growth factor release rates were inversely proportional to the hydrogel concentration. Caccavo et al. (2015) found that as the effective pore size increases during the degradation process, the drug release rate can be manipulated using varying hydrogel degradation rates. In addition, the drug and the hydrogel necklace are linked by degradable covalent bonds, and the release system can be regulated by adjusting the ratio of the drug to the binding site and the affinity between the drug and the hydrogel.

Li et al. (2018) loaded paclitaxel-encapsulated liposomes into collagen microchannel scaffolds, which prolonged the sustained release time of paclitaxel. Fingolimod promotes NSC proliferation and induces the favorable differentiation of NSCs, thereby promoting remyelination. It is used in bioscaffolds to be co-implanted with NSCs in SCI lesions (Wang et al., 2015). Injectable hydrogels represented by thermosensitive hydrogels are suitable for treating nerve repair because their injection can minimize the damage to the injured area, fill the cavity generated by the lesion and ensure that the drug is carried directly into the lesion site (Panzer et al., 2020). Zhang et al. (2018) use dpolysialic acid (PSA) to control the developmental properties of the CNS by

regulating cell adhesion and promoting axonal growth. They prepared a PSA/PCL scaffold to encapsulate methylprednisolone (MP). The composite scaffold was transplanted into a rat SCI model, and the findings showed that PCL/PSA/MP with MP could inhibit the expression of axonal demyelination and glial fibrillary acidic protein but promote the recovery of motor function (Zhang et al., 2018).

### 4.3.2 Hydrogel + Growth Factor

Neurotrophic factors can promote neuronal survival and axonal growth during embryonic development, protect damaged neurons and promote the proliferation and differentiation of NSCs (Zhang et al., 2016; Zweckberger et al., 2016). Moreover, they play an important role in preventing microenvironment-induced secondary injury. Many studies have focused on loading neurotrophic factors into bioscaffolds to improve the safety and targeting of damaged nerve repair (Perale et al., 2011). This method helps growth factors overcome the difficulty of passing through the blood-brain barrier and the risks associated with long-term administration (Bajaj et al., 2014; Kondiah et al., 2016). Dai's team used coaxially arranged collagen fiber bundles to functionally bind factors and drugs such as NT3, BDNF, bFGF, LDN193189, SB431542, CHIR99021, P7C3-A20, Eph A4LBD and Plexin B1LBD, and loaded NSCs to repair SCI, significantly reducing the cavitation in the injured area, attenuating the reactive proliferation of glial cells, and promoting axon regeneration and myelination (Han et al., 2019; Liu W. et al., 2020; Yang Y. et al., 2021). Collagen gel complexed with NT-3 can promote axon regeneration in the spinal cord and restore certain functions (Houweling et al., 1998). The copolymer gel that collagen adsorbs NT-3 and FGF-1 to fill poly hydroxyethyl methacrylate, and methyl methacrylate (pHEMA-MMA) promotes the repair of whole SCI in rats (Dewitt et al., 2009). Taylor et al. (2006) implanted a fibrin-loaded NT-3 scaffold into a rat SCI model and reported that fibrin scaffold implantation could significantly reduce glial scarring at the white matter margins of lesions. GDNF was encapsulated in microspheres and delivered to the SCI site *via in situ* injections of sodium alginate gel. The release rate slowed in the rat spinal cord hemi-transaction model; the hydrogel-loaded animals had better functional recovery than the non-GDNF hydrogel-treated group (Ansorena et al., 2013). Zhao et al. (2017) synthesized a new type of heparin-poloxamer (HP) hydrogel, i.e., GDNF bound with temperature-sensitive HP hydrogel. *In situ* injections of GDNF-HP to the injured spinal cord had beneficial effects, including promoting GDNF on the proliferation of NSCs, inhibition of reactive astrogliosis, axon regeneration, neuroprotection against apoptosis, and recovery of bodily functions. Grous et al. (2013) used poly isopropyl acrylamide (PNIPAAAm) and polyethylene glycol (PEG)-cross-linked composite hydrogels to successfully transplant cells or BDNF into the SCI and promote axonal growth and myelination. One-armed or branched PEG is often used as a cross-linking agent to prepare different hydrogel materials (e.g., PEG-cross-linked HA and gelatin composite hydrogels) for transplantating of OPCs into SCI, which can promote their survival and remyelination. Heparin hydrogel was combined with neuroprotective factor (FGF4) to treat SCI in a rat model. The hydrogel released FGF4 in the injured area, which helped inhibit the inflammatory response, increase remyelination, and reduce glial scarring (Wang et al., 2019). EGF-enriched hydrogels promoted synaptic plasticity under local hypoxia after SCI *via* downregulated the *Fbln5* and *Rtl-S3* genes, and upregulated *Clcfl*, *Tgml*, and *Ptgs2* genes (Chan et al., 2019).

### 4.3.3 Hydrogel + Peptide

A new biomaterial, i.e., self-assembled peptide hydrogel has the advantages of moderate mechanical tension and permeability, low cost, good viscoelasticity, good biocompatibility, low immunogenicity, and being non-inflammatory (Rad-Malekshahi et al., 2016). The degradation products of self-assembled peptide hydrogels can be absorbed and are utilized widely in tissue engineering, drug release, hemostasis, and as antibacterial agents. Recent studies have shown that self-loading peptides have neuroprotection after SCI during transplantation, reduce glial scar formation and damage cavity formation, and promote nerve repair.

The chemical properties of hydrogels usually make it difficult to promote cell adhesion and new tissue formation. Certain chemical modifications are usually used for these non-cell-adhesive hydrogels, such as adding natural extracellular matrix components to modulate cell adhesion and growth (Hiraoka et al., 2009). IKVAV-, GYIGSR-, and RGD-modified natural hydrogel materials were shown to promote neural cell adhesion and better direct differentiation (Hiraoka et al., 2009). Agarose hydrogels supplemented with RGD polypeptides can promote cell migration and synapse growth in three-dimensional cultures (Kriebel et al., 2014). Park et al. (2010) designed and synthesized an -IKVAV/-RGD nanofiber hydrogel that can support neural progenitor or neural stem cell differentiation into neurons and astrocytes in a three-dimensional environment. Additionally, this hydrogel provides a more favorable environment for nerve regeneration in sciatic nerve defects, intracerebral hemorrhage, and spinal cord transaction models. Gelain et al. (2012) injected the Ac-FAQ-LDLK12 self-assembled short peptide hydrogel scaffold into an acute SCI model. The results showed that it could promote nerve tissue regeneration and improve motor skills function. Cigognini et al. (2014) and others injected RADA16-4G-BMHP1 and Ac-FAQ-LDLK12 hydrogels into the SCI site. Both short peptides had a hemostatic effect on the third day after the injury, and axon regeneration at the injury and spinal cord hematoma site was significantly improved 28 days after transplantation. Guo et al. (2007) isolated Schwann and nerve cells and implanted them into RADA16 self-assembled short peptide hydrogel scaffolds transplanted into SCI rats. Both Schwann and nerve cells migrated, and spinal cord repair was observed, showing that the self-assembled short peptide hydrogel scaffold played a bridging role in the injured spinal cord tissue. Nanofibrous hydrogel materials linked to IKVAV polypeptides can significantly promote the adhesion of neural cells and the differentiation of stem cells into neurons (Sehgal and Banerjee, 2013). Cheng et al. (2013) found that RADA(16)-IKVAV can self-assemble into a nanofiber morphology with a double-layer β-

sheet structure and form a hydrogel with mechanical stiffness similar to that of brain tissue. Histological analysis showed that RADA(16)-IKVAV self-assembled peptide hydrogels enhanced the survival of loaded NSCs and reduced astrocyte generation. Chitosan hydrogel linked to NT-3 enhanced the ability of NSCs to differentiate into neurons (Yang et al., 2010a). Sodium alginate can generate highly active aldehyde groups grafted with various cytokines and peptides (Le-Tien et al., 2004). Liu et al. (2013) injected K2(QL) and 6K2(QL6) hydrogels into SCI rats and found that it could significantly reduce post-traumatic apoptosis, inflammatory response, and astrogliosis, as well as contribute to organizing protective effects. Liu H. et al. (2020) used RADA16-IKVAV for loading CNTF, a FGF, EGF, and PDGF-AA and RADA16-RGD for loading BDNF, NT3, IGF, b FGF, GDNF, and β-NGF. The prepared functional self-assembling polypeptide hydrogel was implanted into the SCI model, promoting the recruitment and proliferation of endogenous NSCs in the injured area and promoting the regeneration of myelinated axons. Iwasaki et al. (2014) also used the self-assembling polypeptide QL6 series to encapsulate neural progenitor cells (NPCs) to improve the microenvironment after SCI. The QL6 series grafts were effective in acute inflammation of SCI. The protection of MNs in areas adjacent to the injury in a mouse model of SCI was significantly better than that of the control group at 12 weeks after transplantation. Additionally, improved neurobehavioral function, as well as increased activity area and step length, were detected in the forelimbs of rats. Zweckberger et al. (2015) injected QL6 self-assembled peptide scaffolds into the injury site 2 weeks after the acute phase of SCI. They injected NPCs into the adjacent spinal cord, combined with a slow-release growth factor micropump to ensure cell survival. The hydrogel matrix could effectively improve the viability and differentiation potential of the cells and reduce scar tissue formation. The self-assembled short-peptide hydrogel SPG-178 scaffold designed by Ando et al. (2016) can induce neurotrophic factors in the treatment of SCI. *In vitro* studies have shown that SPG-178 can increase the levels of the nerve growth factor brain-derived neurotrophic factor (NT-4), TrkA, and TrkB. *In vivo* studies show that SPG-178 can increase the expression of neurotrophic factors, as well as reduce inflammation and glial scarring. Using N-isopropylacrylamide (NIPAM) monomer and PEG as raw materials to synthesize thermosensitive hydrogels with fast temperature response *via* reversible addition-fragmentation chain transfer (RAFT) polymerization while introducing the polypeptide IKVAV, which has specific biological activity on spinal cord repair, improves the material's biological activity. The constructed gel scaffolds were cultured with NSCs *in vitro*, and the results showed that the gel scaffolds could promote the adhesion of NSCs and the expression of the adhesion gene *Lamb2*, effectively guiding stem cell differentiation into neurons. The results of *in vivo* experiments showed that the motor function of the rats was restored and that the gel scaffold effectively reduced glial scar formation, lesion size, and cyst area (Long et al., 2020).

## 5 CONCLUSION

SCI is typically caused by vertebral body injury, resulting in neurological or motor dysfunction and placing a heavy burden on patients and their families. Traditional treatment methods do not allow drugs to pass the blood-brain barrier and concentrate effective doses on the injured spinal cord. Hydrogels can effectively simulate the local soft tissue environment of injury. Optimized hydrogels that are modified using different methods can be used as scaffolds to load drugs or cells, achieve local long-term release, support and guide axon regeneration, and effectively improve the treatment of spinal cord injury. They also overcome the uncertainty of local drug administration, improve the utilization rate of drugs or cells, and enhance the duration of drug action. The models currently used in SCI mainly include the spinal cord contusion model (the most widely used in scientific research), the spinal cord transection injury model, the spinal cord compression injury model (a common model for SCI), the spinal cord distraction injury model, the transverse spinal cord fracture and dislocation (cervical spinal cord injury) model, and the spinal cord ischemia-reperfusion injury model. Each model varies in its degree of damage performance; therefore, the applied treatment cannot fully evaluate the treatment effect. In addition, the repair effect of hydrogels on models of SCI caused by inflammation or tumor cannot be assessed. Axon regeneration is an important evaluation index for SCI repair; however, whether new axons have biological functions similar to the unique nerve tracts in spinal cord tissue requires further investigation. The microenvironment is another important factor in SCI repair. Future work on hydrogels should focus on how to modify their properties, improve their loading capacity, promote cell proliferation and differentiation, and release drugs and factors reasonably and effectively as well as explore more suitable and effective novel hydrogel scaffold materials, construct a combined treatment of hydrogel-carrying cells and drugs, and improve the microenvironment of the injured area to achieve complete repair of SCI.

## AUTHOR CONTRIBUTIONS

Data curation: ZL. Investigation: ZL. Supervision: SZ. Validation: CD. Writing-original draft: TZ, ZL, and CD. Writing-review and editing: ZL, CD, TZ, and SZ.

## FUNDING

This study was supported by the Department of science and technology of Jilin Province (Grant No. 20190304028YY).

## REFERENCES


Ahmad, Z., Salman, S., Khan, S. A., Amin, A., Rahman, Z. U., Al-Ghamdi, Y. O., et al. (2022). Versatility of Hydrogels: From Synthetic Strategies, Classification, and Properties to Biomedical Applications. *Gels* 8, 167. doi:10.3390/gels8030167

Ando, K., Imagama, S., Ito, Z., Kobayashi, K., Hida, T., Nakashima, H., et al. (2016). Self-assembling Peptide Reduces Glial Scarring, Attenuates Posttraumatic Inflammation, and Promotes Neurite Outgrowth of Spinal Motor Neurons. *Spine (Phila Pa 1976)* 41, E1201–E1207. doi:10.1097/brs.0000000000001611

Ansorena, E., De Berdt, P., Ucakar, B., Simón-Yarza, T., Jacobs, D., Schakman, O., et al. (2013). Injectable Alginate Hydrogel Loaded with GDNF Promotes Functional Recovery in a Hemisection Model of Spinal Cord Injury. *Int. J. Pharm.* 455, 148–158. doi:10.1016/j.ijpharm.2013.07.045

Arlov, O., and Skjak-Braek, G. (2017). Sulfated Alginates as Heparin Analogues: A Review of Chemical and Functional Properties. *Molecules* 22, 778. doi:10.3390/molecules22050778

Ashton, R. S., Banerjee, A., Punyani, S., Schaffer, D. V., and Kane, R. S. (2007). Scaffolds Based on Degradable Alginate Hydrogels and Poly(lactide-Co-Glycolide) Microspheres for Stem Cell Culture. *Biomaterials* 28, 5518–5525. doi:10.1016/j.biomaterials.2007.08.038

Assunção-Silva, R. C., Gomes, E. D., Sousa, N., Silva, N. A., and Salgado, A. J. (2015). Hydrogels and Cell Based Therapies in Spinal Cord Injury Regeneration. *Stem Cells Int.* 2015, 948040. doi:10.1155/2015/948040

Austin, J. W., Kang, C. E., Baumann, M. D., Didiodato, L., Satkunendrarajah, K., Wilson, J. R., et al. (2012). The Effects of Intrathecal Injection of a Hyaluronan-Based Hydrogel on Inflammation, Scarring and Neurobehavioural Outcomes in a Rat Model of Severe Spinal Cord Injury Associated with Arachnoiditis. *Biomaterials* 33, 4555–4564. doi:10.1016/j.biomaterials.2012.03.022

Babaloo, H., Ebrahimi-Barough, S., Derakhshan, M. A., Yazdankhah, M., Lotfibakhshaiesh, N., Soleimani, M., et al. (2019). PCL/gelatin Nanofibrous Scaffolds with Human Endometrial Stem cells/Schwann Cells Facilitate Axon Regeneration in Spinal Cord Injury. *J. Cell. Physiology* 234, 11060–11069. doi:10.1002/jcp.27936

Badner, A., Siddiqui, A. M., and Fehlings, M. G. (2017). Spinal Cord Injuries: How Could Cell Therapy Help? *Expert Opin. Biol. Ther.* 17, 529–541. doi:10.1080/14712598.2017.1308481

Bajaj, P., Schweller, R. M., Khademhosseini, A., West, J. L., and Bashir, R. (2014). 3D Biofabrication Strategies for Tissue Engineering and Regenerative Medicine. *Annu. Rev. Biomed. Eng.* 16, 247–276. doi:10.1146/annurev-bioeng-071813-105155

Balgude, A., Yu, X., Szymanski, A., and Bellamkonda, R. V. (2001). Agarose Gel Stiffness Determines Rate of DRG Neurite Extension in 3D Cultures. *Biomaterials* 22, 1077–1084. doi:10.1016/s0142-9612(00)00350-1

Banerjee, A., Arha, M., Choudhary, S., Ashton, R. S., Bhatia, S. R., Schaffer, D. V., et al. (2009). The Influence of Hydrogel Modulus on the Proliferation and Differentiation of Encapsulated Neural Stem Cells. *Biomaterials* 30, 4695–4699. doi:10.1016/j.biomaterials.2009.05.050

Baptiste, D. C., and Fehlings, M. G. (2006). Pharmacological Approaches to Repair the Injured Spinal Cord. *J. Neurotrauma* 23, 318–334. doi:10.1089/neu.2006.23.318

Barbour, H. R., Plant, C. D., Harvey, A. R., and Plant, G. W. (2013). Tissue Sparing, Behavioral Recovery, Supraspinal Axonal Sparing/regeneration Following Sub-acute Glial Transplantation in a Model of Spinal Cord Contusion. *BMC Neurosci.* 14, 106. doi:10.1186/1471-2202-14-106

Barclay, T. G., Day, C. M., Petrovsky, N., and Garg, S. (2019). Review of Polysaccharide Particle-Based Functional Drug Delivery. *Carbohydr. Polym.* 221, 94–112. doi:10.1016/j.carbpol.2019.05.067

Bertlein, S., Brown, G., Lim, K. S., Jungst, T., Boeck, T., Blunk, T., et al. (2017). Thiol-Ene Clickable Gelatin: A Platform Bioink for Multiple 3D Biofabrication Technologies. *Adv. Mater* 29. doi:10.1002/adma.201703404

Borgens, R. B., Shi, R., and Bohnert, D. (2002). Behavioral Recovery from Spinal Cord Injury Following Delayed Application of Polyethylene Glycol. *J. Exp. Biol.* 205, 1–12. doi:10.1242/jeb.205.1.1

Bozza, A., Coates, E. E., Incitti, T., Ferlin, K. M., Messina, A., Menna, E., et al. (2014). Neural Differentiation of Pluripotent Cells in 3D Alginate-Based Cultures. *Biomaterials* 35, 4636–4645. doi:10.1016/j.biomaterials.2014.02.039

Burdick, J. A., Ward, M., Liang, E., Young, M. J., and Langer, R. (2006). Stimulation of Neurite Outgrowth by Neurotrophins Delivered from Degradable Hydrogels. *Biomaterials* 27, 452–459. doi:10.1016/j.biomaterials.2005.06.034

Caccavo, D., Cascone, S., Lamberti, G., and Barba, A. A. (2015). Modeling the Drug Release from Hydrogel-Based Matrices. *Mol. Pharm.* 12, 474–483. doi:10.1021/mp500563n

Caldwell, A. S., Rao, V. V., Golden, A. C., and Anseth, K. S. (2020). Porous Bio-Click Microgel Scaffolds Control hMSC Interactions and Promote Their Secretory Properties. *Biomaterials* 232, 119725. doi:10.1016/j.biomaterials.2019.119725

Celikkin, N., Mastrogiacomo, S., Jaroszewicz, J., Walboomers, X. F., and Swieszkowski, W. (2018). Gelatin Methacrylate Scaffold for Bone Tissue Engineering: The Influence of Polymer Concentration. *J. Biomed. Mat. Res.* 106, 201–209. doi:10.1002/jbm.a.36226

Chan, S. J., Niu, W., Hayakawa, K., Hamanaka, G., Wang, X., Cheah, P. S., et al. (2019). Promoting Neuro-Supportive Properties of Astrocytes with Epidermal Growth Factor Hydrogels. *Stem Cells Transl. Med.* 8, 1242–1248. doi:10.1002/sctm.19-0159

Chedly, J., Soares, S., Montembault, A., Von Boxberg, Y., Veron-Ravaille, M., Mouffle, C., et al. (2017). Physical Chitosan Microhydrogels as Scaffolds for Spinal Cord Injury Restoration and Axon Regeneration. *Biomaterials* 138, 91–107. doi:10.1016/j.biomaterials.2017.05.024

Chen, G., Hu, Y. R., Wan, H., Xia, L., Li, J. H., Yang, F., et al. (2010). Functional Recovery Following Traumatic Spinal Cord Injury Mediated by a Unique Polymer Scaffold Seeded with Neural Stem Cells and Schwann Cells. *Chin. Med. J. Engl.* 123, 2424–2431.

Chen, J., Chen, Y. Q., Shi, Y. J., Ding, S. Q., Shen, L., Wang, R., et al. (2021). VX-765 Reduces Neuroinflammation after Spinal Cord Injury in Mice. *Neural Regen. Res.* 16, 1836–1847. doi:10.4103/1673-5374.306096

Chen, X., Zhao, Y., Li, X., Xiao, Z., Yao, Y., Chu, Y., et al. (2018). Functional Multichannel Poly(Propylene Fumarate)-Collagen Scaffold with Collagen-Binding Neurotrophic Factor 3 Promotes Neural Regeneration after Transected Spinal Cord Injury. *Adv. Healthc. Mater* 7, e1800315. doi:10.1002/adhm.201800315

Chen, X., Wu, J., Sun, R., Zhao, Y., Li, Y., Pan, J., et al. (2020). Tubular Scaffold with Microchannels and an H-shaped Lumen Loaded with Bone Marrow Stromal Cells Promotes Neuroregeneration and Inhibits Apoptosis after Spinal Cord Injury. *J. Tissue Eng. Regen. Med.* 14, 397–411. doi:10.1002/term.2996

Chen, Z., Han, X., Ouyang, X., Fang, J., Huang, X., and Wei, H. (2019). Transplantation of Induced Pluripotent Stem Cell-Derived Mesenchymal Stem Cells Improved Erectile Dysfunction Induced by Cavernous Nerve Injury. *Theranostics* 9, 6354–6368. doi:10.7150/thno.34008

Cheng, T.-Y., Chen, M.-H., Chang, W.-H., Huang, M.-Y., and Wang, T.-W. (2013). Neural Stem Cells Encapsulated in a Functionalized Self-Assembling Peptide Hydrogel for Brain Tissue Engineering. *Biomaterials* 34, 2005–2016. doi:10.1016/j.biomaterials.2012.11.043

Choo, A. M., Liu, J., Dvorak, M., Tetzlaff, W., and Oxland, T. R. (2008). Secondary Pathology Following Contusion, Dislocation, and Distraction Spinal Cord Injuries. *Exp. Neurol.* 212, 490–506. doi:10.1016/j.expneurol.2008.04.038

Chu, K.-A., Wang, S.-Y., Yeh, C.-C., Fu, T.-W., Fu, Y.-Y., Ko, T.-L., et al. (2019). Reversal of Bleomycin-Induced Rat Pulmonary Fibrosis by a Xenograft of Human Umbilical Mesenchymal Stem Cells from Wharton's Jelly. *Theranostics* 9, 6646–6664. doi:10.7150/thno.33741

Cigognini, D., Silva, D., Paloppi, S., and Gelain, F. (2014). Evaluation of Mechanical Properties and Therapeutic Effect of Injectable Self-Assembling Hydrogels for Spinal Cord Injury. *J. Biomed. Nanotechnol.* 10, 309–323. doi:10.1166/jbn.2014.1759

Collins, M. N., and Birkinshaw, C. (2013). Hyaluronic Acid Based Scaffolds for Tissue Engineering-A Review. *Carbohydr. Polym.* 92, 1262–1279. doi:10.1016/j.carbpol.2012.10.028

Cox, A., Varma, A., and Banik, N. (2015). Recent Advances in the Pharmacologic Treatment of Spinal Cord Injury. *Metab. Brain Dis.* 30, 473–482. doi:10.1007/s11011-014-9547-y

Cregg, J. M., Depaul, M. A., Filous, A. R., Lang, B. T., Tran, A., and Silver, J. (2014). Functional Regeneration beyond the Glial Scar. *Exp. Neurol.* 253, 197–207. doi:10.1016/j.expneurol.2013.12.024

Dadsetan, M., Liu, Z., Pumberger, M., Giraldo, C. V., Ruesink, T., Lu, L., et al. (2010). A Stimuli-Responsive Hydrogel for Doxorubicin Delivery. *Biomaterials* 31, 8051–8062. doi:10.1016/j.biomaterials.2010.06.054

Delmar, K., and Bianco-Peled, H. (2016). Composite Chitosan Hydrogels for Extended Release of Hydrophobic Drugs. *Carbohydr. Polym.* 136, 570–580. doi:10.1016/j.carbpol.2015.09.072

Deng, Q. Y., Li, S. R., Cai, W. Q., and Su, B. Y. (2006). Poly-lactic Acid and Agarose Gelatin Play an Active Role in the Recovery of Spinal Cord Injury. *Neurosci. Bull.* 22, 73–78.

Dewitt, D. D., Kaszuba, S. N., Thompson, D. M., and Stegemann, J. P. (2009). Collagen I-Matrigel Scaffolds for Enhanced Schwann Cell Survival and Control of Three-Dimensional Cell Morphology. *Tissue Eng. Part A* 15, 2785–2793. doi:10.1089/ten.tea.2008.0406

Dimatteo, R., Darling, N. J., and Segura, T. (2018). *In Situ* forming Injectable Hydrogels for Drug Delivery and Wound Repair. *Adv. Drug Deliv. Rev.* 127, 167–184. doi:10.1016/j.addr.2018.03.007

Donnelly, D. J., and Popovich, P. G. (2008). Inflammation and its Role in Neuroprotection, Axonal Regeneration and Functional Recovery after Spinal Cord Injury. *Exp. Neurol.* 209, 378–388. doi:10.1016/j.expneurol.2007.06.009

Donoghue, P. S., Lamond, R., Boomkamp, S. D., Sun, T., Gadegaard, N., Riehle, M. O., et al. (2013). The Development of a ε-Polycaprolactone Scaffold for Central Nervous System Repair. *Tissue Eng. Part A* 19, 497–507. doi:10.1089/ten.tea.2012.0382

Doulames, V., and Plant, G. (2016). Induced Pluripotent Stem Cell Therapies for Cervical Spinal Cord Injury. *Int. J. Mol. Sci.* 17, 530. doi:10.3390/ijms17040530

Duerstock, B. S., and Borgens, R. B. (2002). Three-dimensional Morphometry of Spinal Cord Injury Following Polyethylene Glycol Treatment. *J. Exp. Biol.* 205, 13–24. doi:10.1242/jeb.205.1.13

Egawa, E. Y., Kato, K., Hiraoka, M., Nakaji-Hirabayashi, T., and Iwata, H. (2011). Enhanced Proliferation of Neural Stem Cells in a Collagen Hydrogel Incorporating Engineered Epidermal Growth Factor. *Biomaterials* 32, 4737–4743. doi:10.1016/j.biomaterials.2011.03.033

Ek, C. J., Habgood, M. D., Dennis, R., Dziegielewska, K. M., Mallard, C., Wheaton, B., et al. (2012). Pathological Changes in the White Matter after Spinal Contusion Injury in the Rat. *PLoS One* 7, e43484. doi:10.1371/journal.pone.0043484

Emmez, H., Börcek, A. Ö., Kaymaz, M., Kaymaz, F., Durdağ, E., Çivi, S., et al. (2010). Neuroprotective Effects of Gabapentin in Experimental Spinal Cord Injury. *World Neurosurg.* 73, 729–734. doi:10.1016/j.wneu.2010.04.008

Fan, L., Liu, C., Chen, X., Zou, Y., Zhou, Z., Lin, C., et al. (2018). Directing Induced Pluripotent Stem Cell Derived Neural Stem Cell Fate with a Three-Dimensional Biomimetic Hydrogel for Spinal Cord Injury Repair. *ACS Appl. Mat. Interfaces* 10, 17742–17755. doi:10.1021/acsami.8b05293

Fang, X., and Song, H. (2019). Synthesis of Cerium Oxide Nanoparticles Loaded on Chitosan for Enhanced Auto-Catalytic Regenerative Ability and Biocompatibility for the Spinal Cord Injury Repair. *J. Photochem. Photobiol. B Biol.* 191, 83–87. doi:10.1016/j.jphotobiol.2018.11.016

Fang, X., Xie, J., Zhong, L., Li, J., Rong, D., Li, X., et al. (2016). Biomimetic Gelatin Methacrylamide Hydrogel Scaffolds for Bone Tissue Engineering. *J. Mat. Chem. B* 4, 1070–1080. doi:10.1039/c5tb02251g

Fitch, M. T., Doller, C., Combs, C. K., Landreth, G. E., and Silver, J. (1999). Cellular and Molecular Mechanisms of Glial Scarring and Progressive Cavitation: *In Vivo* and *In Vitro* Analysis of Inflammation-Induced Secondary Injury after CNS Trauma. *J. Neurosci.* 19, 8182–8198. doi:10.1523/jneurosci.19-19-08182.1999

Führmann, T., Tam, R. Y., Ballarin, B., Coles, B., Elliott Donaghue, I., Van Der Kooy, D., et al. (2016). Injectable Hydrogel Promotes Early Survival of Induced Pluripotent Stem Cell-Derived Oligodendrocytes and Attenuates Longterm Teratoma Formation in a Spinal Cord Injury Model. *Biomaterials* 83, 23–36. doi:10.1016/j.biomaterials.2015.12.032

Gao, L., Peng, Y., Xu, W., He, P., Li, T., Lu, X., et al. (2020). Progress in Stem Cell Therapy for Spinal Cord Injury. *Stem Cells Int.* 2020, 2853650. doi:10.1155/2020/2853650

Gelain, F., Cigognini, D., Caprini, A., Silva, D., Colleoni, B., Donegá, M., et al. (2012). New Bioactive Motifs and Their Use in Functionalized Self-Assembling Peptides for NSC Differentiation and Neural Tissue Engineering. *Nanoscale* 4, 2946–2957. doi:10.1039/c2nr30220a

Gros, T., Sakamoto, J. S., Blesch, A., Havton, L. A., and Tuszynski, M. H. (2010). Regeneration of Long-Tract Axons through Sites of Spinal Cord Injury Using Templated Agarose Scaffolds. *Biomaterials* 31, 6719–6729. doi:10.1016/j.biomaterials.2010.04.035

Grous, L. C., Vernengo, J., Jin, Y., Himes, B. T., Shumsky, J. S., Fischer, I., et al. (2013). Implications of poly(N-Isopropylacrylamide)-G-Poly(ethylene Glycol) with Codissolved Brain-Derived Neurotrophic Factor Injectable Scaffold on Motor Function Recovery Rate Following Cervical Dorsolateral Funiculotomy in the Rat. *J. Neurosurg Spine* 18, 641–652. doi:10.3171/2013.3.spine12874

Grulova, I., Slovinska, L., Blaško, J., Devaux, S., Wisztorski, M., Salzet, M., et al. (2015). Delivery of Alginate Scaffold Releasing Two Trophic Factors for Spinal Cord Injury Repair. *Sci. Rep.* 5, 13702. doi:10.1038/srep13702

Günther, M. I., Weidner, N., Müller, R., and Blesch, A. (2015). Cell-seeded Alginate Hydrogel Scaffolds Promote Directed Linear Axonal Regeneration in the Injured Rat Spinal Cord. *Acta Biomater.* 27, 140–150. doi:10.1016/j.actbio.2015.09.001

Guo, J., Su, H., Zeng, Y., Liang, Y.-X., Wong, W. M., Ellis-Behnke, R. G., et al. (2007). Reknitting the Injured Spinal Cord by Self-Assembling Peptide Nanofiber Scaffold. *Nanomedicine Nanotechnol. Biol. Med.* 3, 311–321. doi:10.1016/j.nano.2007.09.003

Hall, E. D., and Springer, J. E. (2004). Neuroprotection and Acute Spinal Cord Injury: a Reappraisal. *Neurotherapeutics* 1, 80–100. doi:10.1602/neurorx.1.1.80

Han, G. H., Kim, S. J., Ko, W.-K., Lee, D., Lee, J. S., Nah, H., et al. (2020). Injectable Hydrogel Containing Tauroursodeoxycholic Acid for Anti-neuroinflammatory Therapy after Spinal Cord Injury in Rats. *Mol. Neurobiol.* 57, 4007–4017. doi:10.1007/s12035-020-02010-4

Han, S., Yin, W., Li, X., Wu, S., Cao, Y., Tan, J., et al. (2019). Pre-Clinical Evaluation of CBD-NT3 Modified Collagen Scaffolds in Completely Spinal Cord Transected Non-human Primates. *J. Neurotrauma* 36, 2316–2324. doi:10.1089/neu.2018.6078

Hejcl, A., Lesný, P., Prádný, M., Michálek, J., Jendelová, P., Stulík, J., et al. (2008). Biocompatible Hydrogels in Spinal Cord Injury Repair. *Physiol. Res.* 57 (Suppl. 3), S121–S132. doi:10.33549/physiolres.931606

Hiraoka, M., Kato, K., Nakaji-Hirabayashi, T., and Iwata, H. (2009). Enhanced Survival of Neural Cells Embedded in Hydrogels Composed of Collagen and Laminin-Derived Cell Adhesive Peptide. *Bioconjugate Chem.* 20, 976–983. doi:10.1021/bc9000068

Horn, E. M., Beaumont, M., Shu, X. Z., Harvey, A., Prestwich, G. D., Horn, K. M., et al. (2007). Influence of Cross-Linked Hyaluronic Acid Hydrogels on Neurite Outgrowth and Recovery from Spinal Cord Injury. *J Neurosurg Spine* 6, 133–140. doi:10.3171/spi.2007.6.2.133

Hosseinkhani, H., Hiraoka, Y., Li, C.-H., Chen, Y.-R., Yu, D.-S., Hong, P.-D., et al. (2013). Engineering Three-Dimensional Collagen-IKVAV Matrix to Mimic Neural Microenvironment. *ACS Chem. Neurosci.* 4, 1229–1235. doi:10.1021/cn400075h

Houweling, D. A., Lankhorst, A. J., Gispen, W. H., Bär, P. R., and Joosten, E. A. J. (1998). Collagen Containing Neurotrophin-3 (NT-3) Attracts Regrowing Injured Corticospinal Axons in the Adult Rat Spinal Cord and Promotes Partial Functional Recovery. *Exp. Neurol.* 153, 49–59. doi:10.1006/exnr.1998.6867

Hu, W., Wang, Z., Xiao, Y., Zhang, S., and Wang, J. (2019). Advances in Crosslinking Strategies of Biomedical Hydrogels. *Biomater. Sci.* 7, 843–855. doi:10.1039/c8bm01246f

Huang, Q., Zou, Y., Arno, M. C., Chen, S., Wang, T., Gao, J., et al. (2017). Hydrogel Scaffolds for Differentiation of Adipose-Derived Stem Cells. *Chem. Soc. Rev.* 46, 6255–6275. doi:10.1039/c6cs00052e

Hurlbert, R. J., Hadley, M. N., Walters, B. C., Aarabi, B., Dhall, S. S., Gelb, D. E., et al. (2015). Pharmacological Therapy for Acute Spinal Cord Injury. *Neurosurgery* 76 (Suppl. 1), S71–S83. doi:10.1227/01.neu.0000462080.04196.f7

Im, J. S., Bai, B. C., Jin In, S., and Lee, Y.-S. (2010). Improved Photodegradation Properties and Kinetic Models of a Solar-Light-Responsive Photocatalyst when Incorporated into Electrospun Hydrogel Fibers. *J. Colloid Interface Sci.* 346, 216–221. doi:10.1016/j.jcis.2010.02.043

Iwasaki, M., Wilcox, J. T., Nishimura, Y., Zweckberger, K., Suzuki, H., Wang, J., et al. (2014). Synergistic Effects of Self-Assembling Peptide and Neural Stem/progenitor Cells to Promote Tissue Repair and Forelimb Functional Recovery in Cervical Spinal Cord Injury. *Biomaterials* 35, 2617–2629. doi:10.1016/j.biomaterials.2013.12.019

Jain, A., Kim, Y.-T., Mckeon, R. J., and Bellamkonda, R. V. (2006). *In Situ* gelling Hydrogels for Conformal Repair of Spinal Cord Defects, and Local Delivery of BDNF after Spinal Cord Injury. *Biomaterials* 27, 497–504. doi:10.1016/j.biomaterials.2005.07.008

Johnson, C. D., D'Amato, A. R., Puhl, D. L., Wich, D. M., Vesperman, A., and Gilbert, R. J. (2018). Electrospun Fiber Surface Nanotopography Influences Astrocyte-Mediated Neurite Outgrowth. *Biomed. Mat.* 13, 054101. doi:10.1088/1748-605x/aac4de

Johnson, P. J., Parker, S. R., and Sakiyama-Elbert, S. E. (2010). Fibrin-based Tissue Engineering Scaffolds Enhance Neural Fiber Sprouting and Delay the

Accumulation of Reactive Astrocytes at the Lesion in a Subacute Model of Spinal Cord Injury. *J. Biomed. Mat. Res.* 92A, 152–163. doi:10.1002/jbm.a.32343

Joung, D., Truong, V., Neitzke, C. C., Guo, S. Z., Walsh, P. J., Monat, J. R., et al. (2018). 3D Printed Stem-Cell Derived Neural Progenitors Generate Spinal Cord Scaffolds. *Adv. Funct. Mater* 28, 1801850. doi:10.1002/adfm.201801850

Jukes, J. M., Van Der Aa, L. J., Hiemstra, C., Van Veen, T., Dijkstra, P. J., Zhong, Z., et al. (2010). A Newly Developed Chemically Crosslinked Dextran-Poly(ethylene Glycol) Hydrogel for Cartilage Tissue Engineering. *Tissue Eng. Part A* 16, 565–573. doi:10.1089/ten.tea.2009.0173

Kataoka, K., Suzuki, Y., Kitada, M., Hashimoto, T., Chou, H., Bai, H., et al. (2004). Alginate Enhances Elongation of Early Regenerating Axons in Spinal Cord of Young Rats. *Tissue Eng.* 10, 493–504. doi:10.1089/107632704323061852

Katoh, H., Yokota, K., and Fehlings, M. G. (2019). Regeneration of Spinal Cord Connectivity through Stem Cell Transplantation and Biomaterial Scaffolds. *Front. Cell. Neurosci.* 13, 248. doi:10.3389/fncel.2019.00248

Katz, J. S., and Burdick, J. A. (2009). Hydrogel Mediated Delivery of Trophic Factors for Neural Repair. *WIREs Nanomed Nanobiotechnol.* 1, 128–139. doi:10.1002/wnan.10

Khajouei, S., Ravan, H., and Ebrahimi, A. (2020). DNA Hydrogel-Empowered Biosensing. *Adv. Colloid Interface Sci.* 275, 102060. doi:10.1016/j.cis.2019.102060

King, V. R., Alovskaya, A., Wei, D. Y. T., Brown, R. A., and Priestley, J. V. (2010). The Use of Injectable Forms of Fibrin and Fibronectin to Support Axonal Ingrowth after Spinal Cord Injury. *Biomaterials* 31, 4447–4456. doi:10.1016/j.biomaterials.2010.02.018

Klapka, N., and Müller, H. W. (2006). Collagen Matrix in Spinal Cord Injury. *J. Neurotrauma* 23, 422–436. doi:10.1089/neu.2006.23.422

Kommareddy, S., and Amiji, M. (2005). Preparation and Evaluation of Thiol-Modified Gelatin Nanoparticles for Intracellular DNA Delivery in Response to Glutathione. *Bioconjugate Chem.* 16, 1423–1432. doi:10.1021/bc050146t

Kondiah, P. J., Choonara, Y. E., Kondiah, P. P., Marimuthu, T., Kumar, P., Du Toit, L. C., et al. (2016). A Review of Injectable Polymeric Hydrogel Systems for Application in Bone Tissue Engineering. *Molecules* 21. doi:10.3390/molecules21111580

Kriebel, A., Rumman, M., Scheld, M., Hodde, D., Brook, G., and Mey, J. (2014). Three-dimensional Configuration of Orientated Fibers as Guidance Structures for Cell Migration and Axonal Growth. *J. Biomed. Mat. Res.* 102, 356–365. doi:10.1002/jbm.b.33014

La Manna, S., Di Natale, C., Onesto, V., and Marasco, D. (2021). Self-Assembling Peptides: From Design to Biomedical Applications. *Int. J. Mol. Sci.* 22, 12662. doi:10.3390/ijms222312662

Lagreca, E., Onesto, V., Di Natale, C., La Manna, S., Netti, P. A., and Vecchione, R. (2020). Recent Advances in the Formulation of PLGA Microparticles for Controlled Drug Delivery. *Prog. Biomater.* 9, 153–174. doi:10.1007/s40204-020-00139-y

Lakard, S., Herlem, G., Propper, A., Kastner, A., Michel, G., Vallès-Villarreal, N., et al. (2004). Adhesion and Proliferation of Cells on New Polymers Modified Biomaterials. *Bioelectrochemistry* 62, 19–27. doi:10.1016/j.bioelechem.2003.09.009

Laverty, P. H., Leskovar, A., Breur, G. J., Coates, J. R., Bergman, R. L., Widmer, W. R., et al. (2004). A Preliminary Study of Intravenous Surfactants in Paraplegic Dogs: Polymer Therapy in Canine Clinical SCI. *J. Neurotrauma* 21, 1767–1777. doi:10.1089/neu.2004.21.1767

Le-Tien, C., Millette, M., Lacroix, M., and Mateescu, M.-A. (2004). Modified Alginate Matrices for the Immobilization of Bioactive Agents. *Biotechnol. Appl. Biochem.* 39, 189–198. doi:10.1042/ba20030054

Li, H., Koenig, A. M., Sloan, P., and Leipzig, N. D. (2014). *In Vivo* assessment of Guided Neural Stem Cell Differentiation in Growth Factor Immobilized Chitosan-Based Hydrogel Scaffolds. *Biomaterials* 35, 9049–9057. doi:10.1016/j.biomaterials.2014.07.038

Li, J., and Mooney, D. J. (2016). Designing Hydrogels for Controlled Drug Delivery. *Nat. Rev. Mater* 1, 16071. doi:10.1038/natrevmats.2016.71

Li, L., Zhang, Y., Mu, J., Chen, J., Zhang, C., Cao, H., et al. (2020). Transplantation of Human Mesenchymal Stem-Cell-Derived Exosomes Immobilized in an Adhesive Hydrogel for Effective Treatment of Spinal Cord Injury. *Nano Lett.* 20, 4298–4305. doi:10.1021/acs.nanolett.0c00929

Li, X., Fan, C., Xiao, Z., Zhao, Y., Zhang, H., Sun, J., et al. (2018). A Collagen Microchannel Scaffold Carrying Paclitaxel-Liposomes Induces Neuronal Differentiation of Neural Stem Cells through Wnt/β-Catenin Signaling for Spinal Cord Injury Repair. *Biomaterials* 183, 114–127. doi:10.1016/j.biomaterials.2018.08.037

Lindsey, S., Piatt, J. H., Worthington, P., Sönmez, C., Satheye, S., Schneider, J. P., et al. (2015). Beta Hairpin Peptide Hydrogels as an Injectable Solid Vehicle for Neurotrophic Growth Factor Delivery. *Biomacromolecules* 16, 2672–2683. doi:10.1021/acs.biomac.5b00541

Liu, A. L., and García, A. J. (2016). Methods for Generating Hydrogel Particles for Protein Delivery. *Ann. Biomed. Eng.* 44, 1946–1958. doi:10.1007/s10439-016-1637-z

Liu, H., Xu, X., Tu, Y., Chen, K., Song, L., Zhai, J., et al. (2020). Engineering Microenvironment for Endogenous Neural Regeneration after Spinal Cord Injury by Reassembling Extracellular Matrix. *ACS Appl. Mat. Interfaces* 12, 17207–17219. doi:10.1021/acsami.9b19638

Liu, S., Sandner, B., Schackel, T., Nicholson, L., Chtarto, A., Tenenbaum, L., et al. (2017). Regulated Viral BDNF Delivery in Combination with Schwann Cells Promotes Axonal Regeneration through Capillary Alginate Hydrogels after Spinal Cord Injury. *Acta Biomater.* 60, 167–180. doi:10.1016/j.actbio.2017.07.024

Liu, W., Xu, B., Xue, W., Yang, B., Fan, Y., Chen, B., et al. (2020). A Functional Scaffold to Promote the Migration and Neuronal Differentiation of Neural Stem/progenitor Cells for Spinal Cord Injury Repair. *Biomaterials* 243, 119941. doi:10.1016/j.biomaterials.2020.119941

Liu, Y., Sui, Y., Liu, C., Liu, C., Wu, M., Li, B., et al. (2018). A Physically Crosslinked Polydopamine/nanocellulose Hydrogel as Potential Versatile Vehicles for Drug Delivery and Wound Healing. *Carbohydr. Polym.* 188, 27–36. doi:10.1016/j.carbpol.2018.01.093

Liu, Y., Ye, H., Satkunendrarajah, K., Yao, G. S., Bayon, Y., and Fehlings, M. G. (2013). A Self-Assembling Peptide Reduces Glial Scarring, Attenuates Post-traumatic Inflammation and Promotes Neurological Recovery Following Spinal Cord Injury. *Acta Biomater.* 9, 8075–8088. doi:10.1016/j.actbio.2013.06.001

Long, Y., Yan, L., Dai, H., Yang, D., Wu, X., Dong, X., et al. (2020). Enhanced Proliferation and Differentiation of Neural Stem Cells by Peptide-Containing Temperature-Sensitive Hydrogel Scaffold. *Mater. Sci. Eng. C* 116, 111258. doi:10.1016/j.msec.2020.111258

Ma, W., Fitzgerald, W., Liu, Q.-Y., O'Shaughnessy, T. J., Maric, D., Lin, H. J., et al. (2004). CNS Stem and Progenitor Cell Differentiation into Functional Neuronal Circuits in Three-Dimensional Collagen Gels. *Exp. Neurol.* 190, 276–288. doi:10.1016/j.expneurol.2003.10.016

Marchand, R., Woerly, S., Bertrand, L., and Valdes, N. (1993). Evaluation of Two Cross-Linked Collagen Gels Implanted in the Transected Spinal Cord. *Brain Res. Bull.* 30, 415–422. doi:10.1016/0361-9230(93)90273-e

Marchand, R., and Woerly, S. (1990). Transected Spinal Cords Grafted with *In Situ* Self-Assembled Collagen Matrices. *Neuroscience* 36, 45–60. doi:10.1016/0306-4522(90)90350-d

Martins, A., Facchi, S., Follmann, H., Pereira, A., Rubira, A., and Muniz, E. (2014). Antimicrobial Activity of Chitosan Derivatives Containing N-Quaternized Moieties in its Backbone: a Review. *Int. J. Mol. Sci.* 15, 20800–20832. doi:10.3390/ijms151120800

Meng, F., Modo, M., and Badylak, S. F. (2014). Biologic Scaffold for CNS Repair. *Regen. Med.* 9, 367–383. doi:10.2217/rme.14.9

Moon, Y. J., Lee, J. Y., Oh, M. S., Pak, Y. K., Park, K.-S., Oh, T. H., et al. (2012). Inhibition of Inflammation and Oxidative Stress by Angelica Dahuricae Radix Extract Decreases Apoptotic Cell Death and Improves Functional Recovery after Spinal Cord Injury. *J. Neurosci. Res.* 90, 243–256. doi:10.1002/jnr.22734

Mothe, A. J., Tam, R. Y., Zahir, T., Tator, C. H., and Shoichet, M. S. (2013). Repair of the Injured Spinal Cord by Transplantation of Neural Stem Cells in a Hyaluronan-Based Hydrogel. *Biomaterials* 34, 3775–3783. doi:10.1016/j.biomaterials.2013.02.002

Nazari, B., Kazemi, M., Kamyab, A., Nazari, B., Ebrahimi-Barough, S., Hadjighassem, M., et al. (2020). Fibrin Hydrogel as a Scaffold for Differentiation of Induced Pluripotent Stem Cells into Oligodendrocytes. *J. Biomed. Mat. Res.* 108, 192–200. doi:10.1002/jbm.b.34378

Nichol, J. W., Koshy, S. T., Bae, H., Hwang, C. M., Yamanlar, S., and Khademhosseini, A. (2010). Cell-laden Microengineered Gelatin Methacrylate Hydrogels. *Biomaterials* 31, 5536–5544. doi:10.1016/j.biomaterials.2010.03.064

O'connor, S. M., Stenger, D. A., Shaffer, K. M., and Ma, W. (2001). Survival and Neurite Outgrowth of Rat Cortical Neurons in Three-Dimensional Agarose and

Collagen Gel Matrices. *Neurosci. Lett.* 304, 189–193. doi:10.1016/s0304-3940(01)01769-4

Oliveira, E., Assunção-Silva, R. C., Ziv-Polat, O., Gomes, E. D., Teixeira, F. G., Silva, N. A., et al. (2017). Influence of Different ECM-like Hydrogels on Neurite Outgrowth Induced by Adipose Tissue-Derived Stem Cells. *Stem Cells Int.* 2017, 6319129. doi:10.1155/2017/6319129

Onyango, I., Bennett, J., and Stokin, G. (2021). Regulation of Neuronal Bioenergetics as a Therapeutic Strategy in Neurodegenerative Diseases. *Neural Regen. Res.* 16, 1467–1482. doi:10.4103/1673-5374.303007

Panzer, K. V., Burrell, J. C., Helm, K. V. T., Purvis, E. M., Zhang, Q., Le, A. D., et al. (2020). Tissue Engineered Bands of Büngner for Accelerated Motor and Sensory Axonal Outgrowth. *Front. Bioeng. Biotechnol.* 8, 580654. doi:10.3389/fbioe.2020.580654

Pardridge, W. M. (2011). Drug Transport in Brain via the Cerebrospinal Fluid. *Fluids Barriers CNS* 8, 7. doi:10.1186/2045-8118-8-7

Parekkadan, B., and Milwid, J. M. (2010). Mesenchymal Stem Cells as Therapeutics. *Annu. Rev. Biomed. Eng.* 12, 87–117. doi:10.1146/annurev-bioeng-070909-105309

Park, J., Lim, E., Back, S., Na, H., Park, Y., and Sun, K. (2010). Nerve Regeneration Following Spinal Cord Injury Using Matrix Metalloproteinase-Sensitive, Hyaluronic Acid-Based Biomimetic Hydrogel Scaffold Containing Brain-Derived Neurotrophic Factor. *J. Biomed. Mater Res. A* 93, 1091–1099. doi:10.1002/jbm.a.32519

Patel, B. B., Sharifi, F., Stroud, D. P., Montazami, R., Hashemi, N. N., and Sakaguchi, D. S. (2019). 3D Microfibrous Scaffolds Selectively Promotes Proliferation and Glial Differentiation of Adult Neural Stem Cells: A Platform to Tune Cellular Behavior in Neural Tissue Engineering. *Macromol. Biosci.* 19, e1800236. doi:10.1002/mabi.201800236

Paves, H., and Saarma, M. (1997). Neurotrophins as *In Vitro* Growth Cone Guidance Molecules for Embryonic Sensory Neurons. *Cell Tissue Res.* 290, 285–297. doi:10.1007/s004410050933

Pedersen, S. L., Huynh, T. H., Pöschko, P., Fruergaard, A. S., Jarlstad Olesen, M. T., Chen, Y., et al. (2020). Remotely Triggered Liquefaction of Hydrogel Materials. *ACS Nano* 14, 9145–9155. doi:10.1021/acsnano.0c04522

Perale, G., Rossi, F., Sundstrom, E., Bacchiega, S., Masi, M., Forloni, G., et al. (2011). Hydrogels in Spinal Cord Injury Repair Strategies. *ACS Chem. Neurosci.* 2, 336–345. doi:10.1021/cn200030w

Perets, A., Baruch, Y., Weisbuch, F., Shoshany, G., Neufeld, G., and Cohen, S. (2003). Enhancing the Vascularization of Three-Dimensional Porous Alginate Scaffolds by Incorporating Controlled Release Basic Fibroblast Growth Factor Microspheres. *J. Biomed. Mat. Res.* 65A, 489–497. doi:10.1002/jbm.a.10542

Piantanida, E., Alonci, G., Bertucci, A., and De Cola, L. (2019). Design of Nanocomposite Injectable Hydrogels for Minimally Invasive Surgery. *Acc. Chem. Res.* 52, 2101–2112. doi:10.1021/acs.accounts.9b00114

Rabchevsky, A. G., Patel, S. P., and Springer, J. E. (2011). Pharmacological Interventions for Spinal Cord Injury: where Do We Stand? How Might We Step Forward? *Pharmacol. Ther.* 132, 15–29. doi:10.1016/j.pharmthera.2011.05.001

Rad-Malekshahi, M., Lempsink, L., Amidi, M., Hennink, W. E., and Mastrobattista, E. (2016). Biomedical Applications of Self-Assembling Peptides. *Bioconjugate Chem.* 27, 3–18. doi:10.1021/acs.bioconjchem.5b00487

Ramer, M. S., Priestley, J. V., and Mcmahon, S. B. (2000). Functional Regeneration of Sensory Axons into the Adult Spinal Cord. *Nature* 403, 312–316. doi:10.1038/35002084

Ren, B., Chen, X., Du, S., Ma, Y., Chen, H., Yuan, G., et al. (2018). Injectable Polysaccharide Hydrogel Embedded with Hydroxyapatite and Calcium Carbonate for Drug Delivery and Bone Tissue Engineering. *Int. J. Biol. Macromol.* 118, 1257–1266. doi:10.1016/j.ijbiomac.2018.06.200

Ruzicka, J., Romanyuk, N., Jirakova, K., Hejcl, A., Janouskova, O., Machova, L. U., et al. (2019). The Effect of iPS-Derived Neural Progenitors Seeded on Laminin-Coated pHEMA-MOETACl Hydrogel with Dual Porosity in a Rat Model of Chronic Spinal Cord Injury. *Cell Transpl.* 28, 400–412. doi:10.1177/0963689718823705

Sehgal, R. R., and Banerjee, R. (2013). Research Highlights: Highlights from the Latest Articles in Nanomedicine. *Nanomedicine* 8, 521–523. doi:10.2217/nnm.13.40

Shi, J., Zhang, X., Zeng, X., Zhu, J., Pi, Y., Zhou, C., et al. (2012). One-step Articular Cartilage Repair: Combination of *In Situ* Bone Marrow Stem Cells with Cell-free poly(L-Lactic-Co-Glycolic Acid) Scaffold in a Rabbit Model. *Orthopedics* 35, e665. doi:10.3928/01477447-20120426-20

Shoichet, M. S., Tator, C. H., Poon, P., Kang, C., and Douglas Baumann, M. (2007). Intrathecal Drug Delivery Strategy Is Safe and Efficacious for Localized Delivery to the Spinal Cord. *Prog. Brain Res.* 161, 385–392. doi:10.1016/s0079-6123(06)61027-3

Shoukat, H., Buksh, K., Noreen, S., Pervaiz, F., and Maqbool, I. (2021). Hydrogels as Potential Drug-Delivery Systems: Network Design and Applications. *Ther. Deliv.* 12, 375–396. doi:10.4155/tde-2020-0114

Silva, N. A., Sousa, N., Reis, R. L., and Salgado, A. J. (2014). From Basics to Clinical: a Comprehensive Review on Spinal Cord Injury. *Prog. Neurobiol.* 114, 25–57. doi:10.1016/j.pneurobio.2013.11.002

Silva, N. A., Sousa, R. A., Fraga, J. S., Fontes, M., Leite-Almeida, H., Cerqueira, R., et al. (2013). Benefits of Spine Stabilization with Biodegradable Scaffolds in Spinal Cord Injured Rats. *Tissue Eng. Part C. Methods* 19, 101–108. doi:10.1089/ten.tec.2012.0264

Song, H. H., Song, T. C., Yang, T., Sun, C. S., He, B. Q., Li, H., et al. (2021). High Mobility Group Box 1 Mediates Inflammatory Response of Astrocytes via Cyclooxygenase 2/prostaglandin E2 Signaling Following Spinal Cord Injury. *Neural Regen. Res.* 16, 1848–1855. doi:10.4103/1673-5374.303039

Staples, N. A., Goding, J. A., Gilmour, A. D., Aristovich, K. Y., Byrnes-Preston, P., Holder, D. S., et al. (2017). Conductive Hydrogel Electrodes for Delivery of Long-Term High Frequency Pulses. *Front. Neurosci.* 11, 748. doi:10.3389/fnins.2017.00748

Stegemann, J. P., and Nerem, R. M. (2003). Altered Response of Vascular Smooth Muscle Cells to Exogenous Biochemical Stimulation in Two- and Three-Dimensional Culture. *Exp. Cell Res.* 283, 146–155. doi:10.1016/s0014-4827(02)00041-1

Stokols, S., and Tuszynski, M. H. (2006). Freeze-dried Agarose Scaffolds with Uniaxial Channels Stimulate and Guide Linear Axonal Growth Following Spinal Cord Injury. *Biomaterials* 27, 443–451. doi:10.1016/j.biomaterials.2005.06.039

Stokols, S., and Tuszynski, M. H. (2004). The Fabrication and Characterization of Linearly Oriented Nerve Guidance Scaffolds for Spinal Cord Injury. *Biomaterials* 25, 5839–5846. doi:10.1016/j.biomaterials.2004.01.041

Sun, W., Incitti, T., Migliaresi, C., Quattrone, A., Casarosa, S., and Motta, A. (2017). Viability and Neuronal Differentiation of Neural Stem Cells Encapsulated in Silk Fibroin Hydrogel Functionalized with an IKVAV Peptide. *J. Tissue Eng. Regen. Med.* 11, 1532–1541. doi:10.1002/term.2053

Sun, X., Zhang, C., Xu, J., Zhai, H., Liu, S., Xu, Y., et al. (2020). Neurotrophin-3-Loaded Multichannel Nanofibrous Scaffolds Promoted Anti-Inflammation, Neuronal Differentiation, and Functional Recovery after Spinal Cord Injury. *ACS Biomater. Sci. Eng.* 6, 1228–1238. doi:10.1021/acsbiomaterials.0c00023

Suzuki, Y., Kitaura, M., Wu, S., Kataoka, K., Suzuki, K., Endo, K., et al. (2002). Electrophysiological and Horseradish Peroxidase-Tracing Studies of Nerve Regeneration through Alginate-Filled Gap in Adult Rat Spinal Cord. *Neurosci. Lett.* 318, 121–124. doi:10.1016/s0304-3940(01)02359-x

Syková, E., Jendelová, P., Urdzíková, L., Lesný, P., and Hejcl, A. (2006). Bone Marrow Stem Cells and Polymer Hydrogels-Ttwo Strategies for Spinal Cord Injury Repair. *Cell Mol. Neurobiol.* 26, 1113–1129. doi:10.1007/s10571-006-9007-2

Tabakow, P., Jarmundowicz, W., Czapiga, B., Fortuna, W., Miedzybrodzki, R., Czyz, M., et al. (2013). Transplantation of Autologous Olfactory Ensheathing Cells in Complete Human Spinal Cord Injury. *Cell Transpl.* 22, 1591–1612. doi:10.3727/096368912x663532

Taylor, S. J., Rosenzweig, E. S., Mcdonald, J. W., and Sakiyama-Elbert, S. E. (2006). Delivery of Neurotrophin-3 from Fibrin Enhances Neuronal Fiber Sprouting after Spinal Cord Injury. *J. Control. Release* 113, 226–235. doi:10.1016/j.jconrel.2006.05.005

Toh, W. S., and Loh, X. J. (2014). Advances in Hydrogel Delivery Systems for Tissue Regeneration. *Mater. Sci. Eng. C* 45, 690–697. doi:10.1016/j.msec.2014.04.026

Trombino, S., and Cassano, R. (2020). Special Issue on Designing Hydrogels for Controlled Drug Delivery: Guest Editors' Introduction. *Pharmaceutics* 12, 57. doi:10.3390/pharmaceutics12010057

Tuszynski, M. H., Gabriel, K., Gage, F. H., Suhr, S., Meyer, S., and Rosetti, A. (1996). Nerve Growth Factor Delivery by Gene Transfer Induces Differential Outgrowth of Sensory, Motor, and Noradrenergic Neurites after Adult Spinal Cord Injury. *Exp. Neurol.* 137, 157–173. doi:10.1006/exnr.1996.0016

Ucar, B., Kajtez, J., Foidl, B. M., Eigel, D., Werner, C., Long, K. R., et al. (2021). Biomaterial Based Strategies to Reconstruct the Nigrostriatal Pathway in Organotypic Slice Co-cultures. *Acta Biomater.* 121, 250–262. doi:10.1016/j.actbio.2020.11.035

Vrana, N. E., Elsheikh, A., Builles, N., Damour, O., and Hasirci, V. (2007). Effect of Human Corneal Keratocytes and Retinal Pigment Epithelial Cells on the Mechanical Properties of Micropatterned Collagen Films. *Biomaterials* 28, 4303–4310. doi:10.1016/j.biomaterials.2007.06.013

Wang, C., Gong, Z., Huang, X., Wang, J., Xia, K., Ying, L., et al. (2019). An Injectable Heparin-Laponite Hydrogel Bridge FGF4 for Spinal Cord Injury by Stabilizing Microtubule and Improving Mitochondrial Function. *Theranostics* 9, 7016–7032. doi:10.7150/thno.37601

Wang, C., Yue, H., Feng, Q., Xu, B., Bian, L., and Shi, P. (2018). Injectable Nanoreinforced Shape-Memory Hydrogel System for Regenerating Spinal Cord Tissue from Traumatic Injury. *ACS Appl. Mat. Interfaces* 10, 29299–29307. doi:10.1021/acsami.8b08929

Wang, J., Wang, J., Lu, P., Cai, Y., Wang, Y., Hong, L., et al. (2015). Local Delivery of FTY720 in PCL Membrane Improves SCI Functional Recovery by Reducing Reactive Astrogliosis. *Biomaterials* 62, 76–87. doi:10.1016/j.biomaterials.2015.04.060

Wang, Y., Wu, M., Gu, L., Li, X., He, J., Zhou, L., et al. (2017). Effective Improvement of the Neuroprotective Activity after Spinal Cord Injury by Synergistic Effect of Glucocorticoid with Biodegradable Amphipathic Nanomicelles. *Drug Deliv.* 24, 391–401. doi:10.1080/10717544.2016.1256003

Wei, W., Qi, X., Liu, Y., Li, J., Hu, X., Zuo, G., et al. (2015). Synthesis and Characterization of a Novel pH-Thermo Dual Responsive Hydrogel Based on Salecan and Poly( N,N-Diethylacrylamide-Co-Methacrylic Acid). *Colloids Surfaces B Biointerfaces* 136, 1182–1192. doi:10.1016/j.colsurfb.2015.11.007

Wong, D. Y., Leveque, J.-C., Brumblay, H., Krebsbach, P. H., Hollister, S. J., and Lamarca, F. (2008). Macro-architectures in Spinal Cord Scaffold Implants Influence Regeneration. *J. Neurotrauma* 25, 1027–1037. doi:10.1089/neu.2007.0473

Wu, S., Xu, R., Duan, B., and Jiang, P. (2017). Three-Dimensional Hyaluronic Acid Hydrogel-Based Models for *In Vitro* Human iPSC-Derived NPC Culture and Differentiation. *J. Mat. Chem. B* 5, 3870–3878. doi:10.1039/c7tb00721c

Xu, Y., Zhang, L., Shao, T., Ruan, L., Wang, L., Sun, J., et al. (2013). Ferulic Acid Increases Pain Threshold and Ameliorates Depression-like Behaviors in Reserpine-Treated Mice: Behavioral and Neurobiological Analyses. *Metab. Brain Dis.* 28, 571–583. doi:10.1007/s11011-013-9404-4

Yang, C., Lim, W., Park, J., Park, S., You, S., and Song, G. (2019). Anti-inflammatory Effects of Mesenchymal Stem Cell-Derived Exosomal microRNA-146a-5p and microRNA-548e-5p on Human Trophoblast Cells. *Mol. Hum. Reprod.* 25, 755–771. doi:10.1093/molehr/gaz054

Yang, D., Xiao, J., Wang, B., Li, L., Kong, X., and Liao, J. (2019). The Immune Reaction and Degradation Fate of Scaffold in Cartilage/bone Tissue Engineering. *Mater. Sci. Eng. C* 104, 109927. doi:10.1016/j.msec.2019.109927

Yang, J., An, H.-W., and Wang, H. (2021). Self-Assembled Peptide Drug Delivery Systems. *ACS Appl. Bio Mat.* 4, 24–46. doi:10.1021/acsabm.0c00707

Yang, Y., Fan, Y., Zhang, H., Zhang, Q., Zhao, Y., Xiao, Z., et al. (2021). Small Molecules Combined with Collagen Hydrogel Direct Neurogenesis and Migration of Neural Stem Cells after Spinal Cord Injury. *Biomaterials* 269, 120479. doi:10.1016/j.biomaterials.2020.120479

Yang, Z., Duan, H., Mo, L., Qiao, H., and Li, X. (2010a). The Effect of the Dosage of NT-3/chitosan Carriers on the Proliferation and Differentiation of Neural Stem Cells. *Biomaterials* 31, 4846–4854. doi:10.1016/j.biomaterials.2010.02.015

Yang, Z., Mo, L., Duan, H., and Li, X. (2010b). Effects of Chitosan/collagen Substrates on the Behavior of Rat Neural Stem Cells. *Sci. China Life Sci.* 53, 215–222. doi:10.1007/s11427-010-0036-1

Yao, M., Li, J., Zhang, J., Ma, S., Wang, L., Gao, F., et al. (2021). Dual-enzymatically Cross-Linked Gelatin Hydrogel Enhances Neural Differentiation of Human Umbilical Cord Mesenchymal Stem Cells and Functional Recovery in Experimental Murine Spinal Cord Injury. *J. Mat. Chem. B* 9, 440–452. doi:10.1039/d0tb02033h

Yao, S., He, F., Cao, Z., Sun, Z., Chen, Y., Zhao, H., et al. (2020). Mesenchymal Stem Cell-Laden Hydrogel Microfibers for Promoting Nerve Fiber Regeneration in Long-Distance Spinal Cord Transection Injury. *ACS Biomater. Sci. Eng.* 6, 1165–1175. doi:10.1021/acsbiomaterials.9b01557

Yoshii, S., Oka, M., Shima, M., Taniguchi, A., Taki, Y., and Akagi, M. (2004). Restoration of Function after Spinal Cord Transection Using a Collagen Bridge. *J. Biomed. Mat. Res.* 70A, 569–575. doi:10.1002/jbm.a.30120

Yuan, N., Tian, W., Sun, L., Yuan, R., Tao, J., and Chen, D. (2014). Neural Stem Cell Transplantation in a Double-Layer Collagen Membrane with Unequal Pore Sizes for Spinal Cord Injury Repair. *Neural Regen. Res.* 9, 1014–1019. doi:10.4103/1673-5374.133160

Yuan, T., Shao, Y., Zhou, X., Liu, Q., Zhu, Z., Zhou, B., et al. (2021). Highly Permeable DNA Supramolecular Hydrogel Promotes Neurogenesis and Functional Recovery after Completely Transected Spinal Cord Injury. *Adv. Mater* 33, e2102428. doi:10.1002/adma.202102428

Zarei-Kheirabadi, M., Sadrosadat, H., Mohammadshirazi, A., Jaberi, R., Sorouri, F., Khayyatan, F., et al. (2020). Human Embryonic Stem Cell-Derived Neural Stem Cells Encapsulated in Hyaluronic Acid Promotes Regeneration in a Contusion Spinal Cord Injured Rat. *Int. J. Biol. Macromol.* 148, 1118–1129. doi:10.1016/j.ijbiomac.2020.01.219

Zhan, X. (2020). Effect of Matrix Stiffness and Adhesion Ligand Density on Chondrogenic Differentiation of Mesenchymal Stem Cells. *J. Biomed. Mater Res.* 108, 675–683. doi:10.1002/jbm.a.36847

Zhang, J., Lu, X., Feng, G., Gu, Z., Sun, Y., Bao, G., et al. (2016). Chitosan Scaffolds Induce Human Dental Pulp Stem Cells to Neural Differentiation: Potential Roles for Spinal Cord Injury Therapy. *Cell Tissue Res.* 366, 129–142. doi:10.1007/s00441-016-2402-1

Zhang, S., Wang, X.-J., Li, W.-S., Xu, X.-L., Hu, J.-B., Kang, X.-Q., et al. (2018). Polycaprolactone/polysialic Acid Hybrid, Multifunctional Nanofiber Scaffolds for Treatment of Spinal Cord Injury. *Acta Biomater.* 77, 15–27. doi:10.1016/j.actbio.2018.06.038

Zhang, Y., Li, L., Mu, J., Chen, J., Feng, S., and Gao, J. (2020). Implantation of a Functional TEMPO-Hydrogel Induces Recovery from Rat Spinal Cord Transection through Promoting Nerve Regeneration and Protecting Bladder Tissue. *Biomater. Sci.* 8, 1695–1701. doi:10.1039/c9bm01530b

Zhao, Y.-Z., Jiang, X., Lin, Q., Xu, H.-L., Huang, Y.-D., Lu, C.-T., et al. (2017). Thermosensitive Heparin-Poloxamer Hydrogels Enhance the Effects of GDNF on Neuronal Circuit Remodeling and Neuroprotection after Spinal Cord Injury. *J. Biomed. Mat. Res.* 105, 2816–2829. doi:10.1002/jbm.a.36134

Zhao, Y., Tan, K., Zhou, Y., Ye, Z., and Tan, W.-S. (2016). A Combinatorial Variation in Surface Chemistry and Pore Size of Three-Dimensional Porous Poly(ε-Caprolactone) Scaffolds Modulates the Behaviors of Mesenchymal Stem Cells. *Mater. Sci. Eng. C* 59, 193–202. doi:10.1016/j.msec.2015.10.017

Zhou, L., Fan, L., Yi, X., Zhou, Z., Liu, C., Fu, R., et al. (2018). Soft Conducting Polymer Hydrogels Cross-Linked and Doped by Tannic Acid for Spinal Cord Injury Repair. *ACS Nano* 12, 10957–10967. doi:10.1021/acsnano.8b04609

Zweckberger, K., Ahuja, C. S., Liu, Y., Wang, J., and Fehlings, M. G. (2016). Self-assembling Peptides Optimize the Post-traumatic Milieu and Synergistically Enhance the Effects of Neural Stem Cell Therapy after Cervical Spinal Cord Injury. *Acta Biomater.* 42, 77–89. doi:10.1016/j.actbio.2016.06.016

Zweckberger, K., Liu, Y., Wang, J., Forgione, N., and Fehlings, M. G. (2015). Synergetic Use of Neural Precursor Cells and Self-Assembling Peptides in Experimental Cervical Spinal Cord Injury. *J. Vis. Exp.* (96), e52105. doi:10.3791/52105

**Conflict of Interest:** The authors declare that the research was conducted in the absence of any commercial or financial relationships that could be construed as a potential conflict of interest.

**Publisher's Note:** All claims expressed in this article are solely those of the authors and do not necessarily represent those of their affiliated organizations, or those of the publisher, the editors and the reviewers. Any product that may be evaluated in this article, or claim that may be made by its manufacturer, is not guaranteed or endorsed by the publisher.

frontiers | Frontiers in Bioengineering and Biotechnology

ORIGINAL RESEARCH
published: 29 June 2022
doi: 10.3389/fbioe.2022.865545

# Effect of Decellularized Extracellular Matrix Bioscaffolds Derived from Fibroblasts on Skin Wound Healing and Remodeling

*Hyo-Sung Kim[1], Hyun-Jeong Hwang[1], Han-Jun Kim[1,2], Yeji Choi[3], Daehyung Lee[3], Hong-Hee Jung[3] and Sun Hee Do[1]**

[1]*Department of Veterinary Clinical Pathology, College of Veterinary Medicine, Konkuk University, Seoul, South Korea,* [2]*Terasaki Institute for Biomedical Innovation, Los Angeles, CA, United States,* [3]*Advanced Medical Device R&D Center, HansBiomed Co. Ltd., Seoul, South Korea*

The mammalian tissue extracellular matrix (ECM) has been used as a scaffold to facilitate the repair and reconstruction of numerous tissues. However, the material properties of decellularized ECM (dECM) from *in vitro* cell cultures and the effect of these properties on wound remodeling remain unclear. To elucidate its biological activity, we extracted dECM from human lung fibroblasts, fabricated it into a patch, and applied it to a full-thickness skin wound. The fibroblast-derived dECM (fdECM) maintained the content of collagen I, collagen IV, and elastin, and the extraction process did not damage its critical growth factors. The fdECM-conjugated collagen patch (COL-fdECM) facilitated wound contraction and angiogenesis in the proliferative phase when applied to the *in vivo* full-thickness skin wound model. Moreover, the COL-fdECM treated wound showed increased regeneration of the epidermal barrier function, mature collagen, hair follicle, and subepidermal nerve plexus, suggesting qualitative skin remodeling. This therapeutic efficacy was similarly observed when applied to the diabetic ulcer model. fdECM was shown to help remodel the tissue by regulating fibroblast growth factors, matrix metalloproteinases, and tissue inhibitors of metalloproteinases via the p38 and ERK signaling pathways in an *in vitro* experiment for understanding the underlying mechanism. These results provide a biological basis for cell-derived ECM as a multi-functional biomaterial applicable to various diseases.

**Keywords: fibroblast, decellularized extracellular matrix (dECM), biomaterial, skin wound, remodeling, diabetic ulcer**

OPEN ACCESS

***Edited by:***
*Zongliang Wang,*
*Changchun Institute of Applied Chemistry (CAS), China*

***Reviewed by:***
*Chandra Kothapalli,*
*Cleveland State University, United States*
*Rúben Pereira,*
*Universidade do Porto, Portugal*

****Correspondence:***
*Sun Hee Do*
*shdo@konkuk.ac.kr*

***Specialty section:***
*This article was submitted to Biomaterials, a section of the journal Frontiers in Bioengineering and Biotechnology*

***Received:*** *30 January 2022*
***Accepted:*** *22 March 2022*
***Published:*** *29 June 2022*

***Citation:***
*Kim H-S, Hwang H-J, Kim H-J, Choi Y, Lee D, Jung H-H and Do SH (2022) Effect of Decellularized Extracellular Matrix Bioscaffolds Derived from Fibroblasts on Skin Wound Healing and Remodeling. Front. Bioeng. Biotechnol. 10:865545. doi: 10.3389/fbioe.2022.865545*

## INTRODUCTION

The decellularized xenogeneic scaffolds using various tissue types such as small intestine submucosa, cartilage, heart valves, and urethra have generated considerable interest in tissue engineering to develop functional bioscaffolds as natural templates (Cui et al., 2019). Although the standard procedure has not been established, the basic principle is to remove cells from tissues or organs using appropriate methods, leaving the bioactive component (Massaro et al., 2021). This organ-derived extracellular matrix (ECM) preserves its natural 3D structure and multidirectional active composition, leaving critical biocompatibility, immunogenicity, cell penetrability, and disease

transmission issues. However, cell-derived ECM containing native bioactive molecules and proteins overcome these organ-derived ECM disadvantages by avoiding pathogen risks and immunogenic molecules (Lu et al., 2011b). Therefore, ECM extraction from *in vitro* cell culture has recently received attention as an alternative to extracting ECM from tissues or organs. This approach allows for the gathering of a sufficient amount of well-characterized ECM and controlling the active ingredient content to support *in vivo* function. Moreover, *in vitro* generated ECM has the advantages of a physiological system with standardizable and customizable modifications toward a specific application. Although 2D-cultured cell-derived ECM lacks 3D architectures, technological advances have supplemented the cell-derived ECM structural limitations by integrating it with other materials, cell aligning, and 3D culture (Kim et al., 2015; Assuncao et al., 2020; Antich et al., 2021). Furthermore, cell-derived ECM may be utilized for autologous ECM preparation and can be combined with different cell-derived ECM types to maximize efficacy (Lu et al., 2011b). However, ECM bioactive functions and mechanisms remain unclear, requiring further elucidation.

In a broad sense, ECM is a union of various materials such as fibrous proteins (collagens), glycoproteins, enzymes, and growth factors. These ECM components are synthesized mainly by fibroblasts that exist most abundantly in connective tissue. The ECM in the connective tissue forms the backbone of the polymer network, providing the tissue with morphology/stability and tensile strength (Assuncao et al., 2020). Therefore, various fibroblasts have been investigated for tissue engineering and biomaterials (Lu et al., 2011a; Bourget et al., 2012). *In vitro* fibroblasts grow for 14 weeks to form thick, multilayered cell sheets and secrete abundant ECM proteins and proteoglycans (Xing et al., 2015). Decellularized ECM (dECM) derived from fibroblast sheets is composed primarily of collagen and is more like natural tissue than conventional biopolymers used in tissue engineering (Assuncao et al., 2020). In addition to a supportive role, previous studies have shown that cell-derived ECM can significantly improve cell adhesion, migration, and proliferation to acquire morphology similar to that of the original tissue (Lu et al., 2011b; Lin et al., 2012). Specifically, fibroblast-derived dECM (fdECM) helps keratinocytes proliferate by maintaining their stem-like state and aiding peripheral nerve regeneration by controlling the neurite outgrowth (Harris et al., 2017; Wong et al., 2019). In addition, fdECM plays a role in angiogenesis by aiding endothelial cell sprouting and lumen formation (Newman et al., 2011). In particular, WI-38 lung fdECM has been reported to be rich in angiogenic factors that help skin wound healing (Du et al., 2020). Moreover, it has been suggested that fdECM help recruit macrophages and/or modulate macrophage phenotype through *in vivo* study (Savitri et al., 2020).

Researchers have attempted to develop biomaterials using these cell-derived ECM characteristics for the regeneration of various tissues, such as blood vessels, tendons, muscles, bones, and cartilages (Lu et al., 2011b; Gu et al., 2014; Kim et al., 2015; Xing et al., 2017; He et al., 2021). However, the integumentary system also needs such tissue engineering to treat wide and intractable skin defects such as burns, pressure ulcers, and diabetic ulcers. Therefore, this study was designed to evaluate the ECM bioactive factors obtained from the well-known, WI-38 human lung fibroblast cultures and investigate the effect of fdECM in chronic wound healing for future applications. Moreover, we elucidated the molecular biological mechanisms underlying the therapeutic efficacy of fdECM, which is yet to be fully understood despite recent advances and efforts in ECM technology.

# MATERIALS AND METHODS

## Preparation of Decellularized Extracellular Matrix

Human lung fibroblast WI-38 (CCL-75, ATCC) were seeded at $2 \times 10^4$ cells/cm$^2$ into a T-175 flask and cultured for five to seven days until confluence (approx. $9 \times 10^4$ cells/cm$^2$) was reached in Dulbecco's Modified Eagle medium (DMEM; #11995-065, Gibco) supplemented with 10% fetal bovine serum (FBS; Gibco) and 1% antibiotics (#15140122, Gibco). The medium was changed every 3 days. After reaching 100% confluency, the cells were washed twice with Dulbecco's phosphate-buffered saline (DPBS; Sigma-Aldrich) and lysed with a 0.25% Triton X-100 solution (#H5141, Promega) containing 10 mM $NH_4OH$ (#221228, Sigma-Aldrich) for 90 s at 37°C. After the decellularization process, 50 U/mL Deoxyribonuclease I (#18047-019, Invitrogen) and RNase A (#12091-039, Invitrogen) was added to the lysate for 90 min, and the resulting solution was frozen overnight in 50 mL conical tubes at -80°C and lyophilized.

## Componential Analysis of Decellularized Extracellular Matrix

For western blot analysis, dECM was washed with PBS and then scraped to collect the sample. The sample was extracted from RIPA buffer containing a protein inhibitor cocktail (#89900, Thermo Fisher Scientific). The total protein quantity before and after decellularization was measured by bicinchoninic acid assay (#23225, Thermo Fisher Scientific). Samples (20 μg) were separated by electrophoresis of a 7.5% polyacrylamide gradient gel, and the separated proteins were transferred to a nitrocellulose membrane (HATF29325, Millipore). The membrane was blocked with 2.5% bovine serum albumin (BSA) in Tris-buffered saline (TBS), and primary and horseradish peroxidase-labeled secondary antibodies: anti-collagen I (1:1,000, ab138492, Abcam), -collagen III (1:1,000, ab184993, Abcam), -collagen IV (1:1,000, ab6586, Abcam), -fibronectin (1:1,000, ab6328, Abcam), -laminin (1:800, ab11575, Abcam), -elastin (1:800, ab213720, Abcam), and -β-actin (1:1,000, ab8226, Abcam) were added, incubated overnight at 4°C and proteins were detected. The membrane was washed, and the protein bands were detected using a chemiluminescence reagent (#32106, Thermo Fisher Scientific). Images were captured using the ImageQuant LAS 500 (GE Healthcare).

Relative growth factor levels were determined using a sandwich immunoassay array kit (ARY007, R&D systems).

**TABLE 1 |** Sequences of human primers used for real-time PCR.

| Target Gene | Forward Primer Sequence | Reverse Primer Sequence |
|---|---|---|
| FGF2 | GCAGAAGAGAGAGGAGTTGTG | CCGTAACACATTTAGAAGCCAG |
| FGF7 | TCTTGCAATGAACAAGGAAGG | CCGTTGTGTGTCCATTTAGC |
| FGF10 | CGTACAGCATCCTGGAGATAAC | CCCTTCTTGTTCATGGCTAAGT |
| MMP1 | TACGAATTTGCCGACAGAGA | AAGCCAAAGGAGCTGTAGATG |
| MMP2 | TTCAAGGACCGGTTCATTTGG | TGCAAAGAACACAGCCTTCTC |
| MMP3 | ACTGTGATCCTGCTTTGTCC | CACGCCTGAAGGAAGAGATG |
| TIMP1 | GATGGACTCTTGCACATCACT | GATAAACAGGGAAACACTGTGC |
| TIMP2 | ATCTCATTGCAGGAAAGGCC | GTACCTGTGGTTCAGGCTCT |
| TIMP3 | CTTCACCAAGATGCCCCATG | ATCATAGACGCGACCTGTCA |
| β-actin | GGCCGAGGACTTTGATTGC | GTGTGGACTTGGGAGAGGAC |
| GAPDH | ATCAAGAAGGTGGTGAAGCAG | GTCGCTGTTGAAGTCAGAGG |
| 18s rRNA | GCCATGCATGTCTGAGTACG | GCGACCAAAGGAACCATAAC |
| β2-microglobulin | CCTGCCGTGTGAACCATGTG | TGCGGCATCTTCAAACCTCC |
| TBP | TGTTGAGTTGCAGGGTGTGG | AAATAATGCCCCTTCCCGGC |

Briefly, the extracted ECM total protein concentration was assessed using a bicinchoninic acid assay, and 200 μg of total protein was used as input for the array. Chemiluminescence was detected using an ImageQuant LAS 500, and the signal intensities were measured using ImageQuant TL software (GE Healthcare).

## Fabrication of Bioactive Scaffolds

The bioactive scaffolds were fabricated using a collagen solution and ECM powder for lyophilization within the mold. Specifically, Type I porcine collagen (MS Collagen; MSBIO) was reconstituted in 0.001N HCl at 5 mg/mL at 4°C under continuous gentle magnetic stirring (COL group). After the collagen was completely dissolved, the solution was mixed with fdECM (0.1%, w/v) (COL-fdECM group). Afterward, the mixture solution either for the COL or COL-fdECM group was poured into the 12 mm diameter mold to form scaffolds, collagen patch or fdECM-supplemented collagen patch, and they were frozen for 1 day at −78°C prior to lyophilization.

## *In Vivo* Full-Thickness Skin Wound Healing Study

All experimental procedures for *in vivo* full-thickness skin wound study were approved by the Institutional Animal Care and Use Committee of Konkuk University (KU18128). Male 6-week-old C57BL/6 mice were purchased from Orient Bio. The mice were housed under controlled conditions at a temperature of 23 ± 2°C, humidity of 50 ± 5%, and a light-dark cycle of 12/12 h. To establish the full-thickness skin wound model, the surgical area was clipped and aseptically prepared using povidone iodine. The surgical excision was made on the dorsal skin of mice using a 10 mm biopsy punch under inhalation anesthesia with isoflurane (3.5% for induction and 1.5% for maintenance). The mice were randomly allocated into three groups ($n$ = 5 per group), including a CON group with non-treatment, a COL group with collagen patch treatment, and a COL-fdECM group with fdECM-collagen patch treatment. After applying the allocated treatment, the skin wound was covered with Tegaderm and Coban to maintain humidity and protect from infection. Treatment was repeated for three consecutive days after the wound was induced, and the wound size was measured after 7 and 14 days. Prophylactic antibiotics (enrofloxacin, 5 mg/kg) and analgesics (meloxicam, 1 mg/kg) were administered subcutaneously after surgery and for 2 days afterward.

## *In Vivo* Diabetic Skin Ulcer Healing Study

All experimental procedures for *in vivo* diabetic skin ulcer healing study were approved by the Institutional Animal Care and Use Committee of Konkuk University (KU18042). To establish the diabetic skin ulcer model, leptin receptor knockout mice (DB), C57BL/6-Lepr$^{em1hwl}$/Korl, were obtained from the National Institute of Food and Drug Safety Evaluation (NIFDS, Cheongju, Korea). Male 10-week-old DB and misty (wild-type) were used, and the same surgical procedure described in section *In Vivo Full-Thickness Skin Wound Healing Study* was applied. The DB mice were randomly allocated into two groups ($n$ = 4 per group), the DB mice with injury-only group (DB/I) and DB mice with fdECM-collagen patch treatment group (DB/COL-fdECM). Misty mice with injury-only group (Wild/I) were used to compare the normal skin wound and diabetic ulcer.

## Histological Analysis

After 7 and 21 days after inducing the skin wound and treatment, dorsal skin samples were obtained and fixed with 10% neutral-buffered formalin (BBC Biochemical). The tissue samples were embedded in paraffin through a routine process and were sectioned at 4 μm thickness. The tissue sections were hydrated by gradient alcohols for routine histological analysis and stained with hematoxylin and eosin. In addition, tissue sections were stained with Masson's trichrome, and specific protein expressions were visualized by immunohistochemistry for further analysis. Briefly, the hydrated tissue sections were boiled using a TintoRetriever pressure cooker (Bio SB) in sodium citrate buffer (pH 6.0) to detect α-SMA, CD34, PGP9.5, loricrin, E-cadherin, and CD31 or in Tris-EDTA buffer (pH 9.0) to detect collagen I and III. For the primary antibodies, anti-collagen I (1:200, ab6308, Abcam), -collagen III (1:200, ab7778, Abcam), -α-SMA (1:1,000, ab7817, Abcam), -CD34 (1:200, MA5-27901, Invitrogen), -PGP9.5 (1:100, ab8189, Abcam), -loricrin (1:200, ab85679, Abcam), -E-cadherin (1:100, #14472, Cell Signaling Technology) and

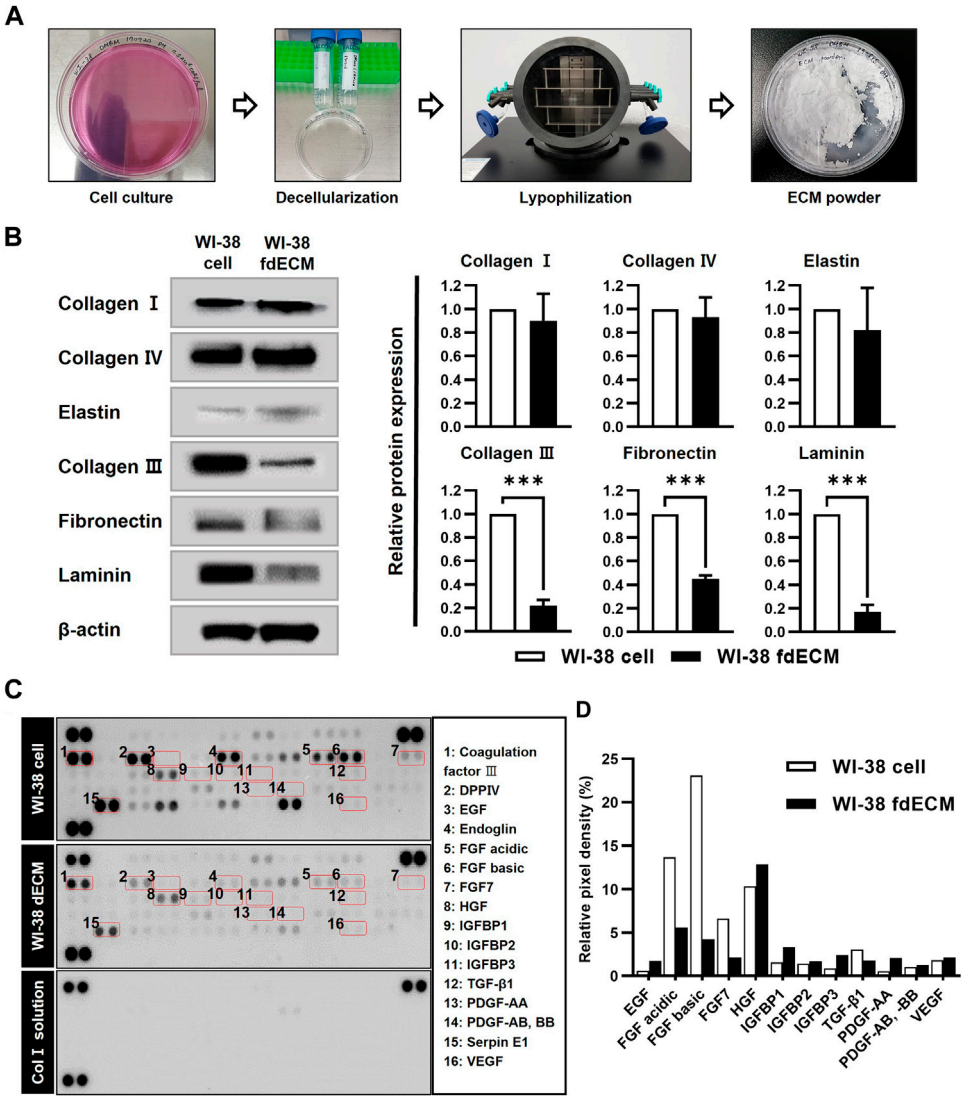


**FIGURE 1 |** Preparation and characterization of fdECM. **(A)** The extraction method of WI-38 fibroblast-derived decellularized extracellular matrix (fdECM). **(B)** Western blot analysis of ECM proteins before and after decellularization with β-actin as an internal control. **(C)** Analysis of angiogenic factors by a semi-quantitative method. Dot blot of the matrix before and after decellularization. The graph of some of the 55 principal angiogenic factors detected (box denotes factors). Results are expressed as mean ± standard deviation (SD). ***$p < 0.001$.

-CD31 (1:100, sc-376764, Santa Cruz Biotechnology) were used. The anti-CD31 antibody-labeled sections were incubated with a Vectastain Elite ABC-Peroxidase kit (Vector Laboratories), and the reactions were visualized by Vector SG (Vector Laboratories). Finally, the sections were counterstained with a nuclear fast red solution (Vector Laboratories) and analyzed under a microscope (Leica Microsystems). To detect proteins other than CD31, the antibody-labeled sections were incubated with secondary antibodies conjugated with Alexa fluor 488 and/or Alexa fluor 594 (Abcam). Then the sections were mounted in 4′-6-diamidino-2-phenylindole (DAPI) containing media (H-1800, Vector Laboratories) and analyzed under a fluorescence microscope (Leica Microsystems) or confocal fluorescence microscope (Zeiss).

## *In Vitro* Wound Healing Study

Human dermal fibroblasts (PCS-201-010, ATCC) were cultured using DMEM, supplemented with 10% FBS, 1% penicillin/streptomycin (#15140122, Gibco), and 2% Mycoeraser (ME05-100, RD tech) at 37°C in a 5% $CO_2$ humidified incubator. The cells were seeded on a 6-well plate at a density of $7.5 \times 10^5$ cells/well and incubated for 24 h to reach the confluency. The scratch wound was made using a commercial scratcher (SPL Life Sciences). The recombinant human epidermal growth factor (rhEGF) (E9644, Sigma-Aldrich) or fdECM powder was dissolved in DPBS. The concentrated solution of rhEGF or fdECM was added to each well to a final concentration of 10 ng/mL. For the control group, the same volume of DPBS was added. Photomicrographs were taken at each time point (0, 18, 24, and 48 h) after applying the treatment.

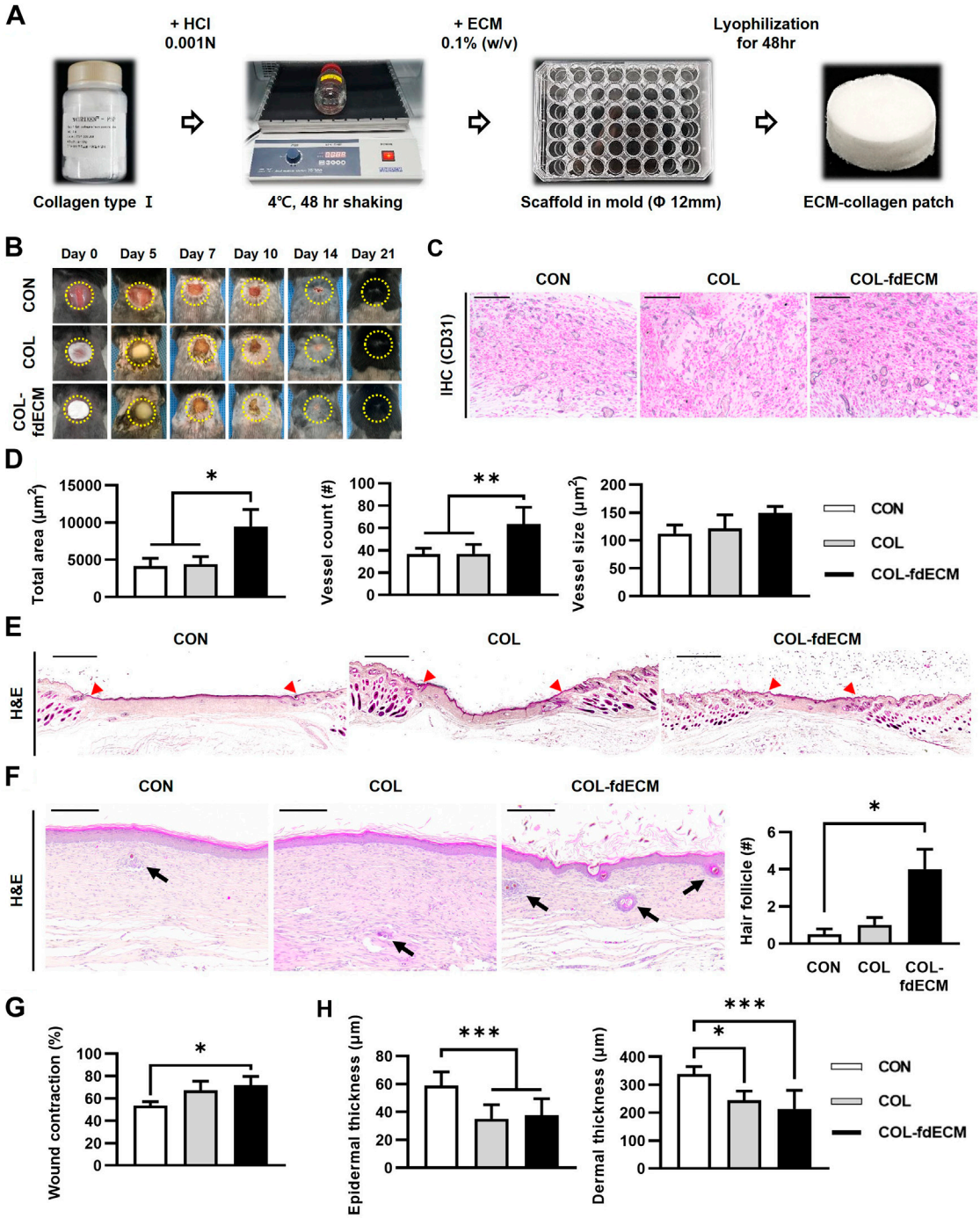


**FIGURE 2 |** *In vivo* evaluation of fdECM scaffolds on full-thickness skin wounds. **(A)** Fabrication of fdECM scaffold by adding collagen I and lyophilization, **(B)** Gross evaluation of skin wounds, **(C)** Immunohistochemistry images stained with anti-CD31 antibody after 7 days of treatment (Gray color indicates a positive reaction), Scale bar represents 200 μm **(D)** Semi-quantitative measurement of blood vessel area, count, and size, after 7 days of treatment. **(E)** Whole-mount image of skin wound stained with hematoxylin and eosin (H&E) after 21 days of treatment. The red arrowhead indicates the initial site of the wound. Scale bar represents 2 mm **(F)** An increased number of hair follicles on regenerated dermis was detected after 21 days of fdECM treatment. Black arrows indicate hair follicles. Scale bar represents 200 μm. **(G)** Wound contraction ratio calculated as ratio of the gap between unaffected tissue to original wound diameter, **(H)** Thickness of epidermis and dermis. Bar in graphs represents the mean ± standard error of mean (SEM). $^{*}p < 0.05$, $^{**}p < 0.01$, $^{***}p < 0.001$.

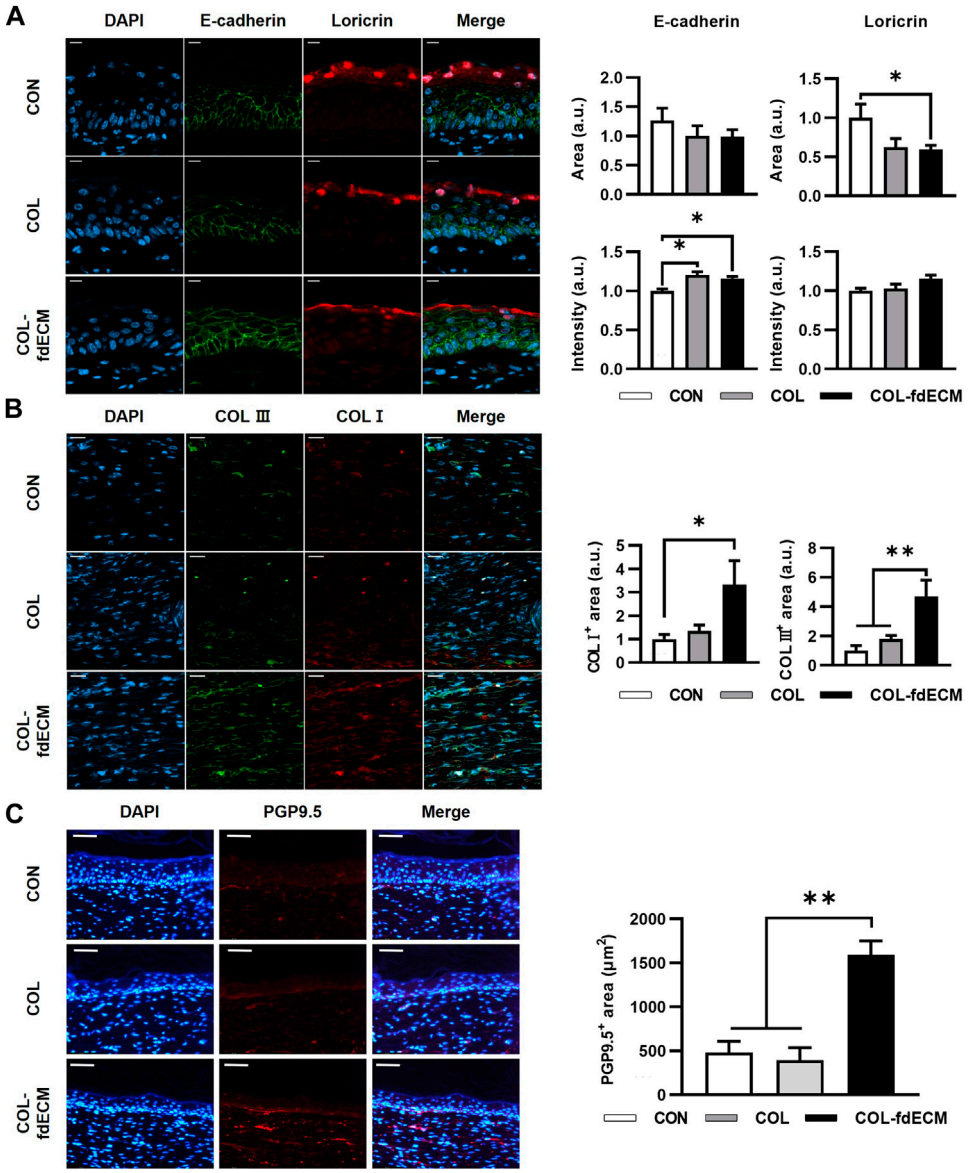


**FIGURE 3 |** Tissue remodeling in skin wound after 21 days of fdECM treatment. **(A)** Immunofluorescence image and semi-quantitative analysis of barrier function of epidermis stained with E-cadherin (green) and loricrin (red). Scale bar represents 10 μm. **(B)** Representative images of double immunofluorescence staining against collagen I (COL I, red) and collagen III (COL III, green). Semi-quantitative analysis was performed by measuring the positive area. Scale bar represents 20 μm. **(C)** Immunofluorescence image and semi-quantitative analysis of nerve fiber in dermis stained with PGP9.5 (red). Scale bar represents 50 μm. Bar represents mean ± standard error of mean (SEM). *$p < 0.05$, **$p < 0.01$.

The relative scratch gap area was measured by using ImageJ software (National Institutes of Health). After 48 h when the scratch gap was restored, the cells were either fixed with 4% paraformaldehyde or the supernatant media and cells were separately harvested and stored at −78°C, for further analysis.

## Immunocytochemistry Analysis

The fixed cells were permeabilized using 0.1% Triton X-100 for immunocytochemistry analysis. The samples were blocked with 2% normal serum and incubated with anti-α-SMA (1:1000), -collagen I (1:200), and -collagen III (1:200). The signals were detected with secondary antibodies conjugated with Alexa fluor 488 or 594, and nuclei were counterstained with DAPI (D9542, Sigma-Aldrich).

## Growth Factor Array

Growth factors secreted by fibroblasts in the media were determined using a human growth factor antibody array kit (ab134002, Abcam), according to the manufacturer's protocol. Two milliliters of supernatant media were used for each quantification. Chemiluminescence was detected using a charged-coupled device

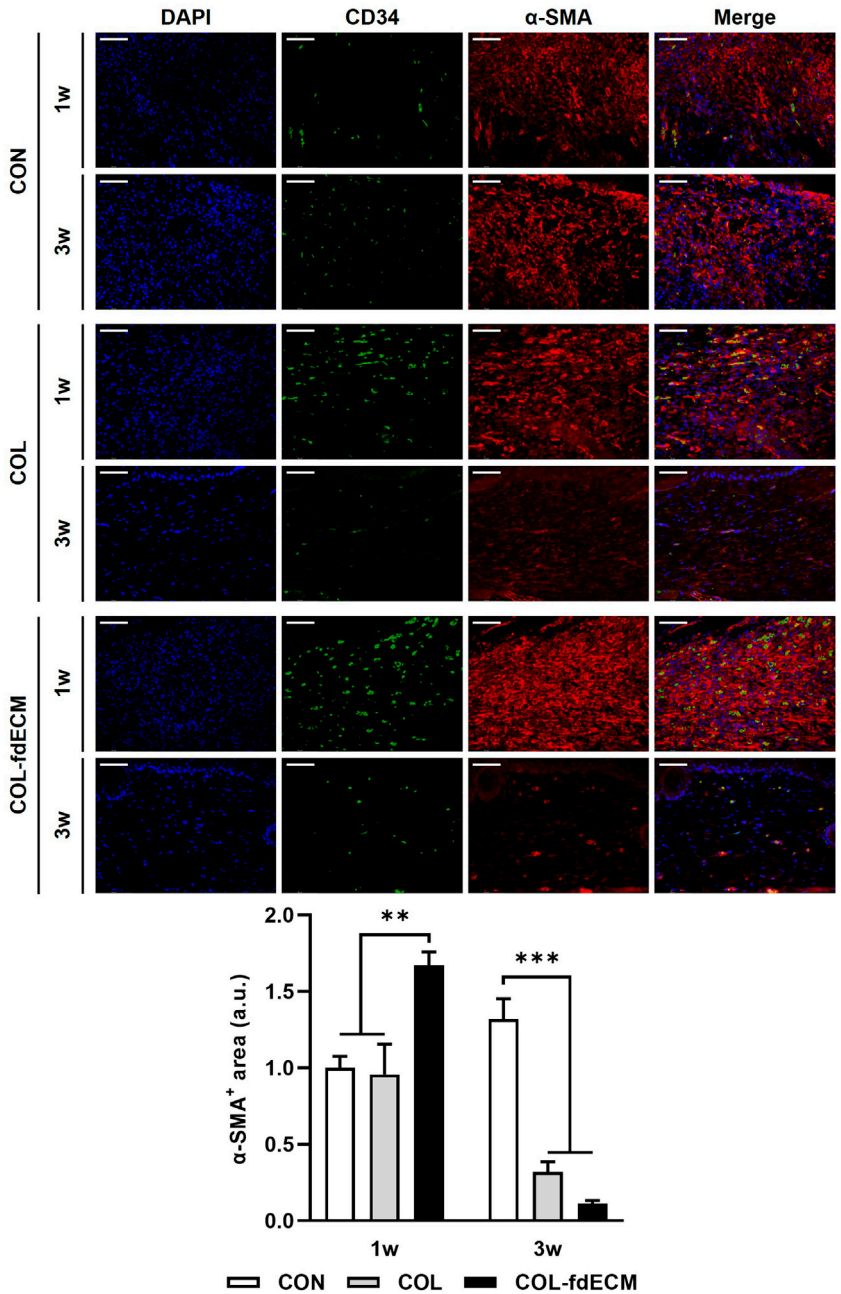


**FIGURE 4 |** Time-varying phenotype change of dermal fibroblasts in full-thickness skin wound after fdECM treatment. Immunofluorescence image and semi-quantitative analysis of dermal fibroblast stained with CD34 (green) and α-SMA (red) on tissue sections. Scale bar represents 50 μm. Bar represents mean ± standard error of mean (SEM). $^{**}p < 0.01$, $^{***}p < 0.001$.

(CCD) camera (Fusion Solo S, Vilber), and the signal intensities were measured using ImageJ.

## Real-Time Polymerase Chain Reaction (qPCR)

The cells were harvested for mRNA expression analysis at -78°C. Total RNA was isolated using the RNeasy Mini kit (#74106, Qiagen) according to the manufacturer's instructions. One microgram of extracted RNA was transcribed into cDNA using the QuantiTect Reverse Transcription Kit (#205311, Qiagen). The primers for the target genes are listed in **Table 1**. The PowerUp SYBR Green Master Mix (A25742, Applied Biosystems) was used to perform real-time PCR (initial denaturation, 5 min at 95°C; recurring denaturation, 15 s at 95°C, and amplification, 30 s at 60°C, for 45 cycles). All

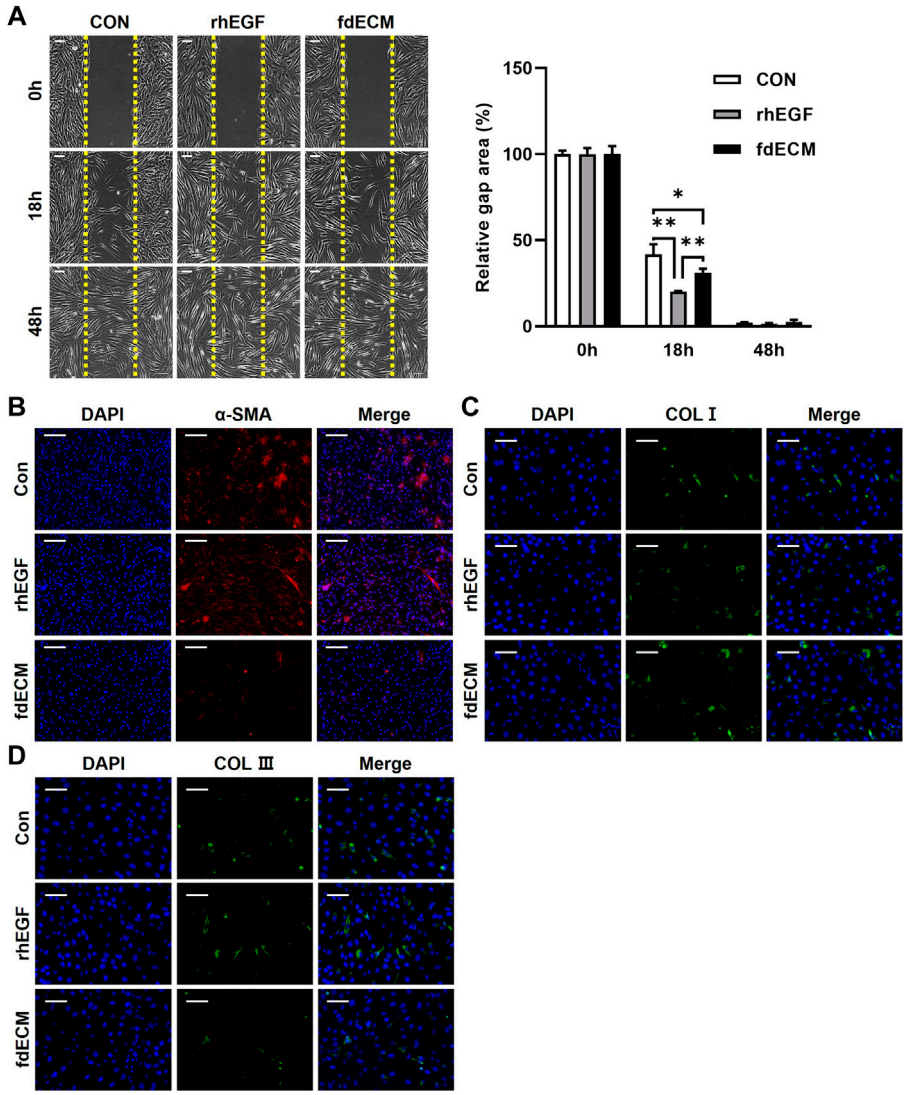


**FIGURE 5 |** Phenotype change of human dermal fibroblasts after fdECM treatment. **(A)** Representative images of scratch wound healing assay using human dermal fibroblasts and semi-quantitative analysis of relative scratch area calculated as ratio for original defect area. Yellow dashed line indicates the original site of the scratch wound. **(B–D)** Immunofluorescence images of α-SMA **(B)**, COL I **(C)**, and COL III **(D)** expression after 48 h of fdECM treatment. Scale bars represent 200 μm **(B)** and 100 μm **(A,C,D)**. Results are expressed as mean ± standard deviation (SD). $^{*}p < 0.05$, $^{**}p < 0.01$.

mRNA levels were normalized to mean values of reference genes, β-actin, GAPDH, 18s rRNA, β2-microglobulin, and TBP, and the results were calculated as fold changes of the cycle threshold (Ct) value relative to the controls using the $2^{-\Delta\Delta Ct}$ method.

## Immunoblot Analysis

To analyze the MAPK, TGF-β/SMAD, JAK/STAT, and PI3K/AKT signaling pathways, total protein was extracted using M-PER (Thermo Fisher Scientific) extraction buffer with Halt phosphatase protease inhibitor (Thermo Fisher Scientific) according to the manufacturer's instruction. The protein concentration was determined using a protein assay kit (Bio-Rad), and the total protein (20 μg) was separated by sodium dodecyl sulfate-polyacrylamide gel electrophoresis (SDS-PAGE) using a 4-20% precast gel (Bio-Rad). The separated proteins were transferred onto polyvinylidene fluoride membranes, followed by western blot analysis. Briefly, the background signals were blocked with EveryBlot Blocking buffer (#12010020, Bio-Rad) and incubated with each primary antibody, purchased from Cell Signaling Technology and diluted to 1:1,000 in 3% BSA/TBST (SMAD3, #9513; p-SMAD3, #9520; ERK1/2, #4695; p-ERK1/2, #4370; JNK, #9252; p-JNK, #4668; p38, #9212; p-p38, #4511; STAT3, #30835; p-STAT3, #9145; AKT, #4691; p-AKT, #4060; β-actin, #4970). After several washing steps, the membranes were incubated with horseradish peroxidase-conjugated secondary antibodies (Cell Signaling Technology). A CCD camera was

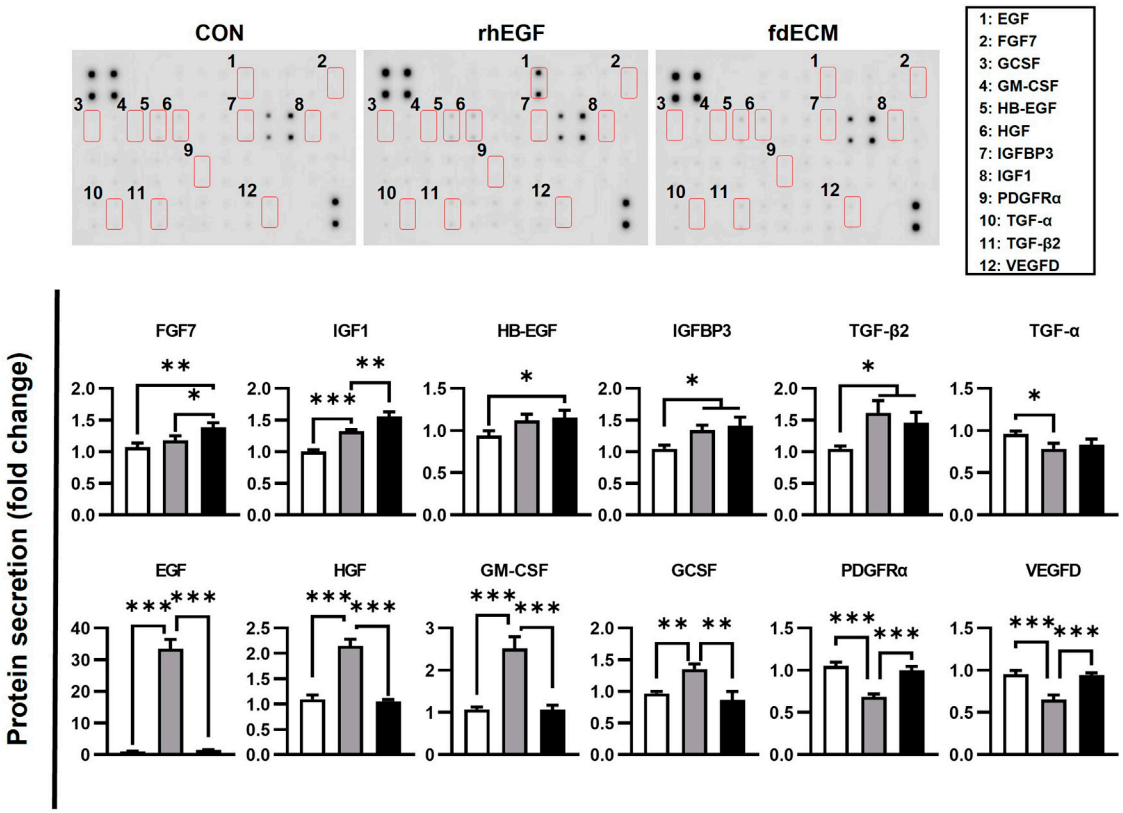


**FIGURE 6 |** Growth factor analysis of fibroblasts after fdECM treatment. Semi-quantitative analysis of growth factors and cytokines of human dermal fibroblast after 48 h of fdECM treatment. Forty-one angiogenic factors were detected, and the significantly changed factors are graphed (box denotes factors). Results are expressed as mean ± standard deviation (SD). *$p < 0.05$, **$p < 0.01$, ***$p < 0.001$.

used to detect immunoreactive bands using a chemiluminescent substrate (Clarity Western ECL Substrate; Bio-Rad). Quantification was performed using ImageJ, and each expression was standardized by the β-actin level.

## Statistical Analysis

Statistical analysis was conducted using Prism V5 (Graphpad Software Inc). Significant differences between groups were determined using one-way analysis of variance (ANOVA) followed by Bonferroni multiple comparisons post hoc test for parametric measures, Kruskal–Wallis test followed by Dunn post hoc test for non-parametric measures, and linear regression for construction of standard curves. Statistical significance was accepted at $p < 0.05$.

# RESULTS

## Bioactive Component Preserved fdECM

A commercially obtained human cell line, WI-38, was used to prepare fdECM. After the cells reached full confluency, we applied an optimal decellularization protocol to remove DNA and nuclei from the cells while maximally preserving ECM content (**Figure 1A** and **Supplementary Figure S1**). The extracted ECM was approximately 100 mg per confluent T-175 flask (571 μg/cm$^2$) and the ECM yield was 220 mg/g protein ($p < 0.001$, compared to extracted protein without decellularization). To verify the preservation of the active ingredients, the protein contents of cells before and after decellularization were compared by western blot. As a result, collagens I, IV, and elastin proteins showed little change, while collagen III, fibronectin, and laminin were reduced to 20, 50, and 20%, respectively, compared to the original cells (**Figure 1B**). In the growth factor array analysis, coagulation factor III, Serpin E1, and dipeptidyl peptidase-4 were the most abundant remaining factors even though the original contents were reduced (**Figure 1C**). However, several growth factors, including epidermal growth factor (EGF), hepatocyte growth factor (HGF), insulin-like growth factor-binding protein (IGFBP), platelet derived growth factor (PDGF), and vascular endothelial growth factor (VEGF) remained without being significantly lost during the decellularization process (**Figure 1D**).

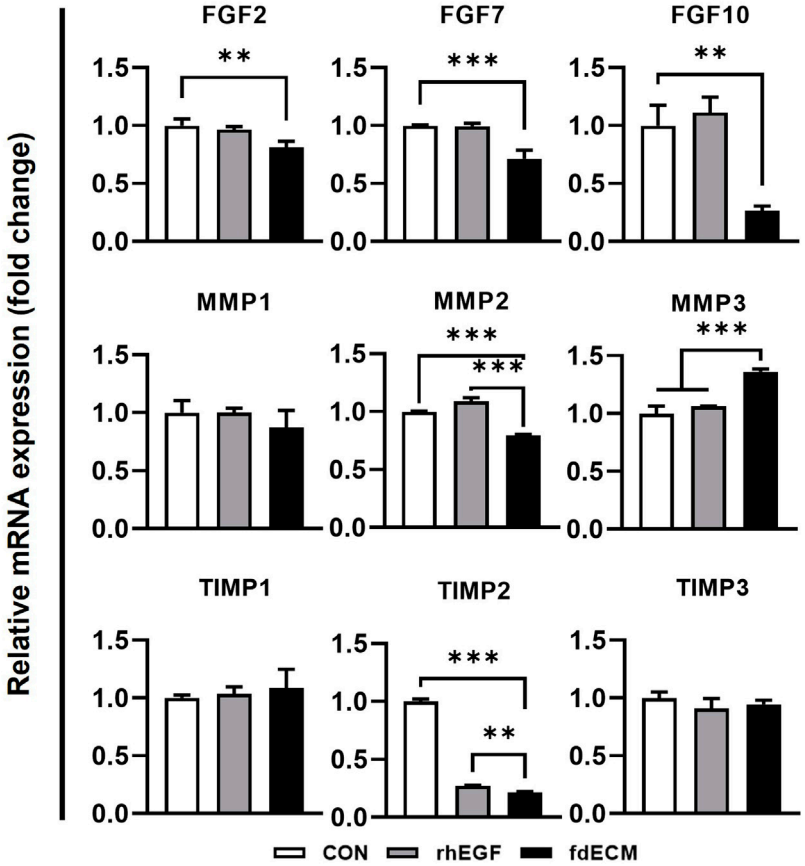


**FIGURE 7 |** mRNA expression pattern of fibroblasts after 48 h of fdECM treatment. Real-time PCR was used to analyze mRNA expression levels after 48 h of rhEGF or fdECM treatment. Results are expressed as mean ± standard deviation (SD). $^{**}p < 0.01$, $^{***}p < 0.001$.

## COL-fdECM Accelerated Skin Wound Healing *via* Neovascularization and Wound Contraction

Based on the fdECM remaining ingredients, we hypothesized that fdECM could accelerate wound healing via angiogenesis (Werner and Grose, 2003). First, we made an fdECM supplemented collagen patch to confirm its effect by adding the extracted fdECM to collagen I for the *in vivo* experiment (**Figure 2A**). The fdECM-collagen patch was observed to have a more homogeneous surface than the control collagen patch. However, the mechanical properties of the fdECM-collagen patch were similar to the control collagen patch, except the slightly increased compressive modulus (**Supplementary Figure S2**). We applied this patch to the full-thickness skin wound model to confirm its biological activities. After 14 days, in the control group (CON), where nothing was applied, the hemorrhagic crust was on the wounded skin (**Figure 2B**). In contrast, the defect area was almost completely epithelialized in the control collagen patch (COL) or fdECM-collagen patch (COL-fdECM) groups, and the wound area appeared smaller in the COL-fdECM group. To confirm the angiogenic efficacy of the prepared fdECM-collagen patch, we analyzed the blood vessels in the granulation tissue by CD31 immunostaining in the sampled tissue on day 7 (**Figure 2C**). As a result, the COL-fdECM group exhibited about twice as much blood vessel area as the other groups because the size and number of the blood vessels were significant (**Figure 2D**). Histological analysis was performed on the sample tissue on day 21 when the proliferation ended and remodeling was active, to confirm the long-term effect on wound healing. In the CON group, most of the defects consisted of immature skin tissue where only a few skin adnexa were observed (**Figure 2E**). However, in the COL-fdECM group, more hair follicles were observed in the center of the wound bed than the CON or COL group (**Figure 2F**). Moreover, the normal skin was closer to the center of the defect in the COL-fdECM group than the control (**Figure 2G**). In addition, when the collagen or fdECM-collagen patch was applied, the thickness of both the epidermis and the dermis was reduced compared to the CON group (**Figure 2H**). These results collectively confirm that the scaffold's regeneration efficacy created with fdECM promoted angiogenesis and contributed to wound contraction. Furthermore, the reduced thickness of the skin and increased hair follicles in the wound bed suggest that the treatment may help wound remodeling. Therefore, we attempted additional analyzes to evaluate it.

## COL-fdECM Assisted in Remodeling the Skin Wound

First, we analyzed the epidermal barrier function by staining cell adhesion molecule E-cadherin and the major component of the

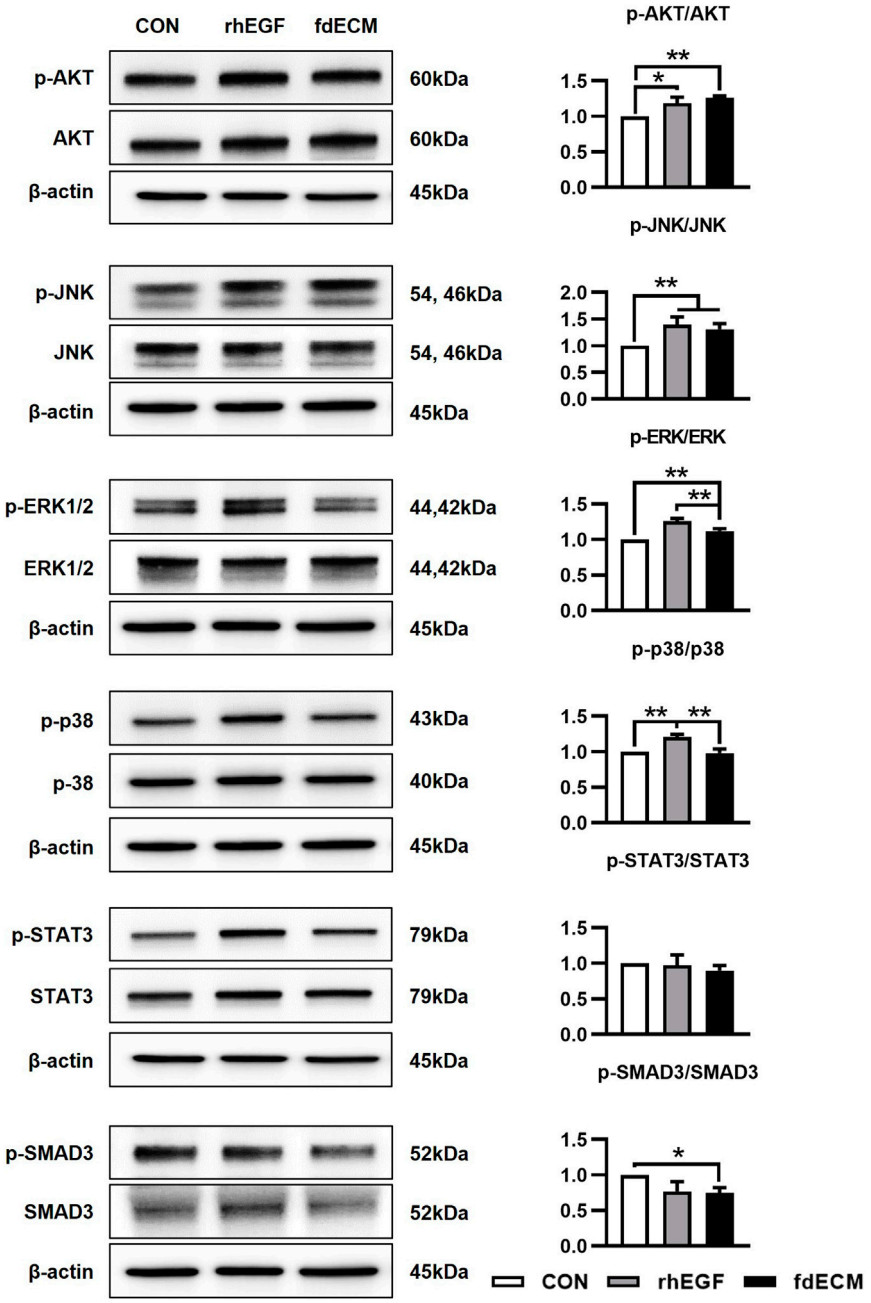


**FIGURE 8 |** Cell signaling pattern of fibroblasts after 48 h of fdECM treatment. Western blotting was used to analyze protein expression and phosphorylation levels after 48 h of rhEGF or fdECM treatment. Results are expressed as mean ± standard deviation (SD). *$p < 0.05$, **$p < 0.01$.

cornified envelope, loricrin (**Figure 3A**) (Tunggal et al., 2005; Abhishek and Palamadai Krishnan, 2016). The E-cadherin positive area seemed larger in the control group because of epidermal thickness. However, the signal intensity was higher in both the COL and COL-fdECM groups, meaning keratinocytes adhered to each other tightly. Loricrin expression in the CON group appeared diffuse and less intense, similar to the E-cadherin expression pattern. However, in the COL-fdECM group, loricrin was expressed in a constant line. Then, we analyzed the content of major components in the dermis, collagen I and III (**Figure 3B**). The immunofluorescence staining confirmed that collagen I and III content in the regenerated dermis was higher in the COL-fdECM group than in the CON and COL groups. We also checked whether the cut nerve fiber re-innervated from the ganglia to the skin. The PGP9.5 positive nerve fiber area was also higher in the superficial dermis of the COL-fdECM group compared to the other groups

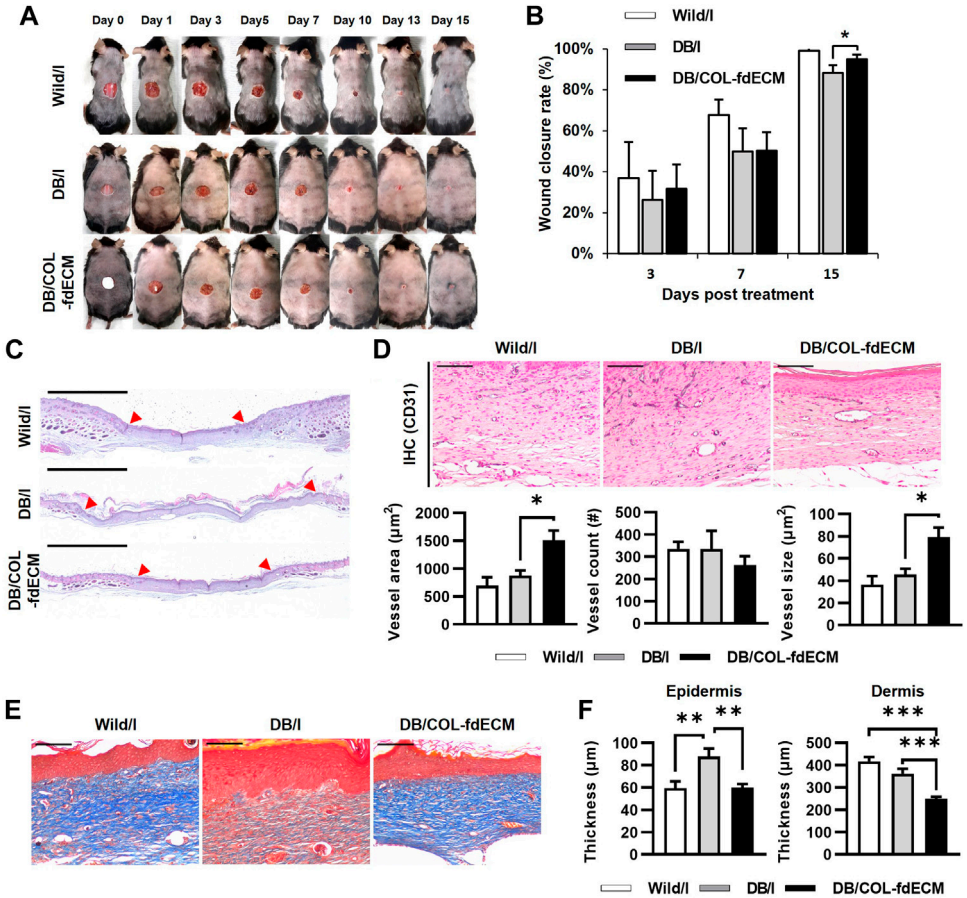


**FIGURE 9 |** *In vivo* evaluation of fdECM scaffolds on regeneration of diabetic skin wound model. **(A)** Gross evaluation of skin wounds after 15 days of fdECM treatment, **(B)** Wound closure rate (%) measured on day 3, 7, and 15, **(C)** Whole-mount images of fdECM treated skin wound stained with hematoxylin and eosin. Red arrows indicate the original defect site. Scale bar represents 2 mm, **(D)** Immunohistochemistry images stained with anti-CD31 antibody after 15 days of treatment (Gray color indicates a positive reaction), Scale bar represents 100 μm, Vessel area, and count were calculated per dermis area ($mm^2$), **(E)** Histological images of upper dermis stained with Masson's trichrome. Scale bars represent 100 μm. **(F)** Epidermal and dermal thickness in wound area. Bar represents mean ± standard error of mean (SEM). $^*p < 0.05$, $^{**}p < 0.01$, $^{***}p < 0.001$.

(**Figure 3C**). These results indicate that the fdECM also helps remodel the skin wounds to the original tissue. To analyze the effect and mechanism of fdECM on wound remodeling, we analyzed the phenotype change of the dermal fibroblast, the cell constituting most of the skin (**Figure 4**). After 7 days, the $\alpha$-SMA$^+$ was highest in the COL-fdECM group, indicating that CD34$^-$ dermal fibroblasts were mostly $\alpha$-SMA$^+$ myofibroblasts. Conversely, their activity was lowest at day 21 in the COL-fdECM group, suggesting dermal fibroblasts reversed their phenotype.

## fdECM Treated Fibroblasts Exhibited a Favorable State After Migration

To validate fdECM's efficacy on fibroblasts, we treated human dermal fibroblasts with unfabricated fdECM and analyzed the behavior. As a positive control, we used rhEGF, commercially available and known for various physiological activities, including angiogenic effect. The fdECM group showed increased cell migration to the scratch gap than the control group 18 h after the scratch wound was induced, although the number of fibroblasts migrating was highest in the rhEGF group (**Figure 5A**). After 48 h, when the scratch wound was completely restored, the fibroblasts of the CON and rhEGF groups remained in their active form, $\alpha$-SMA positive myofibroblasts (**Figure 5B**) (Pilcher et al., 1999). However, most fibroblasts of the fdECM group showed $\alpha$-SMA negative quiescent form, consistent with the *in vivo* results. Although myofibroblasts play a major role in contracting skin wounds, the remaining myofibroblasts, after wound healing, are suspected of causing hypertrophic scar formation (Chitturi et al., 2015). Therefore, the reduced number of myofibroblasts indicates a more favorable state for wound remodeling.

Moreover, it was confirmed that ECM components secreted by fibroblasts were different for each group. The fdECM or rhEGF treated fibroblasts were observed to secrete collagen I more than the control fibroblasts (**Figure 5C**). In contrast, increased collagen III-positive cells were observed in the CON and rhEGF groups and less in the fdECM group (**Figure 5D**). The

major dermal collagen type changes from collagen III to collagen I as the skin wound is remodeled (Volk et al., 2011; Tracy et al., 2016). Therefore, these results indicate fibroblasts treated with fdECM reverse their differentiation to a stable form and secrete collagen I more than collagen III. We also evaluated fibroblasts' growth factor secretion pattern (**Figure 6**). Among the 41 factors tested, fibroblast growth factor 7 (FGF7), insulin-like growth factor 1 (IGF1), insulin-like growth factor-binding protein 3 (IGFBP3), transforming growth factor beta-2 (TGF-β2), and heparin binding epidermal growth factor (HB-EGF) increased in the fdECM group compared to the CON group, but other factors did not differ. In particular, FGF7 and IGF1 were higher than in the rhEGF group, suggesting that these two factors may play a role in wound migration (Haase et al., 2003; Kirfel and Herzog, 2004).

## fdECM Modulated FGFs, MMPs, and TIMPs Expression

To elucidate the underlying mechanism of fdECM on wound remodeling, mRNA expression level and cell signaling were inspected. As shown in a previous study describing that FGFs mRNA increased rapidly after wounding and then decreased as the wound healed [6], FGF-2, -7, and -10 were downregulated in the fdECM treated group after 48 h (**Figure 7**). Matrix metalloproteinases (MMPs) mRNA pattern after 48 h of fdECM treatment was similar to that of the late phase in skin wound healing. Proinflammatory MMPs, such as MMP1 and MMP2, were downregulated, while MMP3, remodeling MMP, was upregulated. Tissue inhibitor of metalloproteinase-2 (TIMP2) was significantly downregulated in fdECM treated dermal fibroblasts, while TIMP1 and TIMP3 were stable.

We also measured the signaling pathway activated by fdECM using immunoblot analysis. Similar to rhEGF, fdECM treated fibroblasts showed increased AKT and JNK phosphorylation and decreased SMAD3 phosphorylation (**Figure 8**). However, the phosphorylation of ERK was decreased compared to the rhEGF group, and the p38 was decreased to the control group level. Together with the other results, these results suggest that adequate remodeling is related to regulating the p-38 and ERK pathways.

## fdECM was Effective in Diabetic Skin Ulcers

Finally, we investigated whether the fdECM efficacy can also be applied to the diabetic skin wound model (**Figure 9A**). After 15 days of inducing the skin wound, the wound closure rate of COL-fdECM treated diabetic mice (DB/COL-fdECM) was higher than the injury-only group (DB/I) (**Figure 9B**). Histopathologically, the wound bed size of the diabetic ulcer model was larger compared to normal mice, and hyperkeratosis was observed (**Figure 9C**). However, the wound closure of diabetic ulcers was improved after applying the fdECM-collagen patch. The CD31 positive vessel area was greater in the DB/COL-fdECM group compared to the DB/I group (**Figure 9D**). However, the increased vessel area was due to the increased size of the blood vessels rather than the number of blood vessels. Because of the progressed wound healing stage compared to previous experiments, this result suggests that the vessels are more mature after COL-fdECM treatment. Moreover, collagen quantity in the regenerated dermis was higher after being treated with an fdECM-collagen patch, suggesting a better quality of dermal regeneration (**Figure 9E**). The thickness of the epidermis and dermis was also significantly reduced compared to the DB/I group (**Figure 9F**). These results support that fdECM and its therapeutic efficacy can be applied to chronic skin wounds such as diabetic ulcers.

# DISCUSSION

ECM-based communication arises from orchestrating biochemical, topological, and biomechanical signals, facilitating interactive dialogue with cells that can respond through ECM remodeling. These multi-dimensional signals enable the ECM to guide complex cellular and tissue processes such as hemostasis, tissue repair, and regeneration in clinical applications. Currently, tissue- or organ-derived dECM is mainly used as a framework for tissue engineering. In addition, ECM can be used for the bare scaffolds and in various forms such as ingredients of hydrogels, polymers, nanoparticles, and in the drug delivery system (Bourget et al., 2012; Du et al., 2014; Kim et al., 2019). This study revealed the cell-derived ECM's biological mechanism and presented the scientific basis for miscellaneous uses. Moreover, the fdECM-collagen scaffold used in this study is stable enough to be stored at room temperature for future use, making the application of regenerative medicine simple and effective.

Many attempts have been made to reveal the efficacy of ECM for tissue engineering. Particularly, the fdECM efficacy on angiogenesis is well known, although the application is different from this study (Newman et al., 2011; Aldemir Dikici et al., 2020; Du et al., 2020). However, previous research was limited in the complex evaluation of diverse tissue components or underlying mechanisms. Furthermore, studies on tissue remodeling and qualitative differences were lacking since the focus was on rapid recovery. Our results showed consistency with previous research and suggested that the effect of the ECM component itself is greater than that of the delivery system. Moreover, to link tissue engineering and biology, we aimed to comprehensively elucidate the mechanisms of proliferation to remodeling and cell signaling to protein expression. Despite such efforts, a few limitations in this study remain. First, the effect of ECM through signaling pathways has not been rigorously validated by other methods using siRNA or inhibitors. Because ECM is not a single molecule but a mixture of countless compositions, further validation methods could not be applied.

Although the skin can be easily touched and observed, it is one of the most complex organs made up of various cells. However, this study did not include all cell types constituting the skin, such as immune cells and melanocytes. However, this study presented the scientific basis for application to various other tissues and diseases by analyzing epithelial cells, fibrous tissue, nerve fibers, and blood vessels, which are typical components of tissues other than the skin. Like diabetic

skin ulcers described in this study, fdECM can be a promising candidate for the treatment of other disorders, such as cardiac diseases (Fan et al., 2012; Zeng et al., 2013; Schmuck et al., 2014). Moreover, it can be used to directly reconstruct the circulatory or nervous system.

It is considered that there is potential for improvement of ECM's efficacy. Various fibroblast types exhibit different phenotypes, protein components, secretion profiles, and mechanical properties (Savitri et al., 2020). Recent studies have demonstrated that ECMs derived from other origins likewise could enhance the function of the target tissue by promoting cell-niche interactions and tissue-specific niches (Kusuma et al., 2017; Davidov et al., 2021). Phenotype-modulation of ECM source cells also exhibited better tissue regeneration (Antich et al., 2021). Coculturing of stromal and endothelial cells also enhanced mesenchymal stem cell differentiation (Carvalho et al., 2019). Moreover, aligning human dermal fdECM for vascular graft also enhanced a-SMA and calponin expression of mesenchymal stem cells (Xing et al., 2017). These papers suggest that cells of the same origin are not necessarily needed and that ECM efficacy can be maximized through various methods. For example, if the characterization is generated dependent on the ECM extracted from different cell types, such as dermal fibroblasts or keratinocytes, or at differentiation stages, the therapeutic efficacy of ECM can be optimized. Furthermore, it is necessary to consider the change in the efficacy of ECM according to the extraction method and application platform (Zhang et al., 2022). When these efforts are implemented, cell-derived dECM can be used as a multi-functional biomaterial that can be applied to various other biomaterials, from scaffolds to hydrogels.

## DATA AVAILABILITY STATEMENT

The original contributions presented in the study are included in the article/**Supplementary Material**, further inquiries can be directed to the corresponding author.

## ETHICS STATEMENT

The animal study was reviewed and approved by Institutional Animal Care and Use Committee of Konkuk University.

## AUTHOR CONTRIBUTIONS

H-SK drafted the manuscript. H-JH did the experiments and performed the analysis. H-JK designed the study and edited the manuscript. YC, DL, and H-HJ prepared the extracellular matrix and analyzed its properties. SD supervised the study and critically revised the manuscript. All authors contributed to the article and approved the submitted version.

## FUNDING

This research was supported by a grant from the Korea Health Technology R&D Project through the Korea Health Industry Development Institute (KHIDI), funded by the Ministry of Health and Welfare (HI17C1234), Republic of Korea.

## ACKNOWLEDGMENTS

We thank NIFDS for providing C57BL/6-Lepr$^{em1hwl}$/Korl mice and their information.

## SUPPLEMENTARY MATERIAL

The Supplementary Material for this article can be found online at: https://www.frontiersin.org/articles/10.3389/fbioe.2022.865545/full#supplementary-material

## REFERENCES

Abhishek, S., and Palamadai Krishnan, S. (2016). Epidermal Differentiation Complex: A Review on its Epigenetic Regulation and Potential Drug Targets. *Cell J* 18 (1), 1–6. doi:10.22074/cellj.2016.3980

Aldemir Dikici, B., Reilly, G. C., and Claeyssens, F. (2020). Boosting the Osteogenic and Angiogenic Performance of Multiscale Porous Polycaprolactone Scaffolds by *In Vitro* Generated Extracellular Matrix Decoration. *ACS Appl. Mater. Inter.* 12 (11), 12510–12524. doi:10.1021/acsami.9b23100

Antich, C., Jiménez, G., Vicente, J., López-Ruiz, E., Chocarro-Wrona, C., Griñán-Lisón, C., et al. (2021). Development of a Biomimetic Hydrogel Based on Predifferentiated Mesenchymal Stem-Cell-Derived ECM for Cartilage Tissue Engineering. *Adv. Healthc. Mater.* 10 (8), 2001847. doi:10.1002/adhm.202001847

Assunção, M., Dehghan-Baniani, D., Yiu, C. H. K., Später, T., Beyer, S., and Blocki, A. (2020). Cell-Derived Extracellular Matrix for Tissue Engineering and Regenerative Medicine. *Front. Bioeng. Biotechnol.* 8, 602009. doi:10.3389/fbioe.2020.602009

Bourget, J.-M., Gauvin, R., Larouche, D., Lavoie, A., Labbé, R., Auger, F. A., et al. (2012). Human Fibroblast-Derived ECM as a Scaffold for Vascular Tissue Engineering. *Biomaterials* 33 (36), 9205–9213. doi:10.1016/j.biomaterials.2012.09.015

Carvalho, M. S., Silva, J. C., Udangawa, R. N., Cabral, J. M. S., Ferreira, F. C., da Silva, C. L., et al. (2019). Co-culture Cell-Derived Extracellular Matrix Loaded Electrospun Microfibrous Scaffolds for Bone Tissue Engineering. *Mater. Sci. Eng. C* 99, 479–490. doi:10.1016/j.msec.2019.01.127

Chitturi, R. T., Balasubramaniam, A. M., Parameswar, R. A., Kesavan, G., Haris, K. T., and Mohideen, K. (2015). The Role of Myofibroblasts in Wound Healing, Contraction and its Clinical Implications in Cleft Palate Repair. *J. Int. Oral Health* 7 (3), 75–80. doi:10.4103/0975-7406.163513

Cui, H., Chai, Y., and Yu, Y. (2019). Progress in Developing Decellularized Bioscaffolds for Enhancing Skin Construction. *J. Biomed. Mater. Res.* 107 (8), 1849–1859. doi:10.1002/jbm.a.36688

Davidov, T., Efraim, Y., Hayam, R., Oieni, J., Baruch, L., and Machluf, M. (2021). Extracellular Matrix Hydrogels Originated from Different Organs Mediate Tissue-Specific Properties and Function. *Ijms* 22 (21), 11624. doi:10.3390/ijms222111624

Du, P., Hwang, M. P., Noh, Y. K., Subbiah, R., Kim, I. G., Bae, S. E., et al. (2014). Fibroblast-Derived Matrix (FDM) as a Novel Vascular Endothelial Growth

Factor Delivery Platform. *J. Controlled Release* 194, 122–129. doi:10.1016/j.jconrel.2014.08.026

Du, P., Da Costa, A. D. S., Savitri, C., Ha, S. S., Wang, P.-Y., and Park, K. (2020). An Injectable, Self-Assembled Multicellular Microsphere with the Incorporation of Fibroblast-Derived Extracellular Matrix for Therapeutic Angiogenesis. *Mater. Sci. Eng. C* 113, 110961. doi:10.1016/j.msec.2020.110961

Fan, D., Takawale, A., Lee, J., and Kassiri, Z. (2012). Cardiac Fibroblasts, Fibrosis and Extracellular Matrix Remodeling in Heart Disease. *Fibrog. Tissue Repair* 5 (1), 15. doi:10.1186/1755-1536-5-15

Gu, Y., Zhu, J., Xue, C., Li, Z., Ding, F., Yang, Y., et al. (2014). Chitosan/silk Fibroin-Based, Schwann Cell-Derived Extracellular Matrix-Modified Scaffolds for Bridging Rat Sciatic Nerve Gaps. *Biomaterials* 35 (7), 2253–2263. doi:10.1016/j.biomaterials.2013.11.087

Haase, I., Evans, R., Pofahl, R., and Watt, F. M. (2003). Regulation of Keratinocyte Shape, Migration and Wound Epithelialization by IGF-1- and EGF-Dependent Signalling Pathways. *J. Cel. Sci.* 116 (Pt 15), 3227–3238. doi:10.1242/jcs.00610

Harris, G. M., Madigan, N. N., Lancaster, K. Z., Enquist, L. W., Windebank, A. J., Schwartz, J., et al. (2017). Nerve Guidance by a Decellularized Fibroblast Extracellular Matrix. *Matrix Biol.* 60-61, 176–189. doi:10.1016/j.matbio.2016.08.011

He, S.-K., Ning, L.-J., Yao, X., Hu, R.-N., Cui, J., Zhang, Y., et al. (2021). Hierarchically Demineralized Cortical Bone Combined with Stem Cell-Derived Extracellular Matrix for Regeneration of the Tendon-Bone Interface. *Am. J. Sports Med.* 49 (5), 1323–1332. doi:10.1177/0363546521994511

Kim, I. G., Hwang, M. P., Du, P., Ko, J., Ha, C.-w., Do, S. H., et al. (2015). Bioactive Cell-Derived Matrices Combined with Polymer Mesh Scaffold for Osteogenesis and Bone Healing. *Biomaterials* 50, 75–86. doi:10.1016/j.biomaterials.2015.01.054

Kim, Y. S., Majid, M., Melchiorri, A. J., and Mikos, A. G. (2019). Applications of Decellularized Extracellular Matrix in Bone and Cartilage Tissue Engineering. *Bioeng. Transl. Med.* 4 (1), 83–95. doi:10.1002/btm2.10110

Kirfel, G., and Herzog, V. (2004). Migration of Epidermal Keratinocytes: Mechanisms, Regulation, and Biological Significance. *Protoplasma* 223 (2-4), 67–78. doi:10.1007/s00709-003-0031-5

Kusuma, G. D., Brennecke, S. P., O'Connor, A. J., Kalionis, B., and Heath, D. E. (2017). Decellularized Extracellular Matrices Produced from Immortal Cell Lines Derived from Different Parts of the Placenta Support Primary Mesenchymal Stem Cell Expansion. *PLoS One* 12 (2), e0171488. doi:10.1371/journal.pone.0171488

Lin, H., Yang, G., Tan, J., and Tuan, R. S. (2012). Influence of Decellularized Matrix Derived from Human Mesenchymal Stem Cells on Their Proliferation, Migration and Multi-Lineage Differentiation Potential. *Biomaterials* 33 (18), 4480–4489. doi:10.1016/j.biomaterials.2012.03.012

Lu, H., Hoshiba, T., Kawazoe, N., and Chen, G. (2011a). Autologous Extracellular Matrix Scaffolds for Tissue Engineering. *Biomaterials* 32 (10), 2489–2499. doi:10.1016/j.biomaterials.2010.12.016

Lu, H., Hoshiba, T., Kawazoe, N., Koda, I., Song, M., and Chen, G. (2011b). Cultured Cell-Derived Extracellular Matrix Scaffolds for Tissue Engineering. *Biomaterials* 32 (36), 9658–9666. doi:10.1016/j.biomaterials.2011.08.091

Massaro, M. S., Pálek, R., Rosendorf, J., Červenková, L., Liška, V., and Moulisová, V. (2021). Decellularized Xenogeneic Scaffolds in Transplantation and Tissue Engineering: Immunogenicity versus Positive Cell Stimulation. *Mater. Sci. Eng. C* 127, 112203. doi:10.1016/j.msec.2021.112203

Newman, A. C., Nakatsu, M. N., Chou, W., Gershon, P. D., and Hughes, C. C. W. (2011). The Requirement for Fibroblasts in Angiogenesis: Fibroblast-Derived Matrix Proteins Are Essential for Endothelial Cell Lumen Formation. *MBoC* 22 (20), 3791–3800. doi:10.1091/mbc.E11-05-0393

Pilcher, B. K., Wang, M., Qin, X.-J., Parks, W. C., Senior, R. M., and Welgus, H. G. (1999). Role of Matrix Metalloproteinases and Their Inhibition in Cutaneous Wound Healing and Allergic Contact Hypersensitivity. *Ann. NY Acad. Sci.* 878, 12–24. doi:10.1111/j.1749-6632.1999.tb07671.x

Savitri, C., Ha, S. S., Liao, E., Du, P., and Park, K. (2020). Extracellular Matrices Derived from Different Cell Sources and Their Effect on Macrophage Behavior and Wound Healing. *J. Mater. Chem. B* 8 (42), 9744–9755. doi:10.1039/d0tb01885f

Schmuck, E. G., Mulligan, J. D., Ertel, R. L., Kouris, N. A., Ogle, B. M., Raval, A. N., et al. (2014). Cardiac Fibroblast-Derived 3D Extracellular Matrix Seeded with Mesenchymal Stem Cells as a Novel Device to Transfer Cells to the Ischemic Myocardium. *Cardiovasc. Eng. Tech.* 5 (1), 119–131. doi:10.1007/s13239-013-0167-1

Tracy, L. E., Minasian, R. A., and Caterson, E. J. (2016). Extracellular Matrix and Dermal Fibroblast Function in the Healing Wound. *Adv. Wound Care* 5 (3), 119–136. doi:10.1089/wound.2014.0561

Tunggal, J. A., Helfrich, I., Schmitz, A., Schwarz, H., Günzel, D., Fromm, M., et al. (2005). E-Cadherin Is Essential for *In Vivo* Epidermal Barrier Function by Regulating Tight Junctions. *Embo J.* 24 (6), 1146–1156. doi:10.1038/sj.emboj.7600605

Volk, S. W., Wang, Y., Mauldin, E. A., Liechty, K. W., and Adams, S. L. (2011). Diminished Type III Collagen Promotes Myofibroblast Differentiation and Increases Scar Deposition in Cutaneous Wound Healing. *Cells Tissues Organs* 194 (1), 25–37. doi:10.1159/000322399

Werner, S., and Grose, R. (2003). Regulation of Wound Healing by Growth Factors and Cytokines. *Physiol. Rev.* 83 (3), 835–870. doi:10.1152/physrev.2003.83.3.835

Wong, C.-W., LeGrand, C. F., Kinnear, B. F., Sobota, R. M., Ramalingam, R., Dye, D. E., et al. (2019). *In Vitro* Expansion of Keratinocytes on Human Dermal Fibroblast-Derived Matrix Retains Their Stem-Like Characteristics. *Sci. Rep.* 9 (1), 18561. doi:10.1038/s41598-019-54793-9

Xing, Q., Yates, K., Tahtinen, M., Shearier, E., Qian, Z., and Zhao, F. (2015). Decellularization of Fibroblast Cell Sheets for Natural Extracellular Matrix Scaffold Preparation. *Tissue Eng. C: Methods* 21 (1), 77–87. doi:10.1089/ten.TEC.2013.0666

Xing, Q., Qian, Z., Tahtinen, M., Yap, A. H., Yates, K., and Zhao, F. (2017). Aligned Nanofibrous Cell-Derived Extracellular Matrix for Anisotropic Vascular Graft Construction. *Adv. Healthc. Mater.* 6 (10), 1601333. doi:10.1002/adhm.201601333

Zeng, Q.-c., Guo, Y., Liu, L., Zhang, X.-z., Li, R.-x., Zhang, C.-q., et al. (2013). Cardiac Fibroblast-Derived Extracellular Matrix Produced *In Vitro* Stimulates Growth and Metabolism of Cultured Ventricular Cells. *Int. Heart J.* 54 (1), 40–44. doi:10.1536/ihj.54.40

Zhang, X., Chen, X., Hong, H., Hu, R., Liu, J., and Liu, C. (2022). Decellularized Extracellular Matrix Scaffolds: Recent Trends and Emerging Strategies in Tissue Engineering. *Bioact. Mater.* 10, 15–31. doi:10.1016/j.bioactmat.2021.09.014

**Conflict of Interest:** YC, DL, and H-HJ were employed by HansBiomed Co. Ltd.

The remaining authors declare that the research was conducted in the absence of any commercial or financial relationships that could be construed as a potential conflict of interest.

**Publisher's Note:** All claims expressed in this article are solely those of the authors and do not necessarily represent those of their affiliated organizations, or those of the publisher, the editors and the reviewers. Any product that may be evaluated in this article, or claim that may be made by its manufacturer, is not guaranteed or endorsed by the publisher.

# Advantages of publishing in Frontiers

**OPEN ACCESS**
Articles are free to read for greatest visibility and readership

**FAST PUBLICATION**
Around 90 days from submission to decision

**HIGH QUALITY PEER-REVIEW**
Rigorous, collaborative, and constructive peer-review

**TRANSPARENT PEER-REVIEW**
Editors and reviewers acknowledged by name on published articles

**Frontiers**
Avenue du Tribunal-Fédéral 34
1005 Lausanne | Switzerland

**Visit us:** www.frontiersin.org
**Contact us:** frontiersin.org/about/contact

**REPRODUCIBILITY OF RESEARCH**
Support open data and methods to enhance research reproducibility

**DIGITAL PUBLISHING**
Articles designed for optimal readership across devices

**FOLLOW US**
@frontiersin

**IMPACT METRICS**
Advanced article metrics track visibility across digital media

**EXTENSIVE PROMOTION**
Marketing and promotion of impactful research

**LOOP RESEARCH NETWORK**
Our network increases your article's readership